Principles of Membrane Bioreactors for Wastewater Treatment

Influent wastewater → Bioreactor — MF or UF — Suction pump → Treated wastewater — Waste activated sludge

Hee-Deung Park
In-Soung Chang
Kwang-Jin Lee
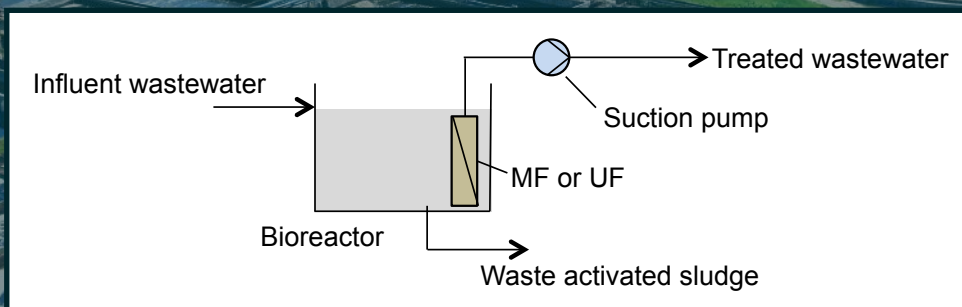
Principles of Membrane Bioreactors for Wastewater Treatment

Principles of Membrane Bioreactors for Wastewater Treatment

Hee-Deung Park
In-Soung Chang
Kwang-Jin Lee

CRC Press
Taylor & Francis Group
Boca Raton London New York

CRC Press is an imprint of the
Taylor & Francis Group, an **informa** business

Visit the Taylor & Francis Web site at
http://www.taylorandfrancis.com

and the CRC Press Web site at
http://www.crcpress.com

Contents

Preface

Membrane bioreactor (MBR) technology is a wastewater treatment method coupling biological treatment and membrane separation. Although MBR technology did not come into the spotlight when it was first introduced by Smith and coworkers in the late 1960s, it has been playing an important role in wastewater treatment and wastewater reuse since the mid-1990s. Stringent regulations on effluent discharge, demands for wastewater reuse, and the reduction of membrane capital costs are regarded as the main drivers for today's widespread use of this technology worldwide.

In accordance with the popularity of MBR technology, students majoring in environmental engineering, or related disciplines, and wastewater engineers are in continuous need of knowledge about the principles and applications of the technology. Nevertheless, good books instructing both students and professionals about MBR technology principles and applications are difficult to find. Only a few MBR books are available at present, and, moreover, the books mostly concentrate on the technological development in MBR operations and full-scale case studies. There is a need for a book that provides concrete principles, appropriate design examples, and operational experiences.

In *Principles of Membrane Bioreactors for Wastewater Treatment*, we focus on the basic principles of MBR technology such as biological treatment, membrane filtration, and membrane fouling. The book also includes applications of MBR such as operation, maintenance, design, and case studies. We wrote the book to impart comprehensive knowledge about MBR technology to students and wastewater engineers via a step-by-step learning process. To this end, there are many examples and problems in the core chapters dealing with the principles of MBR technology.

Principles of Membrane Bioreactors for Wastewater Treatment is a textbook mostly designed for one-semester, graduate-level, or senior undergraduate-level courses. It consists of an introductory chapter (Chapter 1), three core chapters (Chapters 2 through 4), and three application chapters (Chapters 5 through 7). The core chapters deal with basic principles of biological treatment, membrane filtration, and membrane fouling and comprise about two-thirds of the book. Examples in the

book will help the readers understand the basic concepts and principles clearly, while problems are prepared to advance the relevant theories more deeply. Application chapters connect the three main branches of MBR technology handled by the three core chapters, including operation, maintenance, design, and case studies.

MBR processes use their microbiological metabolic potential for treating wastewater. In this sense, MBR processes are similar to conventional activated sludge (CAS) processes. However, if we take a closer look at the design and operation of bioreactors in MBR processes, we will notice several differences between these two processes. For example, MBR processes are designed and operated with much longer solids retention times (SRT) than CAS processes. Longer SRT operation results in different treatment performances and other associated situations. Therefore, Chapter 2 deals with fundamental frameworks for analyzing and interpreting biological processes (e.g., microbiology, stoichiometry, kinetics, and mass balances) of MBR plant bioreactors, which are substantially different from CAS plant bioreactors with respect to design and operation.

MBR processes use microfiltration or ultrafiltration membranes to separate treated water from activated sludge, replacing gravity sedimentation tanks (or secondary sedimentation tanks) in CAS processes. Membrane separation can overcome the limitation of gravity sedimentation tanks and produce nearly particle-free clean effluents. However, the use of membranes entails problems of membrane fouling. The success of MBR processes is largely dependent upon proper design and operation that minimize membrane fouling. Chapters 3 and 4 will be helpful for understanding membrane fouling problems as well as membrane filtration phenomena. Particularly, these chapters deal with filtration theory, membrane materials and geometry, fouling phenomena and properties, and strategies for minimizing fouling.

Chapters 5 through 7 will be of great use for wastewater engineers as well as students. In these chapters, we have included the practical aspects of MBR in terms of operation, maintenance, design, and application. These chapters cover some considerations and examples for designing and operating MBR plants. Here, we adhered to the knowledge and principles provided in the core chapters in explaining the practices related to applications in MBR technology.

Research on MBR technology has matured, and several thousands of full-scale applications of MBRs are operating worldwide. The hope of spreading MBR knowledge and information has inspired us to prepare this textbook. Over the past two years, we have worked toward explaining MBR technology more clearly and understanding the underlying essential MBR principles better. This book is the fruit of our labor, and we hope that our efforts result in increased successful MBR applications.

Additional material is available at the CRC website: http://www.crcpress.com/product/isbn/9781466590373.

We take this opportunity to say a few appreciative words for the people who supported the preparation of this book. First, we thank the graduate students who

took course ACE946 at Korea University. They corrected errors in the drafts of Chapters 2 and 6 and also suggested examples and problems in those chapters. In addition, we thank Sung Jun Hong from Hoseo University for help with the figure drawings. Special thanks to Samantha Reuter, who proofread the entire book and provided useful writing tips. We also thank Li-Ming Leong, acquisitions editor, CRC Press, without whose proposal and encouragement we would not have written this book. Finally, we thank our family members for their endurance and understanding during our long work hours.

Hee-Deung Park

In-Soung Chang

Kwang-Jin Lee

Chapter 1

Introduction

Ardern and Lockett at Savyhulme Sewage Works in the United Kingdom introduced "activated sludge" to the public in 1914, exactly 100 years ago. They found out that aerated sewage in a fill-and-draw reactor produced purified water with the help of biological organisms (i.e., activated sludge). This phenomenal discovery, the sewage treatment process using activated sludge or the "activated sludge process," has revolutionized our society in terms of public health as well as environmental protection.

Activated sludge processes have tremendous merit in treating polluted wastewater as well as sewage. It is a reliable, economical, and robust technology that contributes to our lives daily. Owing to this technology, we are living in a cleaner and safer water environment, although world populations are steadily growing and are concentrated in big cities.

Nevertheless, the demand for a cleaner water environment has increased to protect aquatic life, and effluent standards are getting more stringent. On the other hand, recent climate change has aggravated uneven precipitation and water distribution, making water more precious than ever and accelerating wastewater reuse rates. Wastewater is produced abundantly and stably, which makes it a suitable water resource during water shortages.

Membrane treatment of wastewater can be a solution to satisfy both cleaner effluent and wastewater reuse demands. Membrane bioreactor (MBR) technology couples biological treatment and membrane separation and has emerged as the leading membrane technology that can meet the two requirements mentioned above. MBR has especially gained popularity with the help of dramatic membrane cost reductions (~1/10) over the last two decades.

The MBR market has grown steadily since mid-1990s. Based on the research of Frost & Sullivan, the MBR market was $838.2 million in year 2011 and is

expected to grow to \$3.44 billion by year 2018 with a compound annual growth rate of 22.4%. The market is expected to grow rapidly in locations where water resources are limited such as the Middle East and Asia Pacific regions (Water World, 2014).

This chapter provides a brief overview of MBR technology including principles, history, a comparison between MBR and conventional activated sludge systems (CAS), performance, and the current direction in research and development.

1.1 Introduction of MBR

1.1.1 Principle of MBR

MBR is a technology used to treat wastewater that combines a bioreactor and membrane separation. A bioreactor in an MBR system has the same function as the aerated tank of any activated sludge process in which wastewater is treated by the activity of microorganisms. In an MBR process, instead of separating treated water and microorganisms (i.e., activated sludge) by gravity, porous membranes with 0.05–0.1 μm pore diameters are used to separate treated water and microorganisms. As shown in Figure 1.1a and c, the pore diameter of the membranes used in MBR are small enough to reject activated sludge flocs, free-living bacteria, and even large-size viruses or particles.

Therefore, MBR produces very high-quality treated water containing almost no detectable suspended solids (SSs). The treated water quality is equivalent to tertiary wastewater treatment (i.e., the combination of activated sludge and depth filtration). In addition, membrane filtration in MBR processes obviate gravity sedimentation tanks, which results in a smaller footprint than CAS processes. Other features of MBR processes will be discussed in Sections 1.1.3 and 1.1.4.

Nevertheless, MBR processes, like other membrane processes, have limitations in terms of membrane fouling. Membranes are vulnerable to be fouled by activated sludge, suspended solids, organics, and inorganics during the filtration process (Figure 1.1b). Therefore, controlling membrane fouling is the key for stable MBR operation. Various approaches have been developed to mitigate membrane fouling problems. For example, membrane manufacturers are trying to fabricate fouling-resistant membranes by modifying membrane surface chemistry and/or membrane module geometry, while process engineers modulate filtration cycles, ensure backwashing, and provide scouring aeration.

1.1.2 Brief History of MBR Technology

In 1969, MBR technology was first introduced by Smith et al. (1969), who were assisted by the Dorr–Oliver research program. To develop a wastewater treatment process with high-quality effluent without a sedimentation tank for separating
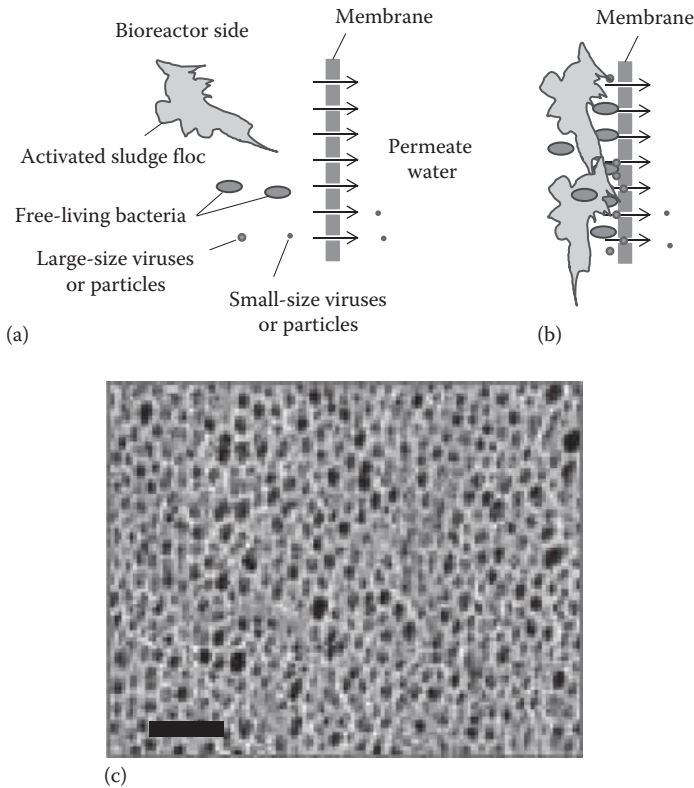
Figure 1.1   Schematic representation of the principles of MBR process: (a) membrane filtration in MBR, (b) membrane fouling in MBR, and (c) surface image of Kolon's Cleanfil-S membrane (scale = 1 μm). (From Kolon Industries Inc., http://kolonmembr.co.kr/, 2014. With permission.)

treated water and activated sludge, they used ultrafiltration membranes. They conducted a feasibility test using a pilot plant treating sewage generated from a manufacturing plant in Sandy Hook, Connecticut, United States, for 6 months.

Membrane units were installed outside the bioreactor and mixed liquor in the bioreactor was recirculated across the membrane surface with high crossflow velocities ranging from 1.2 to 1.8 m/s with 150–185 kPa to reduce fouling and to maintain a stable flux (13.6–23.4 L/m²/h). The effluent quality was typically less than 5 mg/L BOD and achieved 100% removal of coliform bacteria for 90% of the operational time. Although this MBR operational strategy called side-stream configuration (Figure 1.2a) produced very high quality effluent, the technology was applied to very limited cases such as industrial and leachate wastewaters. High energy costs associated with mixed liquor recirculation, membrane fouling,
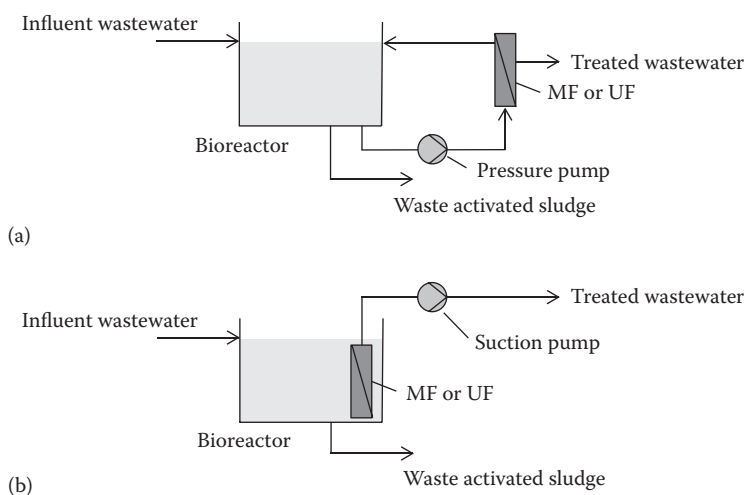
Figure 1.2 Two operational types of MBR technology: (a) side-stream configuration and (b) submersed configuration.

and high membrane capital costs restrained the spread of this technology to general applications such as the treatment of municipal wastewater.

In 1989, Yamamoto et al. (1989) introduced an innovative MBR technology called "direct solid–liquid separation using hollow fiber (HF) membrane in an activated sludge aeration tank." They used 0.1 μm size polyethylene HF membranes for separating treated water in an activated sludge bioreactor. Instead of circulating mixed liquor across a membrane by a pressurized pump installed outside of the bioreactor, they immersed the membranes directly into the bioreactor and applied suction pressure to produce permeate (i.e., treated water).

Treated water was continuously produced with low suction pressure (13 kPa), short hydraulic retention times (4 h), high volumetric loads (1.5 kg COD/m³·days), and relatively long operating periods (120 days) by operating the membrane with intermittent suction (10 min "on" and 10 min of "off"). This operational strategy called the submersed or immersed configuration (Figure 1.2b) resulted in the widespread dissemination of MBR technology used for treating various wastewaters including municipal wastewater, mainly due to the low energy cost in producing permeate.

Since the introduction of MBR technology using the submersed configuration, a number of studies have been conducted to optimize the shape of membrane modules, the pore size of membranes, operations to minimize membrane fouling, and the cleaning of fouled membranes. The appearance of competitive MBR providers (e.g., Zenon, Kubota, Mitsubishi Rayon, and US-Filter), as well as the accumulation

of operational data via academic and field studies have accelerated the application of MBR technology since the mid-1990s.

With the help of significant reductions in membrane costs (~US$400 per m^2 membrane in 1992 → ~US$50 in 2010) and the introduction of high-quality membranes, construction of large-scale MBR plants with capacities greater than 50,000 m^3/day have been initiated in areas where wastewater reuse is necessary, such as the Middle East countries, China, and the United States. Refer to Table 7.1 for a list of large-scale MBR plants built around the world. Although the spread of MBR plants had slowed down due to economic depression worldwide after 2008, considering the need for a better water environment in the future, the prospects are bright for MBR technology.

1.1.3 Comparison of CAS and MBR Processes

CAS processes mainly consist of a bioreactor treating wastewater using activated sludge (i.e., active microorganisms) and a sedimentation tank or secondary clarifier separating the treated water from the mixture of activated sludge (plus some SSs originated from nonbiomass) and treated water.

Sedimentation tanks are not perfect in settling all of the activated sludge. Lighter fraction of activated sludge is washed away with the treated effluent. Typically, the SSs concentration of the supernatant from the sedimentation tank is around 5 mg/L even for properly working secondary clarifiers.

However, in MBR processes all activated sludge is separated from the treated effluent because the pore size of the membranes (<0.1 μm) used are smaller than the activated sludge particles. This results in almost no detectable concentration of SSs in the treated effluent, although dissolved matters can pass through the membrane pores. Therefore, tertiary treatment such as sand filters and microfilters for removing SSs can be omitted in MBR processes.

Both CAS processes and MBR processes utilize the metabolic power of microorganisms in bioreactors for the treatment of wastewater. Therefore, the rate of wastewater treatment is basically proportional to the concentration of active biomass in the bioreactor (we will learn about biological kinetic expressions in detail in Chapter 2). However, in CAS processes it is impossible to increase the concentration of activated sludge greater than a certain level due to the limitations of secondary clarifiers. Clarifiers are operated based on the settling properties of activated sludge governed by gravity and interactions between activated sludge particles.

Settling obligations increase with increasing concentrations of activated sludge in the secondary clarifier. Approximately 5000 mg/L of mixed liquor suspended solids (MLSS) in a bioreactor is regarded as the maximum concentration of activated sludge for operating a secondary clarifier stably. In MBR processes, theoretically, there is no maximum concentration of MLSS in a bioreactor, although 8,000–12,000 mg/L MLSS are regarded as optimal levels. Higher MLSS
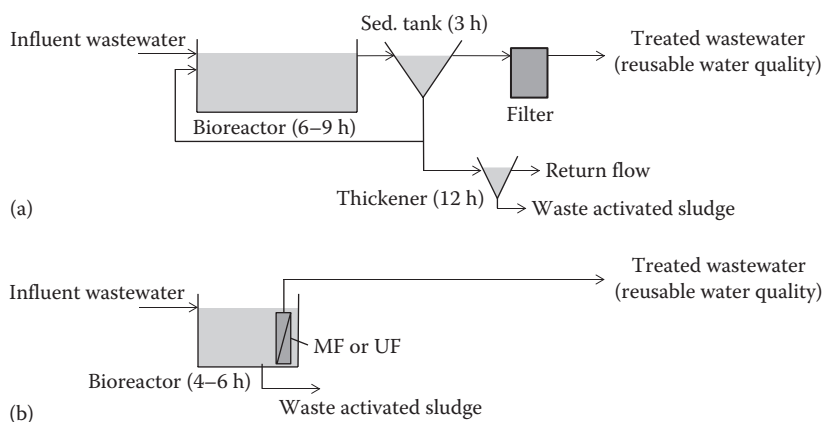
Figure 1.3 Comparison between CAS and MBR processes: (a) CAS and (b) MBR. The times indicated in parenthesis are hydraulic-retention times.

concentrations during MBR operation results in a smaller bioreactor footprint required to treat wastewater to a certain level (i.e., more compact, Figure 1.3), or a higher quality of treated water is obtained from the same volume of bioreactor compared to a CAS process.

The high MLSS-concentration operation of MBR processes also provides benefits by reducing waste sludge production. Microorganisms tend to degrade themselves in bioreactors (i.e., endogenous decay). As the degradation rate is proportional to the concentration of biomass (see Chapter 2 for more details and discussion), MBR processes produce less waste activated sludge (WAS) and, therefore, reduce the cost associated with WAS removal.

Solids retention time (SRT) is an important operating parameter for a bioreactor that determines the quality of treated water and the bioreactor MLSS concentration. SRT is the average retention time of solids in a bioreactor (i.e., the average amount of time a particle spends in a bioreactor). SRT can be estimated from the total MLSS mass (=MLSS concentration times bioreactor volume) in a bioreactor over the WAS removal rate (=WAS concentration times flow rate). In general, with increasing SRT, the wastewater treatment efficiency increases and the substrate concentration decreases. Long SRT operation of MBR processes (typically >20 days) compared with CAS processes (typically 5–15 days) contributes to the high-quality of effluent in MBR processes.

In many CAS cases, SRT is controlled by modulating the WAS rate in the sedimentation tank. However, the concentration of WAS is variable depending on the settling properties of the activated sludge in the sedimentation tank, which makes it difficult to achieve precise SRT control. In MBR, WAS is obtained from the bioreactor directly (i.e., MLSS concentration = WAS concentration). SRT is thus

Table 1.1   Advantages and Disadvantages of MBR over CAS

Advantages	1. Production of high-quality treated water that is reusable. In addition, removal of most of the pathogenic bacteria and some viruses are possible.
	2. Low footprint due to the obviation of secondary sedimentation tank and smaller bioreactor size.
	3. Reduced WAS production.
	4. Fine control of SRT.
Disadvantages	1. Greater operational and process complexity.
	2. Higher capital and operational costs.
	3. Greater foaming propensity.

Source: Judd, S., *Trends Biotechnol.*, 26(2), 109, 2008.

calculated as bioreactor volume over wastage flow rate, which provides a simpler and more precise way to modulate SRT.

As discussed, MBR has advantages such as higher final effluent quality (due to membrane separation of treated water and longer SRT operation), lower treatment plant footprint (due to omitting secondary clarifiers and more compact bioreactors), reduced WAS (due to high-MLSS-concentration operation), and precise control of SRT (due to omitting sedimentation tanks). For all the advantages, MBR also has disadvantages mainly related to the membranes.

Membrane installment results in greater operational and process complexity. The complexity is mostly associated with the maintenance and membrane cleanliness (Judd, 2008). Membranes tend to foul (i.e., clogging of pores by organics and inorganics) with time. It is necessary to provide various operational strategies as well as processes to mitigate the fouling propensity of membranes (see Chapter 5 for more details and discussion).

Membrane installment also requires additional capital cost, although the price of membranes has dramatically reduced over the last 20 years. In addition, anti-fouling strategies such as membrane aeration in submerged MBR and recirculation of MLSS in side-stream MBR require additional operational costs. Sometimes the electrical consumption for MBR operation is greater than twice that of CAS. In addition, MBR produces more bioreactor foams, a nuisance during operation. The advantages and disadvantages of MBR over CAS are summarized in Table 1.1.

1.1.4 Operational Condition and Performance of MBR

As described earlier, MBR processes operate with high MLSS concentrations and long SRTs. These operational conditions allow bioreactors to be operated at higher

Table 1.2   Typical MBR Operational Conditions and Effluent Quality

Classification	Unit	Typical value	Range
Operational condition			
COD loading	kg/m³·day	1.5	1.0–3.2
MLSS	mg/L	10,000	5,000–20,000
MLVSS	mg/L	8,500	4,000–16,000
F/M ratio	g COD/g MLSS·day	0.15	0.05–0.4
SRT	day	20	5–30
HRT	h	6	4–9
Flux	L/m²·h	20	15–45
Suction pressure	kPa	10	4–35
DO	mg/L	2.0	0.5–1.0
Effluent quality			
BOD	mg/L	3	<5
COD	mg/L	20	<30
NH_3	mg N/L	0.2	<1
TN	mg N/L	8	<10
SS	mg/L	0.1	<0.2

Source: Tchobanoglous, G. et al., *Wastewater Engineering: Treatment and Reuse*,
    4th edn., Metcalf and Eddy Inc., McGraw-Hill, New York, 2003.

COD volumetric loadings and lower F/M ratios. Higher COD volumetric loading operation indicates that MBR processes have more compact bioreactors (i.e., shorter HRT) than CAS processes. Also, the lower F/M ratio operation of MBR processes generates conditions for slowly growing bacteria such as nitrifying bacteria. Other operational factors such as the dissolved oxygen level in the aerobic tank (within the bioreactor) and the return flow of MLSS from the aerobic tank for nitrogen removal are similar to the CAS process. Typical MBR-process operational conditions are presented in Table 1.2.

MBR processes produce a higher-quality effluent than CAS processes. The higher effluent quality is primarily due to the near perfect removal of SSs by membrane filtration. Although CAS processes result in ~5 mg/L SS even for a well-operated secondary clarifier, MBR processes can reject most SSs in a bioreactor

by membrane filtration (SS < 0.2 mg/L). If we acknowledge that organic matters, nitrogen, and phosphorus are components of SS, it is no wonder that the effluent quality of MBR processes is better than that of CAS processes. In addition, MBR processes are operated at longer SRT compared to CAS processes, which generates stable nitrification efficiency even during the winter and removes more of slowly biodegradable organic matters. Typical effluent quality values and ranges for MBR processes are presented in Table 1.2.

1.2 Direction in Research and Development (R&D) of MBR

1.2.1 Membranes and Modules

Membrane materials used for MBR processes can be categorized into polymeric and ceramic materials. Although polymeric materials have been commonly used to fabricate membranes, membranes made of ceramic materials have started to gain attention due to their durability and chemical resistance.

Diverse polymer materials including polyethylene (PE), plyvinylidene difluoride (PVDF), polytetrafluoroethylene (PTFE), polypropylene (PP), polyacrylonitrile (PAN), polyethersulfone (PES), and polysulfone (PS) have all been used to fabricate membranes. Among them, PVDF is the most popular. The development of enhanced mechanical-structured PVDF membranes has made it possible to overcome the brittleness of membranes of which the wastewater treatment practitioners often complain. The prolonged lifetime of PVDF membranes has led to widespread installations of MBR plants worldwide.

Cutting-edge and/or high technologies are seldom applied to biological wastewater treatment facilities. However, the developments of innovative technologies in the fields of nanosciences and molecular biology over the last couple of decades show the potential to make MBRs more adaptive to cope with membrane fouling than before. For example, membranes composited with carbon nanotubes or fullerene are known to retard depositions and/or adsorptions of microorganisms onto their surfaces and pores.

Membranes are fabricated into flat sheet (FS), hollow fiber (HF), and multi-tube (MT) (see Chapter 3 for a detailed description) configurations. FS and HF membranes are generally used for the submerged MBR configuration, while MT membranes are exclusively applied to the side-stream MBR configuration. All types of membranes are packaged into modules for application in MBR. Membrane modules have been developed to increase their packing density because more highly packed membrane modules are better in terms of saving footprint. Packing density is mainly increased by increasing the number of stacks (or decks) for the membrane modules adopting FS and by packing (or potting) membrane fibers more densely within a certain area or by increasing the length of membrane fibers for the membrane modules adopting HF (Figure 1.4).

First deck

Second deck

(a)   (b)
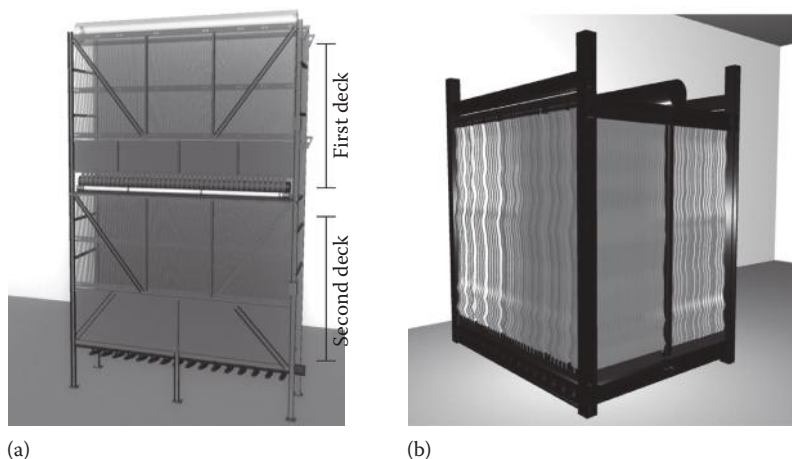
Figure 1.4   Highly packed membrane modules: (a) Kubota's EK-400 (FS) and (b) GE Zenon's Zeeweed 500d (HF). (Images were drawn by Young-Hwan Yang.)

Devices for generating aeration for scouring have been developed to improve scouring efficiency and to save energy associated with aeration. Typically pipes with holes for aeration are placed under membrane modules. Optimum hole size, applied pressure, and air flow rates have been determined mostly experimentally. Cyclic aeration or discontinued aeration is an approach to improve the scouring performance as well as to reduce the energy costs for aeration (see Section 1.2.2).

In addition to typical aerators, membrane module makers try to develop devices for pulsed aeration, which operate over a certain threshold level of air amount. MemPulse (http://www.siemens.com) and LEAPmbr (http://www.gewater.com) are the two representative systems for the devices introduced by Siemens and GE Zenon, respectively. These systems are claimed to be effective in scouring membranes as well as in saving energy costs.

1.2.2 Operation and Maintenance (O&M)

The important issues R&D of MBR currently focus on are the reduction of operation and maintenance (O&M) costs (mainly energy consumption) and controlling membrane fouling. Therefore, the general trend and the state of the art of MBR technology have been focused on the sustainability of MBR in terms of energy consumption and membrane fouling. In practice, the costs associated with power consumption and membrane replacement contribute to the difference in O&M costs between CAS and MBR plants. An estimation of the O&M cost
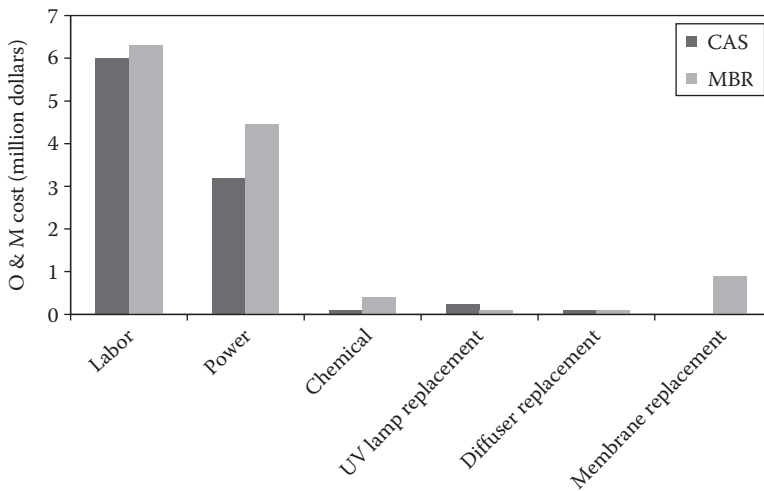
Figure 1.5 Present-worth (2012 US dollars) life cycle O&M cost comparison between CAS and MBR plants. The comparison was conducted based on an influent flow rate of 18,927 m³/day and effluent levels satisfying 20 mg/L BOD, 20 mg/L SS, and 10 mg/L TN. Further, minimum wastewater temperature was 12°C, hourly flow peaking factor was 2.0, and primary sedimentation was omitted for the estimation. The graph was constructed based on Young et al. (2012) dataset.

differences between CAS and MBR plants treating municipal wastewater (Young et al., 2012) is provided in Figure 1.5.

The development of the submersed configuration for MBR has reduced the energy cost compared to the side-stream configuration. Nevertheless, the submerged MBR configuration has an inherent weak point, that is, dead-end filtration. Side-stream MBR obeys cross-flow filtration, so that the accumulation of biosolids deposited on the membrane surface should be retarded to some degree due to the scouring effect of fluids. However, submerged MBR needs an extra shear stress to control the accumulation of biosolids on the membrane surface. This makes the submerged MBR practice coarse bubble aeration.

Coarse bubble aeration entails extensive and excessive aeration to retard biosolids buildup on the membrane surface. However, this leads to considerable energy consumption and deflocculation of activated sludge, which reduces the savings of the configuration compared to side-stream MBR. Therefore, the success of submerged MBR depends on reducing the cost associated with coarse bubble aeration while maintaining the low levels of fouling.

Effective, innovative, and economic coarse bubble aeration devices and systems have been studied and developed academically and commercially. Basic studies on the effect of coarse bubble aeration on fouling reduction have been reported since the late 1990s. A comprehensive study of the effect of aeration on fouling has been

carried out by Ueda et al. (1996) using a submerged MBR adopting HF membrane. They measured air uplift velocity and correlated it to membrane fouling. An optimum airflow rate was identified beyond which further increases had no effect. This finding, the optimum airflow rate is present for fouling control, is an important clue for the design of aeration devices without dissipation of the supplied air.

Moving bed carriers in MBR bioreactors are known to increase the efficiency of coarse bubble aeration. Carriers driven by coarse bubble aeration repeatedly collide with membrane surfaces, and this reduces membrane fouling and enhances MBR performance (Lee et al., 2006). Cyclic aeration introduced by GE Zeon is another innovative way to reduce the energy consumption of coarse bubble aeration. This is achieved by providing air cyclically (e.g., 10 s aeration and 10 s pause), which can reduce the total aeration amount significantly.

Different design ideas for smart aeration have been applied for a long time, and various kinds of aeration strategies are commercially available. There is still much room for improvement in terms of reducing aeration energy consumption, so that each company can try to develop its own aeration tactics and devices without infringing other companies' patents.

In addition to providing coarse bubble aeration, several operational strategies have been proposed. Reversing permeate flow to the membrane (i.e., backwashing) is a primary operational way to reduce fouling and transmembrane pressure. Backwashing combined with an oxidizing chemical (e.g., hypochlorite) can sometimes detach biosolids accumulated on membrane surfaces. Pausing permeation is another approach to release biosolids on membrane surfaces. Several studies have been conducted to optimize times or cycles of backwashing or pausing permeation.

Membrane fouling can be removed or reduced chemically. Selection of appropriate chemicals and their concentrations/contact times is the key in cleaning fouled membranes. High cleaning efficiency increases membrane lifespan as well as reduces the number of cleanings required. Refer to Chapter 5 for a detailed discussion on this.

Direct addition of chemicals or enzymes into a bioreactor can reduce fouling in MBR. Coagulants such as ferric chloride or aluminum sulfate are known to reduce membrane fouling by reducing soluble microbial products and extrapolymeric substances in MBR bioreactors (Mishima and Nakajima, 2009). Nalco Company commercialized the polycationic coagulants named MPE30 and MPE50. These chemicals were identified to be effective in coagulating soluble microbial products and fine particles that are believed to enhance membrane fouling (Yoon et al., 2005). Yoon et al. (2005) demonstrated that the addition of 100 mg/L MPE into an MBR bioreactor reduced polysaccharide levels and suppressed transmembrane pressure increases. The addition of MPE enabled stable MBR process operation under very high levels of solids (e.g., 50,000 mg/L).

Another example is the application of quorum-sensing inhibition between microorganisms for membrane fouling amelioration. Quorum-sensing mechanisms are quite well understood due to the progresses in microbiology. Quorum sensing

is a bacterial communication system based on chemical signals known as autoinducers. Quorum sensing is dependent on population density and involved in biofilm development in many bacteria. Membrane fouling caused by biofilm formation and deposition to membrane surfaces by microorganisms could be directly reduced by adding enzymes that can degrade autoinducers or the microorganisms that can produce such enzymes. Lee's research group at Seoul National University showed the effectiveness of quorum quenching on reducing membrane biofouling in MBR processes using quorum-quenching bacteria encapsulated in microporous membranes (Oh et al., 2012) and also using bead-entrapped quorum-quenching bacteria (Kim et al., 2013). Although these recent applications are still under lab-scale development, they should reach mature stages soon.

1.2.3 Prospect for Future R&D in MBR

Ongoing and future trends in MBR R&D are likely to focus on the most important issue, energy consumption. Membrane fouling is closely related to energy consumption; hence, reducing membrane fouling in MBR while keeping energy consumption as low as possible is the main focus of MBR R&D. Moreover, the need for municipal and industrial wastewater reuse has been increasing due to water shortages suffered in most countries. MBRs have the potential to play a key role in generating water for reuse. Hybrid processes such as MBR + reverse osmosis or MBR + advanced oxidation processes are typical in wastewater reuse practices. However, there is still much improvement necessary to make these processes economical and environmentally benign.

The future directions in R&D are mostly in the fields of membrane/module and operation/maintenance as will be discussed in Sections 2.2.1 and 2.2.2, respectively. In terms of process, MBR technology can be a core technology for producing energy and potable water. Anaerobic digestion using anaerobic microorganisms is a way of generating biogas. High concentrations of anaerobic methanogenic microorganisms can be maintained in digesters by applying microfiltration or ultrafiltration membranes, similar to what was previously introduced. One technical difficulty of anaerobic MBR is scouring biomass accumulated on membrane surfaces. Coarse bubble aeration is the method in aerobic MBR. However, if oxygen is introduced into anaerobic digester via aeration, the activity of anaerobic microorganisms will decrease. Researchers frequently use the produced biogas (without aeration) for generating coarse bubbles for this purpose.

MBR technology can be also combined with reverse osmosis (RO) processes to produce drinking water. Shannon et al. (2008) discussed this possibility. If microfiltration membranes are used in MBR, large amounts of dissolved matters and colloids will pass through the membrane. However, tight ultrafiltration membranes in MBR will produce significantly smaller amounts of those matters, which will allow RO processes to be operated after the MBR. Adding a disinfection facility after an RO process will produce water for drinking.

References

Judd, S. (2008) The status of membrane bioreactor technology, *Trends in Biotechnology*, 26(2): 109–116.

Kim, S.-R., Oh, H.-S., Jo, S.-J., Yeon, K.-M., Lee, C.-H., Lim, D.-J., Lee, C.-H., and Lee, J.-K. (2013) Biofouling control with bead-entrapped quorum quenching bacteria in membrane bioreactors: Physical and biological effects, *Environmental Science and Technology*, 47(2): 836–842.

Kolon Industries Inc., http://kolonmembr.co.kr/, 2014.

Lee, W.-N., Kang, I.-J., and Lee, C.-H. (2006) Factors affecting filtration characteristics in membrane-coupled moving bed biofilm reactor, *Water Research*, 40(9): 1827–1835.

Mishima, I. and Nakajima, J. (2009) Control of membrane fouling in membrane bioreactor process by coagulant addition, *Water Science and Technology*, 59(7): 1255–1262.

Oh, H.-S., Yeon, K.-M., Yang, C.-S., Kim, S.-R., Lee, C.-H., Park, S. Y., Han, J. Y., and Lee, J.-K. (2012) Control of membrane biofouling in MBR for wastewater treatment by quorum quenching bacteria encapsulated in microporous membrane, *Environmental Science & Technology*, 46(9): 4877–4884.

Shannon, M. A., Bohn, P. W., Elimelech, M., Georgiadis, J. G., Marinas, B. J., and Mayes, A. M. (2008) Science and technology for water purification in the coming decades, *Nature*, 452(20): 301–310.

Smith, C. V., Gregorio, D. D., and Talcott, R. M. (1969) The use of ultrafiltration membranes for activated sludge separation, *24th Annual Purdue Industrial Waste Conference*, Lafayette, IN, pp. 130–1310.

Tchobanoglous, G., Burton, F. L., and Stensel, H. D. (2003) *Wastewater Engineering: Treatment and Reuse*, 4th edn., Metcalf and Eddy Inc./McGraw-Hill, New York.

Ueda, T., Hata, K., and Kikuoka, Y. (1996) Treatment of domestic sewage from rural settlements by a membrane bioreactor, *Water Science and Technology*, 34: 189–196.

Water World, http://www.waterworld.com, 2014.

Yamamoto, K., Hiasa, M., Mahmood, T., and Matsuo, T. (1989) Direct solid-liquid separation using hollow fiber membrane in an activated sludge aeration tank, *Water Science and Technology*, 21: 43–54.

Yoon, S.-H., Collins, J. H., Musale, D., Sundararajan, S., Tsai, S.-P., Hallsby, G. A., Kong, J. F., Koppes, J., and Cachia, P. (2005) Effects of flux enhancing polymer on the characteristics of sludge in membrane bioreactor process, *Water Science and Technology*, 51(6–7): 151–157.

Young, T., Muftugil, M., Smoot, S., and Peeters, J. (2012) MBR vs. CAS: capital and operating cost evaluation, *Water Practice & Technology*, 7(4): doi: 10.2166/wpt.2012.075.

Chapter 2

Biological Wastewater Treatment

Membrane bioreactor (MBR) combines biological treatment and membrane separation to produce a very high-quality effluent with extremely low suspended solids concentrations. However, this does not mean that high-quality effluent is always produced stably. High-quality effluent is difficult to produce if optimal conditions for microorganism function are not maintained. This is because the treatment of wastewater pollutants (e.g., organic and particulate biodegradable matters, inorganic nutrients, and nonsettleable colloids) is dependent on the activity of microorganisms in bioreactors in MBR plants. Moreover, the characteristics of microbiological floc (e.g., size and the content of filamentous microorganisms) are influenced by the bioreactor operational conditions, and they affect the fouling properties of the membranes. Proper operation of bioreactors in MBR plants is thus essential to achieve the objective of wastewater treatment. A comprehensive understanding of biological wastewater treatment will provide the fundamentals for designing and operating optimal bioreactors in MBR plants.

This chapter includes the principles of biological wastewater treatment such as microbiology, microbial stoichiometry, kinetics, mass balances, and processes that will provide fundamental frameworks for students to understand bioreactors in MBR plants. The features of biological treatment in MBR plants are somewhat different from those of conventional activated sludge (CAS) plants mainly due to long solids retention times (SRTs) and high concentrations of biomass in MBR bioreactors. This chapter will compare the similarities and differences of biological wastewater treatment between CAS and MBR systems.

2.1 Microorganisms in Bioreactor

Microorganisms in the bioreactors of MBR plants transform dissolved and particulate pollutants found in influent wastewater into less innocuous forms. For example, organic pollutants are oxidized into mostly carbon dioxide and water, while ammonia (an inorganic pollutant) is oxidized into nitrate. Microorganisms can also remove suspended and colloidal solids found in influent wastewater by adsorption onto the surface of microbiological flocs. The transformation and adsorption lead to the production of new biomass and solids, which are removed and disposed of with appropriate methods from the MBR plants.

Microorganisms in the bioreactors of MBR plants exist as mostly microbiological floc and not as free-living planktonic microorganisms. When microbiological floc of a bioreactor is observed with a light microscope, it looks like a brown "cloud" or "cotton candy" to which stalked bell-shaped organisms are often clung (Figure 2.1a). Sometimes free swimming ciliates are moving around the cloudy matters. The microbiological floc mainly consists of bacteria and matrix matters secreted by the bacteria themselves. The bacteria are aggregated by the matrix, which is a biopolymer consisting mostly of carbohydrates with some proteins and nucleic acids.

This matrix is referred to as extracellular polymeric substances (EPS). The bacteria in the floc are difficult to clearly identify by conventional light microscopes, but they are distinguishable from the matrix using a phase contrast microscope after staining with appropriate chemicals or by a fluorescent microscope after staining with appropriate fluorophore such as DAPI (Figure 2.1b). The development of

(a)   (b)
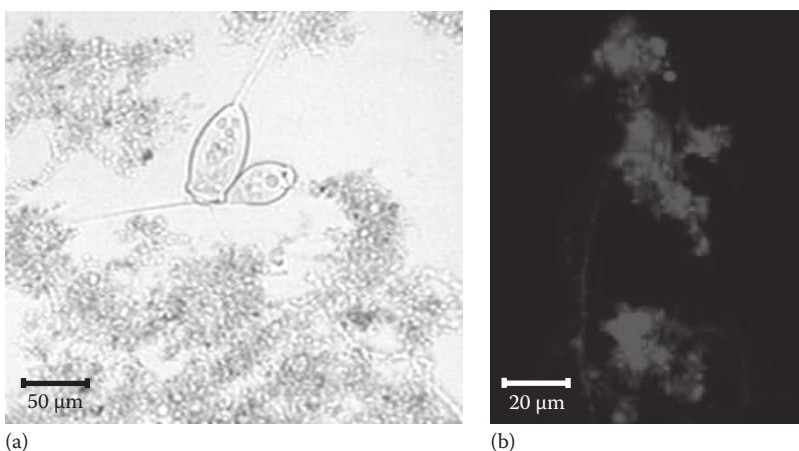
Figure 2.1 Microscopic images of microbiological floc in a bioreactor: (a) an image of microbiological floc observed by a light microscope and (b) microbiological flocs observed by a fluorescent microscope after staining with a fluorophore that can bind to DNA (DAPI). (Images created by Sang-Hoon Lee.)

modern molecular techniques has shed light on the identification, in situ quantification, and functional characterization of bacteria in activated sludge (Wagner and Loy, 2002).

Various types of microorganisms exist in the bioreactors of MBR plants. One main feature of microorganisms in environmental engineering systems, including MBR, is that they are structured into communities consisting of diverse species in an open system, where diverse microorganisms are continuously fed into a bioreactor via influent wastewater and from the atmosphere. This makes the microbial community of a bioreactor very dynamic in terms of structure and composition across time scales and from MBR plant to MBR plant. Nevertheless, specific types of microorganisms can be enriched in bioreactors by imposing specific reactor design and operational conditions. The microbial community structure is believed to be important in determining the function, performance, and stability of bioreactors.

The types of microorganisms and their function in MBRs are basically similar to those of CAS bioreactors. However, the characteristics of microorganisms appear to be somewhat different mainly due to long SRTs maintained for bioreactor operation in MBR plants. Long SRTs generate conditions where slow-growing microorganisms are maintained compared with the relatively shorter SRTs of CAS bioreactors. Maintaining slow-growing microorganisms is advantageous to degrade recalcitrant organic matters biologically, but may harness unwanted microorganisms such as foaming microorganisms. Another effect of the long SRT operation of MBRs is the production of more inert solids, which reduces the fraction of active biomass from the total solids in bioreactor. This will be discussed in Section 2.4.4.

In this section, only a brief description of the microorganisms found in bioreactors will be presented because excellent textbooks are available about the microorganisms, including Madigan et al.'s (2000) Brock: biology of microorganisms and Black's (2008) Microbiology.

2.1.1 Types of Microorganisms

Microorganisms are generally defined as small life forms that cannot be easily identified by the naked eye but are observed with the help of a microscope. Traditionally, microorganisms are classified into prokaryotic and eukaryotic microorganisms based on the existence of a membrane-bound nucleus. Eukaryotic microorganisms have an intracellular membrane-bound nucleus that contains nuclear materials, while prokaryotic microorganisms have their nuclear materials spread in the cytoplasm (e.g., no membrane-bound nucleus). In addition to the nucleus, there are various differences between them including cell size, membrane-bound organelles, cell wall, cell division, and sexual reproduction (Table 2.1). Prokaryotic microorganisms include bacteria and archaea, while eukaryotic microorganisms include fungi, algae, protozoa, and animals (Figure 2.2).

Life forms can be divided into three domains: bacteria, archaea, and eukarya. This classification is based on the phylogenetic analysis of 16S rRNA sequences,

Table 2.1   Comparison between Prokaryotic and Eukaryotic Microorganisms

	Prokaryotes	*Eukaryotes*
Membrane-bound nucleus	Absent	Present
Cell size	0.1–2 µm	10–100 µm
Membrane-bound organelles	Absent	Present (e.g., mitochondria, chloroplast, golgi complex)
Cell wall	Present	Not all
Pili	Present	Absent
Cell division	Binary fission	Mitosis, meiosis
Sexual reproduction	Asexual	Sexual, asexual
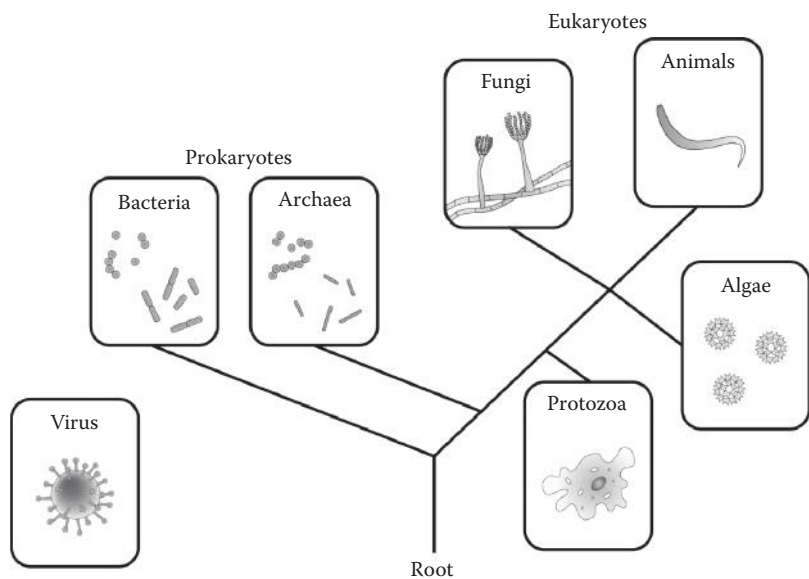
Figure 2.2   Microorganisms in wastewater treatment bioreactors. Each type of microorganisms is positioned in a phylogenetic tree relating evolutionary relationships among types of microorganisms. The root of the tree indicates the ancestral lineage. (Image created by Kang-Hee Park.)

which was first introduced by Woese and Fox (1977). Life forms within the bacteria and the archaea domains are all microorganisms, while some organisms within the eukarya domain are microorganisms (e.g., rotifer). A brief description of the types of microorganisms is provided in the following sections.

2.1.1.1 Bacteria

Bacteria constitute the majority of microorganisms in bioreactors (>90%). Morphologically, they have spherical, rod, and spiral shapes, which are referred to as coccus, bacillus, and spirochete, respectively. Although they can sustain their life living as a single cell, they mostly aggregate into pairs, chains, or clusters. Each cell is approximately 1–2 µm in size.

As shown in Figure 2.3, a bacterium is surrounded by a cytoplasmic membrane, which protects cellular materials from the environment. Because the cytoplasmic membrane is a tight barrier, substances (except for water molecules) cannot penetrate across the membrane freely, which prevents the leakage of cellular substances out of cells as well as prevents the influx of unwanted substances into cells
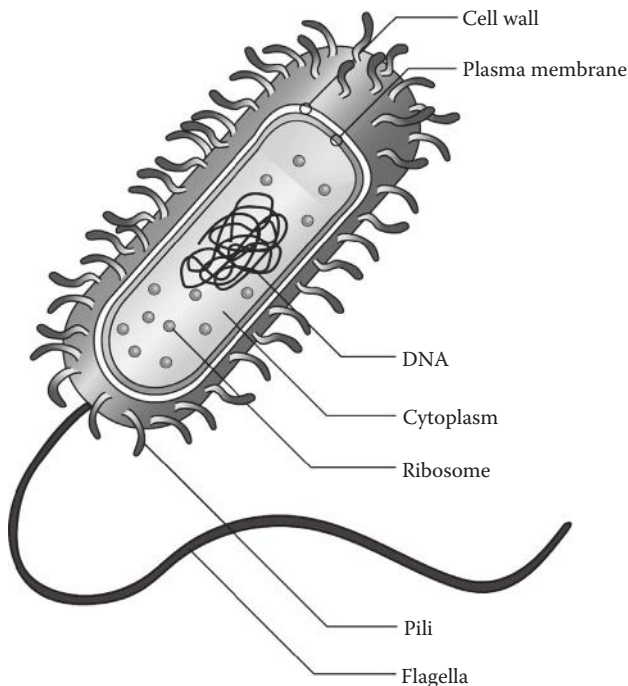
Figure 2.3 Internal structure of a bacterial cell. (Image created by Kang-Hee Park.)

(e.g., permeability barrier). The cytoplasm contains important components for bacteria to maintain their life such as genetic materials, biosynthetic and energy-generating enzymes, and signal transduction molecules. Nutrients are transported into the cytoplasm and wastes are pumped out of the cytoplasm through pores embedded in the cellular membrane.

Diverse enzymes are also located in the membrane such as proteins involved in the electron transport system. Therefore, in addition to providing a permeability barrier, the cytoplasmic membrane provides sites for anchoring proteins (e.g., enzymes and ion channels) and for generating proton motive forces for energy generation.

The cell wall is located outside of the cellular membrane. The cell wall consists of a polymer named peptidoglycan and provides mechanical strength for maintaining the morphology of the bacteria. On the cell wall, diverse cell appendages (e.g., flagella and pili) are attached as well. Flagella play a role helping bacteria move around, while pili are known to allow bacteria to attach onto surfaces.

Bacteria are versatile in terms of metabolism. They can use various sources of energy, electron donors, electron acceptors, and carbon sources. The metabolic versatility of bacteria can be beneficially used to treat diverse organic and inorganic contaminants in wastewater. Harnessing specific groups of bacteria capable of specific functions is the key to achieving the objective of wastewater treatment. For example, phosphorus-accumulating organisms can be enriched in bioreactors by alternating anaerobic and aerobic conditions and can be used for removing phosphorus during wastewater treatment (refer to Section 2.6.2).

Bacteria (and other types of microorganisms) tend to accumulate onto surfaces and form biofilms. Biofilm cells are quite different from planktonic cells. Biofilm cells are embedded by the self-produced matrix material called extracellular polymeric substance (EPS). EPS mostly consists of carbohydrates and proteins, and provides adhesive properties so biofilm can attach onto surfaces. In MBR plants, biofilm formation onto membrane surfaces is a critical issue, and the conditions that favor biofilm formation must be minimized. A better understanding of the biofilm formation mechanisms in bioreactors will help promote a stably operating MBR plant.

Some bacteria produce biosurfactants. Proliferation of those bacteria generates heavy foam on the surface of bioreactors with the help of aeration. Foaming is a very common problem in MBR bioreactors. Although the reason is not clear, the cause is presumed to be that MBR bioreactors are operated with higher aeration rates and/or the longer SRT provides better conditions for foaming bacteria to be maintained.

2.1.1.2 Archaea

Archaea are very similar to bacteria morphologically. They have no nuclear membranes like bacteria but are different from bacteria in various aspects, including evolutionary history, biochemistry, and genetic apparatus. Historically, archaea

were considered to be a group of bacteria, but nowadays archaea are believed to constitute an independent domain of life with bacteria and eukarya.

Archaea are often detected in aerated bioreactors, but the fraction of archaea is generally less than 1% of the total biomass. Bioreactors operated under moderate temperature (<30°C) and aerobic conditions appear to be inappropriate for archaea to inhabit. The detection of archaea might be caused by the return flow from anaerobic digesters and/or by influent wastewater. Anaerobic digesters contain methane-producing archaea, and influent wastewater may contain some archaea found in soils during the transport of sewage to the treatment facilities. Nevertheless, some archaea (e.g., ammonia-oxidizing archaea [AOA]) are known to survive and proliferate in aerated wastewater treatment bioreactors (Park et al., 2006).

2.1.1.3 Viruses

Viruses are very small entities ranging from several dozen to several hundred nanometers in size. Viruses are composed of simple genetic materials (DNA or RNA) and proteins, called capsid, that coat the genetic materials. Some viruses are enveloped by lipid membranes outside the capsid. Viruses infect host organisms (e.g., animals, plants, bacteria) to sustain life as they cannot live without a host. The importance of viruses in activated sludge processes is not clear, although the discharge of some viruses that infect humans to water bodies may endanger human health.

Based on the study of Irving and Smith (1981), which focused on the removal of certain virus groups in an activated sludge wastewater treatment plant, the removal efficiency of enteroviruses, adenoviruses, and reoviruses in chlorinated secondary effluent was 93%, 85%, and 28%, respectively. Compared with CAS wastewater treatment plants, MBR plants adopting membranes with small pore sizes (e.g., ultrafiltration membranes) probably increase the virus removal performance due to the rejection of several hundred size viruses.

Viruses that infect bacteria, called bacteriophages, may influence the performance of bioreactors as well as the bacterial community compositions in activated sludge bioreactors. Barr et al. (2010) observed the decline of phosphorus removal efficiency following the addition of a bacteriophage-rich solution capable of infecting the bacteria removing phosphorus. However, the ability to infect certain bacteria in bioreactors can be beneficially used. Kotay et al. (2011) reported that sludge bulking was controlled by adding bacteriophages that can lysis bacteria responsible for sludge bulking.

2.1.1.4 Fungi

Fungi are nonphototrophic aerobic organisms. They are multicellular organisms composed of filamentous-like structures called hypha (Figure 2.2). They grow slowly but tolerate well in harsh conditions such as low pH, low temperature, and low nutrient levels. Their function and role in wastewater treatment is not well known.

In addition, they are unimportant numerically in wastewater treatment bioreactors including MBR.

2.1.1.5 Algae

Algae are mostly unicellular phototrophic microorganisms and are food sources for protozoa and fish in aquatic environments. They use sunlight for their energy source and dissolved carbon dioxide for their cellular organic substances (photosynthesis). Because water is split into oxygen and protons in photosynthesis, algae can provide oxygen in natural water bodies. However, algae do respire and consume oxygen when light is not available. Algal blooms are the result of an overgrowth of algae in the presence of excess nutrients in water bodies.

The ecological response of water bodies to excess nutrients is called eutrophication. Algal blooms result from eutrophication and cause various adverse effects including endangering organisms by depleting oxygen, decreasing clarity in lakes, increasing sedimentation in lakes and estuaries, generating taste and odors in water supplies, filter clogging in water treatment plants, and interfering with water leisure activities. Algae do not take part in treating wastewater in MBRs, but they are often detected in effluent tanks exposed to sunlight.

2.1.1.6 Protozoa

Protozoa are unicellular and nonphototrophic eukaryotic microorganisms. Some of them are motile and the others are nonmotile. They feed on bacteria and small organic particles. In activated sludge systems, they play the role of effluent polisher. To achieve effluent with low suspended solids, the activity of protozoa is important in CAS. The role of effluent polishers is not so important in MBRs because MBRs can remove suspended solids irrespective of the presence of protozoa using membranes. Another feature of protozoa is their sensitivity to toxic materials in bioreactors. Therefore, protozoa are commonly used as indicators for monitoring toxic material levels.

2.1.1.7 Other Types of Eukaryotic Microorganisms

In the bioreactors of MBR, some micrometer-size multicellular animals can exist such as nematodes, rotifers, and crustaceans. Although these eukaryotic microorganisms are known to predate other microorganisms in bioreactors, the detailed role of these microorganisms is not well reported.

2.1.2 Quantification of Microorganisms

The quantification of microorganisms is very important in designing and operating MBR bioreactors because the rates of pollutant removal and sludge production

are proportional to the mass of microorganisms (refer to Section 2.3.2). Culture-dependent methods (e.g., plate counting) have been traditionally used to quantify microorganisms in bioreactors, but these methods have inherent limitations due to the difficulty to generate a condition in which all of the microorganisms in a bioreactor are able to grow.

Only 1%–15% of bacteria in activated sludge are known to be culturable (Amann et al., 1995). This limitation is therefore apt to underestimate the quantity of microorganisms in a bioreactor. During the last two decades, culture-independent methods based on molecular technology (e.g., fluorescent in situ hybridization and quantitative real-time PCR) have been developed to overcome the limitations of culture-dependent methods, although the molecular methods require well-trained engineers as well as expensive equipment and analytical effort.

Wastewater engineers have frequently used an indirect quantification method. They assume that the quantity of volatile suspended solids (VSS) is closely related to the quantity of microorganisms because dry biomass mostly consists of organic matters. VSS measurements are simple and require relatively short analytical run times. VSS is analyzed by filtering a mixed liquor sample using a micrometer-size glass-fiber filter and then burning the filtered matters at 550°C for ~2 h to measure the burnable mass (e.g., organic content).

VSS includes inert materials originated from influent wastewater and from biomass decay as well as active microorganisms. It is generally known that 50%–80% of VSS is attributable to active microorganisms, although the exact proportion is dependent on the operational conditions and wastewater characteristics. The proportion of active biomass decreases with increasing SRTs and higher concentrations of inert solids in the influent wastewater (refer to Section 2.4.4).

2.1.3 Metabolisms of Microorganisms

Metabolism is defined as the biochemical reactions in living organisms and can be roughly divided into the reactions involved in the degradation of complex molecules for energy generation (catabolism) and those in the synthesis of cell materials from simple molecules using the energy generated from catabolism (anabolism).

Microorganisms extract energy by oxidizing reduced organic and/or inorganic compounds (chemotrophs) or by capturing photons from sunlight (phototrophs). Most of the microorganisms found in wastewater treatment are chemotrophs rather than phototrophic microorganisms, which are rarely used in wastewater treatment. The extracted energy is then used for cell synthesis and for maintenance of the microorganisms. In biological wastewater treatment, the reduced compounds are supplied via influent wastewater. Depending on their primary electron donor (energy source), microorganisms can also be classified into organotrophs (microorganisms using organic compounds as their energy source) and lithotrophs (microorganisms using inorganic compounds as their energy source).

Electrons released by primary electron donors must be accepted by the appropriate electron accepter within the microorganisms to complete energy generation reactions and to extract free energy from the primary electron donor. Microorganisms can use various terminal electron acceptors. Some of them use molecular oxygen (aerobes), while others can use other oxidizing molecules such as nitrite, nitrate, sulfate, and ferric ion (anaerobes).

Environmental engineers further differentiate the anaerobes between anoxic and anaerobic microorganisms. Anoxic microorganisms use chemically bound oxygen (e.g., nitrate), while anaerobic microorganisms use other compounds (e.g., ferric ion) for their electron acceptor. Some microorganisms are able to use either molecular oxygen or other oxidizing molecules for their terminal electron acceptors (facultative anaerobes).

All microorganisms require a carbon source to constitute their cell components. Carbon sources come from organic compounds (heterotrophs) or carbon dioxide (autotrophs). Some use either organic compounds or carbon dioxide (mixotrophs).

Microorganisms can be classified based on the types of microbial metabolisms described earlier. For example, ammonia-oxidizing bacteria (AOB) responsible for nitrification can be classified as aerobic chemolithoautotrophs, because they use ammonia as their energy source (chemotrophs) and as their primary electron donor (lithotrophs), molecular oxygen as their electron acceptor (aerobes), and carbon

Table 2.2   Classification of Microorganisms Based on Their Energy Source, Carbon Source, Primary Electron Donor, and Terminal Electron Acceptor

Criterion	Classification
Energy source	Chemotrophs (chemical energy)
	Phototrophs (light energy)
Carbon source	Heterotrophs (organic matters)
	Autotrophs (carbon dioxide)
	Mixotrophs (organic matters, carbon dioxide)
Primary electron donor	Organotrophs (organic matters)
	Lithotrophs (inorganic matters)
Terminal electron acceptor	Aerobes (oxygen)
	Anoxic microorganisms (bound oxygen other than O_2)
	Anaerobes (no molecular oxygen)
	Facultative microorganisms (O_2 and others)

dioxide as their cell components (autotrophs). The classification of microorganisms based on their energy source, carbon source, primary electron donor, and terminal electron acceptor is summarized in Table 2.2.

2.1.4 Energy Generation in Microorganisms

How do microorganisms extract energy for their reproduction and maintenance? Respiration and fermentation are two common ways for generating energy in microorganisms. Microorganisms oxidize reduced organic or inorganic chemicals (primary electron donors) during which free energy is released and captured by energy carriers such as adenosine triphosphate (ATP). In respiration, oxidation processes release electrons that are then transferred to electron carriers sequentially.

As shown in Figure 2.4, electrons generated from the oxidation of primary electron donors (e.g., glucose) are primarily captured by diffusible electron carriers such as nicotinamide dinucleotide ($NAD^+ + H^+ + 2e^- \rightarrow NADH$) and transferred sequentially to membrane-associated electron carriers (e.g., NADH dehydrogenase, flavoprotein, iron–sulfur protein, cytochrome, and quinine) in the electron transport system. The electrons are finally accepted by terminal electron acceptors (e.g., oxygen).

During the electron transport system, protons (H^+) are pumped out of the cytoplasm. This proton pumping generates an electrochemical proton gradient across
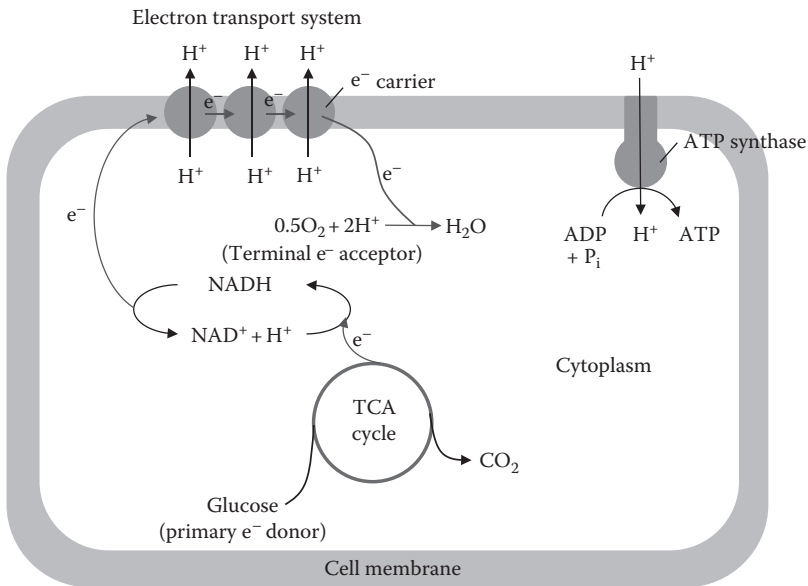
Figure 2.4 **The schematic shows electron transport from the primary electron donor to the terminal electron acceptor. In this schematic, glucose is the primary electron donor and oxygen is the terminal electron acceptor.**

the cell membrane, which drives the protons back across the cell membrane using ATP synthase, which is responsible for ATP synthesis from ADP and phosphate. This type of ATP formation is called oxidative phosphorylation.

Another way microorganisms generate energy is through fermentation. Unlike respiration, fermentation uses an endogenous electron acceptor, not exogenous electron acceptor (e.g., oxygen), to accept the electrons released by the oxidation of the primary electron donors. The end products of fermentation are generally acids, gases, and alcohols. Ethanol (C_2H_5OH) production by yeast is a typical example of microbial fermentation in which acetaldehyde (CH_3COH) is the endogenous electron acceptor ($CH_3COH + 2H^+ + 2e^- \rightarrow C_2H_5OH$). In fermentation, electrons captured by electron carriers (e.g., NADH) are not transported to membrane-associated electron carriers but to the endogenous electron acceptor. During fermentation, ATP synthesis occurs during the transformation of the primary electron donors. This type of ATP formation is called substrate-level phosphorylation.

In fermentation, less energy is generally extracted compared with respiration because most of the free energy is stored in the fermentation products (e.g., ethanol). For example, only 10.17 kJ of free energy is extracted through ethanol fermentation from 1/24 mol of glucose. For the same energy source (e.g., 1/24 mol of glucose), 120.07 kJ of free energy can be extracted via respiration with oxygen as the terminal electron acceptor. The following energy calculation for ethanol fermentation assumes that glucose is oxidized to carbon dioxide (not to acetaldehyde), and carbon dioxide (not acetaldehyde) is reduced to ethanol to simplify the calculation:

$$\frac{1}{24}C_6H_{12}O_6 + \frac{1}{4}H_2O = \frac{1}{4}CO_2 + H^+ + e^- \quad \Delta G^{\circ\prime} = -41.35 \text{ kJ/e}^- \text{ equivalent}$$

$$\frac{1}{6}CO_2 + H^+ + e^- = \frac{1}{12}C_2H_5OH + \frac{1}{4}H_2O \quad \Delta G^{\circ\prime} = 31.18 \text{ kJ/e}^- \text{ equivalent}$$

$$\frac{1}{24}C_6H_{12}O_6 = \frac{1}{12}C_2H_5OH + \frac{1}{4}H_2O \qquad \Delta G^{\circ\prime} = -10.17 \text{ kJ/e}^- \text{ equivalent}$$
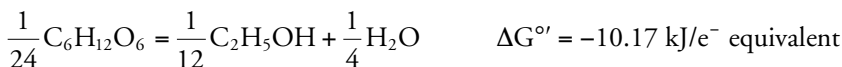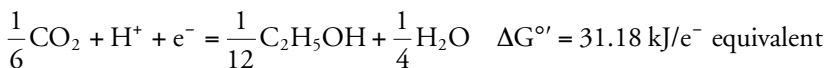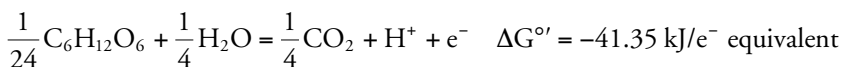
The quantity of energy extracted from the electron transport system during respiration is proportional to the difference in redox potential between the primary electron donor and terminal electron acceptor. For example, at standard state (e.g., all reactants and products are unit molar concentration) and pH = 7.0, 120.07 kJ of free energy can be extracted when glucose ($C_6H_{12}O_6$) is the primary electron donor and oxygen (O_2) is the terminal electron acceptor (calculation based on one electron equivalent), while only 22.2 kJ of free energy can be obtained when glucose is the primary electron donor and sulfate (SO_4^{2-}) is the terminal electron acceptor.

$$\frac{1}{24}C_6H_{12}O_6 + \frac{1}{4}H_2O = \frac{1}{4}CO_2 + H^+ + e^- \quad \Delta G^{\circ\prime} - 41.35 \text{ kJ/e}^- \text{ equivalent}$$

$$\frac{1}{4}O_2 + H^+ + e^- = \frac{1}{2}H_2O \quad \Delta G^{o\prime} = -78.72 \text{ kJ/e}^- \text{ equivalent}$$

$$\frac{1}{24}C_6H_{12}O_6 + \frac{1}{4}O_2 = \frac{1}{4}CO_2 + \frac{1}{4}H_2O \quad \Delta G^{o\prime} = -120.07 \text{ kJ/e}^- \text{ equivalent}$$

$$\frac{1}{24}C_6H_{12}O_6 + \frac{1}{4}H_2O = \frac{1}{4}CO_2 + H^+ + e^- \quad \Delta G^{o\prime} = -41.35 \text{ kJ/e}^- \text{ equivalent}$$

$$\frac{1}{6}SO_4^{2-} + \frac{4}{3}H^+ + e^- = \frac{1}{6}S + \frac{2}{3}H_2O \quad \Delta G^{o\prime} = 19.15 \text{ kJ/e}^- \text{ equivalent}$$

$$\frac{1}{24}C_6H_{12}O_6 + \frac{1}{6}SO_4^{2-} + \frac{1}{3}H^+ = \frac{1}{4}CO_2 + \frac{1}{6}S + \frac{5}{12}H_2O$$
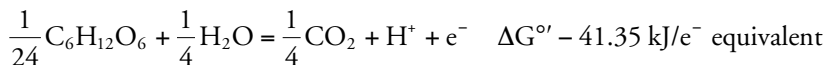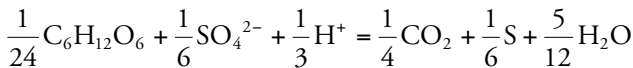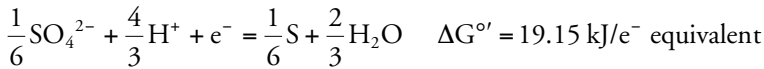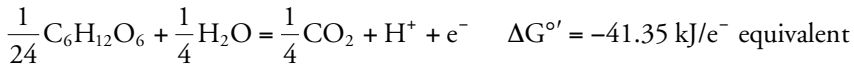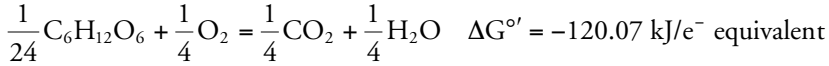
$$\Delta G^{o\prime} = -22.20 \text{ kJ/e}^- \text{ equivalent}$$

Free energy quantities can be estimated using the scales of redox potential as illustrated in Figure 2.5.
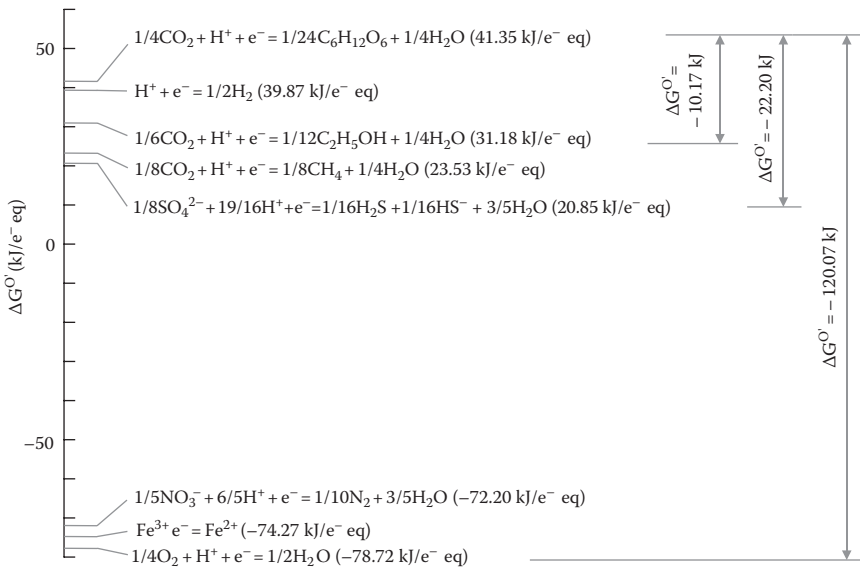
Figure 2.5 Scale of redox potentials of some chemicals. Different quantities of free energy can be extracted for the same primary electron donor (glucose in this example) depending on different terminal electron acceptors.

Example 2.1

Gibbs free energy at standard state and pH$=7.0$ ($\Delta G°'$) can be used to determine whether a biological reaction is occurring spontaneously at the condition. If the value of $\Delta G°'$ is less than 0, the reaction will be occurring spontaneously. Acetate (CH_3COO^-) oxidation to bicarbonate (HCO_3^-) and hydrogen (H_2) can occur spontaneously by certain bacteria in a bioreactor under anaerobic condition, although $\Delta G°'$ of the reaction is greater than 0.

$$CH_3COO^- + 4H_2O \rightarrow 2HCO_3^- + 4H_2 + H^+; \quad \Delta G°' = +104.6 \text{ kJ/mol}$$
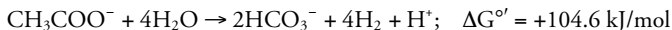
Explain why the reaction is possible in the reactor and propose a condition in which the reaction will be occurring.

Solution

$\Delta G°'$ of a reaction is determined at standard state (i.e., every reactant and product is unit molar concentration at 25°C and pH$=7.0$). Actual criterion for the spontaneity of a reaction is determined by ΔG. ΔG can be calculated by the following equation:

$$\Delta G = \Delta G°' + RT \ln \frac{[HCO_3^-]^2[H_2]^4[H^+]}{[CH_3COO^-]}$$

where $[HCO_3^-]$, $[CH_3COO^-]$, and $[H_2]$ are molar concentrations of bicarbonate, acetate, and hydrogen, respectively.

Acetate oxidation will be occurring spontaneously if ΔG (not $\Delta G°'$) is less than 0. The reaction can occur spontaneously by generating a condition in which ΔG is less than 0. For example, acetate oxidation can occur spontaneously by combining with the reaction that reduces hydrogen concentration and/or increase acetate concentration to certain levels. In reality, there are some archaea (e.g., hydrogenotrophic archaea) that consume the hydrogen produced by acetate-oxidizing bacteria. This cooperative reaction is called syntrophic acetate oxidation.

2.2 Microbial Stoichiometry in Bioreactor

In chemistry, stoichiometry deals with the relative quantities of reactants and products for chemical reactions based on the mass conservation law. Stoichiometry is formed in balanced chemical equations. Just like chemical stoichiometric equations, balanced microbial stoichiometric equations are very useful for estimating the relative quantities of reactants or products in biological treatments. Balanced microbial stoichiometric equations representing biological treatments are basically the same as those of chemical stoichiometric equations except for the production of a catalyst (e.g., microorganisms). Microorganisms not only serve as catalysts for biological treatments but they also produce themselves during treatment via microbial growth.

Two glucose ($C_6H_{12}O_6$) oxidation reactions are presented in the following to provide comparison between chemical and microbial reactions. Under aerobic conditions, glucose can be oxidized chemically or by microorganisms as follows:

$$\text{Chemical reaction: } C_6H_{12}O_6 + 6O_2 \rightarrow 6CO_2 + 6H_2O \tag{2.1}$$

$$\text{Microbial reaction: } C_6H_{12}O_6 + 0.67NH_3 + 2.67O_2 \rightarrow 0.67C_5H_7O_2N$$
$$+ 2.67CO_2 + 4.67H_2O \tag{2.2}$$
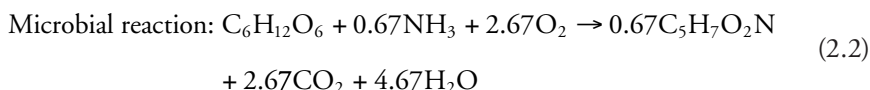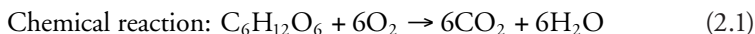
Note that although the chemical reaction of glucose oxidation produces only carbon dioxide and water, the microbial oxidation of glucose generates microorganisms ($C_5H_7O_2N$) as a reaction product as well as carbon dioxide and water. In addition, the microbial reaction requires nutrients (NH_3 in this example) to generate microorganisms. The microbial stoichiometric equation is useful to estimate theoretical oxygen consumption or to determine biomass production during the aerobic treatment. For example, if 1 kg of glucose is treated daily in an MBR plant and the microbial reaction follows the stoichiometric equation presented earlier, 0.47 kg of oxygen ($=[2.67 \cdot 32$ g $O_2/180$ g $C_6H_{12}O_6] \cdot [1$ kg $C_6H_{12}O_6$/day]) would be required daily and 0.42 kg of biomass ($=[0.67 \cdot 113$ g $C_5H_7O_2N/180$ g $C_6H_{12}O_6] \cdot 1$ kg $C_6H_{12}O_6$/day]) would be produced daily.

This microbial stoichiometric equation indicates that glucose is used for biomass synthesis as well as an energy source. Microorganisms use a part of glucose as their energy source by extracting free energy from the oxidation of glucose into carbon dioxide (e.g., $C_6H_{12}O_6 \rightarrow CO_2$) and the rest of the glucose molecule is used for comprising their cell constituents (e.g., $C_6H_{12}O_6 \rightarrow C_5H_7O_2N$) by consuming the free energy extracted from glucose oxidation. The ratio of produced biomass to consumed substrate (glucose in this example) is defined as growth or the biomass yield (Y), which depends on growth conditions and microbial composition.

The growth yield of this example is 0.42 g cells per g glucose ($=0.67 \cdot 113$ g $C_5H_7O_2N/180$ g $C_6H_{12}O_6$). The growth yield can be obtained experimentally or theoretically. This book presents an experimental method for obtaining the growth yield (refer to Section 2.3.4), while theoretical estimations of growth yields based on bioenergetics is described in other excellent textbooks (Rittmann and McCarty, 2000). The growth yields can be used to set up balanced microbial stoichiometric equations, which underlines the importance of growth yields in evaluating biological wastewater treatment.

2.2.1 Balanced Microbial Stoichiometric Equations

To construct a balanced microbial stoichiometric equation, initially it is necessary to identify the elements taking part in the microbial reaction such as the primary electron donor, terminal electron acceptor, nutrients, biomass, and oxidized products.

Nutrients are essential elements for the growth of microorganisms. Nitrogen and phosphorus are the two major nutrients, although various trace elements also constitute microbial cells. Microbial cells are mainly composed of carbon, hydrogen, oxygen, and nitrogen. If we use the chemical formula of $C_5H_7O_2N$ as microorganisms, it is only required to add nitrogen in the stoichiometric equation.

Ammonia is the common nitrogen source for the growth of microorganisms and should be placed on the left side of a stoichiometric equation, although nitrite, nitrate, and organic nitrogen can be used. Phosphorus (e.g., phosphate) as well as other nitrogen sources can be placed in the stoichiometric equation when chemical formulas representing microorganisms containing phosphorus are used (e.g., $C_5H_7O_2NP_{0.1}$). In addition, oxygen should be placed on the left side of the equation for aerobic reactions since oxygen is the terminal electron acceptor for aerobic treatments.

Microorganisms are catalysts for the microbial transformation (treatment) of wastewater, but the catalyst is also produced during the transformation unlike common chemical catalysts as described earlier. Microorganisms are then placed on the right side of the stoichiometric equation because microorganisms are produced overall. Carbon dioxide and water are the two major reaction products of wastewater transformation and should be placed on the right side of the stoichiometric equation. Accordingly, we can set up a simple balanced stoichiometric equation for a wastewater consisting of acetic acid (CH_3COOH) like this:

$$aCH_3COOH + bNH_3 + cO_2 \rightarrow dC_5H_7O_2N + eCO_2 + fH_2O \qquad (2.3)$$

where a, b, c, d, e, and f are stoichiometric coefficients of the microbial stoichiometric equation. If the microbial growth yield of the reaction is known (or estimated experimentally), it is possible to determine the stoichiometric coefficients based on the mass conservation law for each chemical element as follows:

$$\text{Carbon (C): } 2a = 5d + e$$

$$\text{Hydrogen (H): } 4a + 3b = 7d + 2f$$

$$\text{Oxygen (O): } 2a + 2c = 2d + 2e + f$$

$$\text{Nitrogen (N): } b = d$$

Two additional equations are required to solve the equations simultaneously. Assuming the growth yield is 0.4 g cells per gram acetic acid ($= d \cdot$ molecular weight of bacterial cell/$a \cdot$ molecular weight of acetic cell) and $a = 1$, the other stoichiometric coefficients can be determined. Using the growth yield value and the mass balance equations for C, H, O, and N, all of the coefficients can be obtained as follows:

Using the value of Y, $Y = 0.4 = (d \cdot 113)/1 \cdot 60$, $d = 0.2$
Using the mass balance of N, $b = d = 0.2$
Using the mass balance of C, $2 \cdot 1 = 5 \cdot 0.2 + e$, $e = 1$
Using the mass balance of H, $4 \cdot 1 + 3 \cdot 0.2 = 7 \cdot 0.2 + 2f$, $f = 1.6$
Using the mass balance of O, $2 \cdot 1 + 2c = 2 \cdot 0.2 + 2 \cdot 1 + 1.6$, $c = 1$

All of the stoichiometric coefficients are solved as $a = 1$, $b = 0.2$, $c = 1$, $d = 0.2$, $e = 1$, and $f = 1.6$. Therefore, the microbial balanced stoichiometric equation for the oxidation of acetic acid is

$$CH_3COOH + 0.2NH_3 + O_2 \rightarrow 0.2C_5H_7O_2N + CO_2 + 1.6H_2O \qquad (2.4)$$
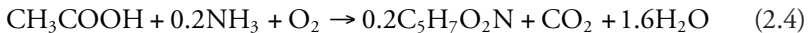
Example 2.2

Determine the stoichiometric coefficients for a balanced equation of aerobic treatment of domestic wastewater. Assume that the chemical formula of wastewater and biomass are $C_{10}H_{19}O_3N$ and $C_5H_7O_2N$, respectively, and the growth yield of biomass is 0.4 g biomass/g wastewater.

Solution

It is assumed that the main reactants are wastewater ($C_{10}H_{19}O_3N$) and oxygen and the main products are biomass ($C_5H_7O_2N$), carbon dioxide (CO_2), ammonia (NH_3), and water (H_2O). In addition, nitrogen is assumed to be supplied by wastewater not by exogenous ammonia. Therefore, the basic stoichiometric equation can be written as follows:

$$C_{10}H_{19}O_3N + aO_2 \rightarrow bC_5H_7O_2N + cCO_2 + dNH_3 + eH_2O$$
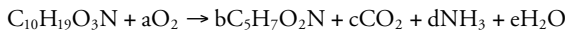
Stoichiometric relations can be set up using the following equations and the equations can be solved simultaneously:

$$\text{Growth yield: } \frac{b \cdot 113}{1 \cdot 201} = 0.4$$

$$C: 10 = 5b + c$$

$$H: 19 = 7b + 3d + 2e$$

$$O: 3 + 2a = 2b + 2c + e$$

$$N: 1 = b + d$$

By solving the equations, all of the coefficients are determined as $a = 8.96$, $b = 0.71$, $c = 6.45$, $d = 0.28$, and $e = 6.60$, and the balanced stoichiometric equation is

$$C_{10}H_{19}O_3N + 8.96O_2 \rightarrow 0.71C_5H_7O_2N + 6.45CO_2 + 0.28NH_3 + 6.60H_2O$$

Example 2.3

A sugar production plant generates 1000 m³ of wastewater daily. It is reported that the main composition of the wastewater is sucrose ($C_{12}H_{22}O_{11}$, MW = 342) at a concentration of 2000 mg COD/L. The wastewater is treated by an MBR plant where the wastewater is completely oxidized into carbon dioxide and water aerobically. Assume that the growth yield is 0.5 g biomass/g sucrose. Operators of the wastewater treatment plant want to estimate the theoretical oxygen requirement (kg O_2/day) and excess biomass production (kg biomass/day) during the wastewater treatment. Calculate the values based on a balanced microbial stoichiometric equation.

Solution

In order to estimate the theoretical oxygen requirement and the excess biomass production, one approach is to determine the balanced microbial stoichiometric equation for sucrose oxidation using the provided conditions. Assuming that the biomass composition is $C_5H_7O_2N$ and ammonia is the nitrogen source for the microbial reaction, the balanced stoichiometric equation can be determined using the method described previously. The balanced equation and mass balance equations for each element are as follows:

$$C_{12}H_{22}O_{11} + aNH_3 + bO_2 \rightarrow cC_5H_7O_2N + dCO_2 + eH_2O$$
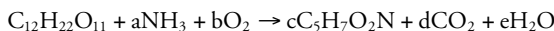
$$\text{Growth yield: } \frac{c \cdot 113}{1 \cdot 342} = 0.5$$

$$\text{C: } 12 = 5c + d$$

$$\text{H: } 22 + 3a = 7c + 2e$$

$$\text{O: } 11 + 2b = 2c + 2d + e$$

$$\text{N: } a = c$$

By solving the equations simultaneously, all of the coefficients are determined as a = 1.5, b = 4.5, c = 1.5, d = 4.5, and e = 8, and the balanced stoichiometric equation is as follows:

$$C_{12}H_{22}O_{11} + 1.5NH_3 + 4.5O_2 \rightarrow 1.5C_5H_7O_2N + 4.5CO_2 + 8H_2O$$
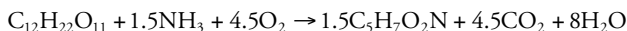
Because the concentration of sucrose wastewater is provided in chemical oxygen demand (COD), it is necessary to change the mass unit into an oxygen unit (e.g., COD) for the calculation. Sucrose is completely oxidized as follows:

$$C_{12}H_{22}O_{11} + 12O_2 \rightarrow 12CO_2 + 11H_2O$$
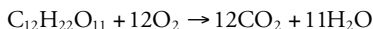
Thus, 1 g of sucrose corresponds to 1.12 g O_2 (COD) (=12 · MW_{O_2}/1 · $MW_{sucrose}$ = 12·32/1·342 = 1.12[gO_2/g sucrose]). Because 342 g of sucrose (1 × $MW_{sucrose}$) consumes 144 g of oxygen (4.5 × MW_{oxygen}) in the balanced stoichiometric equation for sucrose oxidation, the theoretical oxygen demand for a complete oxidation of wastewater in the MBR is

$$\left(\frac{1000\ \text{m}^3}{\text{day}}\right)\left(\frac{1000\ \text{L}}{\text{m}^3}\right)\left(\frac{2000\ \text{mg}\,\text{O}_2}{\text{L}}\right)\left(\frac{\text{mg sucrose}}{1.12\ \text{mg}\,\text{O}_2}\right)\left(\frac{\text{g sucrose}}{1000\ \text{mg sucrose}}\right)$$

$$\times\left(\frac{144\ \text{g}\,\text{O}_2}{342\ \text{g sucrose}}\right)\left(\frac{\text{kg}\,\text{O}_2}{1000\ \text{g}\,\text{O}_2}\right)$$

$$= 752\ \frac{\text{kg}\,\text{O}_2}{\text{day}}$$

Similarly, the excess biomass production can be calculated based on the ratio between sucrose consumption and biomass production (e.g., 169.5 g of biomass is produced for 342 g of sucrose consumption).

$$\left(\frac{1000\ \text{m}^3}{\text{day}}\right)\left(\frac{1000\ \text{L}}{\text{m}^3}\right)\left(\frac{2000\ \text{mg}\,\text{O}_2}{\text{L}}\right)\left(\frac{\text{mg sucrose}}{1.12\ \text{mg}\,\text{O}_2}\right)\left(\frac{\text{g sucrose}}{1000\ \text{mg sucrose}}\right)$$

$$\times\left(\frac{169.5\ \text{g biomass}}{342\ \text{g sucrose}}\right)\left(\frac{\text{kg biomass}}{1000\ \text{g biomass}}\right)$$

$$= 885\ \frac{\text{kg biomass}}{\text{day}}$$

2.2.2 Theoretical Oxygen Demand for Aerobic Bacterial Growth

Oxygen supply in a bioreactor provides the terminal electron acceptor for aerobic microorganisms for oxidizing organic and inorganic matters. Overestimation of oxygen demand wastes energy costs associated with oxygen supply. However, underestimation of oxygen demand may interfere with complete oxidation of oxidizable pollutants in the wastewater. Thus, it is important to estimate the proper amount of oxygen for the optimum design of bioreactors. In practice, oxygen is often provided to the bioreactor through aeration, which constitutes more than half of the electrical consumption during the operation of MBR.

As introduced in Example 2.3, the theoretical oxygen demand for aerobic bacterial growth can be estimated using the balanced stoichiometric equation. We can also estimate the theoretical oxygen demand without knowledge of the balanced microbial stoichiometric equation if we have information about the amount of organic matter removed during the treatment and the growth yield. In aerobic heterotrophic microorganisms, organic matter can be utilized for both energy generation and biomass production. This can be interpreted as the amount of oxygen equivalent.

In other words, the oxygen equivalent of organic matter consists of the oxygen equivalent for generating energy and the oxygen equivalent for biomass production.

Therefore, the theoretical oxygen demand corresponds to the oxygen equivalent for energy generation. The equation for theoretical oxygen demand (OD_{theory}) can be obtained using the growth yield (Y), the influent flow rate (Q), and the organic matter removed ($S_0 - S$) as follows:

$$OD_{theory} = Q \cdot (S_0 - S) - 1.42 \cdot P_{x,bio} \tag{2.5}$$

where
    OD_{theory} is the theoretical oxygen demand, g O_2/day
    Q is the flow rate, m³/day
    ($S_0 - S$) is the organic matter removed, g/m³
    $P_{x,bio}$ is the daily biomass production (=$Y \cdot Q \cdot (S_0 - S)$), g biomass/day

In Equation 2.5, 1.42 is the coefficient for changing a unit of biomass from mass to O_2 based on the chemical reaction for biomass oxidation (see Equation 2.6) in which 113 g of biomass is equivalent to 160 g (=5×32 g) of oxygen (e.g., 1.42 g O_2 (COD) per gram of biomass).

$$C_5H_7O_2N + 5O_2 \rightarrow 5CO_2 + NH_3 + 2H_2O$$

$$113\,g \qquad 5 \cdot 32 = 160\,g \tag{2.6}$$
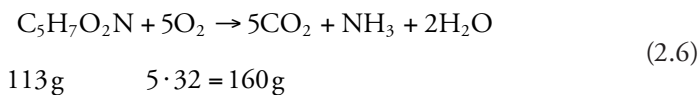
Let's revisit Example 2.3 for the calculation of theoretical oxygen demand. Assuming a complete oxidation of sucrose (e.g., effluent sucrose (S) = 0 g/m³) and 0.5 g biomass/g sucrose is the growth yield of sucrose oxidation, the daily biomass production ($P_{x,bio}$) can be calculated as follows:

$$P_{x,bio} = \left(\frac{0.5\,\text{g biomass}}{\text{g sucrose}} \right)\left(\frac{\text{g sucrose}}{1.12\,\text{g}\,O_2} \right)\left(\frac{1000\,\text{m}^3}{\text{day}} \right)\left(\frac{1000\,\text{L}}{\text{m}^3} \right)\left(\frac{2000\,\text{mg}\,O_2}{\text{L}} \right)$$

$$\times \left(\frac{\text{kg}}{10^6\,\text{mg}} \right) = 893\,\frac{\text{kg biomass}}{\text{day}}$$

Using the Equation 2.5, the theoretical oxygen requirement can be calculated as

$$\text{Oxygen requirement} = \left(\frac{1000\,\text{m}^3}{\text{day}} \right)\left(\frac{1000\,\text{L}}{\text{m}^3} \right)\left(\frac{2000\,\text{mg}\,O_2}{\text{L}} \right)\left(\frac{\text{kg}}{10^6\,\text{mg}} \right)$$

$$- \left(\frac{1.42\,\text{kg}\,O_2}{\text{kg biomss}} \right)\left(\frac{893\,\text{kg biomass}}{\text{day}} \right) = 732\,\frac{\text{kg}\,O_2}{\text{day}}$$

It is noted that the values of theoretical oxygen demand and biomass production are almost identical to those obtained by the microbial balanced stoichiometric equation shown in Example 2.3. In many cases, the approach based on the amount of organic matter removed and growth yield (Equation 2.5) is more convenient than that based on a balanced stoichiometric equation because it can be difficult to estimate the chemical formula for influent wastewater and biomass. On the other hand, Equation 2.5 should be modified when oxidizable inorganic matters such as ammonia and nitrite are present in wastewater. Also, more oxygen would be required if inorganic matters are oxidized during wastewater treatment. The case of nitrification (e.g., oxidation of ammonia to nitrate) is introduced in Section 2.5.1.

2.3 Microbial Kinetics

Although balanced microbial stoichiometric equations are very useful to identify the elements involved in the microbial reactions and to estimate the amounts of elements produced or consumed during the reaction, the stoichiometry itself is unable to provide any information how fast the reactions occur. Environmental scientists and engineers are concerned with the rate of microbial reactions because the rates determine the volume of bioreactor or the biomass concentration required to achieve a certain degree of performance. Rates are also used to estimate the performance of the bioreactor at certain design and operational conditions.

Kinetics is a discipline that studies the speed of chemical reactions. Microbial kinetics largely focuses on the rates of microbial growth and substrate utilization. The kinetic expressions of microbial growth and substrate utilization are used to set up mass balance equations associated with biomass production and substrate utilization, which will be used to estimate a bioreactor's performance (e.g., effluent substrate concentration and the rate of biomass produced) and to design a bioreactor (e.g., reactor volume).

2.3.1 Microbial Growth Rate

Microorganisms grow by metabolizing biodegradable substrates. Microorganisms cannot utilize all matter in influent wastewater, only the biodegradable substrate fraction. Thus, it is essential to characterize wastewater components usable by microorganisms (biodegradable substrate) for better evaluation of microbial kinetics in a bioreactor. The methods for characterization of wastewater are briefly available in Chapter 6 and elsewhere (Rittmann and McCarty, 2000; Tchobanoglous et al., 2003). The rate of microbial growth can be explained as a Monod-type equation as follows:

$$r_g = \frac{dX}{dt} = \frac{\mu_m S X}{K_S + S} \qquad (2.7)$$

where
  r_g is the microbial growth rate, g VSS/m³·day
  X is the biomass concentration, g VSS/m³
  μ_m is the maximum specific growth rate, day⁻¹
  K_s is the half saturation constant for biodegradable substrate, g COD/m³
  S is the biodegradable substrate concentration, g COD/m³

The microbial growth rate (r_g) as a function of biodegradable substrate (S) at a constant biomass concentration is plotted in Figure 2.6. At a low concentration of substrate, the microbial growth rate appears to be linearly proportional to the substrate concentration ($r_g \cong [\mu_m X/K_S] \cdot S$). The increasing trend of microbial growth rate decreases at higher substrate concentrations (e.g., rectangular hyperbolic), and the growth rate reaches a maximum at infinite substrate concentration ($r_g \cong X \cdot \mu_m$). In the kinetic equation, the half saturation constant for substrate (K_s) is defined as
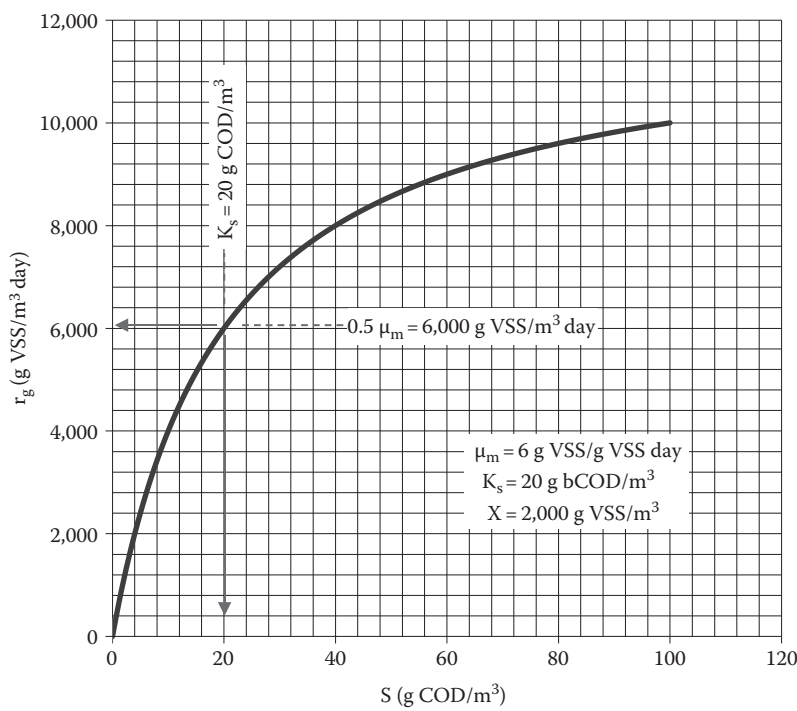
Figure 2.6 Microbial growth rate as a function of substrate concentration.

the substrate concentration to generate half the maximum microbial growth rate at a constant biomass concentration (or the substrate concentration to generate half the maximum specific growth rate).

Microorganisms also tend to decay themselves during growth (e.g., endogenous decay). The rate of biomass decay ($r_{g,decay}$) is known to be proportional to the biomass concentration. Hence, the "net" microbial growth rate ($r_{g,net}$) is the difference between the microbial growth rate (r_g) and the microbial decay rate ($r_{g,decay}$), and can be expressed as follows:

$$r_{g,net} = \frac{dX}{dt} = \frac{\mu_m SX}{K_S + S} - k_d X \tag{2.8}$$

where
$r_{g,net}$ is the net microbial growth rate, g VSS/m³·day
k_d is the decay coefficient, g VSS/g VSS·day

2.3.2 Substrate Utilization Rate

Substrate is the food for microorganisms to grow. In other words, substrate is the biodegradable pollutants in wastewater for microorganisms to treat. Wastewater engineers are more concerned about the rate of substrate removal (e.g., the rate of wastewater treatment) rather than the microbial growth rate.

In practice, the rate of substrate utilization is tightly related to the rate of microbial growth because microorganisms grow by expense of substrate utilization. The biomass yield (Y) introduced in Section 2.2.1 is a coefficient to connect between the rate of microbial growth and the rate of substrate removal. The biomass yield can be estimated as the ratio of the rate of microbial growth to the rate of substrate utilization (e.g., $Y = -r_g/r_u$, where r_u = substrate utilization). Therefore, the rate of substrate removal (r_u) can be expressed using the rate of microbial growth (Equation 2.7) and biomass yield as follows:

$$r_u = \frac{dS}{dt} = -\frac{r_g}{Y} = -\frac{\mu_m SX}{Y(K_S + S)} = -\frac{kSX}{K_S + S} \tag{2.9}$$

where
r_u is the substrate utilization rate, g COD/m³·day
Y is the biomass yield, g VSS/g COD
k is the maximum specific substrate utilization rate ($= \mu_m/Y$), g COD/g VSS·day

Note that the sign of the substrate utilization rate is negative due to the removal of substrate with time, not the production of substrate.

2.3.3 Total VSS Production Rate

It is important to estimate the amount of VSS (or total suspended solids [TSS]) produced per unit time in a bioreactor. The estimation can be used to design and operate the facilities associated with sludge disposal as well as to predict VSS (or TSS) concentration in a bioreactor. VSS of mixed liquor in a bioreactor consists of active biomass and nonbiodegradable VSS (nbVSS). nbVSS can be further classified as the nbVSS from cell debris and that from influent wastewater. Hence, the total VSS production rate can be obtained by adding the three VSS production rates corresponding to the three VSS components: (1) VSS production rate via net microbial growth. The rate is described in Equation 2.8. (2) nbVSS production rate via biomass decay. Most of decay products are used by microorganisms themselves for their substrates, but a fraction of decay products (~10%) cannot be used by microorganisms and accumulate in a bioreactor as nbVSS. The decay products are also called cell debris. The rate of cell debris production is known to be proportional to biomass concentration and is expressed as follows:

$$r_{debris} = \frac{dX}{dt} = f_d k_d X \tag{2.10}$$

where

r_{debris} is the cell debris production rate, g VSS/m³·day

f_d is the fraction of biomass that can be accumulated in a bioreactor during decay, unit less

(3) nbVSS production rate via influent nbVSS. Although the amount of nbVSS in influent wastewater depends on influent wastewater characteristics, generally domestic wastewater contains 60–100 mg nbVSS/L. The rate of nbVSS production is a function of influent nbVSS ($X_{0,i}$), flow rate (Q), and bioreactor volume (V), and is expressed as follows:

$$r_{nbVSS} = \frac{dX}{dt} = \frac{X_{0,1} Q}{V} \tag{2.11}$$

where

r_{nbVSS} is the nbVSS production rate from influent wastewater, g VSS/m³·day

$X_{0,1}$ is the concentration of nonbiodegradable VSS in influent wastewater, g VSS/m³

Q is the influent flow rate, m³/day

V is the bioreactor volume, m³

Therefore, the total VSS production rate ($r_{XT,VSS}$) can be expressed by combining the rate of net biomass growth, the rate of cell debris production, and the rate of nbVSS production from influent wastewater, as shown in the following equation:

$$r_{X_{T,VSS}} = \frac{dX}{dt} = r_{g,net} + r_{debris} + r_{nbVSS} = \frac{\mu_m SX}{K_S + S} - k_d X + f_d k_d X + \frac{X_{0,1}Q}{V} \quad (2.12)$$

where $r_{XT,VSS}$ is the total VSS production rate (g VSS/m³·day).

2.3.4 Effect of Temperature on Microbial Kinetics

Generally, chemical reaction rates increase with increasing temperature. In many cases, the increased reaction rates are explained by increased reaction rate constants. A chemist named Arrhenius first formulated the correlation. Just like chemical reactions, biochemical reactions including microbial growth rates and substrate utilization rates increase with increasing temperature because of increasing biochemical reaction rate constants (e.g., μ_m and k). Environmental engineers adapted the Arrhenius equation to explain the correlation between biochemical reaction rates and temperature, as expressed in the following equation:

$$k_2 = k_1 \theta^{(T_2 - T_1)} \quad (2.13)$$

where
   k_2 is the reaction rate constant at temperature T_2
   k_1 is the reaction rate constant at temperature T_1
   θ is the temperature correction coefficient
   T_1, T_2 are temperatures, °C

Equation 2.13 is very useful to estimate the reaction rate constant for unknown temperature conditions (T_2) when the reaction constant at a certain temperature (T_1) and the temperature correction coefficient (θ) are known. The typical kinetic coefficients and temperature correction coefficients used in activated sludge systems relevant to heterotrophic bacteria are introduced in Table 2.3. However, it should be noted that the biochemical reaction rates cannot increase infinitely with increasing temperature. The rates eventually decrease rapidly above a certain threshold temperature (e.g., 50°C), which is dependent on microbial species. This is mainly due to the rapid loss of biochemical activity at high temperature conditions.

Example 2.4

Biological nitrogen removal (BNR) involves two microbiological processes called nitrification and denitrification. Nitrification is the oxidation of ammonia into nitrate via nitrite, while denitrification is the reduction of nitrate into gaseous nitrogen. AOB are key microorganisms that play an important role in the initial step of nitrification (e.g., the conversion of ammonia into nitrite) and

Table 2.3   Kinetic Coefficients of Activated Sludge for Heterotrophic Bacteria at 20°C Treating Domestic Wastewater

Coefficient	Unit	Range	Typical Value
μ_m	g VSS/g VSS · day	3.0–13.2	6.0
K_S	g bCOD/m³	5.0–40.0	20.0
Y	g VSS/g b COD	0.30–0.50	0.40
k_d	g VSS/g VSS · day	0.06–0.20	0.12
f_d	Unitless	0.08–0.20	0.15
θ values			
μ_m	Unitless	1.03–1.08	1.07
K_S	Unitless	1.00	1.00
k_d	Unitless	1.03–1.08	1.04

Source: Tchobanoglous, G. et al., *Wastewater Engineering: Treatment and Reuse*, 4th edn., McGraw-Hill, New York, 2003.

their growth rates are known to be sensitive to temperature decline. Estimate the maximum specific growth rate of AOB when the temperature of the bioreactor increases to 20°C and decreases to 10°C. It is assumed that the maximum specific growth rate (μ_m) and temperature correction coefficient (θ) of AOB are 0.53 day^{-1} and 1.07, respectively, at 15°C.

Solution

The temperature dependency of the maximum specific growth rate can be estimated using Equation 2.13.

$$\mu_{m,20°C} = 0.53 \cdot 1.07^{(20-15)} = 0.74 \text{ day}^{-1}$$

$$\mu_{m,10°C} = 0.53 \cdot 1.07^{(10-15)} = 0.38 \text{ day}^{-1}$$

At 20°C the maximum specific growth rate of AOB increases from 0.53 to 0.74 day^{-1}, while at 10°C it reduces from 0.53 to 0.38 day^{-1}. It is noted that AOB grow 1.9 times faster at 20°C than at 10°C if all other conditions are the same.

2.4 Mass Balances

Mass balance equations for biomass, substrate, and inert material are very useful to analyze a bioreactor systematically and to provide a basis for evaluating the

performance of bioreactor in MBR plants (e.g., substrate concentration of the per-meate water and biomass concentration in a bioreactor). Mass balance equations are expressed as a set of differential equations that can be solved by solver software. However, if we assume steady-state conditions, it is possible to solve the equations algebraically. A steady-state condition is a state when components (e.g., substrate and biomass) in a bioreactor are unchanging with time.

The following example is a simplified MBR system consisting of a continuous stirred tank bioreactor (CSTR) and an immersed membrane system (Figure 2.7). CSTR assumes that the components entering the reactor are mixed instantaneously and uniformly, and the reaction products leave the reactor with the same concen-trations as those in the reactor. In the schematic diagram presented in Figure 2.7, wastewater is fed to the bioreactor (CSTR) with a flow rate of Q and the treated wastewater is permeated through the immersed membrane with a flow rate of Q_e. The excess VSS is wasted directly from the bioreactor with a flow rate of Q_w. The bioreactor volume is V. For the mass balance analyses, the system boundary includes the bioreactor with the submersed membrane, and the control volume corresponds to the reactor volume. Kinetic parameters used for setting up mass balance equations are also indicated in Figure 2.7.

Figure 2.7 shows the schematic diagram with:

System boundary

Inflow
Q
$X_0 = 0$
$X_{i,0}$
S_0

Bioreactor contents: X, X_i, S, V

Immersed membrane

Outflow
$Q_e = Q - Q_w$
$X_e = 0$
$X_{i,e} = 0$
$S_e = S$

Waste
Q_w
$X_w = X$
$X_{i,w} = X_i$
$S_w = S$

Symbols

Q = flow rate
X = biomass
X_i = inert material
S = substrate
V = volume of bioreactor
0 = influent
e = permeate
w = waste activated sludge

Kinetic parameters

Y = biomass yield
K = half saturation constant for substrate utilization
k = maximum substrate utilization rate
k_d = decay constant
f_d = fraction of biomass that remains as cell debris

Figure 2.7 Schematic diagram of a bioreactor of an MBR plant for setting up mass balance equations.

2.4.1 Mass Balance for Biomass (X)

A mass balance equation for biomass in the bioreactor (around the system boundary) can be simply expressed as follows:

Rate of accumulation of biomass in the bioreactor

= Rate of inflow of biomass − rate of outflow of biomass

+ rate of net biomass production (2.14)

Keep in mind that the units used in the mass balance equations are mass per time (e.g., g VSS/day) not concentration per time. The mass balance equation for biomass can be set up as follows:

$$\frac{dX}{dt}V = QX_0 - \left[(Q - Q_w)X_e + Q_wX\right] + r_{g,net}V \qquad (2.15)$$

where
X_0 is the biomass concentration of feed water, g VSS/m^3
X_e is the biomass concentration of permeate water, g VSS/m^3
X is the biomass concentration of bioreactor, g VSS/m^3

As a result of near perfect removal of biomass by the membrane filtration in MBR plants, the biomass concentration in the permeate water is negligible (e.g., $X_e = 0$). Therefore, the rate of the outflow of biomass via permeate water is zero (e.g., $(Q - Q_w)X_e = 0$). The equation can be further simplified by assuming steady-state conditions for biomass concentration in the bioreactor (e.g., $dX/dt = 0$) and neglecting the influent biomass concentration ($X_0 = 0$). In practice, the concentration of biomass in the influent is very low compared with that in the bioreactor. Steady-state conditions imply that biomass concentrations in the bioreactor at any time point are invariant. The mass balance equation (Equation 2.15) can thus be rearranged using the rate of net biomass growth (Equation 2.8), as expressed in the following equation:

$$Q_wX = r_{g,net}V = \frac{\mu_mSX}{K_S + S}V - k_dXV \qquad (2.16)$$

By dividing VX on both sides of Equation 2.16, the equation can be transformed as follows:

$$\frac{Q_wX}{VX} = \frac{\mu_mS}{K_S + S} - k_d \qquad (2.17)$$

Here, it is required to define an important parameter for bioreactors called solids retention time (SRT). SRT is average retention time of solids in a bioreactor, which is defined as the total biomass in a bioreactor (VX) over the biomass removal rate via

waste biomass ($Q_w X_w$). Because the bioreactor biomass concentration and the waste biomass concentration are the same for MBRs ($X = X_w$, see Figure 2.7), SRT can be expressed as

$$SRT = \frac{VX}{Q_w X_w} = \frac{V}{Q_w} \qquad (2.18)$$

Hence, Equation 2.17 is further transformed using the definition of SRT (Equation 2.18) as

$$\frac{1}{SRT} = \frac{\mu_m S}{K_S + S} - k_d \qquad (2.19)$$

Equation 2.19 is rearranged to give rise to substrate concentration (S) in permeate water as

$$S = \frac{K_S(1 + k_d)SRT}{SRT(\mu_m - k_d) - 1} = \frac{K_S(1 + k_d)SRT}{SRT(Yk - k_d) - 1} \qquad (2.20)$$

Equation 2.20 can be used to estimate substrate concentrations in permeate water (refer to Example 2.5) in MBR plants. Interestingly, the substrate concentration in permeate water is not dependent on the influent substrate concentration (S_0) but is determined by operational conditions (e.g., SRT) and microbial kinetic parameters.

2.4.2 Mass Balance for Substrate (S)

Similar to the mass balance for biomass, the mass balance for substrate can be set up as follows:

> Rate of accumulation of substrate in the bioreactor
>> = Rate of inflow of substrate – rate of outflow of substrate
>> + rate of net substrate production   (2.21)

$$\frac{dS}{dt}V = QS_0 - \left[\left(Q - Q_w\right)S + Q_w S\right] + r_u V = QS_0 - QS + r_u V \qquad (2.22)$$

Unlike biomass, dissolved substrate can pass through the membrane and is detectable as S in permeate water. Assuming steady-state conditions for substrate (e.g., no change in substrate concentration over time, dS/dt = 0), the equation (2.22) is simplified as follows:

$$QS_0 - QS = -r_u V \qquad (2.23)$$

By dividing Q on both sides of Equation 2.23 and substituting r_u as $-kXS/K_S + S$ (Equation 2.9), the equation can be transformed as follows:

$$S_0 - S = \left(\frac{V}{Q}\right)\left(\frac{kXS}{K_S + S}\right) \tag{2.24}$$

Equation 2.24 can be further modified by defining V/Q as τ (hydraulic retention time) and by substituting $S/(K_S + S)$ as $(1 + k_d SRT)/YkSRT$ (see Equation 2.17), generating the following equation:

$$S_0 - S = \tau kX\left(\frac{1 + k_d SRT}{YkSRT}\right) \tag{2.25}$$

Equation 2.25 can be rearranged to generate X as follows:

$$X = \left(\frac{SRT}{\tau}\right)\left[\frac{Y(S_0 - S)}{1 + k_d SRT}\right] = \left(\frac{Q}{Q_w}\right)\left[\frac{Y(S_0 - S)}{1 + k_d SRT}\right] \tag{2.26}$$

Unlike substrate (S), biomass (X) is dependent upon the influent substrate (S_0) as well as operational conditions and microbial kinetic information. Biomass concentration is directly proportional to the substrate removed ($S_0 - S$) in MBRs.

2.4.3 Mass Balance for Inert Material (X_i)

Similar to the mass balances for biomass and substrate, the mass balance for inert material can be set up as follows:

Rate of accumulation of inert material in the bioreactor

= Rate of inflow of inert material-rate of outflow of inert material

+ rate of net inert material production (2.27)

$$\frac{dX_i}{dt} V = QX_{0,i} - \left[(Q - Q_w)X_{e,i} + Q_w X_i\right] + r_{debris} V \tag{2.28}$$

Just like the mass balance for biomass, the concentration of inert material is negligible in the permeate water (e.g., $X_{e,i} = 0$) due to near perfect removal of particulate matters by membrane filtration. Assuming steady-state conditions (e.g., $dX_i/dt = 0$) and substituting the rate of waste of inert material ($Q_w X_i$) as $X_i V/SRT$ using Equation 2.18, the equation is reduced as follows:

$$0 = QX_{0,i} - \frac{X_i V}{SRT} + f_d k_d XV \tag{2.29}$$

where $X_{0,i}$ is the concentration of inert material in influent, g VSS/m³.

Inert biomass (X_i) can be obtained by rearranging Equation 2.29 as follows:

$$X_i = \frac{X_{0,i}SRT}{\tau} + f_d k_d XSRT \tag{2.30}$$

The total volatile solids (X_T) in a bioreactor are the sum of biomass (X) and inert material (X_i), which can be expressed as follows:

$$X_T = X + X_i = \left(\frac{SRT}{\tau}\right)\left[\frac{Y(S_0 - S)}{1 + k_d SRT}\right] + \frac{X_{0,i}SRT}{\tau} + f_d k_d XSRT \tag{2.31}$$

Example 2.5

Calculate the substrate (S), biomass (X), and inert material (X_i) in a bioreactor of an MBR system treating municipal wastewater. The bioreactor operates with a 30-day SRT and a 0.25-day HRT at 20°C. The influent wastewater concentration (S_0) and influent inert material concentration ($X_{0,i}$) are 400 g COD/m³ and 20 g VSS/m³, respectively. The kinetic parameters and their values are as follows:

$$k = 12.5 \text{ g COD/g VSS} \cdot \text{day}$$

$$K_s = 10 \text{ g COD/m}^3$$

$$Y = 0.40 \text{ g VSS/g COD}$$

$$f_d = 0.15 \text{ g VSS/g VSS}$$

$$k_d = 0.10 \text{ g VSS/g VSS} \cdot \text{day}$$

Solution

S, X, and X_i can be calculated using Equations 2.20, 2.26, and 2.30, respectively:

$$S = \frac{K_S(1 + k_d SRT)}{SRT(Yk - k_d) - 1}$$

$$= \frac{(10 \text{ g COD/m}^3)[1 + (0.10 \text{ g VSS/ g VSS} \cdot \text{day})(30 \text{ day})]}{30 \text{ day}[(0.40 \text{ g VSS/g COD})(12.5 \text{ g COD/g VSS} \cdot \text{day}) - 0.10 \text{ g VSS/g VSS} \cdot \text{day}] - 1}$$

$$= 0.27 \text{ g COD/m}^3$$

$$X = \left(\frac{SRT}{\tau}\right)\left[\frac{Y(S_0 - S)}{1 + k_d SRT}\right] = \left(\frac{30 \text{ day}}{0.25 \text{ day}}\right)\left[\frac{0.40 \text{ g VSS/g COD} \cdot (400 \text{ g/m}^3 - 0.27 \text{ g/m}^3)}{1 + (0.10 \text{ g VSS/g VSS} \cdot \text{day})(30 \text{ day})}\right]$$

$$= 4797 \text{ VSS/m}^3$$

$$X_i = \frac{X_{0,i}SRT}{\tau} + f_d k_d X SRT$$

$$= \frac{(20 \text{ g VSS/m}^3)(30 \text{ day})}{0.25 \text{ day}} + (0.15 \text{ g VSS/g VSS})(0.10 \text{ g VSS/g VSS} \cdot \text{day})$$

$$\times (4797 \text{ g VSS/m}^3)(30 \text{ day})$$

$$= 4559 \text{ g VSS/m}^3$$

2.4.4 Effect of SRT on Substrate, Biomass, and Inert Material

One of the main differences of MBR compared with CAS is long SRT operation. The long SRT operation influences the levels of substrate, active biomass, and inert material. It would be valuable to estimate each component for various SRT conditions for a better understanding of MBR. The concentrations of substrate (S), active biomass (X), and inert material (X_i) for various SRTs (5–100 days) are calculated using Equations 2.20, 2.26, and 2.30 in Table 2.4 and plotted in Figure 2.8. The conditions introduced in Example 2.5 are used for all calculations except for SRT.

As shown in Table 2.4 and Figure 2.8, S decreases with increasing SRT, but the magnitude of decrease is not substantial with increasing SRT. A decrease of only 0.42 mg/L of COD corresponds with increasing SRT from 5 to 100 days. On the other hand, X and X_i increase substantially with increasing SRT. X_i increases more than X. X increases from 2,130 to 5,815 mgVSS/L when SRT increases from 5 to 100 days, while X_i increases from 560 to 16,722 mgVSS/L for the same increase in SRT. Interestingly, the concentration of X levels off around 30 days of SRT, while the concentration of X_i increases linearly with increasing SRT.

This suggests that MBR cannot take advantage of long SRT operation greater than 30 days in terms of active biomass for our specified conditions. Rather the increased concentration of solids may exacerbate the membranes' fouling tendency.

Table 2.4   S, X, and X_i for Various SRTs in an MBR

SRT (days)	S (mg/L)	X (mg/L)	X_i (mg/L)	X_T (mg/L)[a]	X/X_T
5	0.64	2130	560	2,690	0.79
10	0.42	3197	1,280	4,476	0.71
20	0.31	4263	2,879	7,142	0.60
30	0.27	4797	4,559	9,355	0.51
40	0.26	5117	6,270	11,387	0.45
50	0.25	5330	7,998	13,328	0.40
100	0.22	5815	16,722	22,537	0.26

[a] $X_T = X + X_i$.
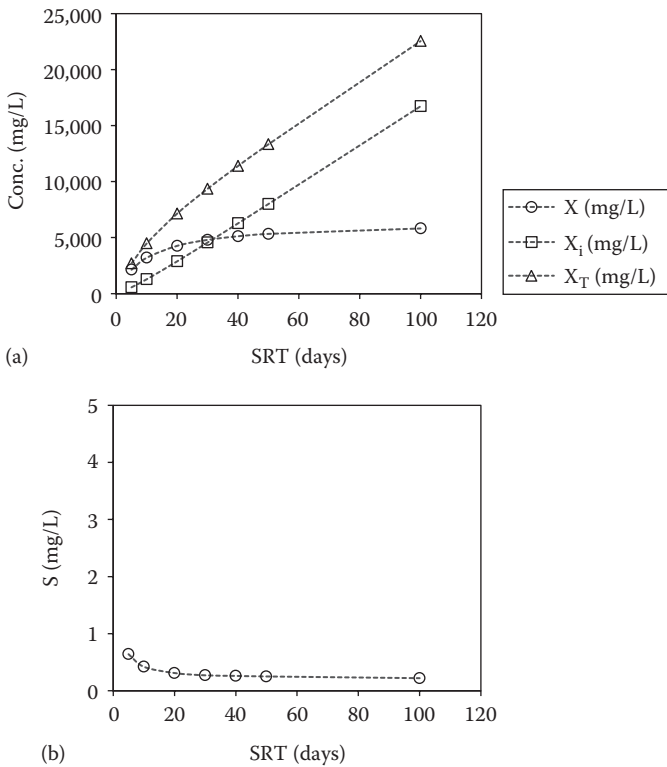
Figure 2.8   Effect of SRT on the concentrations of solids (a) and substrate (b) in an MBR.

The total solids concentration (e.g., sum of X and X_i) shows a similar trend with X_i. Note that the fraction of active biomass (e.g., X/X_T) gradually decreases with increasing SRT and is only 26% at 100 days of SRT.

These calculations are in line with experimental results by Pollice et al. (2008). They operated a laboratory-scale MBR equipped with Zenon hollow fiber membranes with different SRT conditions using municipal sewage. The results demonstrated that biological activity tended to decrease with increasing SRT, while the membrane fouling tendency (e.g., capillary suction time, sludge resistance to filtration, and sludge viscosity) increased at higher SRT operations.

By operating at a long SRT, MBR reduce the volume of waste sludge because SRT is a function of the waste sludge flow rate (SRT = V/Q_w). However, the mass reduction of the sludge wasted daily would not be substantial at very long SRT conditions. This can be verified by calculating the solids production generated daily as a function of SRT. Figure 2.9 shows the correlation for the same conditions described earlier (in Example 2.5) and by assuming that the volume of the
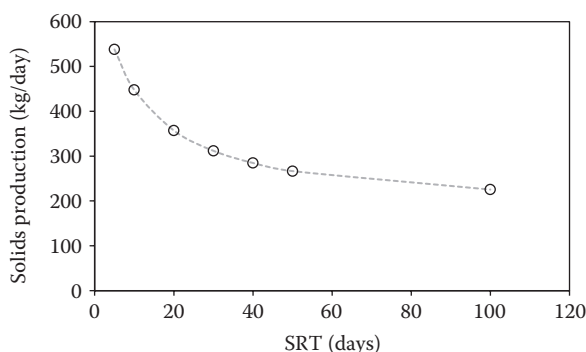
Figure 2.9   Effect of SRT on the daily solids production (or daily solids waste) in an MBR.

bioreactor is 1000 m³. Please see Section 6.3.3 for a detailed description of the calculation for daily solids production.

The daily solids production (or the daily solids waste) reduces with increasing SRT, but it levels off around 40 days of SRT. The daily solids production reduces from 285 to 225 kg/day when SRT increases from 40 to 100 days. This result demonstrates that the benefit of long SRT operation appears to be minimal after a certain point (e.g., 40 days). Moreover, high concentrations of solids in the bioreactor reduce the efficiency of oxygen transfer for microbial growth and require more energy for solids mixing and membrane aeration (see Section 6.4.1), which all lead to additional operating costs.

2.4.5 Effect of Temperature on Substrate, Biomass, and Inert Material

Temperature affects the reaction rates within bioreactors significantly. In biological processes, the rate of microbial growth, substrate removal, and biomass decay are mainly influenced by temperature changes. How temperature affects the reaction rates is already discussed in Section 2.3.4. The effect of temperature on the concentration of substrate, biomass, and inert materials in MBR is illustrated in Example 2.6.

Example 2.6

Calculate the substrate (S), biomass (X), and inert material (X_i) in a bioreactor of an MBR system treating municipal wastewater when the temperature of the bioreactor is reduced from 20°C to 10°C. Assume the operating conditions and kinetic coefficients are the same as those used in Example 2.5. The temperature-dependent rate constants for substrate utilization (k) and biomass decay (k_d) are 1.07 and 1.04, respectively. Assume that the effects of temperature on other kinetic coefficients are negligible.

Solution

The following two equations are used to calculate the temperature corrected reaction rate constants for maximum substrate removal (k) and biomass decay (k_d), respectively.

$$k_{10°C} = k_{20°C}\theta^{(10-20)} = 12.5 \cdot 1.07^{(10-20)} = 6.35 \text{ g COD/gVSS} \cdot \text{day}$$

$$k_{d,10°C} = k_{d,20°C}\theta^{(10-20)} = 0.1 \cdot 1.04^{(10-20)} = 0.07 \text{gVSS/gVSS} \cdot \text{day}$$

Based on these constants and the conditions introduced in Example 2.5, S, X, and X_i can be estimated as follows:

$$S = \frac{K_S(1+k_d SRT)}{SRT(Yk - k_d) - 1}$$

$$= \frac{\left(10 \text{ gCOD/m}^3\right)\left[1+(0.07 \text{ g VSS/g VSS} \cdot \text{day})(30 \text{ day})\right]}{30 \text{ day}\left[(0.40 \text{ g VSS/gCOD})(6.35 \text{ gCOD/g VSS} \cdot \text{day}) - 0.07 \text{ g VSS/g VSS·day}\right] - 1}$$

$$= 0.42 \text{ gCOD/m}^3$$

$$X = \left(\frac{SRT}{\tau}\right)\left[\frac{Y(S_0 - S)}{1 + k_d SRT}\right]$$

$$= \left(\frac{30 \text{ day}}{0.25 \text{ day}}\right)\left[\frac{0.40 \text{ gVSS/g COD} \cdot (400 \text{ g/m}^3 - 0.42 \text{ g/m}^3)}{1 + (0.07 \text{ gVSS/gVSS·day})(30 \text{ day})}\right]$$

$$= 6187 \text{ gVSS/m}^3$$

$$X_i = \frac{X_{0,i} SRT}{\tau} + f_d k_d X SRT$$

$$= \frac{(20 \text{ g COD/m}^3)(30 \text{ day})}{0.25 \text{ day}} + (0.15 \text{ gVSS/gVSS})(0.07 \text{ gVSS/gVSS} \cdot \text{day})$$

$$\times (6187 \text{ gVSS/m}^3)(30 \text{ day})$$

$$= 4349 \text{ gVSS/m}^3$$

The concentrations of S, X, and X_i at 10°C are different from those calculated at 20°C, which is summarized in the following table. S and X increased with decreasing temperature, while X_i decreased slightly. The percent increase or decrease for each parameter with changing temperatures is also indicated in the table. Decreases in both the substrate removal rate and the biomass decay rate due to the lowered temperature result in increases in substrate and biomass concentrations. However, the concentration of inert material did not increase because the decreased decay rates contributed more to the production of inert biomass than the increased biomass did. Nevertheless, the total solids concentration increased by lowering the temperature.

Temperature (°C)	S (mgCOD/L)	X (mgVSS/L)	X_i (mgVSS/L)	X_T (mgVSS/L)
20	0.27	4797	4559	9,355
10	0.42	6187	4349	10,536
	(55.6)[a]	(29.0)[a]	(−4.6)[a]	(12.6)

[a] () indicates the percent increase or decrease by changing the temperature from 20°C to 10°C.

2.4.6 Determination of Kinetic Coefficients

As described in previous sections, four kinetic coefficients (Y, k, K_s, k_d) are important to set up kinetic expressions and mass balances. Although several experimental approaches are available in other textbooks, this book presents a method based on a reactor operation with various SRTs as described in Tchobanoglous et al. (2003). The experimental setup for the determination of kinetic parameters is presented in Figure 2.10.
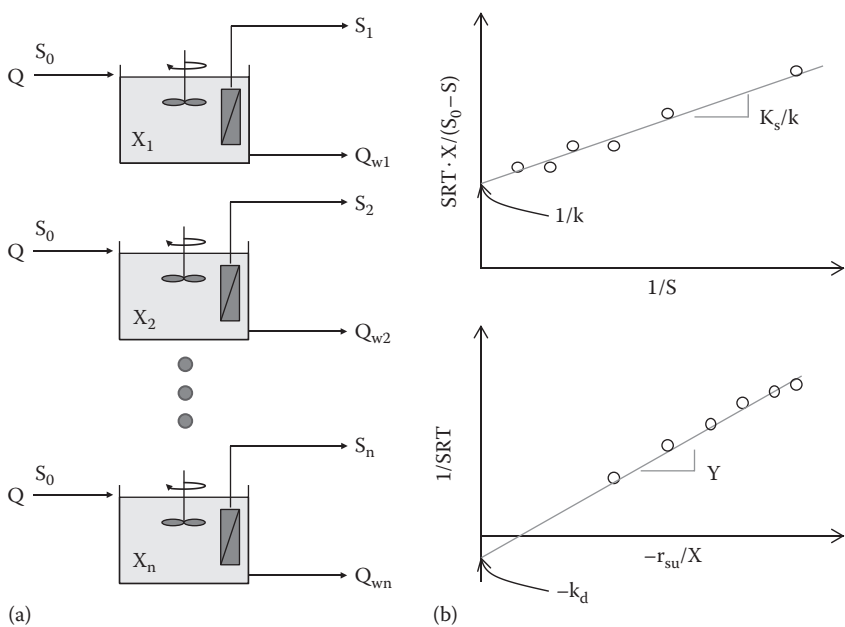
Figure 2.10 Determination of kinetic coefficients: (a) operation of laboratory MBRs with various SRTs and (b) curve fittings for the estimation of kinetic coefficients.

To begin, bioreactors should be operated with various SRTs (e.g., 1–30 days). Control of SRT in MBRs is relatively easier than it is in CAS because the SRT is directly manipulated by changing the wastage flow rate (Q_w) as follows:

$$SRT = \frac{VX}{Q_w X} = \frac{V}{Q_w} \tag{2.32}$$

After steady-state conditions are reached for each SRT condition (e.g., no changes in S and X with time), feed wastewater concentration (S_0), permeate water concentration (S_e), and biomass concentration in bioreactor (X) should be measured. The kinetic coefficients can be obtained by fitting the dataset obtained from the reactor operation to the two equations described in the following. The substrate utilization rate equation (Equation 2.9) can be manipulated as follows:

$$r_u = -\frac{kSX}{K_S + S} = -\frac{S_0 - S}{SRT} \tag{2.33a}$$

Dividing by X on both sides,

$$\frac{kS}{K_S + S} = -\frac{S_0 - S}{SRT \cdot X} \tag{2.33b}$$

Rearranging Equation 2.33b yields

$$\frac{SRT \cdot X}{S_0 - S} = \frac{K_S}{k} \cdot \frac{1}{S} + \frac{1}{k} \tag{2.34}$$

K_s and k can be estimated by fitting the dataset to Equation 2.34. In the plot of SRT·X/S_0 − S as a function of 1/S, the slope and the intercept would correspond to K_S/k and 1/k, respectively. Likewise Y and k_d can be estimated using the following equation:

$$\frac{1}{SRT} = -Y\frac{r_{su}}{X} - k_d \tag{2.35}$$

In the plot of 1/SRT as a function of $-r_{su}$/X, the slope and the intercept would correspond to Y and $-k_d$, respectively.

2.5 Biological Nitrogen Removal

In most countries, nitrogen levels in the effluent of wastewater treatment plants are regulated to mitigate the possible harmful effects of nitrogen discharge in water bodies. The harmful effects include biostimulation of plant and algal growth in surface

waters, depletion of dissolved oxygen (DO) caused by nitrification, ammonia toxicity, public health concerns, and difficulty in reuse of wastewater (US EPA, 1993). Aerobic growth of heterotrophic microorganisms in MBR can remove only a small fraction of nitrogen contained in wastewater. As shown in Example 2.2, ~40% of nitrogen in the wastewater could be incorporated into cell biomass and ~60% of nitrogen was mineralized.

Therefore, it is necessary to remove the mineralized nitrogen such as ammonia using appropriate technology. Nitrogen removal processes are frequently included into MBR plants to reduce the unwanted effects of nitrogen discharge. BNR methods are preferred over physical or chemical nitrogen removal methods such as ammonia stripping or ion exchange mainly due to lower operational cost. Biological methods based on nitrification and denitrification are commonly employed in removing nitrogen contained in wastewater. The purpose of this section is to provide the basic microbiology and mechanisms associated with nitrification and denitrification.

2.5.1 Nitrification

Nitrification is a biochemical process referring to the oxidation of ammonia (NH_3) into nitrate (NO_3^-) via nitrite (NO_2^-). This process is fulfilled by two groups of chemolithoautotrophic bacteria called ammonia-oxidizing bacteria (AOB) and nitrite-oxidizing bacteria (NOB). AOB oxidize ammonia into nitrite, while NOB oxidize nitrite into nitrate. *Nitrosomonas* and *Nitrosospira* are the two AOB genera frequently detected in MBR plants, while *Nitrospira* and *Nitrobacter* are the two common NOB genera. Ammonia-oxidizing archaea (AOA) are also detected in activated sludge bioreactors, but AOA are regarded as minor contributors in the environment of activated sludge (Wells et al., 2009). The following are the stoichiometric equations for ammonia and nitrite oxidation, respectively, without considering the biomass production accompanied with the microbial reactions:

$$\text{AOB: } NH_3 + 1.5O_2 \rightarrow NO_2^- + H_2O + H^+ \tag{2.36}$$

$$\text{NOB: } NO_2^- + 0.5O_2 \rightarrow NO_3^- \tag{2.37}$$

$$\text{Net reaction: } NH_3 + 2O_2 \rightarrow NO_3^- + H_2O + H^+ \tag{2.38}$$
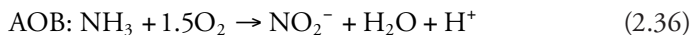
Nitrifying bacteria (AOB and NOB) are strict aerobic bacteria and use oxygen as their terminal electron acceptor. As shown in Equation 2.38, nitrification consumes 4.57 g O_2 per 1 g NH_3–N oxidized ($(2 \cdot 32$ g $O_2)/14$ g NH_3–N$= 4.57$). A balanced nitrification reaction including nitrifying bacterial production is shown in the following equation:

$$NH_3 + 1.89O_2 + 0.0805CO_2 \rightarrow 0.0161C_5H_7O_2N + 0.984NO_3^-$$

$$+ 0.952H_2O + 0.98H^+ \tag{2.39}$$
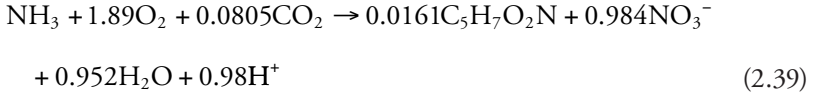
Now, the stoichiometric ratio for oxygen consumption reduces to 4.32 g O_2 per 1 g NH_3–N oxidized ((1.89 · 32 g O_2)/14 g NH_3–N = 4.32). If we have information about the oxidizable ammonia concentration, we can calculate the stoichiometric oxygen requirement using this ratio. At least the stoichiometric amount of oxygen is required for complete nitrification.

The growth or activity of nitrifying bacteria is affected by several bioreactor operational factors including the concentration of the primary electron donor (e.g., ammonia or nitrite), DO concentration, pH, temperature, and the presence of toxic substances. Nitrifying bacteria follow Monod-type growth kinetics for the concentration of the primary electron donor. However, very high concentrations of ammonia are known to inhibit the growth of AOB (>1000 mg NH_3–N/L, US EPA, 1993).

As mentioned earlier, oxygen is the terminal electron acceptor for nitrifying bacteria. DO concentration is therefore a critical factor for the growth of nitrifying bacteria. DO concentration affects the growth rate of nitrifying bacteria in a similar way as the primary electron donor. If we include ammonia and DO as the two growth-limiting components for AOB, the specific growth rate of AOB (μ_{AOB}) can be explained using the following equation:

$$\mu_{AOB} = \left(\frac{\mu_{m,AOB} \cdot NH_3}{K_N + NH_3} \right) \left(\frac{DO}{K_{DO} + DO} \right) - k_{d,AOB} \tag{2.40}$$

where

$\mu_{m,AOB}$ is the maximum specific growth rate of AOB, day^{-1}
NH_3 is the ammonia concentration in bioreactor, mg N/L
K_N is the half saturation constant for ammonia, mg N/L
DO is the dissolved oxygen concentration in bioreactor, mg/L
K_{DO} is the half saturation constant for DO, mg/L
$k_{d,AOB}$ is the decay constant of AOB, day^{-1}

It is generally recommended to maintain greater than 2 mg/L DO in a bioreactor for efficient nitrification. In practice, the aeration system is designed and operated to maintain the DO levels required in the nitrifying zone of bioreactors. pH is also a factor affecting the activity of nitrifying bacteria. The nitrification rate is known to show the highest activity at pH values of 7.5–8.0. During nitrification, pH tends to decrease due to the production of hydrogen ion (refer to Equation 2.39). Nitrification activity decreases to less than 50% of the maximum value under pH 5.

In most cases, municipal wastewater has enough alkalinity to neutralize the hydrogen ions produced by nitrification, but in some industrial wastewater, the alkalinity is not sufficient to maintain a neutral pH in the bioreactor. In such cases, bases

such as NaOH should be provided to the bioreactor to prevent a pH drop. When 1 g of NH_3–N is oxidized, 7.1 g of alkalinity as $CaCO_3$ (= $(1.98 \cdot 50)/14$) is consumed (see Equation 2.39).

Like other microorganisms, the growth of nitrifying bacteria is affected by temperature. Nitrification is known to occur in the temperature range of 4°C–45°C and to be optimum around 35°C (US EPA, 1993). Temperature affects the maximum growth rate constant of nitrifying bacteria. The Arrhenius-type growth rate of AOB can be expressed as follows:

$$\mu_{m,AOB}(T) = 0.75\theta^{(T-20)} \tag{2.41}$$

where θ is the temperature correction factor for the maximum specific growth rate of AOB, and typically it has a value of 1.10 applicable to 5°C–30°C (US EPA, 1993).

Nitrifying bacteria are autotrophs and use dissolved carbon dioxide instead of organic matter as their carbon source to synthesize cell materials. This feature forces them to spend more energy to synthesize cell material than heterotrophs that use organic matter. In addition, nitrifying bacteria are lithotrophs. Less energy is extracted from the oxidation ammonia or nitrite compared with the oxidation of organic matters. Therefore, nitrifying bacteria are slower growing microorganisms than the microorganisms responsible for BOD removal. In order to harness the slow-growing nitrifying bacteria, sufficient SRT should be provided.

Bioreactors of MBR plants are generally operated with long SRTs (>20 days), allowing the nitrifying bacteria to readily inhabit in the bioreactors. Refer to Section 6.3.2 for the calculation of the minimum required SRT for maintaining nitrifying bacteria in a bioreactor. In addition, nitrifying bacteria have lower growth yields than BOD removal bacteria due to similar reasons (e.g., less energy extraction from ammonia or nitrite oxidation and substantial energy consumption for the synthesis of cell materials). A typical value of growth yield is 0.1 g VSS/g NH_3–N.

2.5.2 Denitrification

Nitrifying bacteria in aerobic tanks produce nitrate as the end product of nitrification. In most cases, nitrate must be removed to satisfy the effluent discharge limit in wastewater treatment plants, which are often regulated by total nitrogen. Using denitrification, nitrate is transformed into gaseous nitrogen (N_2), which can be emitted into atmosphere for removal from the system. Denitrification is the microbiological process of reducing nitrate (NO_3^-) into gaseous nitrogen (N_2) via sequential reduction processes involving nitrite (NO_2^-), nitric oxide (NO), and dinitrogen oxide (N_2O), as follows:

$$NO_3^- \rightarrow NO_2^- \rightarrow NO \rightarrow N_2O \rightarrow N_2 \tag{2.42}$$

Denitrification is carried out by phylogenetically diverse microorganisms in oxygen-deficient bioreactors (e.g., anoxic tanks). Most of the denitrifying bacteria

also have aerobic energy generation pathways. They tend to use oxygen as their terminal electron acceptor instead of nitrate in conditions where both oxygen and nitrate are present due to the higher extraction of free energy when using oxygen. Therefore, it is vital to minimize the oxygen concentration in anoxic tanks to achieve efficient denitrification. Denitrifying bacteria are also heterotrophs that use organic matter for synthesizing cell materials. The substrate utilization rate (r_{su}) of denitrifying bacteria can be expressed as functions of substrate, nitrate, oxygen, and denitrifying biomass, as shown in the following equation:

$$r_{su} = -\left(\frac{kXS\eta}{K_S + S}\right)\left(\frac{NO_3^-}{K_S,NO_3^- + NO_3^-}\right)\left(\frac{K_{O_2}}{K_{O_2} + DO}\right) \tag{2.43}$$

where
  k is the maximum specific substrate utilization rate, g COD/g VSS·day
  X is the biomass concentration, g VSS/m³
  S is the biodegradable substrate concentration, g COD/m³
  η is the fraction of denitrifying bacteria in biomass, g VSS/g VSS
  K_S is the half saturation constant for biodegradable substrate, g COD/m³
  NO_3^- is the nitrate nitrogen concentration, g N/m³
  K_{S,NO_3^-} is the half saturation constant for nitrate reduction, g N/m³
  DO is the dissolved oxygen concentration, g/m³
  K_{O_2} is the half saturation constant for DO inhibition of nitrate reduction, g/m³

The organic matter frequently comes from influent wastewater. However, in some wastewater the amount of organic matter is not sufficient to achieve complete denitrification. In such cases, organic matter such as methanol, ethanol, acetic acid, or waste organic material should be externally provided to the anoxic tank to achieve efficient denitrification. The required amount of organic matter can be theoretically estimated based on the reduction half reactions as follows:

$$\frac{1}{4}O_2 + H^+ + e^- = \frac{1}{2}H_2O \tag{2.44}$$

$$\frac{1}{5}NO_3^- + \frac{6}{5}H^+ + e^- = \frac{1}{10}N_2 + \frac{3}{5}H_2O \tag{2.45}$$
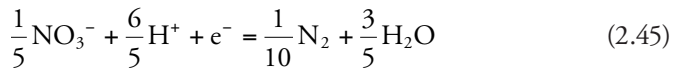
From the half reactions, we can deduce that 1/5 nitrate nitrogen consumes "one electron" for the production of 1/10 gaseous nitrogen, which is equivalent to the transformation of 1/4 oxygen into 1/2 water using "one electron." In other words, 2.8 ($= 1/5 \times 14$) g of nitrate nitrogen is equivalent to 8 ($=\frac{1}{4} \times 32$) g of oxygen (e.g., COD). The theoretical COD requirement for a unit amount of nitrate nitrogen reduction is therefore 2.86 g COD per 1.0 g of nitrate nitrogen (=8/2.8).

Also during denitrification, when 1 g of NO_3-N is denitrified, 3.6 g of alkalinity as $CaCO_3$ (=(1 · 50)/14) is recovered.

Similarly, theoretical amounts of other organic matters such as methanol, ethanol, and acetate for denitrification can be calculated. The reduction half reactions for methanol, ethanol, and acetate are as follows:

$$\text{Methanol: } \frac{1}{6}CO_2 + H^+ + e^- = \frac{1}{6}CH_3OH + \frac{1}{6}H_2O \tag{2.46}$$

$$\text{Ethanol: } \frac{1}{6}CO_2 + H^+ + e^- = \frac{1}{12}CH_3CH_2OH + \frac{1}{4}H_2O \tag{2.47}$$

$$\text{Acetate: } \frac{1}{8}CO_2 + \frac{1}{8}HCO_3^- + H^+ + e^- = \frac{1}{8}CH_3COO^- + \frac{3}{8}H_2O \tag{2.48}$$
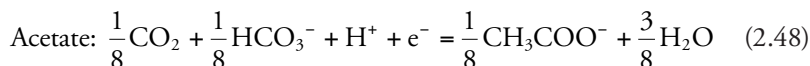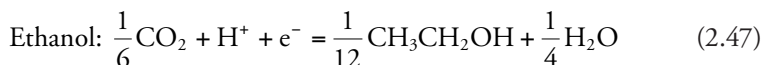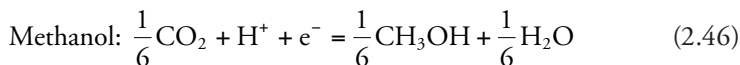
The reduction of 2.8 (=1/5 × 14) g of nitrate nitrogen is equivalent to 5.3 (=1/6 × 32) g of methanol, 3.8 (=1/12 × 46) g of ethanol, and 7.4 (=1/8 × 59) g of acetate. Therefore, the theoretical requirements of methanol, ethanol, and acetate for 1.0 g of nitrate nitrogen reduction are 1.90, 1.36, and 2.63 g, respectively. However, actual requirements of organic matters for denitrification reaction are greater than the theoretical values because the organic matters are also used to synthesize cell mass as well as denitrification.

The growth yield (Y) can be used to adapt the calculation. Y is the ratio of biomass production to substrate consumption, and (1 − α · Y) is the proportion of organic matter used (e.g., substrate) for denitrification, where α is a conversion factor of substrate equivalent to biomass. For example, assuming Y for the bacteria responsible for denitrification using methanol is 0.3 g biomass per 1.0 g of methanol, then α is 0.944 (=(1/6 · 32) g methanol/(1/20 × 113) g biomass) and the fraction used for denitrification is 0.72 g of methanol for 1.0 g of methanol consumption (=1 − (0.944 × 0.3)). For the calculation of α, please refer to Example 2.7. Thus, the theoretical amount of methanol for 1 g of nitrate reduction is 2.64 (=1.90/0.72) g.

A general equation for the requirement of organic matter can be generated based on the earlier discussion. Similar to the approach for estimating theoretical oxygen demand (Equation 2.5), the oxygen equivalent of organic matter consumed (COD) is the sum of the oxygen equivalent for denitrification (2.86 N) and the oxygen equivalent for produced biomass (1.42Y · COD), as shown in the following equation:

$$COD = 2.86N + 1.42Y \cdot COD \tag{2.49}$$

where
   Y is the growth yield, g biomass/g COD
   1.42 is the coefficient for converting mass unit into oxygen unit in biomass
      ($C_5H_7O_2N$), g COD/g biomass

Equation 2.49 can be rearranged as follows:

$$\frac{COD}{N} = \frac{2.86}{1 - 1.42Y} \qquad (2.50)$$

Example 2.7

Waste glucose ($C_6H_{12}O_6$) is produced in a food factory. An engineer wants to use the waste glucose as a carbon source for denitrification. Calculate the theoretical requirement of glucose for 1 g of nitrate nitrogen reduction in g COD/g N. Assume that the growth yield of the bacteria in the denitrifying bioreactor is 0.42 g biomass per 1.0 g of glucose.

Solution

The half reactions for the reduction of glucose and nitrate are as follows:

$$\text{Glucose: } \frac{1}{4}CO_2 + H^+ + e^- = \frac{1}{24}C_6H_{12}O_6 + \frac{1}{2}H_2O$$

$$\text{Nitrate: } \frac{1}{5}NO_3^- + \frac{6}{5}H^+ + e^- = \frac{1}{10}N_2 + \frac{3}{5}H_2O$$
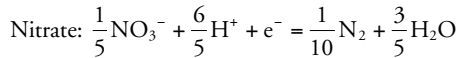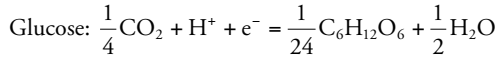
Because the reduction of 2.8 (= 1/5 × 14) g of nitrate nitrogen is equivalent to 7.5 (=1/24 × 180) g of glucose, the theoretical requirements of glucose is 2.68 (=7.5/2.8) g for 1 g of nitrate nitrogen reduction.

Considering the growth yield, we need to calculate the fraction of glucose used for biomass production (i.e., $1 - \alpha \cdot Y$). α is a conversion factor of glucose equivalent to biomass and can be calculated based on the half reactions for glucose and biomass. 1/24 glucose is equivalent to 1/20 biomass. Thus, α is 1.327 (=(1/24 × 180) g glucose/(1/20 × 113) g biomass).

$$\text{Glucose: } \frac{1}{4}CO_2 + H^+ + e^- = \frac{1}{24}C_6H_{12}O_6 + \frac{1}{2}H_2O$$

$$\text{Biomass}: \frac{1}{4}CO_2 + \frac{1}{20}NH_3 + H^+ + e^- = \frac{1}{20}C_5H_7O_2N + \frac{2}{5}H_2O$$
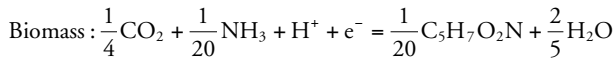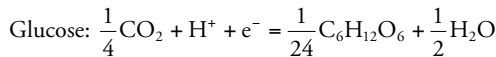
Thus, the theoretical glucose requirement increases to 6.05 (=2.68/ $(1 - 1.327 \cdot 0.42)$) g. It is now required to convert the mass unit of glucose into COD units based on the half reactions for glucose and water.

$$\text{Glucose}: \frac{1}{4}CO_2 + H^+ + e^- = \frac{1}{24}C_6H_{12}O_6 + \frac{1}{2}H_2O$$

$$\text{Water}: \frac{1}{4}O_2 + H^+ + e^- = \frac{1}{2}H_2O$$
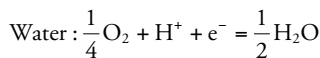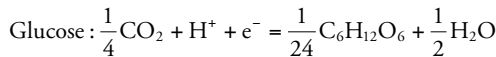
These reactions indicate 7.5 (=1/24 × 180) g of glucose is equivalent to 8 (= 1/4 × 32) g of oxygen (e.g., COD). In other words, 1 g of glucose is equivalent to 1.07 (=8/7.5) g of COD. Therefore, the theoretical requirement of glucose

is 6.47 g COD per 1 g of nitrate nitrogen reduction (=(1.07 g COD/g glucose)·(6.05 g glucose/g nitrate N reduction)).

Alternatively, the theoretical requirement of glucose can be calculated using Equation 2.50. The growth yield for the calculation is 0.39 (=(0.42 g biomass/g glucose)·(7.5 g glucose/8 g COD)) g biomass per g COD.

$$\frac{COD}{N} = \frac{2.86}{1-1.42Y} = \frac{2.86}{1-1.42 \cdot 0.39}$$
$$= 6.41g \ COD \ per \ 1 \ g \ of \ nitrate \ nitrogen \ reduction$$

2.5.3 Nitrogen Removal Performance

As shown in Figure 2.11, BNR processes generally consist of tanks for denitrification (anoxic tanks) and nitrification (aerobic tanks). In practice, the anoxic tank precedes the aerobic tank to utilize organic matters (e.g., primary electron donors) included in influent wastewater (preanoxic denitrification). However, in this configuration nitrate (the terminal electron acceptor) should be provided to the anoxic tank by recycling mixed liquor containing nitrate from the aerobic tank.

Another possible configuration of BNR processes is postanoxic denitrification in which the aerobic tank precedes the anoxic tank. In this configuration, most of the organic matter included in the influent wastewater is utilized by aerobic heterotrophic microorganisms in the aerobic tank, and denitrification would occur mostly by using the organic matters generated by endogenous decay. Postanoxic denitrification is less efficient than preanoxic denitrification due to the lower availability of organic matters. In addition, postanoxic denitrification may require the addition of an external carbon source into the anoxic tank to improve denitrification efficiency.

In the preanoxic denitrification process, nitrified mixed liquor is recycled from the aerobic tank to the anoxic tank to provide nitrate for denitrification reactions. The rate of the mixed liquor recycle from the aerobic tank to the anoxic tank determines the nitrogen removal performance. Higher nitrogen removal performance occurs with higher mixed liquor recycle rates because more denitrification can occur in the anoxic tank.
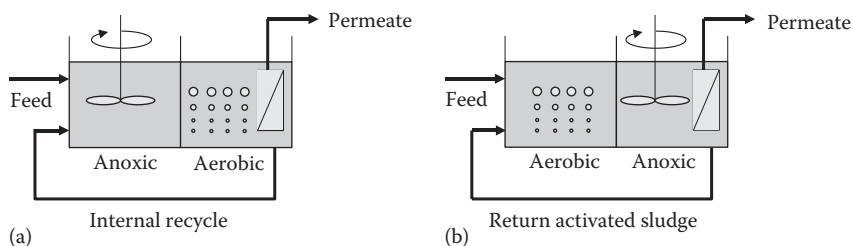
Figure 2.11 **Biological nitrogen removal processes: (a) preanoxic denitrification process and (b) postanoxic denitrification process.**

The mass balance equation around the anoxic–aerobic MBR can be used to estimate the nitrogen removal performance quantitatively. Assuming no nitrate (or nitrite) in the influent, no carbon source limiting conditions for denitrification in the anoxic tank, complete mineralization of organic nitrogen into ammonia in the anoxic tank, and complete nitrification in the aerobic tank, we can setup simple mass balance equations for nitrogen. Figure 2.9 shows a schematic diagram of an MBR plant consisting of an anoxic and an aerobic tank for denitrification and nitrification, respectively. Here are the nitrogen mass balance equations for the anoxic and aerobic tanks (Figure 2.12).

By assuming all of the organic nitrogen is mineralized in the anoxic tank and by considering the nitrogen assimilated in biomass, the nitrogen mass balance equation in the anoxic tank can be expressed as

$$Q \cdot TKN_0 \cdot (1 - f) = NH_{3,ax} \cdot (Q + Q_r) \tag{2.51}$$

$$NH_{3,ax} = \frac{Q \cdot TKN_0 \cdot (1 - f)}{(Q + Q_r)} \tag{2.52}$$

$$NO_{3,ax} = 0 \tag{2.53}$$

where
  TKN_0 is the total Kjeldahl nitrogen (i.e., organic nitrogen + ammonia nitrogen), g N/m^3
  $NH_{3,ax}$ is the ammonia nitrogen concentration in the anoxic tank, g N/m^3
  $NO_{3,ax}$ is the nitrate nitrogen concentration in the anoxic tank, g N/m^3
  f is the fraction of nitrogen assimilated in biomass
  Q is the influent flow rate, m^3/day
  Q_r is the recycle flow rate, m^3/day
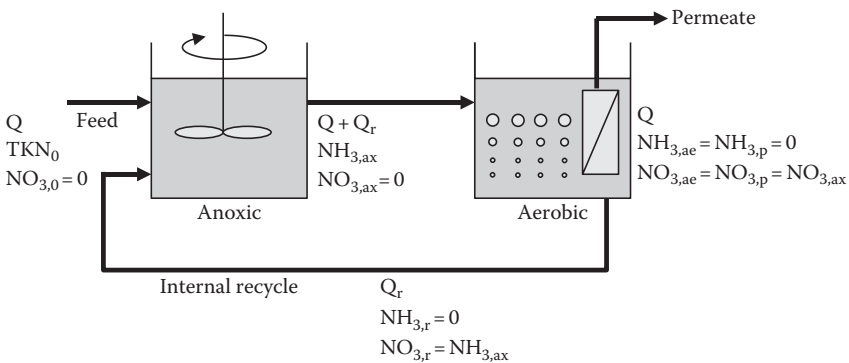
Figure 2.12 Mass balance of nitrogen removal in the preaerobic denitrification process. Waste activated sludge flow is neglected in this schematic.

In the aerobic tank, because all of the ammonia nitrogen is nitrified, the nitrate nitrogen concentration would be the same as the ammonia concentration of the anoxic tank and the ammonia nitrogen concentration (in the aerobic tank) would be zero. The nitrogen mass balance equation in the aerobic tank can be expressed as

$$NO_{3,ae} = NH_{3,ax} \tag{2.54}$$

$$NH_{3,ae} = 0 \tag{2.55}$$

where $NH_{3,ae}$ is the ammonia nitrogen concentration in the aerobic tank, g N/m³.

Using the nitrogen mass balance equations, the total nitrogen removal efficiency can be estimated as follows:

$$\text{Total nitrgen removal efficiency} = \frac{TKN_0 - NO_{3,p}}{TKN_0}$$

$$= 1 - \frac{\left(Q/(Q + Q_r)\right) \cdot TKN_0 \cdot (1 - f)}{TKN_0}$$

$$= 1 - \frac{Q \cdot (1 - f)}{Q + Q_r} \tag{2.56}$$

where $NO_{3,p}$ is the nitrate concentration in the permeate ($NO_{3,ae} = NH_{3,ax}$), g/m³.

The nitrogen removal efficiency of an anoxic–aerobic MBR as a function of the mixed liquor recycle ratio is plotted in Figure 2.13. In this example, we can
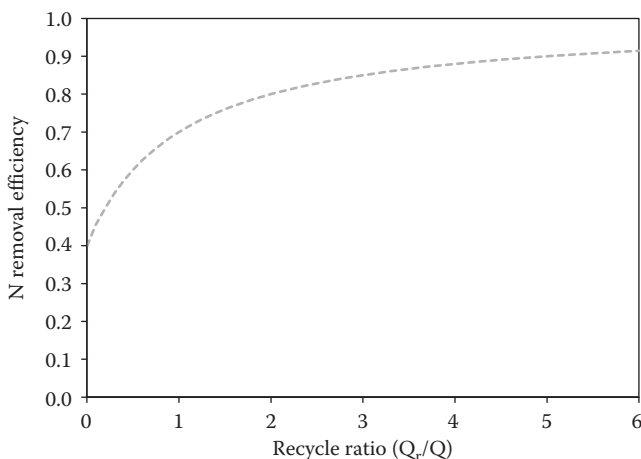
Figure 2.13   Total nitrogen removal efficiency as a function of return ratio (Q_r/Q) when nitrogen assimilation in biomass (f) is 0.4.

estimate that the return ratio (Q_r/Q) should be higher than 2.0 to achieve greater than 80% total nitrogen removal efficiency.

2.6 Biological Phosphorus Removal

2.6.1 Phosphorus Removal by Conventional Biological Activated Sludge Process

Phosphorus is a macronutrient that often limits the growth of aquatic phototrophic organisms when present in low concentrations. Like nitrogen, phosphorus should be appropriately treated to reduce the risk of algal blooms in receiving water bodies. The phosphorus content of the cell mass of CAS is around 2%–3%, which leads to a chemical formula of activated sludge of $C_5H_7O_2NP_{0.1}$ (P is therefore ~2.7% of cell mass).

Let's estimate about phosphorus removal through the assimilation (uptake by the biomass cells) of phosphorus in CAS. Rittmann and McCarty (2000) introduced an equation for calculating effluent phosphorus concentration based on a mass balance of phosphorus in a bioreactor as follows:

$$P = P_0 - \frac{0.0267 \cdot Y \cdot (1 + f_d k_d \theta_x) \cdot \Delta COD}{1 + k_d \theta_x} \tag{2.57}$$

where
   P is the effluent phosphorus concentration, mg P/L
   P_0 is the influent phosphorus concentration, mg P/L
   ΔCOD is the COD removal, mg COD/L

Equation 2.57 is a function of growth yield, SRT, and COD removal. More phosphorus can be removed by increasing the growth yield and COD removal, while less phosphorus can be removed by increasing SRT. Phosphorus removal is plotted in Figure 2.14 for different COD removal rates and SRTs when influent phosphorus concentration = 5 mg P/L, influent COD = 400 mg/L, Y = 0.40 g VSS/g COD, f_d = 0.15 g VSS/g VSS, and k_d = 0.10 g VSS/g VSS·day.

No conditions in Figure 2.14 result in an effluent phosphorus concentration less than 1.0 mg P/L, a typical effluent phosphorus level in municipal wastewater treatment plants. However, the phosphorus concentrations did show a decreasing trend with increasing COD removal and decreasing SRT. It is almost impossible to reduce the phosphorus concentration to less than 3.0 mg/L for the specified conditions if we consider the long SRT values typical of MBR operation (e.g., >20 days). Therefore, it is required to implement enhanced biological phosphorus removal (EBPR) and/or chemical precipitation to reduce the phosphorus concentration further.
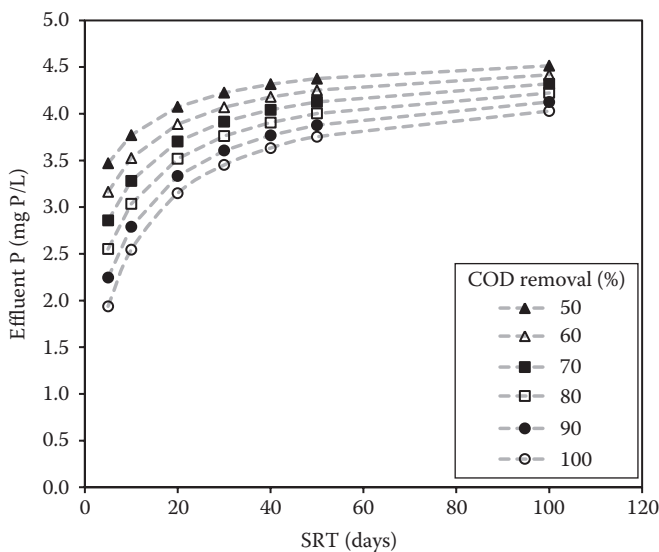
Figure 2.14   Effect of COD removal and SRT on the effluent phosphorous for the specified conditions described in the text.

2.6.2 *Phosphorus Removal by Enhanced Biological Phosphorus Removal Process*

EBPR uses special groups of bacteria that are able to accumulate phosphorus granules inside their cells. The enrichment of these bacteria in a bioreactor leads to an increase in the phosphorus content of the total biomass, which results in greater phosphorus removal compared with the CAS process at the same COD removal and SRT conditions. It is reported that the phosphorus content in the biomass can be increased up to 12.5% based on VSS in very active EBPR process (Mino et al., 1998). The effluent phosphorus concentration can be estimated in EBPR by assuming the increased phosphorus content (8% in this example) and modifying the Equation 2.57 as follows:

$$P = P_0 - \frac{0.08 \cdot Y \cdot (1 + f_d k_d \theta_x) \cdot \Delta COD}{1 + k_d \theta_x} \tag{2.58}$$

Effluent phosphorus concentrations are plotted in Figure 2.15 for the same conditions presented in Figure 2.14 using EBPR. EBPR significantly reduced the phosphorus concentration in the effluent. Nevertheless, not all of conditions reduced the level of phosphorus down to 1 mg P/L. When COD removal is less than 70% and SRT is longer than 20 days, it is still impossible to satisfy the target phosphorus
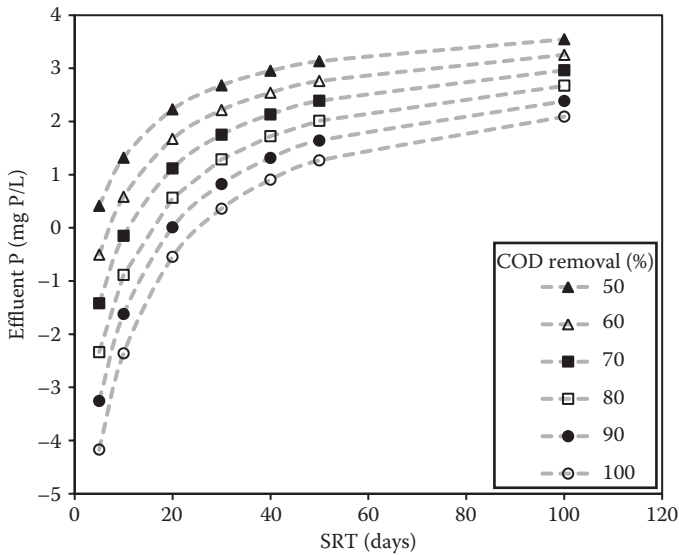
Figure 2.15   Effect of COD removal and SRT on the effluent phosphorous for EBPR. Note: Negative effluent phosphorus values are only included to show the shape of the data curves.

level (<1 mg P/L). In these cases, chemical precipitants are generally added to the bioreactor to meet the stringent effluent regulations in MBR plants.

Example 2.8

What is the maximum SRT in days for reducing the effluent phosphorus level down to 1.0 mg/L of phosphorus? Please use the following conditions for the estimation.

$$\text{Influent phosphorus concentration} = 5 \text{ mgP/L}$$

$$\text{Influent COD} = 400 \text{ mg/L}$$

$$Y = 0.40 \text{ g VSS/g COD}$$

$$f_d = 0.15 \text{ g VSS/g VSS}$$

$$k_d = 0.10 \text{ g VSS/g VSS·day.}$$

$$\text{Phosphorus content of cell mass} = 10\%$$

$$\text{COD removal} = 80\%$$

Solution

Using the mass balance equation for phosphorus around a bioreactor (Equation 2.58), the maximum SRT can be calculated as

$$P = P_0 - \frac{0.1 \cdot Y \cdot (1 + f_d k_d \theta_x) \cdot \Delta COD}{1 + k_d \theta_x}$$

$$1.0 \text{ mg/L} = 5.0 \text{ mg/L} - \frac{0.1 \cdot (0.40 \text{ g VSS/g COD}) \cdot}{1 + 10 \text{ g VSS/g VSS/day} \cdot \theta_x} \cdot 320 \text{ mg/L}$$

$$\theta_x = 42.3 \text{ day}$$

The effluent phosphorus concentration will be higher than 1.0 mg/L when SRT is greater than 42.3 days.

EBPR works when phosphorus accumulating organisms (PAOs) are enriched in the bioreactor. Although nobody has succeeded in obtaining pure-culture PAOs, a great deal of culture-independent molecular analyses has demonstrated that PAOs are mostly affiliated with *Accumulibacter phosphatis* within *Betaproteo bacteria*.

PAOs can be enriched by providing alternating anaerobic and aerobic conditions. The basic biochemical mechanism of PAOs relevant to phosphorus removal is introduced in Figure 2.16. During anaerobic conditions, complex organic matters are initially converted into short-chain fatty acids (e.g., acetate, propionate, butyrate) by fermentation bacteria. PAOs then change the short-chain fatty acids into acetyl-CoA, which is used for synthesizing an intracellular polymer called polyhydroxybutyrate (PHB). The energy for the synthesis of PHB is provided by
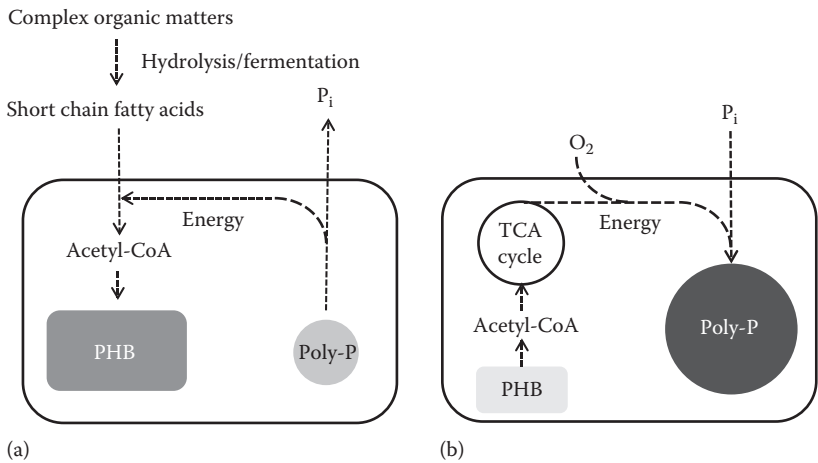
Figure 2.16 Biochemical mechanisms of phosphorus removal by PAOs by alternating (a) anaerobic and (b) aerobic conditions.

hydrolyzing intracellular polyphosphate during which orthophosphate is produced and is transferred to the bulk solution.

During aerobic conditions, PAOs oxidize PHB using oxygen as the terminal electron acceptor to generate reducing power (e.g., NADH) for their growth and maintenance. The reducing power is also utilized for synthesizing intracellular polyphosphate using orthophosphate, which is transferred from the bulk solution. During the synthesis of polyphosphate, more phosphate is absorbed than the phosphate transferred to the bulk solution during anaerobic conditions. This phenomenon is referred to as "luxury uptake of phosphate." By removing the excess biomass containing a high percentage of nitrogen, phosphorus removal is achieved.

Some PAOs can also use nitrate as their terminal electron acceptor for oxidizing PHB in anoxic conditions. These PAOs are called denitrifying PAOs and are useful for removing nitrate from wastewater having low COD/total nitrogen ratios.

2.6.3 Phosphorus Removal by Chemical Precipitation

As discussed in the previous section, chemical addition appears to be unavoidable when phosphorus is regulated stringently. Salts of multivalent cations can be used to precipitate phosphate, which transforms soluble phosphate into suspended solids. Although the precipitants can be added before or after biotreatment, it is common to add the precipitants into the bioreactor directly in MBR plants (Figure 2.17). In case of adding precipitant after biotreatment in MBR, it is known to be difficult to create nuclei for growing floc of precipitation due to extremely low levels of particulate matters to act as precipitation nuclei in the permeate water of MBR.

For precipitation, aluminum (Al(III)), iron (Fe(III)), and calcium (Ca(II)) are frequently used in practice. Aluminum and iron cations can react with phosphate as follows:

$$Al^{3+} + PO_4^{3-} \rightarrow AlPO_4(S)$$

$$Fe^{3+} + PO_4^{3-} \rightarrow FePO_4(S)$$
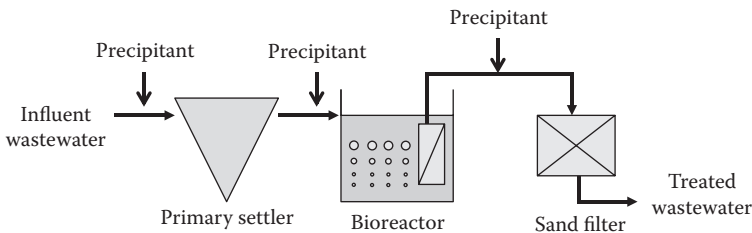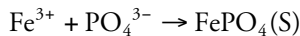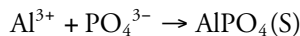
Figure 2.17   **The locations of precipitant addition for phosphorus removal in an MBR plant.**

Although the chemical equations suggest that one mole of aluminum or iron ions are required for the precipitation of one mole of phosphate, in reality, more aluminum or iron ions are required due to competition reactions. Aluminum or iron ions are involved in complex reactions with various ligands including water and hydroxide ions in solution. Therefore, phosphate competes with the ligands for the precipitation reactions. To provide optimum conditions for the precipitation reactions, it is generally required to conduct jar tests for various concentrations of precipitants, pH, and alkalinity.

Calcium ions can also precipitate with phosphate under high pH conditions (>10) as follows:

$$10Ca^{2+} + 6PO_4^{3-} + 2OH^- \rightarrow Ca_{10}(PO_4)_6(OH)_2(S)$$

Because the reaction is only feasible under high pH conditions and the added calcium (generally in the form of lime, $Ca(OH)_2$) should consume alkalinity in solution before precipitation, this method is suitable after biological treatment.

The addition of aluminum or iron salts can affect the membrane fouling propensity. In the bioreactor, the salts neutralize negatively charged colloids and activated sludge particles as well as precipitate phosphate. Neutralizing particles leads to increases in particle size and ultimately reduces the concentration of particles that can clog membrane pores (Song et al., 2008). Therefore, adding aluminum or iron salts is helpful to reduce fouling in MBR. However, too much precipitant addition into the bioreactor may lead to scale formation on the surface of the membrane.

Problems

2.1 Although protozoa such as *Vorticella* are not numerically important microorganisms in activated sludge wastewater treatment, they are routinely monitored by operators of wastewater treatment plants using microscope. What is the importance of protozoa in activated sludge wastewater treatment?

2.2 A wastewater operator wanted to quantify microorganisms in an activated sludge bioreactor. Plate count analysis showed 10^4 microorganisms/mL mixed liquor. However, the number increased to 10^5 for the same volume in microscopic observation. Please explain the discrepancy in quantifying microorganisms between the two methods.

2.3 Glucose ($C_6H_{12}O_6$) is completely oxidized as shown the following chemical equation. Molecular weights of C, H, and O are 12, 1, and 16, respectively.

$$C_6H_{12}O_6 + 6O_2 \rightarrow 6CO_2 + 6H_2O$$
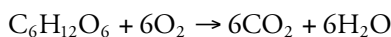
a. If 180 mg of glucose is dissolved in 1 L of deionized water, what is the value of theoretical oxygen demand (ThOD) of the water in mg/L?

    b. A 5-day BOD measurement of the water was 150 mg/L. What is the reason of the difference between the ThOD and BOD?

    c. Some people want to measure the concentration of glucose as the content of carbon, instead of measuring oxygen, which is called "total oxygen carbon (TOC)." What is the concentration of TOC of the water?

2.4 Adenosine triphosphate (ATP) is an energy carrying molecule used for biosynthesis and maintenance of bacteria. How many ATP molecules can be theoretically produced when a glucose molecule is completely oxidized into carbon dioxide and water by aerobic bacteria? Estimate the numbers based on the free energy values of ATP synthesis and glucose oxidation as follows:

$$ADP\,(\text{adenosine diphosphate}) + P_i\,(\text{phosphate}) \rightarrow ATP \quad \Delta G^{\circ\prime} = +32 \text{ kJ}$$

$$\text{Glucose} + 6O_2 \rightarrow 6CO_2 + 6H_2O \quad \Delta G^{\circ\prime} = -2882 \text{ kJ}$$
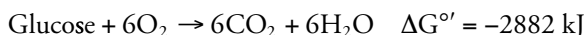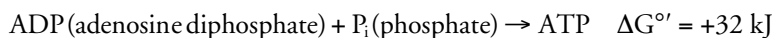
The calculated numbers are known to be much higher than the produced ATP molecules in bacteria. What are the possible reasons of lower numbers of ATP than those of calculation?

2.5 The following are the half reactions and their standard Gibbs free energy at $pH = 7.0$ for electron donors and electron acceptors, respectively. Combination of an electron donor half reaction and an electron can generate a bacterial energy generation reaction. Determine the order of energy generation reactions from the highest to the lowest by free energy at standard state and $pH = 7.0$. Note that oxidized chemicals are presented in the left sides for all of the half reactions.

(Electron donor half reactions)

$$\frac{1}{8}CO_2 + \frac{1}{8}HCO_3^- + H^+ + e^- = \frac{1}{8}CH_3COO^- + \frac{3}{8}H_2O;$$

$$\Delta G^{\circ\prime} = +27.40 \text{ kJ/e}^- \text{ equivalent}$$

$$H^+ + e^- = \frac{1}{2}H_2 \; ; \Delta G^{\circ\prime} = +39.87 \text{ kJ/e}^- \text{ equivalent}$$

$$\frac{1}{6}NO_2^- + \frac{4}{3}H^+ + e^- = \frac{1}{6}NH_4^- + \frac{1}{3}H_2O;$$
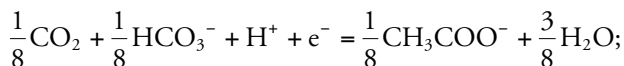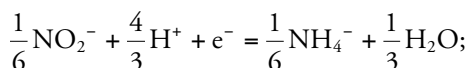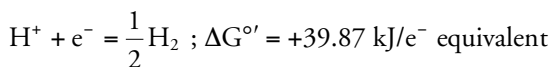
$$\Delta G^{\circ\prime} = -32.93 \text{ kJ/e}^- \text{ equivalent}$$

(Electron acceptor half reactions)

$$\frac{1}{4}O_2 + H^+ + e^- = \frac{1}{2}H_2O; \quad \Delta G^{\circ\prime} = -78.72 \text{ kJ/e}^- \text{ equivalent}$$

$$\frac{1}{5}NO_3^- + \frac{6}{5}H^+ + e^- = \frac{1}{10}N_2 + \frac{3}{5}H_2O; \quad \Delta G^{\circ\prime} = -77.20 \text{ kJ/e}^- \text{ equivalent}$$

$$Fe^{3+} + e^- = Fe^{2+}; \quad \Delta G^{\circ\prime} = -74.27 \text{ kJ/e}^- \text{ equivalent}$$
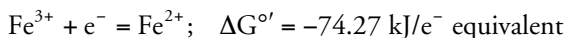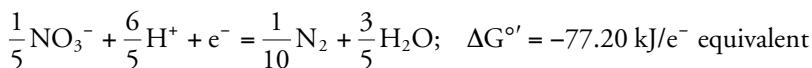
2.6 A chemical plant generates wastewater mostly containing methanol (CH_3OH). The treatment of methanol wastewater requires an external nitrogen addition because the influent wastewater does not contain a nitrogen source. The two nitrogen sources available are ammonia or nitrate. In order to estimate the amount of nitrogen required, an engineer wants to construct a balanced stoichiometric equation representing the microbial treatment of methanol. Determine the stoichiometric equations for methanol wastewater treatment under aerobic conditions for the two different nitrogen sources. Assume that the growth yield is 0.6 g biomass/g methanol irrespective of the nitrogen source. Inclusion of nitrate in a stoichiometric equation may cause imbalance in charges. In this case, balance the charges by including hydrogen ion (H^+).

2.7 To determine growth yield and oxygen consumption for wastewater treatment, an experiment was conducted using domestic wastewater. Experimental data showed 195.8 g carbon dioxide was produced by consuming of 222.4 g oxygen. Assume that bacteria use domestic wastewater as energy and carbon sources and oxygen as electron acceptor. The chemical formula for wastewater and bacteria are $C_{10}H_{19}O_3N$ and $C_5H_7O_2N$, respectively, and ammonia (NH_3) is present in the influent wastewater.

a. Determine the growth yield of the aerobic bacteria.
b. Calculate the theoretical oxygen requirement for treating the domestic wastewater. The wastewater flow rate is 1000 m^3/day and its COD concentration is 500 g COD/m^3.

2.8 A food company produces 1000 m^3 of wastewater daily. The results of a COD analysis of the wastewater were 2000 g/m^3. Wastewater was treated using a bioreactor via the following stoichiometry:

$$C_8H_{12}O_3N_2 + 3O_2 \rightarrow C_5H_7O_2N + NH_3 + 3CO_2 + H_2O$$
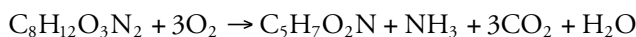
where
$C_8H_{12}O_3N_2$ is the wastewater
$C_5H_7O_2N$ is the produced biomass

a. Calculate the biomass yield in g COD biomass per g COD wastewater treated.
b. Assume that wastewater is completely treated. Estimate the sludge production in kg biomass per day.
c. Assume that wastewater is completely treated. Estimate theoretical oxygen requirement in kg O_2 per day.

2.9 A membrane manufacturer reported that bioreactor solids concentrations greater than 10,000 mg VSS/L would be detrimental to the submersed membrane units due the increased membrane fouling rate. An engineer wants to design a bioreactor operated under the limiting condition of solids concentration (i.e., <10,000 mg VSS/L). Calculate the minimum reactor volume satisfying the solids concentration limit and the following conditions:

▪ Bioreactor number and type: one complete-stirred-tank reactor
▪ Wastewater inflow: 10,000 m^3/day
▪ Wastewater characteristics
   Inert volatile suspended solids concentration: 50 mg/L
   Influent biodegradable COD concentration: 500 mg/L
▪ Kinetic parameters

$$k = 12.5 \text{ g COD/g VSS} \cdot \text{day}$$

$$K_s = 10 \text{ g COD/m}^3$$

$$Y = 0.40 \text{ g VSS/g COD}$$

$$f_d = 0.15 \text{ g VSS/g VSS}$$

$$k_d = 0.10 \text{ g VSS/g VSS} \cdot \text{day}$$

2.10 Calculate the hydraulic retention time (hours) of an MBR bioreactor satisfying the target solids concentration (=10,000 mg VSS/L). Suspended solids concentration indicates the sum of the concentration of active biomass and inert material (i.e., $X_T = X + X_i$). Assume that the influent flow rate is 1000 m^3/day, the influent substrate concentration is 400 mg COD/L, influent inert solids concentration is 30 mg VSS/L, and SRT is 20 days. Use the following kinetic parameters for the calculation:

$$k = 12.5 \text{ g COD/g VSS} \cdot \text{day}$$

$$K_s = 10 \text{ g COD/m}^3$$

$$Y = 0.40 \text{ g VSS/g COD}$$

$$f_d = 0.15 \text{ g VSS/g VSS}$$

$$k_d = 0.10 \text{ g VSS/g VSS} \cdot \text{day}$$

2.11 The food to microorganism (F/M) ratio and the organic volumetric loading rate (OLR) are the two major parameters that have been used for designing the volume of bioreactors. Typical values of the F/M ratio and OLR for designing CAS systems are 0.3–0.6 kg COD/kg MLVSS·day and 1.1–1.6 kg COD/m³·day, respectively. The F/M ratio and OLR are defined as follows:

$$F/M \, ratio = \frac{QS_0}{VX_T}$$

$$OLR = \frac{QS_0}{V(10^3 \, g/kg)}$$

where
    Q is the influent wastewater flow rate
    S_0 is the influent COD (or BOD) concentration
    V is the bioreactor volume
    X_T is the total solids concentration ($=X+X_i$)

Using the conditions provided in the previous problem, calculate the F/M ratio and OLR, and compare the calculated values with the typical values used for designing CAS systems.

2.12 Determine the SRT when the active biomass (X) and inert material (X_i) concentrations are the same in an MBR plant. The influent wastewater concentration (S_0) and influent inert material concentration ($X_{i,0}$) are 400 g COD/m³ and 20 g VSS/m³, respectively. The kinetic parameters are as follows:

$$k = 12.5 \, g \, COD/g \, VSS \cdot day$$

$$K_s = 10 \, g \, COD/m^3$$

$$Y = 0.40 \, g \, VSS/g \, COD$$

$$f_d = 0.15 \, g \, VSS/g \, VSS$$

$$k_d = 0.10 \, g \, VSS/g \, VSS \cdot day$$

2.13 Set up a balanced microbial stoichiometric equation for a reaction occurring in anoxic conditions (e.g., denitrification). Assume the wastewater is the primary electron donor and carbon source, while nitrate is the terminal electron acceptor. Assume that the main reactants are wastewater ($C_{10}H_{19}O_3N$) and nitrate (NO_3^-), while biomass ($C_5H_7O_2N$), carbon dioxide (CO_2), and water (H_2O) are the main reaction products. In addition, the biomass yield is 0.4 g biomass/g wastewater. Using the microbial stoichiometric equation, calculate the theoretical concentration of wastewater per unit concentration of nitrate removal in mg COD/mg NO_3–N.

2.14 In order to determine kinetic parameters used for designing an MBR plant, a set of bioreactors were operated with different SRT conditions. The following table shows the influent substrate, effluent substrate, and biomass concentrations when steady-state conditions were reached. Influent and effluent substrates are mostly consisted of dissolved organic matters. Estimate the four essential kinetic parameters (Y, k, K_s, k_d) using the dataset.

SRT (Days)	S_0 (mg COD/L)	S (mg COD/L)	X (mg VSS/L)
1	400	55.0	160
2	400	8.0	165
3	400	4.1	170
5	400	1.7	190
10	400	0.7	200

2.15 Calculate the SRT of a bioreactor in days satisfying the condition in which the concentrations of biomass (X) and inert biomass (X_i) are same. Assume that the bioreactor is a completely stirred tank reactor with a 0.25-day HRT. The influent wastewater concentration (S_0) and influent inert material concentration ($X_{i,0}$) are 400 g COD/m³ and 20 g VSS/m³, respectively. The kinetic parameters and their values at the operating temperature are as follows:

$$k = 12.5 \text{ g COD/gVSS} \cdot \text{day}$$

$$K_s = 10 \text{ g COD/m}^3$$

$$Y = 0.40 \text{ g VSS/g COD}$$

$$f_d = 0.15 \text{ g VSS/g VSS}$$

$$k_d = 0.10 \text{ g VSS/g VSS} \cdot \text{day}$$

2.16 A wastewater operator wants to use wastewater generated from a food factory for improving denitrification. It is reported that the major component of the wastewater is propionic acid (CH_3CH_2COOH). Calculate the theoretical requirements of propionate for 1.0 g of nitrate nitrogen reduction.

2.17 Estimate the nitrogen removal efficiency for an MBR plant consisting of an anoxic and an aerobic tank. The operating and design conditions are follows:

- Wastewater inflow: 10,000 m³/day
- Recycle flow from the aerobic tank to anoxic tank: 20,000 m³/day

- ■ Wastewater characteristics
  Inert volatile suspended solids concentration: 50 mg/L
  Influent biodegradable COD concentration: 500 mg/L
  Influent total nitrogen: 50 mg/L
- ■ Kinetic parameters

$$k = 12.5 \text{ g COD/g VSS} \cdot \text{day}$$

$$K_s = 10 \text{ g COD/m}^3$$

$$Y = 0.40 \text{ g VSS/g COD}$$

$$f_d = 0.15 \text{ g VSS/g VSS}$$

$$k_d = 0.10 \text{ g VSS/g VSS} \cdot \text{day}$$

Assume that complete nitrification in the aerobic tank and complete denitrification in the anoxic tank.

2.18 Estimate recycle flow from the aerobic tank to the anoxic tank in m³/day required to achieve 80% nitrogen removal efficiency. Assume that the operational conditions and kinetic information are the same as the previous problem except for the recycle activated sludge flow.

2.19 Estimate the maximum SRT required to produce an effluent phosphorus concentration of 2.0 mg/L when the influent phosphorus concentration is 5 mg P/L, COD removal within the bioreactor = 350 mg/L, Y = 0.40 g VSS/g COD, f_d = 0.15 g VSS/g VSS, k_d = 0.10 g VSS/g VSS·day, and P content of cell mass = 6%.

2.20 In 1999, the bacteria responsible for anaerobic ammonium oxidation called anammox bacteria were indentified. Basic stoichiometry of ammonium oxidation by anammox bacteria can be expressed as

$$NH_4^+ + NO_2^- \rightarrow N_2 + 2H_2O$$
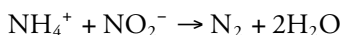
These bacteria can be beneficially used to remove nitrogen during wastewater treatment. The processes utilizing anammox bacteria reduce nitrite (NO_2^-) into gaseous nitrogen (N_2) without using carbon sources for denitrification. In addition, the processes are working without provision of air for nitrification. Nevertheless, the processes need nitrite as the terminal electron acceptor. Nitrite is generally produced by aerobic AOB. The stoichiometric equations for AOB and NOB are as follows:

$$2NH_4^+ + 3O_2 \rightarrow 2NO_2^- + 2H_2O + 4H^+$$

$$2NO_2^- + O_2 \rightarrow 2NO_3^-$$

   a. 1000 kg of NH_4^+–N is continuously fed to a wastewater treatment plant daily. In the treatment plant nitrogen is removed by a postanoxic process (i.e., aerobic and anoxic tanks in series). How much of oxygen is required for the oxidation of ammonium into nitrate using AOB and NOB. Neglect assimilation of ammonium into cells for the estimation.
   b. Calculate the amount of methanol (CH_3OH) in kg per day for denitrification of the nitrate produced by above nitrification step. Assume that there are no carbon sources for denitrification in influent wastewater.
   c. How much of aeration and methanol addition can be saved if the nitrogen removal process is fulfilled by anammox bacteria. Note that ammonium should be initially oxidized into nitrate by AOB for anammox reaction.

References

Amann, R. I., Ludwig, W., and Schleifer, K. H. (1995) Phylogenetic identification and in situ detectionof individual microbial cells without cultivation, *Microbiology and Molecular Biology Reviews*, 59(1): 143–169.

Barr, J., Slater, F. R., Fukushima, T., and Bond, P. L. (2010) Evidence for bacteriophage activity causing community and performance changes in a phosphorus-removal activated sludge, *FEMS Microbiology Ecology*, 74(3): 631–642.

Black, J. G. (2008) *Microbiology*, 7th edn. John Wiley & Sons, Inc., Hoboken, NJ.

Irving, L. G. and Smith, F. A. (1981) One-year survey of enteroviruses, adenoviruses, and reoviruses isolated from effluent at an activated-sludge purification plant, *Applied and Environmental Microbiology*, 41(1): 51–59.

Kotaya, S. M., Dattab, T., Choi, J., and Goel, R. (2011) Biocontrol of biomass bulking caused by *Haliscomenobacter hydrossis* using a newly isolated lytic bacteriophage, *Water Research*, 45(2): 694–704.

Madigan, M. T., Matinko, J. M., and Parker, J. (2000) *Brock: Biology of Microorganisms*. Prentice-Hall Inc., Upper Saddle River, NJ.

Mino, T., van Loosdrecht, M. C. M., and Heijnen, J. J. (1998) Microbiology and biochemistry of the enhanced biological phosphate removal process, *Water Research*, 32(11): 3193–3207.

Park, H.-D., Wells, G. W., Bae, H., Criddle, C. S., and Francis, C. A. (2006) Occurrence of ammonia-oxidizing archaea in wastewater treatment plant bioreactors, *Applied and Environmental Microbiology*, 72(8): 5643–5647.

Pollice, A., Laera, G., Saturno, D., and Giordano, G. (2008) Effects of sludge retention time on the performance of a membrane bioreactor treating municipal sewage, *Journal of Membrane Science*, 317(1–2): 65–70.

Randal, C. W., Barnard, J. L., and Stensel, H. D. (1992) Design of activated sludge biological nutrient removal plants. In *Design and Retrofit of Wastewater Treatment Plants for Biological Nutrient Removal*, Randal, C. W., Barnard, J. L., and Stensel, H. D. (eds.). Technomic Publishing, Lancaster, PA.

Rittmann, B. E. and McCarty, P. L. (2000) *Environmental Biotechnology: Principles and Applications*. McGraw-Hill Higher Education, Boston, MA.

Song, K.-G., Kim, Y., and Ahn, K.-H. (2008) Effect of coagulant addition on membrane fouling and nutrient removal in a submerged membrane bioreactor, *Desalination*, 221(1–3): 467–474.

Tchobanoglous, G., Burton, F. L., and Stensel, H. D. (2003) *Wastewater Engineering: Treatment and Reuse*, 4th edn. McGraw-Hill, New York.

US EPA (1993) Manual: Nitrogen control. Environmental Protection Agency, Washington, DC.

Wagner, M. and Loy, A. (2002) Bacterial community composition and function in sewage treatment systems, *Current Opinion in Biotechnology*, 13: 218–227.

Wells, G. F., Park, H.-D., Yeung, C.-H., Eggleston, B., Francis, C. A., and Criddle, C. S. (2009) Ammonia-oxidizing communities in a highly aerated full-scale activated sludge bioreactor: Betaproteobacterial dynamics and low relative abundance of Crenarchaea, *Environmental Microbiology*, 11(9): 2310–2328.

Woese, C. and Fox, G. (1977) Phylogenetic structure of the prokaryotic domain: The primary kingdoms, *Proceedings of the National Academy of Science of the United States of America*, 74(11): 5088–5090.

Chapter 3

Membranes, Modules, and Cassettes

In membrane bioreactor (MBR) processes, microorganisms and membranes make up the major treatment technologies. We covered microorganisms in Chapter 2, and in this chapter we will discuss membrane technologies. The scope of this chapter includes everything from membrane materials to the basic processes of membrane products.

3.1 Membrane Separation Theories

There are two mechanisms by which particles are separated from liquids via filters: The first is depth filtration and the other is screen filtration.

In depth filtration, while the average pore diameter of a filter is often 10 times bigger than that of the smallest particle that is able to go through the pores, depth filters can separate particles from liquids. Some particles are rejected at small constrictions within the filter, while others by adsorption as they permeate the membrane through a tortuous path. The main mechanism of depth filtration is adsorption. There must be some saturation point of desorption in which particles are no longer removed by the filter. At this point, the filter should be regenerated by flushing out adsorbed particles or by substituting it with a new membrane. Examples of depth filtration include granulated activated carbon column filters, sand filters, and dual-media filters.

Screen filters contain surface pores smaller than the particles to be removed, which is called a sieving mechanism. In this mechanism, when particles in the source water (influent water) side are rejected and accumulate on the surface of

the membrane, particles smaller than the diameter of the surface pores can also be rejected. This results in good rejection performance, but high particle accumulation should be taken into account. Most microfiltration (MF) and ultrafiltration (UF) membranes for MBR processes are screen filters.

When particles in the source water are filtered by membranes, complex transport mechanisms need to be considered, which usually pertain not only to the interaction of particles with the external membrane surfaces and internal pore walls but also to the carrying of influent water. We divided the particle separation phenomenon by membranes into two discussion topics: One is the transport of suspended particles to the surface of MF and UF membranes and the other is the transport of water molecules through the membrane pores.

3.1.1 Transport of Suspended Particles to the Surface of Membranes and Particle–Membrane Interactions

The mechanism of fluid transport in fluid–solid separation is mainly viscous flow in the case of liquid suspensions. Usually, the flow field inside the membrane is calculated as the result of the action of an externally applied pressure drop across both sides of the membrane where influent flows in and effluent flows out as a driving force for particle separation.

Mechanisms of permeation through or rejection from a membrane depend not only on the relative size of the suspended particles and membrane pores but also on particle–wall interactions. Figure 3.1 shows the full transport mechanism of suspended particles to the membrane surface. Suspended particles approach the membrane surface by convection or diffusion. The main stream resulting in
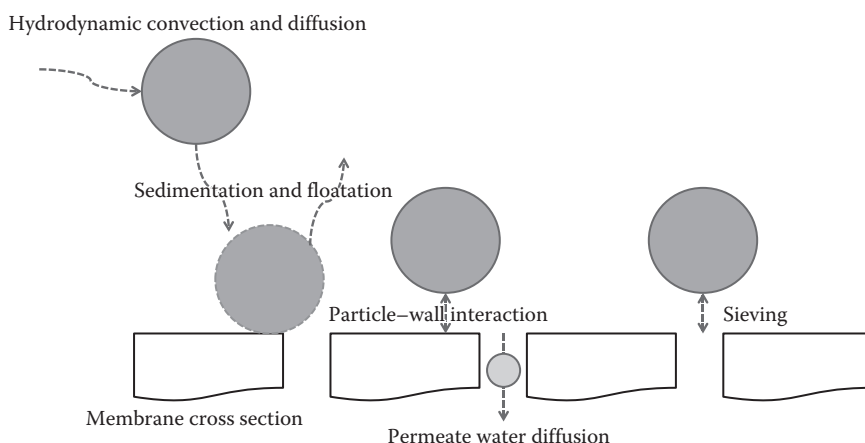
Figure 3.1   Transport mechanism of suspended particles to the surface of membranes.

convection of particles originates from the difference of levels or hydraulic pressure. In the vicinity of the membrane, particles approach (sedimentation) and depart from (flotation) the membrane surface until an equilibrium state is reached where these sedimentation and flotation rates become equal.

Particles approaching or departing from the membrane surface interact with the membrane wall, and there, particles are rejected by the sieving mechanism. Water molecules smaller than the membrane pores go through inner pores by diffusion and in some cases by hydraulic pressure (transmembrane pressure; see Section 3.5.1). The main types of particle transport and particle–membrane interaction mechanisms are summarized later.

3.1.1.1 Hydrodynamic Convection

Particles are, in general, carried along by the hydrodynamic pressure difference between the inflow and permeate flow or concentrate flow. As the particles approach the pore walls, significant hydrodynamic resistance hinders their collision with the solid surface, which increases rapidly with decreasing clearance and tends to infinity upon contact if both the particle and the wall are nonporous. If at least one of the two bodies is permeable, then the hydrodynamic resistance remains finite as the stress that is applied to the fluid is dissipated into the porous body.

Because of the great significance of these phenomena, intensive analytical and numerical efforts have been made to calculate correction factors for the classical Stokes hydrodynamic force expression for both porous and nonporous bodies during normal or tangential motion of the particles relative to the pore wall. It is also interesting to note that in the vicinity of the wall, the hydrodynamic torque becomes considerable giving rise to particle rotation prior to potential capture.

3.1.1.2 Sedimentation and Flotation

Gravitational effects are usually significant for particles larger than about 1 μm. General influent in wastewater treatment contains particles mostly larger than 1 μm. Therefore, gravitation is a dominant mechanism in the approach of particles to a membrane surface utilizing the convection mechanism. Depending on the relative density of particles to that of the carrying fluid, sedimentation or flotation may arise. Nevertheless, in most cases gravitational effects act in combination with other migration mechanisms, like hydrodynamically driven migration. When the distance between particles and membrane wall is very close, other mechanisms begin to be dominant: (1) electrokinetic double-layer interaction and (2) van der Waals force.

3.1.1.3 Particle–Wall Interaction

In the vicinity of the pore walls, particle–surface interactions become significant, and as the particle approaches the wall, they become dominant. Usually, van der

Waals and electrokinetic double-layer interactions determine the motion of particles in the close vicinity of the pore walls. Attraction is caused by the former and, usually, also by the latter in most cases—depending on the sign of surface and solution charges—to a net repulsion at clearances smaller than a critical value due to the switch of the double-layer forces to rapidly increasing repulsive ones.

Despite the obvious need for estimates of the physicochemical constants to describe quantitatively these interactions, it has been shown that once these constants are below or above some critical values, the particle retention rate is not sensitive to the precise value of these constants. It must be stressed that in nanofiltration (NF; later discussed) membranes, where the pore size is usually smaller than 10 nm and many charging particles such as ions are rejected by and accumulated on the membrane surface, such electrokinetic phenomena may become dominant and extend over the entire membrane domain resulting, in many cases, in quite high rejection rates.

3.1.1.4 Sieving

Size exclusion–based separation is theoretically the simplest mechanism of retention of suspended particles that can also lead to very high filtration efficiencies. However, a small pore size usually implies unacceptably low permeation, which decreases further during filter operation due to the creation of a cake, or a buildup of retained particles, on the feed side of the membrane requiring some special treatment for its removal, typically backwashing.

3.1.1.5 Particle Diffusion

In liquid filtration, Brownian diffusion may become a significant transport mechanism for submicron particles (<1 μm). For sufficiently small values of the d_{par}/d_p ratio where d_{par} is the effective particle diameter and d_p is the effective pore diameter, whether particles are rejected by membrane pores or not can be determined by treating the system as a mass diffusion process that can be described by the classical diffusion equation (Equation 3.1). In this case, the ordinary diffusion coefficient is replaced by the Brownian diffusivity (BD), given by

$$BD = \frac{C_s k_B T}{3\pi\mu d_{par}} \tag{3.1}$$

where
  C_s is the Cunningham correction factor, unitless
  k_B is the Boltzmann constant, J/K or $(kg\ m^2/s^2)$ K
  T is the absolute temperature, K
  d_{par} is the effective particle diameter, m
  μ is the viscosity of water, kg/m s

If both hydrodynamic drag and Brownian forces are significant, particle displacement results from the combination of a convective step (determined solely by the local fluid velocity and the time step) and a Brownian step (of random direction and with magnitude that is determined by the BD and the time step).

Example 3.1

Calculate the BD of particles that have 10 μm of diameter flows in water at 20°C in given conditions. Use the information of the Cunningham correction factor C_s at a given temperature in Table 3.1.

Solution

In Table 3.1 two literatures show the Cunningham correction factor of 10.0 μm diameter of particles at a given temperature, which is 1.02, and the viscosity of water at 20°C is 1.002×10^{-3} kg/m s. Therefore the BD of the particles can be calculated using Equation 3.1 as follows:

$$\mathrm{BD} = \frac{C_s k_B T}{3\pi\mu d_{par}} = \frac{(1.02)(1.38 \times 10^{-23} \text{ (kg m}^2/\text{s}^2) \text{ K})(298 \text{ K})}{(3)(\pi)(1.002 \times 10^{-3} \text{ (kg/m) s})(10^{-5} \text{ m})} = 4.44 \times 10^{-14} \text{ m}^2/\text{s}$$

Table 3.1   Cunningham Correction Factors in Two Literatures

d_p (μm)	Cunningham Correction Factor, C_s	
	Davies (1945)	*Allen and Raabe (1982)*
0.01	22.7	22.4
0.02	11.6	11.6
0.05	5.06	5.09
0.1	2.91	2.94
0.2	1.89	1.90
0.5	1.34	1.32
1	1.17	1.16
2	1.08	1.08
5	1.03	1.03
10	1.02	1.02
20	1.01	1.01

3.1.2 Transport Theory of Water Molecules through MF and UF Membranes

The Hagen–Poiseuille equation considers membranes as a number of parallel cylindrical pores perpendicular or oblique to the membrane surface, and there is Laminar flow through a capillary of radius R_p. The water flow per cylindrical pore is given by

$$Q_c = \frac{\pi R_p^4}{8\mu} \times \frac{\Delta P}{\Delta x} \tag{3.2}$$

where
μ is the viscosity of water, Pa s
ΔP is the pressure difference, Pa
Δx is the membrane thickness, μm
R_p is the pore diameter, μm

If the membrane has N number of capillary pores, then the total flow through the membrane (Q_p or Q_w) is

$$Q_p \quad \text{or} \quad Q_w = NQ_c \tag{3.3}$$

And effective membrane pore area (A) is calculated as follows:

$$A = \frac{N\pi R_p^2}{\varepsilon} \tag{3.4}$$

where
N is the number of pores
ε is the porosity of membrane, unitless

The permeate flux through a membrane is the permeate flow divided by the effective area of flow surface and is given by

$$J_w = \frac{NQ_c}{A} = \frac{NQ_c}{\left(N\pi R_p^2/\varepsilon\right)} = \frac{N\left(\left(\pi R_p^4/8\mu\right) \times (\Delta P/\Delta x)\right)}{\left(N\pi R_p^2/\varepsilon\right)} = \frac{\varepsilon R_p^2}{8\mu} \times \frac{\Delta P}{\Delta x} \tag{3.5}$$

In reality, pores are not straight, so the previous equation should include a factor for the tortuosity of pores (τ) and $\varepsilon R_p^2/8\mu\tau$. This factor is abbreviated as K_p and is called hydraulic permeability:

$$J_w = \frac{\varepsilon R_p^2}{8\mu\tau} \times \frac{\Delta P}{\Delta x} = K_p \times \frac{\Delta P}{\Delta x} \tag{3.6}$$

Meanwhile Kozeny and Carman (1939) assumed that membranes are a system of closely packed spheres and derived permeate flux as follows:

$$J_w = \frac{\varepsilon^3}{(1-\varepsilon^2)\mu K S^2} \times \frac{\Delta P}{\Delta x} \tag{3.7}$$

where
  ε is the porosity of the membrane, unitless
  S is the internal surface area, m^2
  K is the Kozeny–Carman constant depending on the shape of pores and tortuosity, unitless

Equation 3.7 is called the Kozeny–Carman equation. Note that the "$\varepsilon^3/(1-\varepsilon^2)$ $\mu K S^2$" term is equal to K_p in the Hagen–Poiseuille equation.

  The real structure of pores of MF and UF membranes are not cylindrical or closely packed spheres but spongelike in the case of non-solvent-induced phase separation (NIPS) membranes (see Section 3.3.1). Therefore, the pore pathway is very complex and not linear, which results in a deviation between the observed permeation flux and the calculated value.

Example 3.2

Assume that the pore shape of a membrane is cylindrical and the membrane has only one pore with a length of 1 mm. Once the inner pore is wet enough and the hydraulic pressure is applied between the two ends of the pore, then water flows from the source water side to the permeate side with a linear velocity of 100 cm/s. Assume that the hydraulic pressure is 0.2 bar and the temperature is a constant 20°C. Calculate the inner diameter of the membrane pore.

Solution

Because the pore shape of the membrane is cylindrical, we can use the Hagen–Poiseuille equation to get the inner diameter of the membrane pore. We have to first calculate the flow rate per cylindrical pore by multiplying the linear velocity of the cross-sectional area:

$$Q_c = v \times \pi R_P^2 = \frac{\pi R_P^4}{8\mu} \times \frac{\Delta P}{\Delta x}$$

$$v = \frac{R_P^2}{8\mu} \times \frac{\Delta P}{\Delta x}$$

$$R_P = \sqrt{8\mu v \times \frac{\Delta x}{\Delta P}}$$

$$R_P = \sqrt{((8)(1.002 \times 10^{-3} \text{ Pa s})(10^3 \text{ μm} \times 10^6 \text{ μm/s})/((\pi)(0.2 \times 10^5 \text{ Pa}))} = 11.3 \text{ μm}$$

Therefore the inner diameter of the membrane pore is 11.3 μm.

Example 3.3

When a membrane that has N numbers of cylindrical pores permeates water at a flow rate of 45.0 mL/min, the transmembrane pressure is 0.4 bar and the membrane pore size is 0.1 μm. If the membrane thickness is 0.12 mm and both the width and length are 5.0 mm, calculate the pore density as a unit of the number of pores per membrane area. During the operation, the temperature is 20°C and is constant.

Solution

When we combine Equations 3.2 and 3.3, the pore density can be expressed as follows:

$$Q_P = N \times Q_c = N \times \frac{\pi R_P^4}{8\mu} \times \frac{\Delta P}{\Delta x}$$

$$N = Q_P \times \frac{8\mu}{\pi R_P^4} \times \frac{\Delta x}{\Delta P}$$

$$\text{Pore density} = \frac{N}{A} = \frac{Q_P}{W \times L} \times \frac{8\mu}{\pi R_P^4} \times \frac{\Delta x}{\Delta P}$$

$$\text{Pore density} = \frac{45.0/60 \text{ cm}^3/\text{s}}{(0.5 \text{ cm})(0.5 \text{ cm})} \times \frac{(8)(1.002 \times 10^{-3} \text{ Pa s})}{(\pi)(0.1 \times 10^{-4} \text{ cm})^4} \times \frac{0.012 \text{ cm}}{0.2 \times 10^5 \text{ Pa}}$$

Therefore, the pore density is 4.59 ea/cm².

3.2 Membrane Materials

A survey of the scientific and patent literature indicates that over 130 materials have been used to manufacture membranes. However, only a few have been commercialized. In water and wastewater treatment, there are several limitations that reduce the number of materials available. Membranes are expected to have high acidic, basic, chemical, and mechanical durability for more than 5 years of operation. Membranes should be operated in the pH range of 4–10, but membranes can be exposed to pH values of 1–12 during recovery cleaning. They might be exposed to diverse kinds of unknown toxic chemicals including oxidants such as chlorine and hypochlorite, along with high shear forces from water and air during long periods of operation.
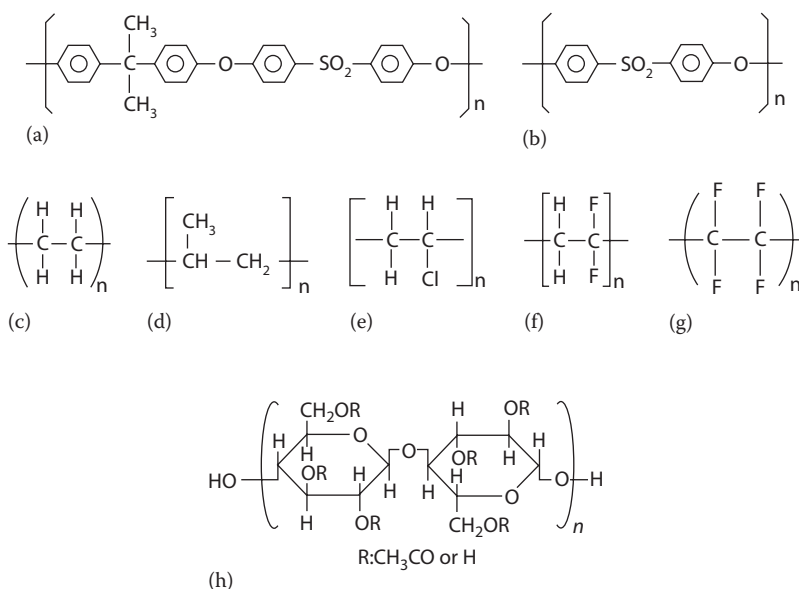
Figure 3.2 Molecular structure of the most commonly used polymers for membranes: (a) PSF, (b) PES, (c) PE, (d) PP, (e) PVC, (f) PVDF, (g) PTFE, and (h) CA.

Therefore, we must use robust materials such as engineering plastics, stainless steel, and ceramic materials to satisfy these operating conditions. In this chapter we focus on polymer-based membranes that dominate the water and wastewater treatment membrane market, including MBR. Figure 3.2 shows the molecular structures of the most commonly used polymers for membrane construction in water and wastewater treatment. Table 3.2 shows the properties of polymers for membrane fabrication.

3.2.1 Polysulfone

Polysulfones (PSFs) are one of the widely used engineering plastics and were introduced in 1965 by Union Carbide. Due to the high cost of raw materials and processing, PSFs are used in specialty applications and often are a superior replacement for polycarbonates. As a membrane material, PSFs were earlier adapted to medical and pharmaceutical processes such as dialysis and separation of pyrogen because of their minimal leaching during operation compared to other materials. Additionally, filter cartridges made from PSF can be sterilized with inline steam or in an autoclave up to 50 times without loss of integrity. Furthermore, it is easy to control the wide range of pore sizes within the UF to MF range, and even the pore structure can be controlled because of the fast gelation time (hardening time; see Section 3.3.3) of PSF by nonsolvent-induced phase separation.

Table 3.2 Membrane Materials

Polymer	Fabrication	Advantage	Disadvantage
PSF	NIPS	• Easy to form structure • Safe from leaching • High mechanical strength	• Rigid/brittle • Low chemical durability
PES	NIPS	• Easy to form structure • Safe from leaching • High mechanical strength	• Rigid/brittle • Low chemical durability
PE	MSCS	• Low material cost • High elongation	• Wide pore size distribution
PP	MSCS	• Low material cost • High elongation	• Wide pore size distribution
PVC	MSCS	• Low material cost • High elongation	• Wide pore size distribution • Side effect by additives
PVDF	NIPS, TIPS	• Narrow pore size distribution • High chemical durability	• Not easy to form structure • Weak to basic condition
PTFE	MSCS	• High water permeability • Highest chemical durability • Low fouling potential	• Difficult module fabrication • High material cost
CA	NIPS	• Hydrophilic (easily wet) • Easy to from structure	• Low acid/base durability • Low chemical durability

Due to its sulfonated aromatic backbone, PSF has a high degree of rigidity that provides higher mechanical strength, creep resistance, and a higher heat deflection temperature to the membranes. PSF has wider temperatures and pH stability range compared to cellulose acetate (CA). PSF can endure temperatures up to 75°C and can be operated in pH values from 1 to 13. PSF has fairly good chlorine resistance too. However, its chemical durability is weaker than that of polyvinylidene

difluoride (PVDF), polytetrafluoroethylene (PTFE), and polyolefins, so you need to be careful in chemical cleaning PSF with strong acids or bases.

3.2.2 Polyethersulfone

Polyethersulfone (PES) has similar properties to PSF. It is a heat-resistant, transparent, amber, noncrystalline engineering plastic. Natural grade PES can be used up to 100°C. PES is inherently hydrophilic, and PES membranes wet quickly for filtration. The hydrophilic nature of PES leads to no addition of wettability-increasing surfactants (see Section 3.4.2.1). But PES membranes are more brittle than PSF membranes because of their higher glass transition temperature (T_g) and melting point (T_m). This brittleness leads to less durability during long periods of membrane operation even if the stiffness is reduced after the membrane is made wet by water.

3.2.3 Polyolefins: Polyethylene, Polypropylene, and Polyvinylchloride

The best advantage of these materials is directly related to cost. They are popular commodity plastics and can be supplied at very low cost. They show similar tensile strength as PSF or PES but higher tensile strength elongation, so it can be said that they have higher mechanical strength. During operation of polyethylene (PE), polypropylene (PP), or polyvinylchloride (PVC) membranes for water and wastewater treatment, the most serious problem related to permeate quality comes from concentrated source water leakage through broken membrane holes. But as long as the membrane is not broken, even if it is elongated, the permeate quality can be guaranteed. The higher elongation comes from higher elastic properties. Some membrane suppliers apply this property to stronger backwashing processes with relatively higher air pressure to raise the efficiency of membrane performance recovery.

PE, PP, and PVC are more hydrophobic than any other membrane material, and this property makes the membrane pores not easily wet before filtration. It needs an additional wetting agent treatment. Section 3.4 will cover this wetting issue in detail. In addition, their membranes need a different fabrication process (melt spinning cold stretching [MSCS]) that produces a comb-like pore shape. It is not easy to control pore sizes using this method, so most of the membranes made of these materials have 0.2–0.4 μm pore sizes.

3.2.4 Polyvinylidene Difluoride

Compared to conventional membrane materials, such as CA, PSF, and PES, PVDF is now the most widely used membrane material for water and wastewater treatment. PVDF membranes are only available in a narrow range of pore sizes because of their long gelation time during fabrication. However, the long gelation time results in very uniform pore size distributions. Commercialized PVDF membranes

have pore sizes from 0.02 (loose UF) to 0.4 μm (MF). Also PVDF membranes show the highest chemical and chlorine durability among commercialized membranes.

3.2.5 Polytetrafluoroethylene

PTFE is considered the most promising membrane material to replace PVDF membranes in water and wastewater treatment. It is the most stable membrane material to strong acids, bases, chlorine, and most solvents. PTFE membranes also have the widest range of operation pHs (from 1 to 13) and operational temperatures (from –100°C to 260°C). It is extremely hydrophobic, so it gives some range of slip boundary condition that accelerates water flux through membrane pores resulting in extraordinary higher water permeation flux through the pores of PTFE membranes. This is the main reason why PTFE-based membranes show the highest water permeability. But this superhydrophobicity results in poor adhesion properties resulting in an additional potting process (see Section 3.6.1).

3.2.6 Cellulose Acetate

CA was the first material used in membrane fabrication. CA can be obtained from natural sources such as wood pulp or cotton linters, which might be the reason why it became popular initially as a membrane material. CA can provide the widest range of pore sizes and it is also the only material used to manufacture all kinds of membranes in water treatment including MF, UF, NF, and reverse osmosis (RO) membranes. CA is a low-cost, hydrophilic material that minimizes fouling potential.

However, CA has some limitations for wider application. It has a narrow operational temperature and pH range. The maximum allowable operation temperature suggested is 30°C. It can be raised up to 40°C by blending CA with cellulose triacetate (CTA). Normal membrane operation conditions demand, especially in MBR applications, a wide range of operational pH values. Membranes need to be cleaned periodically with chemicals such as acids, bases, and chlorine in order to recover its performance after irreversible fouling has occurred on the surface.

Normal pH values during membrane operation changes from 5 to 9 and during cleaning from 2 to 11, but most CA membranes are restricted to pH 2–8, which is not suitable for recovery chemical cleaning. In addition, CA is highly biodegradable and it is not easy to guarantee a long life span or long-term operation.

3.3 Membrane Fabrication

3.3.1 Membrane Fabrication Methods

There are three major membrane fabrication methods: NIPS, MSCS, and thermal-induced phase separation (TIPS).

NIPS uses the solubility difference of polymers in solvents. There are two solvents used: One is "good solvent," in which the polymer dissolves well in the solvent, and the other is "poor solvent" or nonsolvent, in which the polymer is incompatible with the solvent. However, the two solvents are compatible with each other. When the polymer and "good solvent" solution are injected into the "poor solvent," the "good solvent" is extracted inside of the polymer and "good solvent" solution and forms a solution with the "poor solvent," resulting in the gelation (or hardening) of the polymer.

During the gelation of the polymer, the space where the "good solvent" occupied is converted into membrane pores. After rinsing to remove the residual "good solvent" and "poor solvent" solution and additives, the polymer is dried and acts as a membrane. The shape and dimension of the injection nozzle and the composition of the polymer and "good solvent" in the solution decide the membrane's outer and inner diameter. Most polymers that have "good solvents" and "poor solvents" are adapted in this method. Figure 3.4a shows pores on a membrane surface fabricated by the NIPS process.

Figure 3.3 shows the general structure of polymers. Generally, polymers have either a crystalline lamella structure (rigid) or an amorphous interlamella structure (flexible). Polymers have two transition temperatures: One is the glass transition temperature (T_g) and the other is the melting point (T_m). Generally, T_m is higher than T_g. The amorphous structure becomes very active (more "liquid-like") at temperatures above the T_g, and the crystalline structure becomes very active at temperatures above T_m.

MSCS uses the T_m of polymers that do not have any "good solvents" at room temperature. Melted polymers are cooled to just under the T_m and one or two directional stretching are applied. The crystalline lamella structure in the polymer retains its morphology, but the amorphous interlamella structure in the polymer is lengthened and has larger spaces that can act as membrane pores.

Figure 3.4b shows that these membranes have very anisotropic pore shapes, resulting at a wider pore size distribution than any other method unfavorable for membrane integrity. It is very difficult to control the pore size using this method and it is impossible to make UF membranes. General average pore sizes of commercial membranes fabricated using MSCS are about 0.4 µm. For this reason, MSCS membranes are mainly applied to MBR processes and not drinking water treatment. However, MSCS can produce the cheapest membranes because the price of the main polymers for MSCS, such as PE or PP, is cheap.

TIPS has the intermediate position between NIPS and MSCS in terms of fabrication mechanisms. TIPS uses the difference between solubility and thermal melting point. The TIPS polymer is dissolved by solvents or diluted by diluents at a high temperature, and then it is quenched in cold liquid that extracts the solvents or diluents and induces membrane pores. Sometimes a stretching process is followed to give mechanical strength to the membrane. All polymers that can be used in NIPS or MSCS methods are applicable.
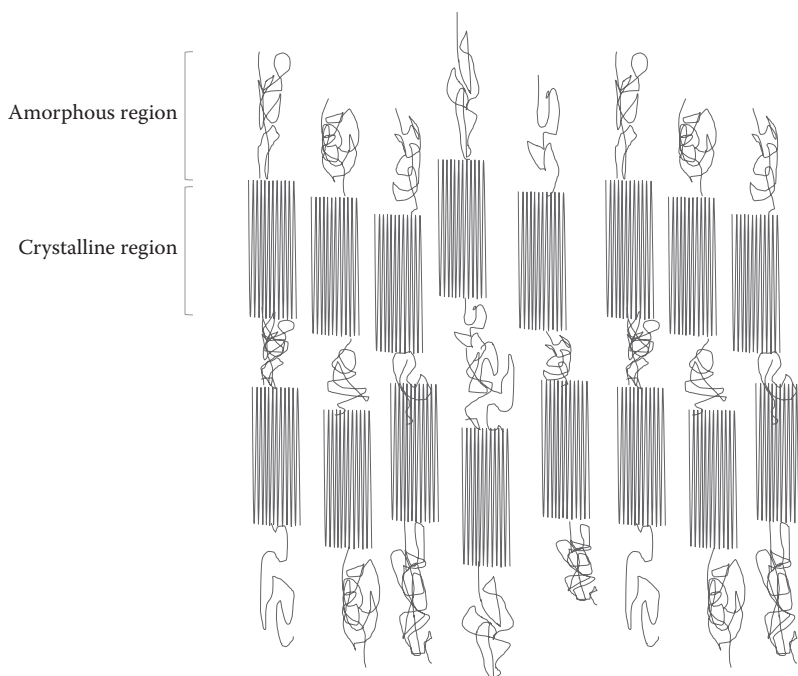
Figure 3.3 Amorphous and crystalline regions in a polymer. Note that the crystalline region (crystallite) has an orderly arrangement of molecules. The higher the crystallinity, the harder, stiffer, and less ductile is the polymer.

Recently, TIPS has been studied intensely in order to address the mechanical weakness of TIPS membranes, which is one of its major problems. But the most popular membrane fabrication method is NIPS. New membranes that both have strong points of TIPS and NIPS have been developed and are braid reinforced membranes. They have a support layer called a braid and membrane layer fabricated by the NIPS process on the surface of the braid. They show the highest tensile strength among all membranes. Their tensile strength is 20–30 kgf/cm² and is 30 times higher than that of any membrane, and they do not easily break during operation.

For the NIPS method, we choose one polymer as the membrane material and two kinds of solvents, a "good solvent" that has a similar solubility parameter to the polymer and a "poor solvent" that does not have a similar solubility parameter.

3.3.2 Solubility Parameter for NIPS and TIPS Processes

The compatibility of a solvent to a polymer, that is to say, the intensity of the dissolution tendency of a polymer into a solvent, is also known as the "solubility
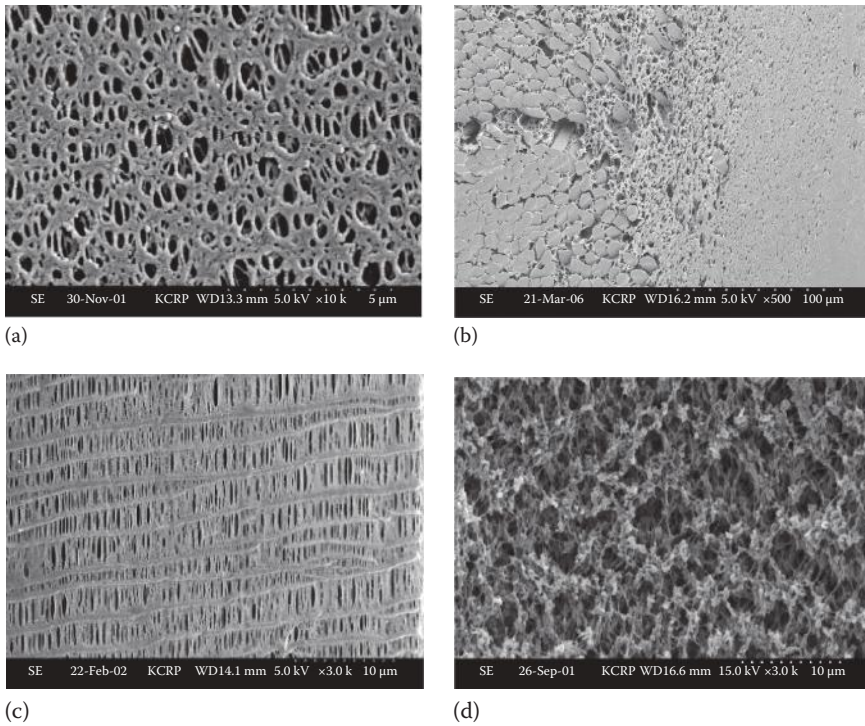
Figure 3.4   Pictures of membranes fabricated by (a) the membrane surface by NIPS, (b) cross section of the reinforced membrane, (c) membrane surface by MSCS, and (d) membrane surface by TIPS.

parameter." A polymer becomes more soluble in a solvent when their relative solubility parameters are close to each other and vice versa. The dissolution of polymers is accompanied by a free energy change, ΔG (J/mol), which can be written as

$$\Delta G = \Delta H - T\Delta S \qquad (3.8)$$

where
   ΔH is the heat of mixing, J/mol
   T is the absolute temperature, K
   ΔS is the entropy of mixing, J/mol K

Since the polymer dissolution involves large changes in entropy, whether ΔG is plus or minus is determined primarily by the magnitude of ΔH. Several methods have been proposed to evaluate ΔH. Among others the following equation proposed by Hildebrand and Scott (1950) is by far the most popular:

$$\Delta H_M = V_M \left[\left(\frac{\Delta E_1}{V_1} \right)^{1/2} - \left(\frac{\Delta E_2}{V_2} \right)^{1/2} \right]^2 \Phi_1 \Phi_2 \qquad (3.9)$$

where
  ΔH_M is the total heat of mixing, J/mol
  V_M is the total molar volume of the mixture, m³/mol
  ΔE is the heat of vaporization or cohesive energy, J/mol
  V is the molar volume, m³/mol
  Φ is the volume fraction
  Subscripts 1 and 2 represent components 1 and 2 of the solution mixture

A physical interpretation of ΔE is the degree of attraction between molecules in a liquid. $\Delta E/V$ in Equation 3.9 is equal to the density of the heat of vaporization and is called the "internal pressure" or "cohesive energy density" of the substance. The quantity $(\Delta E/V)^{1/2}$ is defined as the "solubility parameter" and can be obtained both for the polymer repeating unit and for the solvent and is denoted by δ_{sp}. The solubility parameter can be calculated roughly from the chemical structure of the polymer repeat unit and solvent but can usually be obtained easily from the literature. The solubility parameter can be divided into three components, with each component representing a molecular interaction force of a different kind:

$$\delta_{sp}^2 = \delta_d^2 + \delta_p^2 + \delta_h^2 \qquad (3.10)$$

where
  δ_d^2 is the van der Waals force
  δ_p^2 is the dipole moment
  δ_h^2 is the hydrogen bonding force component

Example 3.4

See solubility parameters in Tables 3.3 and 3.4 and suggest the compatibility of solvents (hexane, N,N-dimethyl formamide (DMF) and water) with each given polymer:
    (a) PE, (b) PAN, and (c) CA (56% acetate groups)

Solution

In Table 3.3 we can see the solubility parameters of hexane, DMF, and water, which are 7.3, 12.1, 23.4 cal/cm³, respectively. In Table 3.4 the solubility parameters of PE, PAN, and CA are 8.0, 12.5, and 27.8 cal/cm³. The best matchups will be PE–hexane, PAN–DMF, and CA–water. We can expect the worst compatibility between water and PE because their solubility parameter difference is the biggest.

Table 3.3   Solubility Parameters for Solvents Commonly Used for Membrane Fabrication

Solvent	δ (cal/cm³)F	H-Bonding Strength
Acetone	9.9	m
Acetonitrile	11.9	p
Amyl acetate	8.5	m
Aniline	10.3	s
Benzene	9.2	p
Butyl acetate	8.3	m
Butyl alcohol	11.4	s
Butyl butyrate	8.1	m
Carbon disulfide	10.0	p
Carbon tetrachloride	8.6	p
Chlorobenzene	9.5	p
Chloroform	9.3	p
Cresol	10.2	s
Cyclohexanol	11.4	s
Diamyl ether	7.3	m
Diamyl phthalate	9.1	m
Dibenzyl ether	9.4	m
Dibutyl phthalate	9.3	m
Dibutyl sebacate	9.2	m
1,2-Dichlorobenzene	10.0	p
Diethyl carbonate	8.8	m
Di(ethylene glycol)	12.1	s
Di(ethylene glycol) monobutyl ether (butyl Carbitol®)	9.5	m
Di(ethylene glycol) monoethyl ether (Carbitol®)	10.2	m
Diethyl ether	7.4	m

Table 3.3 (*Continued*)   Solubility Parameters for Solvents Commonly Used for Membrane Fabrication

Solvent	δ *(cal/cm³)F*	*H-Bonding Strength*
Diethyl ketone	8.8	m
Diethyl phthalate	10.0	m
Di-*n*-hexyl phthalate	8.9	m
Diisodecyl phthalate	7.2	m
N,N-Dimethylacetamide	10.8	m
Dimethyl ether	8.8	m
N,N-dimethylformamide	12.1	m
Dimethyl phthalate	10.7	m
Dimethylsiloxanes	4.9–5.9	p
Dimethyl sulfoxide	12.0	m
Dioctyl adipate	8.7	m
Dioctyl phthalate	7.9	m
Dioctyl sebacate	8.6	m
1,4-Dioxane	10.0	m
Di(propylene glycol)	10.0	s
Di(propylene glycol) monomethyl ether	9.3	m
Dipropyl phthalate	9.7	m
Ethyl acetate	9.1	m
Ethyl amyl ketone	8.2	m
Ethyl *n*-butyrate	8.5	m
Ethylene carbonate	14.7	m
Ethylene dichloride	9.8	p
Ethylene glycol	14.6	s
Ethylene glycol diacetate	10.0	m

(Continued)

Table 3.3 (*Continued*)   Solubility Parameters for Solvents Commonly Used for Membrane Fabrication

Solvent	δ (cal/cm³)F	H-Bonding Strength
Ethylene glycol diethyl ether	8.3	m
Ethylene glycol dimethyl ether	8.6	m
Ethylene glycol monobutyl ether (butyl Cellosolve®)	9.5	m
Ethylene glycol monoethyl ether (Cellosolve®)	10.5	m
Furfuryl alcohol	12.5	s
Glycerol	16.5	s
Hexane	7.3	p
Isopropyl alcohol	8.8	m
Methanol	14.5	s
Methyl amyl ketone	8.5	m
Methylene chloride	9.7	p
Methyl ethyl ketone	9.3	m
Methyl isobutyl ketone	8.4	m
Propyl acetate	8.8	m
1,2-Propylenecarbonate	13.3	m
Propylene glycol	12.6	s
Propylene glycol methyl ether	10.1	m
Pyridine	10.7	s
1,1,2,2-Tetrachloroethane	9.7	p
Tetrachloroethylene (perchloroethylene)	9.3	p
Tetrahydrofuran	9.1	m
Toluene	8.9	p
Water	23.4	s

Table 3.4   Solubility Parameters for Polymers Commonly Used for Membrane Fabrication

Repeating Unit	$\delta\ (cal/cm^3)^{1/2}$
Alphabetical sequence	
Acrylonitrile	12.5
Butyl acrylate	9.0
Butyl methacrylate	8.8
Cellulose	15.6
Cellulose acetate (56% Ac groups)	27.8
Cellulose nitrate (11.8% N)	14.8
Chloroprene	9.4
Dimethylsiloxane	7.5
Ethyl acrylate	9.5
Ethylene	8.0
Ethylene terephthalate	10.7
Ethyl methacrylate	9.0
Formaldehyde (oxymethylene)	9.9
Hexamethylene adipamide (Nylon 6/6)	13.6
n-Hexyl methacrylate	8.6
Isobornyl acrylate	8.2
1,4-*cis*-Isoprene	8.0
Isoprene, natural rubber	8.2
Isobutylene	7.8
Isobornyl methacrylate	8.1
Isobutyl methacrylate	7.2
Lauryl methacrylate	8.2
Methacrylonitrile	10.7
Methyl acrylate	10.0
Methyl methacrylate	9.5
Octyl methacrylate	8.4

(*Continued*)

Table 3.4 (*Continued*)   Solubility Parameters for Polymers Commonly Used for Membrane Fabrication

Repeating Unit	δ (cal/cm³)$^{1/2}$
Propyl acrylate	9.0
Propylene	9.3
Propylene oxide	7.5
Propyl methacrylate	8.8
Stearyl methacrylate	7.8
Styrene	8.7
Tetrafluoroethylene	6.2
Tetrahydrofuran	9.4
Vinyl acetate	10.0
Vinyl alcohol	12.6
Vinyl chloride	9.5
Vinylidene chloride	12.2
Increasing δ value sequence	
Tetrafluoroethylene	6.2
Isobutyl methacrylate	7.2
Dimethylsiloxane	7.5
Propylene oxide	7.5
Isobutylene	7.8
Stearyl methacrylate	7.8
Ethylene	8.0
1,4-*cis*-Isoprene	8.0
Isobornyl methacrylate	8.1
Isoprene, natural rubber	8.2
Lauryl methacrylate	8.2
Isobornyl acrylate	8.2
Octyl methacrylate	8.4

<div align="right">(<i>Continued</i>)</div>

Table 3.4 (*Continued*) Solubility Parameters for Polymers Commonly Used for Membrane Fabrication

Repeating Unit	δ *(cal/cm³)¹ᐟ²*
n-Hexyl methacrylate	8.6
Styrene	8.7
Propyl methacrylate	8.8
Butyl methacrylate	8.8
Ethyl methacrylate	9.0
Butyl acrylate	9.0
Propyl acrylate	9.0
Propylene	9.3
Chloroprene	9.4
Tetrahydrofuran	9.4
Methyl methacrylate	9.5
Ethyl acrylate	9.5
Vinyl chloride	9.5
Formaldehyde (oxymethylene)	9.9
Methyl acrylate	10.0
Vinyl acetate	10.0
Methacrylonitrile	10.7
Ethylene terephthalate	10.7
Vinylidene chloride	12.2
Acrylonitrile	12.5
Vinyl alcohol	12.6
Hexamethylene adipamide (Nylon 6/6)	13.6
Cellulose nitrate (11.8% N)	14.8
Cellulose	15.6
Cellulose acetate (56% Ac groups)	27.8

Example 3.5

Estimate the solubility parameter components δ_d, δ_h, and δ_{sp} of (a) PVA and (b) ethanol using Table 3.5. The structures of the repeat unit of the polymer and ethanol are

$$(a)\ -CH_2-C(OH)H-\quad and\quad (b)\ CH_3CH_2OH$$
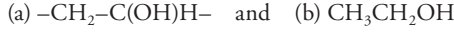
respectively, including 1 ($-CH_2-$), 1 ($-CH-$), 1 ($-OH$) moiety for the repeat unit of PVA and 1 ($-CH_3$), 1 ($-CH_2-$), 1 ($-OH$) moiety for ethanol. Suggest the compatibility of ethanol with PVA.

Solution

$$\delta_d = \frac{\sum F_d}{V_m} = \frac{499.8 \times 1000^{0.5}\ J^{0.5}\ L^{0.5}/mol}{28.1\ L/mol} = 562.5\ J^{0.5}/L^{0.5}$$

$$\delta_p = \frac{\sqrt{\sum F_p^2}}{V_m} = \frac{400.0 \times 1000^{0.5}\ J^{0.5}\ L^{0.5}/mol}{28.1\ L/mol} = 450.1\ J^{0.5}/L^{0.5}$$

$$\delta_h = \sqrt{\frac{\sum E_h}{V_m}} = \sqrt{\frac{4000.0\ J/mol}{28.1\ L/mol}} = 11.93\ J^{0.5}/L^{0.5}$$

$$\delta_{sp}^2 = \delta_d^2 + \delta_p^2 + \delta_h^2 = 316,406\ J/L + 202,590\ J/L + 142\ J/L = 519,138\ J/L$$

Therefore, $\delta_{sp} = 720.5$ J/L.

$$\delta_d = \frac{\sum F_d}{V_m} = \frac{703.8 \times 1000^{0.5}\ J^{0.5}\ L^{0.5}/mol}{62.6\ L/mol} = 355.3\ J^{0.5}/L^{0.5}$$

$$\delta_p = \frac{\sqrt{\sum F_p^2}}{V_m} = \frac{400.0 \times 1000^{0.5}\ J^{0.5}\ L^{0.5}/mol}{62.6\ L/mol} = 202.1\ J^{0.5}/L^{0.5}$$

$$\delta_h = \sqrt{\frac{\sum E_h}{V_m}} = \sqrt{\frac{4000.0\ J/mol}{62.6\ L/mol}} = 7.99\ J^{0.5}/L^{0.5}$$

$$\delta_{sp}^2 = \delta_d^2 + \delta_p^2 + \delta_h^2 = 126,238\ J/L + 40,844\ J/L + 64\ J/L = 167,146\ J/L$$

Therefore, $\delta_{sp} = 408.8$ J/L.

Table 3.5 Group Contribution Parameters and Associated Molar Volumes for the Estimation of the Solubility Parameter Component of Organic Chemicals

Group Parameter	n	F_d $((J\,m^3)^{1/2}/mol)$	F_p $((J\,m^3)^{1/2}/mol)$	E_h (J/mol)	V_m (L/mol)
–CH₃	21	336.6	0.0	0.0	33.5
–CH₂–	35	234.6	0.0	0.0	16.1
–CH–	31	132.6	0.0	0.0	–1.0
⟩C⟨	4	–214.2	0.0	0.0	–19.2
=CH–	44	255.0	38.0	0.0	13.5
=C⟨	46	–56.7	20.0	0.0	–5.5
Phenyl	7	1515.0	50.0	20.9	71.4
Phenylene	16	1173.0	63.7	40.4	52.4
–COOH	3	561.0	833.0	14,645.0	28.5
–COOH adjacent*	3	450.0	180.0	9,000.0	24.0
–COOH aromatic*	3	335.0	200.0	8,800.0	26.0
–COOR	1	204.0	450.0	12,500.0	18.0
–CHO	1	198.9	4,351.2	27,783.7	22.8
–CO–	5	105.0	600.0	9,500.0	10.8
–O–	1	76.5	1,225.0	101.0	3.8
–O– adjacent	8	30.0	407.0	277.8	4.5
–OH	7	76.5	1,225.0	6,060.0	10.0
–OH adjacent	22	132.6	400.0	4,000.0	13.0
–OH phenyloge*	2	51.0	1,300.0	12,000.0	12.0
–CO–NH–*	6	225.0	400.0	11,000.0	11.0
–CO–NR–*	5	360.0	930.0	9,250.0	15.0
–NH₂	3	132.6	1,176.0	11,541.8	17.5
–NH–	2	122.4	700.7	1,500.0	4.5
=N⟨	11	30.0	150.0	750.0	–9.0

(*Continued*)

Table 3.5 (*Continued*)   Group Contribution Parameters and Associated Molar Volumes for the Estimation of the Solubility Parameter Component of Organic Chemicals

Group Parameter	n	F_d $((J m^3)^{1/2}/mol)$	F_p $((J m^3)^{1/2}/mol)$	E_h (J/mol)	V_m (L/mol)
–N=	12	380.0	100.0	250.0	5.0
–S–	1	815.9	196.0	297.5	12.0
–SO$_2$–	3	295.8	4,361.0	200.0	51.0
–F	6	102.0	493.9	6,544.3	18.0
–Cl aromatic*	9	397.8	1,477.2	4,706.0	26.0
Ring 3–4	1	204.0	0.0	0.0	18.0
Ring 5–	32	142.8	0.0	0.0	16.0
Double bond	49	15.0	14.3	83.5	–2.2
Group Parameter		F_d $((J m^3)^{0.5}/mol)$	F_p $((J m^3)^{0.5}/mol)$	E_h (J/mol)	V_m (L/mol)
(a) PVA: From the above, we can acquire the following values:					
–CH$_2$–		234.6	0	0	16.1
–CH–		132.6	0	0	–1.0
–OH		132.6	400.0	4,000.0	13.0
Total		499.8	400.0	4,000.0	28.1
(b) Ethanol: From the above, we can acquire the following values:					
–CH$_2$–		234.6	0	0	16.1
–CH$_3$		336.6	0	0	33.5
–OH		132.6	400.0	4,000.0	13.0
Total		703.8	400.0	4,000.0	62.6

3.3.3 *Phase Separation and Triangular Phase Diagram*

In the NIPS process, the main components of the phase separation are polymer, "good solvent," and "poor solvent." The whole phase separation process can be described as a change of the composition of these components in a quenching tank, and it is expressed by a ternary nonsolvent (N), solvent (S), and polymer (P)

composition diagram. The composition diagram is expressed by a triangular phase diagram and is shown in Figure 3.6.

Since the separation of a given composition into two phases of different compositions that are in equilibrium is a thermodynamic process, some thermodynamic consideration is necessary to draw a phase boundary line. On the other hand, the composition change on the ternary diagram is affected by the speed of solvent evaporation and by the speed of the "good solvent"–"poor solvent" exchange during the quenching step. Hence, kinetic consideration is necessary to draw a line of composition change on the ternary diagram. Therefore, theoretical treatment of the membrane formation by the phase separation technique consists of two aspects: (1) the thermodynamic and (2) the kinetic aspect. In this chapter we will deal with qualitatively understanding phase separation as a change of composition in a triangular phase diagram (Figure 3.5).

The quenching (gelation) process of a polymer solution is described as the composition change from A to B. A has no poor solvent and B has no good solvent in composition. There are infinite pathways from A to B, and if the curvature is concave up, it means the quenching speed or good solvent extraction speed is slower. If the composition has too much poor solvent, the system becomes unstable, so the unstable or metastable region is closed to the polymer and poor solvent boundary. Polymer quenching begins at the borderline between the stable and unstable region of the polymer. This borderline will change as each component changes.

If we want to increase the porosity of a membrane, then we reduce the polymer concentration. In Figure 3.6, the initial composition of the polymer solution is moved from A to B when we reduce the polymer concentration and generally most of pathway and final composition are moved upward too. As a result, the
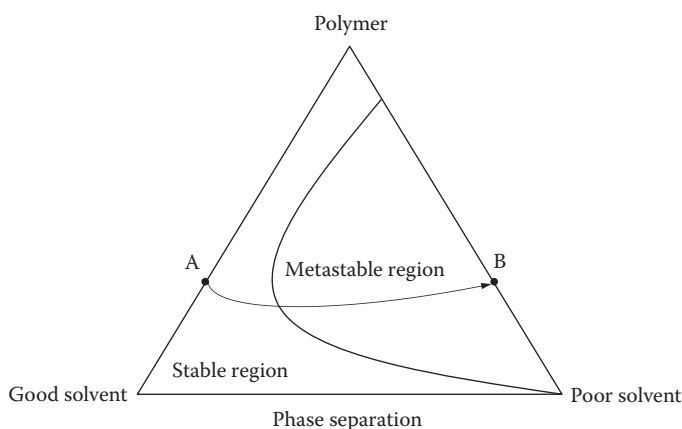
Figure 3.5   Triangular phase diagram of a polymer/good solvent/poor solvent system.
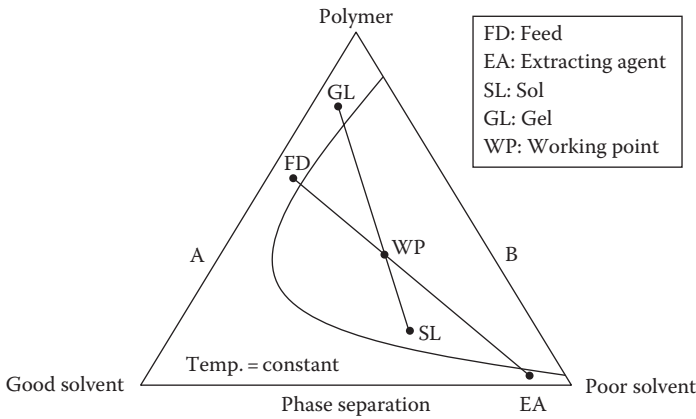
Figure 3.6   Role of polymer concentration in the polymer solution.

final composition has a higher poor solvent ratio compared to the polymer, that is, much more voids.

Example 3.6

See the triangular phase diagram (Figure 3.6). If we change solvent S to another S′ that has a higher compatibility with polymer P, what will be changed in the diagram?

Solution

The higher compatibility a solvent has with the polymer, the wider the area of stable region in the triangular phase diagram (Figure 3.6).

3.3.4 Fabrication of Hollow Fiber and Flat Sheet Membrane

The NIPS process has five major steps: (1) preparation of the polymer solution, (2) injection and molding, (3) quenching, (4) rinsing, and (5) drying. In the fabrication process of hollow fiber or flat sheet membranes, there are little differences in the conceptual equipment. The main differences are the injection nozzles and the molding parts. Dual spinning nozzles are used for injection and molding to produce hollow fiber membranes. The nozzles have one hole in the center and one donut in the cross section. The polymer–good solvent solution goes through the donut-shaped hole and the poor solvent goes through the center hole. The inner side of the polymer solution meets the poor solvent with the help of the center hole.

Flat sheet membranes have independent injection and molding parts. The polymer–good solvent solution is added to a porous support nonwoven fabric and then is submerged into the quenching tank. The gap between the knife (or blade)

(a)

(b)
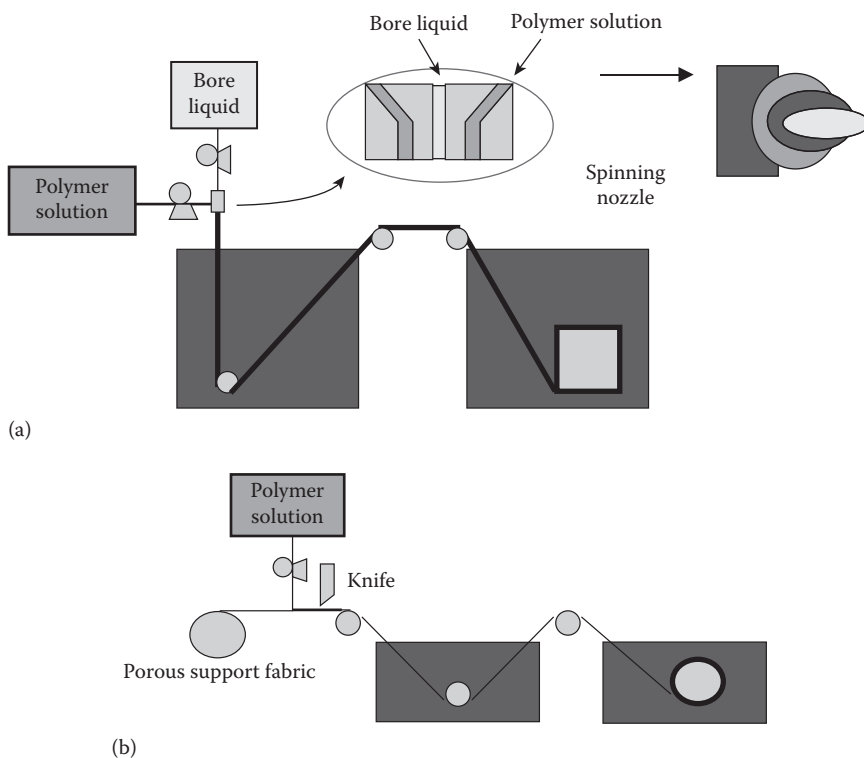
Figure 3.7   Schematic of (a) hollow fiber and (b) flat sheet membrane fabrication process.

and the support is used to control the thickness of the membranes with the control of the concentration of the polymer solution (Figure 3.7).

3.4 Membrane Characterization

3.4.1 Dimensions

There are two major shapes of membranes: (1) hollow fiber and (2) flat sheet type. The outer diameter, inner diameter, and membrane length are the main dimensions of hollow fiber membranes. Hollow fiber membranes are frequently divided into two groups based on a 3 mm membrane diameter. Membranes with a diameter larger than 3 mm are called tubular membranes, while membranes with diameters smaller than 3 mm are called hollow fiber membrane.

In the case of flat sheet membranes, the thickness, length, and width are considered. Flat sheet membranes are used as flat sheets and sometimes are wound tightly

to form spiral wound membranes in modules. All dimensions can be measured by deliberate rulers such as micrometers or calipers, and field emission scanning electron microscope (FE-SEM) sometimes is used for measurement. Most hollow fiber membranes have 0.8–2 mm of outer diameters, 0.4–1.6 mm of inner diameters, and 300–3000 mm of length in modules.

With these dimension parameters we can calculate the effective membrane surface area as follows:

$$A = (2\pi r) \times L \quad \text{(hollow fiber or cylindrical type)} \tag{3.11}$$

$$A = W \times L[\times 2]^{\dagger} \quad \text{(flat-sheet type)} \tag{3.12}$$

where
    A is the effective membrane surface area, m^2
    r is the radius of the cross-sectional circle of the membrane, m
    L is the length of the membrane, m
    W is the width of the membrane, m
    † is adapted when both sides of flat sheet–type membranes are active

In the case of hollow fiber–type membranes, we have to consider the membrane morphology, which is divided into two groups: (1) out-to-in permeation type and (2) in-to-out permeation type. The former has active sites for rejection on the outer surface, which means the membrane meets the source water on the outer surface of the membrane and permeate water comes through into the inner holes of the hollow fiber. The latter is in contact with the source water at the inner surface, and permeate is pulled to the outer surface. The radius of out-to-in membranes is half of the outer diameter and the radius of in-to-out membranes is half of the inner diameter.

Example 3.7

Calculate the effective area of the two types of membranes:

(a) *Hollow fiber membrane* (*out-to-in permeation*): The inner diameter is 0.80 mm, outer diameter is 1.2 mm, and membrane length is 50 cm.
(b) *Flat sheet membrane*: The width is 0.50 m, length is 1.0 m, and thickness is 0.70 mm. Both sides can act as a membrane.

Solution

(a) The effective *membrane* area of the hollow fiber type is calculated by

$$A = (2\pi r) \times L$$

where the radius of the cross-sectional circle of the membrane (r) is 0.60 mm and the membrane length (L) is 50 cm. Then the effective membrane area A is

$$A = (2\pi)(0.60 \times 10^{-3} \text{ m})(50 \times 10^{-2} \text{ m}) = 1.9 \times 10^{-3} \text{ m}^2$$

(b) The effective membrane area of the flat sheet type is calculated by

$$A = W \times L \times 2$$

where the width of the membrane (W) is 0.50 m and the membrane length (L) is 1.0 m. Then the effective membrane area A is

$$A = (0.50 \text{ m})(1.0 \text{ m})(2) = 1.0 \text{ m}^2$$

3.4.2 Pore Size Distribution

The direct way to evaluate the pore size distribution of membranes is to measure all pores with a ruler in a picture of a membrane surfaces by an electric microscope (FE-SEM). But no matter how many pictures of a membrane surface we acquire, the total area captured will be a small fraction of the entire membrane surface. Therefore, it is difficult to represent the total pore size distribution by measuring FE-SEM images of the membrane surface. We need bulk information of the pore size distribution and there are three methods that can satisfy these needs.

3.4.2.1 Bubble Point

This method is based on the bubble point theory. A dry membrane means that all pores are occupied by air. Once the membrane pores are fully wetted by a liquid that has enough surface tension to fill all of the pores occupied by air, there needs to be more pressure so that air goes through the membrane pores again. The larger the pore size, the lower the inlet air pressure that needs to force the air back through the membrane pores. The lowest pressure required is called the "bubble point," and this pressure is directly related to the largest membrane pore diameter, the surface tension of the retained liquid, and the contact angle between the pore and the liquid.

The relation of the parameters describing the bubble point (Figure 3.8) is described by Cantor's equation:

$$P = \frac{4k\sigma\cos\theta}{d} \tag{3.13}$$

where
  P is the lowest applied air pressure, psi
  k is the pore shape correction factor, unitless
  σ is the surface tension at the liquid/air interphase, dyn/cm
  θ is the wetting angle, °
  d is the diameter of the largest pore, μm
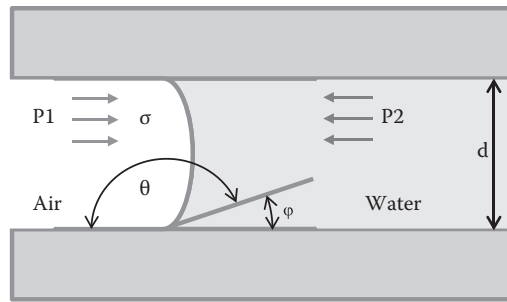
Figure 3.8   Schematic diagram of the bubble point test.

k has the value between 0 and 1, with the value of 1 corresponding to when the pores have a perfectly cylindrical shape. When there are exact data of the pore shape, the k value usually has 1. The surface tension of water is mainly dependent on the water temperature and does not change much during the water treatment operation, which is typically from 1°C to 40°C (Figure 3.9).

The wetting angle, that is, the liquid–solid contact angle, is very diverse with respect to the membrane chemistry. It can range from 0° to 90°; thus its cosine value can be between 0 and 1. Equation 3.13 changes dramatically depending on the wetting angle value.

The morphology of most membranes for water and wastewater treatment is mainly of the hollow fiber type. Compared to flat sheet–type membranes, it is not easy to measure their wetting angles. Recently the dynamic contact angel measuring equipment has been developed and provides proper wetting values for hollow fiber–type membranes. Nowadays, most membrane suppliers provide these values with their products. The higher the wetting values are, the lower their cosine values, and less applied pressure is required (Figure 3.10).

Once we obtain σ and θ by independent analysis and increase the applied pressure slowly and detect the pressure when the air flows abruptly through the membrane pores, the largest membrane pore diameter can be calculated using the earlier equation. Generally the air loss resulting from dissolution into the liquid in the pore is ignored.
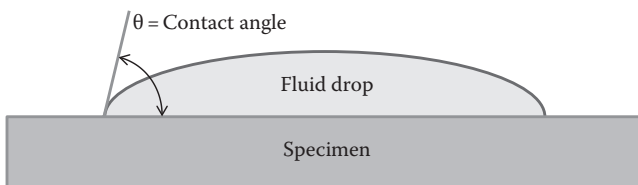
Figure 3.9   Contact angle of fluid drop.
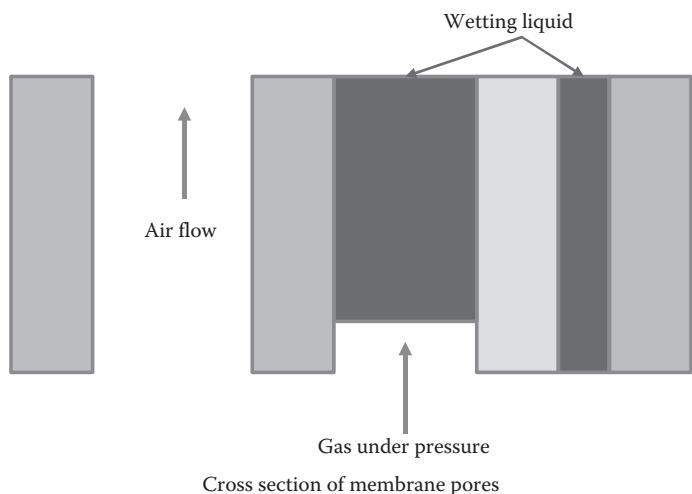
Figure 3.10   Illustration of the principle of capillary flow porometry.

Some bubble point analyzers produce more information about the membrane pores. They measure not only the maximum pore size but also the pore size distribution of the membrane. The pore size distribution comes from the relationship between the applied pressure and airflow. When the pressure keeps increasing beyond the lowest required applied pressure to produce bubbles, the airflow increases. Figure 3.11 is a graph of the volume of airflow versus applied pressure, and it shows that the volume of air flowing at a given pressure is proportional to the volume of space of a given pore size. Figure 3.11b shows the membrane pore size distribution curve converted from raw data (Figure 3.11a).
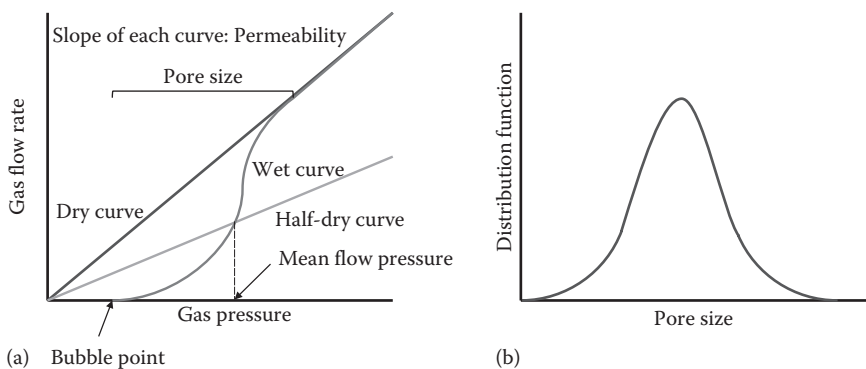
Figure 3.11   Characteristics measurable by capillary flow porometry: (a) pore diameter and permeability and (b) pore distribution.

The main advantage of this test is that it is the fastest and simplest among other related methods. After a membrane sample is set up into the required equipment, the total run takes 30 min. Generally, the calculated pore size is no bigger than the real one.

One of the deviations from this equation is related to the following assumptions. Firstly, pores are assumed to have a cylindrical structure, but all membrane pores produced using phase separation processes are composed of very complex channels. Additional pressure is therefore required to expel the retained liquid out of the membrane pores. This additional pressure results in smaller calculated membrane pore sizes than the actual sizes. In case of membranes that have smaller pores and do not have enough mechanical strength to endure rather high applied pressures, it is impossible to acquire any information about the membrane pore size and pore size distribution due to breakage of the membranes in the middle of the test.

Example 3.8

In measuring the contact angle of the sample, a droplet of deionized water falls on the flat surface of a sample. See its cross section in Figure 3.8 and calculate what the $\cos \theta$ is when the contact angle of the sample is 45.0°.

Solution

Because the contact angle of the membrane sample is 45.0°, the $\cos \theta$ is $\cos 45.0° = 0.707$.

Example 3.9

See the schematic of the capillary test. Suppose the hollow fiber membrane has cylindrically shaped pores. Assume the membrane has a 2.83 μm maximum pore size and shows 1.00 bar of bubble point pressure. Calculate the surface tension from the given parameters using the contact angle that was obtained in Example 3.8. Finally, report the temperature of the system.

Solution

In Equation 3.13,

$$P = \frac{4k\sigma \cos \theta}{d}$$

where $P = 1.00$ bar, $k = 1$, $\cos \theta = 0.707$, and $d = 2.83$ μm.
Therefore,

$$\sigma = \frac{P \times d}{(4k \times \cos \theta)} = \frac{(1.00 \times 10^6 \text{ dyn/cm}^2) \times (2.83 \times 10^{-4} \text{ cm})}{(4 \times 1 \times 0.707)} = 72.0 \text{ dyn/cm}$$

Water has 72.0 dyn/cm at 25°C. Therefore, the temperature of the system is 25°C.

Example 3.10

We conducted bubble point tests with several pore sizes of membranes. Calculate the bubble point pressures of the diverse range of membrane pore sizes. The surface tension of water is 72.0 dyn/cm. All of the membrane samples have the same contact angle of 75°:

(a) Pore diameter is 0.00500 μm (UF).
(b) Pore diameter is 0.0100 μm (MF or UF).
(c) Pore diameter is 0.100 μm (MF).

Solution

In Equation 3.13,

$$P = \frac{4k\sigma\cos\theta}{d}$$

(a) where $k=1$, $\sigma=72.0$ dyn/cm, $\cos 75°=0.259$, and $d=0.00500$ μm

$$P = \frac{4k\sigma\cos\theta}{d} = \frac{(4)(1)(72.0 \text{ dyn/cm})(0.259)}{(5.00\times10^{-7} \text{ cm})}$$

$$= 1.49\times10^8 \text{ dyn/cm}^2 = 149 \text{ bar}$$

(b) where $k=1$, $\sigma=72.0$ dyn/cm, $\cos 75°=0.259$, and $d=0.0100$ μm

$$P = \frac{4k\sigma\cos\theta}{d} = \frac{(4)(1)(72.0 \text{ dyn/cm})(0.259)}{(1.00\times10^{-6} \text{ cm})}$$

$$= 7.46\times10^7 \text{ dyn/cm}^2 = 74.6 \text{ bar}$$

(c) where $k=1$, $\sigma=72.0$ dyn/cm, $\cos 75°=0.259$, and $d=0.100$ μm

$$P = \frac{4k\sigma\cos\theta}{d} = \frac{(4)(1)(72.0 \text{ dyn/cm})(0.259)}{(1.00\times10^{-5} \text{ cm})}$$

$$= 7.46\times10^6 \text{ dyn/cm}^2 = 7.46 \text{ bar}$$

3.4.2.2 Particle Rejection

There is also an indirect method to measure the pore size of a membrane (Figure 3.12). There is an assumption that the size of the smallest rejected particles is the same as the membrane pore size. To use this assumption, several sizes of particle emulsion or suspension standards whose concentrations are known are required. Each standard emulsion or suspension is filtered by a sample membrane, and then the concentration of the permeated water is measured by a ultraviolet-visible spectroscopy (UV-VIS) absorption photometer, reflective index
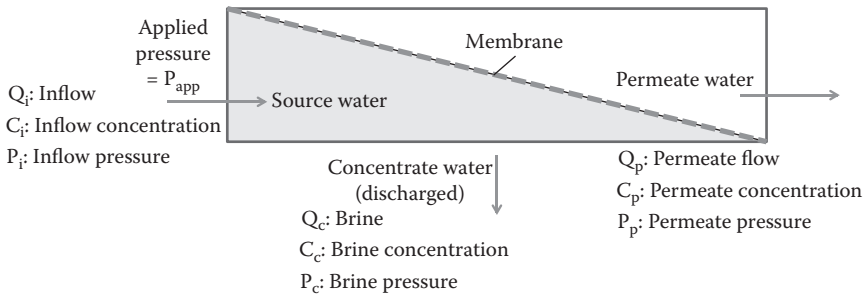
Figure 3.12   Diagram of the membrane operation process.

detector, evaporative light scattering detector, etc. The rejection ratio R is calculated from the before and after filtering concentrations as follows:

$$R = \frac{(C_{in} - C_{out})}{C_{in}} \times 100\% \tag{3.14}$$

where
   C_{in} is the reference concentration, %
   C_{out} is the concentration of permeated water, %

We have a dotted graph of rejection versus the size of standard particles and connected the points and fit calibration curve. Through the graph we find the relative linear relationship between the two parameters and the size of standard particles where the rejection ratio was 90% (some membrane companies use a 95% standard). This size is called the nominal membrane pore size.

   Many studies have shown that a membrane can reject slightly smaller particles than its pore size, because the rejection mechanism is not solely related to the membrane pore size. Interactions between the particles and the surface and/or the pores of a membrane also affect rejection including charge differences, dipole, hydrophilicity, and roughness. Therefore, the result of this method to determine pore sizes might result in smaller calculated membrane pore sizes than the actual sizes.

Example 3.11

See Figure 3.13. Calculate the rejection from the given parameters:

   (a) The inlet concentration of particles is 100.0 mg/L and the permeate concentration is 2.00 mg/L.
   (b) The inlet concentration of particles is 100.0 mg/L and the concentrate concentration is 99.00 mg/L. Recovery is 50.0%, that is, the flow rates of the concentrate and permeate are equal.
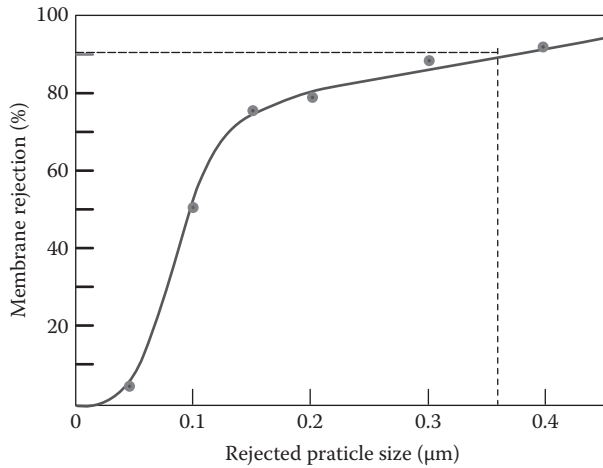
Figure 3.13 Membrane rejection versus particle size.

(c) The inlet concentration of particles is 100.0 mg/L and its flow rate is 10.00 mL/min. The concentrate concentration is 900.0 mg/L, and the recovery rate is 90.00%.

Solution

From Equation 3.14,

$$R = \frac{(C_{in} - C_{out})}{C_{in}} \times 100\%$$

(a) where $C_{in} = 100.0$ mg/L and $C_{out} = 2.00$ mg/L
Therefore, R = (100.0 – 2.00 mg/L)/(100.0 mg/L) × 100% = 98.0%.

(b) where $C_{in} = 100.0$ mg/L, $C_{conc} = 99.00$ mg/L, and recovery rate = 50%
In membrane operation, the rate of mass change of particles flowing in the membrane is the summation of the rate of mass changes of particles flowing out in two ways. That is to say,

$$\frac{dM_{in}}{dt} = \frac{dM_{conc}}{dt} = \frac{dM_{out}}{dt} \tag{3.15}$$

And dM/dt = C × Q, where C is the concentration of the particle solution and Q is the flow rate of the particle solution. So Equation 3.15 can be converted to

$$C_{in} \times Q_{in} = C_{conc} \times Q_{conc} + C_{out} \times Q_{out} \tag{3.16}$$

Because the rejection rate is 50%, $Q_{conc} = Q_{out} = 0.5 \times Q_{in}$

$(100.0 \text{ mg/L}) \times Q_{in} = (99.00 \text{ mg/L}) \times (0.5 \times Q_{in}) + C_{out} \times (0.5 \times Q_{in})$

$$C_{out} = \frac{(100.0 - 49.50 \text{ mg/L})}{(0.5)} = 25.25 \text{ mg/L}$$

Therefore, $C_{out} = 25.25 \text{ mg/L}$.

Therefore, $R = (C_{in} - C_{out})/C_{in} \times 100\% = (100.0 - 25.25 \text{ mg/L})/100.0 \text{ mg/L} \times 100\% = 74.75\%$.

(c) where $C_{in} = 100.0 \text{ mg/L}$, $Q_{in} = 10.00 \text{ mL/min}$, $C_{conc} = 900.0 \text{ mg/L}$, and recovery rate $= 90.00\%$.

Because the rejection rate is 90.00%, $Q_{conc} = 0.1 \times Q_{in}$, $Q_{out} = 0.9 \times Q_{in}$.

From Equation 3.16,

$$C_{in} \times Q_{in} = C_{conc} \times Q_{conc} + C_{out} \times Q_{out}$$

$(100.0 \text{ mg/L})(10.00 \text{ mL/min})(\text{L}/1000 \text{ mL})$

$= (900.0 \text{ mg/L})(1.000 \text{ mL/min})(\text{L}/1000 \text{ mL}) + C_{out}$

$\times (9.000 \text{ mL/min})(\text{L}/1000 \text{ mL})$

$$C_{out} = \frac{(1.000 - 0.900 \text{ mg/min})}{(0.009000 \text{ L/min})} = 11.11 \text{ mg/L}$$

Therefore, $C_{out} = 11.11 \text{ mg/L}$.

Therefore, $R = (100.0 - 11.11 \text{ mg/L})/100.0 \text{ mg/L} \times 100\% = 88.89\%$.

Example 3.12

See Figure 3.13. When we change the cutoff standard from 90% to 80% calculate the nominal membrane pore size from the particle rejection result.

Solution

When we interpolate 80% of membrane rejection, we get 0.2 μm of the rejected particle size. So the nominal membrane pore size is 0.2 μm.

3.4.2.3 Polymer Rejection

Polymer rejection is another indirect method of measuring the pore size of a membrane. The basic mechanism of polymer rejection is the same as that of particle rejection, but there are two major differences between the two.

One difference is the state of sample solution. Particle standards are in an emulsion or suspension, so when their concentrations are measured by an optical detector, there is a deviation caused by unwanted interactions between the optical equipment and the suspended particles that alter the results. Unwanted interactions are anything that causes light intensity loss that is not absorption like diffraction or reflection. Beer–Lambert's law, which is a simple but very precise equation, represents the linear relationship between the solution concentration and absorption:

$$A = abc \tag{3.17}$$

$$T = \frac{I}{I_0}, \quad A = -\log T \tag{3.18}$$

where
  A is the absorption, unitless
  a is the absorptivity, $cm^{-1}\ M^{-1}$
  b is the cell constant, the light path length, cm
  c is the sample concentration, molality, M
  I_0 is the incident intensity, unitless
  I is the transmitted intensity, unitless
  T is the transmittance, unitless

However, optical detector values are correct when a sample is fully dissolved. Fully dissolved is defined as the size of particles, including ions, in the liquid that is smaller than the wavelength of the source light, and the only possibility for light intensity loss is via absorption. The source light wavelength range used in this method is 200–800 nm, which is in submicrometers. If any particles are larger than 0.1 μm, there will be other interactions, such as diffraction or reflection of source light in addition to absorption that will affect readings. The extra interactions result in higher absorption measurements than the real value. For this reason, there should be a little nonlinear curve in a particle rejection test (Figure 3.14).

The other difference between polymer and particle rejection is the detection method. Sample solutions include continuous size spectrum depending on the molecular weight of the polymer. The molecular weight distribution of each sample and permeate solution is measured by gel permeation chromatography (GPC). Unlike particle rejection, this method shows the linear relation between rejection and molecular weight. If all the molecular weight data need to be converted to particle size information, there are additional analysis methods available such as static laser light scattering spectroscopy (Figure 3.15).
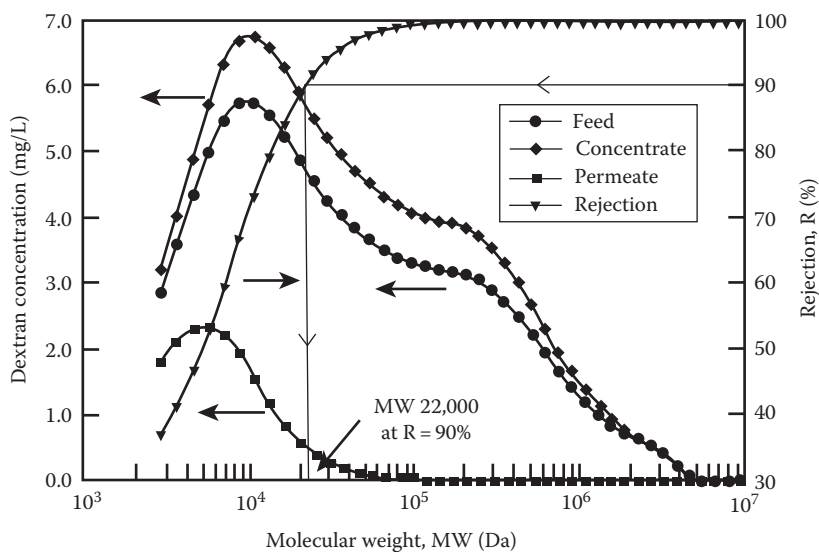
Figure 3.14   The molecular weight distribution curve of standard and permeate solution and the rejection curve.

Figure 3.15   Pictures of GPC and laser light scattering spectroscopy instrument.

Example 3.13

Figure 3.16 shows the relationship between absorbance and sample concentration. From the graph, calculate the absorptivity of the sample in solution. Assume the cell length is 1.00 cm and use the given point.

Solution

From Equation 3.17, when we use the given point from Figure 3.16,

$$0.45 = a \times (1.00 \text{ cm}) \times (2.8 \times 10^{-3} \text{ M})$$

Therefore, the absorptivity of the sample in solution is

$$a = \frac{(1.00 \text{ cm})(2.8 \times 10^{-3} \text{ M})}{0.45} = 6.2 \times 10^{-3} \text{ cm}^{-1} \text{ M}^{-1}$$

Example 3.14

See Figure 3.17. The absorbance of the sample differs with the wavelength of inlet light. Find the maximum wavelength (λ_{max}) of the sample in solution. Discuss why it is better to use λ_{max} compared to all other wavelengths.

Solution

In Figure 3.17, the maximum wavelength (λ_{max}) of the sample in solution is about 304 nm. Among the spectrum of inlet lights, λ_{max} shows the highest absorbance that corresponds to the highest sensitivity. Therefore, λ_{max} can measure the lowest concentration of the sample solution.
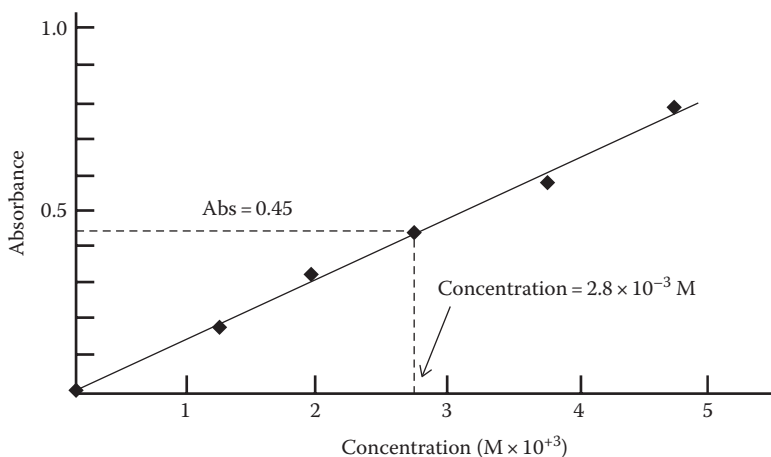
Figure 3.16 **UV–VIS result: absorbance versus concentration of the sample solution.**
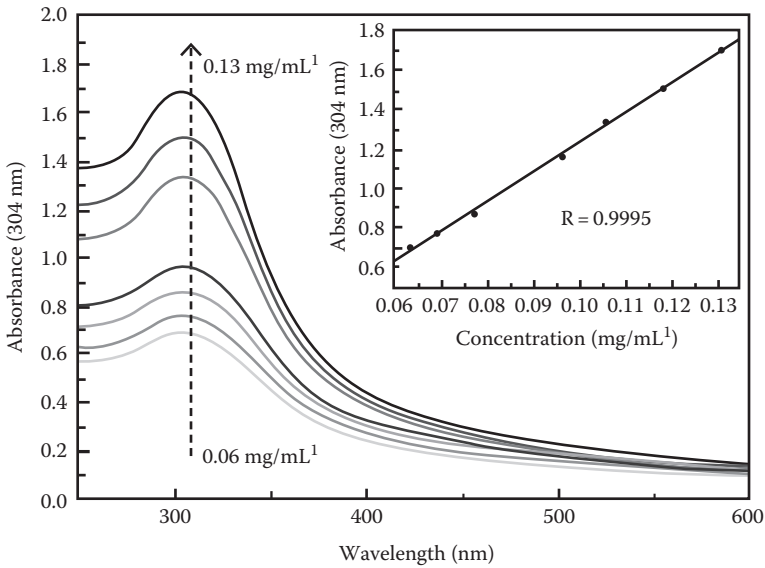
Figure 3.17   Absorbance versus inlet wavelength of the sample solution.

Example 3.15

Convert the given transmittances to absorbance using Equation 3.18 and discuss the advantages and disadvantages of transmittance and absorbance:

(a) T = 10%
(b) T = 25%
(c) T = 50%
(d) T = 75%
(e) T = 100%

Solution

From Equation 3.18, the transmittances can be converted to absorbances:

$$A = -\log T$$

(a) A = –log 0.10 = 1.0
(b) A = –log 0.25 = 0.60
(c) A = –log 0.50 = 0.30
(d) A = –log 0.75 = 0.12
(e) A = –log 1.0 = 0.00

Absorbance can be directly converted to solution concentration as a unit of molality but transmittance cannot be. However, transmittance is preferred when detecting for the presence of very dilute (very low absorbance values) solutes or particles because it is more sensitive at low concentrations as it is the inverse of absorbance.

Table 3.6   UV–VIS Results Example: Absorbance versus Concentration of Sample Solution

Sample Concentration (×10⁻³ M)	Absorbance
0.0	0.00
1.22	0.18
2.00	0.32
2.80	0.45
3.80	0.60
4.80	0.80

Example 3.16

See Figure 3.16 and Table 3.6, which both show absorbance data and concentration of sample solutions of a standard material. Obtain a calibration curve of sample concentration from Table 3.6 as a function of absorbance data and R^2 value using the method of linear least squares. Is it reliable or not?

Solution

The independent variable is A, which represents absorbance, and the dependent variable is C, which represents concentration. From Table 3.6 we can make a function of f(A, C) with the help of a calculator or spreadsheet program such as Microsoft Excel:

$$C = 6.03 \times A + 0.0753, \quad R^2 = 0.998$$

Using this function, whenever we measure any sample solution, we can calculate its concentration with very high confidence because the R^2 value function is very close to 1.

Example 3.17

See Figure 3.14 for the absorbance graph versus molecular weight permeated and measure the nominal membrane pore size assuming the standard of molecular weight cutoff (MWCO) is 90%.

Solution

In Figure 3.14, when we interpolate 90% membrane rejection, we get 22,000 of rejected molecular weight. So the nominal membrane pore size (MWCO) is 22,000.

3.4.3 Hydrophilicity (Contact Angle)

Most polymer-based membranes are hydrophobic. Hydrophobic membranes are not easily wetted by water, or the air in the membrane pores is not easily substituted

by water. Unless the membrane is wetted, there cannot be water permeation through the pores. Some providers supply the membranes already wetted by a glycerin aqueous solution to allow the initial permeation of water. Without the help of a wetting agent such as glycerin or alcohol, hydraulic pressure will be required to expel the air out of pores.

We can calculate the minimum hydraulic pressure required through Equation 3.13 when we know the diameter of the pores, the surface tension of the water, and the contact angle. The contact angle represents the hydrophilicity of the membrane:

$$P = \frac{4k\sigma\cos\theta}{d} \tag{3.13}$$

The most serious disadvantage of hydrophobic membranes is the high fouling potential. The major foulants in MBR are biomass in the forms of activated sludge floc and some organic matters produced by microbes. They are usually hydrophobic, so there is a very strong adhesive potential between foulants and hydrophobic membranes. In order to lessen this problem, some hydrophilic additives are supplied to the membrane in fabrication to reduce hydrophobicity (e.g., the contact angle).

The contact angle of a planar membrane sample is usually measured by a goniometer. The sample is placed on the platform of the machine, and water is dropped on the sample. The side view of the sessile drop is monitored through a contact lens. Figure 3.18 shows a picture of a sessile drop, and the contact angle is automatically measured directly.

The advantage of this method is the smaller piece of membrane sample needed and independent information for each side of the samples. But this method may be affected by some error factors such as roughness and nonuniformity of the sample surface. In the case of hollow fiber–type membranes, the dynamic contact angle is useful.

Example 3.18

We measured the contact angles through five different sessile drops. Say which membrane surface is the most hydrophilic and hydrophobic (Figure 3.19).

Solution

The smaller the contact angle we measure from the sample, the more hydrophilic the sample is and vice versa. A zero degree contact angle represents the most hydrophilic and 180° contact angle the most hydrophobic.

3.4.4 Charge Characters (Zeta Potential)

In solution all materials have their own surface electric charge including membranes and foulants. Along with hydrophilicity and roughness, the surface electric charge is closely related to fouling. Foulants are typically divided into four groups:
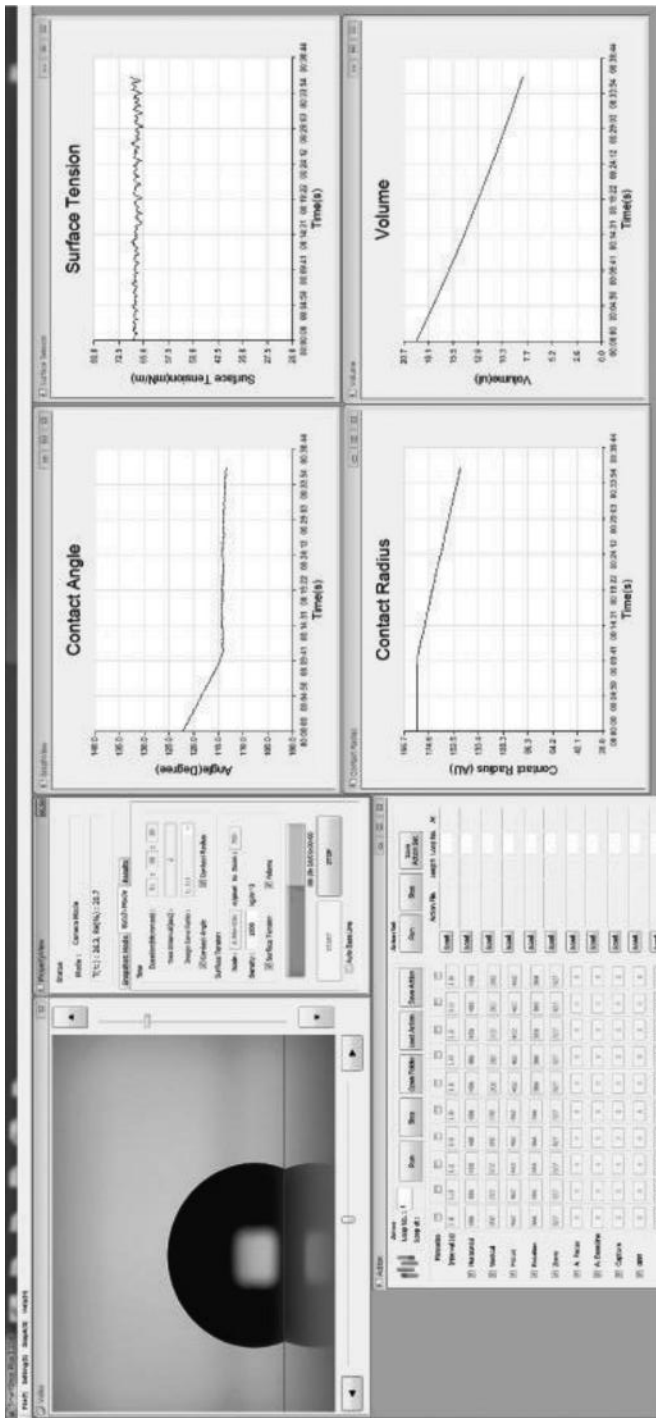
Figure 3.18 Sessile drop and the contact angle measuring machine.
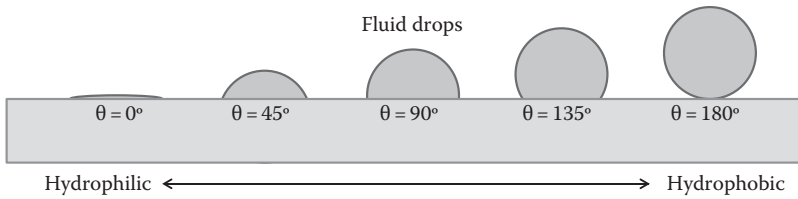
Figure 3.19   Sessile drops on surfaces of samples.

(1) particles, (2) organic matters, (3) scaling ionic salts, and (4) microbes. The major foulants of MF or UF membrane are organic matters. Generally, organic matters have negative surface charges in water, so the higher the negative charge a membrane surface has, the less fouling potential the membrane experiences. The zeta potential is the quantitative value representing the electric charge on a membrane surface.

Zeta potential is measured by several methods including electrophoresis, electroosmosis, streaming potential, and sedimentation potential characteristics (Stumm, 1992). Recently, the streaming potential has been used frequently to measure the zeta potential (Figures 3.20 and 3.21).
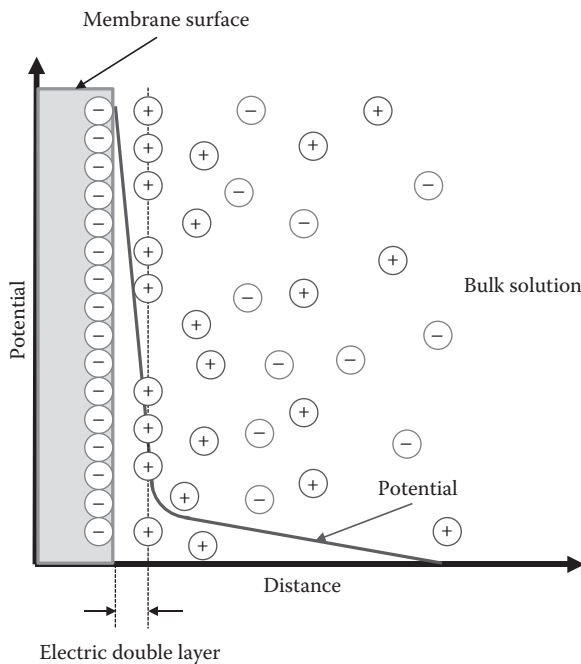
Figure 3.20   The structure of an electric double layer on a membrane surface and zeta potential.
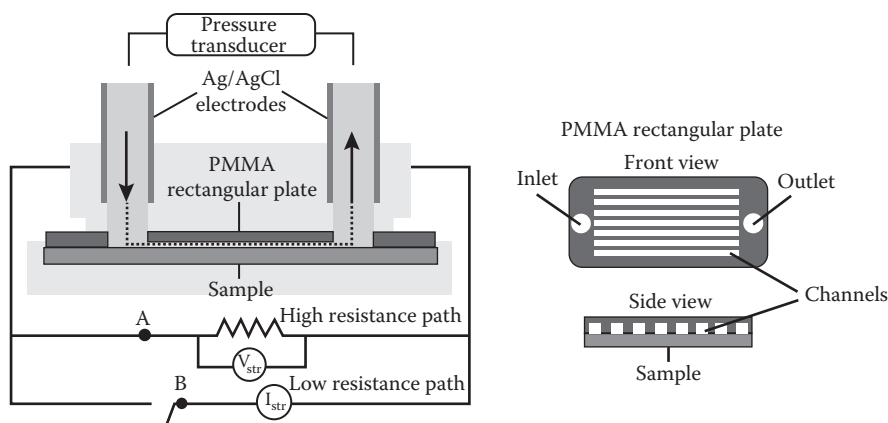
Figure 3.21 The basic concept of streaming potential measurements.

The streaming potential is the potential occurring when electrolytes in aqueous solution flow between two materials. It can be related by the following equation:

$$\frac{\Delta E}{\Delta P} = \frac{\varepsilon \zeta}{\eta \lambda} \tag{3.19}$$

where
 ΔE is the voltage difference, mV
 ΔP is the pressure difference, mbar
 ε is the dielectric constant of the electrolyte, unitless
 ζ is the zeta potential, mV
 η is the viscosity of the electrolyte, MPa/s
 λ is the conductivity of the electrolyte, mS/m

If we use the known conductivity, viscosity, and dielectric constant of electrolytes and measure the dependence of the voltage on the pressure applied, we can calculate the zeta potential (Figure 3.22).

3.4.5 Roughness (Atomic Force Microscopy)

The roughness of a membrane surface is an important parameter for fouling. Generally, the rougher a membrane surface is, the more serious membrane fouling will be owing to wider contact areas and more intense interactions between foulants and the membrane surface. Therefore, understanding the roughness of the
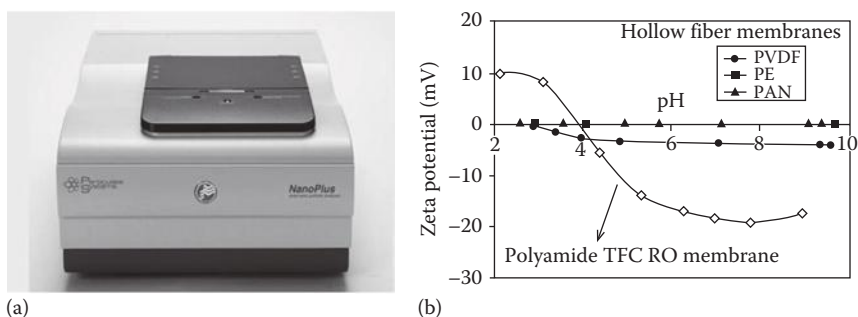
Figure 3.22 **(a) Zeta potential tester and (b) zeta potential curve versus pH of a solution.**

membrane surface and the particle size distribution of the source water should be done before the application.

The roughness of MF or UF membranes is measured by an atomic force microscope (AFM). AFMs are a type of scanning probe microscopes (SPMs). SPM is a newly developed microscope following the electronic microscope by Binning, Roher, Gerber, and Welbel in 1962. It uses a very sharp probe to scan the sample surface. There are many types of probes available and they each have different chemical and physical properties that interact with diverse sample surfaces. According to the properties of the sample surfaces, proper probes can be chosen.

Generally, different kinds of SPMs are classified by the types of probes and are made to measure the roughness (AFM), magnetic force (magnetic force microscope [MFM]), atomic arrangement (scanning tunneling microscope [STM]), lateral force (lateral force microscope [LFM]), force modulation (force modulation microscope [FMM]), electrostatic force (electrostatic force microscope [EFM]), capacitance (scanning capacitance microscope [SCM]), etc.

AFM uses a cantilever with a 30 nm end tip as the probe and can scan roughness larger than the tip size of the cantilever (30 nm). The interaction between the end tip and the membrane surface is dominated by van der Waals forces. The tip uses the repulsive interaction of van der Waals forces in the contact mode or attractive interaction in the noncontact mode.

There is also an intermittent-contact mode called tapping mode. The position of the cantilever is monitored by reading the phase difference of a laser reflected from the tip, and this position is converted to membrane roughness. MF and UF have rather high roughness and the contact mode may not cover the range and could damage a sample surface, so the noncontact or tapping mode is preferable (Figures 3.23 through 3.25).
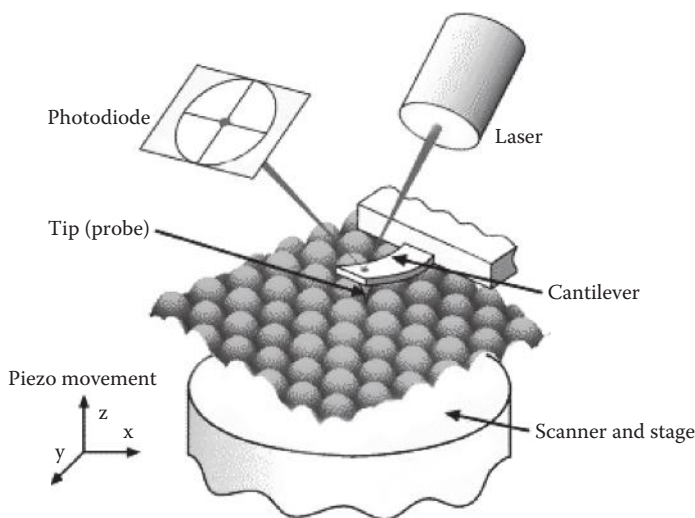
Figure 3.23 The interaction between the cantilever and sample surface.

3.5 Membrane Performance

There are two main performance criteria for membranes: One is how much clean water is permeated, or produced through the membrane, and the other is how many of the contaminants are rejected by the membrane, or how clean is the permeate water. The former is expressed by permeability and the latter is expressed using rejection ratios. During operation, membranes may shrink due to the hydraulic pressure of permeation. Hydraulic pressure reduces the pore size resulting in decreased permeated water flow. Fouling of the membrane is the most important parameter influencing membrane permeability, and it is expressed as the rate of change in permeability or fouling resistance with time.

3.5.1 Permeability

The definition of permeability is as follows:

$$L_p = \frac{J}{\Delta P} \tag{3.20}$$

where
   L_p is the water permeability of the membrane, LMH/bar
   J is the water flux of the membrane, LMH, L/m^2 h
   ΔP is the transmembrane pressure (TMP), bar

(a)

(b)
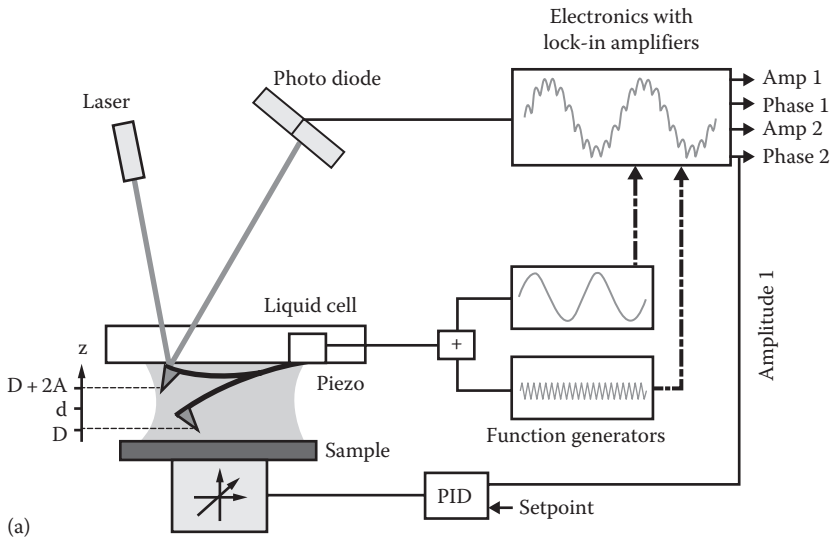
Figure 3.24   (a) Schematic of AFM measurements and (b) picture of an AFM machine.

Phase

Scan size: 2.5 μm × 2.5 μm.

Topography

Scan size: 2.5 μm × 2.5 μm.

(a)

(b)

(c)
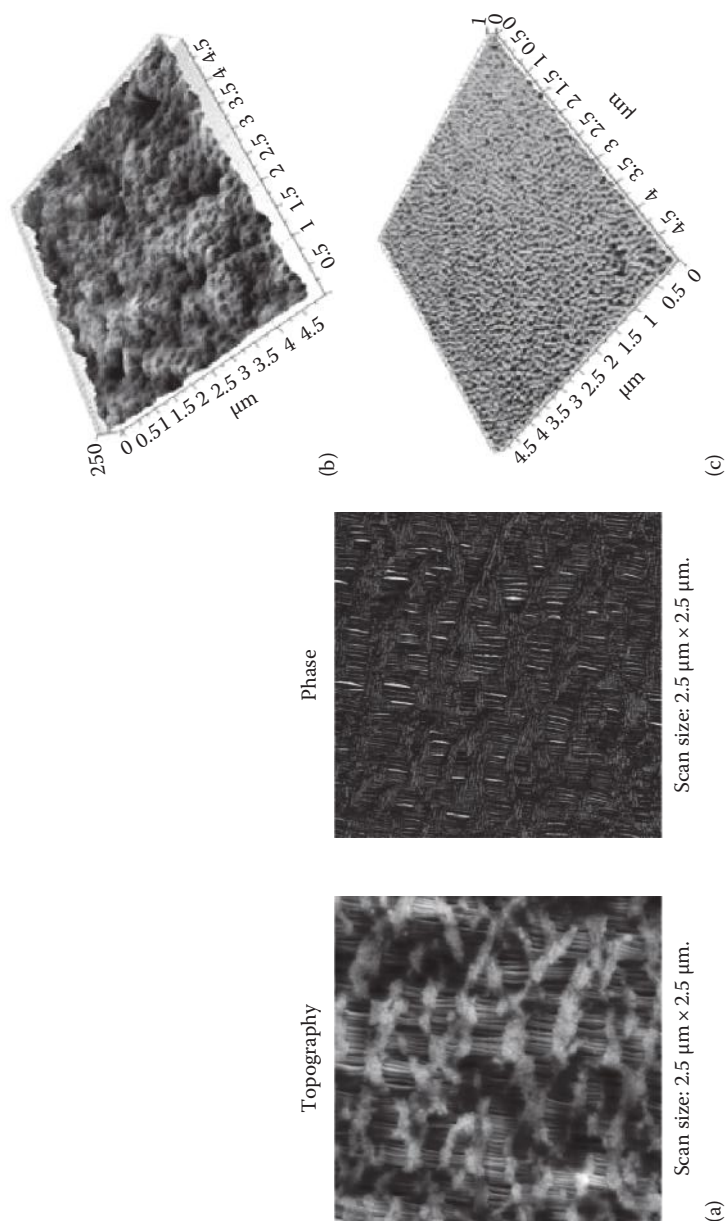
Figure 3.25 **AFM images of different MF membrane surfaces: (a) MSCS membranes, (b) NIPS membranes, and (c) TIPS membranes.**
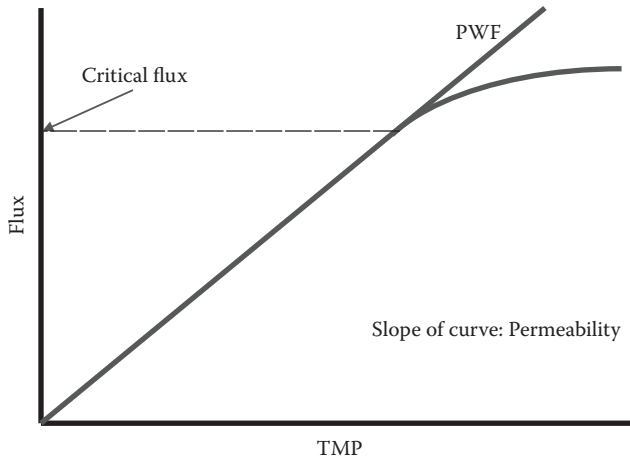
Figure 3.26 Flux versus ∆P at constant temperature.

TMP is calculated from pressures measured during membrane operation. In Figure 3.26, TMP is defined using the following equation:

$$\text{TMP} = \Delta P = P_{\text{perm}} - P_{\text{source-water-side}} = P_{\text{perm}} - \frac{(P_{\text{in}} + P_{\text{conc}})}{2} \tag{3.21}$$

where

P_{perm} is the pressure measured at the permeate water side of the membrane
$P_{\text{source-water-side}}$ is the pressure measured at the source water side of the membrane
P_{in} is the pressure measured at the inlet of the source water
P_{conc} is the pressure measured at the concentrate water

If there is no cross flow (no concentrate water flow), TMP is the differences between the pressures of the outflow or permeate and the inflow or inlet side. So P_{conc} equals zero and $P_{\text{source-water-side}}$ is equal to P_{in}. But in a crossflow system, the inflow is divided into two streams: One stream is the inlet flow from the source water to the active layer of the membrane and the other is the outlet flow of concentrate water exposed to the whole area of the membrane active layer and then pushed out. During cross flow, $P_{\text{source-water-side}}$ has to be calculated as the average value of P_{in} and P_{conc}. Usually P_{in} is no less than P_{conc} because water pressure is reduced through the membrane surface from the inlet to the concentrate side.

Membrane permeability can be acquired from water flux dependence on TMP at constant temperature. When we rewrite Equation 3.20, $J = L_p \times \Delta P$, J has a linear dependence to ΔP. When we acquire several points of $(\Delta P, J)$ at constant

Table 3.7 Membrane Fluxes at Each TMP

TMP (bar)	(a) MF (LMH)	(b) UF (LMH)	(c) NF (LMH)	(d) RO (LMH)
0.00	0.00	0.00	0.00	0.00
0.25	125	55	1.29	0.42
0.50	252	102	2.60	0.81
0.75	371	151	3.75	1.19
1.00	505	195	5.10	1.60

temperature and draw a graph of J versus ΔP, the points should show a linear relationship and L_p is the slope of the curve.

Most MF membranes have clean water permeabilities that range from 200 to 1000 LMH/bar and UF membranes from 100 to 500 LMH/bar at room temperature.

Example 3.19

Four types of membranes are operated at given TMPs at a constant temperature (20°C) with deionized water as the source water, and the corresponding permeate water fluxes are shown in Table 3.7. Calculate the membrane permeabilities of the individual membranes.

Solution

When we draw graphs of permeate water flux versus TMP for each membrane and get the calibrated functions, the results are as follows:

(a) MF: $J = 502 \times \Delta P$, so clean water permeability of MF is 502 LMH/bar. $R^2 = 0.9997$.
(b) UF: $J = 199 \times \Delta P$, so clean water permeability of UF is 199 LMH/bar. $R^2 = 0.9998$.
(c) NF: $J = 5.09 \times \Delta P$, so clean water permeability of NF is 5.09 LMH/bar. $R^2 = 0.9995$.
(d) RO: $J = 1.60 \times \Delta P$, so clean water permeability of RO is 1.60 LMH/bar. $R^2 = 0.9996$.

3.5.2 Rejection

The definition of rejection rate is shown in Equation 3.14. The main target of MF and UF membranes are colloidal solids and microbial flocs. Colloidal solids are frequently turbidity (NTU) or suspended solids (SSs, mg/L). The effluent of conventional wastewater plants shows 1–10 NTU or mg/L of turbidity or SS,

while MBR plants show <0.2 NTU or 1 mg/L. The permeate water quality from the MBR process is 5–10 times better than that of the conventional type. Sometimes conventional plants suffer from sludge bulking resulting in discharging reduced water quality, but MBR plants guarantee permeate water qualities such as turbidity and SSs under any trouble conditions.

3.5.3 Compaction

Because there is an equilibrium state in membrane compaction, commercial membranes are supplied after full compaction to guarantee constant permeation performance. Nevertheless when the membrane meets a higher hydraulic pressure or a membrane deteriorates after long operation times, further compaction occurs (Figure 3.27).

3.5.4 Fouling Property

When a membrane is fouled, it shows a reduction of permeate flux at the same temperature and TMP. To recover the shortage, TMP should be increased. All membranes have their own TMP limitation for sustainable operation, and their TMP limit stimulates irreversible fouling, which is not easily cleaned by normal processes. Most irreversible fouling can be removed by high concentrations of
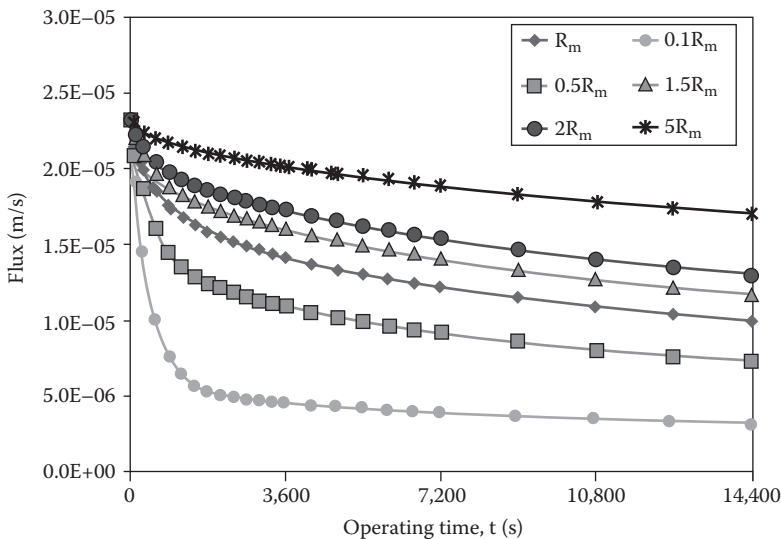
Figure 3.27   Permeation flux curve with respect to time at constant TMP.

chemicals with intense physical flushing, but some irreversible fouling cannot be removed. This fouling is called irrecoverable fouling. Furthermore, frequent chemical recovery cleaning reduces the life span of membranes because of increasing irrecoverable fouling and deterioration of the membrane material.

Fouling is the most important parameter to control for sustainable operation of membrane processes, and it is tightly dependent on the source water quality and the membrane operation process. There is no systematic evaluation process to anticipate membrane fouling given diverse source water qualities and membrane operation processes.

There are two criteria that can express fouling intensity. One is permeate flux and the other is fouling resistance. Fouling resistance is calculated from the permeate flux and TMP using the equation derived in the resistance-in-series (RIS) model:

$$J = \frac{\Delta P}{\eta \times R} \qquad (3.22)$$

where
  J is the permeation flux, LMH
  ΔP is the TMP, bar
  η is the viscosity of water, bar s
  R is the resistance, m^{-1}

This equation is available when the TMP and the operation temperature are constant.

Flux and resistance are inversely related and have their own characteristics. In terms of sensitivity to fouling, flux shows better sensitivity than resistance at initial operation, but as fouling goes on, resistance becomes more sensitive. Resistance is directly related to the fouling intensity. Using the RIS model, fouling can be understood in more detail. Unlike flux, resistance is the sum of several numbers in series independently. The relation among the resistances is as follows:

$$R_t = R_m + R_r + R_{ir} \qquad (3.23)$$

where
  R_t is the total fouling resistance
  R_m is the membrane resistance
  R_r is the reversible fouling resistance
  R_{ir} is the irreversible resistance

Sometimes R_r is represented as R_c, cake layer resistance, and R_{ir} can be represented as R_p or R_b, resistance by pore plugging or resistance by pore blocking.
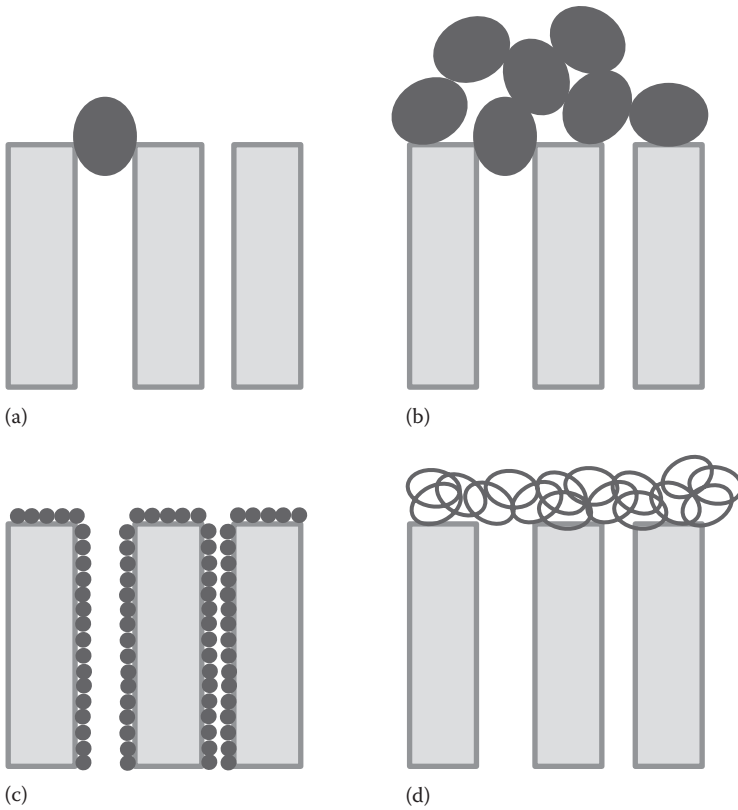
Figure 3.28 **Hermia's membrane fouling mechanism: (a) complete blocking, (b) internal pore blocking, (c) intermediate blocking, and (d) cake formation.**

$R_r + R_{ir}$, $R_c + R_p$ or $R_t - R_m$ is sometimes called R_f, membrane fouling resistance (Figure 3.28).

Example 3.20

From Example 3.19, convert clean water permeabilities to membrane resistances (R_m).

Solution

Using Equation 3.22,

$$J = \frac{\Delta P}{\eta \times R}$$

In Equation 3.22, R is substituted by R_m because there is no membrane fouling. We can get R_m from the conversion of Equation 3.22 as follows:

$$R_m = \frac{\Delta P}{\eta \times J} = \frac{1}{\eta \times (J/\Delta P)} = \frac{1}{\eta \times L_p}$$

The viscosity of water at 20°C is 1.002×10^{-7} bar s.

(a) MF: $L_p = 502$ LMH/bar. So

$$R_m = \frac{1}{\eta \times L_p} = \frac{1}{(1.002 \times 10^{-7} \text{ bar s})(502 \text{ LMH/bar})(1 \text{ h}/3600 \text{ s})(1 \text{ m/h}/1000 \text{ LMH})}$$

$$= \frac{1}{0.140 \times 10^{-10} \text{ m}} = 7.14 \times 10^{10} \text{ m}^{-1}$$

(b) UF: $L_p = 199$ LMH/bar. So

$$R_m = \frac{1}{\eta \times L_p} = \frac{1}{(1.002 \times 10^{-7} \text{ bar s})(199 \text{ LMH/bar})(1 \text{ h}/3600 \text{ s})(1 \text{ m/h}/1000 \text{ LMH})}$$

$$= \frac{1}{0.0554 \times 10^{-10} \text{ m}} = 1.81 \times 10^{11} \text{ m}^{-1}$$

(c) NF: $L_p = 5.09$ LMH/bar. So

$$R_m = \frac{1}{\eta \times L_p} = \frac{1}{(1.002 \times 10^{-7} \text{ bar s})(5.09 \text{ LMH/bar})(1 \text{ h}/3600 \text{ s})(1 \text{ m/h}/1000 \text{ LMH})}$$

$$= \frac{1}{1.42 \times 10^{-13} \text{ m}} = 7.04 \times 10^{12} \text{ m}^{-1}$$

(d) RO: $L_p = 1.60$ LMH/bar. So

$$R_m = \frac{1}{\eta \times L_p} = \frac{1}{(1.002 \times 10^{-7} \text{ bar s})(1.60 \text{ LMH/bar})(1 \text{ h}/3600 \text{ s})(1 \text{ m/h}/1000 \text{ LMH})}$$

$$= \frac{1}{4.45 \times 10^{-14} \text{ m}} = 2.25 \times 10^{13} \text{ m}^{-1}$$

Example 3.21

When a fresh membrane is filtering (a) initially deionized water at 420 LMH and then (b) surface water in turn to produce drinking water at 60.0 LMH of permeate water flux, calculate (a) the membrane resistance and (b) fouling resistance of the surface water.

Assume viscosities of all kinds of waters have the same value and all operations are conducted at a constant temperature (20.0°C) and TMP is 1.00 bar.

Solution

(a) The membrane is not contaminated and the source water is deionized. So the total resistance only consists of the membrane resistance:

$$R_m = \frac{\Delta P}{\eta \times J} = \frac{1.00 \text{ bar}}{(1.002 \times 10^{-7} \text{ bar s})(420 \text{ LMH})(1 \text{ h}/3600 \text{ s})(1 \text{ m/h}/1000 \text{ LMH})}$$

$$= \frac{1}{0.000117 \times 10^{-7} \text{ m}} = 8.55 \times 10^{10} \text{ m}^{-1}$$

(b) The source water is not clean and so the permeate water flux will be lower than that of clean water. So we will use the total fouling resistance (R_t) at first:

$$R_t = \frac{\Delta P}{\eta \times J} = \frac{1.00 \text{ bar}}{(1.002 \times 10^{-7} \text{ bar s})(60.0 \text{ LMH})(1 \text{ h}/3600 \text{ s})(1 \text{ m/h}/1000 \text{ LMH})}$$

$$= \frac{1}{0.0000167 \times 10^{-7} \text{ m}} = 5.99 \times 10^{11} \text{ m}^{-1}$$

Because $R_t = R_m + R_f$, we can acquire R_f from R_m and R_t, which we already calculated:

$$R_f = R_t - R_m = 5.99 \times 10^{11} \text{ m}^{-1} - 8.55 \times 10^{10} \text{ m}^{-1} = 5.14 \times 10^{11} \text{ m}^{-1}$$

3.6 Membrane Modules

When fabricating modules with membranes, there are several important parameters to consider. First, it is very important to minimize the loss of essential performance properties resulting from scaling up from single membrane operation to module operation. Second, the membranes need to maintain integrity during long periods of operation. No matter how robust or well designed the membrane materials and module parts are, the long exposure times to high concentrations of chemicals and stress from the continuous vibration during operation may result in broken parts and adherents between module parts may detach. These effects will result in the loss of module integrity. Third, to optimize module performance, the membrane packing density (see Section 3.6.4) must be considered. Some experts in membrane operation and maintenance believe that easy membrane module setup with a simple and reduced number of components is very helpful in membrane maintenance.

3.6.1 Chemistry

The main parts of modules are made of robust plastics such as polyvinylchloride (PVC), acrylonitrile–butadiene–styrene (ABS) copolymer, and polycarbonate

(PC). They compose frameworks, permeation water channels, and connectors. ABS is the cheapest material and easiest to mold into diverse shapes, but the mechanical and chemical durability is less than the other options. PVC is the second most popular material. It is brittle but can be easily changed by controlling the composition of acrylate, butadiene, and styrene or mixing with diverse additives and plasticizers. However, sometimes these additives and plasticizers cause leaching issues.

Potting resin (similar to glue) is another important part of membrane housing. For flat sheet membrane modules, potting resin acts as a glue to seal the two sheets together. For hollow fiber membrane modules, potting resin glues the ends of the fibers to the module to seal fibers. Potting is a separation process to divide space between the inlet and permeate sides. Once the end of the interstitial spaces between membranes is filled with the potting resin, most of the membrane is exposed to the inlet side and the gate hole of the end of the membrane is connected to the permeate space. Potting resin needs to be not only mechanically robust and chemically durable but also a strong adhesive between the membrane and module material.

3.6.2 Morphologies

There are two types of morphologies of membrane modules: cylindrical and rectangular. The two module shapes can accommodate hollow fiber, tubular and even flat sheet membranes. Cylindrical modules composed of flat sheet membranes are spiral wound modules. The advantage of cylindrical modules is tighter potting because of uniform distribution and easy connection to pipes. However, rectangular modules have higher packing density and are easier to expand to form larger cassettes (Figure 3.29).

(a) (b) (c)
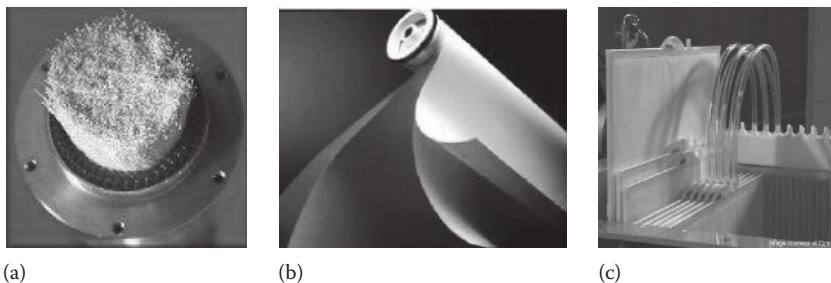
Figure 3.29 (a) Cylindrical module of hollow fiber membrane, (b) cylindrical (spiral wound) module of flat sheet membrane, and (c) rectangular module of flat sheet membrane.

3.6.3 Membrane Effective Area

There are more than two membranes in membrane modules. So if we add the number of membranes into the effective area equation, we can then calculate the total membrane effective area of a membrane module as follows:

$$A = 2\pi \times r \times L \times N \quad \text{(hollow fiber or cylindrical type)} \qquad (3.24)$$

$$A = W \times L \times N \quad \text{(flat-sheet type)} \qquad (3.25)$$

where
  A is the effective membrane surface area, m^2
  r is the radius of the cross-sectional circle of the membrane, m
  L is the length of the membrane, m
  W is the width of the membrane, m
  N is the number of membranes in the module, unitless

In general, commercial membrane modules for MBR have 5–100 m^2/module for hollow fiber membranes and 0.4–1 m^2/module for flat sheet membranes.

Example 3.22

Calculate the effective area of the two types of membrane modules:

(a) *Hollow fiber membrane module*: Inner diameter is 0.80 mm, outer diameter is 1.20 mm, and membrane length is 50 cm. The total number of membrane fibers is 3600. The membrane is operated with an out-to-in flow (the active layer is on the outer side of the membrane).
(b) *Flat sheet membrane*: Width is 0.50 m, length is 1.0 m, and thickness is 0.70 mm. Both sides can act as a membrane. The total number of membrane sheets is 100.

Solution

(a) For the hollow fiber membrane modules, the effective membrane area of each module (A) is as follows:

$$A = 2\pi \times r \times L \times N$$

where r = 0.6 mm, L = 50 cm, N = 3600.
  Therefore, $A = (2\pi) \times (0.6 \times 10^{-3} \text{ m}) \times (50 \times 10^{-1} \text{ m}) \times (3600) = 6.8 \text{ m}^2$.

(b) For flat sheet membrane modules, the effective membrane area of each modules (A) is as follows:

$$A = W \times L \times N \times 2$$

where W = 0.50 m, L = 1.0 m, N = 100. The multiple 2 is present because both sides of the membrane are used as active layers.
  Therefore, $A = (0.50 \text{ m}) \times (1.0 \text{ m}) \times (100) \times (2) = 1.0 \times 10^2 \text{ m}^2$.

3.6.4 Packing Density

There are two types of parameters that represent the packing density of modules: One is based on footprint and the other is based on the space a module occupies. Their exact definitions are the effective membrane area of a module divided by the footprint and the space a module occupies. The most ideal term that can express the exact packing density of a module is based on space, but in MBR the reactor is high enough to accommodate modules or cassettes, so the packing density based on footprint is more practical. We can easily calculate them from the dimensions of the membranes and modules.

Example 3.23

Calculate the packing density of the following modules by the footprint and volume each module occupies:

(a) *Hollow fiber membrane module*: Inner diameter is 0.80 mm, outer diameter is 1.20 mm, and membrane length is 50 cm. The total number of membrane fibers is 12,379. Module dimension: width is 0.10 m, length is 1.0 m, and height is 0.70 m.

(b) *Flat sheet membrane module*: Width is 0.50 m, length is 1.0 m, and thickness is 0.70 mm, and both sides can act as an active layer of the membrane. The total number of membrane sheets is 20. Module dimension: width is 0.10 m, length is 1.0 m, and height is 0.70 m.

(c) *Cylindrical membrane module*: Inner diameter is 1.8 mm, outer diameter is 3.2 mm, and membrane length is 50 cm. The total number of membrane fibers is 1741. Module dimension: width is 0.10 m, length is 1.0 m, and height is 0.70 m.

(d) *Spiral wound membrane module*: Width is 0.50 m, length is 20.0 m, and thickness is 0.70 mm, and both sides can act as a layer of the membrane. One sheet is wound to form a cylindrical module. Module dimension: width is 0.10 m, length is 1.0 m, and height is 0.70 m.

Solution

(a) The effective membrane area of module (A) is as follows:

$$A = 2\pi \times r \times L \times N$$

where $r = 0.6$ mm, $L = 50$ cm, $N = 12,379$.

Therefore, $A = (2\pi) \times (0.6 \times 10^{-3} \text{ m}) \times (5.0 \times 10^{-1} \text{ m}) \times (12,379) = 23 \text{ m}^2$.

Because the module shape is rectangular, the footprint and volume of the module (A) are

$$F = W \times L = (0.10 \text{ m}) \times (1.0 \text{ m}) = 0.10 \text{ m}^2$$

$$V = W \times L \times H = (0.10 \text{ m}) \times (1.0 \text{ m}) \times (0.70 \text{ m}) = 0.070 \text{ m}^3$$

Therefore, the packing densities of module A by footprint (PD_F) and volume (PD_V) are

$$PD_F = \frac{A}{F} = \frac{(23 \text{ m}^2)}{(0.10 \text{ m}^2)} = 2.3 \times 10^2 \text{ m}^2/\text{m}^2$$

$$PD_V = \frac{A}{V} = \frac{(23 \text{ m}^2)}{(0.070 \text{ m}^3)} = 3.3 \times 10^2 \text{ m}^2/\text{m}^3$$

(b) For flat sheet–type membrane modules, the effective membrane area of each module (A) is as follows:

$$A = W \times L \times N \times 2$$

where $W = 0.50$ m, $L = 1.0$ m, $N = 20$. The multiple 2 is applied because the membrane uses both sides as active layers.

Therefore, $A = (0.50 \text{ m}) \times (1.0 \text{ m}) \times (20) \times (2) = 2.0 \times 10$ m^2.

Because the module shape is rectangular, the footprint and volume of module (A) are

$$F = W \times L = (0.10 \text{ m}) \times (1.0 \text{ m}) = 0.10 \text{ m}^2$$

$$V = W \times L \times H = (0.10 \text{ m}) \times (1.0 \text{ m}) \times (0.70 \text{ m}) = 0.070 \text{ m}^3$$

Therefore, the packing densities of module A by footprint (PD$_F$) and volume (PD$_V$) are

$$PD_F = \frac{A}{F} = \frac{(2.0 \times 10 \text{ m}^2)}{(0.10 \text{ m}^2)} = 2.0 \times 10^2 \text{ m}^2/\text{m}^2$$

$$PD_V = \frac{A}{V} = \frac{(2.0 \times 10 \text{ m}^2)}{(0.070 \text{ m}^3)} = 2.9 \times 10^2 \text{ m}^2/\text{m}^3$$

(c) The effective membrane area of module (A) is as follows:

$$A = 2\pi \times r \times L \times N$$

where $r = 1.6$ mm, $L = 50$ cm, $N = 1741$.

Therefore $A = (2\pi) \times (1.6 \times 10^{-3} \text{ m}) \times (5.0 \times 10^{-1} \text{ m}) \times (1741) = 8.8$ m^2.

Because the module shape is rectangular, the footprint and volume of module (A) are

$$F = W \times L = (0.10 \text{ m}) \times (1.0 \text{ m}) = 0.10 \text{ m}^2$$

$$V = W \times L \times H = (0.10 \text{ m}) \times (1.0 \text{ m}) \times (0.70 \text{ m}) = 0.070 \text{ m}^3$$

Therefore, the packing densities of module A by footprint (PD$_F$) and volume (PD$_V$) are

$$PD_F = \frac{A}{F} = \frac{(8.8 \text{ m}^2)}{(0.10 \text{ m}^2)} = 8.8 \times 10 \text{ m}^2/\text{m}^2$$

$$PD_V = \frac{A}{V} = \frac{(8.8 \text{ m}^2)}{(0.070 \text{ m}^3)} = 1.3 \times 10^2 \text{ m}^2/\text{m}^3$$

(d) For flat sheet–type membrane modules, the effective membrane area of each modules (A) is as follows:

$$A = W \times L \times N \times 2$$

where $W = 0.50$ m, $L = 20.0$ m, $N = 1$. The multiple 2 is applied because the membrane uses both sides as active layers.

Therefore, $A = (0.50 \text{ m}) \times (20.0 \text{ m}) \times (1) \times (2) = 2.0 \times 10 \text{ m}^2$.

Because the module shape is rectangular, the footprint and volume of module (A) are

$$F = W \times L = (0.10 \text{ m}) \times (1.0 \text{ m}) = 0.10 \text{ m}^2$$

$$V = W \times L \times H = (0.10 \text{ m}) \times (1.0 \text{ m}) \times (0.70 \text{ m}) = 0.070 \text{ m}^3$$

Therefore, the packing densities of module A by footprint (PD_F) and volume (PD_V) are

$$PD_F = \frac{A}{F} = \frac{(2.0 \times 10 \text{ m}^2)}{(0.10 \text{ m}^2)} = 2.0 \times 10^2 \text{ m}^2/\text{m}^2$$

$$PD_V = \frac{A}{V} = \frac{(2.0 \times 10 \text{ m}^2)}{(0.070 \text{ m}^3)} = 2.9 \times 10^2 \text{ m}^2/\text{m}^3$$

The packing densities of each style of membrane modules in Example 3.23 show very different values even though all types of membrane modules have the same total membrane volume of 7.0×10^{-3} m³. Hollow fiber–type membrane modules have the highest effective membrane area. Furthermore, hollow fiber–type membranes require the smallest volume of modules and therefore the highest packing compared to other membranes.

3.6.5 Operation Types

The driving force separating liquids and particles via membranes is usually hydraulic pressure. We have two chances to provide pressure to induce permeate water from the source water through a membrane. Since permeate water is held at atmospheric pressure, if we can provide hydraulic pressure to the source water, a pressure differential will develop between the two sides, and flow from the source
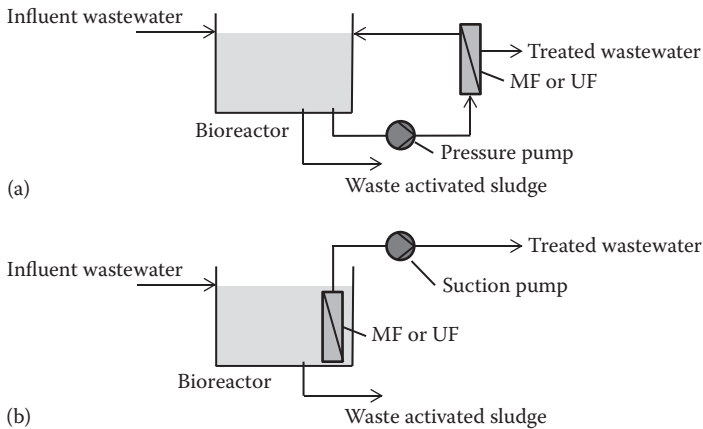
Figure 3.30 Membrane process schemes of (a) pressurized and (b) submerged membrane modules.

water side to the permeate water side will occur. This is the operational principle of pressurized modules. In case of submerged membrane modules, a pump creates a slight vacuum on the permeate side, which induces the pressure difference also causing water to flow. Each method has advantages depending on project specifics (Figure 3.30).

3.6.5.1 Submerged Type

In general, submerged membrane modules are directly installed into the source water tank. In MBR systems the modules are located in the bioreactor or in a separated membrane tank right after the bioreactor. Even in the latter case, the membrane tank is filled with biomass. Submerged setups can reduce the footprint and the need for an extra source water tank. The membranes are exposed to source water and can move freely. This setup is easy to maintain and experiences less fouling because of extra aeration provided from aerators installed below the modules.

The energy of the suction pump producing permeated water is lower than that of a pressurizing pump at the same permeability given constant temperature. The only disadvantage of submerged membrane modules is a narrow permeate flux range. They are operated at 70% flux compared to pressurized membrane modules. In MBR systems, permeate flux is generally in the range of 10–40 LMH at 20°C.

Unlike flat sheet membranes, hollow fiber membrane modules have orientations (Figure 3.31). Vertically oriented membrane modules show less accumulation tendency or activated sludge flocs on the membrane surface. However, a portion
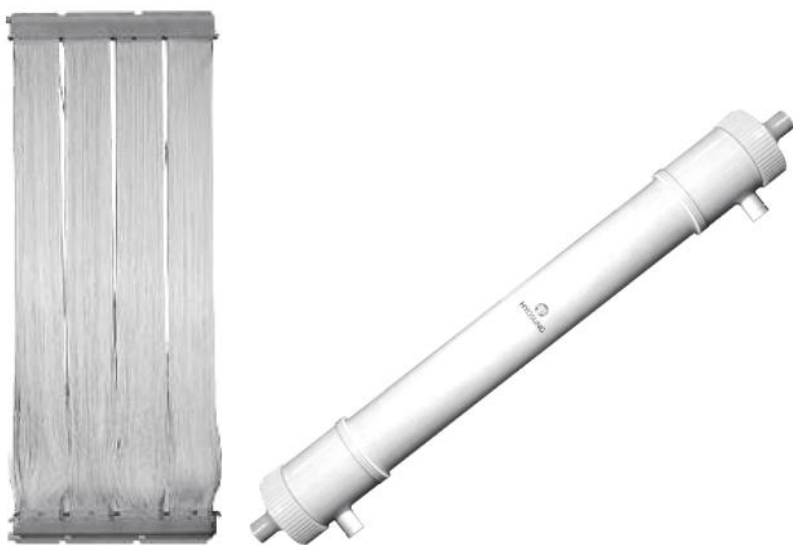
Figure 3.31 The vertically and horizontally oriented submerged hollow fiber membrane modules.

of the system footprint has to be left available for an aeration channel because they have permeate water channels at the bottom that hinder the air bubbles from the aerators. Horizontally oriented ones have permeate water channels on both sides, so they do not consume any footprint for membrane installation; thus, they show higher packing densities than vertically oriented ones. However, horizontally oriented modules have a higher fouling potential and may experience easy accumulation of foulants or activated sludge flocs.

3.6.5.2 Pressurized Type

Most pressurized membrane modules are cylindrical and can have either flat sheet– or hollow fiber–type membranes. Pressurized modules have to endure higher hydraulic pressure and accommodate thousands of membrane fibers to satisfy larger effective membrane areas, and the cylindrical shape is the most adequate. Flat sheet membranes are wound tightly with spaces of proper thickness to secure source and permeate water channels inside. Finally, they are fabricated into spiral wound membrane modules and have a cylindrical shape. Spiral wound membranes can be laid vertically or horizontally because they are wound tightly with narrow water channels resulting in high flow velocities. Inside to out–type hollow fiber membrane modules have as many orientation choices as spiral wound ones, but outside to in–type hollow fiber membrane modules have to be installed vertically to avoid unfilled water channels.

The biggest advantage of pressurized membrane modules is higher permeate water flux rates. Unlike drinking water treatment membranes, MBR membranes endure high concentrations of biomass—5,000 to 15,000 mg/L—higher operating pressures, and flux, all of which accelerate membrane fouling. Pressurized membranes cannot be scrubbed by aeration during permeation, so they tend to foul more quickly. To solve this problem they are operated at higher cross flows instead of aeration, but higher cross flows result in too much energy loss from overdesigned crossflow pumps that have 5–15 times higher flow capacity than that of the permeate flow. At least in MBR, pressurized membrane modules have problems that need to be solved to guarantee higher permeate water flux at high influent water flux rates.

3.7 Membrane Cassettes

The price of membranes dramatically decreased over the last 20 years from about 500 to 50 USD/m^2 in 2013, and the prices continue to fall. The reduced prices are a result of scale-up and greater automation of the membrane module manufacturing processes. To optimize the efficiency of manufacturing membranes and modules, there should be a limitation on their size. Size limits can not only save membrane footprints but also encourage lots of automatic/manual valves and pipes including related components. But the market needs bigger cassettes coinciding with the trend of expanding the application of membrane plants to larger water and wastewater treatment plants (WTPs and WWTPs). Engineers and membrane providers have begun to satisfy this necessity with membrane cassette. Cassettes are preengineered "building blocks" or sets of modules containing some extra parts for essential membrane operation and sometimes called "membrane skids."

3.7.1 Components and Materials

Membrane cassettes consist of a mainframe, connectors to permeation pipe, aeration pipe, and, in the case of pressurized types, source water and concentrate pipe and aerators, in case of submerged types. The major purposes of developing membrane cassettes are to enlarge the effective membrane area, to maintain operation during maintenance of a single membrane or module, and to promote robustness over long periods of operation. Because membrane cassettes are very heavy, they have a very strong loop on top for conveyance by hoist.

Stainless steel is a good material for the mainframe, including the loop on top, unless there is a possibility of a corrosive problem (e.g., seawater desalination). Stainless steel supports many membrane modules against continuous impact (e.g., vibration from strong aeration systems) and sometimes acts as a pipe for water or air. Pipes are made of stainless steel or PVC. PVC gives higher chemical durability and easy maintenance in accidents such as breakage.

Figure 3.32   Schematic of the submerged membrane cassettes and the aerators.

In submerged membrane systems, aeration is one of the most important processes. Coarse bubbles are much more favorable for scrubbing foulants away from membrane surfaces. But because no matter how big the hole sizes of the aerators are, there is a saturation point of bubble size due to water pressure. Furthermore, the bigger the hole sizes of the aerators, the more difficult to control the evenness of the amount of air released from the hole. Therefore, we must optimize the hole size and its configuration for best performance and energy use. Major parameters for the optimization of the hole size are the space between holes, the angles of holes on the aerators, and the space between the holes and membranes (Figures 3.32 and 3.33).

3.7.2 Setup and Maintenance

Usually the setup of membrane cassettes is conducted on-site. This is because membrane cassettes are too big to deliver and handle from the manufacturing factory to the site. Sometimes even the mainframe of a membrane cassette is assembled on-site. After all parts are delivered, the mainframes are assembled, then the membrane modules are set up onto the mainframes, and finally the other parts are connected. Most membrane cassette manufacturers provide easy installation methods for installing membrane modules onto membrane cassettes. Figures 3.34 and 3.35 show the pictures of assembled membrane cassettes.

Figure 3.33   Schematic of the pressurized membrane cassettes and the aerators.
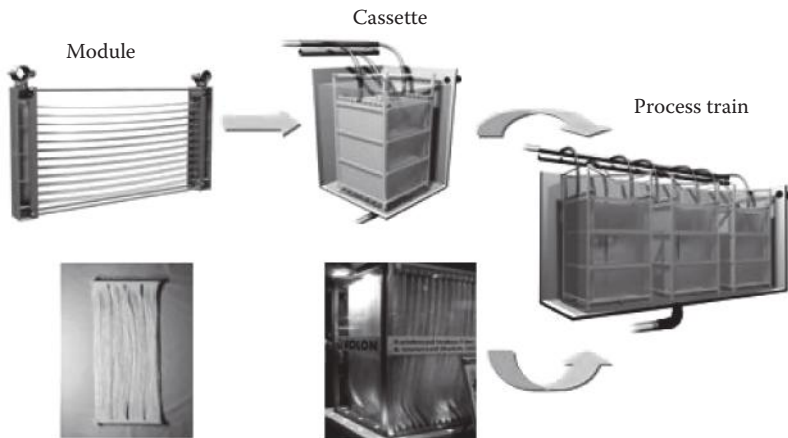
Figure 3.34   Installation of submerged membrane cassette.
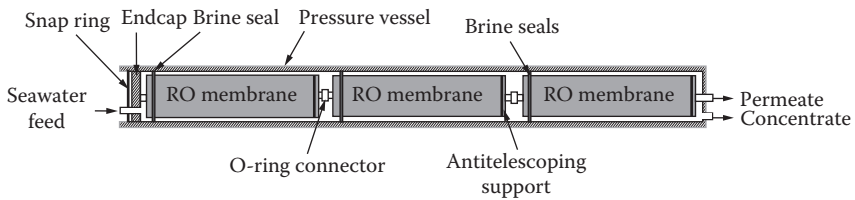
Figure 3.35   Installation of pressurized membrane modules (RO).

A membrane module has hundreds to thousands of membranes, and there are dozens to hundreds of membrane modules in membrane cassettes. If there are broken membranes in a membrane cassette, operators should find the exact module and then membrane and replace the module from the cassette with a new one and then fix the membrane while keeping membrane operation going. Small damages on a membrane surface can be plugged by operation with particles or biomass flocs, but comparably larger breakages need to be repaired. During the operation of WWTP whose capacity is 10,000 m^3/day, operators may meet dozens of membrane breakages a year. Of course several membrane breakages do not influence the permeate water quality seriously, so generally operators can repair membranes during the regular recovery cleaning term, which may take more than a week in a 10,000 m^3/day of WWTP. The recovery cleaning cycle is 3–6 months a year, and it changes as the source water quality and plant operation conditions change.

3.7.3 Membrane Effective Area and Packing Density

The membrane effective area of a membrane cassette is easily acquired. We just consider one parameter, the number of membrane modules per membrane cassette. Because most membrane cassettes are rectangular, we can measure the length, width, and height of the cassette to calculate the packing density of the membrane cassette. Even though they typically have some curvatures, the packing density of membrane cassettes is acquired as if they are rectangular for convenience.

3.7.4 Aeration

3.7.4.1 Aerator

There are several kinds of fouling inhibition processes adapted to membrane operation. They are cross flow, backwash, relaxation, maintenance cleaning (or chemical enhanced backwash), recovery cleaning, and aeration. When we compare the efficiency of fouling inhibition or removal of foulants from the membrane surface, chemical-based cleaning processes, maintenance, and recovery cleaning are the best. But among non-chemical-based cleaning processes, aeration is the most efficient because of the very effective scrubbing between two different phases (liquid and gas).

3.7.4.2 Air Demand

Nevertheless, the energy cost in generating and supplying air to membranes is not negligible and there should be some optimum range of air supplied, which is expressed by specific air demand (SAD). There are two SAD values: (1) SAD_m (SAD per membrane area) whose units are N m^3/(h m^2) and (2) SAD_p (SAD per permeate volume) whose units are m^3 air/m^3 permeate. Most membrane cassettes have a SAD_m in the range of 0.3–0.8 N m^3/(h m^2) and a SAD_p in the range of 10–90 m^3 air/m^3 permeate.

Example 3.24

When air is supplied to each module at 15 N m³/h of flow, calculate SAD_m and SAD_p. Each membrane permeates 0.5 m³/h of water. Use the effective membrane area of each membrane in Example 3.23.

Solution

(a) The effective membrane area of module (A) is 23 m².
Therefore SAD_m and SAD_p are

$$SAD_m = \frac{Q_a}{A} = \frac{(15 \text{ N m}^3/h)}{(23 \text{ m}^2)} = 0.65 \text{ N m}^3/(h \text{ m}^2)$$

$$SAD_p = \frac{Q_a}{Q_w} = \frac{(15 \text{ N m}^3/h)}{(0.5 \text{ m}^3/h)} = 30 \text{ N m}^3/\text{m}^3$$

(b) The effective membrane area of module (A) is 2.0×10 m².
Therefore, SAD_m and SAD_p are

$$SAD_m = \frac{Q_a}{A} = \frac{(15 \text{ N m}^3/h)}{(2.0 \times 10 \text{ m}^2)} = 0.75 \text{ N m}^3/h \text{ m}^2$$

$$SAD_p = \frac{Q_a}{Q_w} = \frac{(15 \text{ N m}^3/h)}{(0.5 \text{ m}^3/h)} = 30 \text{ N m}^3/\text{m}^3$$

(c) The effective membrane area of module (A) is 8.8 m².
Therefore, SAD_m and SAD_p are

$$SAD_m = \frac{Q_a}{A} = \frac{(15 \text{ N m}^3/h)}{(8.8 \text{ m}^2)} = 1.7 \text{ N m}^3/h \text{ m}^2$$

$$SAD_p = \frac{Q_a}{Q_w} = \frac{(15 \text{ N m}^3/h)}{(0.5 \text{ m}^3/h)} = 30 \text{ N m}^3/\text{m}^3$$

(d) The effective membrane area of module (A) is 2.0×10 m².
Therefore, SAD_m and SAD_p are

$$SAD_m = \frac{Q_a}{A} = \frac{(15 \text{ N m}^3/h)}{(2.0 \times 10 \text{ m}^2)} = 0.75 \text{ N m}^3/h \text{ m}^2$$

$$SAD_p = \frac{Q_a}{Q_w} = \frac{(15 \text{ N m}^3/h)}{(0.5 \text{ m}^3/h)} = 30 \text{ N m}^3/\text{m}^3$$

Problems

3.1 *Membrane separation theories*: Dr. M develops a novel technique to increase the number of pores in MF and UF membranes. Using this technique, Dr. M is able to double the number of pores in a certain MF membrane. In this process, there is no change in pore radius. The membrane filtration experiment is performed with a feed solution containing 2000 mg/L NaCl and the result is given in the following figure and table.

Water flux (10^{-5} m/s)

Pressure (bar)	Original membrane	New membrane
0.10	0.8	1.0
0.20	1.6	2.0
0.30	2.4	3.0
0.40	3.2	4.0
0.50	4.0	5.0
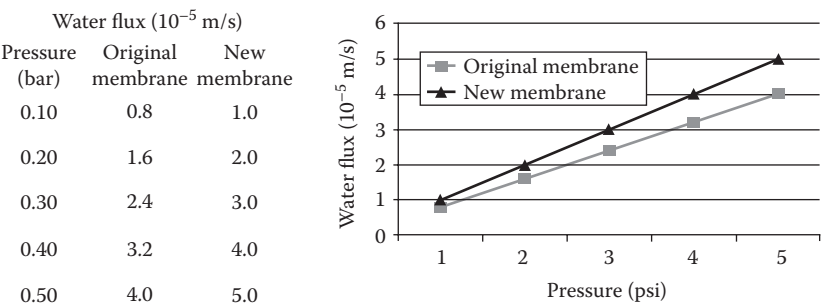
Calculate the tortuosity of the new MF membrane. Assume the original MF membrane has cylindrical pores perpendicular to the membrane surface.

3.2 *Membrane materials and fabrication*: B in Table 3.8 shows different membrane polymers and their mechanical and thermal properties. When we fabricate membranes using these materials, choose the best polymer and proper reason for the following questions (Table 3.8):

a. Choose the best polymer for the NIPS process in fabricating the membrane and explain the reason for the choice.

Table 3.8 Polymers for Membrane and Their Mechanical Thermal Properties

Polymer	A	B	C
T_g, °C	80	120	180
T_m, °C	100	150	250
Solvent miscibility	Good	Medium	Bad
Tensile strength, MPa	100	200	300
Tensile elongation, %	100	50	30
Contact angle, °	180	90	30
Chemical durability	Good	Good	Good

b. Choose the best polymer for the MSCS process in fabricating the membrane and explain the reason for the choice.

c. When we apply the membrane to hot water (80°C) treatment, is there any polymer that is not proper to the application? Why do you think?

d. For long-term (least over 5 years) operation for municipal wastewater treatment, mechanical, thermal, and chemical durability should be considered. Which polymer will be the best for the purpose? Why?

e. Hydrophilicity is related to the water permeability and fouling potential. Which polymer will show higher water permeability? Why? Which polymer will show better antifouling property against natural organic matters? Why?

3.3 *Membrane performance*: Equations 3.2 and 3.4 show the flow and flux of permeate water. Equation 3.22 shows that the permeate water flux is inversely related to resistance. Drive the resistance from Equation 3.2 or 3.4.

3.4 *Membrane characterization*: A UF membrane is used to filter a macromolecular waste with a concentration of 2%.

3.5 *Membrane modules*: C in Table 3.8 shows the specifications of different morphologies of membranes and modules.
C in Table 3.8 is the specifications of different morphologies of membranes and modules.

3.6 *Membrane cassettes*: The following is the basic operation information on G WWTP with a capacity larger than 5000 m³/day. Based on the information given in Tables 3.9 through 3.11, determine the following missing parameters:

a. Pure water permeability at 25°C

b. Minimum intake rate

c. Total membrane surface area installed in the plant

d. Operating flux at emergency

e. Recovery under normal operating condition (feedwater containing below 200 NTU)

Table 3.9 Overview of the Membrane Module

Index	Content	Remark
Pore size	0.05 μm	
Effective membrane area	72 m²/module	
Pure water flux	4.60 m³/m² day (1°C)	TMP 0.5 kgf/cm²
	8.95 m³/m² day (25°C)	

Table 3.10 Overview of the Membrane System

Index	Design	Remark
Water supply	30,000 m³/day	
Recovery	Minimum 90%	
Filtration rate	0.95 m³/m² day (TMP 1.0 kgf/cm², 1°C)	Normally, 4 systems online Emergency, 3 systems online
Number of membrane	4 systems (6 unit/system, 20 modules/unit)	

Table 3.11 Operation Condition Difference

Index	Normal Operating Condition	High Turbidity Operating Condition
Filtration mode	Dead end (below 200 NTU)	Dead end (200–400 NTU) Cross flow (above 400 NTU)
Filtration rate	0.94 m³/m² day	0.98 m³/m² day

References

Allen, M. D. and Raabe, O. G. (1982) Re-evaluation of Millikan's oil drop data for the motion of small particles in air. *J. Aerosol Sci.*, 13: 537.

Davies, C. N. (1945) Definitive equations for the fluid resistance of spheres. *Proc. Phys. Soc.*, 57: 259–270.

Hildebrand, J. H. and Scott, R. L. (1950) *The Solubility of Non-Electrolyte*, 3rd edn. Reinhold, New York, pp. 123–124.

Stumm, W. W. (1992) Dissolution kinetics of kaolinite in acidic aqueous solutions at 25 C, *Geochimica et Cosmochimica Acta*, 56: 3339–3355.

Chapter 4

Membrane Fouling

Membrane fouling is a major problem encountered during the application of membrane separation processes in water and wastewater treatment. Exactly like all other pressure-driven membrane filtration processes, there are inherent problems encountered and a main limiting step in membrane bio-reactors (MBRs) is membrane fouling. Therefore, the success of MBR operation is largely dependent upon how to cope with membrane fouling, which is affected by many factors such as the wastewater influent water quality, membrane characteristics, bioreactor operational conditions, and membrane cleaning methods.

In order to further understand membrane fouling in MBR, this chapter first describes the basics of the membrane fouling phenomena including the classification of foulants, dominant foulants, and factors affecting membrane fouling. The chapter also explains how to determine membrane fouling quantitatively in MBRs.

4.1 Fouling Phenomena

Membrane fouling can be perceived by a decrease in permeation flux or an increase in transmembrane pressure (TMP) according to the operation mode (constant flux or constant pressure mode, respectively). That is, membrane fouling happens when the TMP increases to keep a specific operating flux (constant flux mode) or when permeate flux decreases under the constant pressure mode. Constant pressure filtration behavior is typified by a rapid flux decline at the start of filtration followed by a more gradual decrease until a steady-state or a pseudo-steady-state flux is reached.
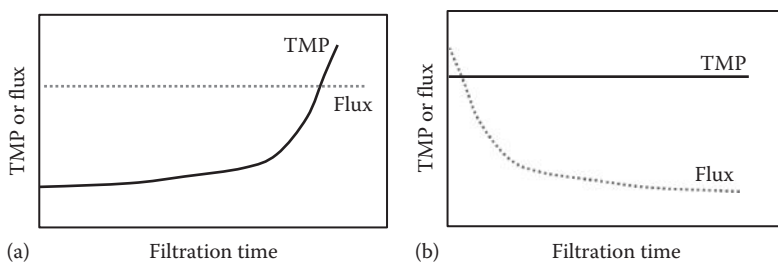
Figure 4.1 Two methods for tracking membrane fouling encountered in MBRs according to operation modes: (a) constant flux mode and (b) constant pressure mode.

Figure 4.1 shows the typical pattern of the fouling phenomena according to the operation mode in MBR. TMP in the constant flux mode and flux in the constant pressure mode should be monitored along with operation run time to perceive fouling in MBR. It is very natural that the lines in Figure 4.1a and b are exactly opposite because TMP and flux reciprocate each other as discussed later in this chapter (resistance-in-series [RIS] model described in Section 4.5.1)

Since most wastewater treatment plants (WWTPs) are operated in constant flux mode, fouling is generally recognized by monitoring TMP variation with time. Slow and gradual increases in TMP are the first symptom of membrane fouling in MBR. Whether proper cleaning has been provided during the operation of MBRs or not, an abrupt increase in the TMP will be observed following the gradual rise in the TMP. Figure 4.2a shows the typical pattern of the slow TMP rise and then the abrupt jump. This TMP pattern is commonly called the two-stage TMP rise-up. The time lapse to the breakthrough point is dependent upon how the cleaning strategy is set up. Appropriate physicochemical cleaning can prolong the time to reach the abrupt TMP rise.
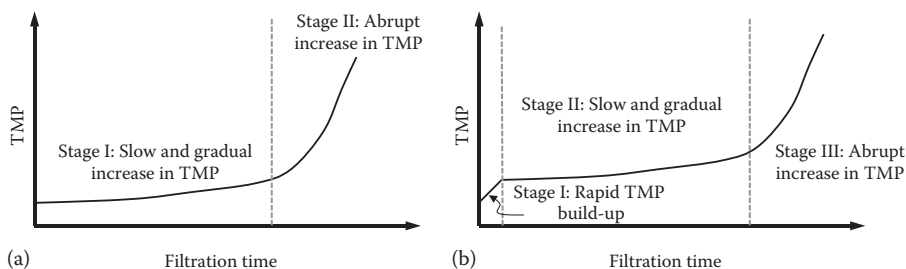
Figure 4.2 Typical TMP jump patterns found in MBR: (a) two-stage TMP jump and (b) three-stage TMP jump.

This characteristic two-stage TMP jump has been explained using two different theories:

1. The TMP jump is due to the local fluxes that are higher than the critical flux.

   During the first step fouling gradually occurs on the porous membrane surface under subcritical flux conditions. In this period, the local filtration flux is still lower than the critical flux, and the number of open pores decreases continuously, and TMP buildup is hydraulically irreversible; this is attributed to the adsorption of solutes and particulates to membrane pore walls and surfaces. After long periods of operation, an abrupt increase in TMP occurs when the local filtration flux exceeds the critical flux. This moment is the onset of the second stage of the TMP profile.

2. TMP jump is due to the extracellular polymeric substance (EPS) change in the cake layer on the membrane surface.

   The second stage TMP jump is closely related to the sudden increase in EPS concentration at the bottom layer of the cake on the membrane surface. The abrupt TMP increase at the second stage under subcritical flux conditions is attributable mainly to a substantial generation of EPSs in the lower layer of the cake over long periods of operation.

TMP is also reported to increase in three stages as shown in Figure 4.2b. Small and rapid TMP increases are commonly observed at the initiation of the MBR operation, which is attributed to rapid blockages of the membrane pores by sludge particles, concentration polarization, and membrane compaction happening at the very early stages of filtration. This first stage TMP increase is often buried by the following second stage increase, so that the overall TMP increase looks like the two-stage TMP profile. The remaining second and third stages occur with the same mechanisms mentioned earlier.

The second stage of TMP buildup is a slow and gradual increase in TMP due to the deposition of microbial flocs and particles on the membrane surface, whereas first stage fouling is the passive adsorption of solutes onto the membrane surfaces and pore walls. The rapid TMP buildup at the third stage is known to be correlated with a reduction in porosity arising from (1) a compression that has been exerted on the cake during the course of operation time as well as (2) increased contents of EPSs interior to the cake layer.

4.1.1 Fouling Rate

Fouling rates are often referred to and used as criteria for membrane fouling. Four consecutive steps can be defined during fouling: (1) blockage of the smallest pores, (2) coverage of the larger pores' inner surface, (3) superimposition of
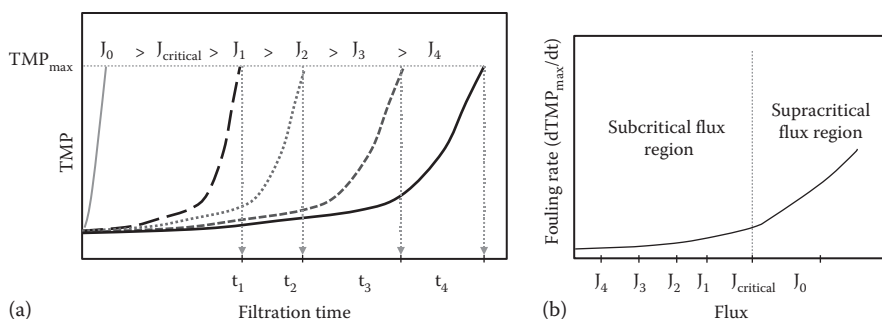
Figure 4.3   (a) Typical TMP rise pattern and (b) fouling rate as a function of flux.

particles and direct blockage of larger pores, and (4) creation of the cake layer. Since each step cannot be readily identified or quantified, determining the overall fouling propensity is generally practiced instead of characterizing each individual fouling step.

The easiest way to have an insight into the fouling propensity is to express the fouling rate. As shown in Figure 4.3a, the derivative form of TMP buildup at a particular time (i.e., dTMP/dt) is the commonly used term to represent the fouling rate. Thus, the unit should be kPa/h or psi/h. A calculated fouling resistance (R) instead of the TMP could be used to express the fouling tendency at a particular time. In this case, the unit of the fouling rate should be $m^{-1} h^{-1}$.

The fouling rate is dependent on the operating flux as shown in Figure 4.3b, i.e., the higher is the operating flux maintained, the faster is the fouling rate. As the operating flux increases ($J_4 \rightarrow J_3 \rightarrow J_2 \rightarrow J_1$), the fouling rate increases until the breakthrough point flux, $J_{critical}$, which is normally called the critical flux. The fouling rate abruptly increases beyond this critical flux, which is called the supracritical flux region. Typical critical flux values, which divide the sub- and supracritical region in MBR plants for domestic wastewater treatment, are usually between 10 and 40 LMH. If the MBR plant treats industrial wastewater or highly variable influent feed stream, the critical flux may differ.

4.2 Classification of Fouling

Membrane fouling in MBR is too complicated to fully understand, and thus, it cannot be described by a single mechanism. There have been many classifications of membrane fouling in MBR by many researchers, but still unified terms describing fouling phenomena have not been set yet. Therefore, membrane fouling in MBR can be classified into different categories according to what the classifying criterion is applied to.

Table 4.1 provides classifications of membrane fouling in MBR. The most simple and easiest way to classify fouling is to consider the reversibility of flux after a simple cleaning operation. According to this criterion fouling is divided into reversible, irreversible, and irrecoverable fouling. Based on the second criterion, the place where the fouling occurs, fouling can be classified into clogging, cake layer deposition, and internal pore fouling. Strictly speaking, the clogging or blocking of membrane channels severely by accumulated suspended solids (SSs) is not classified as membrane fouling because it occurs outside the membrane surface. However, it deteriorates the membrane filtration performance so it is often dealt together with fouling. The pattern of solid buildup is the last criterion. Cake layer formation, pore narrowing, and pore blocking fall into this fouling class. Although membrane compaction is not classified as a kind of fouling, it deteriorates the membrane filtration performance like clogging.

4.2.1 Reversible versus Irreversible and Recoverable versus Irrecoverable Fouling

Traditionally, categorizing membrane fouling into reversible and irreversible is common and even simple. This classification is based on the capability of flux recovery after conventional cleaning steps. Reversible fouling literally means that the flux is recovered after simple cleaning such as backwashing, pressure relaxation, and air scouring, but the flux is recovered only after chemical cleaning when irrecoverable fouling has occurred. On the other hand, irreversible fouling means that the flux cannot be recovered by any means of cleaning (Figure 4.4).

Summarizing this relationship, the following equation on fouling can be expressed:

Total fouling = reversible fouling + irreversible fouling

= recoverable fouling + irrecoverable fouling + irreversible fouling

(4.1)

As membrane filtration starts, TMP increases gradually until the end of stage I. Periodic cleaning, typically backflushing, maintains the TMP as low as possible. Recoverable fouling can be restored easily by simple cleaning (e.g., backwashing or air scouring) during this stage. Irrecoverable fouling might originate from the gel layer, which has been consolidated at the interface between the membrane surface and the cake layer as well as from the strong adsorption of solutes to the pores and/or pore walls. The gel layer and the adsorbed layer in the pores are not easily removed by conventional cleaning protocols but need to be removed by chemical cleaning. Irreversible fouling is relatively smaller than reversible fouling at the initial stage, but it will gradually develop thereafter.

Table 4.1   Classification of Membrane Fouling in MBRs

Criteria Classifying Fouling	Fouling Phenomena	Description
Flux recovery after cleaning	Reversible fouling	Flux is recovered after simple or chemical cleaning.
	Irreversible fouling	Flux is not recovered by any kind of cleaning.
	Recoverable fouling	Flux is recovered after simple cleaning such as backwashing or relaxation.
	Irrecoverable fouling	Flux is recovered only by chemical cleaning.
Places of fouling occurrence	Clogging	Sludge accumulation between hollow fibers and flat sheet membrane channels inside the module.
	Cake layer deposition	Sludge deposition on the membrane surface.
	Internal pore fouling	Adsorption of solutes smaller than the pores to the membrane pore walls.
Solids deposition pattern	Cake layer formation	Vertical buildup of layer on the membrane surface.
	Pore narrowing	Narrowed pore size due to the accumulation of solutes inside pore walls.
	Pore blocking (or plugging)	Particle blockage of the entrance of pores or pore walls.
Solute fouling	Concentration polarization	Concentration gradient of solutes near the membrane surface.
	Gel layer formation	Consolidation of the initially adhered solutes (as well as solids) on the membrane surface.
Nonfouling	Compaction	Compression of membrane structure by the applied pressure.
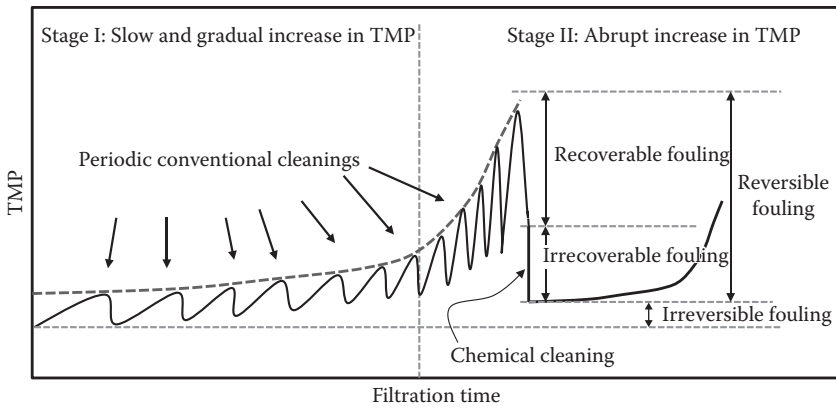
Figure 4.4   TMP profile according to the fouling classification.

TMP abruptly jumps at the onset of stage II and rapidly reaches the maximum allowable TMP. The fouling developed during this short period is mostly reversible fouling (=recoverable fouling + irrecoverable fouling). Chemical cleaning using oxidizing agents such as sodium hypochlorite will decrease the TMP again.

Different types of fouling patterns are shown in Figure 4.5. A ratio of reversible to total fouling, $a/(a + b)$ is not the same for the two different types even though the overall degree of fouling $(a + b)$ is the same. Ratio 1 is higher than ratio 2 as shown in Figure 4.5, which means reversible fouling is more dominant in Figure 4.5a compared to b. This ratio is dependent on what kind of chemical cleaning is used and how severely and/or often the precedent backwashings have been carried out before chemical cleaning. More frequent and severe backwashing before chemical cleaning will result in higher ratios.
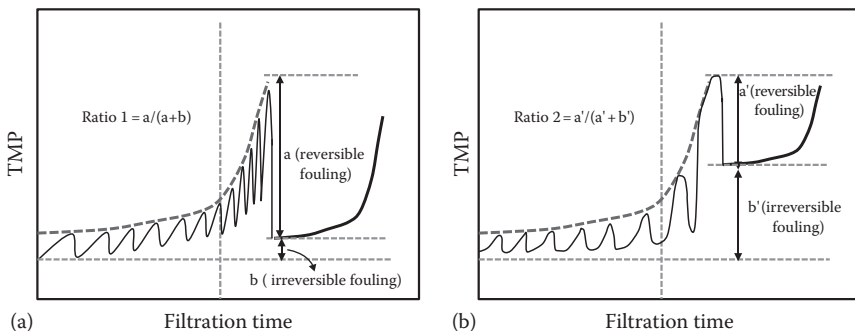
Figure 4.5   Different types of TMP profile according to their fouling pattern: (a) reversible fouling dominant and (b) big irreversible fouling.
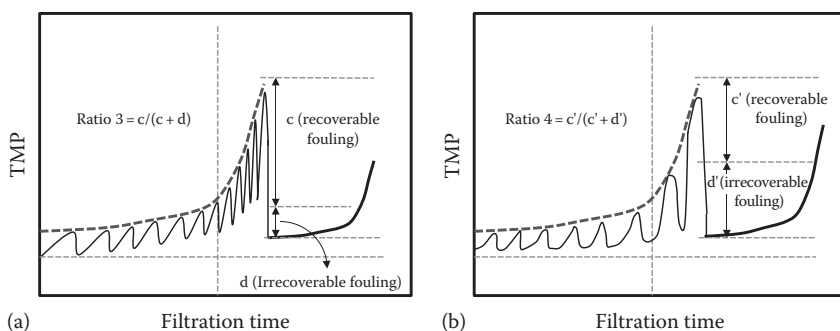
Figure 4.6   Different levels of recoverable fouling: (a) recoverable fouling dominant and (b) high irrecoverable fouling.

Even though the level of reversible fouling is the same for two different TMP buildup patterns, the ratio of the recoverable to the reversible fouling, c/(c + d), is not the same for two cases as shown in Figure 4.6. The ratio is mainly dependent on what kinds of the chemicals are used for the chemical cleaning, how frequently, and how severely the chemical cleaning is carried out.

4.2.2 Classification of Fouling by Location of Fouling

The location where fouling occurs is another criteria to classify membrane fouling: clogging, cake layer deposition, and internal pores fouling. Clogging occurs at the outer space of the membrane bundle, typically between the membrane channels. The cake layer is formed on the membrane surface, which contributes to the most important fouling, whereas internal pore fouling develops inside the membrane.

4.2.2.1 Clogging

Sludge flocs, small particles, and debris in bulk solution are easily migrated and then accumulated to the spaces within the hollow fibers or flat sheet membranes inside a membrane module. Thus, the stream to the membrane surface is choked up completely. This is called clogging, as shown in Figure 4.7, and it blocks the convection flow to the membrane surfaces, which results in the reduction of permeation flux. Clogging is mainly due to a mal-pretreatment of SSs and debris. Clogging could be also attributed to poorly designed membrane modules. If clogging does not occur, the membrane module configuration is properly designed to support good flow from the bulk solution to the membrane surface, and accumulating solids and debris are apt to progress inside the module. Clogging should not be classified into fouling, but it obviously leads to the same result (i.e., the flux reduction or the TMP buildup like other fouling phenomena).
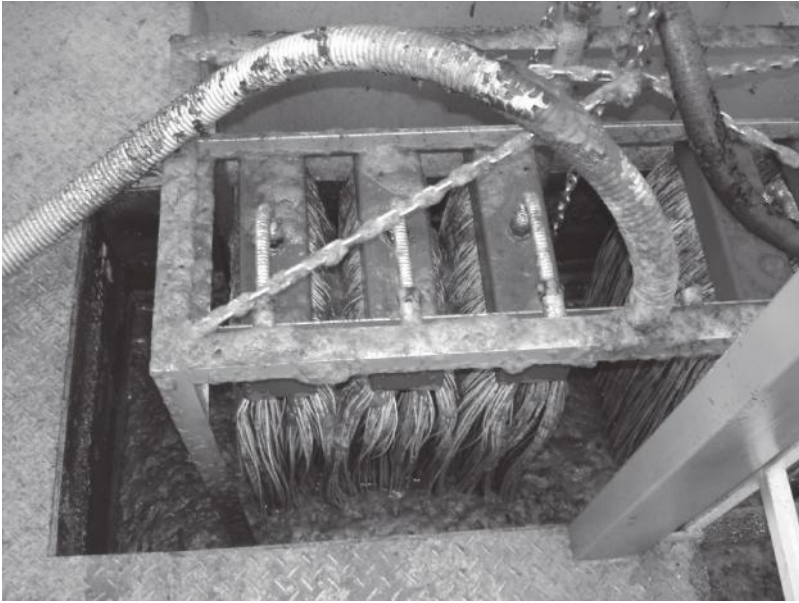
Figure 4.7 **Photo of typical clogging in the hollow fiber membrane channels.**

Membrane clogging in MBRs has been largely unexplored academically because it is difficult to scientifically and quantitatively evaluate even though it has been widely recognized as a key impediment to sustainable MBR operation. Proper preliminary treatments for the influent wastewater such as screens, bar racks, and grit chambers could reduce clogging problems.

4.2.2.2 Cake Layer

Cake layer formation on membrane surfaces has been known to be a predominant fouling mechanism in MBR regardless of membrane type, wastewater characteristics, and operating conditions. Mixed liquors and SSs in the aeration basin start to deposit onto the membrane surface from the beginning of filtration due to the convective flows from bulk solution to the membrane.

The thickness of the cake layer increases at the initial stage of cake deposition, but it reaches a plateau. Hydrodynamic conditions near the membrane surface resulting from extensive coarse aeration do not allow the cake layer to develop further. Cake layer thicknesses range from several to hundreds of micrometers, mainly depending on the membrane applied pressure and aeration intensity. Generally speaking, a thicker cake layer could induce higher cake resistance. However, the cake layer thickness is not the sole factor determining membrane filterability.

For example, cake resistance (R_c), which is closely related with membrane filterability, is a function of the specific cake resistance (α) of the cake layer and the weight of the biomass (M) on the membrane surface:

$$R_c = \frac{\alpha \cdot m}{A_m}$$

(4.2)

where
   α is the specific cake resistance of the biofilm, m/kg
   m is the mass of the biofilm, kg
   A_m is the membrane area, m^2

According to the Carman–Kozeny equation, both the size of particles (e.g., microbial flocs) and porosity are key parameters determining the specific cake resistance of a cake layer:

$$\alpha = \frac{180(1-\varepsilon)}{\rho_p . d_p^2 \cdot \varepsilon^3}$$

(4.3)

where
   ε is the porosity of the cake layer
   ρ_p is the density of particles, kg/m^3
   d_p is the particle diameter, m

Since the density of activated sludge (ρ_p) is not greatly changed in most biological wastewater treatment environments, the most predominant factor affecting the specific cake resistance is the particle size (d) and the porosity (ε). Therefore, the filterability of a thick cake would be greater than that of a thin cake if the latter is made of finer and smaller particles than the former.

Figure 4.8 shows the image of a cake layer formed on a hollow fiber membrane using confocal laser scanning microscopy (CLSM) and the reconstructed 3D structure from the images.

Among the various techniques to analyze the cake layer structure, CLSM allows for nondestructive in situ examination of cake layers on a membrane surface. This technique can be effectively used for visualization and quantification when combined with a fluorescent probe, which can be achieved using different staining techniques for the bio-cake components (Bressel et al., 2003). The bacteria in the cake layer should be stained first with some commercial staining agents that are specific to nucleic acids. After dye addition the cake layer is incubated for 30 min at room temperature in the dark and then washed with phosphate-buffered saline solution. The stained cake layer is immediately observed using CLSM and the signals are recorded.

(a) (b)
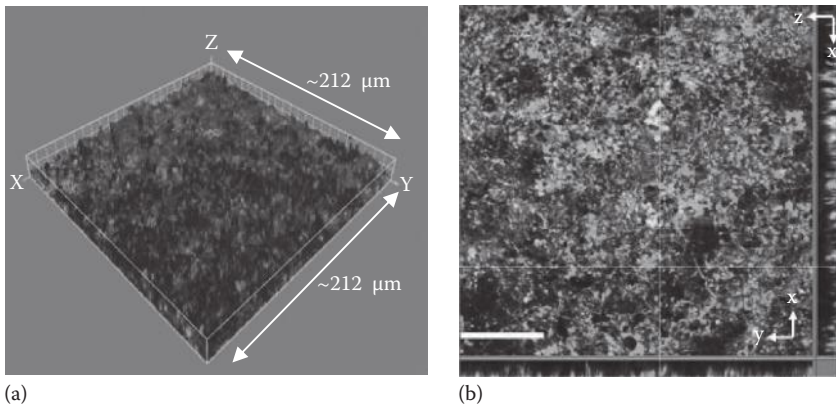
Figure 4.8   3D structure reconstructed from the CLSM images and (b) CLSM projection image of a cake layer formed on the membrane using CLSM: bright gray, bacterial cell; dark gray, EPS (polysaccharide); and black, void.

For observation and visualization of the bio-cake, the CLSM assistant software supplied by the manufacturer or commercial visualization software can be used to develop the 3D digitized image. The CLSM images from top to bottom in depth are reconstructed to visualize the bio-cake. Figure 4.9 shows one example of 3D cake layer images reconstructed by one of the commercially available software. The software ISA-2, developed by Beyenal et al. (2004), is an image analyzer used to
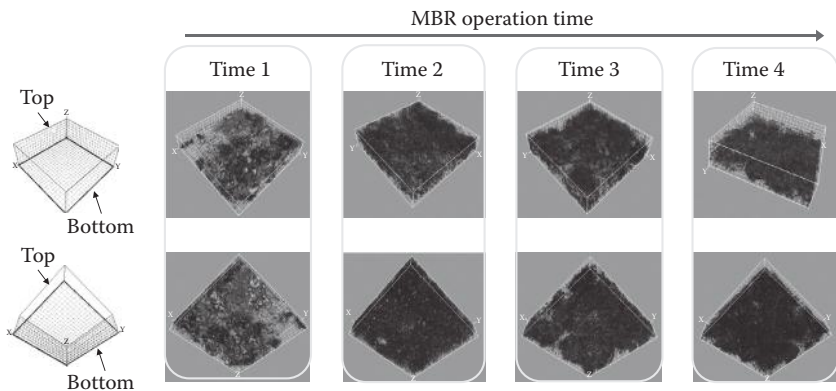
Figure 4.9   Volumetric 3D reconstructed images of bacterial cells and polysaccharides present in a cake layer on a membrane surface in an MBR: bright gray, bacterial cells, and dark gray, polysaccharides.

determine the structure of the cake layer and can be used to calculate the porosity of the cake layer.

4.2.2.3 Internal Pore Fouling

Dissolved solute and fine particulate adsorption to internal pore walls govern internal fouling. From the early stage of filtration, adhesion occurs when dissolved matter and colloidal particles in mixed liquor begin to attach to the pore entrance and pore walls of the membranes, narrowing the pore diameter. After sufficient cake buildup on the membrane surface, the dissolved matter and fine particulates are prone to attach preferentially to the sticky cake layer prior to being transported to the membrane pore walls, also called cohesion.

Generally speaking, the predominant fouling resistance is the cake layer resistance (R_c) rather than the internal fouling (R_f). Several to tens of times larger cake resistances compared to internal fouling have been reported in most cases of MBRs.

4.2.3 Solids Deposit Pattern

According to the pattern on how the solids and solutes are deposited onto the membrane, fouling can be classified into (1) cake layer formation, (2) pore narrowing, and (3) pore plugging as shown in Figure 4.10.

Cake layer formation occurs on the membrane surface and entrance channels and has been already explained in the previous section. As the name indicates, pore plugging occurs when particles become stuck in the pores of a membrane, i.e., the pore plugging (or blocking) occurs when particles (mainly activated sludge flocs) and/or microbial cells slightly bigger than the pore size block the entrance of pores,
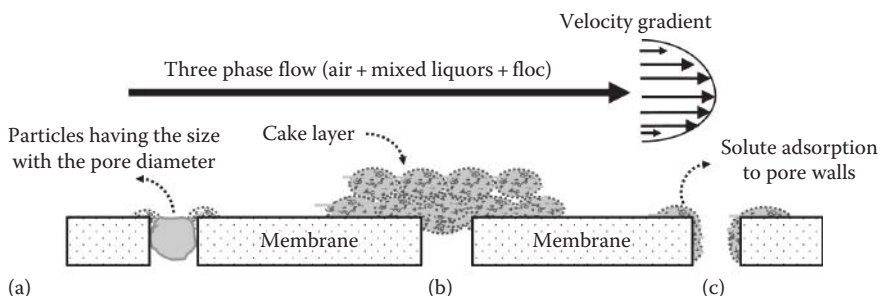
Figure 4.10 Membrane fouling pattern in MBR (a) pore clogging (or plugging) caused by particles with sizes similar to the pore, (b) cake layer deposition, and (c) pore narrowing mainly caused by dissolved solutes.

or when particles of the same size as the pore size are caught in pores, resulting in jammed particles in pores. Pore narrowing also happens when solute and particulates smaller than the pore diameter deposit onto the surface of a membrane as well as in the interior pore walls.

These individual fouling patterns never happen separately or independently, but they always occur simultaneously (i.e., they coexist). The individual fouling patterns cannot be observed in activated sludge filtration.

4.2.4 Solute Fouling

4.2.4.1 Concentration Polarization

Concentration polarization due to concentration gradients formed near the membrane surface also happens in MBR as like all other membrane filtration processes. However, concentration polarization exists in a very limited range of distance close to the membrane surface so that it is buried underneath the cake layers. Therefore, it cannot be distinguished well from the cake layer, and as a result, concentration polarization is not considered important in MBR operation.

4.2.4.2 Gel Layer Formation

Gel layers are often confused with the cake layers. Strictly speaking, a gel layer consists of highly concentrated solutes and macromolecules rather than particulates. As the concentration polarization progresses near the membrane surface, the gel layer forms and expands. However, gel layers are easily incorporated into cake layers so it is difficult to distinguish the two. Gel layers are simple and consolidated cake layers.

4.3 Types of Foulants

Membrane fouling in MBR is attributed to the physicochemical interactions between biofluids and membranes. In order to get an insight of the possible foulants, it is necessary to scrutinize the biofluid constituents. Unlike the simple and well-defined chemical nature of membrane properties, mixed liquor in an aeration basin has complex characteristics because it consists of many constituents that are not easily defined.

Figure 4.11 summarizes each constituent present in mixed liquor as potential candidates for foulants. Basically the mixed liquor in the aeration tank where a membrane unit is immersed consists of particulates (insoluble parts) and soluble matter. Particulates can be divided further into three parts: sludge flocs, individual microbial cells, and debris. The origin of soluble matter is divided into three parts: unmetabolized feed components from influents of wastewater, soluble microbial products (SMPs) secreted by microorganisms, and soluble inorganics.
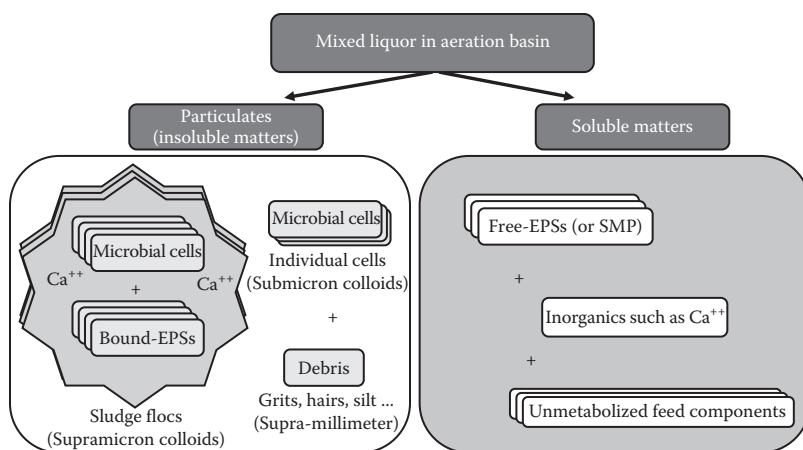
Figure 4.11 Conceptual illustration showing each component of activated sludge mixed liquor.

4.3.1 Particulates

Since membrane filtration is basically a sort of solid–liquid separation, the particulates in an aeration basin should be primarily considered as important foulants in the MBR. The majority of particles in the mixed liquor based on mass are the activated sludge flocs, although individual microbial cells and debris are also present in the mixed liquor.

4.3.1.1 Flocs

An activated sludge floc can be defined as a microbial entity that is formed by different species. Individual microbial cells are interconnected by EPSs and cations such as Ca^{2+} ions. This leads to a formation of a 3D structural matrix, or "flocs." The constituents of the flocs are embedded in a polymeric network of EPSs.

Mixed liquor suspended solids (MLSS) is a basic component comprising bulk solution in activated sludge. Therefore, the effect of MLSS concentration on membrane fouling has been investigated thoroughly for the last couple of decades. MLSS concentration is believed strongly to have a correlation with fouling (i.e., degree of fouling increases as MLSS concentration increases). Because the viscosity of mixed liquor increases as the MLSS concentration increases, filtration resistance increases according to the RIS model, which will be described in Section 4.5.1. However, inconsistent and contradictory fouling tendencies associated with MLSS concentration are found in some cases, which are attributed to other fouling factors prevailing against the MLSS influences.

Debris such as grit, hair, and plastic materials are categorized into particulates. One of the notorious troubles of submerged MBR plants is the entanglement of hairs with membrane fibers, which can result in entire system shutdowns. Proper preliminary treatments such as screens and/or grit chambers can solve these kinds of problems.

4.3.1.2 Floc Size

Figure 4.12 is one example diagram showing floc size distribution of activated sludge suspensions with different MLSS concentrations. As shown in the figure, the typical size of sludge flocs agglomerated from individual cells range from a micrometer up to several hundred micrometers regardless of MLSS concentration. Particles that are between 1 and 100 μm in size are often classified as supracolloidal solids, and particles >100 μm are called settleable solids. Colloidal particles are between 0.001 and 1 μm in size (Guo et al., 2012).

In terms of floc size, the majority of the mixed liquor of activated sludge seems to belong to the settleable solids based on sludge volume frequency. However, the number of small (>10 μm) and colloidal (>1 μm) particles is greater than that of the settleable solids. Particularly, individual activated sludge cells in the bulk solution typically range from submicron to several microns because the majority of microbial cells are bacteria. Colloidal particles including individual cells and small flocs adversely affect membrane filterability in MBRs because the size of these fine
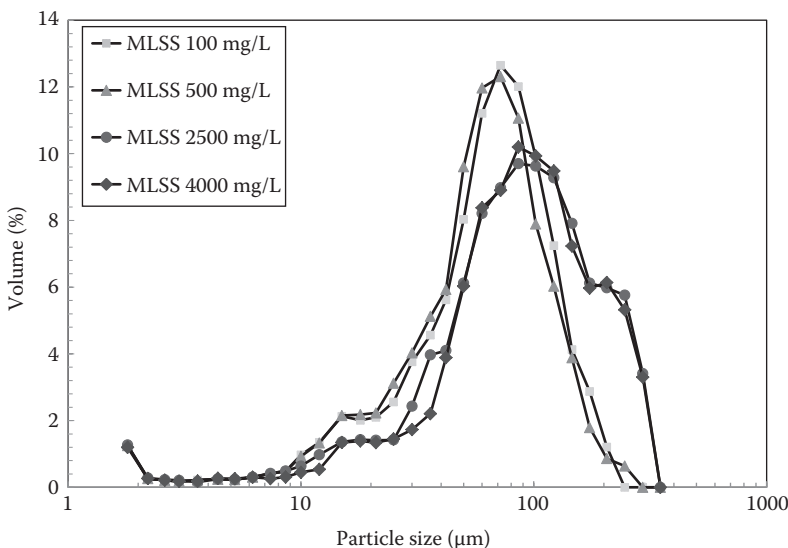
Figure 4.12   Typical particle size distribution of activated sludge with different MLSS concentrations.

particles is similar to the membrane pore sizes. Most membranes used in MBR plants for wastewater treatment belong to either MF or UF, in which they have a submicron pore size, so that the similarity in size of the membrane pores and feed stream particles leads to severe membrane fouling—pore blocking—making it difficult to recover the permeate flux by conventional physicochemical cleaning methods.

There is another reason why fine particles are important to understanding the fouling phenomena. The particles in the cake layer deposited on membrane surfaces are compressed by the convection flow toward membrane surfaces. However, the particles move backward from the cake layer to the bulk solution simultaneously due to diffusion caused by concentration gradients, which is called back transport. In general, the fine particles have a small back-transport velocity. Therefore, the smaller the particle size is, the slower back transport is. This results in a diminished scouting impact on the cake layer, leading to insufficient cleaning (i.e., fouling is worsened).

Therefore, particle size is one of the most important parameters related to membrane fouling in MBRs. The average floc size found in conventional submerged-type MBR is typically around 80–160 μm depending on the microbial physiology, influent characteristics, and WWTP site. But the average floc size in sidestream MBR is much smaller than that of submerged-type MBR because of the recirculation of mixed liquor from the aeration basin to the membrane module that is present outside the tank. This transfer provides the flocs a shear force, and the flocs experience disintegration (or deflocculation), which results in smaller particle sizes than that of submerged MBRs. Therefore, sidestream MBR designs must consider how to avoid severe membrane fouling due to small floc sizes.

Evaluating the fouling propensity by the mean particle sizes based on the volume frequency as shown in Figure 4.12 might not always be adequate. The average particle size (or median value) is decided by several big particles, that is, a small number of bigger particles occupy most of the total volume. Even though the overall volume occupied by fine particles is much smaller than that of the big particles, the number of fine particles is obviously greater than that of the bigger particles. Because the contribution of smaller particles to membrane fouling is more important than that of bigger particles as mentioned previously, understanding or describing a fouling phenomenon with average particle size based on the volume frequency could often fail.

Figure 4.13 is an example showing the importance of choosing the appropriate method to express particle size distribution when considering the fouling potential. Two bioreactors (designated as sludge 1 and 2) employing identical membranes show different fouling propensities. Sludge 1 shows more fouling tendency than sludge 2. The difference in the particle size distribution between them based on the volume frequency (Figure 4.13a) does not appear to correlate the fouling propensity and the particle size. Thus, the data in Figure 4.13a based on the volume frequency are transformed into that based on the number frequency (Figure 4.13b). In this
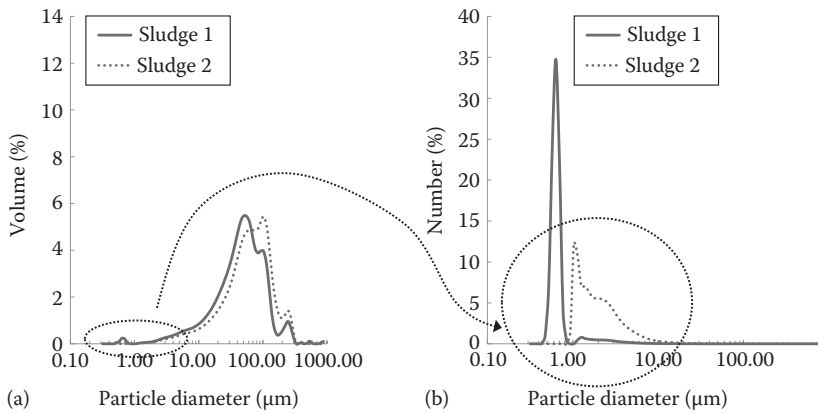
Figure 4.13 Expression of particle size distribution based on (a) volume frequency and (b) number frequency.

case, it is clearly seen that in the range of 0.1–10 μm, the fraction of smaller particles in sludge 1 is much greater than that in sludge 2, indicating that severe fouling in sludge 1 is attributed to the fine and submicron particles. This example emphasizes the importance of interpreting particle size based on the number frequency.

4.3.1.3 Extracellular Polymeric Substances

Microbial EPSs are high-molecular-weight mucous secretions from microbial cells. EPSs play an important role in floc formation of individual cells and include heterogeneous polymeric materials including polysaccharides, proteins, lipids, and humic-like substances as major components and phospholipids and nucleic acids such as DNA and RNA as minor constituents. Among these components, polysaccharides and proteins play a significant role in membrane fouling.

Since EPSs provide a highly hydrated gel matrix in which microorganisms are embedded, they provide a significant barrier to permeate flow in MBRs. Therefore, EPSs have been considered as one of the most important foulants in MBR processes. In addition, trace deposition of polysaccharides also contributes to the initial slow TMP increase during subcritical filtration condition. Generally speaking, high concentrations of EPSs inside flocs as well as in bulk solution are responsible for rapid fouling buildup. The EPSs inside flocs are often called bound EPSs in order to differentiate them from the free EPSs that are present in the bulk solution in a soluble state.

Internal pore fouling due to pore narrowing or pore blocking plays an important role in fouling, but it can be prevented to occur partially by means of pretreatments of feeds and proper selection of pore size. Therefore, predominant filtration resistance is normally attributed to the cake layers on membrane surfaces due to

convection flow. The bound EPSs tightly maintain the internal structure of the cake layer and act as a barrier of the permeation flow to the membrane surface. Therefore, the amounts of bound EPSs in the cake layer have been considered one of the important fouling indexes in MBRs.

4.3.1.4 EPS Extraction and Quantitative Analysis of EPS Components

Quantitative determination of foulant concentrations is important for setting up a strategy for fouling control. Therefore, identifying what the key foulants are and determining the concentration of components of bound EPSs are the initial steps for fouling control.

Figure 4.14 shows a general protocol for EPS extraction from fouled membranes in MBR. To analyze the bound EPSs in the cake layer quantitatively, first you must detach the cake layer from the membrane surface. To do this, membranes are taken out of the MBR reactor and repeatedly washed and resuspended with saline buffer solution until all biomass from the cake layer has been transferred from the membrane to the suspension.

The next step is to separate the particulates from this detached solution by means of centrifugation near $4000 \times g$ and/or filtration using a 0.2 µm membrane filter. To reduce thermal damage to microbial cells, centrifugation is usually carried out
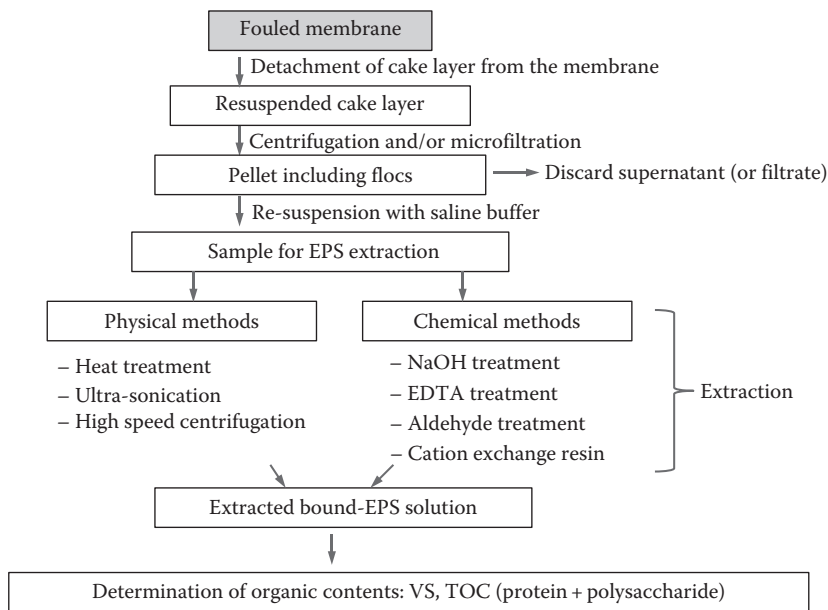
Figure 4.14 EPS extraction procedure for a fouled membrane in MBRs.

under 4°C. After discarding the supernatant, the remaining pellet, which is comprised mainly of sludge flocs and microbial cells, is to be resuspended with a saline solution such as a TRIS buffer. This is the starting point of the next of EPS extraction and further extraction procedures use the resuspended solution as a basic sample.

Various kinds of EPS extraction methods from activated sludge flocs have been developed. The methods are simply classified into physical and chemical extraction. Heat treatment, ultrasonication, and high-speed centrifugation belong to physical extraction. Chemical methods include treatments with NaOH, aldehyde, cation exchange resin (CER), and ethylenediaminetetraacetic acid (EDTA). Heat treatment over 80°C–100°C for 1–2 h can release the interior EPSs out of the resuspended pellet. Ultrasonication over 40 W for 2–10 min can also satisfy the purpose of EPS extraction. High-speed centrifugation is carried out at high gravity normally over 20,000×g. Remember that the gravity force for supernatant separation is around 4000×g, but it was found that high-speed centrifugation did not guarantee a good release of EPSs without cell damage, so it is not used anymore.

Addition of a strong alkaline solution such as NaOH leads to alkaline hydrolysis, which weakens the bonds between cells and exopolymers. Aldehyde (such as formaldehyde or glutaraldehyde) is an auxiliary chemical added with the alkaline solution or ultrasonication. The EPSs are interconnected by multivalent cations such as Ca^{2+} in the sludge matrix. The addition of CER or EDTA to the sample removes the Ca^{2+} ion, making the bonds between the EPSs and Ca^{2+} weak, leading to a release of EPSs out of the flocs.

A good extraction procedure should cause minimal cell lysis and not disrupt the exopolymers. Details and comparisons between each method are summarized well in literature. Because each method of extraction yield and cell lysis has positives and negatives, there is no current standardized method.

Whatever extraction methods are used, the EPSs are transferred from the resuspended pellet into the aqueous phase. This is the extracted bound EPS solution in Figure 4.14. Determining the organic contents of this solution is the final step of the procedure. For example, analysis of the volatile solids (VSs), total organic carbon (TOC), or (protein + polysaccharide) concentration is a common way to examine the organic content of the extracted EPSs. Therefore, several units are used to express the total amount of bound EPSs according to the methods employed for the quantitative determination of organic contents. In order to compensate for the sample's mass of microorganisms, organic contents have to be divided by the MLSS concentration of the sample as follows:

- mg VS/g mixed liquor of volatile suspended solids (MLVSS)
- mg TOC/g MLSS
- mg (proteins + polysaccharides)/g MLSS

If information on the chemical composition of the bound EPSs is needed to understand fouling behavior, quantitative analyses on the extracted bound EPS solution

should be carried out. As mentioned earlier, the main components of EPSs that affect membrane fouling are proteins and polysaccharides. Carbon 13 isotope nuclear magnetic resonance (^{13}C-NMR) analysis confirmed that foulants are rich in proteins and polysaccharides. Fourier transform infrared (FTIR) analysis also confirmed the presence of amide I and II peaks (1638 and 1421 cm^{-1}) and a carbohydrate-like substance peak (Yamamura et al., 2007). In most cases, the observed protein concentration ranging from 10 to 120 mg/g MLSS is greater than the typical polysaccharide concentration, typically 6 to 40 mg/g MLSS (Le-Clech et al., 2006).

The Lowry method (Lowry et al., 1951) and the phenol sulfuric method (Dubois et al., 1956) are the basic procedures used for the quantitative analysis of proteins and polysaccharides. The principle of both methods is based on absorbance measurements using a spectrophotometer, so both methods require standards to calibrate for proteins and polysaccharides. Bovine serum albumin (BSA) and glucose are the most common standards for model compounds. But the real bound EPSs contain various kinds of proteins and polysaccharides. Therefore, explaining fouling with EPS data obtained from analyses using some specific standard is inherently very limited.

Although the total amount of bound EPSs is crucial to understanding fouling mechanisms, the ratio of the proteins and polysaccharides has also been considered an important factor affecting fouling in MBRs. Yao et al. (2010) reviewed multiple studies and reported that the ratio of proteins/polysaccharides varies from 1 to near 10. Sludge with higher ratios of proteins and polysaccharides in the bound EPS resulted in higher stickiness, stimulating the cake formation and increasing membrane fouling.

The molecular weight distribution of bound EPSs could be identified by chromatographic analyses, such as size-exclusion chromatograph (or gel permeation chromatograph). Gorner et al. (2003) revealed that the proteins' molecular weight ranged from 45 to 670 kDa. However, the polysaccharides had very small sizes of <1 kDa and were present in smaller amounts than the proteins.

Example 4.1

To analyze the bound EPS concentration in the activated sludge suspension in an MBR plant, 1000 mL of mixed liquor was taken from the aeration basin in the plant and delivered to a laboratory. The mixed liquor was immediately centrifuged at 3500 rpm, and the supernatant was discarded. The pellet was washed several times by TRIS buffer solution and then resuspended within it. The resuspended solution was heat-treated at 90°C for 2 h in the oven and then was cooled to room temperature. Two hundred milliliters of the chilled solution was transferred to a melting pot in order to measure the VS contents according to the standard methods (American Public Health Association, American Water Works Association, Water Environment Federation). Calculate the bound EPS concentration of the sample of the activated sludge suspension with the following data:

- MLVSS concentration: 8000 mg/L
- Mass of the melting pot: 20.000 g

■ Mass of the melting pot after evaporation in the drying oven: 21.050 g
■ Mass of the melting pot after ignition in the muffle furnace: 20.330 g

Solution

1. Calculation of VS of the extracted solution

$$VS\left(\frac{mg}{L}\right) = \frac{\text{mass of volatile solids}}{\text{sample volume}}$$

$$= \frac{(21.050 - 20.330)\text{g}}{200\ \text{mL}} \times \frac{10^3\ \text{mg}}{\text{g}} \times \frac{10^3\ \text{mL}}{\text{L}} = \frac{3,600\ \text{mg}}{\text{L}}$$

2. Calculation of the bound EPS

$$\text{Bound EPS}\left(\frac{mg\ VS}{g\ MLVSS}\right) = \frac{\text{VS of extracted solution}}{\text{sample MLVSS}}$$

$$= \frac{3600\ \text{mg VS}}{\text{L}} \frac{\text{L}}{8000\ \text{mg MLVSS}} \frac{10^3\ \text{mg}}{\text{g}}$$

$$= 450\ \frac{mg\ VS}{g\ MLVSS}$$

Remark

The calculated value of the bound EPS concentration is 450 mg VS/g MLVSS, which seems a lot (i.e., 450 mg of bound EPSs is present in 1 g of MLVSS). This is due to the nature of the extraction method chosen. Heat treatment for 2 h at 90°C is high enough to damage the cell structure, so this treatment can release not only the bound EPS on the cells but also inner cell plasma, individual cells, and cell debris. That is, the heating broke apart cells that were then measured as EPS. Therefore, a precipitation procedure is needed to exclude the cell and/or cell debris from the extracted solution. For example, acetone or ethanol is used for precipitation with the extracted EPS solution. The precipitated bound EPSs are separated from the solution and analyzed further, which would represent a more exact level of the bound EPS.

4.3.2 Soluble Matter

The origin of soluble matter is divided into two categories: unmetabolized feed components from influent wastewater and SMPs secreted by microorganisms. Both the SMPs and the soluble EPSs (or sometimes called free EPSs) are used to express the soluble organic solutes in bulk solution originating from microbial excretion. They are sometimes interchangeable terms. SMP is a more comprehensive term than soluble EPSs because soluble EPSs indicate only the macromolecules. However, it is very difficult to distinguish both of them by chemical analysis because their basic chemical composition is similar, the proteins and polysaccharides.

4.3.2.1 SMPs or Free EPSs (Soluble EPSs)

The terms SMPs and soluble EPSs are used with confusion when they are used to describe key membrane foulants in MBRs. Basically SMPs represent all kinds of soluble organics excreted from microbial metabolism including monomers, oligomers, or polymers. EPSs obviously have a polymeric nature, but the borderline dividing polymers and oligomers is obscured to some extent. Moreover, unmetabolized feed components are not related to microbial excretion products, but they are categorized into SMPs or soluble EPSs when they are chemically analyzed. Practically, it is difficult to analyze or differentiate SMPs and EPSs no matter where they originate (either cells or feed solution). Therefore, some research groups categorize all EPSs and SMPs into a single group called biopolymeric cluster (BPC).

Exact definitions for EPSs, bound EPSs, loosely bound EPSs, extracted EPSs (eEPSs), soluble EPS, free EPS, BPC, and SMP are not set up, and they are often used confusedly. Le-Clech et al. (2006) distinguished between EPSs and SMP as shown in Figure 4.15, and they proposed a method for EPS and SMP extractions and measurements. They simply divide EPSs into EPS extracted artificially from biological cell flocs (eEPS) and SMPs. They reported that SMPs are easily obtained by simple solid–liquid separation of mixed liquor such as centrifugation and subsequent 1.2 μm filtration.
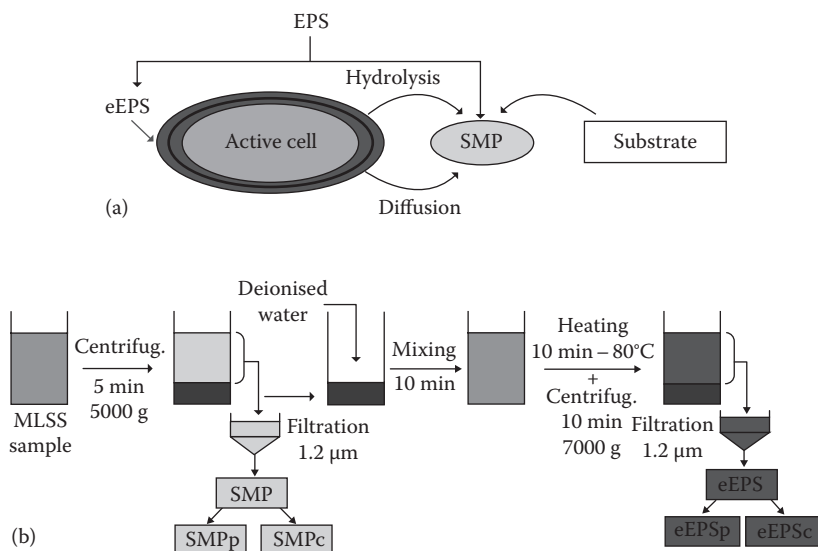
Figure 4.15 (a) Simplified illustration of EPSs, eEPS, and SMP and (b) a proposed method for EPS and SMP extractions and measurements. (Adapted from Le-Clech, P. et al., *J. Membr. Sci.*, 284, 17, 2006.)

However, the unmetabolized feed solution is still present in the mixed liquors. Strictly speaking, the SMPs obtained by this method do not represent only pure microbial products. According to this procedure, the feed components, soluble EPSs, and SMPs are not separated and distinguished from each other. The protein and carbohydrate components of the SMPs are analyzed further and designated as either SMPp or SMPc. The pellet remaining after centrifugation is resuspended by de-ionized water and the eEPSs (i.e., bound EPSs) are extracted by one of the procedures described previously. Finally, they are separated into eEPSp (proteins) and eEPSc (carbohydrates).

It is well known that the EPSs play a key role in membrane fouling in MBRs. However, it is difficult to correlate every EPS component to a fouling parameter because the quantitative and qualitative characterization of the bound EPSs, the free EPSs, and the loosely bound EPSs is practically impossible.

As indicated previously, the bound EPSs act as a permeation flow barrier in the cake layer on the membrane surface. Therefore, the concentration of the bound EPSs is directly proportional to cake layer fouling. However, soluble EPSs are present in the bulk solution, so they play an important role in internal membrane fouling rather than cake layer fouling. Adsorption of soluble EPSs to pore walls leads to internal pore narrowing.

Many studies have reported that high concentrations of free EPSs deteriorate membrane performance (i.e., free EPSs are closely related to fouling). However, the fouling caused by the free EPSs is believed to be less severe than that of the fouling caused by bound EPSs because the predominant fouling in MBRs is usually dependent on the extent of cake layer fouling.

Quantitative determination of free EPS concentrations is similar to the procedure described for EPS extraction as mentioned previously. Activated sludge suspension from the aeration basin is filtered or centrifuged first to remove the particulates. The supernatant remaining after centrifugation or filtration is mixed with a solution mixture (1:1) of acetone and ethyl alcohol. The solution is then transferred to a refrigerator and kept at 4°C for a day. The free EPSs are precipitated during storage, that is, they are salted out and released to the solution. Finally, the precipitated EPSs are ready for determination of mass or further analyses of their chemical components by chromatography.

Attempts to correlate the molecular weight (MW) of free EPS and membrane fouling have been tried. The MW of EPSs is commonly analyzed by gel permeation chromatography. Wang and Wu (2009) reported that the MW of EPS in MBR was 2.2–2,912 kDa, and conventional activated sludge systems contained MWs that ranged from 2.4 to 18,968 kDa. They pointed out that many parameters such as solids retention time (SRT), temperature, gas sparging, substrate composition, and loading rate can influence the EPS concentration and composition in the mixed liquors of both MBR and conventional activated sludge (CAS) processes. Thus, the same parameters could affect the MW distribution of EPS.

Therefore, it is very difficult to obtain a general relationship between the MW of EPS and membrane fouling.

Fluorescence excitation emission matrix (FEEM) spectroscopy can characterize the chemical structural components of soluble organic matter. It is has been proven to be a rapid, selective, sensitive, and useful technique to differentiate the changes and transformations of organic matter in natural environments. FEEM spectroscopy can inform us of the fluorescence characteristics of samples, which are obtained by changing the excitation and emission wavelength simultaneously.

FEEM spectroscopy could be useful in studying the chemical and physical characteristics of dissolved organic matter (DOM) and in interpreting the DOM fluorescence properties due to its high sensitivity, good selectivity, and nondestruction of samples. Therefore, it has been used to compare the chemical structures of influent SMPs and membrane foulants in MBRs, where the spectral similarities between the organic matter in SMPs and foulants have been observed. According to the fluorescence of different spectral regions, it could be also used to distinguish the fluorescent compounds present in the SMPs and the foulants.

Henderson et al. (2011) proposed that seven major components of activated sludge samples can be identified by the excitation and emission wavelength ($\lambda_{ex/em}$) positions of FEEM spectroscopy. They tried to understand the effects of organic matter on membrane fouling by correlating the spectrum of the bulk solution in the aeration basin and the foulants:

1. 390/472 nm—Terrestrial humic-like fluorescence
2. 310/392 nm—Microbially derived humic-like fluorescence
3. 350/428 nm—Wastewater/nutrient enrichment tracer
4. 250/304 nm—Associated with proteins, fluorescing in the same region as tyrosine standards
5. >250/348 nm—Associated with proteins, fluorescing in the same region as tryptophan standards
6. 290/352 nm—Associated with proteins, fluorescing in the same region as tryptophan standards
7. 270/304 nm—Associated with proteins, fluorescing in the same region as tyrosine standards

The basic principle of the FEEM technology is to correlate the output spectra with the library spectra of known foulant groups. The EPSs play an important role in membrane fouling and are major constituents of membrane foulants. Therefore, the fluorescence characteristics of soluble EPSs in the MBR basin are well correlated with the FEEM spectra of membrane foulants.

For example, peak A in Figure 4.16 observed in the FEEM spectra of membrane foulants originated from organic substances with similar fluorescence characteristics as the soluble organic matter of the aeration basin (Wang et al., 2009). The two
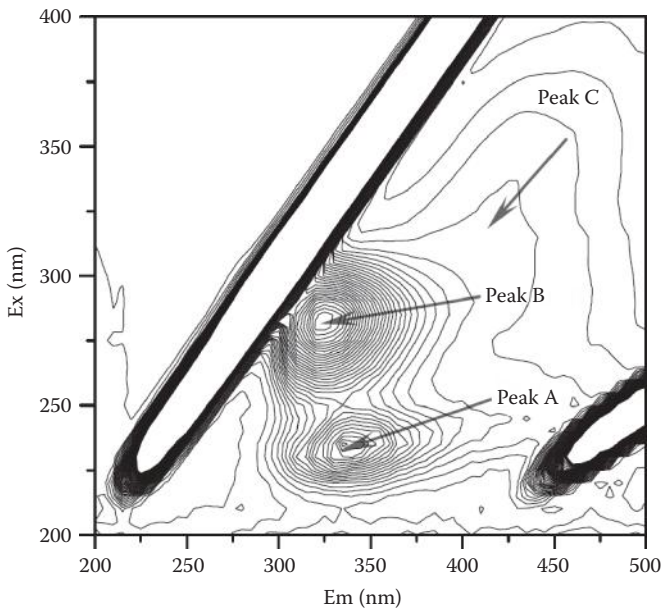
Figure 4.16 Example of the FEEM spectra of membrane foulants in MBRs. (Adapted from Wang, Z. et al., *Water Res.*, 43(6), 1533, 2009.)

main peaks (peak A and B are protein-like peaks) in Figure 4.16 similarly appeared in the existing FEEM spectra in the EPS samples, but their specific locations were slightly different.

4.4 Factors Affecting Membrane Fouling

Although it is difficult to establish a general rule about membrane fouling in MBRs, the nature and extent of fouling are strongly influenced by three factors, as shown in Figure 4.17 (Chang et al., 2002): the characteristics of mixed liquor in membrane tank, the membrane and module type, and the operating conditions, which are considered in the following sections.

Individual fouling factors affect membrane fouling separately and/or mutually. They influence each other as shown in the figure. For example, important operating conditions such as the hydraulic retention time (HRT) and SRT influence membrane fouling directly. They affect the microbial characteristics simultaneously such as EPS production or MLSS concentration, which are important factors controlling membrane fouling.
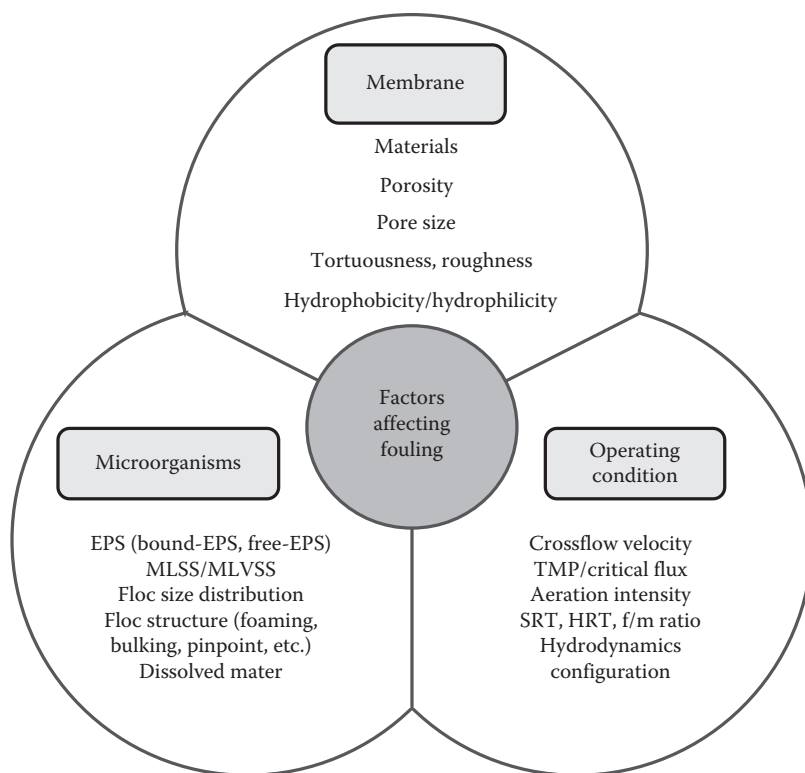
Figure 4.17 Factors affecting membrane fouling in MBRs.

4.4.1 Membrane and Module

Membrane characteristics that affect fouling in MBRs are pore size, porosity, surface energy, charge, roughness, raw materials, hydrophilicity/hydrophobicity, etc. Each factor listed has been known to directly impact membrane fouling.

4.4.1.1 Pore Size

The effect of pore size on fouling intercorrelates with the feed solution characteristics, particularly the particle size distribution of the activated sludge suspension. Larger pore sizes do not always lead to greater flux rates due to internal fouling (i.e., the flux produced from smaller pore sizes can be higher than that from larger pore sizes). This is due to the size similarity of the pores and the particles in the feed. If the average pore size is similar to the size of the particles, pore plugging (or clogging) described in Figure 4.10 is likely to happen, which will fatally reduce the permeate flux. The typical lower size range of activated sludge suspension particles

is submicrometer (i.e., nearly close to the pore size of conventional microfiltration membranes). Therefore, ultrafiltration membranes that have smaller pore sizes than microfiltration membranes are often used in MBRs.

4.4.1.2 Hydrophilicity/Hydrophobicity

Hydrophilic membranes usually yield higher fluxes than hydrophobic membranes. Since hydrophobic membranes interact more strongly with the feed solution's components than hydrophilic ones do, fouling is more likely to occur in hydrophobic membranes, and this is called "hydrophobic interaction." Commercially available membranes are in most cases polymeric membranes even though ceramic membranes have become increasingly popular these days. The raw materials of polymeric membranes used in MBRs have a hydrophobic nature. The most frequently used membrane materials in MBRs are polyethylene, polypropylene, and polyvinyledendifluoride. All of these materials have a hydrophobic nature because they do not have polar groups in their molecular structures. Therefore, hydrophobic parts in the feed solution preferentially adsorb to the hydrophobic membrane surface. To minimize membrane fouling due to hydrophobic interactions, hydrophilically surface-modified membranes often present a decrease in biofouling and an increase in solute retention compared with the unmodified membranes.

Membrane hydrophobicity is quantified by measuring the contact angle between a water droplet and the membrane surface. On the other hand, the hydrophobicity of the floc particles in the activated sludge suspension is quantified by measuring the "relative hydrophobicity," which will be discussed in Section 4.4.2. Consequently, hydrophobic interaction is important for fouling in terms of the membrane and the sludge hydrophobicity.

4.4.1.3 Membrane Raw Materials

The membranes used in MBRs are mostly polymeric materials that have inherent limitations to cope with extreme conditions. Particularly, polymeric membranes are very vulnerable to wide ranges of pH values and oxidizing agents when chemical cleaning is carried out like Cleaning In Place (CIP). Therefore, ceramic (or inorganic) membranes showing superior hydraulic, thermal, and chemical resistance compared to polymeric materials have received attention lately.

Inorganic materials such as alumina (Al_2O_3), zirconia (ZrO_2), silicon carbide (SiC), and titanium oxide (TiO_2) have been developed for membrane separation and are used today in food and dairy industries. The application of inorganic membranes to MBRs has been limited due to their cost and module manipulation limitations. Most inorganic membrane modules have the geometry of tubular monoliths, resulting in much lower packing densities than hollow fiber bundles with the same volume. If this difficulty is overcome, applications of inorganic

membranes to MBR would be widespread because simple and powerful cleaning options using chemicals under extreme conditions such as high/low pH, high temperature, and strong oxidizing agents can be applied to control membrane fouling.

4.4.1.4 Charge

Membrane charge is considered an important parameter in determining the permeability of charged ions in nanofiltration or reverse osmosis processes because the rejection mechanism is strongly correlated with the static charge interaction between the membrane and transported solutes. Even though the flocs in MBRs are slightly negatively charged particles, the charge interaction between the membrane and flocs is not good enough to overcome the pressurized convection to the membrane.

4.4.1.5 Module

An important design parameter of hollow fiber membrane modules in MBRs is the packing density, which is defined by the membrane surface area per unit cross-sectional area of the module header (m^2/m^2) or by the membrane surface area per module volume (m^2/m^3). High packing densities reduce the number of membrane modules and/or the footprint of the module in the aeration tank of the MBR. However, overpacked modules can badly influence the mass transfer efficiency within the fiber bundles, resulting in a decreased design flux.
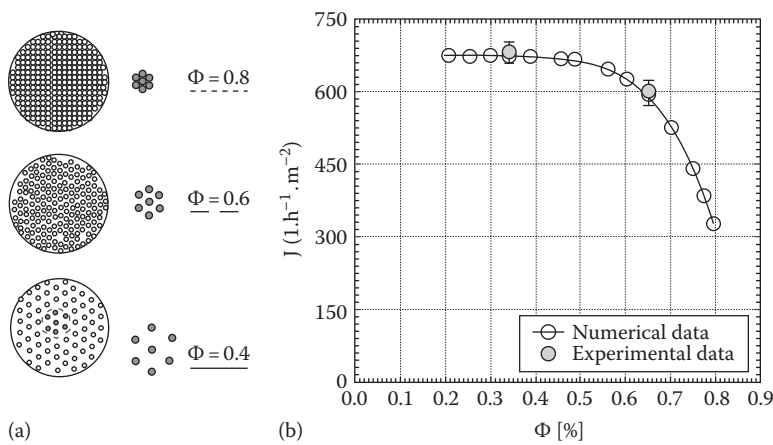
Figure 4.18 (a) Conceptual diagram of packing density and (b) the effect of packing density on flux. (Adapted from Gunther, J. et al., *J. Membr. Sci.*, 348, 277, 2010.)

Moreover, the impact of air scouring could be inhibited as well, leading to the development of sludge clogging within the modules. Therefore, proper packing density design is important to keep the flux high and prevent clogging within the module in MBRs.

Recent developments in computational fluid dynamics (CFD) provide more insight to this packing density. Figure 4.18 is one example showing the effect of packing density on the water flux although the experiments were not for MBR. Numerically predicted data that were assisted by a CFD simulator and real filtration data are shown together, and they match well. An increase in packing density above 55% leads to a strong decrease in filtration flux. Therefore, a compromise must be found regarding the packing density between a higher filtration area and the deterioration of filtration performance. In this figure, a packing density between 0.5 and 0.6 would provide a good compromise.

4.4.2 Microbial Characteristics

Mixed liquor of activated sludge is a complex and variable heterogeneous suspension containing unmetabolized feed components, metabolites produced during biological reactions, as well as actual biomass. Many individual components of the mixed liquor, ranging from biomass solids to dissolved polymers such as EPSs, can contribute to membrane fouling.

As indicated previously, each microbial factor affecting membrane fouling is strongly influenced by operating conditions. If operating conditions such as HRT change, microbial characteristics such as MLSS or EPS concentrations change accordingly. Therefore, the microbial characteristics that appear to be the most important factors are greatly dependent on the operating conditions (i.e., two important factors, operating conditions and biomass characteristics, influence each other).

4.4.2.1 MLSS

The biomass concentration in MBR tanks is represented by the MLSS concentration. Figure 4.19 shows high normalized flux (J/J_{iw}) values for batch-type filtrations as the MLSS concentration decreases. As shown in Figure 4.20, the TMP buildup for a submerged continuous–type bioreactor increases rapidly as the MLSS concentration decreases.

The general consensus follows that MLSS concentration is directly proportional to membrane fouling if other important microbiological factors are kept constant. This is because the cake layer is thicker (or denser) when the biomass concentration becomes greater. However, this hypothesis is only true under very limited conditions as the MLSS concentration could be responsible for membrane fouling.
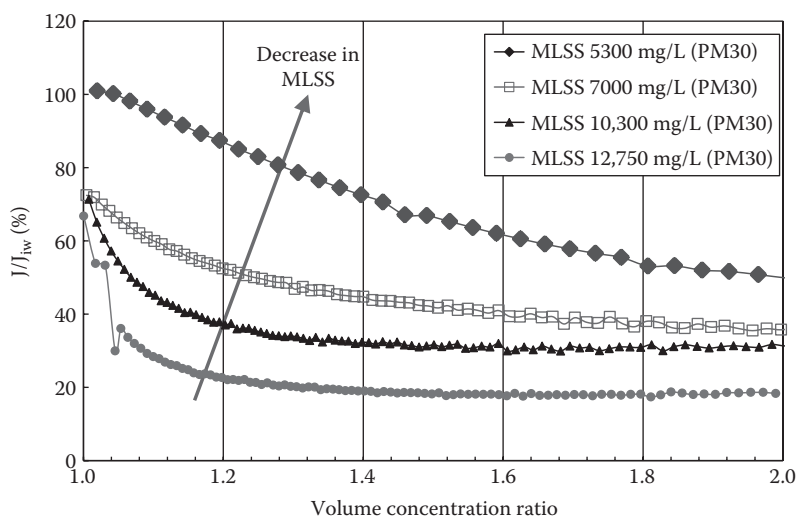
Figure 4.19 **Effect of MLSS concentration on normalized flux (J/J_{iw}) in batch filtrations of activated sludge having different MLSS concentrations with the PM30 membrane.**
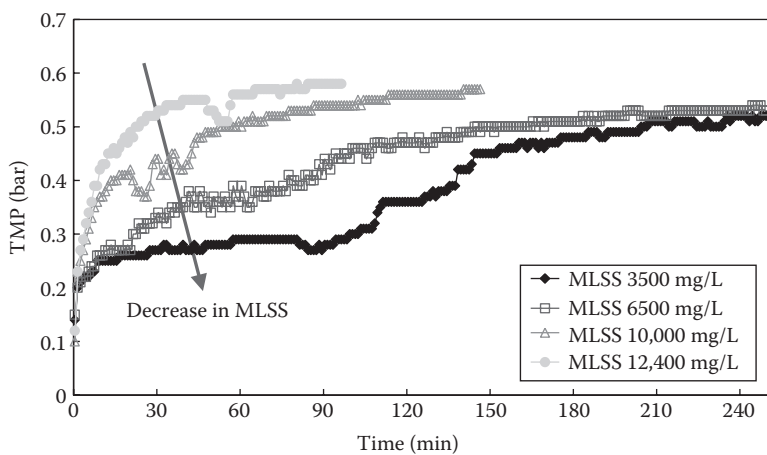
Figure 4.20 **Effect of MLSS concentration on the TMP in a continuous filtration system as a function of time.**

Many papers published in the early stage of MBR studies (i.e., in the 1990s) modeled flux as a function of MLSS concentration. For example, Krauth and Staab (1993) proposed the following equation accounting for the influence of the MLSS and MLVSS for a sidestream MBR:

$$J = J_0 \, e^{k(MLSS - MLVSS)\,Re/MLVSS} \tag{4.4}$$

where
J_0 is the initial flux, $L/(m_2\ h)$
k is the empirical constant depending on TMP
Re is the Reynolds number

Chang and Kim (2005) reported that cake resistance, R_c, decreased as MLSS concentration decreased. The specific cake resistance (α) increased as the MLSS concentration decreased (i.e., R_c and α behaved inversely), indicating that the MLSS concentration directly impacts cake layer resistance, as surmised from the conventional cake filtration theory. Cake resistance, R_c (m^{-1}), is often expressed as

$$R_c = \alpha \cdot v \cdot C_b = \alpha \cdot (m/A) \tag{4.5}$$

where
α is the specific cake resistance, $m\ kg^{-1}$
v is the permeate volume per unit membrane area, $m^3\ m^{-2}$
C_b is the bulk MLSS concentration, $kg\ m^{-3}$
m is the mass of solids, kg
A is the membrane area, m^2

However, membrane fouling is not always proportional to the MLSS concentration. There have been many studies contradicting that membrane fouling is always a function of MLSS concentration. As an example, Wu and Huang (2009) reported that MLSS concentration correlates well with membrane filterability when it is higher than 10,000 mg/L. However, MLSS had almost no effect on the filterability when it is lower than 10,000 mg/L. This might be due to the relationship between MLSS and viscosity, which they proposed as follows:

$$\log(\mu) = 0.043(MLSS) - 0.294 \tag{4.6}$$

where
μ is the viscosity, Pa s
MLSS is the MLSS concentration, g/L

They explained that the viscosity of the mixed liquor increased sharply over 90 MPa s when the MLSS was higher than 10,000 mg/L. Consequently, the decreased permeability is due to the high viscosity when the MLSS is over 10,000 mg/L. Although the MLSS concentrations for aerobic MBRs typically range from 5,000 to 15,000 mg/L, some MBR plants run at MLSS concentrations over 20,000 mg/L. These plants should have potential to experience an abrupt increase in viscosity, which would lead to system failure due to severe membrane fouling.

Since the cake layers on the membrane surface are exposed to shearing forces in most MBR plants, regardless of configuration, either sidestream or submerged, the cake layers repeat a cycle of deposition and sloughing to the bulk solution, prohibiting the continuous accumulation of biosolids to form cake layers, keeping the thickness of cake layers constant during operation. Even if the MLSS concentration is high enough to form a thick cake layer, the cake layer will not grow vertically. This phenomenon helps explain why the MLSS is not directly responsible for irreversible fouling. Rather than the direct effect of MLSS on the cake layer thickness, an increase in the MLSS preferentially leads to an increase in EPS or SMP production, which are directly responsible for irreversible fouling.

4.4.2.2 Floc Size

Among the various factors affecting membrane fouling in MBRs, the most dominant one is presumably floc size. Since the conventional filtration theory can exactly estimate head loss with any given size of filter media, many researchers have used the filtration equation to interpret the fouling phenomena in MBRs. Head loss (h_L) in the conventional filtration theory is an analogy to resistance in membrane filtration:

$$h_L = \frac{f}{\varphi} \frac{1-\varepsilon}{\varepsilon^3} \frac{L}{d} \frac{v^2}{g} \tag{4.7}$$

where
  f is the friction factor
  φ is the shape factor
  ε is the media porosity
  d is the media diameter, m
  L is the filter length, m
  g is the gravity acceleration, m/s^2
  v is the superficial velocity, m/s

According to the well-known Carman–Kozeny equation in a conventional filtration, specific resistance (α) is a function of particle diameter (d_p), porosity of the cake layer (ε), and particle density (ρ) as follows:

$$\alpha = \frac{180(1 - \varepsilon)}{\rho \cdot d_p^2 \cdot \varepsilon^3} \qquad (4.8)$$

The specific resistance (α) is directly correlated with the cake layer resistance (R_c) in the RIS model as follows:

$$R_c = \frac{180(1 - \varepsilon)}{(\rho \cdot d_p^2 \cdot \varepsilon^3) \cdot \nu \cdot C_b} \qquad (4.9)$$

R_c is thus strongly dependent on cake particle sizes (d); the smaller the floc particle size, the greater the cake resistance. In general, particle sizes of activated sludge flocs range from submicron to several hundred micrometers. However, the shearing force arising from either pumping in sidestream MBR or coarse aeration in submerged MBRs results in floc breakups, generating fine colloids and cells that then form a denser cake layer.

Wisniewski et al. (2000) showed that the suspension produced after a floc breakup consists mainly of particles having a size of around 2 µm, which corresponds to flux declines. Cicek et al. (1999) revealed the average diameter of particles in a sidestream MBR to be ~3.5 µm, with 97% of the particles being smaller than 10 µm, whereas the mixed liquor of the conventional activated sludge contained flocs ranging from 20 to 120 µm. On the other hand, the floc sizes in submerged MBRs appear to be greater than that of sidestream systems due to reduced shear stresses.

The porosity of the cake layer (ε) is also an important parameter determining the cake layer resistance. Figure 4.21 shows the effect of porosity (ε) on the cake
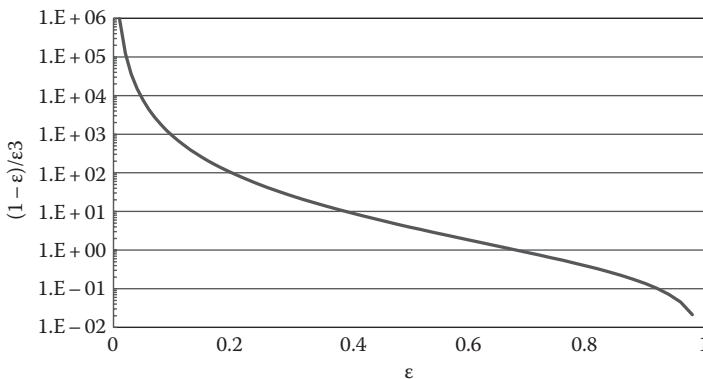
Figure 4.21   Effect of the porosity (ε) of a cake layer on the $(1 - \varepsilon)/\varepsilon^3$ ratio.
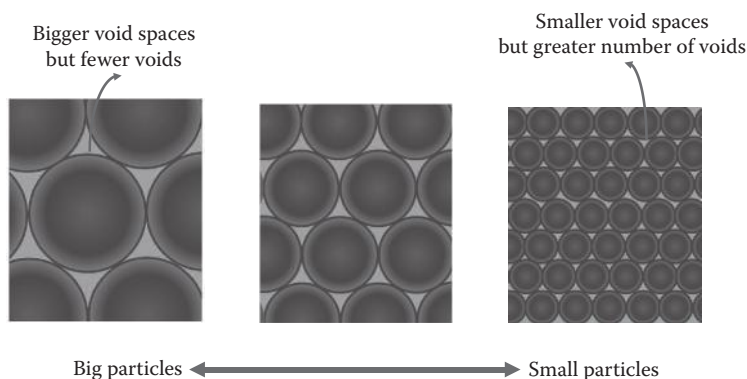
Figure 4.22   Relationship between the particle size and porosity.

layer resistance (R_c). The term $(1 - \varepsilon)/\varepsilon^3$ in Equation 4.9 decreases substantially as the porosity moves from 0 to 1, which means that the cake layer resistance (R_c) also dramatically decreases as the porosity approaches to 1. After all, the porosity is another key factor determining the cake layer resistance.

Two important factors determine the cake layer resistance, the particle size (d_p), and the porosity of the cake layer (ε), and their mutual influence should be noted. The general consensus is that porosity decreases if the particle size (d_p) increases. However, porosity remains constant as the particle size increases or decreases; otherwise, cake layer volume is equal. The size of the particles does not make any changes in the porosity as shown in Figure 4.22.

Figure 4.22 illustrates how the porosities of big and small particles are constant. Bigger particles have a small amount of large void spaces, while smaller particles have greater numbers of narrow void spaces. However, the overall void spaces are equal for both large and small particles; therefore, cake layer porosities are equal regardless of the particle size.

Example 4.2

In order to prove that the overall void spaces in a cake layer are the same for large and small particles as shown in Figure 4.21, compute and compare the porosities of cake layers made of different particle sizes. Assume that the sludge flocs in the activated sludge suspension resemble spheres (shape factor, $\varphi = 1$) and the sludge suspensions have different floc sizes with mean floc diameters of 2, 5, 10, 50, 100, and 500 μm. The suspensions are filtrated by dead-end-type membranes. All sludge feed volumes are 1 L, the mixed liquor feed density is 1003 kg/m³, and the MLSS concentration is 3000 mg/L for all samples. Assume that the degree of compression by pressurization is the same for all samples.

Solution

1. First, calculate the volume of the cake layer on the membrane surface.
   a. For the cake layer volume

   $$V_{cake} = \frac{3000 \text{ mg}}{L} \times 1 \text{ L} \times \frac{kg}{10^6 \text{ mg}} \times \frac{m^3}{1003 \text{ kg}} = 3 \times 10^{-6} \text{ m}^3$$

2. Determine the porosity of the cake layer made of 2 μm spheres (radius is 1×10^{-6} m).
   a. For the volume of one sphere,

   $$V_s = \frac{4}{3} \times \pi \times (10^{-6} \text{ m})^3 = 4.19 \times 10^{-18} \text{ m}^3/\text{sphere}$$

   Assume that one cube contains one sphere within it and the width (or length and depth) of the cube is the same as the diameter of the sphere.
   b. For the volume of one cube containing one sphere within it,

   $$V_{cube} = (2 \times 10^{-6} \text{ m})^3 = 8.00 \times 10^{-18} \text{ m}^3/\text{cube}$$

   c. For the void volume of one cube,

   $$V_{c,v} = V_c - V_s = 8.00 \times 10^{-18} - 4.19 \times 10^{-18} = 3.81 \times 10^{-18} \text{ m}^3/\text{cube}$$

   d. For the number of cubes available in the cake layer,

   $$N_{cube} = \frac{V_{cake}}{V_{cube}} = \frac{3 \times 10^{-6} \text{ m}^3}{8.00 \times 10^{-18} \text{ m}^3/\text{cube}} = 3.79 \times 10^{11}$$

   e. For total void volume in the cake layer,

   $$V_{void} = V_{c,v} \times N_{cube}$$

   $$= 3.81 \times 10^{-18} \frac{\text{m}^3}{\text{cube}} \times 3.79 \times 10^{11} \text{ cube} = 1.42 \times 10^{-6} \text{ m}^3$$

   f. Therefore, the porosity of the cake layer is

   $$\varepsilon = \frac{V_{void}}{V_{cake}} = \frac{1.42 \times 10^{-6} \text{ m}^3}{3 \times 10^{-6} \text{ m}^3} = 0.476$$

   The following table was obtained for different floc sizes by a series of calculations similar to those mentioned earlier:

Floc Size (μm)	2	5	10	50	100	500
Radius of floc, r (m)	1.00E–06	2.50E–06	5.00E–06	2.50E–05	5.00E–05	2.50E–04
Volume of one floc sphere, V_s (m³/cube)	4.19E–18	6.54E–17	5.24E–16	6.54E–14	5.24E–13	6.54E–11
Volume of one floc cube, V_{cube} (m³/cube)	8.000E–18	1.250E–16	1.000E–15	1.250E–13	1.000E–12	1.250E–10
Void volume of one cube, $V_{c,v}$ (m³)	3.811E–18	5.955E–17	4.764E–16	5.955E–14	4.764E–13	5.955E–11
Number of cube in cake, N_{cube} (ea)	3.739E+11	2.393E+10	2.991E+09	2.393E+07	2.991E+06	2.393E+04
Total void volume of cake, V_{void} (m³)	1.42E–06	1.42E–06	1.42E–06	1.42E–06	1.42E–06	1.42E–06
Cake porosity, ε	0.476	0.476	0.476	0.476	0.476	0.476

As shown in the table, all of the porosity values for the different floc sizes are the same (0.476), indicating that porosity is not affected by particle size. Although the bigger particles have larger void spaces, the smaller particles have a greater number of voids.

Example 4.3

Six different activated sludge suspensions with different floc sizes are filtrated with membranes having a surface area of 0.1 m². To gain an insight on how dramatically the floc size affects the cake layer resistance (R_c), plot the R_c versus the floc size (d_p) using the following data:

■ Average floc sizes: 2, 5, 10, 50, 100, and 500 μm.
■ Assume that the density of particles (ρ_p) of all sludge suspensions is 1003 kg/m³.
■ Assume that the MLSS concentration of each sludge suspension is 3000 mg/L.
■ Assume that 1 L of sludge suspension is filtrated by the same membranes with a dead-end filtration mode.

Solution

Calculate the specific cake resistance (α) value of the bio-cakes made from the 2 μm flocs using Equation 1:

$$\alpha = \frac{180(1-\varepsilon)}{\rho_p \cdot d_p^2 \cdot \varepsilon^3} \tag{E4.1}$$

$$\alpha_1 = \frac{180(1-\varepsilon)}{1003 \text{ kg/m}^3 \cdot (2.0 \times 10^{-6})^2 \text{ m}^2 \cdot \varepsilon^3} = 4.487 \times 10^{10} \frac{1-\varepsilon}{\varepsilon^3} \text{ m/kg}$$

Using the calculated α and Equation 4.5, calculate the cake layer resistance (R_c) value of 2 μm bio-cakes:

$$R_c = \frac{\alpha \cdot M}{A_m} \tag{2}$$

$$R_{c1} = \frac{\alpha_1 \cdot M}{A_m} = 4.487 \times \frac{10^{10} \text{ m}}{\text{kg}} \cdot \frac{3 \text{ g}}{0.1 \text{ m}^2} \frac{\text{kg}}{1000 \text{ g}} \cdot \frac{1-\varepsilon}{\varepsilon^3} = 1.346 \times 10^9 \cdot \frac{1-\varepsilon}{\varepsilon^3} \text{ m}^{-1}$$

The following were obtained using the same calculation methods as earlier and are summarized by the following table:

$$\alpha_2 = \frac{180(1-\varepsilon)}{1003 \text{ kg/m}^3 \cdot (5.0 \times 10^{-6})^2 \text{ m}^2 \cdot \varepsilon^3} = 7.178 \times 10^9 \frac{1-\varepsilon}{\varepsilon^3} \text{ m/kg}$$

$$R_{c2} = \frac{\alpha_2 \cdot M}{A_m} = 2.154 \times 10^8 \frac{1-\varepsilon}{\varepsilon^3} \cdot \frac{M}{A_m} \text{ m}^{-1}$$

$$\alpha_3 = \frac{180(1-\varepsilon)}{1003 \text{ kg/m}^3 \cdot (1.0 \times 10^{-5})^2 \text{ m}^2 \cdot \varepsilon^3} = 1.795 \times 10^9 \frac{1-\varepsilon}{\varepsilon^3} \text{ m/kg}$$

$$R_{c3} = \frac{3 \cdot M}{A_m} = 5.384 \times 10^7 \frac{1-\varepsilon}{\varepsilon^3} \cdot \frac{M}{A_m} \text{ m}^{-1}$$

$$\alpha_4 = \frac{180(1-\varepsilon)}{1003 \text{ kg/m}^3 \cdot (5.0 \times 10^{-5})^2 \text{ m}^2 \cdot \varepsilon^3} = 7.178 \times 10^7 \frac{1-\varepsilon}{\varepsilon^3} \text{ m/kg}$$

$$R_{c4} = \frac{\alpha_4 \cdot M}{A_m} = 2.154 \times 10^6 \frac{1-\varepsilon}{\varepsilon^3} \cdot \frac{M}{A_m} \text{ m}^{-1}$$

$$\alpha_5 = \frac{180(1-\varepsilon)}{1.003 \text{ kg/m}^3 \cdot (1.0 \times 10^{-4})^2 \text{ m}^2 \cdot \varepsilon^3} = 1.795 \times 10^7 \frac{1-\varepsilon}{\varepsilon^3} \text{ m/kg}$$

$$R_{c5} = \frac{5 \cdot M}{A_m} = 5.384 \times 10^5 \frac{1-\varepsilon}{\varepsilon^3} \cdot \frac{M}{A_m} \text{ m}^{-1}$$

$$\alpha_6 = \frac{180(1-\varepsilon)}{1.003 \text{ kg/m}^3 \cdot (5.0 \times 10^{-4})^2 \text{ m}^2 \cdot \varepsilon^3} = 7.178 \times 10^5 \frac{1-\varepsilon}{\varepsilon^3} \text{ m/kg}$$

$$R_{c6} = \frac{\alpha 6 \cdot M}{A_m} = 2.154 \times 10^4 \frac{1-\varepsilon}{\varepsilon^3} \cdot \frac{M}{A_m} \text{ m}^{-1}$$

Particle Size (μm)	2	5	10	50	100	500
$\alpha \cdot \left(\dfrac{1-\varepsilon}{\varepsilon^3}\right)$(m/kg)	4.487×10^{10}	7.178×10^9	1.795×10^9	7.178×10^7	1.795×10^7	7.178×10^5
$R_c \cdot \left(\dfrac{1-\varepsilon}{\varepsilon^3}\right)$(m^{-1})	1.346×10^9	2.154×10^8	5.384×10^7	2.154×10^6	5.384×10^5	2.154×10^4

The following figure is created by plotting the particle size versus $R_c \times ((1-\varepsilon)/\varepsilon^3)$ data from the table.

(a)
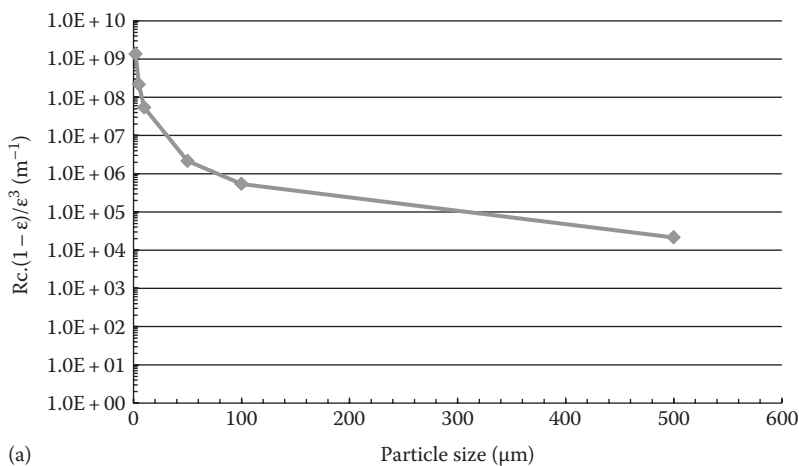
We concluded previously that porosity is not affected by particle size. Assuming that the porosity (ε) is equal to 0.5 for every particle size, we have the following figure of R_c versus particle diameter (d).

Particle Size (μm)	2	5	10	50	100	500
α (m/kg)	1.79×10^{11}	2.87×10^{10}	7.18×10^9	2.87×10^8	7.18×10^7	2.87×10^6
R_c (m^{-1})	5.38×10^9	8.61×10^8	2.15×10^8	8.61×10^6	2.15×10^6	8.61×10^4

(b)
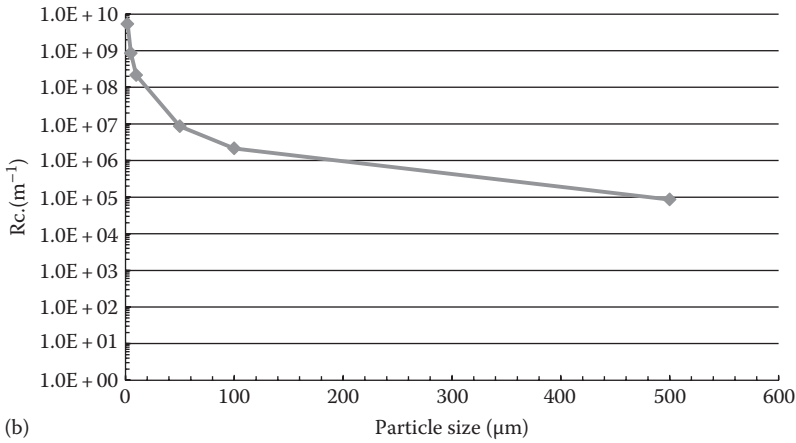
4.4.2.3 Compressibility of the Cake Layer

In conventional filtration using filter media such as sand or anthracite rather than membranes, specific cake resistance (α) has been used to express the filterability of media. As indicated in Equation 4.7, α is a function of particle diameter (d_p), cake layer porosity (ε), and particle density (ρ):

$$\alpha,\ m/kg = \frac{180(1-\varepsilon)}{\rho \cdot d_p^2 \cdot \varepsilon^3} \qquad (4.10)$$

If high pressure is applied for membrane filtration, the cake layer on the membrane surface will be compressed. Thus, an index to express the compressibility of the cake layer is introduced as follows:

$$\alpha = \alpha_o \cdot P^n \qquad (4.11)$$

where
  n is the cake compressibility index
  P is the applied pressure, kPa

This power relationship is suitable to determine the cake layer compressibility from the experimentally measured specific cake resistances. The constant n can be determined by plotting $\log \alpha$ versus $\log P$ by taking log for both sides of Equation 4.11 as

$$\log(\alpha) = \log \alpha_o + n \cdot \log P \qquad (4.12)$$

The compressibility index, n, is determined by a series of filtration experiments carried out under different applied pressures. Figure 4.23 shows how to obtain the
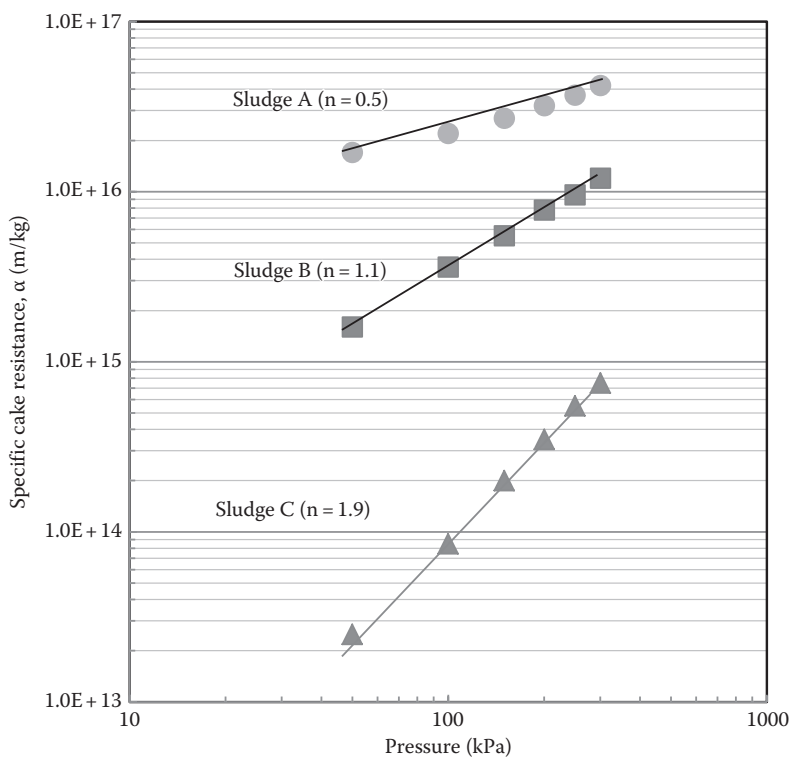
Figure 4.23   Determination of cake layer compressibility (n) using the equation $\log(\alpha) = \log(\alpha_o) + n \log(P)$: the slope of the straight line is n, which represents the compressibility of the cake.

compressibility index n. The slope of a log α versus log P plot corresponds to the compressibility index, n.

4.4.2.4 Dissolved Matter

DOM present in the aeration basin of MBR plants include unmetabolized feed components and metabolites produced during biological reactions such as SMPs and free EPSs. In terms of membrane fouling, they cannot be distinguished from each other based on the chemical structure.

DOM in aeration basins significantly influence membrane fouling. They impact both internal and external fouling, the latter being promoted by concentration polarization. DOM can be adsorbed to the pores' surfaces and walls, which is responsible for inner membrane fouling rather than cake layer formation. This happens mostly at the initial stage of filtration. However, DOM can

be adsorbed in the interstices of the cake layers during their free paths to the membrane. This results in a consolidation of the cake layer, which can make fouling severe.

As shown in Figure 4.24, the sludge flocs are the main building blocks of the cake layer on the membrane surface. Soluble matter including DOM can fill the interstices of the building blocks present inside the cake layer, resulting in the formation of dense cake layers. DOM act as glue, just like the role of cement in the walls made of blocks, consolidating the cake layer.

In the early stages of MBR development, there were several studies investigating the effect of dissolved organic carbon (DOC) on membrane fouling. For example,
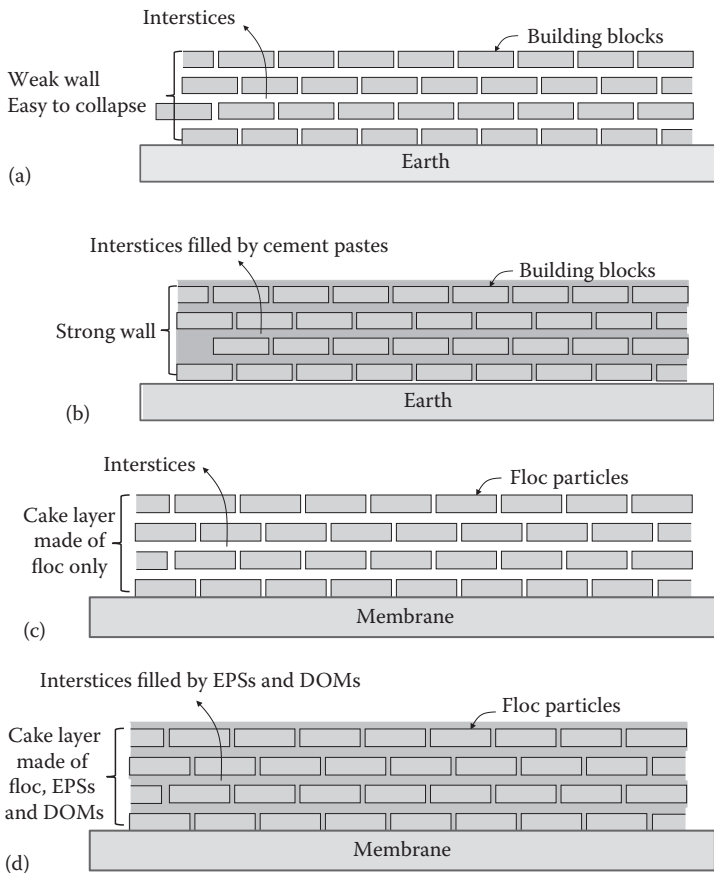
Figure 4.24   Conceptual illustration of the analogy of blocks–wall construction (a, b) and cake layer formation (c, d).

Ishiguro et al. (1994) proposed the following general correlation between flux and DOC where a and b are empirical constants:

$$J = a + b \cdot \log(DOC) \tag{4.13}$$

However, the earlier equation is not universal but is very specific because flux (or fouling) is not determined solely based on DOC. Many other parameters that affect membrane fouling coexist simultaneously. That kind of equation is only valid under specific circumstances. For instance, if other important fouling factors are kept constant, the earlier equation can predict the flux based on the DOC concentration. Sato and Ishii (1991) proposed the following empirical relationship describing filtration resistance in terms of MLSS, chemical oxygen demand (COD), TMP, and viscosity (η) for a sidestream MBR:

$$R = 842.7 \, TMP \, (MLSS)^{0.926} (COD)^{1368} (\eta)^{0.326} \tag{4.14}$$

The soluble EPS (or SMP) concentration had been considered a more important factor for fouling rather than the DOC (or soluble COD). The effect of free EPSs on fouling has been described in detail previously.

4.4.2.5 Flocs Structure (Foaming, Pinpoint Floc, and Bulking)

The structure of activated sludge flocs depends mostly on the physicochemical characteristics of biomass, nutrient balance, and feed characteristics. As shown in Figure 4.25, the floc structure of activated sludge is classified into three types

(a)   (b)   (c)
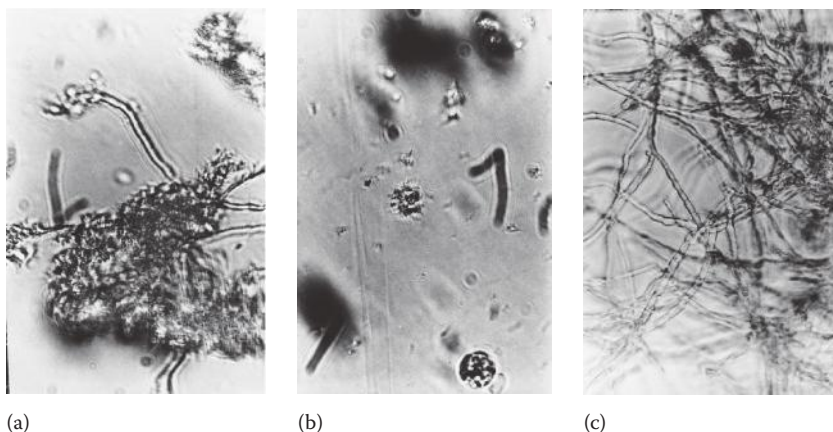
Figure 4.25 Photos of three structure types of sludge flocs: (a) normal sludge, (b) pinpoint flocs, and (c) bulking sludge.

according to the balance of floc-forming and filamentous bacteria (i.e., bulking, pinpoint, and ideal normal flocs).

A proliferation of filamentous microorganisms leads to bulking sludge, while the filamentous bacteria are not observed in pinpoint sludge flocs. On the other hand, normal activated sludge shows a good balance of filamentous and floc-forming bacteria. Activated sludge with the three previously mentioned kinds of floc structures can be obtained by controlling the HRT, SRT, and F/M ratio. The sludge volume index (SVI) can be used to check the settling ability, which is directly related to the floc structure:

$$SVI,\ mL/g = SV_{30} \cdot 1000/MLSS \tag{4.15}$$

where
  SV_{30} is the sludge volume after 30 min settling, mL/L
  MLSS is the mixed liquor suspended solids, mg/L

Typical SVI values for pinpoint floc, normal sludge, and bulking sludge range from <50, 100–180, and >200 mL/g, respectively. The SSs and the turbidity of the supernatant after settling could be indirectly related to the floc structures because pinpoint flocs have a very turbid supernatant while bulking sludge has a relatively clear supernatant.

According to the studies of Chang et al. (1999), the order of fouling tendency was found to be normal sludge < pinpoint sludge < bulking sludge. They explained that the key factors controlling cake resistance were the shape, the size of the activated sludge flocs, and the porosity of the cake layer accumulating on the membrane surface. However, Wu and Huang (2009) reported that the zeta potential and SVI have no effect on membrane filterability. Contradictory results are often found in literature dealing with membrane fouling in MBRs just like the two previously mentioned studies. This is attributed to the oversimplification of microbial conditions. In other words, the effect of different factors (SVI in the two previously mentioned studies) on membrane fouling is only highlighted even though the physiological and operational conditions were different between each study. Since it is almost impossible to cultivate activated sludge suspensions exhibiting different SVI values but with all other parameters affecting membrane fouling kept constant such as MLSS, f/m ratio, and HRT, the impact of SVI on fouling cannot be explained by itself, making it difficult to study membrane fouling in MBRs.

4.4.2.6 Influent Characteristics

The composition of influents to an MBR directly influences microbial metabolism. There are no major differences in sewage compositions worldwide; however, the composition of industrial wastewater differs from site to site. Domestic wastewater has a typical composition that does not vary by location. Typical nutrient ratios for

the growth of microorganisms are known to be 1:5:100 for P/N/C, which represents the phosphorus, nitrogen, and carbon, respectively. More practically, a simple C/N ratio is also recommended to evaluate the balance of influent composition. Obviously, unbalanced nutrient conditions negatively affect microbial activity, leading to partial failures in WWTPs.

4.4.2.7 Sludge Hydrophobicity

Various functional groups of proteins and polysaccharides, which are the main components of EPSs, are exposed on the surface of sludge flocs. Thus, hydrophobic interactions between flocs and the membrane surface are present. The more hydrophobic the flocs are, the more prone they are to be adsorbed to the membrane surface. The flocs' hydrophobicity is decided by the balance of the hydrophilic and hydrophobic nature of the functional groups on the flocs' surface.

Foaming sludge, which is usually caused by a feed stream containing lots of lipid constituents, is strongly hydrophobic. Foaming sludge is known to have troubles in settling as well as scum formation in secondary sedimentation tanks, leading to poor filterability.

Although the hydrophobicity of membranes can be determined by measuring the contact angle of the water droplet on a membrane surface, it is not easy to measure the sludge flocs' hydrophobicity directly. Instead, relative hydrophobicity (or hydrophilicity) tests using an organic solvent are recommended for measuring sludge hydrophobicity. The principle of the determination of relative hydrophobicity is based on solvent extraction from aqueous solution using organic solvents, that is, when an aqueous solution is intimately mixed with an immiscible organic solvent, the solutes (flocs in this case) in the aqueous phase distribute themselves according to its solubility in the two solvents.

Figure 4.26 shows the basic procedure for determining the relative hydrophobicity of a sludge sample. A separation funnel is filled with a sludge sample and then an organic solvent such as hexane, octanol, or diethyl ether is poured into the funnel. Moderate manual (or mechanical) agitation is provided for a sufficient amount of time to allow both (organic and aqueous) layers to mix thoroughly. Extra time is given for the transfer of the sludge flocs migrating from the aqueous to the organic solvent phase, and then the aqueous phase in the lower part of the funnel is decanted and collected. Finally, the collected aqueous phase is ready for further analysis.

The next step is the determination of the MLSS concentration before and after solvent extraction, that is, the relative hydrophobicity is typically expressed as a ratio of the MLSS concentration in the aqueous phase after emulsification ($MLSS_f$) to the MLSS concentration in the aqueous phase before emulsification ($MLSS_i$):

$$\text{Relative hydrophobicity}(\%) = 100 \times (1 - MLSS_f / MLSS_i) \qquad (4.16)$$
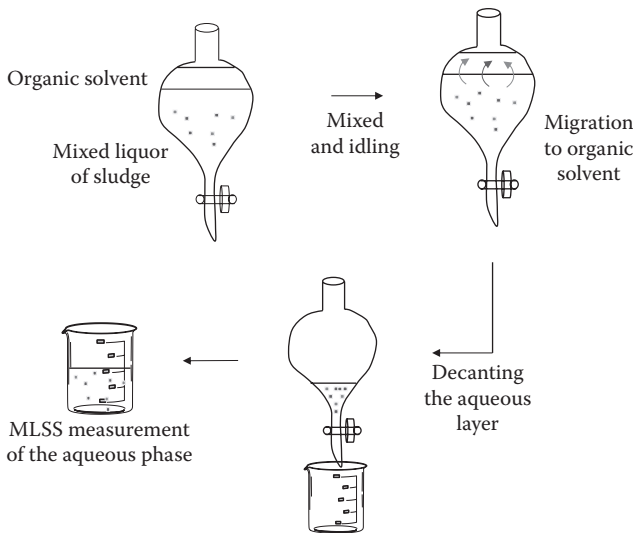
Figure 4.26 **Schematic illustration of the procedure of measuring relative hydrophobicity of activated sludge using organic solvent.**

Chang et al. (1999) reported that the relative hydrophobicity of a normal activated sludge was 54%–60% (57% average), while the foaming sludge was 62%–93% (81% average), which was quite a bit higher than the normal sludge.

4.4.3 Operation

As indicated several times in the previous section, many operating conditions directly affect microbiological characteristics such as MLSS, EPS (or SMP) productions, and floc structures. The most dominant parameters determining membrane fouling in MBRs are microbial characteristics; however, microbial characteristics are strongly influenced by operating conditions.

4.4.3.1 HRT

HRT is defined by the reactor volume (m³) divided by the influent flow rate (m³/h). HRT is a key operating parameter that determines reactor performances of both continuous stirred tank reactors (CSTRs) and plug flow reactors (PFRs). As the HRT of a biological reactor such as an activated sludge basin decreases, the possibility of washout also increases. Therefore, it is important to maintain a proper HRT. Typical HRTs in MBR plants range from 2 to 5 h. Generally speaking, the biodegradation of organics in the influent becomes more stable as the HRT increases.

HRT is directly related to the F/M ratio, which is defined as the ratio of food per microorganisms:

$$F/M\,(kg\ BOD/kg\ MLSS \cdot d) = \frac{QS_o}{VX} = \frac{S_o}{\theta X} \qquad (4.17)$$

where
 Q is the flow rate, m^3/d
 S_o is the influent substrate concentration, kg BOD/m^3
 V is the bioreactor volume, m^3
 θ is the HRT, day
 X is the biomass concentration, kg $MLSS/m^3$

The F/M ratio decreases as the HRT increases according to the earlier equation, which results in direct changes in microbial characteristics because the biomass growth rate strongly depends on the F/M ratio, as shown in Figure 4.27. The effluent water quality such as biochemical oxygen demands (BOD) and SS deteriorates and the settling ability becomes poor as the F/M ratio increases. On the other hand, oxygen consumption becomes increased at low F/M ratios because the microorganisms in the endogenous phase require huge amounts of oxygen for the autooxidation of biomass. Chang and Lee (1998) reported that membrane fouling of microorganisms in the exponential growth phase was more severe than the biomass in the endogenous phase. Therefore, HRT affects membrane fouling indirectly via the change in microbial characteristics.
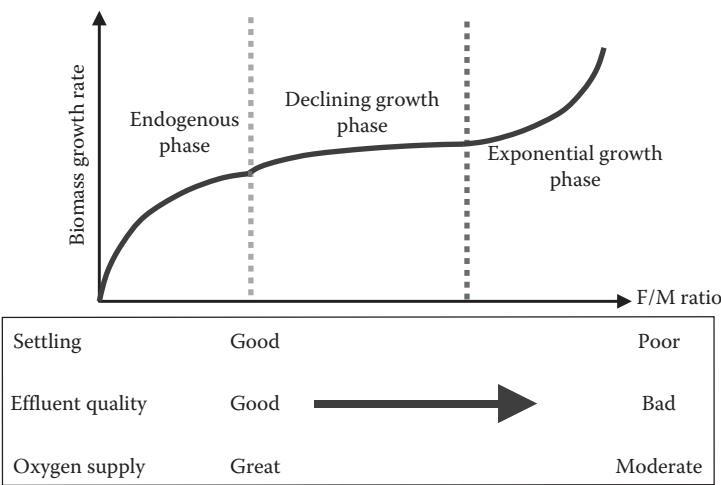
Figure 4.27 Relationship of the F/M ratio and microbial characteristics and performances.

4.4.3.2 SRT

Solutes entering, existing, and exiting a continuous tank reactor have a mean residence time. Regardless of the state of solutes (i.e., solid, liquid, or gas and particulates or dissolved matter), the solutes residence time (τ_E) in a reactor is defined as follows:

$$\tau_E = \frac{E}{|dE/dt|} \tag{4.18}$$

where

  E is the mass of solutes, kg
  t is the time, h

If the solution in a reactor does not contain any solutes, the solute residence time (τ_E) becomes HRT as follows:

$$\tau_w = \frac{E}{|dE/dt|} = \frac{V}{|dV/dt|} = \frac{V}{Q} = HRT \tag{4.19}$$

If microorganisms are in a bioreactor present just like in a conventional activated sludge system, the solute residence time becomes the SRT, which means the mean cells' residence time in a bioreactor. SRT is a function of the mass of cells in a bioreactor ($X \cdot V$) and the solids wasting rate from the secondary clarifier (Q_w) and from effluents ($Q - Q_w$). Therefore, SRT is expressed as follows:

$$SRT_{CAS} = \frac{E}{|dE/dt|} = \frac{X \cdot V}{|X_r \cdot Q_w + X_e \cdot (Q - Q_w)|} \tag{4.20}$$

where
  X_r is the solids concentration of the circulating stream from the secondary clarifier to the aeration basin, mg/L
  X_e is the solids concentration of the supernatant flowing out of the clarifier, mg/L

Since no solids flow out in MBR plants due to the excellent solid–liquid separation by the membranes, X_e becomes zero. Furthermore, there is no recirculation from a secondary clarifier to the bioreactor in MBR systems, so X_r is equal to X. Thus, the earlier equation can be changed as follows for MBR systems:

$$SRT_{MBR} = \frac{E}{|dE/dt|} = \frac{X \cdot V}{|X_r \cdot Q_w + X_e \cdot (Q - Q_w)|}$$

$$= \frac{X \cdot V}{|X \cdot Q_w + 0|} = \frac{V}{|Q_w|} = \frac{V}{Q_w} \tag{4.21}$$

SRT is directly related to the MLSS concentration in a bioreactor. Extended SRT operation leads to an increase in cell residence times, resulting in increased MLSS concentrations (i.e., MLSS tends to increase in accordance with the SRT). This means that the SRT directly influences the MLSS concentration, which was already discussed in the previous section as an important microbial factor affecting membrane fouling. Therefore, the effect of altering SRT on membrane fouling is attributed to the corresponding microbial characteristic changes. In other words, SRT affects membrane fouling indirectly via changing the microbial characteristics.

Typical SRT values for conventional activated sludge systems are around 10 days, but common MBR plants have SRTs that are over 30 days. This prolonged SRT obviously leads to a large MLSS concentration of over 10,000 mg/L, which in turn lowers F/M ratio, which makes the microorganisms in the bioreactor endogenous. Therefore, membrane fouling becomes less severe under this extended SRT situation. Chang and Lee (1998) showed that membrane fouling decreased as SRT increased from 3 to 33 days. Broeck et al. (2012) also reported that a higher SRT contributes to better activated sludge bioflocculation and, as a consequence, to lower fouling rates within the tested SRT range (10–50 days). However, contradictory results have been reported elsewhere, indicating that membrane fouling is not determined by one or two factors.

On the other hand, the free EPS (or SMP) level decreases as the SRT goes to infinity because most of the substrates are consumed for the maintenance needs of microorganisms. This could be one reason why a low membrane fouling propensity is observed at high SRT values. However, the MLSS concentration increases as the SRT increases, leading to an increase in the viscosity of the mixed liquor. This situation deteriorates membrane fouling; moreover, it requires excessive aeration. Therefore, optimum SRT selection is needed to control membrane fouling properly.

4.4.3.3 Shear Stress

In a sidestream MBR, a recirculation loop from the bioreactor to the membrane module, which is present outside the bioreactor, is formed by a pressurized pump (or recirculation pump) in order to give shearing forces to the membrane surface to scour the cake layer. The flocs and microorganisms in the loop as well as in the bioreactor are exposed to steady shear stresses arising from the recirculation flow. The shear forces directly influence the microbial characteristics such as altering the microbial morphology and size, releasing intracellular or extracellular compounds, and affecting microbial viability. Obviously, these microbial changes affect membrane filterability.

According to Newton's law of viscosity, shear stress (τ) acting on fluids between two plates is defined as follows:

$$\tau = \frac{F}{A} = \mu \frac{dv}{dy} \tag{4.22}$$

where
  τ is the shear stress, N/m²
  F is the force acting on a plate, N
  A is the surface area of the plate, m²
  μ is the viscosity, N s/m²
  dv/dy is the shear rate (σ) or simply the velocity gradient (1/s) of fluids between
    two plates

This equation says that the shear stress (τ) is linearly proportional to the velocity gradient dv/dy and the proportional coefficient is the viscosity of the fluids.

The wall shear stress (τ_w) in a flow channel of a recirculation loop in a sidestream MBR is calculated from the following equation:

$$\tau_w = \frac{f\rho\omega^2}{8} \tag{4.23}$$

where
  f is the friction factor
  ρ is the liquid density, kg/m³
  ω is the flow velocity in the middle of the channel, m/s

Example 4.4

For a sidestream MBR, determine the wall shear stress (τ_w) acting on the fluids flowing through a tubular-type membrane module that is located outside the bioreactor. Assume that the crossflow mean velocity flowing in the module is always kept at 0.12 m/s and the density of the mixed liquor is 999 kg/m³. The inner diameter of the tubular membrane module is 2 cm.

Solution

To calculate the wall shear stress (τ_w), friction factor (f), and centerline flow velocity (ω), the Reynolds number should be defined first according to the flow regime. The Reynolds number (Re) can be calculated as follows:

$$Re = \frac{\rho \cdot d \cdot v}{\mu}$$

$$= \frac{(999 \text{ kg/m}^3) \cdot (0.02 \text{ m}) \cdot (0.12 \text{ m/s})}{(1.2 \times 10^{-3} \text{ N} \cdot \text{s/m}^2)} = 1998$$

Because the calculated Reynolds number is below 2100, the flow is laminar.

The friction factor, f, is dependent on the Reynolds number of the flow. For circular pipes, $\omega = 2 \cdot v$ and $f = 64/Re$ at laminar flow, assuming a parabolic flow

front with a mean flow velocity of v. Therefore, the wall shear stress (τ_w) can be calculated as follows:

$$\tau_w = \frac{f \cdot \rho \cdot \omega^2}{8}$$

$$= \frac{\frac{64}{Re} \cdot \rho \cdot \omega^2}{8}$$

$$= \frac{\left(\frac{64}{1998}\right) \cdot \left(\frac{999 \text{ kg}}{\text{m}^3}\right) \cdot \left(2 \times 0.12 \text{ m/s}\right)^2}{8}$$

$$= 0.23 \text{ N/m}^2$$

The wall shear stress, τ_w, is 0.23 N/m^2. On the other hand, ω is the same as v and $f = 0.316/(Re)^{0.25}$ if the flow is turbulent.

The most dramatic effect of shear stress is floc breakage. The fragile microbial flocs are easily broken into smaller flocs producing colloidal and fine particulates. Due to shear stresses, floc structures can collapse and the size of the flocs will therefore decrease, particularly during the initial stages of pump operation. As a sidestream MBR keeps running, floc breakup ceases and floc size reduction is stabilized. Kim et al. (2001) reported that the average floc size decreased from several hundreds to 20 μm within 144 h of operation of a sidestream MBR system. As indicated in the previous section, the size of the flocs is the key parameter that determines membrane fouling (i.e., the smaller the floc sizes, the more severe fouling is). Therefore, floc size reduction due to shear stresses in the recirculation loop definitely negatively impacts filtration performance.

Another impact of floc breakup is the release of EPSs from the flocs to the bulk solution. Lots of EPSs interconnecting the microbial cells can be damaged by floc breakage and can be released to the bulk solution. As discussed extensively in the previous section, the EPS concentration is one of the most important factors determining membrane fouling. Therefore, the EPS release arising from shear stresses in the recirculation loop obviously leads to a nonbeneficial impact on membrane filtration.

Many types of hydraulic pumps recirculating the biofluids in the aeration tank to the outside membrane module are used in MBR operations. Kim et al. (2001) also found that the shear stresses imposed on microbial flocs by a rotary-type pump would be certainly more severe than those by a centrifugal pump. In other words, an adequate selection of pumping device is also important to control membrane fouling in MBRs.

4.4.3.4 Aeration

In submerged MBRs, there are no shear stresses originating from the recirculation pump. Instead, coarse aeration is widely practiced aiming at controlling membrane

fouling as well as supplying air to the microorganisms in the aeration basin. The coarse air supply can efficiently remove or at least reduce the cake layer on membrane surfaces. To provide shearing forces (or scouring) to a membrane surface, coarse aeration should be extensive and excessive. This is why unbeneficial impacts on microorganisms due to coarse aeration are reported. For example, deflocculation by coarse aeration is the most commonly reported problem. Floc size reduction by deflocculation leads to severe membrane fouling, so extensive and excessive coarse aeration should be restrained. The success of submerged MBR plants depends on how the fouling control strategy is implemented. If coarse aeration is too extensive, the operating costs will increase and deflocculation would be anticipated. On the other hand, if coarse aeration is not sufficient, membrane fouling will also become severe.

The aeration intensity (m/h), which is one of the important design parameters for submerged MBRs, refers to the ratio of the supplied airflow rate (m³/h) to the membrane area (m²). Increasing the aeration intensity more than an order of magnitude does not always yield a commensurate increase in flux. Therefore, optimization of aeration intensity allowing sufficient shear force to reduce the cake layer is needed.

4.4.3.5 Flux (Critical Flux)

The basic idea of critical flux suggested by Field in the mid-1990s has been widespread in all areas of membrane processes including MBR application. If the initial operating flux in an MBR starts as low as possible, the rate of fouling would be retarded. There have been many controversies about what the exact meaning of critical flux is. However, the concept of critical flux in MBRs is simple—the highest initial flux for which TMP remains stable during operation of the MBR.

Several methods for determining the critical flux have been suggested but no single protocol has been accepted. A common practice to determine the critical flux is the flux step method—to incrementally increase the flux for a fixed duration as long as each flux step leads to a stable TMP. Critical flux is determined by the flux when the TMP increases with time. The TMP increase indicates a greater resistance to permeation provided by a growing cake formation and internal fouling. TMP is dependent on fouling parameters described previously such as MLSS, membrane materials, and system hydrodynamics.

4.5 Quantitative Determination of Fouling

Quantitatively determining the fouling propensity is an important step to set up a fouling control strategy. Continuous and precise monitoring of how fouling advances in MBR can allow the operator to anticipate future troubles and to take

appropriate antifouling or cleaning action. There are several ways to express the degree of fouling both theoretically and practically.

4.5.1 Resistance in the Series Model

Analyzing filtration resistances makes it easy to understand the fouling phenomena in MBRs. The RIS model is the most frequently used method to analyze fouling mechanisms in laboratory-scale MBR studies. It is an empirical model that is not theoretically driven. A series of filtration experiments and calculations for each resistance value with the filtration data provides us an insight into what kind of fouling existed and was predominant.

The basic idea of this model is that the permeate flux, J, is proportional to the driving force for membrane filtration and inversely proportional to the sum of all the resistances:

$$J = \frac{\text{driving force}}{\sum \text{resistances}} \qquad (4.24)$$

This model states that the driving force for membrane filtration is the TMP, and the resistance to permeation is the sum of resistances and the permeate viscosity:

$$J = \frac{\Delta P_T}{(\eta \cdot R_t)} \qquad (4.25)$$

where
   J is the permeation flux, L/m^2 h
   ΔP_T is the TMP, kg m/s^2 cm^2
   η is the viscosity of the permeate, kg/m s ($= N \ s/m^2$)
   R_T is the total resistance, m^{-1}

Total resistance (R_T) consists of intrinsic membrane resistance (R_m) and resistance arising from all kinds of fouling ($R_{fouling}$) as in Equation 4.25:

$$J = \frac{\Delta P_T}{\eta(R_m + R_{fouling})} \qquad (4.26)$$

Even though the fouling resistance ($R_{fouling}$) could be subdivided further by many criteria categorizing the fouling phenomena, the most common and clearest method is to divide it only into cake layer resistance (R_f) and internal fouling resistance (R_f) as depicted in Figure 4.28.
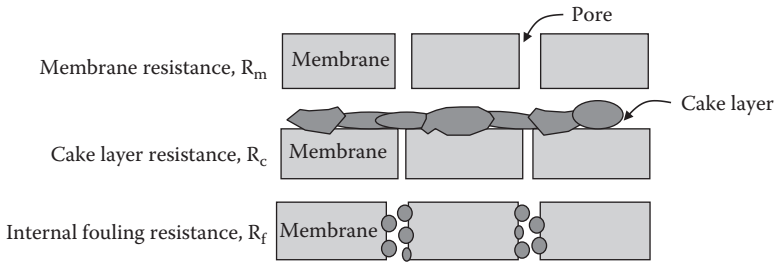
Figure 4.28   Schematic of the RIS model. (Adapted from Chang, I.-S. et al., ***Desalin. Water Treat.***, **8(1), 31, 2009.)**

The RIS model equation is expressed as follows:

$$J = \frac{\Delta P_T}{\eta \cdot R_T}$$

$$= \frac{\Delta P_T}{\eta \cdot (R_m + R_c + R_f)} \qquad (4.27)$$

where
R_c is the cake layer resistance on the membrane surface, m^{-1}
R_f is the internal fouling resistance caused by solute adsorption onto the membrane pores and walls, m^{-1}

Fundamental forms of this model tell us that the flux, J, and the permeate flow rate are directly proportional to the applied pressure and inversely proportional to the permeate viscosity as well as the sum of each resistance. Dividing the fouling resistance ($R_{fouling}$) into two resistances ($R_c + R_f$) is very easy to understand, and it is convenient to get each resistance value by conducting a series of filtration experiments. However, more strict criteria dividing $R_{fouling}$ into its constituent resistances have been often reported. For example, Handerson et al. (2011) divided the fouling resistance into three resistances, R_{Rinsed}, $R_{Backwashed}$, and $R_{Desorbed}$, as shown in Figure 4.29.

The basic equation (4.25) of this model has an analogy to the well-known Ohm's law, which states that the rate of flow of electrical charge through an electrical resistor is proportional to the difference in voltage (V) measured across the resistor:

$$I = \frac{V}{R} \qquad (4.28)$$

where
I is the electric current, ampere, representing the flow rate of the electrical charge
V is the potential, volt, which is the difference in voltage across the resistor
R is the resistance, Ω
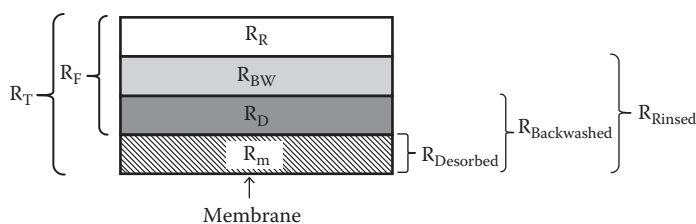
Figure 4.29 Conceptualization of the hydraulic resistance obtained from foulant layers on a membrane surface and the associated nomenclature. (Adapted from Hendersona, R.K. et al., *J. Membr. Sci.*, 382, 50, 2011.)

Flux (J) is the analog of the current (I) because both flux and current are the rate for the flow rate of the permeate (L/s) and the charge (C/s), respectively. TMP (ΔP_T), the difference in pressure across the membrane, is the analog of the potential (V) as both terms represent driving forces for permeation and electric currents. Total resistance (R_T), the sum of all resistances inhibiting the flow of permeate, is obviously the analog of resistance (R) of an electric resistor. Figure 4.30 clearly shows the analogy presented between Ohm's law and the RIS model.

Each resistance value (R_m, R_c, and R_f) can be obtained through Equations 4.28 through 4.30 and can be determined experimentally utilizing J_{iw}, J_{fw}, and J:

$$R_m = \frac{\Delta P_T}{(\eta \cdot J_{iw})} \tag{4.29}$$

Current, I, is the rate expression, coulomb/time		Flux, J, is the rate expression, volume/time
Voltage, V, is the driving force of circuit	*vs.*	TMP is the driving force of filtration
Resistance to electrons flow		Resistance to fluids flow
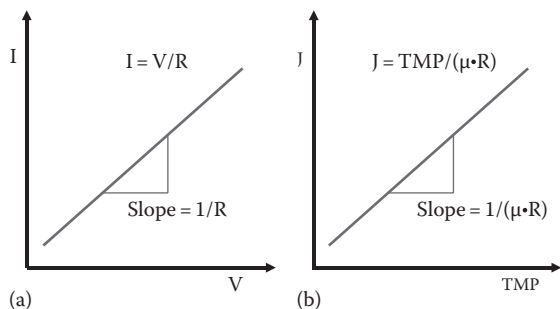
Figure 4.30 Analogy of (a) Ohm's law and the (b) RIS model.

$$R_f = \frac{\Delta P_T}{(\eta \cdot J_{fw}) - R_m} \tag{4.30}$$

$$R_c = \frac{\Delta P_T}{(\eta \cdot J) - (R_m + R_f)} \tag{4.31}$$

J_{iw} is the measured initial water flux of a new (or cleaned) membrane before the feed filtration experiments, J is the measured permeate flux of the feed solution, and J_{fw} is the final water flux measured after removing the cake layer of the fouled membrane.

Example 4.5

The following equation is very useful to conveniently evaluate fouling propensity using raw membrane filtration data such as filtration volume, V, and time, t:

$$\frac{t}{V_p} = \frac{\mu \cdot R_m}{A \cdot \Delta P} + \frac{\mu \cdot C_0 \cdot \alpha}{2A^2 \cdot \Delta P} V_p$$

where
  V_p is permeate volume, mL
  t is the time, s
  μ is the viscosity, kg/m s or Pa s
  A is the membrane surface area, m^2
  C_0 is the initial concentration of the feed solution, kg/m^3
  ΔP is the TMP, kPa

Derive the equation using the RIS model and other relevant equations. Assume that the filtration test runs under constant pressure conditions and the cake layer contributes only to fouling and neglect internal adsorption fouling. Thus, there is only cake layer resistance (R_c), not internal fouling resistance (R_f).

Solution

According to the RIS model ($J = \Delta P/\mu R$) and the derivative form of the flux ($J = dV_p/Adt$), the membrane permeation flux, J, can be expressed as follows:

$$J = \frac{\Delta P}{\mu R} = \frac{dV_p}{Adt}$$

where V_p is the total permeate volume, m^3.
  Remembering the assumption that the pressure is constant, ΔP does not vary with time. Therefore, rearrange the variables (t and V_p) on both sides of the equation and take the integrals as follows:

$$\Delta P \cdot A \int dt = \int \mu \cdot R \cdot dV_p$$

According to the notes and assumptions given in this example, the total resistance, R, is the sum of only the membrane resistance and the cake resistance:

$$R = R_m + R_c$$

Recalling the relationship (4.5),

$$R_c = \frac{\alpha \cdot m}{A} \qquad (4.5)$$

where
   m is the solute mass, kg
   A is the membrane surface area, m²
   α is the specific cake resistance, m/kg

Substitute $R_m + R_c$ for the total resistance, R, and $m\alpha/A$ for R_c as follows:

$$\Delta P \cdot A \int dt = \int \mu \cdot (R_m + R_c) \cdot dV_p$$

$$\Delta P \cdot A \int dt = \int \mu \cdot \left(R_m + \frac{\alpha \cdot m}{A} \right) \cdot dV_p$$

Rearranging the relationship, $C_0 = A \cdot m/V_p$, the following equation is obtained: $m = C_0 \cdot V_p/A$. Substitute m to $C_0 \cdot V_p/A$:

$$\Delta P \cdot A \int dt = \int \mu \cdot \left(R_m + \frac{\alpha \cdot C_0 \cdot V_p}{A^2} \right) \cdot dV_p$$

where C_0 is the initial concentration, kg/m³.
   Integrate both sides:

$$\Delta P \cdot A \cdot t = \mu \cdot R_m \cdot V_p + \frac{\mu \cdot \alpha \cdot C_0}{2A^2} V_p^2$$

After rearranging the equation, we finally obtain the following equation:

$$\frac{t}{V_p} = \frac{\mu \cdot R_m}{A \cdot \Delta P} + \frac{\mu \cdot C_0 \cdot \alpha}{2A^2 \cdot \Delta P} V_p$$

Remarks

This equation is frequently used to obtain a modified fouling index (MFI) experimentally. If we plot t/V_p versus V_p with the raw filtration data, we get a typical MFI curve as shown in the following figure.

(a)
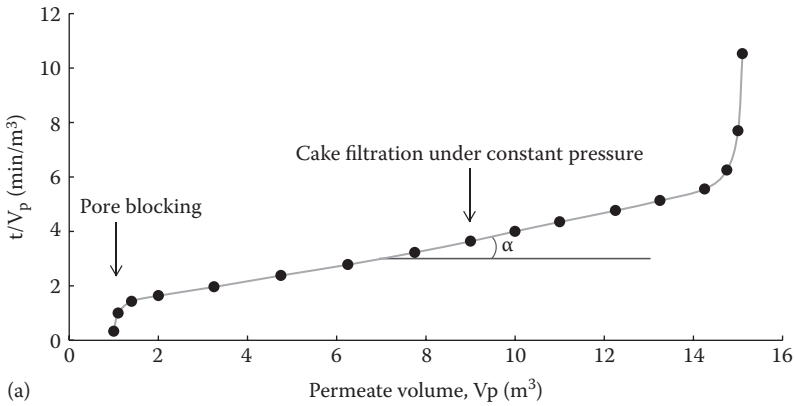
A straight line in the middle of the curve corresponds to cake filtration and the slope of this line represents the MFI. On the right side of the final equation, the slope of the straight line should be $\mu \cdot C_0 \cdot \alpha / 2A^2 \cdot \Delta P$. The graph is divided into three different regions: the first region is where pore blocking and cake filtration occur simultaneously, the second region corresponds to cake filtration under constant filtration pressure, and the final region is where cake (or gel) condensation or compression occurs. Like the silt density index (SDI), MFI is often used as a criterion for verifying if pretreatment prior to an reverse osmosis process is necessary for the tested water or not.

4.5.1.1 Stirred-Batch Filtration Cell

The easiest, most convenient, and fastest way to allow operators to have an insight into the current fouling propensity in an MBR plant is to make them determine each resistance value in their laboratory. Each resistance is obtained by a series of membrane filtration tests with pure water and samples of the activated sludge suspension delivered from the aeration basin to the laboratory using a stirred-batch filtration cell as depicted in Figure 4.31. Because the stirred cell normally only holds up to 250 mL of feed solution, a small volume of the sample is enough to be test-filtrated.

The fresh membrane being tested is first rinsed by letting it float skin side down in ultrapure water for over 1 h to remove residual chemicals on the membrane. The rinsing water is changed two or three times during this cleaning period. The cleaned membrane is placed in the stirred cell. The stirred-batch cell is connected to an electronic top-loading balance in order to read the permeate mass in real time. The permeate flux was determined by weighing permeates on the balance connected to a personal computer equipped with an autoreading program. TMP is regulated using a nitrogen gas cylinder, and the stirring speed is controlled by the stirrer speed.
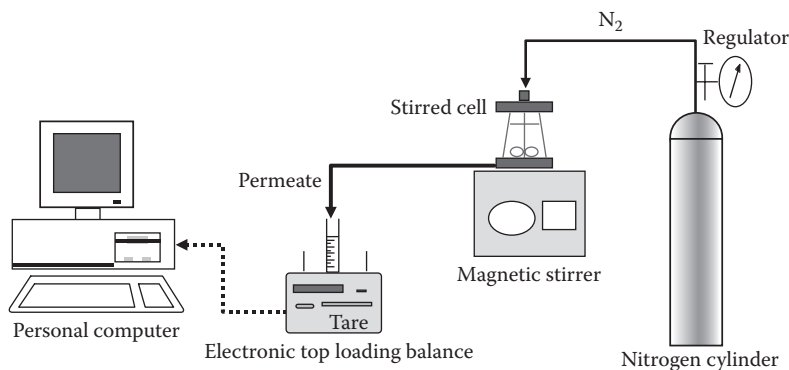
Figure 4.31   Schematic of stirred-batch filtration cell system in laboratory use.

**Example 4.6: Determining Resistance Values Using a
Stirred-Batch Filtration Cell**

To assess the filterability of an activated sludge suspension, a series of batch-type membrane filtrations was carried out using a stirred-cell apparatus in a laboratory. Determine each resistance value—R_m, R_c, and R_f—using the following dataset that was obtained from a series of filtration experiments with pure water and activated sludge suspension:

- The membrane surface area, 30.2 cm²
- Applied pressure, 9.8 kg m/s² cm²
- Temperature, 20°C
- Permeate viscosity, 1.009×10^{-3} kg/m s
- Assume that the permeate density is 1 g/mL.

Permeate volume versus filtration time data

	Mass of Permeate (g)		
Time (s)	Pure Water Filtration before Sludge Filtration	Activated Sludge Filtration	Pure Water Filtration after Cleaning the Cake Layer on the Membrane Surface
15	5.23126	5.18117	6.79102
30	12.69046	10.37136	14.25824
45	20.07453	14.69701	21.60023
60	27.40851	18.44565	29.03840
75	34.70142	21.78456	36.29023
90	41.96227	24.80591	43.50300

Time (s)	Mass of Permeate (g)		
	Pure Water Filtration before Sludge Filtration	*Activated Sludge Filtration*	*Pure Water Filtration after Cleaning the Cake Layer on the Membrane Surface*
105	49.19608	27.58182	50.57151
120	56.39782	30.15538	57.60396
135	63.58555	32.56163	64.60034
150	70.75524	34.82965	71.57669
165	77.89888	36.97444	78.52499
180	85.03050	39.01606	85.46026
195	92.14209	40.96150	92.36248
210	99.23565	42.81779	99.26069
225	106.31718	44.61497	106.27110
240	113.38770	46.34603	113.12523
255	120.44419	48.02000	119.83711
270	127.47062	49.64086	126.67522
285	134.49005	51.21265	133.47225
300	141.49845	52.74035	140.28130
315	148.49484	54.22097	147.07132
330	155.49122	55.67254	153.83028
345	162.45955	57.09506	160.58624
360	169.42789	58.51758	167.33819
375	176.39622	59.94009	174.09014
390	183.36456	61.36261	180.84209
405	190.33289	62.78513	187.59404

Solution

To determine the resistance values quantitatively, three flux values—the initial pure water flux (J_{iw}), the flux of the activated sludge suspension (J), and the final water flux (J_{fw}) after a proper cleaning of the fouled membrane surface—are needed.

First, the initial pure water flux (J_{iw}) has to be calculated in a spreadsheet. Because of the repetitive nature of the calculations, a spreadsheet is ideal for solving this kind of problem.

To determine the initial water flux (J_{iw}) graphically, we must plot the filtration time versus flux. Figure 4.32 shows the water flux graph. Since pure water (or distilled water) was used, it was anticipated that the flux would not decrease with filtration time.

However, the water flux did gradually decrease until it stabilized and finally reached a plateau after nearly 300 s. The flux decline during the early stage of filtration was not due to membrane fouling but compaction of the membrane.

Also, the top-loading balance reading of the permeate mass needs time to stabilize. Because the container receiving the permeate located on the top of the balance was still empty during the initial stage of filtration, the mass data vibrated badly. This resulted in fluctuation of the mass data. Therefore, we should ignore the early-stage flux data when determining the exact value of J_{iw}. We choose 554 L/h m², the stabilized flux as J_{iw} (Table 4.2).

Second, the flux of the activated sludge suspension (J) has to be calculated in a similar way as J_{iw}. Table 4.3 is the spreadsheet showing the procedure of how to calculate the J value.

Figure 4.33 shows the plot of time versus the calculated flux (J) using the spreadsheet shown in Table 4.3.

The flux decreased sharply at first and then gradually decreased. The abrupt flux decline at the early stage of filtration and then the subsequent gradual flux decline are typical patterns exhibited in a common membrane filtration. The flux was stabilized and reached plateau after nearly 330 s. The average value up to this point was calculated to be 114 L/h m², which was chosen as the stabilized flux, J.

Table 4.4 shows the calculated flux of the final water flux (J_{fw}) after proper cleaning of the fouled membrane surface using the same method as earlier.

Figure 4.34 shows the plot of time versus the calculated final pure water flux (J_{fw}). The stabilized water flux appeared after 300 s like the initial water flux determination. We choose 537 L/h m² for the stabilized flux, J_{fw}.

(a)
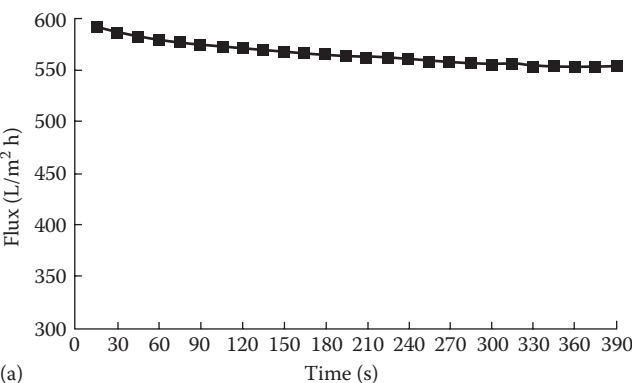
Figure 4.32 Initial water flux profile.

Table 4.2 **Calculation of the Initial Pure Water Flux, J_{iw}**

Time (s)	Volume (mL)	Volume Difference (mL)	mL/s	L/h	Flux (L/h m²)
		Initial Pure Water Flux, J_{iw} (L/h m²), Calculation			
15	5.23126	7.459	0.497	1.790	592.784
30	12.69046	7.384	0.492	1.772	586.813
45	20.07453	7.334	0.489	1.760	582.833
60	27.40851	7.293	0.486	1.750	579.569
75	34.70142	7.261	0.484	1.743	577.021
90	41.96227	7.234	0.482	1.736	574.872
105	49.19608	7.202	0.480	1.728	572.324
120	56.39782	7.188	0.479	1.725	571.210
135	63.58555	7.170	0.478	1.721	569.777
150	70.75524	7.144	0.476	1.714	567.707
165	77.89888	7.132	0.475	1.712	566.751
180	85.03050	7.112	0.474	1.707	565.159
195	92.14209	7.094	0.473	1.702	563.726
210	99.23565	7.082	0.472	1.700	562.771
225	106.31718	7.071	0.471	1.697	561.895
240	113.38770	7.056	0.470	1.694	560.781
255	120.44419	7.026	0.468	1.686	558.392
270	127.47062	7.019	0.468	1.685	557.835
285	134.49005	7.008	0.467	1.682	556.959
300	141.49845	6.996	0.466	1.679	556.004
315	148.49484	6.996	0.466	1.679	556.004
330	155.49122	6.968	0.465	1.672	553.775
345	162.45955	6.968	0.465	1.672	553.775
360	169.42789	6.968	0.465	1.672	553.775
375	176.39622	6.968	0.465	1.672	553.775
390	183.36456	6.968	0.465	1.672	553.775
405	190.33289				$J_{iw} = 554$

Table 4.3   Calculation of the Activated Sludge Suspension Flux, J

Time (s)	Activated Sludge Suspension Flux, J (L/h m²), Calculation				
	Volume (mL)	Volume Difference (mL)	mL/s	L/h	Flux (L/h m²)
15	5.18117	5.190	0.346	1.246	412.465
30	10.37136	4.326	0.288	1.038	343.761
45	14.69701	3.749	0.250	0.900	297.905
60	18.44565	3.339	0.223	0.801	265.344
75	21.78456	3.021	0.201	0.725	240.107
90	24.80591	2.776	0.185	0.666	220.602
105	27.58182	2.574	0.172	0.618	204.521
120	30.15538	2.406	0.160	0.578	191.226
135	32.56163	2.268	0.151	0.544	180.240
150	34.82965	2.145	0.143	0.515	170.447
165	36.97444	2.042	0.136	0.490	162.247
180	39.01606	1.945	0.130	0.467	154.605
195	40.96150	1.856	0.124	0.446	147.519
210	42.81779	1.797	0.120	0.431	142.822
225	44.61497	1.731	0.115	0.415	137.568
240	46.34603	1.674	0.112	0.402	133.030
255	48.02000	1.621	0.108	0.389	128.811
270	49.64086	1.572	0.105	0.377	124.910
285	51.21265	1.528	0.102	0.367	121.407
300	52.74035	1.481	0.099	0.355	117.665
315	54.22097	1.452	0.097	0.348	115.356
330	55.67254	1.423	0.095	0.341	113.048
345	57.09506	1.423	0.095	0.341	113.048
360	58.51758	1.423	0.095	0.341	113.048
375	59.94009	1.423	0.095	0.341	113.048
390	61.36261	1.423	0.095	0.341	113.048
405	62.78513				*J = 114*

(b)
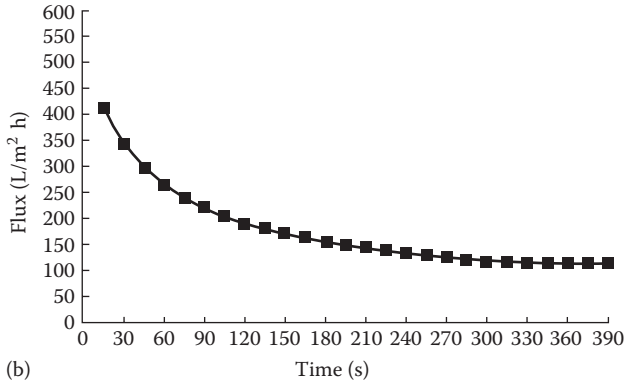
Figure 4.33 **Flux profile of the activated sludge filtration.**

Summarizing the earlier calculations, we got the following three flux values that are needed to calculate the resistance values: $J_{iw} = 554$ L/h m², $J = 114$ L/h m², $J_{iw} = 537$ L/h m².

The next step is the calculation of each resistance value using the RIS model and the previously mentioned flux data:

1. Determination of membrane resistance (R_m) using the following equation:
   $R_m = \Delta P / \eta \cdot J_{iw}$
   a. Insert each value, $J_{iw} = 554$ L/h m², $\Delta P = 9.8$ kg m/s² cm², and $\eta = 1.009 \times 10^{-3}$ kg/m s, into the following equation:

$$R_m = \frac{\Delta P}{\eta \cdot J_{fw}} = \frac{9.8 \, kg \cdot m}{s^2 \cdot cm^2} \frac{m \cdot s}{1.009 \times 10^{-3} \, kg} \frac{m^2 \cdot hr}{554 L} \frac{3600 \, s}{hr} \frac{10^3 L}{m^3} \frac{10^4 cm^2}{m^2}$$

$$= 0.6 \times 10^{12} \, m^{-1}$$

$$\therefore R_m = 0.6 \times 10^{12} \, m^{-1}$$

2. Determination of fouling resistance (R_f) using the following equation:
   $R_c = (\Delta P / \eta \cdot J) - R_m$
   a. Insert $J_{fw} = 537$ L/h m² into the following equation:

$$R_f = \frac{\Delta P}{\eta \cdot J_{fw}} - R_m = \frac{9.8 \, kg \cdot m}{s^2 \cdot cm^2} \frac{m \cdot s}{1.009 \times 10^{-3} \, kg} \frac{m^2 \cdot hr}{537 L} \frac{3600 \, s}{hr} \frac{10^3 \, L}{m^3} \frac{10^4 \, cm^2}{m^2} - R_m$$

$$= 0.7 \times 10^{12} \, m^{-1} - R_m$$

$$\therefore R_f = (0.7 - 0.6) \times 10^{12} \, m^{-1} = 0.1 \times 10^{12} \, m^{-1}$$

Table 4.4 Calculation of the Flux after Backwashing, J_{fw}

Time (s)	Flux after Backwashing, J_{fw} (L/h m²), Calculation				
	Volume (mL)	Volume Difference (mL)	mL/s	L/h	Flux (L/h m²)
15	6.79102	7.668	0.511	1.840	609.343
30	14.45859	7.442	0.496	1.786	591.431
45	21.90076	7.438	0.496	1.785	591.112
60	29.33893	7.051	0.470	1.692	560.383
75	36.39041	7.113	0.474	1.707	565.239
90	43.50300	7.069	0.471	1.696	561.736
105	50.57151	7.032	0.469	1.688	558.870
120	57.60396	6.996	0.466	1.679	556.004
135	64.60034	6.976	0.465	1.674	554.412
150	71.57669	6.948	0.463	1.668	552.183
165	78.52499	6.935	0.462	1.664	551.148
180	85.46026	6.902	0.460	1.657	548.521
195	92.36248	6.898	0.460	1.656	548.202
210	99.26069	7.010	0.467	1.682	557.119
225	106.27110	6.854	0.457	1.645	544.699
240	113.12523	6.712	0.447	1.611	533.394
255	119.83711	6.838	0.456	1.641	543.425
270	126.67522	6.797	0.453	1.631	540.161
285	133.47225	6.809	0.454	1.634	541.117
300	140.28130	6.790	0.453	1.630	539.604
315	146.06954	6.759	0.451	1.622	537.136
330	153.83028	6.756	0.450	1.621	536.897
345	160.58624	6.752	0.450	1.620	536.579
360	167.33819	6.752	0.450	1.620	536.579
375	174.09014	6.752	0.450	1.620	536.579
390	180.84209	6.752	0.450	1.620	536.579
405	187.59404				$J_{fw} = 537$

Figure 4.34 **Final water flux profile after removing the cake layer.**

3. Determination of cake resistance (R_c) using the following equation:

$$R_c = \frac{\Delta P}{\eta \cdot J} - (R_m + R_f)$$

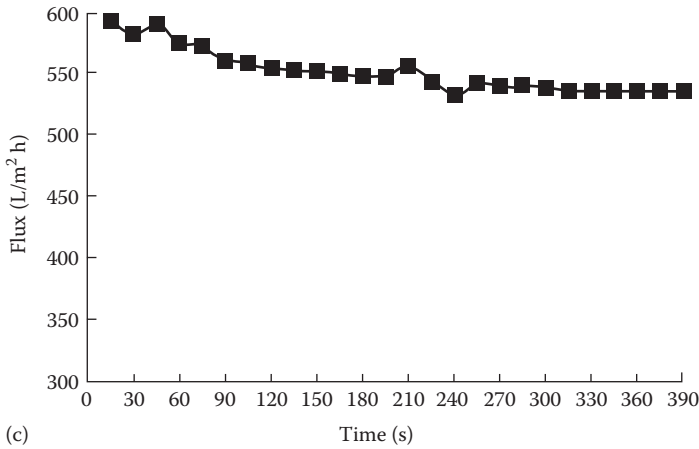a. Insert the flux of the activated sludge filtration, $J = 114$ L/h m², into the following equation:

$$R_c = \frac{\Delta P}{\eta \cdot J} = \frac{9.8\,\text{kg} \cdot \text{m}}{\text{s}^2 \cdot \text{cm}^2} \frac{\text{m} \cdot \text{s}}{1.009 \times 10^{-3}\,\text{kg}} \frac{\text{m}^2 \cdot \text{hr}}{114\,\text{L}} \frac{3600\,\text{s}}{\text{hr}} \frac{10^3\,\text{L}}{\text{m}^3} \frac{10^4\,\text{cm}^2}{\text{m}^2} - (R_m + R_f)$$

$$= 3.1 \times 10^{12}\,\text{m}^{-1} - (R_m + R_f)$$

$$\therefore R_c = \left\{ 3.1 - (0.6 + 0.1) \right\} \times 10^{12}\,\text{m}^{-1} = 2.4 \times 10^{12}\,\text{m}^{-1}$$

$$\therefore \text{Total resistance, } R_T = 3.1 \times 10^{12}\,\text{m}^{-1}$$

$$\text{Membrane resitance, } R_m = 0.6 \times 10^{12}\,\text{m}^{-1}$$

$$\text{Cake layer resistance, } R_c = 2.4 \times 10^{12}\,\text{m}^{-1}$$

$$\text{Fouling resistance, } R_f = 0.1 \times 10^{12}\,\text{m}^{-1}$$

Example 4.7

A bench-scale submerged MBR is running in a laboratory under a constant flux mode (Table 4.5). Determine each resistance value, R_m, R_c and R_f, using the following dataset that was obtained from a series of filtration experiments with pure water and activated sludge suspension (assume that the permeate density is 1 g/mL):

- MLSS concentration, 3500 mg/L
- The membrane surface area, 0.05 m²

Table 4.5 TMP versus Filtration Time Data

Time (s)	Monitored Pressure (bar)		
	Pure Water Filtration before the MBR Run	*MBR Run with Activated Sludge*	*Pure Water Filtration after Cleaning the Cake Layer on the Membrane Surface*
15	0.020	0.656	0.039
30	0.042	1.675	0.045
45	0.046	2.389	0.068
60	0.061	3.199	0.079
75	0.063	3.918	0.091
90	0.070	4.631	0.121
105	0.071	5.348	0.137
120	0.073	5.953	0.145
135	0.073	6.361	0.149
150	0.073	6.662	0.191
165	0.076	6.863	0.192
180	0.077	6.862	0.195
195	0.077	6.861	0.198
210	0.077	6.862	0.199
225	0.078	6.862	0.201
240	0.078	6.863	0.203
255	0.078	6.863	0.204
270	0.078	6.862	0.204
285	0.078	6.861	0.203
300	0.078	6.863	0.203
315	0.078	6.862	0.204
330	0.078	6.863	0.203

- The pore size of the hollow membrane, 0.4 μm
- Initial water flux (J_{iw}), 30 L/m² h
- Flux (J), 20 L/m² h (LMH)
- Final water flux (J_{fw}), 24 L/m² h
- Temperature, 20°C
- Permeate viscosity, 1.009×10^{-3} kg/m s

Solution

Three TMP values are needed to calculate each resistance; the stabilized TMP for pure water filtration (TMP_i), the stabilized TMP for activated sludge filtration (TMP), and the stabilized TMP for pure water filtration after cleaning the cake layer (TMP_f). Each stabilized TMP value should be determined first before calculating the resistances.

The TMP_i has to be found using the pressure dataset, which was obtained from pure water filtration. The unit of pressure should be converted from bar to kg m/s² cm² for the calculation of resistance values. Because of the repetitive nature of the calculations, a spreadsheet calculation is recommended. Table 4.6 shows the converted pressure dataset expressed in SI units using the relationship 1 bar = 9.996 kg m/s² cm².

To see the TMP profile of the pure water filtration graphically, the data in Table 4.6 were plotted as TMP versus the filtration time (Figure 4.35). Since the pure water (or distilled water) was used, the TMP was not anticipated to increase along with the filtration time. However, the TMP increased continuously due to the initial compaction of the membrane and finally stabilized to a plateau value, 0.7797 kg m/s² cm², which is the TMP_i value for the R_m calculation.

Second, the stabilized TMP for the filtration of an activated sludge suspension has to be determined in a similar way as the TMP_i determination. The third column in Table 4.6 contains the pressure data converted into SI units. Figure 4.36 shows the plot of time versus the calculated TMP using data from the spreadsheet. The flux increase during the early stage of filtration is a typical pattern exhibited in common membrane filtration. The flux was stabilized and reached plateau after nearly 150 s. The average value after this point was calculated to be 68.6025 kg m/s² cm², which is representative of the stabilized TMP value for the $R_c + R_f$ calculation.

The fourth column in Table 4.6 shows the calculated TMP obtained after proper cleaning of the fouled membrane surface, for example, after backwashing. Figure 4.37 shows the plot of time versus the calculated TMP using the spreadsheet in Table 4.6. The stabilized TMP is calculated to be 2.0292 kg m/s² cm².

Through the procedure earlier, the three TMP values that were required to calculate the resistance values were obtained: $TMP_i = 0.7797$ kg m/s² cm², TMP = 68.6025 kg m/s² cm², and $TMP_f = 2.0292$ kg m/s² cm². The next step is the calculation of each resistance value using the RIS model and the TMP data:

1. Determination of membrane resistance (R_m) using the following equation:
   $R_m = \Delta P / \eta \cdot J_{iw}$
   a. Insert each value, $J_{iw} = 30$ L/h m², $TMP_i = 0.7797$ kg m/s² cm², and $\eta = 1.009 \times 10^{-3}$ kg/m s, into the following equation and calculate it:

$$R_m = \frac{0.7797 \text{ kg} \cdot \text{m}}{\text{s}^2 \cdot \text{cm}^2} \times \frac{\text{m} \cdot \text{s}}{1.009 \times 10^{-3} \text{ kg}} \times \frac{\text{m}^2 \cdot \text{h}}{30 \text{ L}} \times \frac{3600 \text{ s}}{\text{h}} \times \frac{100^2 \text{ cm}^2}{\text{m}^2} \times \frac{10^3 \text{ L}}{\text{m}^3}$$

$$R_m = 0.09 \times 10^{13} \text{ m}^{-1}$$

Table 4.6   Determination of Each TMP Value Using the Filtration Data

	TMP		
	Pure Water Filtration before the MBR Run	*MBR Run with Activated Sludge*	*Pure Water Filtration after Cleaning the Cake Layer on the Membrane Surface*
Time (s)	*Pressure (kg m/s² cm²)*	*Pressure (kg m/s² cm²)*	*Pressure (kg m/s² cm²)*
15	0.151999	6.5574	0.3898
30	0.4198	16.7433	0.4498
45	0.4598	23.8804	0.6797
60	0.6098	31.9772	0.7897
75	0.6297	39.1643	0.9096
90	0.6997	46.2915	1.2095
105	0.7097	53.4586	1.3695
120	0.7297	59.5062	1.4494
135	0.7297	63.5846	1.4894
150	0.7297	66.5934	1.9092
165	0.7597	68.6025	1.9192
180	0.7697	68.5926	1.9492
195	0.7697	68.5826	1.9792
210	0.7697	68.5926	1.9892
225	0.7797	68.5926	2.0092
240	0.7797	68.6025	2.0292
255	0.7797	68.6025	2.0392
270	0.7797	68.5926	2.0392
285	0.7797	68.5826	2.0292
300	0.7797	68.6025	2.0292
315	0.7797	68.5926	2.0392
330	0.7797	68.6025	2.0292
TMP	$TMP_i = 0.7797$ (kg m/s² cm²)	$TMP = 68.6025$ (kg m/s² cm²)	$TMP_f = 2.0292$ (kg m/s² cm²)

(a)
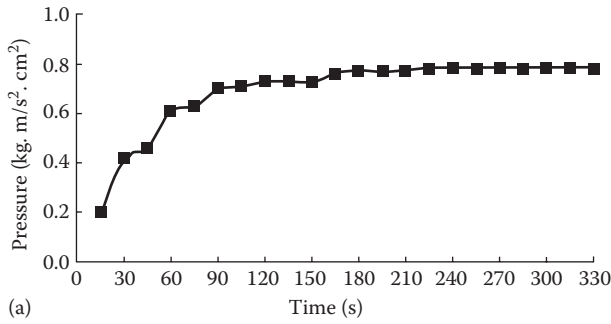
Figure 4.35 TMP$_i$ profile of the pure water filtration.

(b)
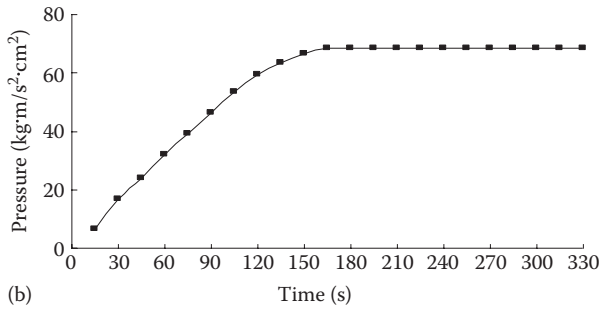
Figure 4.36 TMP profile of the filtration of activated sludge.

(c)
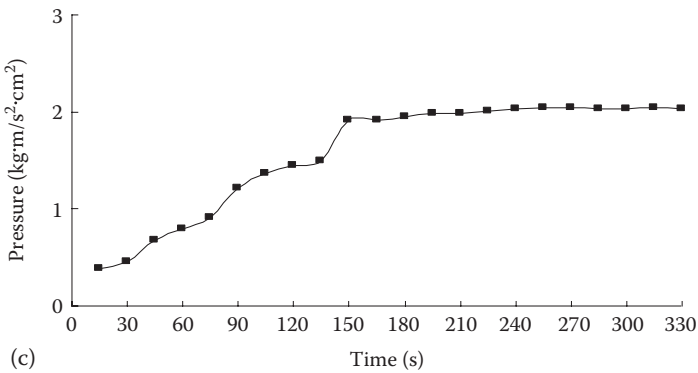
Figure 4.37 TMP$_f$ profile of the pure water filtration after removing the cake layer.

2. Determination of fouling resistance (R_f) using the following equation:
   $R_f = \Delta P / \eta \cdot J_{fw} - R_m$
   a. Insert each value, $J_{fw} = 24$ L/h m^2, $TMP_f = 2.0292$ kg m/s^2 cm^2, and $\eta = 1.009 \times 10^{-3}$ kg/m s, into the following equation:

$$R_f = \frac{2.0292 \text{ kg} \cdot \text{m}}{\text{s}^2 \text{ cm}^2} \times \frac{\text{m} \cdot \text{s}}{1.009 \text{ } 10^{-3} \text{ kg}} \times \frac{\text{m}^2 \cdot \text{h}}{24 \text{ L}} \times \frac{3600 \text{ s}}{\text{h}}$$

$$\times \frac{100^2 \text{ cm}^2}{\text{m}^2} \times \frac{10^3 \text{ L}}{\text{m}^3} - 0.09 \times 10^{13}$$

$$R_f = 0.3 \times 10^{13} \text{ m}^{-1} - 0.09 \times 10^{13} \text{ m}^{-1}$$

$$\therefore R_f = 0.21 \times 10^{13} \text{ m}^{-1}$$

3. Determination of cake resistance (R_c) using the following equation:$R_c = (\Delta P / \eta \times J) - (R_m + R_f)$
   a. Insert each value, $J_{fw} = 20$ L/h m^2, $TMP = 68.6025$ kg m/s^2 cm^2, and $\eta = 1.009 \times 10^{-3}$ kg/m s, into the following equation:

$$R_c = \frac{68.6025 \text{ kg} \cdot \text{m}}{\text{s}^2 \cdot \text{cm}^2} \times \frac{\text{m} \cdot \text{s}}{1.009 \times 10^{-3} \text{ kg}} \times \frac{\text{m}^2 \cdot \text{h}}{20 \text{ L}} \times \frac{3600 \text{ s}}{\text{h}} \times \frac{100^2 \text{ cm}^2}{\text{m}^2} \times \frac{10^3 \text{ L}}{\text{m}^3}$$

$$- (0.09 + 0.21) \times 10^{13}$$

$$R_c = 12.2 \times 10^{13} \text{ m}^{-1} - \left(0.09 + 0.21\right) \times 10^{13} \text{ m}^{-1}$$

$$\therefore R_c = 11.9 \times 10^{13} \text{ m}^{-1}$$

Summarizing each resistance, the membrane resistance, $R_m = 0.09 \times 10^{13}$ m^{-1}; the cake layer resistance, $R_c = 11.9 \times 10^{13}$ m^{-1} and the fouling resistance, $R_f = 0.21 \times 10^{13}$ m^{-1}:

$$\therefore \text{Total resistance, } R_T = R_m + R_c + R_f$$

$$= 0.09 \times 10^{13} \text{ m}^{-1} + 11.9 \times 10^{13} \text{ m}^{-1} + 0.21 \times 10^{13} \text{ m}^{-1}$$

$$= 12.2 \times 10^{13} \text{ m}^{-1}$$

4.5.1.2 Cautious Use of the Resistance in the Series Model

Although the RIS model is very convenient and is an easy way to evaluate and predict membrane fouling quantitatively, there is a need to be cautious when using the RIS model, particularly when it is used to determine the relative values of the main membrane fouling components of an activated sludge suspension:

$$J = \frac{\Delta P_T}{\eta \cdot R_T}$$

$$= \frac{\Delta P_T}{\eta \cdot (R_m + R_c + R_f)} \qquad (4.27)$$

The total resistance, R_T, is taken as the sum of each resistance ($R_T = R_m + R_c + R_f$). However, this summation is only possible if each resistance is additive. In order to be additive, the individual resistances (R_m, R_c, and R_f) must work independently without interferences.

Sometimes this model has been used to link the resistances that are not independent in the components of an activated sludge suspension. For example, it is used to investigate what components of the activated sludge suspension dominate the total resistance. Similar to the classification previously shown in Figure 4.11, the activated sludge suspension in an MBR consists of three components: SSs, colloidal matter, and soluble solutes. Therefore, the resistance of the activated sludge suspension in an MBR could be considered to be equal to the sum of each components' resistance as follows:

$$R_{AS} = R_{SS} + R_{COL} + R_{SOL} \qquad (4.32)$$

where
  R_{AS} is the resistance of the activated sludge
  R_{SS} is the resistance of the SSs
  R_{COL} is the resistance of the colloids
  R_{SOL} is the resistance of the solutes

Many studies have attempted to investigate the relative contribution of the resistances from each component (Bae et al., 2005; Bouhabila et al., 2001; Defrance et al., 2000; Lee et al., 2003; Meng et al., 2007; Wisniewski and Grasmik, 1998). Their studies assumed that activated sludge consists of solutes, colloids, and SSs, and they used an equation similar to Equation 4.32 for their analysis to compare each component's contribution to membrane fouling. Those kinds of attempts and their equations seem to be very feasible considering that an activated sludge suspension is comprised of different components. However, the basic assumption "total resistance of the activated sludge suspension is a sum of the individual resistances of each component" is very questionable. In other words, it should be confirmed that the sum of individual resistances ($R_{SS} + R_{COL} + R_{SOL}$) is equal to the total resistance of an activated sludge suspension (R_{AS}).

Chang et al. (2009) confirmed that the sum of the resistances of each fraction of an activated sludge suspension is different from that of a complete activated sludge suspension. They pointed out that most of the published works assume resistance additivity and two of the three individual resistances are measured and the third is

simply inferred, not measured. They emphasized that activated sludge suspensions are not simple mixtures of individual components but a conjugate closely correlated with each component. When the fractionation of an activated sludge suspension is carried out, the unique characteristics of the individual components could be lost.

Many studies on the membrane filtration of proteins, bio-cells, and their mixtures have also reported that the sum of individual resistances of proteins and cells are different than that of the mixture solution. For example, Guell et al. (1999) concluded that the sum of the individual resistances of a protein and yeast cell suspension is greater than the resistance of the mixture solution. Hughes et al. (2006) also reported that the sum of individual resistances of BSA and ovalbumin is over two times greater than the resistance of their protein mixture. That is, the sum of the resistances of individual components is usually greater than the resistance of a simple mixture of proteins and cells.

Convenience does not imply applicability, and the RIS model should be used cautiously, particularly when used to analyze the individual resistances of the sludge components. Even if an effective fractionation of an activated sludge suspension into its components is accomplished successfully, which is actually very difficult, additivity of individual resistances is not guaranteed. Consequently, determining individual resistances to evaluate and compare the relative contribution of each component to the overall resistance should be used with caution.

4.5.1.3 Cautious Use of the Resistance in the Series Model to Determine Cake Layer Resistance (R_c)

The RIS model should be used cautiously, particularly when determining the cake layer resistance (R_c) experimentally, which is calculated using flux data obtained empirically before and after removing the cake layer on the membrane surface. The calculated R_c values are very dependent upon the cleaning methods used for removing the cake layer from the membranes.

According to the study of Han and Chang (2014), there are big differences in R_c depending on the cake layer removal method. After a series of batch filtrations of the activated sludge suspensions, four different cleaning methods were employed to remove the cake layer on the membrane surface:

1. Water rinsing in a vibrating shaker
2. Manual water rinsing
3. Sponge scrubbing
4. Ultrasonications at different power levels

The ratio of the cake layer resistance to the total fouling resistance, $R_c/(R_c + R_f)$, was calculated and compared in Figure 4.38. The total fouling resistance, $R_c + R_f$, should be identical regardless of the removal options. Because the same feed was
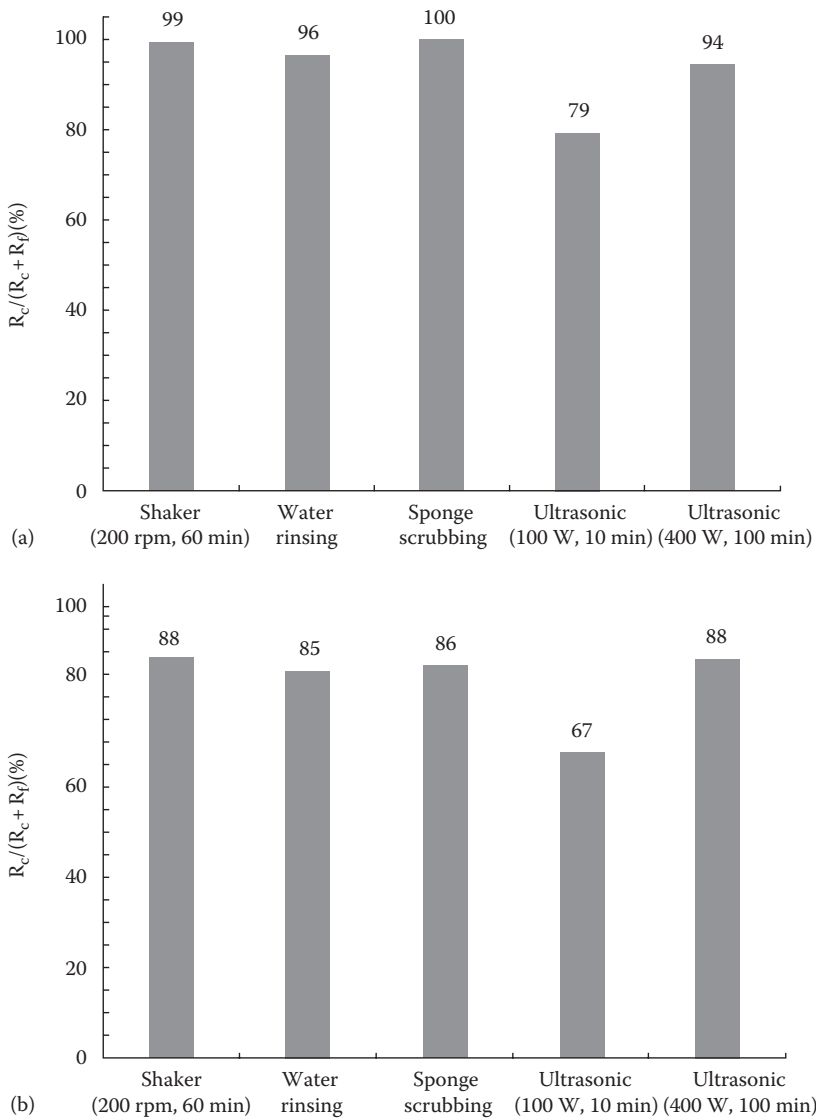
Figure 4.38   Comparison of the resistance ratio, $R_c/(R_c + R_f)$, for the five different cleaning methods using (a) the YM30 membrane and (b) the PM30 membrane. (From Han, S.-H. and Chang, I.-S., *Separat. Sci. Technol.*, 49, 2459, 2014.)

filtered, the total extent of fouling should be identical, theoretically. The decisive parameter for comparing the removal efficiencies between each removal option is not the individual resistance values but the ratio of R_c to the total fouling resistance (i.e., $R_c/(R_c + R_f)$). This ratio decreases in the case of incomplete cake layer removal but increases with proper cake layer removal.

For YM30 membranes, sponge scrubbing removed the cake layer completely ($R_c/R_c + R_f = 100\%$), whereas other methods showed removal efficiencies ranging from 79% to 99%. For the PM30 membrane, none of the options achieved complete cake layer removal. In addition, sponge scrubbing was not the best option for cake removal, indicating that even a method with the potential to completely remove the cake layer on a specific membrane is not universal for every kind of membrane.

The extent of cake layer removal varies by the individual cleaning method regardless of the membrane type, indicating that a wrong explanation about the fouling phenomena could be drawn if an incomplete dataset of resistance values is used. Consequently, a standardized method for cake layer removal to determine cake resistance (R_c) is needed for correct interpretation of the fouling phenomena with the RIS model.

4.5.2 TMP Buildup

Monitoring the TMP buildup with time is a typical and practical way to obtain information about the fouling propensity in a full-scale MBR. The derivative form of the TMP variation with time, dTMP/dt, represents fouling rates similar to head loss (h_L) buildup in conventional sand filtration. That is, fouling advances as the dTMP/dt steepens with operation time.

The fouling rate, dTMP/dt, is dependent upon the operating flux. As shown in Figure 4.3a, the dTMP/dt of J_0 shows the steepest slope among the other fluxes. J_0 is the highest operating flux relative to the others ($J_0 > J_{critical} > J_1 > J_2 > J_3 > J_4$). The fouling rate, dTMP/dt, decreases as the operating flux decreases. Le-Clech et al. (2006) collected fouling rate data in literatures and summarized it. According to their work, typical fouling rates range from 0.004 to 0.6 kPa/h under subcritical flux conditions.

When sidestream MBRs are operated, the permeability represents the flux per applied pressure and is expressed in units of $L/(m^2 \, h \, bar)$ or $m/(h \, kPa)$. Permeability is useful when comparing the relative membrane filterability between fouled membranes. Since sidestream MBRs run under different recirculating velocities and the applied pressure is controlled by back-pressure valves, direct comparison of flux without pressure compensation results in misinformation on membrane fouling. On the other hand, the permeability of submerged MBRs is a little bit confusing. Since the suction pressure is always negative and changes along the operation time, permeability is not frequently used to represent the fouling propensity.

4.6 Fouling Control Strategy

Stable and reliable operation of MBR plants requires careful management of membrane fouling because membrane fouling cannot be completely avoided. Recent developments and improvements in fouling control technologies have led to more favorable projections of membrane life and significantly reduced overall maintenance and operation costs.

Basically, fouling control includes all kinds of implementation strategies to keep the flux as high as the design level. Thus a pretreatment of the feed solution could be considered as an essential tool for fouling control in MBRs. There are numerous methods of fouling control that have been practiced in MBR plants. Most of the attempted methods can be categorized into chemical, physical, biological, or others (electric and membrane and module development). Chemically cleaning membranes certainly restores membrane filtration performance. Strong acids, caustics, and/or oxidizing agents recover the membrane's deteriorated performance nearly completely. However, chemical cleaning cannot avoid secondary contamination, which is the generated waste chemicals that require further treatment and eventual disposal. Moreover, safety regulations for the transport, storage, and usage of chemicals have become stringent nowadays, so that alternative cleaning options are encouraged instead of chemical cleaning.

Therefore, physical cleaning methods are recommended because they do not produce secondary contaminants that require further treatment. For example, after backwashing, the most widely practiced physical cleaning method, backwashing wastes can be redirected to the aeration tank. However, frequent backwashing leads to damages of the membrane structure and particularly collapses the anisotropic membrane structure. On the other hand, physical cleaning such as coarse aeration that is widely practiced in submerged MBR systems consumes great amounts of energy. Most operation and maintenance (O&M) costs in MBR plants are attributed to the electrical energy consumption of the blower supplying coarse air to the membrane surfaces.

Biological fouling control has been developed recently. Innovative developments in the field of molecular biology over the last couple of decades show a potential for MBRs to become more able to cope with membrane fouling than before. For example, the application of quorum sensing between microorganisms to ameliorate membrane fouling has been reported recently. The quorum sensing mechanism is quite well understood by the progress in modern molecular biology. The principal idea of the quorum sensing application to fouling control in MBR is "quorum quenching." The microorganisms in the bio-cakes on membrane surfaces communicate with each other using signal molecules known as autoinducers. Membrane fouling caused by biofilm formation and deposition on membrane surfaces by microorganisms could be inhibited by the addition of autoinducer-inhibiting chemicals. Other types of biological control techniques besides quorum quenching are (1) nitric oxide to induce biofilm dispersal, (2) enzymatic disruption of EPSs, and (3) disruption

of biofilm formation by bacteriophages. Although these recent applications are still developing in the laboratory scale, they could arrive at mature stages soon.

All the fouling control options introduced here and other techniques such as electrical coagulation–aided MBR will be explained in detail in Chapter 5.

Problems

4.1 A data plot with filtration data is needed to have an insight into the fouling propensity of a feed solution. Plotting flux (or TMP) on the y-axis versus filtration volume (or time) on the x-axis is a common way to plot the data. Sometimes the volume concentration ratio (VCR) is used to show how the feed solution has been concentrated during the progress of filtration.
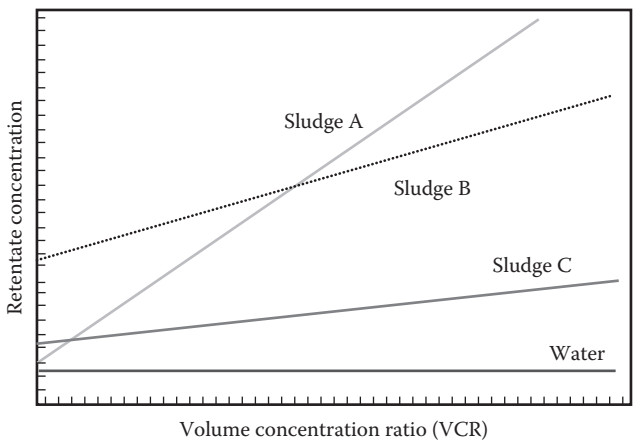
You are to plot your filtration data by VCR versus retentate concentration similar to the figure shown earlier. You are to obtain your raw filtration data (i.e., permeate volume [V]) along with the filtration time (t). You are to transfer the raw data onto a spreadsheet. Derive the equations expressing the VCR and concentration of the retentate (C_c) with your raw data. Make functions calculating the VCR and C_R on your spreadsheet using relevant notations, for example, the permeate volume (V_p), volume of concentrate (V_c), feed solution volume (V_F), initial concentration (C_0), permeate concentration (C_p), and t.

	A	B	C	D
1	Time, t (s)	Volume, V_p (mL)	VCR	Retentate concentration, C_R
2	⋮	⋮	⋮	⋮
3	⋮	⋮	⋮	⋮

4.2 The filtered permeate of MBR becomes a secondary effluent. Since submicron-sized microfiltration or ultrafiltration membranes are used in MBRs, the total suspended solids (TSS) in the effluent of MBRs must be 0 because the typical pore size of the filter papers used to measure TSS is bigger than 1.2 μm. However, the TSS of an MBR effluent is often reported to be between 1 and 4 mg/L. Discuss why the TSS of the MBR effluent exceeds 0 mg/L. Exclude the possibility of membrane defects and experimental errors for measuring TSS.

4.3 The MFI is the most widely applied method to evaluate the particulate fouling potential of feedwater. The utilization of the fouling index enables engineers to determine pretreatment requirements without conducting a pilot study that consumes considerable time and expense.

Dead-end filtration at 30 psi, through a 47 mm diameter MF membrane with an average pore size of 0.45 μm, was conducted on a feed source to determine the MFI. During filtration experiments, feed and permeate samples were collected and analyzed for concentration. Determine the MFI using the following filtration data.

Time (min)	Volume (m³)
0.33	1.00
1.83	1.10
2.78	1.40
4.58	2.00
9.46	3.25
17.40	4.75
27.65	6.25
40.16	7.75
52.33	9.00
63.17	10.00
75.09	11.00
91.42	12.25
105.58	13.25
120.76	14.25
130.53	14.75
142.86	15.00
167.78	15.10

4.4 Determine the wall shear stress (τ_w) produced by fluids flowing through a tubular membrane module that is located outside the bioreactor (i.e., side-stream MBR). The diameter of the pipe carrying the fluids is 10 cm and the flow rate is 34 L/min. The outer diameter of the tubular membrane is 7 cm. The inner diameter of the tube in the membrane module is 1.5 cm. The module consists of 10 tubes as shown in the following figure. The density of the mixed liquor is 1012 kg/m³. The viscosity is 1.14×10^{-3} N s/m².
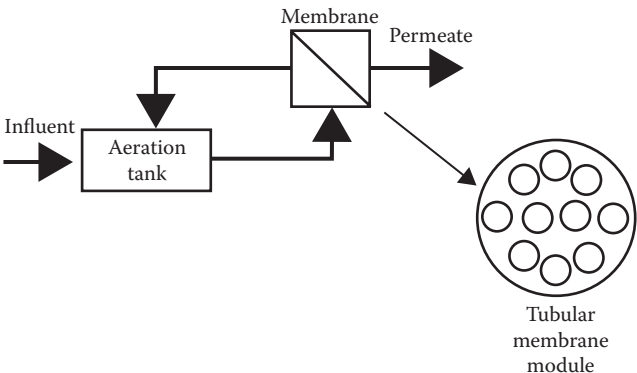
4.5 MBR has many advantages over CAS. One of them is that MBR never suffers from settling problems such as sludge bulking, foaming, rising, and pinpoint flocs. However, membrane fouling is closely related to the settling problems encountered in secondary clarifiers (i.e., membrane permeability deteriorates when the bulking and foaming issues arise). Thus, MBR operators should carefully observe the sludge settling properties. The SVI is the most widely used criteria to evaluate the settling properties of activated sludge. Determine the SVI values of the activated sludge suspensions withdrawn from an MBR tank using the following data. Estimate if the fouling propensity will deteriorate or not with the calculated SVI values.

	MLSS (mg/L)	*SV$_{30}$ (mL/L)*
Sludge 1	2000	450
Sludge 2	3500	480
Sludge 3	8000	530

4.6 Nonwoven fabrics such as nonwoven polypropylene could be used as a filter because they have micropores to pass water. They are also cheaper than synthetic polymeric membranes made of the same materials (i.e., they are low-cost filters). Even though some published papers have already reported that

they can be used for solid–liquid separation in MBR, they are not currently used in MBR. Why aren't they used in MBR?

4.7 A lab-scale sidestream MBR equipped with a tubular membrane module is set up to evaluate the system's performance. The permeate flow rate of pure water through a 100 cm² membrane is 23.5 mL/min at 15°C. The measured pressures at the inlet and outlet of the module are 2500 and 2200 kPa, respectively. Determine the intrinsic membrane resistance values at 15°C and 20°C.

4.8 To check the membrane filterability of mixed liquor in an MBR plant, activated sludge sample is taken and delivered to a lab. Determine the resistance values of R_m, R_c, and R_f using the following data obtained by a series of membrane filtration. Assume the following:

■ The membrane surface area, 32.1 cm²
■ Applied pressure, 9.5 kg m/s² cm²
■ Temperature, 20°C
■ Permeate viscosity, 1.013×10^{-3} kg/m s

Time (s)	Mass of Permeate (g)		
	Pure Water Filtration before the Sludge Filtration	Activated Sludge Filtration	Pure Water Filtration after Cleaning the Cake Layer on the Membrane Surface
15	4.154	4.275	5.964
30	12.682	9.188	14.502
45	21.117	13.226	22.918
60	29.480	16.720	31.248
75	37.789	19.804	39.515
90	46.056	22.575	47.730
105	54.291	25.133	55.905
120	62.502	27.505	64.044
135	70.693	29.719	72.152
150	78.871	31.801	80.232
165	87.033	33.764	88.286
180	95.183	35.629	96.322
195	103.316	37.401	104.334
210	111.434	39.089	112.325

Time (s)	Mass of Permeate (g)		
	Pure Water Filtration before the Sludge Filtration	Activated Sludge Filtration	Pure Water Filtration after Cleaning the Cake Layer on the Membrane Surface
225	119.539	40.724	120.300
240	127.633	42.300	128.261
255	135.713	43.823	136.209
270	143.784	45.298	144.138
285	151.848	46.727	152.052
300	159.902	48.117	159.955
315	167.948	49.462	167.851
330	175.979	50.778	175.738
345	183.998	52.073	183.621
360	192.017	53.368	191.499
375	200.036	54.663	199.377
390	208.055	55.958	207.255
405	216.074	57.253	215.133

4.9 The total resistance (R_T) in the RIS model is a sum of each resistance that acts as a barrier to the permeation flow. Differentiating the total resistance into three resistances ($R_m + R_c + R_f$) is the most popular form when applying the model to evaluate the fouling phenomena in MBRs:

$$J = \frac{TMP}{\mu \cdot R_T} = \frac{TMP}{\mu \cdot (R_m + R_C + R_f)} \tag{4.27}$$

where
  R_m is the membrane resistance
  R_c is the cake resistance
  R_f is the internal fouling resistance

Design an experimental procedure to determine each resistance value if the total resistance is expressed as a sum of $R_m + R_{rev} + R_{irr}$. That is, the fouling resistance is divided into reversible resistance (R_{rev}) and irreversible

resistance (R_{irr}). Discuss the differences in the procedure obtaining each resistance between $R_m + R_{rev} + R_{irr}$ and $R_m + R_c + R_f$.

4.10 Water reuse issues have gained a great deal of attention recently due to the water resource shortage problems. Particularly, water reuse of secondary effluents using membrane separation technologies has been widely applied. A pilot-scale plant employing ultrafiltration membranes is running to reuse the secondary effluents from a domestic wastewater treatment facility. The membrane plant operates at a constant flux mode (i.e., 40 LMH) and the applied pressure is 0.25 bar when no fouling is present. The TSS concentration of the secondary effluent is 15 mg/L. After 60 min of operation, the pressure (i.e., TMP) reaches 0.3 bar. If the pressure rise is entirely due to cake formation on the membrane surface, calculate the specific cake resistance. Assume the temperature is 20°C.

References

Bae, T.H. and Tak, T.M. (2005) Interpretation of fouling characteristics of ultrafiltration membranes during the filtration of membrane bioreactor mixed liquor, *Journal of Membrane Science*, 264: 151–160.

Beyenal, H., Donovan, C., Lewandowski, Z., and Harkin, G. (2004) Three-dimensional biofilm structure quantification, *Journal of Microbiological Methods*, 59: 395–413.

Bouhabila, E.H., Ben Aim, R., and Buisson, H. (2001) Fouling characterization in membrane bioreactors, *Separation and Purification Technology*, 22–23: 123–132.

Bressel, A., Schultze, J.W., Khan, W., Wolfaardt, G.M., Rohns, H.P., Irmscher, R., and Schoning, M.J. (2003) High resolution gravimetric, optical and electrochemical investigation of microbial biofilm formation in aqueous systems, *Electrochimica Acta*, 48: 3363–3372.

Chang, I.-S., Field, R., and Cui, Z. (2009) Limitations of resistance-in-series model for fouling analysis in membrane bioreactors: A cautionary note, *Desalination and Water Treatment*, 8(1): 31–36.

Chang, I.-S. and Kim, S.N. (2005) Wastewater treatment using membrane filtration—Effect of biosolids concentration on cake resistance, *Process Biochemistry*, 40: 1307–1314.

Chang, I.-S., Le-Clech, P., Jefferson, B., and Judd, S. (2002) Membrane fouling in membrane bioreactors for wastewater treatment, *Journal of Environmental Engineering*, 128(11): 1018–1029.

Chang, I.S. and Lee, C.H. (1998) Membrane filtration characteristics in membrane coupled activated sludge system-the effect of physiological states of activated sludge on membrane fouling, *Desalination*, 120(3): 221–233.

Chang, I.S., Lee, C.H., and Ahn, K.H. (1999) Membrane filtration characteristics in membrane coupled activated sludge system: The effect of floc structure on membrane fouling, *Separation Science Technology*, 34: 1743–1758.

Cicek, N., Franco, J.P., Suidan, M.T., Urbain, V., and Manem, J. (1999a) Characterization and comparison of a membrane bioreactor and a conventional activated sludge system in the treatment of wastewater containing high molecular weight compounds, *Water Environment Research*, 71: 64–70.

Defrance, L., Jaffrin, M.Y., Gupta, B., Paullier, P., and Geaugey, V. (2000) Contribution of various constituents of activated sludge to membrane bioreactor fouling, *Bioresource Technology*, 73: 105–112.

Dubois, M., Gilles, K.A., Hamilton, J.K., Rebers, P.A., and Smith, F.(1956) Colorimetric method for determination of sugars and related substances, *Analytical Chemistry*, 28: 350–356.

Gorner, T., de Donato, P., Ameil, M.-H., Montarges-Pelletier, E., and Lartiges, B.S. (2003) Activated sludge exopolymers: Separation and identification using size exclusion chromatography and infrared micro-spectroscopy, *Water Research*, 37: 2388–2393.

Guell, C., Czekaj, P., and Davis, R.H. (1999) Microfiltration of protein mixtures and the effects of yeast on membrane fouling, *Journal of Membrane Science*, 155: 113–122.

Gunther, J., Schmitz, P., Albasi, C., and Lafforgue, C. (2010) A numerical approach to study the impact of packing density on fluid flow distribution in hollow fiber module, *Journal of Membrane Science*, 348: 277–286.

Guo, W., Ngo, H.-H., and Li, J. (2012) A mini-review on membrane fouling, *Bioresource Technology*, 122: 27–34.

Han, S.-H. and Chang, I.-S. (2014) Comparison of the cake layer removal options during determination of cake layer resistance (R_c) in the resistance-in-series model, *Separation Science and Technology*, 49, 2459–2464.

Hendersona, R.K., Subhi, N., Antony, A., Khan, S.J., Murphy, K.R., Leslie, G.L., Chen, V., Stuetz, R.M., and Le-Clech, P. (2011) Evaluation of effluent organic matter fouling in ultrafiltration treatment using advanced organic characterisation techniques, *Journal of Membrane Science*, 382: 50–59.

Hughes, D., Cui, Z.F., Field, R.W., and Tirlapur, U. (2006) In situ three-dimensional membrane fouling by protein suspension using multiphoton microscopy, *Langmuir*, 22: 6266–6272.

Ishiguro, K., Imai, K., and Sawada, S. (1994) Effects of biological treatment conditions on permeate flux of UF membrane in a membrane/activated sludge wastewater treatment system, *Desalination*, 98: 119–126.

Kim, J.-S., Lee, C.-H., and Chang, I.-S. (2001) Effect of pump shear on the performance of a crossflow membrane bioreactor, *Water Research*, 35(9): 2137–2144.

Krauth, K.H. and Staab, K.F. (1993) Pressurized bioreactor with membrane filtration for wastewater treatment, *Water Research*, 27: 405–411.

Le-Clech, P., Chen, V., and Fane, T.A.G. (2006) Fouling in membrane bioreactors used in wastewater treatment, *Journal of Membrane Science*, 284, 17–53.

Lee, W., Kang, S., and Shin, H. (2003) Sludge characteristics and their contribution to microfiltration in submerged membrane bioreactors, *Journal of Membrane Science*, 216: 217–227.

Lowry, O.H., Rosebourgh, N.J., Farr, A.R., and Randall, R.J. (1951) Protein measurement with the folin phenol reagent, *Journal of Biological Chemistry*, 193: 265–275.

Meng, F. and Yang, F. (2007) Fouling mechanisms of deflocculated sludge, normal sludge and bulking sludge in membrane bioreactor, *Journal of Membrane Science*, 305: 48–56.

Sato, T. and Ishii, Y. (1991) Effects of activated sludge properties on water flux of ultrafiltration membrane used for human excrement treatment, *Water Science and Technology*, 23: 1601–1608.

Van den Broeck, R., Van Dierdonck, J., Nijskens, P., Dotremont, C., Krzeminski, P., van der Graaf, J.H.J.M., van Lier, J.B., Van Impe, J.F.M., and Smets, I.Y. (2012) The influence of solids retention time on activated sludge bioflocculation and membrane fouling in a membrane bioreactor (MBR), *Journal of Membrane Science*, 401–402: 48–55.

Wang, Z. and Wu, Z. (2009) Distribution and transformation of molecular weight of organic matters in membrane bioreactor and conventional activated sludge process, *Chemical Engineering Journal*, 150(2–3): 396–402.

Wang, Z., Wu, Z., and Tang, S. (2009) Characterization of dissolved organic matter in a submerged membrane bioreactor by using three-dimensional excitation and emission matrix fluorescence spectroscopy, *Water Research*, 43(6): 1533–1540.

Wisniewski, C. and Grasmik, A. 1998. Floc size distribution in a membrane bioreactor and consequences for membrane fouling, *Colloids and Surfaces A: Physicochemical and Engineering Aspects*, 138: 403–411.

Wisniewski, C., Grasmik, A., and Cruz, A.L. (2000) Critical particle size in membrane bioreactors case of a denitrifying bacterial suspension, *Journal of Membrane Science*, 178: 141–150.

Wu, J. and Huang, X. (2009) Effect of mixed liquor properties on fouling propensity in membrane bioreactors, *Journal of Membrane Science*, 342: 86–96.

Yamamura, H., Kimura, K., and Watanabe, Y. (2007) Mechanism involved in the evolution of physically irreversible fouling in microfiltration and ultrafiltration membranes used for drinking water treatment, *Environmental Science and Technology*, 41: 6789–6794.

Yao, M., Zhang, K., and Cui, L. (2010) Characterization of protein–polysaccharide ratios on membrane fouling, *Desalination*, 259: 11–16.

Chapter 5

MBR Operation

This chapter includes principles and operational parameters for biotreatment and membrane separation in membrane bioreactor (MBR). Particularly, membrane cleaning methods are intensively discussed.

5.1 Operation Parameters

Essentially, MBR systems are biological wastewater treatment processes except membrane unit replaces the secondary setting tank. The membrane unit plays the role of solid–liquid separation just like the secondary setting tank in conventional activated sludge (CAS). Therefore, MBR operation is similar to that of the CAS systems. The operational parameters related to the microbial operation currently used in CAS can be directly applied to MBR operation.

Operation parameters involved in membrane separation will be dealt with in this chapter. However, the microbial parameters directly influence on the performances of the membrane separation. For example, typical microbial floc issues in aeration basin and settling tank of CAS systems such as sludge bulking, foaming, and pinpoint floc formation deteriorate membrane separation performance. These phenomena are caused by low dissolved oxygen (DO) or low nutrient (N and/or P) concentrations, but DO and nutrient concentrations are not recognized as membrane operation parameters. Therefore, important operation parameters with respect to microbial characteristics should be monitored in MBR operation in terms of membrane fouling.

5.1.1 HRT

Hydraulic retention time (HRT) is a basic design and operational factor in biological wastewater treatment engineering. Normal design HRT in CAS for domestic wastewater treatment ranges from 4 to 10 h depending on the characteristics of the influent wastewater. Longer HRT will be required if industrial wastewaters including recalcitrant molecules or nonbiodegradable substances inflow to the wastewater treatment plant (WWTP) or biological nutrient removal (BNR) processes are employed.

The HRT in MBR does not significantly differ with that of CAS. Reduced HRT operation can be possible in MBR because the concentration of microorganisms (i.e., MLVSS) in MBR is much greater than that of CAS. Organic removal in MBR is faster and more stable than CAS due to the high concentrations of biomass. If the designed f/m ratio (f/m$=S_o$/HRT$\cdot$X) remains constant, the HRT could be reduced because the biomass concentration (X) in MBR is greater than that of the CAS. However, MBR normally runs at similar HRT as CAS to give a sufficient time to degrade the organic influents.

5.1.2 SRT

Solids retention time (SRT) is a key operating parameter for operators to control the sludge production rate and to maintain a constant biomass concentration in the bioreactor. Typical SRT values of CAS range from 4 to 10 days, which literally means that the solids (i.e., the biomass) reside 4–10 days in the bioreactor and secondary clarifier. However, the perfect retention of microorganisms in MBR by membranes makes the SRT quite longer, typically over 30 days of SRT. Without sludge being withdrawn in membrane tank, the SRT of MBR will be infinite. This is not possible in CAS because the effluent from the secondary clarifier contains at least several mg/L of suspended solids due to the limitation of settling tanks within the common retention time 2–4 h.

Wastewater treatment engineers want their system to be operated under short HRT and long SRT without loss of system performance. More influents can be treated as HRT shortens and SRT increases. However, this situation, short HRT and long SRT, is a difficult goal to achieve in CAS operation due to the imperfect separation capabilities of secondary clarifiers. Longer SRT (i.e., over 30 days) operation in CAS is not readily achieved due to the loss of microorganisms in the secondary clarifier, that is, HRT and SRT are closely coupled. On the other hand, HRT and SRT can be decoupled in MBR operation because the membrane separates the microorganisms perfectly.
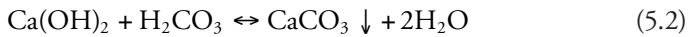
This longer SRT operation in MBR produces less excess sludge than CAS. Considering that the costs for further sanitary treatments of the excess sludge have increased and the regulation for sludge disposal is stricter than before, the long SRT operation seems to provide many benefits.

The longer SRT operation in MBR makes the microorganisms in the aeration tank old, which means the microbial growing state shifts to endogenous phase. The older the sludge, the more oxygen it requires. Since auto-oxidation of microorganisms advances significantly at the endogenous phase, much greater amounts of air should be supplied. However, extensive coarse aeration is commonly practiced in membrane tanks for fouling control in MBR, so the extra requirements of air for the auto-oxidation of sludge could be negligible.

A key issue in longer SRT operation in MBR is related to phosphorus (P) removal. Most BNR–MBR plants operating currently cope with P removal. In the aeration tank of CAS, phosphorus is stored inside the cells by means of biological luxury P uptake. The phosphorus in cells is then removed with the excess sludge withdrawals. However, the sludge in MBR is not removed at a high rate, so P removal is limited. The longer the SRT is, the less P is removed. Therefore, most MBR plants employ extra treatment facilities for P removal. For example, lime $(Ca(OH)_2)$ can be added to the MBR effluent to precipitate the P out as hydroxyl-apatite, $Ca_{10}(PO_4)_6(OH)_2$, as shown in the following equation:

$$10Ca^{2+} + 6PO_4^{3-} + 2OH^- \leftrightarrow Ca_{10}(PO_4)_6(OH)_2 \downarrow \qquad (5.1)$$
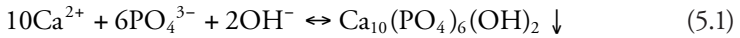
Alkalinity such as bicarbonate (HCO_3^-) or carbonate (CO_3^{2-}) is reacted first with the added lime as shown in Equation 5.2. Thus, sufficient lime is required for P precipitation to raise the pH above 10–11. Most of the P will only precipitate as hydroxylapatite once all of the alkalinity is removed.

$$Ca(OH)_2 + H_2CO_3 \leftrightarrow CaCO_3 \downarrow + 2H_2O \qquad (5.2)$$

$$Al^{3+} + PO_4^{3-} \leftrightarrow AlPO_4 \downarrow \qquad (5.3)$$

If alum is added, as shown in Equation 5.3, the insoluble aluminum phosphates, $AlPO_4$, are obtained. Although the theoretical mole ratio of Al/P is 1:1, much higher mole ratio up to 1.4 to 2.3 is required due to preferential interferences with alkalinities and other ions. Separate lab (or pilot) tests are needed to determine the optimum doses of alum. Sometimes, electrocoagulation (EC) process, which will be described in Section 5.4, is followed by MBR for P precipitation.

5.1.3 Recirculation Ratio, α

The recirculation ratio, $\alpha = Q_r/Q$, is defined as the ratio of the recirculation flow rate from the secondary clarifier to the bioreactor (Q_r) and the influent flow rate (Q). In CAS, α is an important operational parameter controlling the flow of the return activated sludge (RAS) stream. Engineers working in biological WWTPs

control a system's performance by regulating both α and SRT. Typical values of α range from 0.1 to 0.4. Higher α values result in more reliable biodegradation but higher pumping costs.

Obviously, there is no concept of α in submerged MBR where sludge return is not necessary. However, there is an analogy of α in sidestream MBR because a membrane unit outside an aeration tank in sidestream MBR plays the exact same role as a secondary clarifier as shown in Figure 5.1.

Flow analysis makes the analogy clear. If there is sludge withdrawal in sidestream MBR (Figure 5.1b), the flow rate of the returning stream to the aeration tank is $Q_c - Q_w$, which corresponds to Q_r of CSA. Thus, the recirculation ratio, α, in a sidestream MBR with the same flow configuration, as shown in Figure 5.1b, is $(Q_c - Q_w)/Q$.

(a)

(b)

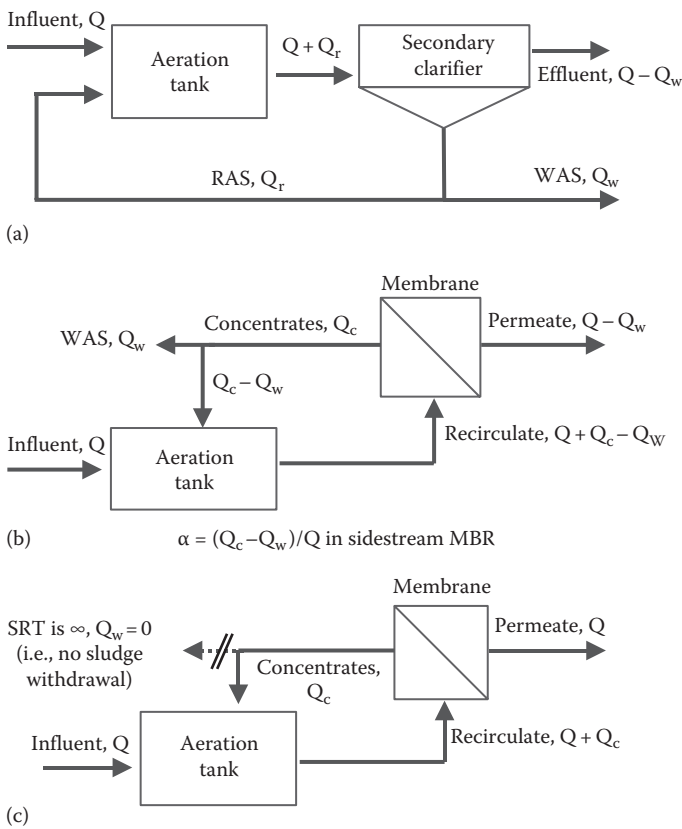$\alpha = (Q_c - Q_w)/Q$ in sidestream MBR

(c)

Figure 5.1 Analysis of flow: (a) CAS, (b) sidestream MBR, and (c) sidestream MBR with infinite SRT (no sludge withdrawal).

If a sludge withdrawal is not carried out in sidestream MBR (i.e., SRT is infinite, Figure 5.1c) the flow rate of the returning stream to the aeration tank is Q_c and the recirculation ratio, α, is Q_c/Q. In conventional membrane filtration operation, "recovery," r, is defined as the ratio of permeate to feed stream flow, $r = Q_{permeate}/Q_{feed}$. If we limit the system boundary to the membrane unit in Figure 5.1c, the recovery, r, is $Q/(Q + Q_c)$. We can get a relationship between r and α.

$$r = \frac{Q}{Q + Q_c} \tag{5.4}$$

Take the reciprocal forms of both sides and rearrange it.

$$\frac{1}{r} = \frac{Q + Q_c}{Q} = 1 + \frac{Q_c}{Q} = 1 + \alpha \tag{5.5}$$

Rearrange the equation to

$$r = \frac{1}{1 + \alpha} \tag{5.6}$$

Since the engineers working in the field of membrane separation are familiar with the terminology, recovery (r) and α can be converted to each other using Equation 5.6.

5.1.4 Temperature

Temperature is not classified as an operational parameter because the operator does not control it. However, temperature is an important factor determining MBR system performance, particularly the rate of microbial metabolism. The mixed liquor of activated sludge in CAS and MBR is affected by temperature.

The low temperature of influent during winter severely deteriorates the biological system performance. Thus, WWTPs suffer from difficulties in the biological treatment. Particularly, the slow-growing nitrogen-oxidizing bacteria and denitrification bacteria are very vulnerable to low temperature, so that nitrogen removal efficiency drops in winter.

Temperature also decides how much gas dissolves in water. Henry's law just describes how much gas can be dissolved in water under atmospheric pressure conditions. Henry's law constant (K_H) depends on temperature, so that the saturated oxygen concentration in water decreases during summer. Since air is always supplied to the bioreactor, the more important issue is the oxygen transfer rate. As temperature changes, the mass transfer rate of gases to water responds accordingly. On the contrary, the mass transfer "rate" of gases to water increases as

temperature increases. For example, the overall gas transfer rate coefficient ($K_{L,a}$) determining the gas transfer rate follows the van't Hoff–Arrhenius equation, which is used to model the effect of temperature on reaction rate as follows:

$$k_{L,a(T)} = k_{L,a(20)} \times \theta^{T-20} \tag{5.7}$$

where
  $k_{L,a(T)}$ is the overall gas transfer rate coefficient at temperature T°C (s^{-1})
  $k_{L,a(20)}$ is the overall gas transfer rate coefficient at 20°C (s^{-1})
  θ is the temperature activity coefficient, typically ranged from 1.013 to 1.040
  T is the temperature, °C

5.1.5 Temperature Dependence of Flux

Permeation flux is strongly dependent on temperature because the viscosity of the feed solution changes according to temperature. Instead of the common van't Hoff–Arrhenius equation, the flux at temperature T_1 can be converted to the flux at temperature T_2 using the following equation, because the viscosity is reciprocally proportional to the temperature:

$$J_{T1} = J_{T2} \left(\frac{\eta_{T2}}{\eta_{T1}} \right) \tag{5.8}$$

where
  J_{T1} is the flux at temperature T_1
  J_{T2} is the flux at temperature T_2
  η_{T1} is the viscosity at temperature T_1
  η_{T2} is the viscosity at temperature T_2

When the resistance values (R) are determined by a series of filtration experiments, the temperature of the feed solution might not be the same at every time of filtrations. If the temperature difference between the activated sludge suspension and pure water or between each sludge suspension is over or under 3°C, a temperature correction for the flux should be carried out before calculating resistances.

  Example 5.1

  New membranes arrive and the initial water flux is tested in a laboratory. The initial water flux is measured at 100 LMH. The water temperature is equilibrated with the room temperature of the laboratory, which is maintained at 25°C for the filtration period. The water temperature of the outside MBR plant is 15°C. Estimate the initial water flux at 15°C.

Solution

Temperature and the flux are reciprocally proportional to each other. Using the viscosity presented in Table 5.1, calculate the water flux at 15°C:

$$J_{T1} = J_{T2} \left(\frac{\eta_{T2}}{\eta_{T1}} \right)$$

$$J_{15} = J_{25} \cdot \frac{\eta_{25}}{\eta_{15}}$$

$$J_{15} = 100 \text{ LMH} \cdot \frac{0.8949 \text{ mPa} \cdot \text{s}}{1.1447 \text{ mPa} \cdot \text{s}} = 78.2 \text{ LMH}$$

The initial water flux at 15°C is calculated to be 78.2 LMH.

Remark

It should be noted that the temperature dependence of the flux follows the van't Hoff–Arrhenius equation style. The effect of temperature on viscosity follows the Arrhenius equation style:

$$\frac{\eta_T}{\eta_{20}} = 1.024^{20-T}$$

Table 5.1   Temperature Dependecy of Water on Viscosity

Temperature (°C)	Viscosity (Centipoise)	Temperature (°C)	Viscosity (Centipoise)
11	1.2735	21	0.9843
12	1.2390	22	0.9608
13	1.2061	23	0.9380
14	1.1748	24	0.9161
15	1.1447	25	0.8949
16	1.1156	26	0.8746
17	1.0876	27	0.8551
18	1.0603	28	0.8363
19	1.0340	29	0.8181
20	1.0087	30	0.8004

Therefore, the flux at a different temperature other than 20°C can be corrected as follows:

$$\frac{J_{20}}{J_T} = \frac{\eta_T}{\eta_{20}} = 1.024^{20-T}$$

$$J_{20} = J_T \cdot 1.024^{20-T}$$

5.1.6 TMP and Critical Flux

Transmembrane pressure (TMP) is the most important parameter for operation of a submerged MBR under constant flux mode. Only after TMP monitoring can operators make an appropriate diagnosis for a TMP jump or other kinds of abnormal TMP behaviors and can take immediate and proper action for the ongoing fouling phenomena.

Figure 5.2 shows the relationship between flux and TMP during the filtration of activated sludge suspension. Flux and TMP are linearly dependent of each other in water filtration (i.e., no fouling conditions). This is called the pressure controlled region (i.e., TMP dependent region). In filtration of activated sludge suspension, flux increases along with TMP within a certain range of TMP; thereafter, the rate of flux increase drops. This is due to the fouling on the membranes, where the flux is mainly controlled by the mass transfer of foulants (solutes) toward the membranes. This is called the mass transfer controlled region (or the TMP independent region). It is difficult to divide the boundary exactly between both regions because the flux increases a little bit by pressure even in the mass transfer controlled region. There are many factors affecting the mass transfer of foulants in bulk solution to the membranes. For example, lower mixed liquor suspended
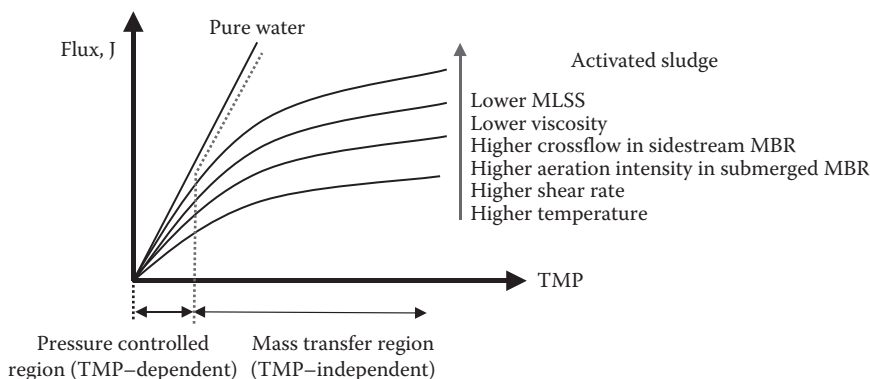
Figure 5.2   Relationship of TMP and flux: the pressure controlled region and the mass transfer controlled region.

solids (MLSS) concentration, lower viscosity, higher crossflow velocity in side-stream MBR, higher aeration intensity in submerged MBR (or higher shear rate), and higher temperature are favorable conditions to increase the mass transfer of activated sludge suspension.

It is crucial to determine the critical flux level at the startup of MBR. Running MBR under critical flux conditions provides stable and reliable operation while minimizing the fouling rate. Even though the strict meaning of critical flux (i.e., no fouling occurs under the critical flux) does not exist in MBR, several experimental protocols have been proposed for determining the critical flux in MBR. The most simple and easiest way is to increase the flux incrementally as shown in Figure 5.3.

The test starts with a lab scale MBR run with a flux as low as possible while TMP is monitored. If an abrupt increase in TMP is not observed for the given observation period (i.e., dTMP/dt = 0), the flux is elevated to the next higher level. The same procedure repeats continually until abrupt TMP increase (i.e., dTMP/dt > 0) is observed. Then the elevated flux reverts to the previous flux level. And then, the same procedure is repeated in reverse—observe the TMP and then revert the flux to a previous level again. The critical flux ($J_{critical}$) is determined by the highest flux for which TMP remains stable for the whole test period.

As indicated in Chapter 4.1, TMP increases slowly at the initial stage of filtration and then increases abruptly at the breakthrough point. Therefore, if the time interval between each flux step is too short to observe the TMP buildup, this method, flux stepping, could give bad information on the critical flux. Three possible examples are depicted in Figure 5.4.
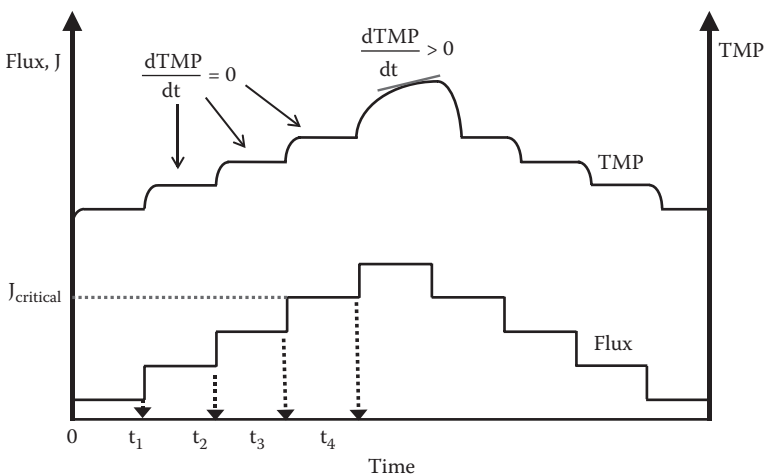
**Figure 5.3 Determination of critical flux using step increase in flux.**
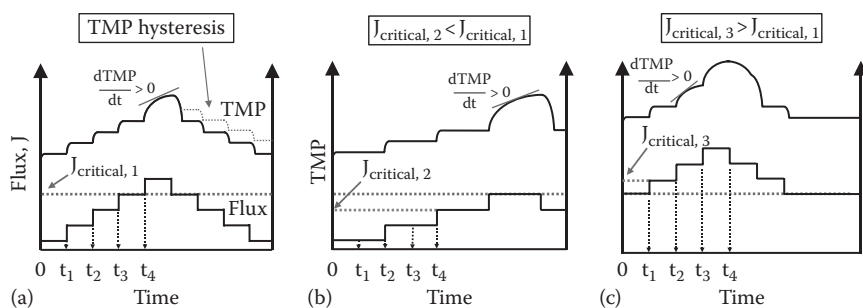
Figure 5.4 **Abnormal TMP behaviors during determination of critical flux using the flux step method: (a) TMP hysteresis during step down of the flux, (b) underestimation of $J_{critical}$, and (c) overestimation of $J_{critical}$.**

First of all, "TMP hysteresis" could happen during the course of stepping down the flux (Figure 5.4a). TMP would not show the same trajectory after passing by the highest flux. Since the fouling developed over a long period of time, higher TMP would be observed than the previous TMP before the highest flux condition. In this case, the determined critical flux would be very suspicious.

If a longer duration of each flux step is given, the critical flux will be underestimated as shown in Figure 5.4b. The duration in Figure 5.4b is given to t_4, which is the same as the duration in Figure 5.4a, but the test is run under much lower flux conditions. If the extended duration from t_1 to t_2 is not good enough to fully develop the fouling, less severe fouling would be observed. Even though the test runs by the flux ($J_{critical,2}$), which is lower than the critical flux ($J_{critical,1}$) determined in Figure 5.4a, the TMP increase rate, dTMP/dt would be zero. The region showing dTMP/dt > 0 would be delayed. In this case, the critical flux ($J_{critical,2}$) would be lower than the $J_{critical,1}$.

If the initial starting flux is chosen sufficiently high near the determined critical flux 1 ($J_{critical,1}$), the critical flux will be overestimated as depicted in Figure 5.4c. Even though the overall duration is given to t_4, which is the same as the duration in Figure 5.4a, more severe fouling would be observed because the running flux is so high. That is, the time to reach the region showing dTMP/dt > 0 would be shortened in this case. Eventually, the critical flux ($J_{critical,3}$) will be higher than the $J_{critical,1}$.

To overcome the imitation associated with the flux step method, modified methods are proposed as shown in Figure 5.5. The first is the flux stepping method with pauses between the flux increments (Figure 5.5a). Distinctively with the "flux stepping without pause" described in Figure 5.3, a pause (or idle time) is given to the membrane for the purpose of removing the already-developed fouling just prior to an increase in flux. Pausing can give the membrane pressure relaxation,
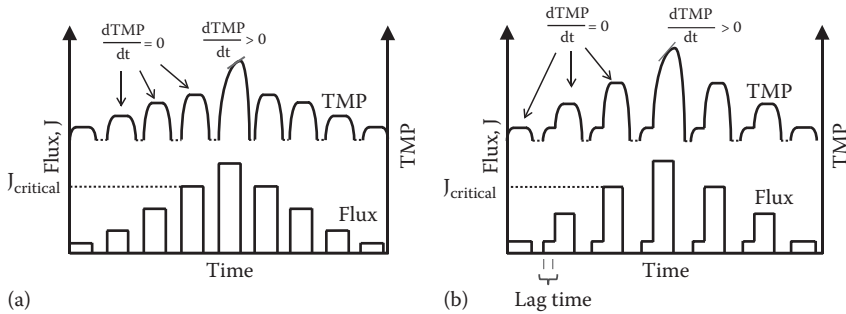
Figure 5.5 **Other protocols determining critical flux: (a) step increase of flux with pauses and (b) step increase of flux with lag phase and pauses.**

and thus, the back transport to bulk solution would be accelerated. During this idle time, cleaning can be another option to restore the already-developed fouling. Figure 5.5b depicts a "step increase of flux with lag phase and pauses," which employs an extra time with the lowest flux prior to an increase in flux. The extra time (or lag time) operation can provide the membrane a low fouling environment before the subsequent flux increase.

Although both modified methods more or less can overcome the limitation of the flux stepping method, the inherent problems stated previously are not perfectly solved. Even though the standardized method determining critical flux without abnormal TMP behavior stated previously is accepted, the critical flux is highly dependent on physicochemical properties of the mixed liquor. Moreover, since the determined critical flux varies by the specific MBR hydrodynamics, the critical flux value determined by the hollow fiber module would be different than that of the plate and frame modules. However, these methods have been practiced commonly to identify the critical flux in fields or laboratories due to the convenience to perform their protocols.

5.2 Aeration for Biotreatment and Membrane Aeration

Aeration serves a number of useful purposes in WWTP. For example, aeration has been widely practiced in odor control (such as H_2S removal), aeration to aerobic microorganisms, dissolved air flotation (DAF), aerated grit chamber, removal of volatile organic compounds (VOC), etc. In MBR plants, aeration might be the most important unit operation, supplying the oxygen to microorganisms for their metabolism as well as to the membrane surface for fouling control. Fine bubbles with extended surface areas are beneficial for effective oxygen transfer to cells

whereas coarse aeration with large-sized bubbles is adequate for effectively vibrating and scouring the membrane bundles.

5.2.1 Fine Bubble Aeration

To supply oxygen to cells effectively, fine bubble aeration is practiced in WWTP because the extended surface area of fine bubbles is favorable to accelerate the mass transfer of oxygen. Although there are many types of aerators, compressed air supply through diffusers underneath the water surface is the most widely used for aeration tanks in MBR. Other types of aerators are well documented in other wastewater treatment engineering books.

Since air is the terminal electron acceptor of the aerobic bacteria treating organic wastewater, a sustainable air supply is needed. Devices for fine bubble aeration are made of porous ceramics or plastics that can release air. Porous plates, tubes, or nozzles are attached to air piping on the bottom of the aeration tank. Delivered air is first dissolved in the wastewater by diffusion or mechanical aeration. Then the DO is taken up by the microorganisms. Although the oxygen demand depends on the amounts of organics and ammonia present in the wastewater, at least 1 mg/L of oxygen should be maintained in the aeration basin, typically 2–3 mg/L.

Oxygen consumption by the microorganisms should be considered important in determining oxygen transfer rate in the aeration tank. The rate of oxygen transfer is as follows:

$$\frac{dC}{dt} = k_{L,a}(C_s - C) - r_m \tag{5.9}$$

where
  C is the oxygen concentration in wastewater (mg/L)
  C_s is the saturated oxygen concentration given by Henry's law (mg/L)
  $k_{L,a}$ is the overall oxygen transfer coefficient (s^{-1})
  r_m is the rate of oxygen consumed by microorganisms (mg/L s)

If the oxygen concentration is maintained at a constant level thanks to the aeration devices (i.e., steady-state condition, $dC/dt = 0$), Equation 5.9 is simplified as follows:

$$r_m = k_{L,a}(C_s - C) \tag{5.10}$$

In this case, C_s is constant and not variable with time, so that r_m can be obtained by the determination of $K_{L,a}$. The overall oxygen transfer coefficient, $K_{L,a}$, can be obtained by simple experiments as the following example demonstrates.

Example 5.2

An aeration system has been monitored to determine $K_{L,a}$. The monitored data for dissolved oxygen versus time is shown in the following table. Assume that the saturation dissolved oxygen concentration (C_s) is 9.0 mg/L at this temperature. Use the data to determine $K_{L,a}$.

Time (min)	C_t (mg/L)
0	1.20
4	2.68
8	3.92
12	4.89
16	5.71
20	6.35
24	6.88
28	7.32
32	7.66
36	7.93
40	8.14
44	8.31
48	8.45
52	8.56
56	8.65
60	8.72

Solution

The oxygen transfer rate in clean water without oxygen consumption by microorganisms is expressed as follows:

$$\frac{dC}{dt} = k_{L,a}(C_s - C) \tag{E2.1}$$

Separating the variable and integrating the previous equation yields

$$\int_{C_o}^{C_t} \frac{1}{C_s - C}\,dC = \int_0^t k_{L,a}\,dt \tag{E2.2}$$

$$\frac{C_s - C_t}{C_s - C_o} = e^{-k_{L,a} \cdot t} \tag{E2.3}$$

$$\ln\left(\frac{C_s - C_t}{C_s - C_o}\right) = -k_{L,a} \cdot t \tag{E2.4}$$

As indicated in Equation E2.4, a plot of $\ln (C_s-C_t/C_s-C_o)$ versus t is needed to determine $K_{L,a}$. The slope of the straight line of best fit is the value of $K_{L,a}$. The best fit is obtained simply by regression using an engineering calculator or spreadsheet program.

C_o is the initial concentration, which is 1.2 mg/L (time at zero), and C_t is the concentration at time t. The results of the calculations are shown in the spreadsheet table as follows.

Time (min)	C_t (mg/L)	$\dfrac{C_s - C_t}{C_s - C_o}$	$k_{L,a}$ (/min)
0	1.20	1.000	—
4	2.68	0.810	0.053
8	3.92	0.651	0.054
12	4.89	0.527	0.053
16	50.71	00.422	00.054
20	6.35	0.340	0.054
24	6.88	0.272	0.054
28	7.32	0.215	0.055
32	7.66	0.172	0.055
36	7.93	0.137	0.055
40	8.14	0.110	0.055
44	8.31	0.088	0.055
48	8.45	0.071	0.055
52	8.56	0.056	0.055
56	8.65	0.045	0.055
60	8.72	0.036	0.055

A plot of ln $(C_s - C_t/C_s - C_o)$ versus t is shown in the figure. The slope, which is equal to $K_{L,a}$, is calculated to be 0.055 per min or 3.3 per h.
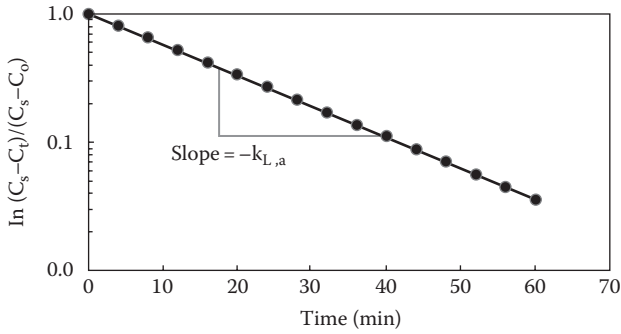

5.2.2 Oxygen Transfer

The oxygen transfer coefficient, $K_{L,a}$, depends on mixing intensity, geometry of the aeration basin, temperature, altitude ($\propto$ atmospheric pressure), surface tension, and characteristics of the wastewater. The effects of temperature were already dealt with in a previous section (refer to Equation 5.7). All factors affecting the coefficient ($K_{L,a}$) except temperature are difficult to generalize and express mathematically on a theoretical basis. Instead, correction factors that can be obtained experimentally are used. The actual amount of oxygen required in plants should be calculated with the corrected equation, which will be discussed further in Chapter 6.4.

5.2.3 Oxygen Demand

Since MBR is basically a biological processes, the oxygen demand should account for the biological oxygen demand (BOD) and ammonia demand. The oxygen demand in CAS is determined by the difference between the influent and effluent BOD, that is, $(BOD_i - BOD_e)$. The wasted sludge should be subtracted from the total oxygen demand because the cells consuming oxygen are wasted as excess sludge. The representative chemical formula of cell is $C_5H_7NO_2$, so that the cell oxidation can be described as the following reaction:

$$C_5H_7NO_2 + 5O_2 \leftrightarrow 5CO_2 + 2H_2O + NH_3 \tag{5.11}$$
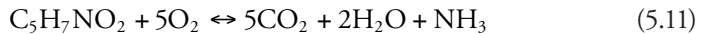
Since 5 mol of oxygen per 1 mol cell are required, 1.42 ($= 5 \times 32/113$) g of oxygen is required for oxidation of 1 g of sludge cell. Therefore, oxygen demand for carbonaceous biodegradation is

$$O_2 \text{ demand} (\text{kg} \, O_2/\text{day}) = Q \, (BOD_i - BOD_e) - 1.42 \, (P_s) \qquad (5.12)$$

where
 O_2 demand is the carbonaceous oxygen demand (kg/day)
    Q is the wastewater flow rate to the aeration basin (kg/day)
    BOD_i is the influent BOD to aeration basin (mg/L)
    BOD_e is the effluent BOD from the secondary clarifier (mg/L)
    P_s is the rate of sludge waste (kg/day)

During the course of full nitrification, ammonia (NH_3) converts to nitrate (NO_3^-) consuming 2 mol of oxygen by nitrifying bacteria, as shown in the following:

$$NH_3 + 2O_2 \leftrightarrow NO_3^- + H_2O + H^+ \qquad (5.13)$$
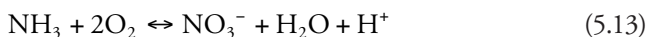
The oxygen demand corresponding to full nitrification is calculated to be 4.6 mg/L (=2 mol O_2/1 mol of nitrogen = 2×32 g O_2/14 g-N). Therefore, the total oxygen demand for a biological process is as follows:

$$O_2 \text{ demand, } \text{kg} \, O_2/\text{day} = Q(BOD_i - BOD_e) - 1.42(P_s) + 4.6 \cdot Q \cdot (NO_x) \qquad (5.14)$$

where NO_x is the total nitrogen concentration in influent (mg/L).

    Sludge production (P_s) in MBR is significantly lower than CAS because MBR operates at long SRT. Therefore, the oxygen demand for MBR must be greater than that of the CAS. If the SRT of MBR is infinite, the oxygen demand in Equation 5.14 could be simplified as

$$O_2 \text{ demand in MBR with infinite SRT, } \text{kg} \, O_2/\text{day}$$
$$= Q(BOD_i - BOD_e) + 4.6 \cdot Q \cdot (NO_x) \qquad (5.15)$$

5.2.4 Coarse Aeration

Membrane aeration is primarily responsible for maintaining membrane permeability. The dual purposes of coarse aeration in membrane tanks are to (1) vibrate the fiber bundles to prevent sludge clogging inside the module and (2) scour the membrane surfaces to prevent deposition of sludge on the membranes. To achieve both effectively, intensive and big-sized air bubbles are needed. Orifices or nozzles are adequate for generating coarse bubbles instead of porous materials for fine bubbling.

    Shear intensity (often called the shear rate and denoted as σ), G (s^{-1}), induced by aeration is given by the following equation:

$$G = \sqrt{\frac{\rho \cdot g \cdot U_a}{\mu_s}} \qquad (5.16)$$

where
   ρ is the sludge density (kg/m³)
   g is the gravitational acceleration (m/s²)
   U_a is the aeration intensity (L/m² s)
   μ_s is the viscosity of the sludge suspension (kg/m s, Pa s or N s/m²)

The shear intensity, G, is analogous to the "velocity gradient," which is used as a criteria for liquids mixing.

$$G = \sqrt{\frac{P}{\mu \cdot V}} \qquad (5.17)$$

$$= \sqrt{\frac{1/V \cdot P}{\mu}} = \sqrt{\frac{1/V((\text{Force}/1) \cdot (\text{distance}/\text{time}))}{\mu}}$$

$$= \sqrt{\frac{1/V((\text{mass}/1) \cdot g \cdot (\text{distance}/\text{time}))}{\mu}}$$

$$= \sqrt{\frac{\text{mass}/V \cdot g \cdot \text{distance}/\text{time}}{\mu}} = \sqrt{\frac{\rho \cdot g \cdot \text{distance}/\text{time}}{\mu}}$$

$$= \sqrt{\frac{\rho \cdot g \cdot (m^3/m^2 \, s)}{\mu}} = \sqrt{\frac{\rho \cdot g \cdot U_a}{\mu}}$$

where
   P is the power of the agitator (N m/s)
   μ is the viscosity of water (kg/m s, Pa s or N s/m²)
   V is the volume of container (m³)

Equation 5.16 expects that the shear intensity (G) will root-proportionally increase as the superficial air intensity ($U_a^{1/2}$) increases. Thus, the permeability (or flux) improvement would follow the trajectory of the shear intensity (G) as the U_a increases. This is the scenario 1 as shown in the dotted line of Figure 5.6.

However, the reality supported by many studies is different as shown in the solid line of Figure 5.6 (i.e., the flux improvement does not increase continually as the superficial velocity increases). Flux can be enhanced but only within a limited range
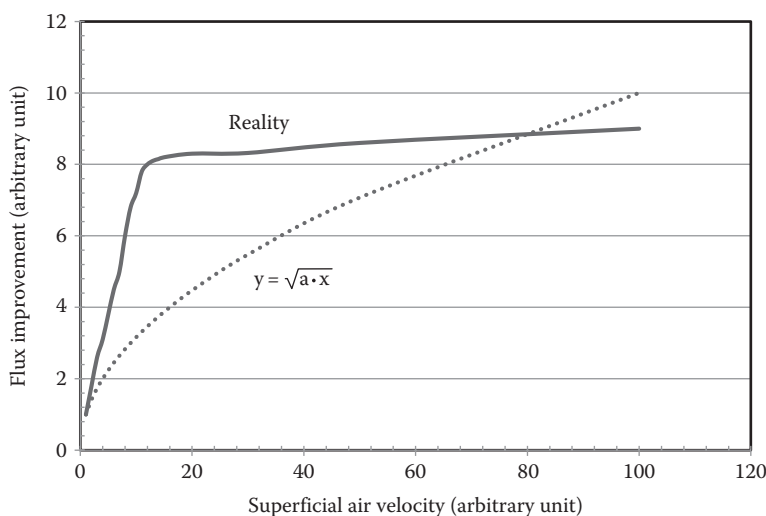
Figure 5.6 Effect of superficial air velocity on fouling reduction in MBR: dotted line refers to Equation 5.16 expressing that shear rate or flux improvement (y-axis) is root proportional to superficial air velocity (x), and the solid line represents the reality advocating that flux improved only to a limited range of aeration velocity.

of aeration intensity. Theoretical optimization for appropriate selection of aeration intensity is difficult because the module configuration is different for each manufacturer and the hydrodynamic behavior of a three-phase fluid (air + liquid + solid) is very complicated to model. Therefore, air intensity is usually selected by bench or pilot scale experiments site by site.

5.2.5 Aeration Demand and Energy

One of the important issues in MBR is the energy costs caused by aeration. A significant part of operational costs arise from aeration in the membrane tank. For conventional submerged MBR operation, membrane aeration usually counts for 30%–50% of the whole plant power consumption.

Specific aeration demand (SAD) is a popularly accepted criteria for comparing aeration requirements in MBR. Two types of SAD, SAD_m and SAD_p, are used to express the aeration demands. SAD_m is the aeration demand based on membrane area, Nm^3 of air/(h m^2), whereas SAD_p is the aeration demand based on permeate volume, Nm^3 of air/(m^3 of permeate). SAD_p is a unitless parameter. The "Nm^3 of air" designates the air volume at normal state (0°C, 1 atmospheric pressure, the N does not mean the force unit Newton). Since flux, J, has the unit of m^3 of permeate/(h m^2), the mutual relationship of both demands is as follows:

$$SAD_p = \frac{SAD_m}{J} \tag{5.18}$$

In most submerged MBR plants, SAD_p exceeds 10 and can be as high as 50 at some sites (Judd, 2008). Some plants even show over 90. This is because the SAD_p strongly depends on module configuration and packing density and frequency of chemical cleanings.

The blower power consumed by aeration in submerged MBR is calculated as follows:

$$P_{blower} = \frac{p_a \times Q_{air}}{\eta} \tag{5.19}$$

where
  P_{blower} is the power of blower (Watt $=$ N m/s)
  p_a is the air pressure (N/m²)
  Q_{air} is the air flow rate (m³/h)
  η is the efficiency of blower and pump (unitless)

Note: N designates force, Newton ($=$kg m/s²), not the normal state.

Air pressure (p_a) is a sum of (1) the pressure loss at the outlet of the blowers and diffusers ($=\delta p$) and (2) the underwater pressure at depth, h. The underwater pressure $\chi \cdot h (= \rho \cdot g \cdot h) \cdot \chi$ is specific volume of water (N/m³). The blower power is rewritten as follows:

$$P_{blower} = \frac{p_a \cdot Q_{air}}{\eta} = \frac{(\delta p + \rho \cdot g \cdot h) \cdot Q_{air}}{\eta} \tag{5.20}$$

where
  ρ is the water density (kg/m³)
  g is the gravity acceleration (m/s²)

Therefore, the energy required for aeration can be calculated as follows:

Energy required for aeration (kW h or 3600 kJ) $= P_{blower}$ (kW) $\times$ operating time (h)

$$\tag{5.21}$$

Specific energy consumption is the energy consumed for treatment of a unit volume of wastewater. It is commonly expressed in units of kWh/m³. This is a useful index to compare the efficiency of energy consumptions for WWTPs. Unfortunately, specific energy consumption data for only aeration is not commonly available.

Instead, specific energy consumptions of whole WWTPs employing MBR have been reported to be between 0.5 and 8 kWh/m^3, quite a broad span, depending on the influent characteristics and plant capacities. Although there have been many efforts to reduce the specific energy consumption by upgrading aeration modules and introducing cyclic aeration, MBR's energy consumption is still quite high compared to the specific energy consumption of CAS, which typically ranges from 0.2 to 0.4 kWh/m^3.

5.2.6 Packing Density

The packing density of a membrane module or cassette is defined by the membranes surface area per unit cross-section area of module header (m^2/m^2) or by the membrane surface area per module volume (m^2/m^3). Packing density is important for systems with coarse aeration in membrane tanks. High membrane module packing densities reduce the footprint of membrane tanks but also lead to unfavorable hydrodynamic air conditions, requiring extensive aeration to put the air through the membrane bundles. Consequences of overpacked modules are increased fouling and sludge clogging within the module.

The average packing densities of commercial submerged hollow fiber and plate and frame membrane modules are 141 and 77 m^2/m^3, respectively (Santos et al., 2011). But the standard deviation of the survey was relatively high, 41%–48%, indicating that diverse types of commercial modules compete in the market with unique configurations and packing densities.

5.3 Fouling Control

The most important operation and maintenance (O&M) routine in MBR plants is membrane cleaning. If the membranes are not maintained clean, the overall plant seriously suffers and could be shutdown eventually. Therefore, membrane cleaning precedes other routines. Setting up the cleaning strategy during the plant design stages should be considered a key step for the design MBR plants.

As cleaning is closely related to membrane fouling, which is extensively dealt in the previous chapter, precise understanding of membrane fouling phenomena is crucial for setting up a cleaning operation. However, a standardized and systematic explanation about membrane fouling mechanisms as well as a fouling model is not currently available in MBR because many physicochemical, biological, and operational factors are involved in membrane fouling. Therefore, universal cleaning methods cannot solve all of the fouling problems encountered in all MBR plants.

Many approaches for fouling control have been studied and implemented in laboratory and/or MBR plants, so that numerous cleaning options have been reported over the last couple of decades. All of the methods reported can be classified into two groups: membrane cleaning and fouling prevention. Membrane cleaning refers to the cleanings conducted normally after membrane fouling has been developed,

while fouling prevention represents all kinds of means to prevent membrane fouling. This classification is based on how to set up a fouling control strategy.

A more familiar way of categorizing fouling control is through chemical, physical, biological, electrical, and membrane and module developments. This classification focuses on the characteristic nature of cleaning materials or methods. It is easy to imagine what types of options are available for chemical, physical, and biological cleaning. Electrical methods refer to an electrical application to control fouling such as in situ EC MBR. Membrane and module developments include developments of antifouling membrane materials or module devices. Table 5.2 summarizes the categories of fouling control, some of which are going to be described in more detail in the following sections.

5.3.1 Chemical Control

Membrane cleaning using many different kinds of chemicals has been widely practiced for a long time due to the immediate and excellent capabilities restoring deteriorated filtration performance. In spite of the merits, chemical cleanings have inherent disadvantages. First of all, chemical cleanings always accompany secondary contamination. The added chemicals itself or conjugated with foulants definitely increase the amount of waste. These waste pollutants should be treated further or disposed of after the chemical cleaning. The regulations on the waste chemicals have become stringent for the purpose of environmental protection, so that treatment and disposal costs have increased. Moreover, safety concerns about chemicals related to their transportation, storage, preparation, and uses have increased nowadays, leading to increasing O&M and safety costs.

Notwithstanding the safety concerns, chemical cleanings for fouling control are still used as a primary tool to restore membrane permeability in MBR. That is, the convenience of using chemicals still outweighs the inherent and unavoidable problems as well as the environmental burden.

It is well known that the reversible fouling caused by cake layer deposition of sludge flocs can be partly prevented by subcritical flux operation and removed by air scouring. However, the irrecoverable fouling caused by adsorption and/or physicochemical bonding (or interaction) between the internal pores walls and foulants cannot be managed by simple subcritical flux operation or other physical cleanings. This is the basic reason why periodical chemical cleanings are still practiced in MBR plants.

5.3.1.1 Cleaning Protocol

Chemical cleanings are carried out by two different cleaning protocols: (1) off-line cleaning and (2) cleaning-in-place (CIP). In the off-line cleaning, membranes or membrane modules are taken out of the bioreactor by hoister and then transferred nearby to a separate tank full of cleaning reagents. The immersed membrane modules in the tank are cleaned. Or the membrane module stays in the aeration tank

Table 5.2   Classification of the Fouling Control in MBR

Fouling Control Strategy	Details Methods of Fouling Control	Classification of Cleaning Methods
Direct membrane cleaning	Chemicals	
	• Acid/base, ozone, H_2O_2, NaOCl, PAC	Chemical
	• Fouling reducer (polyelectrolytes)	Chemical
	Coarse aeration, intermittent aeration	Physical
	Two-phase flow	Physical
	Backwashing	Physical
	Chemically enhanced backwashing	Physical + chemical
	HVI	Electrical
Fouling prevention	Pretreatment of debris, hair, and grit	Physical
	Critical flux operation	Physical
	HRT, SRT, f/m, DO, and MLSS control	Biological
	Development of antifouling membrane	Membrane/module
	Development of antifouling module	Membrane/module
	Shear (rotating disc, helical membrane, etc.)	Membrane/module
	In situ EC	Electrical
	Quorum quenching	Chemical/ biological
	Nitric oxide	Chemical/ biological
	DC induction	Electrical

after draining off all the activated sludge suspension, and the module is immersed in chemical agents for cleaning.

On the other hand, in the CIP cleaning mode, chemical agents are directly injected into the membrane modules in the reverse direction to the normal filtration while the membrane modules are still submerged in the bioreactor. Compared with the off-line cleanings, CIP is much simpler and cheaper (Wei et al., 2011a). The periodic CIP are often called maintenance cleanings, which is the basic cleaning option most MBR plants employ since it as a primary tool for fouling control.

**Example 5.3: Determination of Resistances after
Periodic Chemical Cleanings**

A pilot-scale submerged MBR is running under constant flux mode. Whenever the TMP reaches 70 kg m/s² cm², a chemical cleaning is carried out for 144 min (100 min sodium hypochlorite cleaning and then 44 min water rinsing) to restore the elevated TMP. Determine resistance values after 5, 10, and 15 days of operation using the following data. If data are necessary for the membrane filterability, use the data of Example 4.7 in the previous chapter.

- The membrane surface area, 0.05 m²
- Initial water flux (J_{iw}) measured before MBR operation with pure water: 30 L/m² h
- Operating flux (J): 20 L/m² h (LMH)
- Temperature: 20°C
- Permeate viscosity: 1.009×10^{-3} kg/m s
- Assume that the permeate density is 1 g/mL and the 1 bar is 9.996 kg m/s² cm² (Table 5.3)

Solution

To calculate the resistances, the pressure unit should be changed from bars to the SI unit as shown in Table 5.4. And operating time versus TMP profile is plotted using the table.
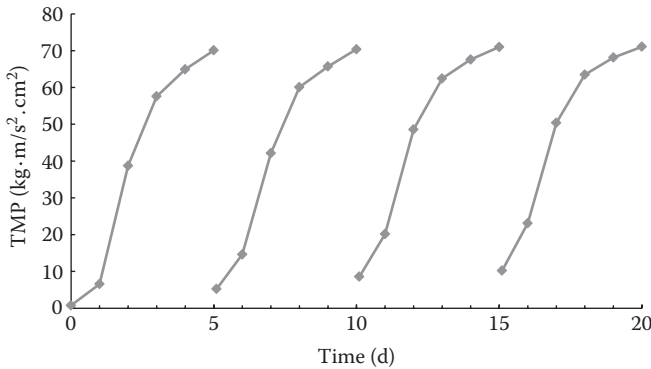
As stated in Chapter 4 and Example 4.7, each resistance value is determined by the following model equations:

$$R_m = \frac{TMP_1}{(\eta \times J_{iw})} \tag{E3.1}$$

$$R_f = \frac{TMP_2}{(\eta \times J_{fw})} - R_m \tag{E3.2}$$

$$R_c = \frac{TMP_3}{(\eta \times J)} - (R_m + R_f) \tag{E3.3}$$

Table 5.3   TMP Data along the Operating Time

Time (Day)	TMP (Bar)	Cleanings
0	0.078	—
1	0.656	—
2	3.875	—
3	5.759	—
4	6.496	—
5	7.012	Chemical cleaning
5.1	0.524	—
6	1.463	—
7	4.214	—
8	6.012	—
9	6.573	—
10	7.041	Chemical cleaning
10.1	0.857	—
11	2.015	—
12	4.861	—
13	6.247	—
14	6.762	—
15	7.104	Chemical cleaning
15.1	1.024	—
16	2.312	—
17	5.041	—
18	6.351	—
19	6.817	—
20	7.111	—

J_{iw} is the predetermined initial pure water flux of the new membrane before the MBR opration. J is the operating runnng flux and J_{fw} is the final water flux after the removal of cake layers. In order to calculate three resistances (i.e., membrane resistance, R_m, the cake layer resistance, R_c and the fouling resistance, R_f, respectively), three TMPs (TMP_1, TMP_2, and TMP_3) are needed.

Table 5.4   TMP Expressed in SI Units as a Function of Operating Time

Time (Day)	Recorded TMP (Bar)	Pressure (kg·m/s² cm²)	Cleaning
0	0.078	0.77969	
1	0.656	6.55738	
2	3.875	38.73450	
3	5.759	57.56696	
4	6.496	64.93402	
5	7.012	70.09195	Chemical cleaning
5.1	0.524	5.23790	
6	1.463	14.62415	
7	4.214	42.12314	
8	6.012	60.09595	
9	6.573	65.70371	
10	7.041	70.38184	Chemical cleaning
10.5	0.857	8.56657	
11	2.015	20.14194	
12	4.861	48.59056	
13	6.247	62.44501	
14	6.762	67.59295	
15	7.104	71.01158	Chemical cleaning
15.1	1.024	10.23590	
16	2.312	23.11075	
17	5.041	50.38984	
18	6.351	63.48460	
19	6.817	68.14273	
20	7.111	71.08156	

First, information on the TMP_1 and the J_{iw} is necessary for the calculation of R_m: TMP_1 was indicated in Example 4.7, 0.7797 kg m/s² cm², and J_{iw} is given by 30 L/m² h in this example:

- Membrane resistance (R_m) is equal to Example 4.7.
- To calculate R_m, put each value, $J_{iw} = 30$ L/h m², $TMP_i = 0.7797$ kg m/s² cm² and $\eta = 1.009 \times 10^{-3}$ kg/m s into Equation E3.1.

$$R_m = \frac{0.7797 \text{ kg} \cdot \text{m}}{s^2 \cdot \text{cm}^2} \times \frac{\text{m} \cdot \text{s}}{1.009 \times 10^{-3} \text{ kg}} \times \frac{\text{m}^2 \cdot \text{h}}{30 \text{ L}} \times \frac{3600 \text{ s}}{\text{h}} \times \frac{100^2 \text{ cm}^2}{\text{m}^2} \times \frac{10^3 \text{ L}}{\text{m}^3}$$

$$R_m = 0.09 \times 10^{13} \text{ m}^{-1}$$

To obtain R_f, both values of TMP_2 and J_{fw} are required according to the resistance in series model as shown in the solution of Example 4.6 (J_{fw} is the pure water flux after the removal of a cake layer). However, the water flux after chemical cleaning was not determined in this MBR operation.

Chemical cleaning was carried out in this example rather than the cake layer removal option such as water rinsing or sponge scrubbing. Chemical cleaning can remove internal foulants on the pore walls as well as the cake layer. Generally speaking, the internal foulants are removed partially by chemical cleaning, but the cake layers are almost entirely removed. The unremoved internal foulants are classified as the irreversible fouling as explained in Section 4.1.

Assuming that the cake layer is removed perfectly, but the internal foulings are only partially removed by the chemical cleaning, the internal fouling resistance (R_f) could be divided further by the reversible fouling resistance ($R_{f, re}$) and the irreversible fouling resistance ($R_{f, ir}$) by a chemical cleaning.

$$J = \frac{TMP}{\eta(R_m + R_c + R_f)} \tag{E3.4}$$

$$J = \frac{TMP}{\eta(R_m + R_c + R_{f,re} + R_{f,ir})} \tag{E3.5}$$

First, the $R_c + R_f$, called "total fouling resistance (R_{Tf})," means the overall resistances developed until the onset of the chemical cleanings can be calculated as follows:

- Total fouling resistance, $R_c + R_f$, at day 5.
- TMP_5 is the pressure measured just prior to the chemical cleaning on day 5, which is 70.09195 kg m/s² cm².
- J_5 is the operating flux at day 5. However, the flux is always 20 L/h m² under the constant flux mode.
- Rearrange Equation E3.4 to the resistance form and insert the corresponding values into it.
- $R_c + R_f = TMP_5/(\eta \cdot J_5) - R_m$

$$= \frac{70.09195 \times \text{kg} \times \text{m}}{\text{s}^2 \times \text{cm}^2} \times \frac{\text{m} \times \text{s}}{1.009 \times 10^{-3}\,\text{kg}} \times \frac{\text{m}^2\ \text{h}}{20\text{L}} \times \frac{3600\text{s}}{\text{h}} \times \frac{100^2\,\text{cm}^2}{\text{m}^2} \times \frac{10^3\,\text{L}}{\text{m}^3}$$

$$-0.09 \times 10^{13}$$

$$= 12.5 \times 10^{13}\,\text{m}^{-1} - 0.09 \times 10^{13}\,\text{m}^{-1}$$

- ■ $R_c + R_f = 12.41 \times 10^{13}\ \text{m}^{-1}$

Second, the $R_{f,re}$ and the $R_{f,ir}$ are calculated using the filtration data collected after chemical cleaning. After chemical cleaning, the cake layers and the reversible internal foulants are removed. Therefore, the following equation can be applied to calculate the flux just after chemical cleaning at day of 5.1.

$$J_{5.1} = \frac{TMP_{5.1}}{\eta(R_m + R_{f,ir})} \tag{E3.6}$$

- ■ The irreversible internal fouling resistance ($R_{f,ir}$).
- ■ $TMP_{5.1}$ is the pressure measured just after the chemical cleaning of day 5.1, which is 5.23790 kg·m/s² cm².
- ■ $J_{5.1}$ is the operating flux at day 5.1, which is always 20 L/h m² under the constant flux mode.
- ■ Shuffle Equation E3.6 until the resistance form appears and insert the corresponding values into it.
- ■ $R_{f,ir} = TMP_{5.1}/(\eta \cdot J_{5.2}) - R_m$

$$= \frac{5.23790\ \text{kg} \cdot \text{m}}{\text{s}^2 \cdot \text{cm}^2} \times \frac{\text{m} \cdot \text{s}}{1.009 \times 10^{-3}\,\text{kg}} \times \frac{\text{m}^2 \cdot \text{h}}{20\ \text{L}} \times \frac{3600\ \text{s}}{\text{h}} \times \frac{100^2\,\text{cm}^2}{\text{m}^2} \times \frac{10^3\ \text{L}}{\text{m}^3}$$

$$-0.09 \times 10^{13}$$

$$= 0.93 \times 10^{13}\ \text{m}^{-1} - 0.09 \times 10^{13}\ \text{m}^{-1}$$

- ■ $R_{f,ir} = 0.84 \times 10^{13}\,\text{m}^{-1}$

Summarizing the calculated resistances, the total fouling resistance ($R_{TF} = R_c + R_f$) and the irreversible internal fouling resistance at day 5 are $12.41 \times 10^{13}\ \text{m}^{-1}$ and $0.84 \times 10^{13}\ \text{m}^{-1}$, respectively.

In a similar manner, the following table was obtained by a series of resitance value calculations at day 10 and 15.

	Resistance Values (x10¹³ m⁻¹)			
	R_m	$R_{f,ir}$	$R_c + R_f$	R_T
Day 5	0.09	0.84	12.41	12.50
Day 10	0.09	1.44	12.46	12.55
Day 15	0.09	1.73	12.58	12.67

(b)
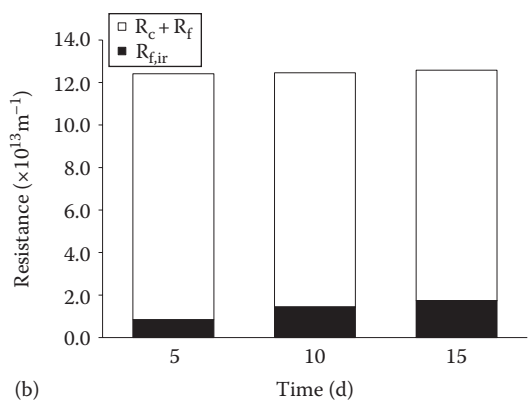
Remark

It should be noted that the cake layer resistance (R_c) and internal fouling resistance (R_f) cannot be obtained separately in this example. Irreversible internal fouling resistance ($R_{f,ir}$) increased along with operation time, indicating that the chemical cleaning was not sufficient to restore the irreversible fouling completely. The total fouling resistance, $R_c + R_f$, are always similar to 12.5×10^{13} m^{-1} at day 5, 10, and 15 because the membrane filtration stopped whenever TMP reached 70 kg m/s^2 cm^2 and then chemical cleaning started.
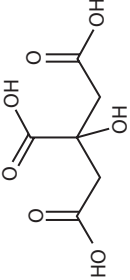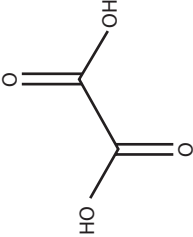
5.3.1.2 Classification of Cleaning Chemicals

Table 5.5 summarizes the chemicals used in MBR cleaning. Chemical cleaning reagents used for fouling control in MBR are categorized into the following groups:

- Oxidizing agents
- Acids and bases
- Enzymes
- Chelating agents
- Detergents (or surfactants)
- Coagulants

Oxidizing agents target mainly the organic foulants attached to membranes surfaces, internal pores, as well as cake layers. Sodium hypochlorite (NaOCl), ozone (O_3), and hydrogen peroxide (H_2O_2) are the most popular oxidizing agents used for fouling control in MBR. Oxidative potential (OP) of a species indicates the power of an oxidant, with a higher value indicating higher reactivity. OP of the hypochlorite, ozone, and hydrogen peroxide are 0.9, 2.07, and 1.76 V, respectively. In addition to their high OP, ozone and hydrogen peroxide produce a hydroxyl radical ($\cdot$OH), which has the highest OP (2.8 V). The $\cdot$OH radical is a strong and nonspecific oxidant and therefore able to rapidly oxidize a large number of recalcitrant molecules.
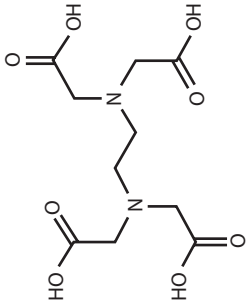
Ozonation is a well-proven technology for excess sludge reduction and treatment of recalcitrant molecules. For this reason, many studies have introduced ozone to

Table 5.5 Chemical Reagents Commonly Used in Membrane Cleanings in MBR

Category	Chemicals Name	Molecular Formula	Molecular Weight	Chemical Structure
Oxidizing agents	Sodium hypochlorite	NaOCl	74.5	
	Calcium hypochlorite	Ca(OCl)$_2$	143.0	
	Ozone	O$_3$	48.0	
	Hydrogen peroxide	H$_2$O$_2$	34.0	
Inorganic acids	Sulfuric acid	H$_2$SO$_4$	98.0	
	Hydrogen chloride	HCl	36.5	
Organic acids	Citric acid	C$_6$H$_8$O$_7$	192.1	
	(2-hydroxypropane-1,2,3-tricarboxylic acid)			
	Oxalic acid (ethanedioic acid)	H$_2$C$_2$O$_4$	90.0	

(Continued)

Table 5.5 (*Continued*)   Chemical Reagents Commonly Used in Membrane Cleanings in MBR

Category	Chemicals Name	Molecular Formula	Molecular Weight	Chemical Structure
Chelating agent	EDTA	$(HO_2CCH_2)_2NCH_2CH_2N(CH_2CO_2H)_2$	292.4	
Surfactants	Sodium dodecyl sulfate (SDS)	$CH_3(CH_2)_{11}OSO_3Na$	288.4	
Enzyme	Protease, hydrolase, glycolytic enzyme	—		—
PAC	Powdered activated carbon	C	—	—

MBR to control membrane fouling. Huang and Wu (2008) reported the effect of ozonation on membrane fouling in an MBR running in laboratory. The membrane permeability was improved by ozonation with a dosage less than 0.7 gO_3/kg MLSS. During their long-term operation of MBR, ozonation did not affect COD and ammonia removal, which means ozonation did not influence the microbial activity within the ozone dosage applied. Later they found that the best dosage of ozone was 0.25 gO_3/kg MLSS at 1 day intervals (Wu and Huang, 2010).

However, ozonation to microbial sludge does have potential to disrupt microbial cells, which leads to cell lysis. He et al. (2006) reported that ozone disrupted the cell walls and caused the release of plasma from the cells, and ozonation also increased the soluble contents of nitrogen and phosphorus as a result of cell lysis. According to their study, a suitable ozone dosage of 0.16 kgO_3/kg MLSS was suggested. Compared with the results of Huang and Wu (2008), the discrepancy is too big to choose a proper ozone dosage. Considering the difficulty in fine-tuning of ozone dosage, ozonation in MBR is believed to have a limitation for precise control of membrane fouling without microbial damages.

Many of the safety concerns related to the use of gaseous chlorine (Cl_2) or ozone (O_3) are loosened by the use of salt form chlorine such as sodium hypochlorite (NaOCl) or calcium hypochlorite (Ca(OCl)$_2$). Hypochlorites are the most commonly used oxidizing agents for both the off-line cleaning and the CIP even though the OP is the lowest among the three candidates (i.e., O_3, H_2O_2, and OCl$^-$). Sodium hypochlorite is relatively easy to handle and stock. On the other hand, ozone needs to be prepared on sites and the ozone generation consumes huge amounts of the electricity. Hydrogen peroxide, liquid at room temperature, is more expensive than hypochlorite.

Typical concentrations of sodium hypochlorite for the maintenance cleanings performed by weekly or monthly are from 300 to 1000 mg/L, depending on the membrane materials employed, whereas the concentration of sodium hypochlorite for the purpose of irreversible flux recovery performed by quarterly or biennially is much higher than the routine maintenance cleanings (i.e., usually 2500–5000 mg/L). The concentration span looks a little bit high due to the low OP compared with the other oxidizing agents. However, membrane damage should be considered in long-term consecutive exposures to sodium hypochlorite. In the case of periodic CIP, lethal damage to the microorganisms is possible too. Particularly, synthetic polymeric membranes are apt to be damaged by free and combined chlorine, so that the chlorine resistance is an important criterion when selecting proper membranes for water and wastewater treatment. Most membrane manufacturers provide their membrane's specifications with chlorine resistances.

Wang et al. (2010) studied the impact of hypochlorite cleaning on the characteristics of polyvinylidene fluoride (PVDF) membranes, which is the most frequently used membrane material in MBR plants worldwide. Similar to conventional disinfection kinetics, they established a standardized value to evaluate the impact of hypochlorite exposure on membranes, C × t, where C is a hypochlorite

concentration and t is the exposure time. They concluded that sodium hypochlorite cleanings did not damage the chemical structure of PVDF membranes but had impacts on the membrane surface properties. Even though they emphasized that the PVDF membranes they used could stand normal chemical cleaning conditions over several years, it might be difficult to generalize their findings because of the complexity in membrane fouling phenomena. For example, if the fouling level is quite higher than theirs, more severe chemical cleanings will be required, leading to shortening the lifetime of the PVDF membranes.

Periodic CIP is needed to lower the elevated TMP during MBR operation. These maintenance cleanings use NaOCl solution or a combined NaOCl solution with acids. NaOCl takes the role of removing organic foulants while the acids solubilize the inorganics such as scales and metal oxides. Mineral (sulfuric acid) or organic acids (citric acid) are often used. Occasionally, CIP is carried out by the form of a chemically enhanced backwashing, where chemicals are added to the backflushing stream to enhance the cleaning efficiency by means of physicochemical synergistic cleaning effect.

5.3.1.3 Hypochlorite Chemistry

The most popular oxidizing agents used for chemical cleanings in MBR, sodium hypochlorite (NaOCl) or calcium hypochlorite ($Ca(OCl)_2$), dissociate into their anion, hypochlorite (OCl^-), and the corresponding cations.

$$NaOCl \leftrightarrow Na^+ + OCl^- \tag{5.22}$$

$$Ca(OCl)_2 \leftrightarrow Ca^{2+} + OCl^- \tag{5.23}$$

The hypochlorite, of course, establishes equilibrium with hydrogen ions in aqueous solution, forming hypochlorous acid (HOCl). The following equation expresses the ionization of HOCl:

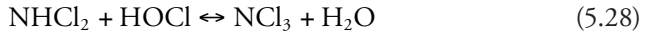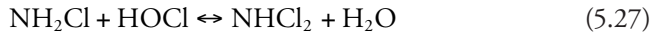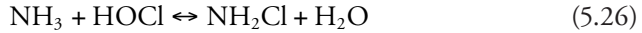$$HOCl \leftrightarrow OCl^- + H^+ \tag{5.24}$$

Both compounds, hypochlorite and HOCl, are in equilibrium, which is apt to be shifted in accordance with the change in pH. The equilibrium constant, K_a, for the dissociation reaction is

$$K_a = \frac{[OCl^-] \cdot [H^+]}{[HOCl]} = 2.7 \times 10^{-8} \text{ mol/L at } 20°C \tag{5.25}$$

The "free available chlorines" refer to the total quantity of HOCl and OCl^- existing in aqueous solution. On the other hand, "combined available chlorines" are formed by the reaction of free chlorines with ammonia, which are often called

chloramines. The reactions are stepwise giving monochloramine (5.26) followed by dichloramines (5.27) and finally nitrogen dichlorides (5.28). These consecutive reactions are as follows:

$$NH_3 + HOCl \leftrightarrow NH_2Cl + H_2O \tag{5.26}$$

$$NH_2Cl + HOCl \leftrightarrow NHCl_2 + H_2O \tag{5.27}$$

$$NHCl_2 + HOCl \leftrightarrow NCl_3 + H_2O \tag{5.28}$$

These reactions are dependent upon pH, temperature, and contact time. In most cases, monochloramine (NH_2Cl) and dichloramine ($NHCl_2$) are the predominate compounds among the three chloramines. The relative distribution of the dichloramine to the monochloramine depends on the ratio of chlorine to ammonia in the water or the wastewater. The amount of nitrogen trichloride is negligible up to chlorine-to-nitrogen ratios of 2.0. Since the dichloramines are quite unstable, they decompose readily to nitrogen gas (N_2) and chloride (Cl^-) as the following reaction (5.30):

$$NHCl_2 + NHCl_2 + H_2O \leftrightarrow HOCl + 3H^+ + 3Cl^- + N_2 \uparrow \tag{5.29}$$
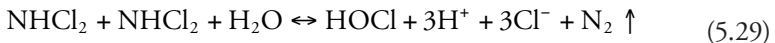
The free chlorines and the combined chlorines have a disinfection potential, which means they serve as disinfectants killing live microorganisms. The order of disinfection efficiency of these chlorine compounds is as follows:

$$HOCl > OCl^- > Chloramines(NH_2Cl, NHCl_2, NCl_3) > Cl^- \tag{5.30}$$
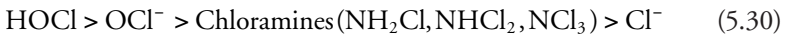
The chloride ion does not have disinfection potential because its oxidation state (–1) is too low to accept electrons from other compounds. Since the oxidation state of the free chlorines ($HOCl$ and OCl^-) and chloramines are all +1, they have a disinfection potential. However, their disinfection efficiency is quite different from each other. For example, the disinfection efficiency of the free chlorines is greater than that of the slow-reacting chloramines. Moreover, the disinfection efficiency of $HOCl$ is about 40–80 times that of OCl^-, so that the relative distribution of the two compounds is very important to setting up a successful disinfection strategy.

Example 5.4

Derive the equation expressing the ratio of hypochlorous acid ($HOCl$) and hypochlorite, $[OCl^-]/\{[OCl^-] + [HOCl]\}$, as a function of pH and K_a. Plot the graph showing the change in the relative distribution of $HOCl$ as a function of pH at two different temperatures, 0°C and 25°C.

Solution

The relative distribution of the two species, $[OCl^-]/\{[OCl^-] + [HOCl]\}$, is a function of pH because the equilibrium in Equation 5.24 can be shifted by pH change.

As the pH increases the reaction shifts to the right, conditions are more favorable to forming hypochlorite, OCl^-. On the contrary, if the reaction shifts to the left side, conditions more favorable to forming HOCl as the pH decreases.

The relative distribution of two the compounds, $[OCl^-]/\{[OCl^-] + [HOCl]\}$, is calculated by means of pH and K_a, as follows:

Dividing the ratio, $[OCl^-]/\{[OCl^-] + [HOCl]\}$, by the $[HOCl]$ for both the denominator and the numerator,

$$\frac{[HOCl]}{[HOCl] + [OCl^-]} = \frac{1}{1 + [OCl^-]/[HOCl]}$$

Rearranging Equation 5.25 for the dissociation of hypochlorous acid, $K_a = [OCl^-] \times [H^+]/[HOCl]$, the ratio in the denominator, $[OCl^-]/[HOCl]$, could be replaced by $K_a/[H^+]$.

$$\frac{[HOCl]}{[HOCl] + [OCl^-]} = \frac{1}{1 + [OCl^-]/[HOCl]} = \frac{1}{1 + K_a/[H^+]}$$

Rearranging the pH definition, $pH = -\log[H^+]$, $K_a/[H^+]$ is replaced by $K_a/10^{-pH}$.

$$\frac{[HOCl]}{[HOCl] + [OCl^-]} = \frac{1}{1 + [OCl^-]/[HOCl]} = \frac{1}{1 + K_a/[H^+]} = \frac{1}{1 + K_a/10^{-pH}}$$

The following graph shows the relative distribution of HOCl and OCl^- as a function of pH and can be plotted by using the final equation.
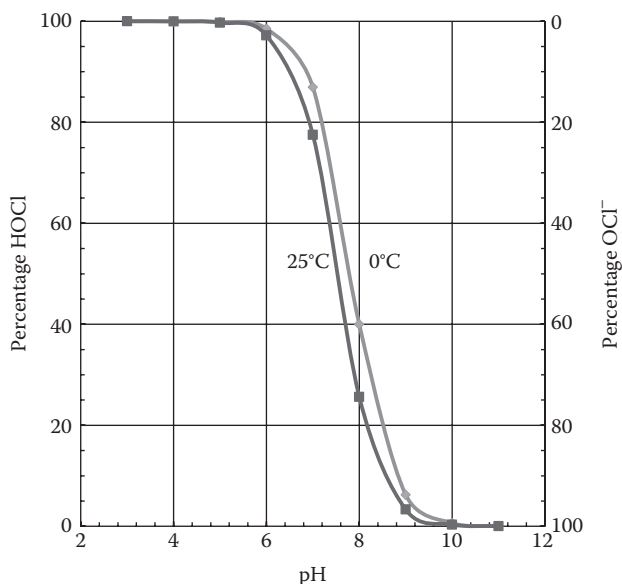
The relative portion of HOCl expressed in percentage decreases as the pH increases whereas the OCl⁻ shows the opposite trend. Considering that the usual pH in water treatment ranges from 4.5 to 7, most free chlorines present are in the form of HOCl. The distribution line shifts to the left as temperature increases from 0°C to 25°C, which means that the portion of the more powerful oxidizing agent, HOCl, increases, indicating that the disinfection efficiency would increase along with temperature increases under constant pH conditions.

5.3.1.4 Actual Chlorine and Available Chlorine

The term "actual chlorine" refers to the actual chlorine content of the compounds containing chlorine. It is used to represent the effectiveness of chlorine compounds. The percent actual chlorine is defined as follows:

$$(Cl_2)_{actual}, \% = \frac{\text{Weight of chlorine in compounds}}{\text{Molecular weight of compounds}} \times 100 \qquad (5.31)$$

The term "available chlorine" is used to compare the oxidizing power of chlorine compounds. The available chlorine given by the following equation is defined by the "chlorine equivalent" times "actual chlorine":

$$(Cl_2)_{available}, \% = Cl \text{ equivalent} \cdot (Cl_2)_{actual} \qquad (5.32)$$

$$= Cl \text{ equivalent} \times \frac{\text{Weight of chlorine in compound}}{\text{Molecular weight of compounds}} \times 100$$

The "chlorine equivalent" represents the oxidation power of chlorine compounds, which means the total number of electrons involved in their oxidation reaction. For example, the half cell reaction for hypochlorite is

$$OCl^- + H_2O + 2e^- \rightarrow Cl^- + 2OH^- \qquad (5.33)$$

or

$$OCl^- + 2H^+ + 2e^- \rightarrow Cl^- + H_2O \qquad (5.34)$$
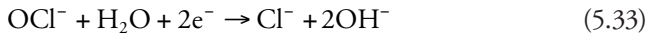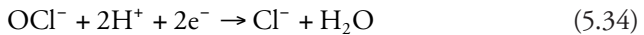
The OCl⁻ must take two electrons to complete the oxidation reaction, that is, the oxidizing agent OCl⁻ should be reduced by accepting two electrons. The chlorine equivalent, the number of electrons involved in the oxidation by OCl⁻, is 2. Therefore, the actual chlorine of OCl⁻ is 68.9% ($= 35.5/51.5 \times 100$) and the available chlorine is calculated to 137.8% as follows:

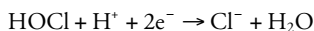$$Cl_{2 available}, \% = Cl \text{ equivalent} \cdot (Cl_2)_{actual} = 2 \times 68.9 = 137.8\%$$

Example 5.5

Determine the "actual chlorine" and the "available chlorine" of the following species: HOCl, NaOCl, and Ca(OCl)$_2$.

Solution

1. HOCl

$$\text{Actual chlorine for HOCl} = \frac{\text{Weight of chlorine in compounds}}{\text{Molecular weight of compounds}} \times 100$$

$$= \frac{35.5}{(1 + 16 + 35.5)} \times 100 = 67.6\%$$

$$HOCl + H^+ + 2e^- \rightarrow Cl^- + H_2O$$

As shown in the previous equation, the electron change is 2. Thus, the Cl equivalent is 2.

$$(Cl_2)_{\text{available}}, \% = \text{Cl equivalent} \cdot (Cl_2)_{\text{actual}} = 2 \times 67.6 = 135.2\%$$

2. NaOCl

$$\text{Actual chlorine for NaOCl}, \% = \frac{\text{Weight of chlorine in compounds}}{\text{Molecular weight of compounds}} \times 100$$

$$= \frac{35.5}{(23 + 16 + 35.5)} \times 100 = 47.7\%$$

$$NaOCl + 2H^+ + 2e^- \rightarrow Na^+ + Cl^- + H_2O$$
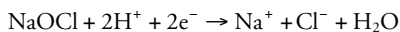
As shown in the previous equation, the electron change is 2. Thus, the Cl equivalent is 2.

$$(Cl_2)_{\text{available}}, \% = \text{Cl equivalent} \cdot (Cl_2)_{\text{actual}} = 2 \times 47.7 = 95.4\%$$

3. Ca(OCl)$_2$

$$\text{Actual chlorine for Ca(OCl)}_2, \% = \frac{\text{Weight of chlorine in compounds}}{\text{Molecular weight of compounds}} \times 100$$

$$= \frac{35.5 \times 2}{40 + 16 \times 2 + 35.5 \times 2} \times 100 = 49.7\%$$

$$Ca(OCl)_2 \rightarrow Ca^{2+} + 2OCl^-$$

$$2OCl^- + 2H_2O + 4e^- \rightarrow 2Cl^- + 4OH^-$$
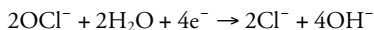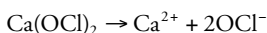
Adding these two reactions, the OCl$^-$ in both equations are deleted and the following reaction is obtained.

$$Ca(OCl)_2 + 2H_2O + 4e^- \rightarrow Ca^{2+} + 2Cl^- + 4OH^-$$
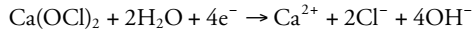
The total electron change for one $Ca(OCl)_2$ molecule looks like four. However, the chlorine equivalent, the net number of electrons involved in one chlorine, is 2 (= 4 electrons/2 chlorines).

$$(Cl_2)_{available}, \% = Cl \text{ equivalent} \cdot (Cl_2)_{actual} = 2 \times 49.7 = 99.4\%$$

Example 5.6

Determine the monthly requirements of sodium hypochlorite (NaOCl) for periodic maintenance cleaning (i.e., routine CIP in MBR plants). A batch cleaning test showed that cleaning with NaOCl solution restored the declined flux sufficiently to the preset operating flux. Assume the following conditions:

- Batch cleaning test with NaOCl solution
  - 0.2% of NaOCl solution for 2 h recovered to the previous set flux
  - Membrane surface area: 1 m^2
  - Volume of the NaOCl cleaning solution: 0.01 m^3
  - Purity of NaOCl solution: 85%
  - Density of NaOCl solution: 1000 kg/m^3
- Operating flux: 30 LMH.
- Chemical cleanings were carried out for every 10 days when the flux was reduced to 20 LMH.
- Influent flow rate (Q) of the MBR plant: 10,000 m^3/day.
- Total membrane area was 500 m^2.

Solution

The initial operating flux was set to 30 LMH, but it was reduced to 20 LMH over 10 days, indicating that the loss of 10 LMH corresponds to the membrane fouling. Therefore, the membrane area loss by 10 days of fouling should be one-third of the original membrane area, that is, $1/3 \times 500$ $m^2 = 167$ m^2.

The membrane area loss by 10 days of fouling is 167 m^2. Therefore, the NaOCl requirement for one cycle of chemical cleaning is

$$167 \text{ m}^2 \times \frac{0.01 \text{ m}^3 \text{ NaOCl solution}}{1 \text{ m}^2 \text{ membrane area}} \times \frac{\text{NaOCl 1000 kg}}{\text{NaOCl m}^3} \times \frac{0.2}{100} \times \frac{1}{0.85} = 3.93 \text{ kg}$$

Since three chemical cleanings are required every 1 month, 3.93 kg × 3 = 11.8 kg of pure NaOCl solution is required.

If 0.2% NaOCl solution, which should be made of 85% purity NaOCl, is used for the cleanings, the NaOCl requirement for one cycle of chemical cleaning is

$$167 \text{ m}^2 \times \frac{0.01 \text{ m}^3 \text{ NaOCl solution}}{1 \text{ m}^2 \text{ membrane area}} \frac{\text{NaOCl 1000 kg}}{\text{NaOCl m}^3} = 1670 \text{ kg}$$

Therefore, 1670 kg × 3 = 5010 kg of 0.2% NaOCl cleaning solution is required for 1 month.

5.3.1.5 Other Chemical Agents

Inorganic and organic acids can serve as cleanings agents. Acids such as sulfuric and citric acid dissolve inorganic precipitated foulants and scales. Bases can be used for organic foulants removal. Surfactants (detergents) are also used for cleaning organic foulants by emulsification. The acid/base tolerance of the membranes and modules should be considered before the cleanings. Moreover, pH neutralization should be considered after the acid/base cleanings. Enzymes aiming at specific organic foulants such as proteins and polysaccharides can also be used for cleaning. They are not used alone but formulated with other reagents. Chelating reagents such as ethylenediaminetetraacetic acids (EDTA) can be used as ligand material for complexing inorganic foulants. Chelating agents are not used for fouling control in MBR because of pH adjustment requirement and possible interferences by cations present in the wastewater. Cost is another factor preventing the use of chelating agents.

5.3.1.6 Activated Carbon

Direct addition of powdered activated carbon (PAC) to a membrane tank is often tried to mitigate membrane fouling in MBR. The membrane permeability of the PAC-added MBR is obviously enhanced compared with the non-PAC-added MBR. The addition of PAC leads to a decrease not only in the compressibility of sludge flocs but also in the content of extracellular polymeric substances (EPSs) inside the microbial flocs. This increases porosity of the cake layer and thus enhances the membrane flux (Kim et al., 1998). Satyawali and Balakrishnan (2009) showed that PAC addition mitigates membrane fouling and enhances the biodegradation of recalcitrants or slowly biodegradable compounds.

5.3.1.7 Chemical Pretreatment and Additives

Chemical pretreatment is considered mandatory to improve the membrane permeability for drinking water treatment. Potential foulants are removed by chemical precipitation prior to the main membrane filtration processes. However, it has not been often tried in MBR applications for wastewater treatment. In special cases, for example, piggery wastewater including high concentration of suspended solids coagulation prior to MBR is reported (Kornboonraksa and Lee, 2009). Instead of pretreatment by coagulation, in situ EC techniques are combined to MBR, which will be discussed later in this section.

Electrolytic polymers have been reported to be effective in fouling mitigation. Several electrolytes improving membrane permeability in MBR are commercialized and available in the market. For example, some commercial cationic polyelectrolytes can improve filterability up to 150% with the doses of several hundreds ppm. The addition of these chemicals makes the cake layer porous and induces a

decrease in soluble EPS. Moreover, soluble constituents in the bulk solution, which are potential foulants, are entrapped in sludge flocs during the flocculation process. However, the MBR market does not use these chemicals frequently due to the lack of a long-term evaluation as well as cost.

5.3.2 Physical (Hydrodynamic or Mechanical)

5.3.2.1 Preliminary Treatment

One of the notorious troubles in submerged MBRs is the entanglements of hairs with the membrane fibers, which results in entire system shutdown. Therefore, debris such as grit, particulates, hair, and plastic materials should be removed prior to the main membrane reactor in MBR. Proper selection of the preliminary treatments should be considered more importantly at the design stage of MBR than for conventional wastewater treatment systems. Operation of the preliminary treatment such as screens, bar racks, and grit chamber is described well in other wastewater treatment textbooks.

5.3.2.2 Backwashing (or Backflushing)

The same principles of the backwashing (or backflushing) for conventional media filtration (sand and/or anthracite filtration for water treatment processes), a reverse direction of water flow expels the foulants from the filter media, can also be applied to membrane separation. Membrane backwashing is the most frequently used tool to maintain a steady flux in membrane filtration processes due to simplicity and controllability. Therefore, backwashing has been considered a primary tool for fouling control in most MBR plants.

Basically, backwashing is carried out with permeate or pure water. Occasionally, chemicals are added to the backwashing solution to enhance the cleaning efficiency, which is called chemically enhanced backwashing. The backwashing frequency and pressure applied depends on the membranes and module design. The membrane manufacturers give an indication of the maximum pressure allowed for the backwashing.

If backwashing is periodically repeated in conventional filtration, the filter media is lost out of the filtration beds. For example, some of the filter media such as sand is swept away with the backwashing water, so that makeup sand is needed for the routine maintenance of filtration. Just like the case of sand filtration, periodic repeating of backwashing in MBR could result in severe damages to the membrane structure. In particular, asymmetric membranes constructed by skin and supporting layers have relatively weaker structure than the microporous membranes, so that they should be backwashed cautiously. That is, periodic backflushing can cause disintegration of membranes and/or modules, so that the lifetime of membranes should be considered first before backwashing.

The backwashing facilities in MBR plants should include valves, pipes, and pressure gauges for the air and/or water. Moreover, backwash pumps and backwash water storage tanks are needed. The generated backwashing wastewaters normally return to the aeration tank unless chemicals are used for the backwashing.

5.3.2.3 Air Scouring (Coarse Aeration)

Most submerged MBRs employ coarse aeration as a fundamental tool for fouling control. The basic idea is that coarse aeration in a membrane tank accomplishes dual goals: (1) air transfer to cells for microbial growth and metabolism (2) and aeration for fouling control. Excessive and extensive coarse aeration onto the membrane surfaces has been practiced commonly to vibrate the submerged membranes mechanically and remove sludge cakes on the membrane surfaces. However, coarse aeration consumes large amounts of energy for air blowing. Depending on MBR sites, aeration consumes about 49%–64% of the total energy required for MBR plant operation (Barllion et al., 2011; Janot et al., 2011).

Coarse aeration for fouling control inevitably introduces strong shear forces to the microbial flocs, so that the sludge flocs are apt to experience floc disintegration. Since membrane fouling worsened by decreases in particle size arising from floc disintegration, segregation of the coarse aeration and fine bubbling for the cells is often tried: locating the coarse aeration diffusers just beneath the membrane module and locating the fine bubble aerator out of the module. Nevertheless, coarse aeration is still frequently practiced in MBR plants because it is easy to install and the dual goals (air transfer to cells and fouling control) are readily achieved by single aeration devices.

Various kinds of devices and methods have been attempted to overcome the huge energy consumption problem. The air cycling system in LEAPmbr™ (GE) is one of the commercially developed examples. For the purpose of vibrating and scouring the membrane fibers, intermittent aeration is supplied to the membrane modules in 20 or 40 s intervals of air on and off in order to reduce the energy cost for aeration in MBR (Adams et al., 2011).

Another example of effective use of air is the introduction of a two-phase (air+liquid) flow to MBR as shown in Figure 5.7. Different flow regimes are formed according to the ratio of flow rates of air and liquid: bubble, slug, churn, annular, and mist flow. The flow regime changes from bubble to mist as the ratio increases. The slug flow is known to be the most effective flow for flux enhancement among the various air–liquid multiphase flow patterns. The slug flow, air pockets formed in the shape of a slug, enhances mass transfer near the membrane surface and scours the cake layers, and thus, fouling is mitigated.

The introduction of slug flow in tubular membrane modules enhances the flux significantly (~43%) in the MBR for domestic wastewater treatment (Chang and Judd, 2002). Application of the two-phase flow to a plate and frame (P+F) module MBR was also studied by Zhang et al. (2011). They reported that the slug
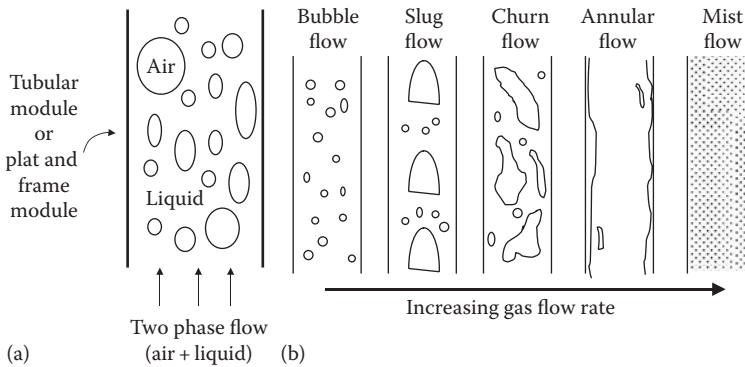
Figure 5.7   Schematic of two-phase flow in membrane module (a) flow regimes according to gas flow rate (b).

flow exhibited a better antifouling performance than free bubbling. They also addressed that the slug flow prevented irreversible as well as reversible fouling. All of these results are attributed to the increased wall shear stress incurred by the two-phase flow. However, the multiphase aeration still remains incompletely understood because the flow in MBR is actually a three-phase flow consisting of solids (sludge flocs) + liquids + gas phase. The three-phase flow is more complex to model. Moreover the solids, microbial flocs, are difficult to characterize because it changes with time. Due to this reason, "air lift" is the more widely accepted term describing the multiphase aeration in MBR, instead of two-phase MBR.

One commercial example is the MemPulse™ MBR system (Evoqua Water Technologies, 2014) employing a pulse device that introduces irregular pulses of air to the MBR module. The supplied air bubbles blend with the mixed liquor and rise up onto membrane fibers, creating plug flow and providing effective scouring to the membrane surface to prevent solids buildup.

5.3.2.4 Intermittent Suction

Since membrane separation is as pressure-driven processes, abrupt pressure relaxation (or retardation) can cause a temporary back transport of permeates, which then helps to dislodge cake layers away from the membrane surfaces. Instant cessation of suction pressure in submerged MBR or stopping pressurization in sidestream MBR has been used widely for fouling prevention in MBR.

An intermittent suction (i.e., temporary cessation of suction) can provide an alternative tool for suppression of membrane fouling in MBR. This technique is called a cyclic filtration because on and off suctions repeat periodically. Intermittent suction is economical for fouling prevention because suction energy can be saved during the off-suction periods. However, disadvantages originating from control

complexity could compromise the merits of the fouling prevention and energy savings. For example, installation of a programmable logic controller (PLC) and solenoid valves to perform the on and off duties makes the system complicated and expensive.

Although big progress in understanding particle deposition on membrane surfaces based on force balance of particles has been accomplished, determining time intervals for on and off filtrations mainly depends on experimental data and not by theoretical analysis of hydrodynamics.

5.3.2.5 Abrasion

Prevention of membrane fouling in MBR can also be achieved by an abrasion mechanism. Free moving materials in membrane tanks can rub the membrane surface, helping to dislodge cake layers off the membrane. They move freely to cake layers and then take them off by mechanical scouring, leading to increased membrane permeability. Soft sponge balls (or cubes) or hard plastic media have been used for the free moving media causing abrasion.

For the purpose of making biological activated carbon (BAC), granular activated carbon (GAC) is added to MBR. The BAC has dual duties: (1) original duty of providing spaces for biomass attachment and growth and (2) moving carriers for abrasion. The attached microorganisms show enhanced microbial performances due to the increased population on the carriers BAC, leading to better effluent water quality than the suspended growth microorganisms. Simultaneously, the BAC carriers move around the membrane tank and can work as abrasive particles, reducing membrane fouling. This system, an MBR-containing BAC, is often called a biofilm MBR.

The use of moving carriers in MBR prevents a sudden rise of TMP by producing extra shear forces and reducing the deposition of fine particles onto the membrane surface by scouring. Commercially developed MBR systems employing scouring carriers are available on the market. The BIO-CEL®-MCP process uses inert organic materials, MCP granulate, that is added directly to the MBR tank. The continuous airflows in the membrane tank bring the MCP granulates to the membranes and the direct contact of granulates cleans the membrane surfaces mechanically.

5.3.2.6 Critical Flux Operation

Field et al. (1995) introduced the critical flux concept and subcritical flux operation in membrane separation processes for the purpose of retarding (or reducing) membrane fouling. Since its introduction, it has been applied to all kinds of membrane systems. After their pioneering works, many controversies about the strict meaning of critical flux were addressed and have being continued today. Notwithstanding that strict definition of the critical flux is not accepted yet, the critical flux in an MBR system denotes the operating flux where no fouling occurs under the proper fouling control conditions. Even though MBR systems run under the critical flux

conditions, membrane fouling still obviously develops. If the strict meaning of critical flux—the flux where no fouling occurs—is applied to MBR, a significantly lower flux would be identified as the critical flux. Therefore, the flux that endure severe and rapid fouling even with employing a proper fouling control strategy such as coarse aeration and periodic cleanings is regarded as the critical flux in MBR. This kind of flux is often called sustainable flux in order to differentiate it from the strict definition of critical flux.

Typical values of critical flux in MBR plants range from 10 to 40 LMH depending on the various factors affecting membrane fouling. As indicated in Chapter 4, numerous factors influence fouling directly or indirectly, for example, characteristics of the activated sludge mixed liquor, membrane properties, flow regime (sidestream or submerged type), module configuration (hollow fiber or flat sheet), influent wastewater characteristics, microbial community (BNR or CAS), and hydraulic conditions (HRT, f/m ratio, and SRT). Several methods determining the critical flux have been suggested, as shown in Figures 5.3 and 5.5. However, no single protocol has been agreed upon to measure critical flux, making comparison of published data difficult.

5.3.3 Biological Control

Biological fouling control has been developed recently thanks to the innovative developments in the fields of molecular biology over the last couple of decades. They show a potential for MBRs to become more able to cope with membrane fouling than ever before. A representative biological fouling control development is quorum quenching technology.

5.3.3.1 Quorum Quenching

The quorum sensing (QS) mechanism is quite well understood due to the progresses in modern microbiology and molecular biology. QS is a means of bacterial communication by signal molecules called autoinducers (AIs) emitted by bacteria. QS is triggered when AI molecules exceed a critical threshold, after which point the AIs bind to receptors on the bacteria and make the whole bacteria population express certain kinds of genes together. Biofilm formation is a typical example of QS. As the microorganisms adhere to a surface, they keep signaling to each other. Once they sense a quorum, genes are regulated and sticky exopolysaccharides are produced that "glue" the bacteria together (Marx, 2014).

The principle idea of application of QS to fouling control in MBR is "quorum quenching." The microorganisms in the bio-cakes on membrane surfaces communicate with each other using AIs. Membrane fouling caused by biofilm formation and deposition to membrane surfaces by microorganisms could be inhibited by the addition of AIs inhibitors. Based on this idea, Professor Lee's group at Seoul National University has provided a potential solution for fouling control in MBR. They isolated

signal-quenching bacteria and immobilized them in free moving beads keeping the bacteria in, but letting the AIs pass through. When it is placed near the membrane in MBR, the beads help to stop biofilm formation (Kim et al., 2013). They found that the time to reach TMP of 70 kPa was extended 10 times compared with the control, indicating the fouling rate was significantly reduced due to the use of beads.

5.3.3.2 Other Biological Control

Other types of biological control techniques besides quorum quenching are (1) nitric oxide to induce biofilm dispersal, (2) enzymatic disruption of EPSs, and (3) disruption of biofilm by bacteriophages.

1. Addition of low levels of nitric oxide (NO) causes dispersal of biofilms, indicating that it can be used as a potential alternative for fouling control. However, it has not been investigated for fouling control in MBR. Further studies are needed.
2. Since EPSs are mainly composed of proteins and polysaccharides, EPSs could be hydrolyzed to their building blocks by some specific enzymes such as protease and polysaccharases. If the EPSs are readily degraded by enzymes addition, less membrane fouling would be anticipated. Several studies have indicated that this kind of enzyme cleaning showed better cleaning efficiency than alkaline cleaning. However, many limitations are still present to applying enzyme cleaning techniques to MBR.
3. The addition of bacteriophages reduces microbial attachment to membrane surfaces in MBR by disrupting biofilm formation, which is caused by infection of host bacteria. However, further and wider studies on characteristics of specific parasites between the bacteria and phages are needed to apply MBR.

Although further studies are needed for these recent applications, each biological approach looks like a promising alternative for fouling control in MBR. In particular, the quorum quenching techniques are still being developed in lab and field scale tests and they could arrive at mature stages soon.

5.3.4 Electrical Control

Electricity has been used for conventional pressure-driven membrane filtration processes. Particularly, attention to fouling control using an electrical application in MBR has been paid extensively. The application of electricity to enhance membrane filtration performance is categorized into three groups:

1. Induction of electric field
2. In situ EC
3. High-voltage impulse

5.3.4.1 Electric Field

An electric field applied across membranes can minimize a movement of charged particles to membrane surface, leading to mitigation of membrane fouling. The mechanism is based on the electric negativity of particles. Suspended, fine, and colloidal particles have negative charges in aqueous solution. The charged particles including activated sludge suspension move from the membrane surface to electrodes if a direct current (DC) electric field is applied across the membrane, as shown in Figure 5.8. Induction of a DC electric field facilitates migration of the charged particles on the membrane surface to the counter (+) electrode. This backward transport of the particles off the membrane could ameliorate membrane fouling.

Recently, many studies on the electric field application to improve filtration performance in MBR have been reported. The introduction of minute electric fields from 0.036 to 0.073 V/cm to submerged MBR enhanced the permeate flux
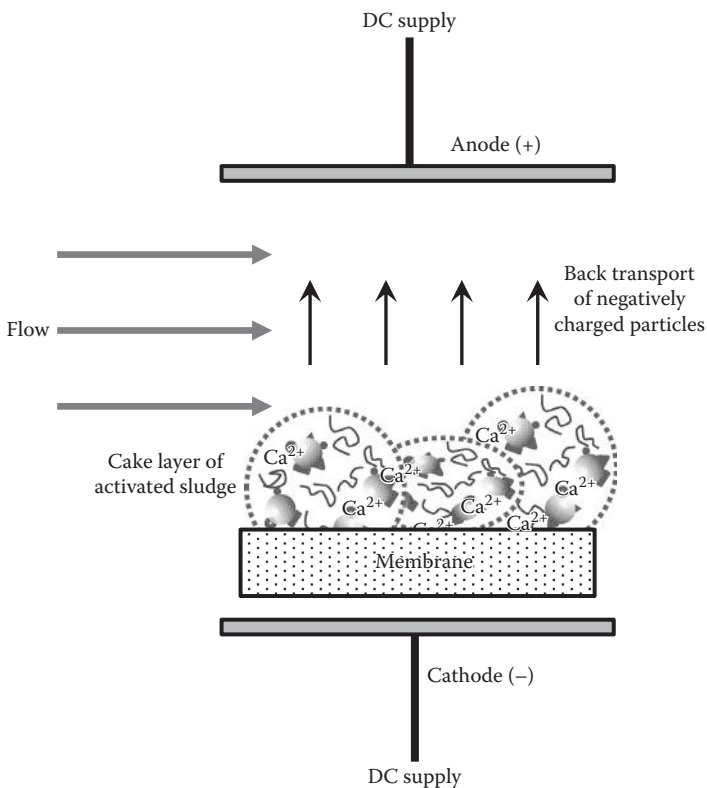
Figure 5.8 Schematic of the DC induction on membrane filtration system to facilitate the back transport away from the membrane surface.

significantly (Liu et al., 2012a). They explained the low electric fields improved microbial growth and activity and thus reduced EPS production, leading to retarded fouling.

Electric field is defined as a ratio of electric potential (volts) per distance between electrodes (cm) as follows:

$$E = \frac{V}{d} \tag{5.35}$$

where E is the electric fields (V/cm), V is the electric potential (V), and d is the distance between electrodes (cm). The closer the distance between electrodes is, the stronger the formed electric fields are.

Applying an electric field to the mixed liquor of activated sludge has the potential to change the microbial activity and physicochemical characteristics of the sludge such as particles size, sludge volume index (SVI), and zeta potential. Liu et al. (2012b) emphasized that operating MBR with low electric fields can reduce inadvertent interferences with MBR performance while simultaneously decreasing energy costs.

Intermittent electric field induction (i.e., on and off electric fields) to MBR systems proposed by Akamatsu et al. (2010) kept the permeate flux as much as 3.5 times higher than the no-electric-field MBR case. Since they found no gases bubbles near the cathode, they concluded that the electrolysis of water did not occur, indicating that the higher flux was not owing to gases scouring sludge onto the membrane surface but to the electric field. They explained that the repulsive force between the membrane surface and the negatively charged activated sludge particles prevents their adhesion to the membrane surface. However, they applied relatively high electric fields, 4–6 V/cm, compared to other researchers. Long-term studies on the effect of electric fields on microbial activity and other various physicochemical characteristics of biomass are needed. Chen et al. (2007) applied much higher electric fields to a hollow-fiber-submerged MBR. They found the flux enhancement was proportional to the electric field strength between 15 and 20 V/cm as the flux remained constant after 20 V/cm.
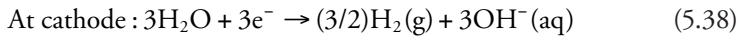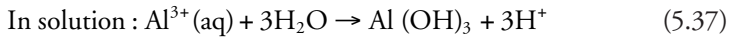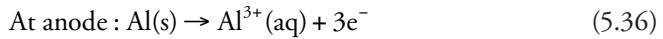
However, they applied the electric fields for a very limited time within a day. Long-term effects of electric fields on microbial activity should be investigated. The advantages of membrane filterability gained by the electric field should overcome or at least compensate the disadvantages caused by possible damages to microorganisms, which could lead to a decline of metabolism or wastewater biodegradation.

Further investigations are needed for a wide application of the electric field to MBR plants. First of all, the flux enhancement, thanks to the electric field induction, should compromise its energy consumption. Although many studies emphasized the enhanced filterability by the use of electric field, data on the energy consumption is not available. In addition, energy consumption of electric field induction should be compared with the conventional aeration for fouling control.

Evaluation of the electric field MBR and the conventional aerated MBR should be compared in terms of energy consumption and flux performance. Another unresolved issue is the lifetime of the electrodes. Since electrodes are very vulnerable to contamination and corrosion, they will likely require frequent cleanings and replacement. Since most studies currently are carried out in laboratory for over a short time duration, long-term data about electrode contamination, corrosion, and cleaning are needed. Finally, long-term effects of electric fields on the microbial activity and physicochemical characteristics of microorganisms should be investigated. No severe microbial damages by electric fields should be guaranteed.

5.3.4.2 In Situ Electrocoagulation

Attention to EC has increased recently because it can run in the reactors (i.e., in situ operation is possible). Particularly, application of EC focusing on membrane fouling control in MBR has a growing research interest. The EC mechanism is based on in situ formation of cations at an anode such as aluminum (Al^{3+}) and ferric (Fe^{3+}) ions, which could work as coagulating agents in aqueous solution to reduce the electrical double layer of the negatively charged colloidal particles. When aluminum (Al) is used as an electrode material, the reactions are as follows (Aouni et al., 2009):

$$\text{At anode}: Al(s) \rightarrow Al^{3+}(aq) + 3e^{-} \tag{5.36}$$

$$\text{In solution}: Al^{3+}(aq) + 3H_2O \rightarrow Al(OH)_3 + 3H^{+} \tag{5.37}$$

$$\text{At cathode}: 3H_2O + 3e^{-} \rightarrow (3/2)H_2(g) + 3OH^{-}(aq) \tag{5.38}$$

The mechanism of EC is similar to conventional coagulation. $Al^{3+}(aq)$ ions are generated at the anode and dissolved to bulk solution, whereas reduction occurs at the cathode generating hydrogen gas (H_2). Similar to alum, $Al_2(SO_4)_3 \cdot 18H_2O$, the most frequently used coagulant in water treatment processes, the $Al^{3+}(aq)$ ions react with water molecules to form various kinds of hydrolyzed aluminum ions as well as aluminum hydroxide, $Al(OH)_3$. Al^{3+} and the hydrolyzed aluminum ions coagulate the negatively charged colloidal matters via a charge neutralization mechanism. The gelatin-like insoluble aluminum hydroxides, $Al(OH)_3$, work as coagulants by enmeshment of colloidal particles to their free-falling bodies in solution (sweep floc mechanism).

Bani-Melhem and Elektorowicz (2010) proposed a new configuration of submerged membrane electro-bioreactor (SMEBR). Figure 5.9 shows the schematic of SMEBR mainly consisting of a DC power supply, hollow fiber membrane module, and cylindrical iron mesh electrodes. The inside of the bioreactor was divided into zone I and II. Zone I is located between the external wall of the reactor and the anode, whereas zone II is between the cathode and the anode. In zone I,
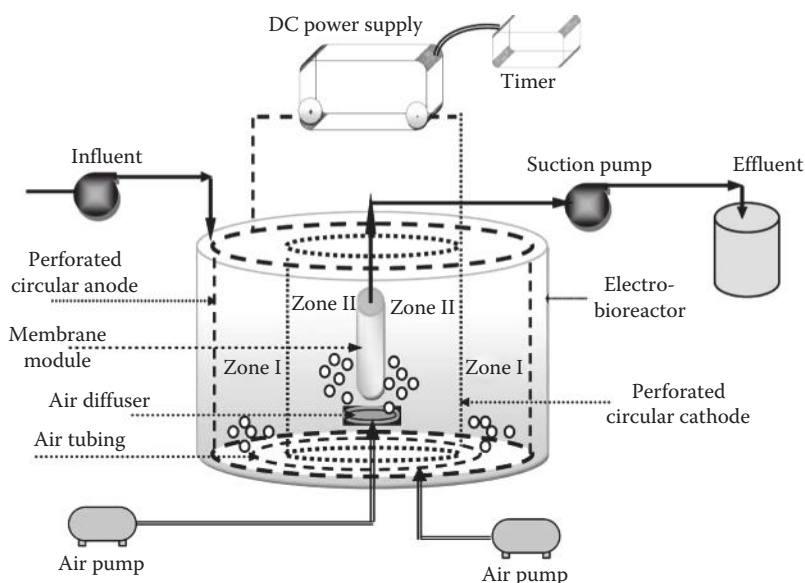
Figure 5.9 **Simplified illustration of submerged membrane electro-bioreactor (SMEBR). (From Bani-Melhem, K. and Elektorowicz, M.,** *Environ. Sci. Technol.,* **44, 3298, 2010.)**

biodegradation and EC take place, whereas biodegradation and membrane filtration are carried out in zone II.

With this novel configuration, 1 V/cm of electric field was applied with a periodic on and off mode (15 min on and 45 min off). They found that membrane filterability was enhanced by reducing the fouling rate up to 16.3% without any backflushing. They explained the cause of the improvement in membrane filterability was closely associated with a decrease in zeta potential of the mixed liquor flocs from −30.5 to −15.3 mV. The increased zeta potential meant that the colloidal particles that are responsible for the cake layer fouling in MBR were coagulated and removed from bulk solution. Moreover, the dissolved matters responsible for membrane pore fouling were removed by the coagulation.

Like DC current induction, information on the microbial activity should be given for EC-MBR. According to the study on the effect of electric current density on microbial activity by Wei et al. (2011), the bacterial viability was not significantly affected until the current density reached 6.2 A/m² for 4 h. However, the percentage of live cells dropped by 15% and 29% at current densities of 12.3 and 24.7 A/m², respectively. They noticed the key role of pH for cell viability. In general, hydroxide (OH⁻) is generated at the cathode as shown in Equation 5.38 due to the electrolysis of water. As the current density increases, the solution pH increases accordingly due to the electrochemical reaction occurring at the cathode.

Obviously alkaline conditions exceeding the normal pH range are harmful for the microorganisms in MBR tanks.

It should be noted that huge amounts of inorganic and/or organic sludge are produced during the course of EC-MBR. In general, metal hydroxides, $M(OH)_3$, are precipitated in bulk solution due to the dissolution of metal ions from the electrode. "Heavy" sludge containing metals is produced. Moreover, any excess metal ion (Me^{2+} or Me^{3+}) has an opportunity to react with soluble phosphate ions (PO_4^{3-}) in bulk solution to form $Me_3(PO_4)_2$ (or $MePO_4$) precipitates. For example, aluminum, $AlPO_4$ (s), is precipitated as the following reaction:

$$Al^{3+} + PO_4^{3-} \rightarrow AlPO_4(s) \downarrow \tag{5.39}$$
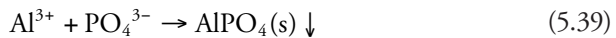
Eventually, great amounts of $M(OH)_3$, $MePO_4$, as well as the coagulated organic sludge are produced in EC-MBR. The MLSS concentration in EC-MBR is likely to be higher than the normal MBR plant. According to the work by Bani-Melhem and Elektorowicz (2011), the MLSS concentration in lab-scale EC-MBR using aluminum electrodes increased from 3500 to 5000 mg/L within 30 days of operation. They also found that the MLVSS/MLSS ratio was nearly 70%, which was relatively lower than the normal ratio of activated sludge, 80%–93%. MLSS represents total organic and inorganic solids of the mixed liquor, whereas MLVSS refers to organic solids (i.e., only microbial cells). The low ratio is definitely attributed to the inorganic sludge production containing either aluminum hydroxide, $Al(OH)_3$, or aluminum phosphates, $AlPO_4$.

Even though the produced sludge differs in its composition depending on the electrodes materials, solution pH, and organic contents of the bulk solution in MBR, a strategy for disposal of the produced metal containing heavy sludge and cost considerations should be taken into account at the initial stage of designing an EC-MBR.

Nutrients (nitrogen and phosphorus) removal is a primary concern in domestic wastewater treatment nowadays. Most MBR plants employing BNR processes suffer from low efficiency of phosphorus removal. Phosphorus should be removed mainly by sludge withdrawals. However, the SRT of MBR is significantly long, so that phosphorus removal by sludge withdrawal is very limited in MBR. Therefore, many BNR-MBR plants employ chemical posttreatments for phosphorus removal such as alum and ferric precipitation. However, enhanced phosphorus removal can be expected in EC-MBR because phosphorus is subjected to be precipitated by metal phosphate. For example, $FePO_4$ (s) in iron electrodes or $AlPO_4$ (s) in aluminum electrodes. This is one of the advantages of the EC-MBR process.

5.3.4.3 High Voltage Impulse

The high voltage impulse (HVI) technique, with typical electric field strength of 20–80 kV/cm and nano- to microsecond pulse duration, has been practiced
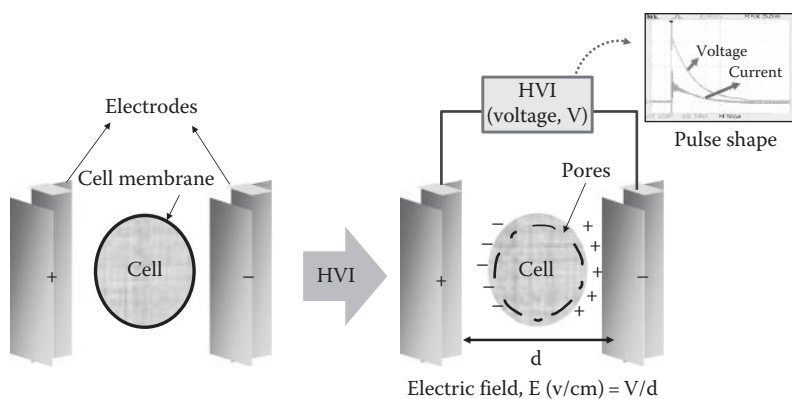
Figure 5.10 Schematic illustration of electroporation mechanism of bacterial cell membrane by HVI.

to inactivate microorganisms. HVI has also been known as pulsed electric fields (PEFs) in the food industry and has been used for nonthermal sterilization of foods. As shown in Figure 5.10, bacterial cell membranes are damaged by HVI and thus torn and finally pin-holed (electroporation). This electroporation of cell membrane by HVI has been proposed as a main mechanism of this microorganism inactivation.

Kim et al. (2011) studied the disinfection of *Escherichia coli* using HVI. They used square-wave pulses of 5–20 kV/cm of electric field to inactivate the model microorganisms. They suggested disinfection kinetics and showed a possibility of membrane biofouling control by HVI. The HVI technique was introduced by Lee and Chang (2014) for the purpose of fouling control in MBR. HVI was applied to mixed liquor of activated sludge instead of a model microorganism. Exponentially decayed-wave form pulses for 10–20 kV/cm of electric field and 20–70 μs pulse durations were used. They reported that the flux recoveries after HVI induction were always higher than those of the control. They also found that the MLSS concentration decreased with increasing HVI contact time, while the concentrations of soluble COD, total nitrogen (TN), total phosphorus (TP), polysaccharide, and protein in the bulk solution increased, strongly indicating that the flocs and cells were damaged by the HVI induction. These results suggest that HVI induction led to sludge solubilization, which loosened the tightly deposited cake layer on the membrane surface, hence allowing it to be easily dislodged from the membrane surface. HVI induction resulted in mitigation of biofouling by means of removing the solubilized bio-cake on the membrane surface. Even though the HVI application to MBR is still in its initial stage of research and development, this study supports the potential use of the HVI technique as an alternative strategy for fouling control in MBRs and for sludge.

## 5.3.5 Membranes and Module Modification

5.3.5.1 Membranes Modification

Physicochemical modifications of membrane materials have been tried to improve performances of membrane processes for a long time. Although surface morphology, structure, charge, and roughness of membranes are subject to be changed, an improvement of surface hydrophilicity is a key factor to get a better flux and antifouling performance. Surface modifications of hydrophobic to hydrophilic membranes are usually achieved by coating or grafting a functional group on the prepared membrane surface. Numerous studies dealing with surface modification of membranes have focused on changes in hydrophilicity through versatile methods. Surface modification of PVDF, the most frequently used membrane material in MBR plants worldwide, is well reviewed and documented by Liu et al. (2011). Patterned morphology on membrane surfaces such as pyramid, prism, and embossing patterns, using a lithographic method, was developed recently (Won et al., 2012). Deposition of microbial cells on the patterned membrane was significantly reduced compared to that on the flat membrane in MBR. They explained this was attributed to hydraulic resistance of the apex of the patterned surface, which induced local turbulences.

In contrary to the conventional ways of surface modification, researchers are focusing on the application of nanomaterials to modify the membrane properties thanks to the recent remarkable developments of nanotechnologies. Silver nanoparticles (nAg), titanium oxide (TiO_2) nanoparticles, carbon nanotube (CNT), and fullerene (C_{60}) could be potential candidates expected to show an improved performance when used to modify the membrane properties.

For a long time, it has been well known that silver has bactericidal abilities. Yang et al. (2009) proposed a biofouling control approach by surface modification of a reverse osmosis (RO) membrane and spacer with nAg coating. They showed that the nAg coated membranes and spacers performed better than the unmodified membrane and spacer in terms of slower decrease in permeate flux and TDS rejection. They concluded that the nAg coating technique is challenging for biofouling control in seawater desalination. Chae et al. (2009) investigated the effect of fullerene C_{60} on biofouling of microfiltration membranes with a model microorganism *E. coli* K12. They reported that C_{60} inhibited microbial respiratory activity and/or attachment to the membrane surface. They suggested that C_{60} might be useful as an antifouling agent to prevent membrane biofouling. Kwak et al. (2001) fabricated hybrid organic/inorganic RO membranes composed of aromatic polyamide thin films underneath titanium dioxide (TiO_2) nanosized particles. They found that the TiO_2 composite membrane showed improved water flux and photocatalytic bactericidal efficiency under UV illumination. Kim et al. (2012) synthesized a thin-film nanocomposite membrane through an interfacial polymerization of a support layer containing multiwall carbon nanotubes

(MWCNTs) and a thin-film layer containing nAg particles. They found that membrane permeability of the composite membrane was enhanced compared to a non-CNT matrix through the diffusive tunnel effects of MWCNTs. The nAg particles in the thin-film layer enhanced membrane permeability and surface hydrophilicity, and provided the composite membrane with antibacterial and antifouling properties. Celik et al. (2011) synthesized a blended membrane with MWCNTs and polyethersulfone (PES) by phase inversion. Increased hydrophilicity of the blended membrane led to a higher flux and slower fouling rate than intact PES membrane.

It has been known that TiO_2 shows a self-assembly behavior on the surface of polymeric membranes having the functional groups such as carboxyl, sulfone, and ether. Self-assembled composite membrane can be made by bonding the sulfone group (or ether groups) in the membrane surface to Ti^{4+}; nanoparticles. Figure 5.11 shows the self-assembly mechanism of TiO_2 nanoparticles: (a) sulfone and ether groups bond to Ti^{4+}; (b) hydrogen bonds between sulfone and ether to the surface hydroxyl group of TiO_2. Luo et al. (2005) reported that modification of a PES membrane by self-assembled TiO_2 nanoparticles enhanced the membrane hydrophilicity, suggesting it as a positive antifouling composite membrane. Kim and Bruggen (2010) reviewed the manufacturing procedures and performance evaluation of the hybrid nanoparticle membranes.
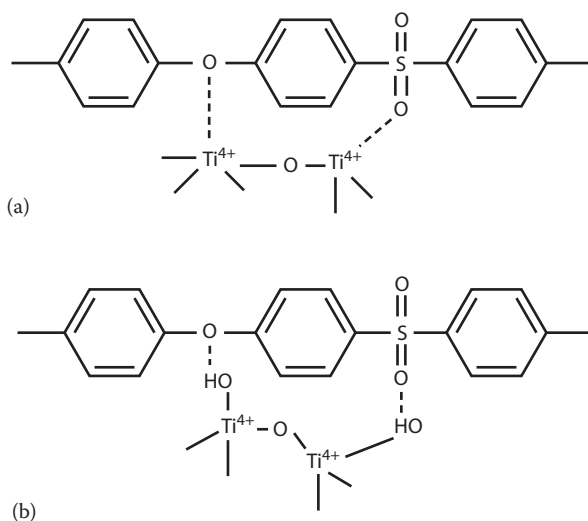

Figure 5.11   Mechanism of self-assembly of TiO_2 nanoparticles: (a) by a coordination of sulfone group and ether bond to Ti^{4+}; (b) by a hydrogen bond between sulfone group and ether bond and surface hydroxyl group of TiO_2. (Adapted from Luo, M.-L. et al., *Appl. Surf. Sci.*, 249, 76, 2005.)

Although many studies have been made to develop low fouling membranes using nanoparticles or nanotubes, direct application of those technologies to MBR or water treatment plants has not been reported yet, indicating that further research work and development is still needed.

5.3.5.2 Modification of Membranes Module

Optimization and modification of module configuration attempts to improve membrane performance. Particularly, membrane fouling can be reduced by increasing turbulence near membrane surfaces via rotation of the membrane or spacer or using a helical membrane.

Figure 5.12 shows the detail structure of a vortex generating membrane module (FMX, BKT Inc.). The vortex generators placed between membranes are driven by the center drive shaft. They create Kármán vortices at the membrane interface without being in contact with the membranes, which maintains the foulants in suspension to be swept away by the bulk flow. Kang et al. (2011) used flat UF membranes equipped with rotating vortex generators for the filtration of anaerobic digestion sludge, which allows the membrane system to cope with high solid concentration feeds up to 5%. Helical-structured membrane systems proposed by Jie et al. (2012) showed increased flux without increasing aeration intensity. The system consists of helical-supporting spacers and membranes. They explained that rotational flows near membrane surfaces were generated due to the helical structure. The enhanced wall shear stresses resulted in increased membrane permeability.
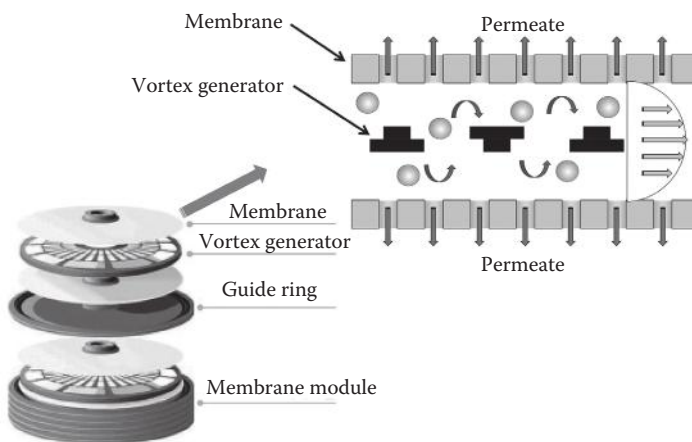
Figure 5.12   Schematic of the vortex generating membrane module. (Photo courtesy of BKT Inc.)

Problems

5.1   Complete the following table.

Compounds	Molecular Weight	Chlorine Equivalent	Actual Chlorine (%)	Available Chlorine (%)
NaOCl	74.5	2	47.7	95.4
Cl$_2$				
ClO$_2$				

5.2   A WWTP treating 2000 m³/day of municipal wastewater employs a submerged MBR equipped with flat and frame-type membrane modules. Calculate the SAD$_m$, SAD$_p$, and the specific energy consumption (kWh/m³) required for 1 day of aeration in the membrane tank only. Assume the following:

   a.   The pressure loss at the outlet of the blower is 90,600 N/m².
   b.   Depth of the blowers is 3 m.
   c.   The efficiency of the blowers and pump is 0.4.
   d.   Air flow rate 120 Nm³ of air/h.
   e.   Mean operating flux is 30 LMH.
   f.   HRT in aeration tank is 4 h.
   g.   Water density is 1000 kg/m³.

5.3   To determine the compressibility of activated sludge suspensions that are delivered from different WWTPs, specific cake resistance values are determined by a series of filtration experiments. Using the data in the following table, calculate the compressibility of each activated sludge suspension.

Pressure (kPa)	Specific Cake Resistance (α, m/kg)		
	Solution A	Solution B	Solution C
100	1.20E+11	2.00E+13	5.20E+14
200	4.00E+11	3.90E+13	6.40E+14
300	7.40E+11	5.95E+13	7.70E+14
400	1.10E+12	8.06E+13	9.05E+14
500	1.56E+12	1.02E+14	1.03E+15
600	1.92E+12	1.25E+14	1.19E+15

5.4 Sodium hypochlorite (NaOCl) is a chemical frequently used in MBR cleanings. NaOCl dissociates to hypochlorate (OCl⁻) and sodium ion in solution. The hypochlorate equilibrates with hypochlorous acid (HOCl) and protons (H⁺) in aqueous solution. If the total concentration of hypochlorous acid (C_T) is 10 mM, determine pH and the equilibrium concentration of HOCl and OCl⁻ at 20°C. The dissociation constant of hypochlorous acid at this temperature is 2.7×10^{-8} mol/L.

5.5 EC-MBR is one of the alternatives for fouling control using applied DC to a membrane system. An EC-MBR is designed and made at lab scale. Determine the electricity consumed per unit time of operation and the amount of aluminum that dissolves from the electrodes. Assume the following:

a. Electrodes (one anode and cathode pair) are made of aluminum
b. Electrode area: 7×5 cm²
c. 0.7 A of current is applied to the aluminum electrodes
    i. Applied voltage is 30 V
    ii. Volume of the activated sludge tank is 1 L
    iii. 60 min of operation

5.6 Hypochlorite is selected as a chemical to control fouling in an MBR plant. Preliminary studies found that the chlorine dose, 1000 mg/L, is good enough for recovering the declined flux. The hypochlorite solution is 75% available chlorine and has a specific gravity of 1.25. If 1 m³/day of the hypochlorite solution is needed for chemical cleaning, how many tons (m³) of hypochlorite are used per day to make a hypochlorite cleaning solution for chemical cleaning in this MBR plant?

5.7 An MBR plant is currently producing excess sludge at a rate of 0.4 kg sludge/m³ of influent. The average daily wastewater flow rate is 5500 m³/day. What will be the total amount of sludge produced per month in m³?

5.8 Regulations on the allowable nutrient concentration in secondary effluent have continually become more stringent due to concerns about the eutrophication of receiving water bodies. An MBR plant obtaining low levels of P removal due to long SRT operation is going to install a posttreatment chemical addition process for P removal. Ferric chloride, $FeCl_3$, is selected as the chemical to precipitate the phosphates in the effluent. Determine the daily requirements of $FeCl_3$ and the sludge production. Assume the following:

a. Orthophosphate concentration in permeate is 2.5 mg/L.
b. Effluent flow rate is 12,000 m³/day.

5.9 Determine the daily sludge production (kg sludge/day) of an MBR plant. The influent flow rate is 2000 m³/day. The MLSS concentration in the aeration tank is 4500 m/L and the aeration time (HRT) is 12 h. The SRT is 35 days and the TSS of the effluent is negligible.

5.10 Determine the shear intensity, G (s^{-1}), induced by aeration in a membrane tank. The air flow rate supplied to the tank is 2.5 L/min, the diameter of the pipe delivering the air is 0.05 m^2, the viscosity of the sludge suspension is 1.005×10^{-3} kg/m s, and the sludge density is 999 kg/m^3.

5.11 An MBR plant is operated at a constant flux mode, 45 LMH at 15°C. Correct the flux for 20°C.

5.12 Since permeate flux depends on the applied pressure, "membrane permeability" is often used to compare membrane filtration capabilities at the same pressure. Thus, the membrane permeability is defined as the flux per unit pressure. Discuss the usefulness and limitations of this term in MBR.

References

Adams, N., Cumin, J., Marschall, M., Turák, T. P., Vizvardi, K., and Koops, H. (2011) Reducing the cost of MBR: The continuous optimization of GE's ZeeWeed Technology, *Proceedings of 6th IWA Specialist Conference on Membrane Technology for Water & Wastewater Treatment*, Aachen, Germany, IWA (International Water Association), 4–7 October.

Akamatsu, K., Lu, W., Sugawara, T., and Nakao, S.-H. (2010) Development of a novel fouling suppression system in membrane bioreactors using an intermittent electric field, *Water Research*, 44: 825–830.

Aouni, A., Fersi, C., Ali, M., and Dhabbi, M. (2009) Treatment of textile wastewater by a hybrid electrocoagulation/nanofiltration process, *Journal of Hazardous Materials*, 168: 868–874.

Bani-Melhem, K. and Elektorowicz, M. (2010) Development of a novel submerged membrane elecro-bioreactor (SMEBR): Performance for fouling reduction, *Environmental, Science and Technology,* 44: 3298–3304.

Bani-Melhem, K. and Elektorowicz, M. (2011) Performance of the submerged membrane elecro-bioreactor (SMEBR) with iron electrodes for wastewater treatment and fouling reduction, *Journal of Membrane Science*, 379: 434–439.

Barllion, B., Ruel, S. M., and Lazarova, V. (2011) Full scale assessment of energy consumption in MBRs, *Proceedings of 6th IWA Specialist Conference on Membrane Technology for Water & Wastewater Treatment*, Aachen, Germany, IWA (International Water Association), 4–7th October.

Celik, E., Park, H., Choi, H., and Choi, H. (2011) Carbon nanotube blended polyethersulfone membranes for fouling control in water treatment, *Water Research*, 45: 274–282.

Chae, S.-R., Wang, S., Hendren, Z. D., Wiesner, M. R., Watanabe, Y., and Gunsch C. K. (2009) Effects of fullerene nanoparticles on *Escherichia coli* K12 respiratory activity in aqueous suspension and potential use for membrane biofouling control, *Journal of Membrane Science*, 329: 68–74.

Chang, I.-S. and Judd, S. (2002) Air sparging of a submerged MBR for municipal wastewater treatment, *Process Biochemistry*, 37(8): 915–920.

Chen, J.-P., Yang, C.-Z., Zhou, J.-H., and Wang, X.-Y. (2007) Study of the influence of the electric field on membrane flux of a new type of membrane bioreactor, *Chemical Engineering Journal*, 128: 177–180.

Evoqua Water Technologies (2014) Web page http://www.evoqua.com/en/products/ biological_treatment/membrane_biological_reactor_systems_mbr/Pages/envirex_ product_integrated_mbr.aspx.

Field, R. W., Wu, D., Howell, J. A., and Gupta, B. B. (1995) Critical flux concept for micro-filtration fouling, *Journal of Membrane Science*, 100, 259–272.

He, S., Xue, G., and Wang, B. (2006) Activated sludge ozonation to reduce sludge production in membrane bioreactor (MBR), *Journal of Hazardous Materials*, B135, 406–411.

Huang, X. and Wu, J. (2008) Improvement of membrane filterability of the mixed liquor in a membrane bioreactor by ozonation. *Journal of Membrane Science*, 318: 210–216.

Janot, A., Drensia, K., and Engelhardt, N. (2011) Reducing the energy consumption of a large-scale membrane bioreactor, *Proceedings of Sixth IWA Specialist Conference on Membrane Technology for Water & Wastewater Treatment*, Aachen, Germany, IWA (International Water Association), 4–7th October.

Jie, L., Liu, L., Yang, F., Liu, F., and Liu, Z. (2012) The configuration and application of helical membrane modules in MBR, *Journal of Membrane Science*, 392–393: 112–121.

Judd, S. (2008) The status of membrane bioreactor technology. *Trends in Biotechnology*, 26(2): 109–116.

Kang, S. J., Olmstead, K., Schraa, O., Rhu, D. H., Em, Y. J., Kim, J. K., Min, J. H. (2011) Activated anaerobic digestion with a membrane filtration system, *Proceedings of 84th Annual Conference and Exhibition of Water Environment Federation (WEFTECH)*, Los Angeles, USA, WEF (Water Environment Federation), 15–19th October.

Kim, E.-S., Hwang, G., El-Din, M.G., and Liu, Y. (2012) Development of nanosilver and multi-walled carbon nanotubes thin-film nanocomposite membrane for enhanced water treatment, *Journal of Membrane Science*, 394–395: 37–48.

Kim, J. and Bruggen, B. V. (2010) The use of nanoparticles in polymeric abd ceramic membrane structure: Review of manufacturing procedures and performance improvement for water treatment, *Environmental Pollution*, 158, 2335–2349.

Kim, J.-S., Lee, C.-H., and Chun, H.-D. (1998) Comparison of ultrafiltration characteristics between activated sludge and BAC sludge, *Water Research*, 32, 3443–3451.

Kim, J.-Y., Lee, J.-H., Chang, I.-S., Lee, J.-H., and Yi, J.-W. (2011) High voltage impulse electric fields: Disinfection kinetics and its effect on membrane bio-fouling, *Desalination*, 283, 111–116.

Kim, S. R., Oh, H. S., Jo, S. J., Yeon, K. M., Lee, C. H., Lim, D. J., Lee, C. H., and Lee, J. K. (2013) Biofouling control with bead-entrapped quorum quenching bacteria in MBR: Physical and biological effects, *Environmental Science & Technology*, 47(2), 836–842.

Kornboonraksa, T. and Lee, S. J. (2009) Factors affecting the performance of membrane bioreactor for piggery wastewater treatment, *Bioresource Technology*, 100, 2926–2932.

Kwak, S.-Y., Kim, S., and Kim, S. (2001) Hybrid organic/inorganic reverse osmosis (RO) membrane for bactericidal anti-fouling. 1. Preparation and characterization of TiO_2 nanoparticle self-assembled aromatic polyamide thin-film-composite (TFC) membrane, *Environmental Science and Technology*, 35: 2388–2394.

Lee, J.-S. and Chang, I.-S. (2014) Membrane fouling control and sludge solubilization using high voltage impulse (HVI) electric fields, *Process Biochemistry*, 49: 858–862.

Liu, F., Hashim, N.-A., Liu, Y.-L., and Li, M.-A. (2011) Review: Progress in the production and modification of PVDF membranes, *Journal of Membrane Science*, 375: 1–27.

Liu, L., Liu, J., Bo, G., Yang, F., and Chellam, S. (2012b) Fouling reductions in a membrane bioreactor using an intermittent electric field and cathodic membrane modified by vapor phase polymerized pyrrole, *Journal of Membrane Science*, 394–395: 202–208.

Liu, L., Liu, J., Gao, B., and Yang, F. (2012a) Minute electric field reduced membrane fouling and improved performance of membrane bioreactor, *Separation and Purification Technology*, 86: 106–112.

Luo, M.-L., Zhao, J.-Q., Tang, W., and Pu, C.-S. (2005) Hydrophilic modification of poly(ether sulfone) ultrafiltration membrane surface by self-assembly of TiO_2 nanoparticles, *Applied Surface Science*, 249: 76–84.

Marx, V. (2014) Stop the microbial chatter, *Nature*, 511: 493–497, 24 July.

Santos, A., Ma, W., and Judd, S. (2011) Membrane bioreactors: Two decades of research and implementation, *Desalination,* 273: 148–154.

Satyawali, Y. and Balakrishnan, M. (2009) Performance enhancement with powdered activated carbon (PAC) addition in a membrane bioreactor (MBR) treating distillery effluent, *Journal of Hazardous Materials*, 170, 457–465.

Wang, P., Wang, Z., Wu, Z., Zhou, Q., and Yang, D. (2010) Effect of hypochlorite cleaning on the physiochemical characteristics of polyvinylidene fluoride membranes, *Chemical Engineering Journal*, 162: 1050–1056.

Wei, C.-H., Huang, X., Aim, R.B., Yamamoto, K., and Amy, G. (2011a) Critical flux and chemical cleaning-in-place during the long-term operation of a pilot-scale submerged membrane bioreactor for municipal wastewater treatment, *Water Research*, 45: 863–871.

Wei, V., Elektorowicz, M., and Oleszkiewicz, J. A. (2011b) Influence of electric current on bacterial viability in wastewater treatment, *Water Research,* 45: 5058–5062.

Wu, J. and Huang, X. (2010) Use of ozonation to mitigate fouling in a long-term membrane bioreactor, *Bioresource Technology*, 101, 6019–6027.

Yang, H.-L., Lin, J.-C., and Huang, C. (2009) Application of nanosilver surface modification to RO membrane and spacer for mitigating biofouling in seawater desalination, *Water Research*, 43: 3777–3786.

Young-June, W., Jaewoo, L., Dong-Chan, C., HeeRo, C., Inae, K., Chung-Hak, L., and In-Chul, K. (2012) Preparation and application of patterned membranes for wastewater treatment, *Environmental Science and Technology*, 46(20): 11021–11027.

Zhang, K., Wei, P., Yao, M., Field, R. W., and Cui, Z. (2011) Effect of the bubbling regimes on the performance and energy cost of flat sheet MBRs, *Desalination*, 283, 221–226.

Chapter 6

Design of MBR

Over the last two decades, a surge of membrane bioreactor (MBR) installations worldwide has led to a rapid increase in MBR design and operational knowledge. Many aspects of MBR design procedures overlap with those of conventional activated sludge (CAS) systems; however, the design procedures for the pretreatment, aeration, and membrane systems vary from CAS systems and require special attention. Appropriately designing these processes leads to an increase in permeate water quality reliability, overall system robustness, and can also significantly reduce energy consumption and prolong the life of the membranes. The purpose of this chapter is to provide considerations and protocols for designing MBR plants including design principles for pretreatment systems, bioreactors, aeration systems, and membrane equipment. A design example is also provided at the end of the chapter.

6.1 Process Flow of Wastewater Treatment Plants Using MBR

Wastewater treatment using MBR technology is somewhat different from a CAS process. Primary and secondary sedimentation tanks can be omitted in MBR plants, and it reduces the footprint of the entire wastewater treatment plant significantly. Nevertheless, often a primary sedimentation tank is installed to reduce the burden of organic and solids loadings in biotreatment in MBR plants. In towns adopting combined sewer collection systems, primary sedimentation tanks can also be used to treat stormwaters as stormwater is treated by primary sedimentation tanks during heavy rain periods.
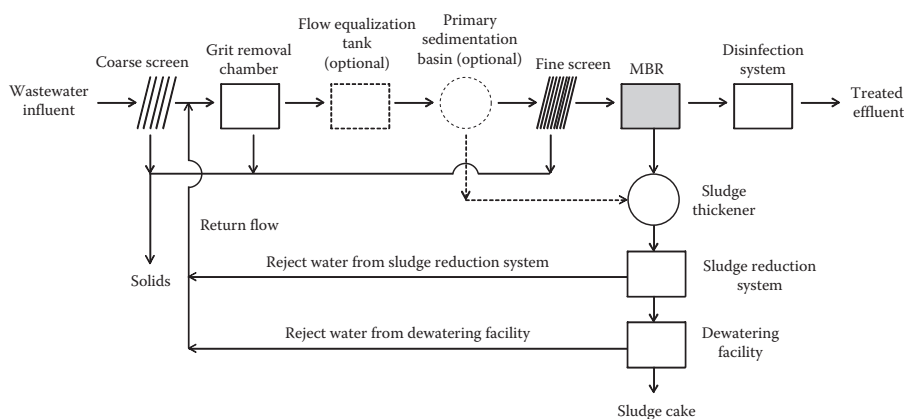
Figure 6.1 **Process flow diagram for an MBR wastewater treatment plant.**

Figure 6.1 shows a process flow schematic of a general MBR wastewater treatment plant. Wastewater collected from the wastewater collection system initially flows through coarse screens to remove large solids, and then the wastewater combined with return flow from the sludge reduction system is fed to the grit removal chamber to eliminate grit. Next, the wastewater passes through flow equalization and primary sedimentation tanks sequentially, which, however, are optional depending on the site's particular conditions. The main objective of a flow equalization tank is to generate stable flows downstream, while a primary sedimentation tank removes settleable and floating solids.

The supernatant from the primary sedimentation tank is fed to the bioreactor through fine screens that are needed to remove small-size debris to protect the membranes from fouling. In the bioreactor, oxygen-depleting organic and inorganic matters are oxidized by microorganisms. The treated water is permeated through membranes either submersed within or equipped outside the bioreactor. The final step is the disinfection system for inactivating pathogens in the permeate water. The permeate water is then discharged into receiving water bodies or beneficially reused as reclaimed water.

Solids generated during wastewater treatment should be treated or disposed of properly. Solids are generated from coarse screening, grit removal, primary sedimentation, fine screening, and bioreactor treatment. In general, solids generated from coarse screening, grit removal, and fine screening are collected and transported to a landfill site, while primary sludge from the primary sedimentation tank (Figure 6.1) and waste activated sludge from the bioreactor are further processed by thickening and dewatering before transportation to a landfill site or incinerator. After aging, dewatered sludge can also be used as fertilizer for agricultural applications.

In large-scale wastewater treatment plants, primary and waste activated sludge are often used to produce biogas via anaerobic digesters.

6.2 Pretreatment System Design

6.2.1 Wastewater Flow Rate

Determining wastewater flow rates is important for designing wastewater treatment facilities because it affects the hydraulic characteristics, sizing, and operation of the facilities (Tchobanoglous et al., 2003). For example, hydraulic retention time (HRT) is one of the design criteria for a bioreactor. A range of HRTs should be provided for proper biological treatment, and HRT is calculated by dividing the influent flow rate by the volume of bioreactor. The determination of the number of membrane modules required is another design criterion that relies on flow rates. The number of membrane modules (or required membrane surface area) is estimated by design water flux values recommended by membrane manufacturers. Because water flux is defined as the permeate flow rate per unit membrane area, reliable wastewater flow rate data is critical for the estimation.

In most cases wastewater is produced unevenly with time. In industrial settings, wastewater is produced mostly during the work hours, while minimal wastewater is produced during off hours. In municipal settings, wastewater is produced more evenly than in industrial settings. Nevertheless, the production of municipal wastewater tends to decrease after midnight until daybreak. Typical hourly variation of flow rates (diurnal variation) for a municipal wastewater treatment plant is illustrated in Figure 6.2. The variation is comparatively larger in small towns than in big cities.

Wastewater flow rates also vary daily, seasonally, and annually. If so, how can we determine the wastewater flow rates and flow rate variations quantitatively to produce a good design? Measurements of flow rates over a period of time would be the best way for the determination. However, if it is impossible to measure the flow rates directly, the determination should be based on previous experiences and/or statistical data. For industrial settings, there are several datasets available for different industries. For example, cheese production factories produce 0.7–2.0 m^3 wastewater per ton of cheese production and its concentration is generally 1–2 kg BOD_7 per m^3 of wastewater (Henze et al., 2000). Therefore, we can project the wastewater flow rate and loading rate (BOD_7 concentration) based on cheese production.

For municipal settings, population data along with wastewater volume production per capita and loading rates per capita are used to estimate the wastewater flow and loading rates. In addition, we need to acknowledge the variation in
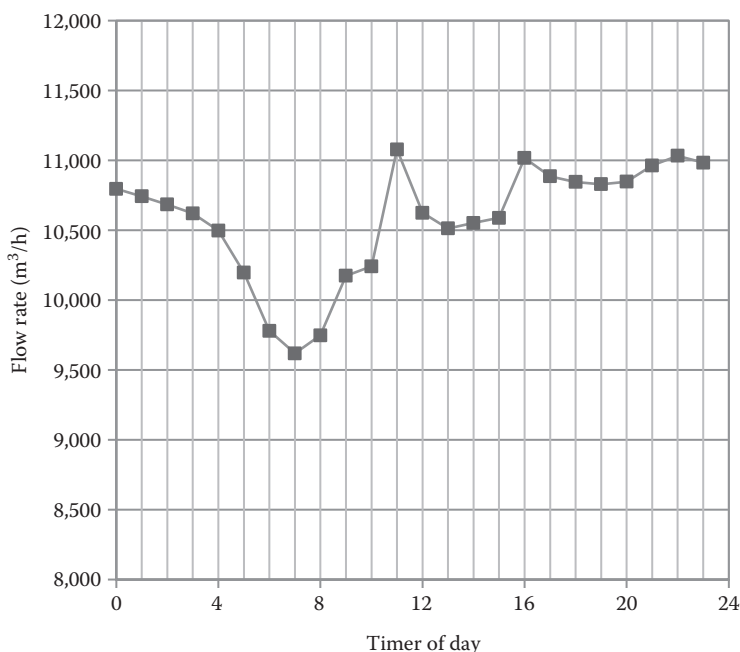
Figure 6.2 Typical hourly variation of flow rate in a large-scale municipal WWTP. (The data were obtained from the Jungnang WWTP in Seoul, Korea, December 2013.)

water consumption for different countries and wastewater origins (e.g., domestic, industrial, infiltration, stormwater, etc.). Detailed data about wastewater flow rates depending on industrial source, country of origin, infiltration, exfiltration, etc., are available in other excellent books including *Wastewater Engineering Treatment and Reuse* (Tchobanoglous et al., 2003) and *Wastewater Treatment* (Henze et al., 2000).

   Flow rate measurements collected over a period time can be analyzed using statistical methods to estimate various flow rates including daily average flow rate and daily maximum flow rate. Municipal wastewater flow rates are generally distributed normally or lognormally, which can be evaluated graphically. Probability curves are used for the analysis following the procedure described:

1. Collect flow rates periodically (e.g., daily, weekly, monthly, etc.).
2. Order the values of flow rates from the lowest to the highest. Then, assign ranks serially to the measurements.
3. Calculate the percentile of the flow rates (i.e., the probability of a flow rate equal or less than the designated flow rate) based on the following equation:

$$\text{Percentile (\%)} = \left(\frac{m}{n+1}\right) \times 100 \qquad (6.1)$$

where
   m is the rank serial number
   n is the number of total measurements (flow rates)

4. Plot the data using arithmetic- or log-probability-scaled graph paper. Plot the percentiles on the y-axis and the flow rates on the x-axis. (To test the lognormal distribution using spreadsheet software, first plot the normal distribution then transform the x-axis to a log scale.)

If the dataset shows a linear trend in the arithmetic paper, the flow rates are assumed to be distributed normally. If the linearity is better in the log-probability paper, the flow rates are assumed to be distributed lognormally. The average and the standard deviation of the wastewater flow rates can also be estimated from the probability plots. For a dataset showing normal distribution, the average ($\overline{X}$) and standard deviation(s) can be obtained using the following equations:

$$\overline{X} = P_{50} \qquad (6.2)$$

$$s = P_{84} - P_{50} \quad \text{or} \quad P_{50} - P_{16} \qquad (6.3)$$

where
   P_{50} is the flow rate corresponding to 50% probability
   P_{84} is the flow rate corresponding to 84% probability
   P_{16} is the flow rate corresponding to 16% probability

For a dataset showing lognormal distribution, the geometric average ($\overline{X}$) and geometric standard deviation (s) can be obtained using the following equations:

$$\log \overline{X} = \log P_{50} + 1.1513 \,(\log s)^2 \qquad (6.4)$$

$$\log s = \log P_{84} - \log P_{50} \text{ or } \log P_{50} - \log P_{16} \qquad (6.5)$$

The average flow rate is generally used to design a bioreactor, while the maximum flow rate (flow rate corresponding to a probability of ~90%) is used to design the pretreatment systems such as the screening and grit chamber. Both the average and maximum flow rates are used for the design of primary sedimentation tank and membrane system. Specifically, the peak flow rate and its duration are important in the design of the membrane systems.

Example 6.1

The data in the following table are the average monthly influent flow rates for a period of one year at a local wastewater treatment plant: (1) How are the monthly flow rates distributed following a normal or lognormal distribution? Use graphical methods by plotting the monthly influent flow rates vs. the corresponding probabilities on arithmetic and log-probability papers and check the linearity. (2) What is the monthly flow rate average and standard deviation? If the data are distributed normally, determine the arithmetic mean and standard deviation; if the data are lognormally distributed, determine the geometric mean and geometric standard deviation. (3) Compare the values determined by the graphical method with the values calculated by statistical formulas.

Month	Flow Rate (m^3/month)
January	24,300
February	30,400
March	37,800
April	50,100
May	42,700
June	35,500
July	62,500
August	54,000
September	40,000
October	45,700
November	33,000
December	27,500

Solution

For the graphical solution, initially the flow rate values should be arranged in order and the probability of a flow rate equal to or less than the designated flow rate should be determined as shown in the following table:

Number (Rank)	Probability (%)	Flow Rate (m^3/month)
1	7.7	24,300
2	15.4	27,500

Number (Rank)	Probability (%)	Flow Rate (m³/month)
3	23.1	30,400
4	30.8	33,000
5	38.5	35,500
6	46.2	37,800
7	53.8	40,000
8	61.5	42,700
9	69.2	45,700
10	76.9	50,100
11	84.6	54,000
12	92.3	62,500

The dataset can now be plotted following the arithmetic and log-probability papers to test whether the flow rates are distributed normally or lognormally. As shown in the following plots, it is evident that the dataset shows a better linear relationship in the log-probability plot than in the arithmetic-probability plot, which suggests the wastewater flow rates are lognormally distributed.

(a)

(b)
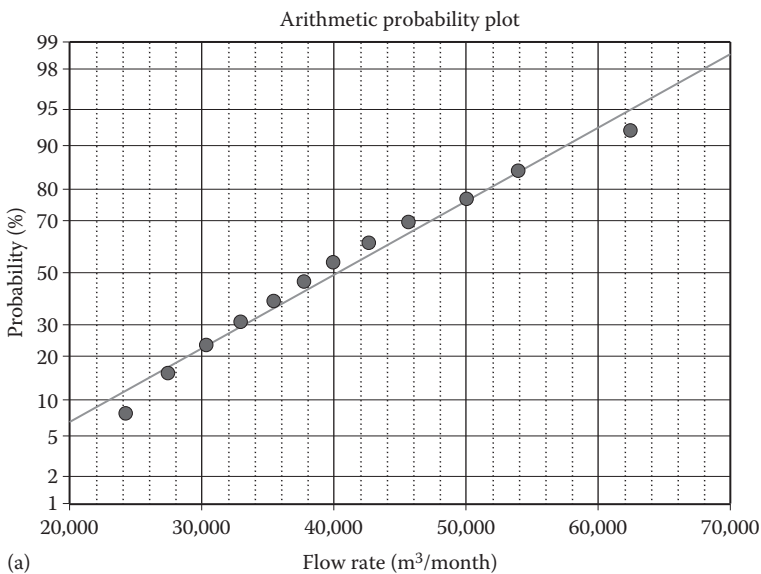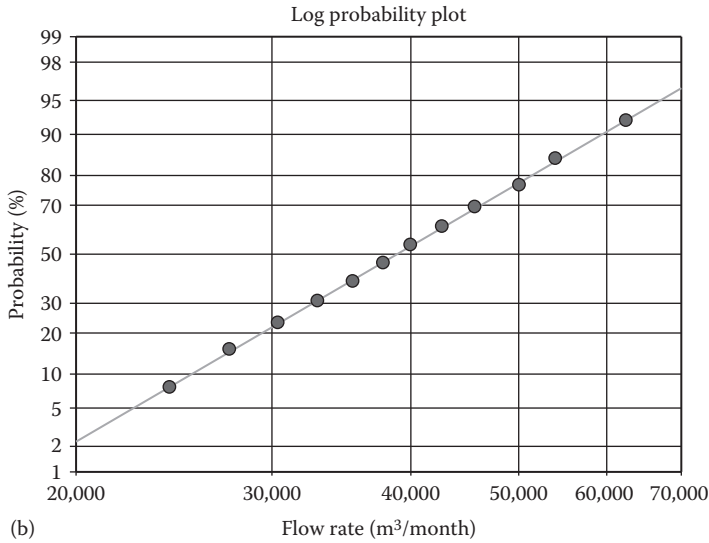
The geometric average and standard deviation can be determined graphically using the probability plot as follows:

$$\log s = \log P_{84} - \log P_{50} = \log(53{,}500) - \log(39{,}000) = 0.137$$

$$s = 1.37 \text{ m}^3/\text{month}$$

$$\log \overline{X} = \log P_{50} + 1.1513(\log s)^2 = \log(39{,}000) + 1.1513(\log 1.37)^2 = 4.61$$

$$\overline{X} = 40{,}738 \text{ m}^3/\text{month}$$

The geometric average and standard deviation can also be calculated based on statistical equations as follows:

$$\log \overline{X} = \frac{\sum \log X_i}{n} = 4.590$$

$$\overline{X} = 38{,}864 \text{ m}^3/\text{day}$$

$$\log s = \sqrt{\frac{\sum (\log X_i - \log \overline{X})^2}{n-1}} = 0.122$$

$$s = 1.325 \text{ m}^3/\text{day}$$

As we saw in this example, the graphical approach is an intuitive method to determine whether the flow rates are distributed normally or lognormally and the average and standard values obtained from the graphical approach are similar enough to those obtained using statistical equations.

6.2.2 Screens

Without proper removal, the coarse objects (rags, papers, plastics, metals, etc.) found in influent wastewater may damage downstream equipment, reduce treatment reliability, and contaminate waterways (Tchobanoglous et al., 2003). Coarse screens are installed at the headworks of wastewater treatment plants primarily to remove these materials.

In addition, hairs and fibrous matters found in influent wastewater may affect the membrane systems, especially in MBRs adopting submersed hollow-fiber membranes. The hairy and fibrous matters can wraparound the hollow-fiber bundles and inhibit the shaking movement driven by upward membrane aeration, which accelerates membrane fouling. It is a known fact that the removal of these matters is crucial for successful operation. Therefore, in many MBR designs, fine screens are installed just before the bioreactors to remove the hairy and fibrous matter.

6.2.2.1 Coarse Screens

The width of the clear openings in coarse screens range from 6 to 150 mm. Mechanically cleaned bar screens are often installed as coarse screens. The purpose of this type of screen is to accumulate the coarse objects from the wastewater inflow on the surface of the bars. Then, the mechanically operated rakes remove the accumulated objects. The location of screens, approach flow velocity, flow velocity through the racks, the clear opening width between bars, headloss through the screen, screen raking, control, etc., should all be considered when designing bar screens.

Coarse screens are often installed at the beginning of wastewater facilities because coarse objects may foul the subsequent processes. The approach velocity should be large enough to prevent the settling of coarse objectives before the bars in the channel (generally, >0.4 m/s), while the flow velocity through the racks should be less than a certain value to minimize the passage of coarse objectives through the bars (generally, <0.9 m/s) (Tchobanoglous et al., 2003). General guidelines for the design of mechanically cleaned bar screens are introduced in Table 6.1 and Figure 6.3.

The accumulation or clogging of coarse objects on the bars increases headloss across the bar screen. Headloss buildup exceeding a certain level may endanger the stability of the bar screen structure and/or increase the risk of an overflow of wastewater from the channel onto the ground. Cleaning the accumulated or clogged coarse objects from the bar screen regularly by detecting headloss buildup or by a set time interval is thus required. Headloss of 150 mm is generally used as a maximum value for triggering a screen cleaning. Headloss can be calculated based on the approach velocity and the velocity through the racks using the following equation:

Table 6.1 Design Factors and Their Recommended Design Values for Mechanically Cleaned Coarse Bar Screens

Design Factors	Values
Approach velocity, m/s	0.4–0.6
Velocity through rack, m/s	0.6–1.0
Bar size	
Width, mm	8–10
Depth, mm	50–75
Clear spacing between bars, mm	10–50
Slope from horizontal (Figure 6.3),°	75–85
Allowable head loss (clogged screen), mm	150
Maximum head loss (clogged screen), mm	800

Source: Qasim, S., *Wastewater Treatment Plants: Planning, Design, and Operation*, 2nd edn., CRC Press, Boca Raton, FL, 1998.
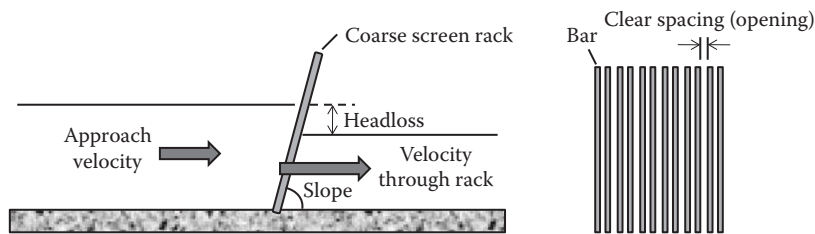
Figure 6.3 Schematic showing the design considerations for coarse screen racks.

$$h_L = \frac{1}{C}\left(\frac{V^2 - v^2}{2g}\right) \tag{6.6}$$

where
  h_L is the headloss, m
  C is the discharge coefficient, unitless
  V is the approach velocity, m/s
  v is the velocity through rack, m/s
  g is the acceleration due to gravity, 9.81 m/s^2

The discharge coefficient (C) is determined experimentally. Typical values of the coefficient are 0.7 for clean water with completely clean screens and 0.6 for clogged screens (Tchobanoglous et al., 2003).

6.2.2.2 Fine Screens

The width of clear spacing in mesh wire screens or the diameter of the holes in perforated plate screens typically range from 0.2 to 6 mm. Generally, MBR plants using hollow-fiber membranes are more sensitive to fouling from hairy materials than those using flat-sheet membranes and therefore require finer screens. Based on a survey of MBR plants operated in Europe by Schier et al. (2009), perforated-hole or meshed-hole-type fine screens are preferred over slit-type fine screens (Figure 6.4) as the former showed better performance than the latter in removing hairy materials. The design criteria and estimation of headloss across fine screens are quite different from those of coarse screens and usually follow the manufacturers' specific guidelines. Typical fine screens equipped in MBR plants are presented in Figure 6.5.

(a)   (b)   (c)   (d)
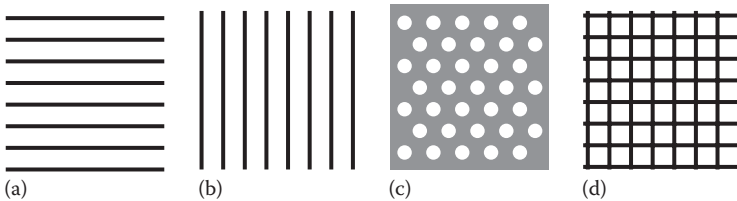
Figure 6.4   Types of fine screens used in MBR plants: (a) horizontal slit, (b) vertical slit, (c) perforated hole, and (d) meshed hole. (Adapted from Frechen, F.B. et al., *Desalination*, 231, 108, 2008.)


(a)   (b)   (c)
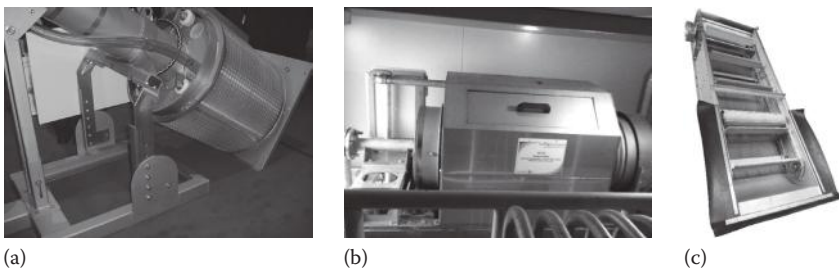
Figure 6.5   Recommended fine screens in MBR plants: (a) Huber's Rotamat screen (Photographed by Dong Myung Engineering and Construction), (b) rotary drum screen (Photographed by TSK water), and (c) Incla panel screen. (Courtesy of Blue Whales Screen.)

Fine screens also remove biological oxygen demand (BOD) and total suspended solids (TSS) in wastewater during the removal of small-sized particulate matters as well as hairy or fibrous materials. Although the removal of BOD and TSS varies depending on wastewater collection systems, wastewater travel time, and types of screen, typically, 5%–50% of BOD and 5%–45% of TSS can be removed via fine screens (Tchobanoglous et al., 2003). It is, therefore, required to consider the removal of BOD and TSS by fine screening during the design of bioreactors.

6.2.3 Grit Removal Chamber

Wastewater influent includes heavy solid materials such as sand, gravel, and cinders (collectively we call this grit). Grit should be properly removed from wastewater influent to protect downstream mechanical equipment from abrasion and accompanying malfunction. Although some MBR plants, especially small-scale MBR plants, omit grit removal facilities, grit removal chambers are generally installed in MBR plants.

Horizontal-flow grit removal chambers and aerated grit removal chambers are the two common types of systems for large-scale MBR plants (Figure 6.6a, b).
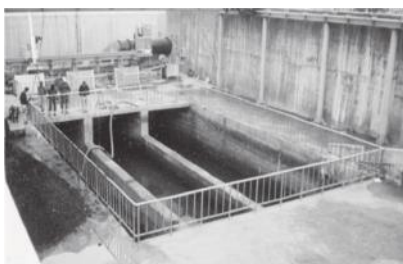
(a)   (b)

(c)

Figure 6.6   Grit removal chambers: (a) horizontal-flow grit removal chamber, (b) aerated grit removal chamber, and (c) vortex-type grit removal chamber. (All of the pictures were photographed by Dong Myung Engineering and Construction.)

Vortex-type grit removal chambers are typically installed at small-scale plants (Figure 6.6c). Horizontal-flow grit removal chambers include a long rectangular tank in which grit settles to the bottom of the tank during the travel of the influent flow. Engineers assume that the settlement of grit follows type 1 settling (i.e., independent settling), so the settling velocity of the smallest grit that is removed 100% of the time is an important parameter in designing a horizontal-flow grit removal chamber.

In grit removal chambers, the settled grit tends to be coated with organic materials which tend to be putrefied and generate bad odors. It is generally required to wash the coated organic matters to avoid odors during disposal. On the other hand, in the aerated grit removal chambers, the organic materials are scraped off the grit due to shear stress imposed on the grit surface when the wastewater influent travels through the rectangular tank.

In an aerated grit removal chamber, aeration diffusers are installed along one side of the tank to generate a spiral wastewater flow pattern perpendicular to the flow during which lighter particles pass through the tank, while heavier particles (generally, >0.21 mm diameter) settle to the bottom of the tank. Design information is available for the two types of grit removal chambers in other references (Reynolds and Reynolds, 1996; Tchobanoglous et al., 2003).

6.2.4 Flow Equalization Tank

As discussed in Section 6.2.1, wastewater flow rates vary hourly especially in wastewater treatment plants especially located in small towns. Membranes are vulnerable to fouling especially during high-flux operational periods so it is recommended to operate the membranes below the critical flux (refer to Section 4.1). Although it is possible to design the bioreactor and the number of membrane modules based on the hourly peak flow, this approach tends to result in an overly designed bioreactor and membrane system, which increases capital expenditure for construction of the MBR plant.

If the peaking factor (e.g., hourly peak flow per average daily flow) is >1.5, generally, it is economical to install a flow equalization tank instead of increasing the size of the bioreactor and the number of membrane modules. Flow variation can be dampened by installing a flow equalization tank, which reduces the required size of the bioreactor and the number of membrane modules. In addition to dampening flow variation, a flow equalization tank moderates solids and organic loadings. It is generally reported that 23%–47% of suspended solids and 10%–20% of BOD are dampened by flow equalization tanks (Reynolds and Reynolds, 1996), which in turn enhances the wastewater treatment efficiency and reliability.

Two types of arrangements for the flow equalization tank are available: in-line and side-line arrangements (Figure 6.7). In the in-line arrangement, all of the wastewater is directly fed to the flow equalization tank where it is pumped downstream by a controlled-flow pumping system to generate a constant flow rate. In the side-line arrangement, wastewater is diverted to the flow equalization tank only
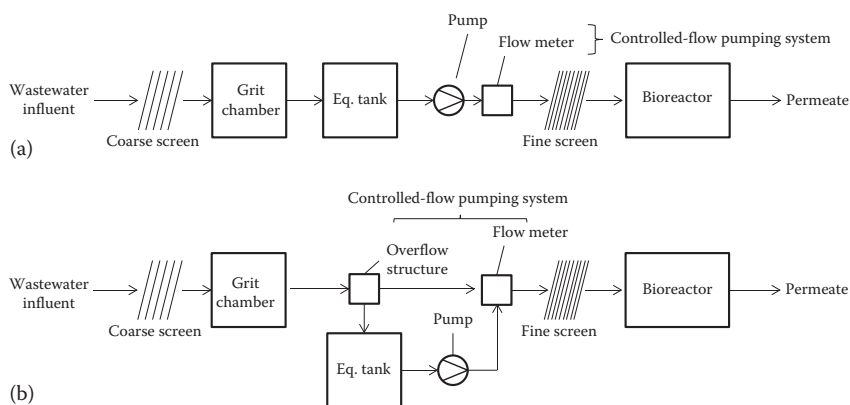
Figure 6.7 Flow equalization tank: (a) in-line arrangement and (b) side-line arrangement.

when the flow rate is greater than the average hourly flow rate. Wastewater in the flow equalization tank is then pumped into the mainstream by a controlled-flow pumping system when the flow rate is less than average hourly flow rate. The side-line arrangement of flow equalization results in lesser stabilization of suspended solids and a BOD than that of an in-line flow equalization.
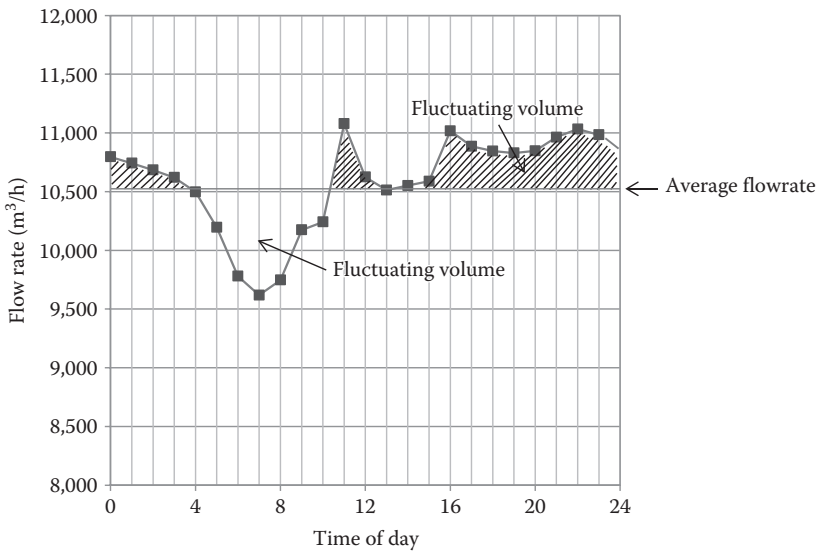
The volume of the flow equalization tank is designed based on the fluctuating flow volume that can be determined based on a hydrograph recording the flow rate distribution over a time period. Figure 6.8 shows an example of flow rate changes in a day. By drawing a parallel line indicating the average hourly flow rate, it is possible to calculate the fluctuating volume of a flow equalization tank. The shaded area over the parallel line is the same as the sum of areas below the parallel line and corresponds to the fluctuating volume. The area can be approximated by segmenting the area and then adding up the areas of the segments above the average flow rate line (refer to Example 6.2).

Example 6.2

The data in the following table are wastewater flow rate distributions for a day in a wastewater treatment plant. Assuming the observed distribution of the flow rates is a typical pattern for the wastewater treatment plant, calculate the fluctuating volume (or minimum tank volume required) of an in-line flow equalization tank:

Time	Flow Rate (m³/h)	Time	Flow Rate (m³/h)
0 midnight	1300	12 noon	1900
1	1100	13	1800

Figure 6.8   Determining the fluctuating flow volume for designing a flow equal-ization tank using a hydrograph.

Time	Flow Rate (m³/h)	Time	Flow Rate (m³/h)
2	930	14	1750
3	760	15	1650
4	650	16	1630
5	600	17	1600
6	700	18	1640
7	900	19	1680
8	1200	20	1700
9	1500	21	1720
10	1800	22	1600
11	1950	23	1540

Solution

In order to estimate the fluctuating volume or tank volume, initially a hydro-graph and the average hourly flow rate should be calculated. The average hourly flow rate for the 24 measurements is 1400 m³/h. The fluctuating volume is

then estimated by calculating the area above the average hourly flow rate in the hydrograph. The volume can be approximated by summing up the differential volumes (Figure 6.9).

$$\text{Fluctuating volume} = 100 + 400 + 550 + 500 + 400 + 350 + 250 + 230 + 200$$

$$+ \ 240 + 280 + 300 + 320 + 280 + 140 = 4460 \ \text{m}^3$$

The volume calculated based on the area above the line of average hourly flow rate is the same as the volume calculated based on the area below the line of average hourly flow rate.

$$\text{Fluctuating volume} = -100 - 300 - 470 - 640 - 750 - 800 - 700 - 500 - 200$$

$$= -4460 \ \text{m}^3$$

Time	Flow Rate (m³/h)	Differential Flow Rate[a] (m³/h)	Differential Volume[b] (m³)
0 midnight	1300	−100	−100
1	1100	−300	−300
2	930	−470	−470
3	760	−640	−640
4	650	−750	−750
5	600	−800	−800
6	700	−700	−700
7	900	−500	−500
8	1200	−200	−200
9	1500	100	100
10	1800	400	400
11	1950	550	550
12 noon	1900	500	500
13	1800	400	400
14	1750	350	350
15	1650	250	250
16	1630	230	230

Time	Flow Rate (m³/h)	Differential Flow Rate[a] (m³/h)	Differential Volume[b] (m³)
17	1600	200	200
18	1640	240	240
19	1680	280	280
20	1700	300	300
21	1720	320	320
22	1600	200	200
23	1540	140	140

[a] Differential flow rates are the differences between measured and average hourly flow rates.

[b] Differential volumes are the multiplication between the differential volume and time difference (i.e., 1 h).
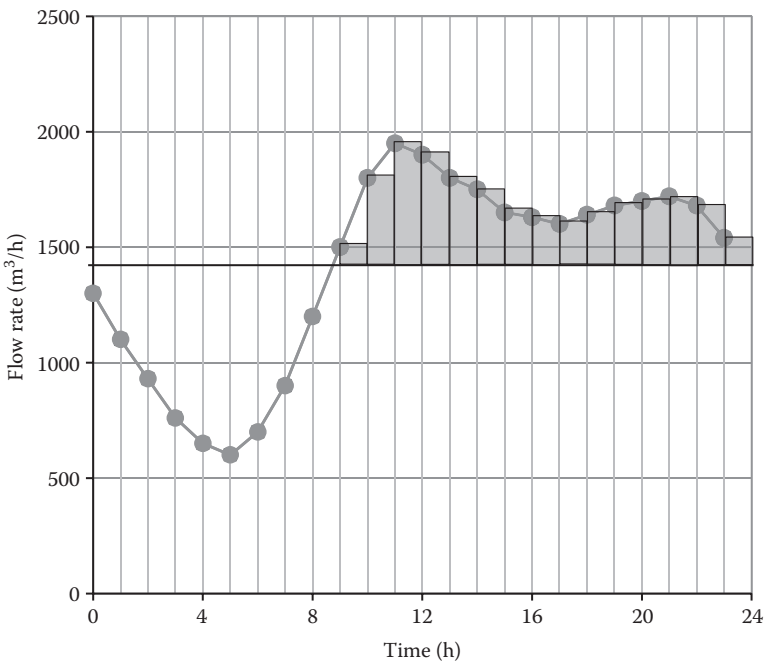
Figure 6.9 **Estimation of fluctuating volume using the profile of hourly flow rates.**

6.3 Bioreactor Design

Designing a bioreactor includes determining the reactor size and oxygen requirement for aerobic treatment of oxygen-depleting contaminants based on the characterization of the influent wastewater, permeate water quality requirements, and daily sludge production. The protocol for the design of a bioreactor is quite different depending on whether the bioreactor is a newly built one or is a retrofitted reactor.

Reactor volume is difficult to change when retrofitting existing treatment plants, while it is quite flexible for a newly built one. For a newly built bioreactor, the target mixed liquor suspended solids (MLSS) concentration and solid retention time (SRT) are determined beforehand. Then, sizing the bioreactor and determining the oxygen requirement follow. For a retrofitted bioreactor, the MLSS concentration is determined during the design process based on the predetermined reactor volume and design SRT. Figure 6.10 shows a general procedure for the design of a bioreactor for the two cases.

6.3.1 Characterization of Influent Wastewater Quality: Determination of Biodegradable COD and TKN

The appropriate design for a bioreactor and accurate estimation of permeate water quality start from the characterization of the influent wastewater quality. Conventionally, organic, nitrogenous, and phosphorus matter in the influent wastewater should be determined. This book uses chemical oxygen demand (COD) for the organic matter instead of BOD like other design books because COD is more accurate than BOD measurements and is much quicker to obtain. The influent COD is often classified based on its filterability, through a 1 μm-size GF/C filter (soluble vs. particulate COD), and biodegradability (biodegradable vs. nonbiodegradable COD). Therefore, the total COD of influent wastewater can be calculated as follows:

$$\text{Total COD} = \text{Soluble and biodegradable COD} \,(S_{0,b})$$
$$+ \text{Particulate and biodegradable COD} \,(X_{0,b})$$
$$+ \text{Soluble and nonbiodegradable COD} \,(S_{0,i})$$
$$+ \text{Particulate and nonbiodegradable COD} \,(X_{0,i})$$

$S_{0,b}$ is readily biodegradable organic matter which can be metabolized by microorganisms quickly, while $X_{0,b}$ cannot be readily used for the growth of microorganisms but can be used after microbial disintegration and hydrolysis. Although $S_{0,b}$ and $X_{0,b}$ are different in terms of the microbial degradation rate, for simplicity, the
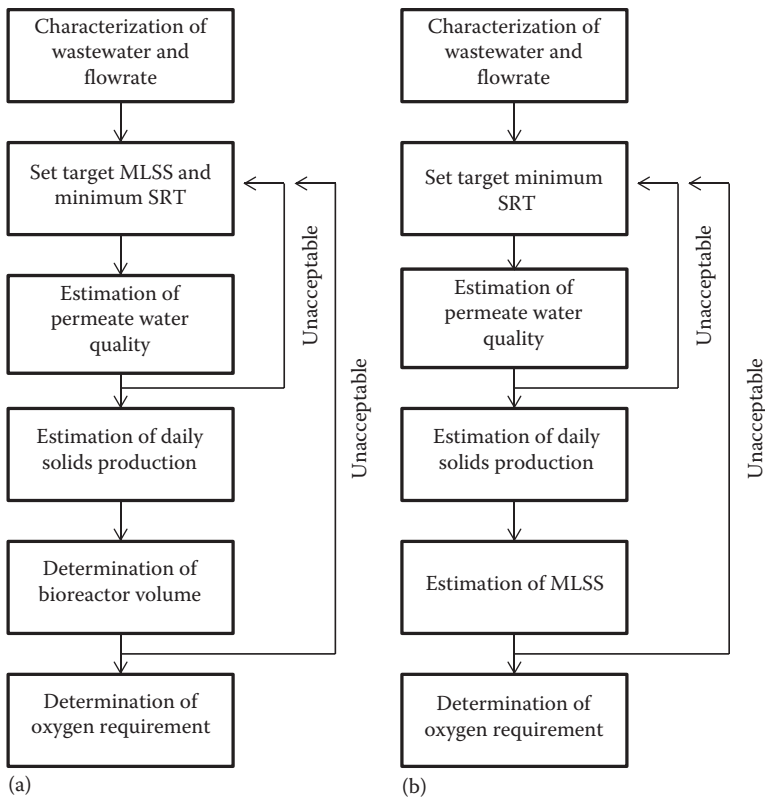
Figure 6.10 **Design process outline for a (a) newly built bioreactor and (b) for a fixed-volume (retrofitted) reactor.**

sum of them $(S_0 = S_{0,b} + X_{0,b})$ is used for the calculation of solids production in this book (refer to Section 2.3).

$S_{0,i}$ cannot be metabolized by microorganisms so $S_{0,i}$ tends to be discharged with the permeate water due to its smaller size than the membrane pore diameter. However, $X_{0,i}$ tends to be discharged with the waste activated sludge because $X_{0,i}$ cannot pass through membranes. Various methods have been proposed to analyze S_0 in the influent wastewater such as the respirometric method (Henze et al., 2000).

One simple method to classify the influent wastewater quality is to operate a laboratory-scale batch reactor filled with activated sludge and influent wastewater (unfiltered or filtered with 1 μm-size GF/C filter) for 15–20 days. For the unfiltered wastewater, the initial COD is the sum of all of the four components $(= S_{0,b} + X_{0,b} + S_{0,i} + X_{0,i})$ and the final COD corresponds to $S_{0,i}$. In addition, if we assume that the biomass increase during the experiment is negligible,

then the difference of the solids concentration between the initial and finial stages corresponds to $X_{0,i}$.

For filtered wastewater, the initial COD is the sum of two soluble components $(=S_{0,b}+S_{0,i})$ and the final COD corresponds to $S_{0,i}$. The difference between the initial and final COD values is $S_{0,b}$. The difference between total COD and the three COD components $(S_{0,i}+X_{0,i}+S_{0,b})$ corresponds to $X_{0,b}$.

Influent nitrogen is frequently classified based on organic and inorganic characteristics. Organic nitrogen in municipal wastewater mostly originates from proteins, amino acids, and urea. Around 60% of organic nitrogen is mineralized into ammonia when the wastewater reaches a treatment plant. The degree of mineralization is dependent on the length of the sewer collection system (i.e., hydraulic residence time), temperature, and wastewater characteristics. Inorganic nitrogen includes ammonia (NH_3), nitrite (NO_2^-), and nitrate (NO_3^-). However, nitrite and nitrate concentrations are very low and negligible in most influent wastewater. Therefore, total Kjeldahl nitrogen (TKN), the sum of organic nitrogen and ammonia/ammonium nitrogen, is frequently used to measure the amount of nitrogen in influent wastewater (e.g., total nitrogen $\cong$ TKN).

Similarly, the influent nitrogen can be divided into groups similar to influent COD (i.e., biodegradable vs. nonbiodegradable and soluble vs. particulate), but engineers often assume that organic nitrogen is readily biodegradable (e.g., the quantity of nonbiodegradable TKN is negligible) and soluble (e.g., the quantity of particulate TKN is negligible). During wastewater treatment, influent TKN (TKN_0) is assimilated into biomass and used as an energy source for ammonia-oxidizing bacteria (AOB).

Figure 6.11 shows the fractionation of COD and nitrogen of influent wastewater and typical corresponding values for municipal wastewater. We can deduce that influent wastewater approximately consists of 80% biodegradable COD and 20% nonbiodegradable COD. Around half of the nonbiodegradable COD ($S_{0,i}$) is expected to pass through the membranes and the other half of it ($X_{0,i}$) will contribute to solid production. For the nitrogen part, around 96% of the influent nitrogen (TKN_0) is biodegradable and nitrite and nitrate concentrations are negligible in influent wastewater.

Along with nitrogen, phosphorus is an important nutrient inducing algal blooms in water bodies if the amount of discharge is substantial. Phosphorus in wastewater exists in the form of orthophosphate, polyphosphate, and organic phosphorus, although orthophosphate constitutes the majority. pH conditions determine the form of orthophosphate (e.g., PO_4^{3-}, HPO_4^{2-}, $H_2PO_4^-$, or H_3PO_4) and also affects the efficiency of chemical precipitation when a precipitant is added for phosphorus removal. Polyphosphate is a polymer of several phosphate groups that can undergo hydrolysis in the bioreactor to form orthophosphate. Organic phosphorus can also be hydrolyzed into orthophosphate, although the magnitude of
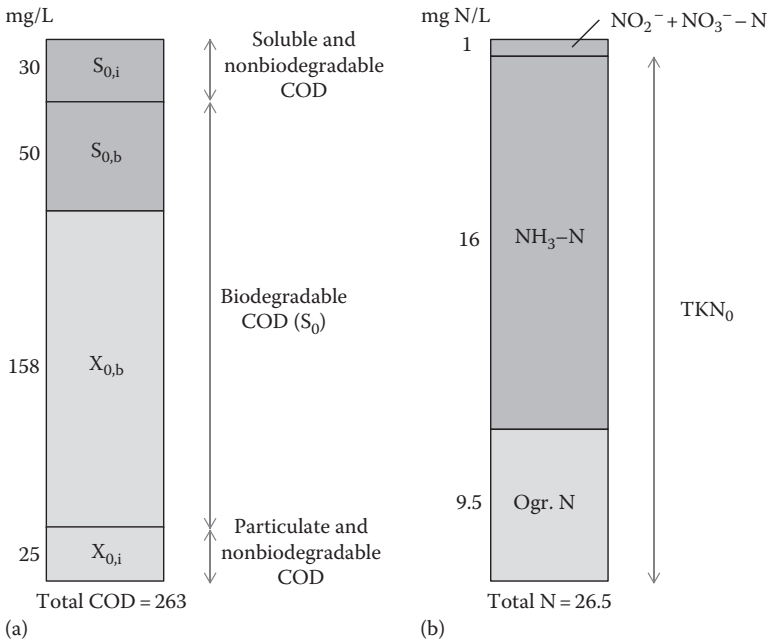
Figure 6.11 Typical fractionation and values of (a) COD and (b) nitrogen in municipal wastewater influent. (The classification and values were adapted based on the data introduced in Henze, M. et al., *Activated Sludge Models ASM1, ASM2, ASM2d and ASM3*, IWA Publishing, London, U.K., 2000.)

hydrolysis varies depending on the characteristics of the organic phosphorus and the operating conditions of the bioreactor.

6.3.2 Check Minimum SRT

The average retention time of solids in a bioreactor affects the concentration of total solids in the bioreactor and the permeate water quality. In addition, SRT can be used as an initial decision point for designing the size of a bioreactor. In principle, SRT should be long enough to retain the slowly growing microorganisms responsible for wastewater treatment. Generally, nitrifying bacteria are the limiting microorganisms that dictate the SRT required.

Nitrifying bacteria consist of two groups of aerobic autotrophic bacteria: ammonia-oxidizing bacteria (AOB) and nitrite-oxidizing bacteria (NOB). If the SRT is not long enough to retain nitrifying bacteria, nitrifying bacteria will be washed away with the waste activated sludge. It is thus required to check whether

the predetermined SRT is long enough to achieve nitrification for the given design conditions. Refer to Chapter 2 for detailed information about nitrifying bacteria. Because AOB grow slower than NOB, the growth kinetic equation for AOB is generally used to estimate the minimum SRT required for an aerobic bioreactor. The specific growth rate of AOB (μ_{AOB}) as a function of ammonia and dissolved oxygen (DO) concentrations can be explained with the following equation:

$$\mu_{AOB} = \left(\frac{\mu_{m,AOB} \cdot NH_3}{K_N + NH_3} \right) \left(\frac{DO}{K_{DO} + DO} \right) - k_{d,AOB} \tag{6.7}$$

where
  $\mu_{m,AOB}$ is the maximum specific growth rate of AOB, day^{-1}
  NH_3 is the ammonia nitrogen concentration in bioreactor, mg N/L
  K_N is the half-saturation constant for ammonia, mg N/L
  DO is the DO concentration in bioreactor, mg/L
  K_{DO} is the half-saturation constant for DO, mg/L
  $k_{d,AOB}$ is the decay constant of AOB, day^{-1}

$\mu_{m,AOB}$ is dependent upon temperature and can be calculated as follows:

$$\mu_{m,AOB}(T_2) = \mu_{m,AOB}(T_1)\theta^{(T_2 - T_1)} \tag{6.8}$$

where
  $\mu_{m,AOB}(T_2)$ is the maximum specific growth rate of AOB at temperature T_2, day^{-1}
  $\mu_{m,AOB}(T_1)$ is the maximum specific growth rate of AOB at temperature T_1, day^{-1}
  θ is the temperature correction factor, unitless

In addition to the maximum specific growth rate, other kinetic coefficients such as the half-saturation constant and the decay constant are also influenced by temperature. Table 6.2 shows the kinetic coefficients and their temperature correction coefficients for AOB applicable to MBR plants.

  SRT is equivalent to the inverse of the specific growth rate ($(dX/dt) \cdot (1/X)$) because the specific growth rate is defined as the amount of produced biomass by growth per unit biomass for a unit time, the inverse of specific growth rate is biomass per biomass production rate. Remember that SRT can be calculated as the total biomass (or solids) per biomass removal (or production) rate. Therefore, SRT can be estimated using the following equation:

$$SRT = \frac{1}{\mu_{AOB}} \tag{6.9}$$

Table 6.2   Kinetic Coefficients of Activated Sludge for AOB at 20°C

Coefficient	Unit	Range	Typical Value
$\mu_{m,N}$	g VSS/g VSS day	0.20–0.90	0.75
K_N	g NH_3–N/m³	0.5–1.0	0.74
Y_N	g VSS/g NH_3–N	0.10–0.15	0.12
$k_{d,N}$	g VSS/g VSS day	0.05–0.15	0.08
K_{DO}	g/m³	0.40–0.60	0.50
Parameters to calculate θ values			
$\mu_{m,N}$	Unitless	1.06–1.123	1.07
K_N	Unitless	1.03–1.123	1.053
$k_{d,N}$	Unitless	1.03–1.08	1.04

Source: Tchobanoglous, G. et al., *Wastewater Engineering: Treatment and Reuse*, 4th edn., McGraw-Hill, New York, 2003.

The minimum SRT required for retaining nitrifying bacteria is therefore estimated by calculating the specific growth rate of AOB based on ammonia and DO concentrations under minimum temperature conditions. Also, keep in mind that the minimum SRT based on AOB maintenance is generally long enough to maintain heterotrophic bacteria (e.g., bacteria responsible for the removal of organic matters) because most heterotrophic bacteria grow faster than nitrifying bacteria. If the predetermined SRT is shorter than the calculated minimum SRT (i.e., SRT estimated by the growth of AOB at design conditions), it is necessary to reset the SRT to greater than the minimum SRT.

In addition, because SRT affects the concentration of permeate COD (refer to Equation 2.20), check that the COD concentration at the design SRT meets the allowable maximum permeate COD concentration. SRT also influences the solids concentration in the bioreactor. It is necessary to maintain an appropriate solids concentration in the bioreactor to minimize membrane fouling, which is dependent on solids concentrations. In practice, SRT is designed to maintain solids concentrations within the range of 8,000–12,000 mg/L as MLSS to avoid membrane fouling associated with high solids concentrations.

Example 6.3

Calculate the minimum SRT for maintaining two groups of microorganisms in a bioreactor: heterotrophic and AOB. Use the following kinetic parameters for the

two groups of microorganisms for your calculation. Assume that the temperature during winter days reaches down to 5°C and that the DO level is not limiting the growth of two groups of microorganisms.

1. Heterotrophic bacteria
   a. Maximum specific growth rate at 5°C: 2.2 g VSS/g VSS day
   b. COD concentration in bioreactor: 5.0 g bCOD/m³
   c. Half-saturation constant for COD at 5°C: 20 g bCOD/m³
   d. Decay constant at 5°C: 0.07 g VSS/g VSS day
2. AOB
   a. Maximum specific growth rate at 5°C: 0.27 g VSS/g VSS day
   b. Ammonia concentration in bioreactor: 0.5 g NH_3–N/m³
   c. Half-saturation constant for ammonia at 5°C: 0.34 g NH_3–N/m³
   d. Decay constant at 5°C: 0.04 g VSS/g VSS day

Solution

The specific growth rate of the heterotrophic bacteria and AOB can be calculated based on the kinetic parameters corrected for 5°C as follows:

◼ Specific growth rate of heterotrophic bacteria

$$\mu = \left(\frac{\mu_m \cdot N}{K_S + N} \right) - k_d = \left(\frac{(2.2 \text{ g/g} \cdot \text{day})(5.0 \text{ g/m}^3)}{(20 + 5.0) \text{ g/m}^3} \right) - 0.07 \text{ g/g} \cdot \text{day}$$
$$= 0.37 \text{ g/g} \cdot \text{day}$$

◼ Growth rate of AOB

$$\mu_{AOB} = \left(\frac{\mu_{m,AOB} \cdot NH_3}{K_N + NH_3} \right) - k_{d,AOB} = \left(\frac{(0.27 \text{ g/g} \cdot \text{day})(0.5 \text{ g/m}^3)}{(0.34 + 0.5) \text{ g/m}^3} \right) - 0.04 \text{ g/g} \cdot \text{day}$$
$$= 0.12 \text{ g/g} \cdot \text{day}$$

Therefore, the minimum SRT (e.g., reciprocal of the maximum specific growth rate) is 2.7 and 8.3 days for the heterotrophic and AOB, respectively. In practice, a safety factor of 1.5–2.0 is applied to the calculation, which results in 4.1–5.4 and 12.5–16.6 days for the heterotrophic and AOB, respectively. Because the minimum SRT for AOB is much longer than that of heterotrophic bacteria, the design size of the bioreactor should be based on the minimum SRT for AOB. The minimum required SRT for the AOB in the bioreactor (i.e., 12.5–16.6 days) will not be limiting because SRT for MBR systems is generally designed for >20 days.

6.3.3 Estimation of Daily Solids Production

It is important to estimate the daily solids production in a bioreactor to design the facilities associated with solids processing such as dewatering facilities, sludge

drying equipment, and a sludge incineration plant. The solids estimation is based on the equation for total solids (X_T). In Chapter 2, we discussed how the total solids concentration in a bioreactor is estimated. Let's recap some of the important concepts of the estimation.

We can calculate the total solids concentration based on kinetic parameters, wastewater characteristics, and operational conditions of the bioreactor as follows:

$$X_T = X + X_i = \underbrace{\left(\frac{SRT}{\tau}\right)\left[\frac{Y(S_0 - S)}{1 + k_d SRT}\right]}_{\text{Active biomass solids}} + \underbrace{\frac{X_{0,i} SRT}{\tau}}_{\substack{\text{Inert materials from} \\ \text{influent inert solids}}}$$

$$+ \underbrace{f_d k_d \left(\frac{SRT}{\tau}\right)\left[\frac{Y(S_0 - S)}{1 + k_d SRT}\right] SRT}_{\text{Inert materials generated from biomass decay}} \tag{6.10}$$

where
  X_T is the total solids, mg VSS/L
  X is the biomass solids, mg VSS/L
  X_i is the inert solids, mg VSS/L
  τ is the HRT, day
  Y is the microbial growth yield, mg VSS/mg COD
  S_0 is the biodegradable substrate, mg COD/L
  S is the permeate substrate, mg COD/L
  k_d is the decay constant, day^{-1}
  $X_{0,i}$ is the inert material in influent wastewater, mg VSS/L
  f_d is the fraction of biomass that can be accumulated in a bioreactor during decay, unitless

The total solids in a bioreactor (X_T) consist of active biomass solids (X) and the solids associated with inert materials (X_i). Inert materials can be further be subdivided into two components: inert materials from influent inert solids ($X_{0,i}$) and the inert solids generated from biomass decay. All of the units for solids are mass per volume.

The daily solids production (unit: mass per time) can be estimated based on flow rate (Q), SRT, and the total solids concentration (X_T) obtained from Equation 6.10. SRT is defined as the mass of total solids in a bioreactor ($X_T V$) over the total solids wastage rate (e.g., SRT = $X_T V$/total solids wastage rate). At steady-state conditions in a bioreactor, total solids production rate should be the same as the total solids wastage rate. Therefore, the daily solids production rate (P_{X_T}) is equivalent to the total solids wastage rate and can be estimated as the following equation:

$$P_{X_T} = \frac{X_T V}{SRT} = \left(\left(\frac{SRT}{\tau}\right)\left[\frac{Y(S_0 - S)}{1 + k_d SRT}\right] + \frac{X_{0,i} SRT}{\tau} + f_d k_d\right)$$

$$\times \left(\frac{SRT}{\tau}\right)\left[\frac{Y(S_0 - S)}{1 + k_d SRT}\right] SRT\right)\left(\frac{V}{SRT}\right)$$

$$= \frac{QY(S_0 - S)}{1 + k_d SRT} + QX_{0,i} + f_d k_d \frac{QY(S_0 - S)}{1 + k_d SRT} SRT \qquad (6.11)$$

where
    Q is the influent flow rate, m³/day
    V is the bioreactor volume, m³

Example 6.4

Determine the daily solids production rate in a bioreactor for two different SRT conditions (20 vs. 30 days). The reactor should be designed based on the following conditions:

■ Solids retention time = 20 or 30 days
■ Flow rate = 1000 m³/day
■ Solids concentration in the bioreactor = 8000 mg VSS/L

The influent wastewater is characterized as follows:

■ Biodegradable COD concentration = 400 g COD/m³
■ Inert organic material concentration = 20 g VSS/m³

Use the following kinetic parameters for the calculation:

$$k = 12.5 \text{ g COD/g VSS day}$$

$$K_S = 10 \text{ g COD/m}^3$$

$$Y = 0.40 \text{ g VSS/g COD}$$

$$f_d = 0.15 \text{ g VSS/g VSS}$$

$$k_d = 0.10 \text{ g VSS/g VSS day}$$

Solution

Equation 6.11 can be used to calculate the daily solids production. It is necessary to estimate the effluent COD concentration (S) to use Equation 6.11. The effluent COD concentration for 20 days of SRT can be obtained using Equation 2.20.

$$S = \frac{K_S(1 + k_d SRT)}{SRT(Yk - k_d) - 1}$$

$$= \frac{\left(10 \text{ g COD/m}^3\right)\left[1 + \left(0.10 \text{ g VSS/g VSS day}\right)(20 \text{ days})\right]}{20 \text{ days}\left[\left(0.40 \text{ g VSS/g COD}\right)\left(12.5 \text{ g COD/g VSS day}\right) - 0.10 \text{ g VSS/g VSS day}\right] - 1}$$

$$= 0.31 \text{ g COD/m}^3$$

$$P_{X_T} = \frac{QY(S_0 - S)}{1 + k_d SRT} + QX_{0,i} + f_d k_d \frac{QY(S_0 - S)}{1 + k_d SRT} SRT$$

$$= \frac{(1,000 \text{ m}^3/\text{day})(0.4 \text{ g VSS/g COD})\left((400 - 0.31) \text{ g COD/m}^3\right)}{1 + (0.1 \text{ g VSS/g VSS})(20 \text{ days})}$$

$$+ (1,000 \text{ m}^3/\text{day})(20 \text{ g VSS/m}^3) + (0.15 \text{ g VSS/g VSS})(0.1 \text{ g VSS/g VSS})$$

$$\times \left[\frac{(1,000 \text{ m}^3/\text{day})(0.4 \text{ g VSS/g COD})\left((400 - 0.31) \text{ g COD/m}^3\right)}{1 + (0.1 \text{ g VSS/g VSS})(20 \text{ days})}\right](20 \text{ days})$$

$$= (53,292 + 20,000 + 15,988) \text{ g VSS/day}$$

$$= 89,280 \text{ g VSS/day} \cong 89.3 \text{ kg VSS/day}$$

Similarly, the effluent COD concentration and daily solids production can be estimated for 30 days of SRT.

$$S = 0.27 \text{ g COD/m}^3$$

$$P_{X_T} = 78.0 \text{ kg VSS/day}$$

It should be noted that a lower daily solids production rate is obtained for an SRT of 30 days compared to an SRT of 20 days. We will also learn how the difference in SRT affects a bioreactor volume in Example 6.5.

For a bioreactor to accomplish nitrification as well as COD removal, we need to include nitrifying biomass production and inert solids generated from the decay of nitrifying biomass in the calculation of daily solids production. When we estimate the value in practice, we only include the nitrifying biomass production because the inert solids generated from the decay of nitrifying biomass are negligible. Equation 6.11 is therefore modified as follows:

$$P_{X_T} = \underbrace{\frac{QY(S_0 - S)}{1 + k_d SRT}}_{\substack{\text{Solids production from} \\ \text{heterotrophic biomass}}} + \underbrace{\frac{QY_n N_{ox}}{1 + k_{dn} SRT}}_{\substack{\text{Solids production from} \\ \text{nitrifying biomass}}} + \underbrace{QX_{0,i}}_{\substack{\text{Solids production from} \\ \text{influent inert material}}} + \underbrace{f_d k_d \frac{QY(S_0 - S)}{1 + k_d SRT} SRT}_{\substack{\text{Solids production from endogenous} \\ \text{decay of heterotrophic biomass}}}$$

(6.12)

where

    Y_n is the growth yield of nitrifying bacteria, g VSS/g COD

    N_{ox} is the oxidizable ammonia concentration, g N/m$_3$

    k_{dn} is the decay constant of nitrifying bacteria, day^{-1}

The oxidizable ammonia concentration (N_{ox}) in Equation 6.12 can be estimated from a nitrogen mass balance as the following equation:

$$N \text{ oxidized} = N \text{ influent} - N \text{ effluent} - N \text{ in biomass}$$

$$QN_{ox} = Q(TKN_0) - QN_e - 0.12P_{X,bio}$$

$$N_{ox} = \frac{TKN_0 - N_e - 0.12P_{X,bio}}{Q} \tag{6.13}$$

where

    TKN_0 is the influent TKN concentration, g N/m³

    N_e is the effluent ammonia nitrogen concentration, g N/m³

    $P_{X,bio}$ is the daily solids production rate due to microbial growth and decay, g VSS/day

    0.12 is the fraction of nitrogen in biomass, unitless

Engineers frequently use TSS over volatile suspended solids (VSS) during the estimation of daily solids production. Information based on experiences is generally used to estimate daily solids production based on TSS. Tchobanoglous et al. (2003) assume that 85% of TSS in the biomass and the inert material generated from the decay of biomass is attributed to VSS. However, it is required to conduct an experiment for a better estimation of the ratio of VSS to TSS. TSS from the influent inert solids can be estimated by measuring influent TSS (TSS_0) and VSS (VSS_0). Therefore, the daily solids production based on TSS can be obtained using the following equation:

$$P_{X_T} = \left[\frac{QY(S_0 - S)/(1 + k_d SRT)}{0.85} \right] + \left[\frac{QY_n N_{ox}/(1 + k_{dn} SRT)}{0.85} \right]$$

$$+ \left[QX_{0,i} + Q(TSS_0 - VSS_0) \right] + \left[\frac{f_d k_d (QY(S_0 - S)/(1 + k_d SRT))SRT}{0.85} \right] \tag{6.14}$$

6.3.4 Determining the Volume of Aerobic Tank

After determining the design SRT and estimating the daily solids production rate, the volume of the bioreactor can be calculated. Bioreactor volume can be expressed as the ratio of the mass of solids in the bioreactor to the total solids concentration in the bioreactor (Equation 6.15). The mass of solids in the bioreactor can be

calculated by multiplying the daily solids production rate (P_{X_T}) by the design SRT (Equation 6.16), while the total solids concentration in the bioreactor is a design value.

$$V = \frac{\text{Mass of solids in a bioreactor}}{\text{Total solids concentration in a bioreactor}} \tag{6.15}$$

$$\text{Mass of solids in a bioreactor} = P_{X_T} \cdot \text{SRT} \tag{6.16}$$

The procedure introduced here estimating the volume of a bioreactor is based on the design solids concentration. In the case of retrofitting an existing bioreactor operated within a CAS process, in most cases the existing bioreactor is used without altering the volume of the bioreactor. In this case, the solids concentration can be determined based on the fixed volume of the bioreactor and the calculated mass of solids.

Example 6.5

Determine the required volume of a bioreactor for two different SRT conditions (20 vs. 30 days). Assume there is no need for nitrification in this example. The conditions for the reactor design, wastewater characteristics, and kinetic parameters are the same as in Example 6.4 except for the following information:

- Design solids concentration = 10.0 kg TSS/m^3
- VSS fraction of TSS in X and the inert material generated from the decay of biomass = 85%
- TSS_0 = 60 g/m^3
- VSS_0 = 50 g/m^3

Solution

For the determination of the volume of bioreactor required, we need to calculate the daily solids production using Equation 6.14 (TSS-based calculation) and the mass of solids in the bioreactor using Equation 6.16.

$$P_{X_T} = \left[\frac{QY(S_0 - S)/(1 + k_d SRT)}{0.85} \right] + \left[QX_{0,i} + Q(TSS_0 - VSS_0) \right]$$

$$+ \left[\frac{f_d k_d (QY(S_0 - S)/(1 + k_d SRT))SRT}{0.85} \right] = \frac{53,292 \text{ g VSS/day}}{0.85 \text{ g VSS/g TSS}} + 20,000 \text{ g VSS/day}$$

$$+ 1,000 \text{ m}^3/\text{day}\,(60 - 50)\,\text{g/m}^3 + \frac{15,988 \text{ g VSS/day}}{0.85 \text{ g VSS/g TSS}}$$

$$= 111,506 \text{ g TSS/day} \approx 111.5 \text{ kg TSS/day}$$

$$\text{Mass of solids in a bioreactor} = P_{X_T} \cdot \text{SRT} = (111.5 \text{ kg TSS/day})(20 \text{ days})$$

$$= 2230 \text{ kg TSS}$$

Now, the volume of reactor can be estimated using Equation 6.15 as follows:

$$V = \frac{\text{Mass of solids in a bioreactor}}{\text{Total solids concentration in a bioreactor}} = \frac{2230 \text{ kg TSS}}{10 \text{ kg TSS/m}^3} = 223 \text{ m}^3$$

Similarly, the volume of the reactor can be estimated for 30 days of SRT:

$$P_{X_T} = 98.2 \text{ kg TSS/day}$$

$$\text{Mass of solids in the reactor} = 2946 \text{ kg TSS}$$

$$V = 295 \text{ m}^3$$

It should be noted that increasing SRT from 20 to 30 days resulted in a 14.5% reduction in daily solids production mainly due to an increased decay of biomass, but the calculated bioreactor volume increased by 32.3%.

6.3.5 Determining the Volume of Anoxic Tank

Determining the volume of the anoxic tank is based on the nitrogen mass to be denitrified and on the specific denitrification rate (SDNR) in the tank. The nitrogen mass to be denitrified is estimated based on the oxidizable ammonia concentration (N_{ox}, Equation 6.13) and the target effluent nitrate concentration or the maximum discharge nitrate concentration limit ($NO_{3,p}$) as the following equation:

$$\text{Nitrogen mass to be denitrified} = Q \cdot (N_{ox} - NO_{3,p}) \tag{6.17}$$

SDNR is affected by the availability of organic matter and can be expressed as an equation as a function of the F/M ratio in the anoxic tank (F/M_{ax}) (Equation 6.18). The equation shows a linear relationship between SDNR and F/M_{ax} as shown in Figure 6.12 and can be formulated as Equation 6.19.

$$\frac{F}{M_{ax}} = \frac{QS_0}{V_{ax} X_{ax}} \tag{6.18}$$

where
  V_{ax} is the volume of anoxic tank, m³
  X_{ax} is the solids concentration of anoxic tank, g VSS/m³

$$\text{SDNR} = 0.019 \left(\frac{F}{M_{ax}} \right) + 0.029 \tag{6.19}$$

Because F/M_{ax} is dependent on the volume of the anoxic tank, the calculation for the volume of the anoxic tank is an interactive approach. General protocol for this

The graph shows a plot with x-axis labeled "Anoxic F/M ratio (gCOD/gMLVSS/day)" ranging from −7.22E−16 to 0.4, and y-axis labeled "SDNR (gNO$_3^-$–N/gMLVSS/day)" ranging from 0 to 0.04. A dashed line shows the relationship:

$$SDNR = 0.094(F/M_{ax}) + 0.043$$
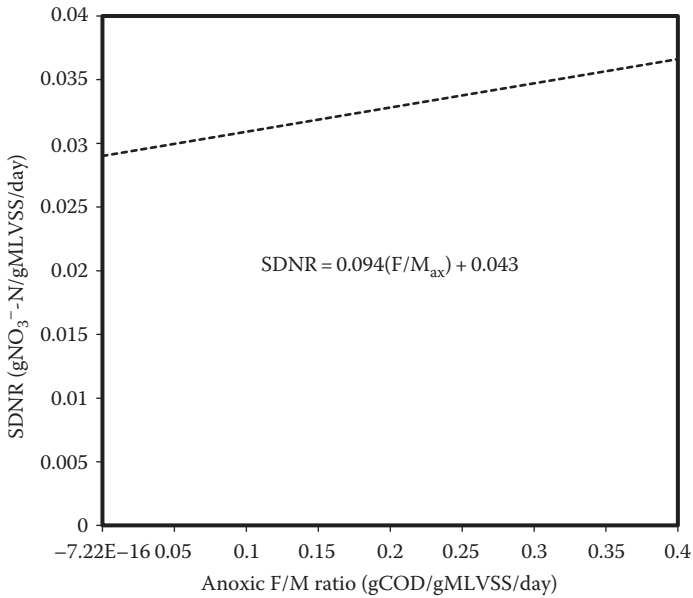
Figure 6.12   SDNR as a function of anoxic F/M ratio. (The relationship was adapted from Tchobanoglous, G. et al., *Wastewater Engineering: Treatment and Reuse***, 4th edn., McGraw-Hill, New York, 2003.)**

approach is summarized in Figure 6.13. Initially, the volume of the anoxic tank is to be assumed to be a certain value. F/M_{ax} and SDNR are thus calculated using the assumed value. Based on the nitrogen mass to be denitrified and the solids concentration in the anoxic tank, the volume of the anoxic tank can be estimated (Equation 6.20). This procedure should be iterated until the estimated value is the same as the assumed value.

$$V_{ax} = \frac{\text{Solids required for denitrification}}{\text{Solids concentration in the anoxic tank}} = \frac{Q\left(N_{ox} - NO_{3,p}\right)\big/SDNR}{X}$$

(6.20)

The flow rate for internal recycling from the aerobic tank back to the anoxic tank can be estimated based on Equation 2.56 that relates total nitrogen removal (TNR) efficiency to the influent flow rate (Q), the internal recycle flow rate (Q_r), and the fraction of nitrogen to be assimilated (f) based on a complete nitrification assumption in the aerobic tank as the following equations:

$$Q_r = \frac{Q(TNR - f)}{1 - TNR}$$

(6.21)

Figure 6.13 shown as a flowchart:

- Set solids concentration of anoxic tank (X_{ax})
- Assume the vol. of anoxic tank (V_{ax})
- Calculation of anoxic F/M ratio (FM_{ax}) — $F/M_{ax} = \dfrac{QS_0}{V_{ax} X_{ax}}$
- Calculation of anoxic SDNR — $SDNR = 0.094\,(F/M_{ax}) + 0.043$
- Calculation of the vol. of anoxic tank (V_{ax}) — $V_{ax} = \dfrac{Q\,(N_{ox} - NO_{3,e})/SDNR}{X}$
- Assumed $V_{ax} \neq$ calculated V_{ax}
- Assumed $V_{ax} =$ calculated V_{ax}
- Calculation of internal recycling rate (V_{ax})
- Calculation of oxygen credit
- Check alkalinity requirement
- Iteration

Figure 6.13   A desktop protocol for designing an anoxic tank.

$$TNR = \frac{TKN_0 - NO_{3,p}}{TKN_0} \tag{6.22}$$

$$f = \frac{TKN_0 - N_{ox}}{TKN_0} \tag{6.23}$$

As discussed in Sections 2.5.1 and 2.5.2, alkalinity is consumed during nitrification (7.1 mg $CaCO_3$ per mg NH_3–N oxidized) and recovered during denitrification (3.6 mg $CaCO_3$ per mg NO_3^-–N reduced). It is thus necessary to check whether supplemental alkalinity is needed or not.

During the design of the anoxic tank, we also need to calculate the oxygen savings from denitrification because some COD is used for denitrification. Note that the denitrification reaction is occurring in anoxic conditions. Oxygen savings reduce the oxygen requirement exerted for COD removal in the aerobic tank. As discussed in Section 2.5.2, 1.0 g of nitrate nitrogen denitrified saves 2.86 g of oxygen. The oxygen savings are estimated by multiplying the coefficient (i.e., 2.86) by the nitrogen mass to be denitrified in the anoxic tank (Equation 6.17).

6.4 Aeration Design

In aerobic bioreactors, aerobic microorganisms use oxygen provided by aeration as their terminal electron acceptor to oxidize organic and inorganic pollutants. In addition, aeration plays a role in mixing the activated sludge and generating turbulent flow for membrane cleaning (in case of submerged MBR).

Aeration is the largest energy consumer in biological wastewater treatment. Around 50% of the energy required in CAS systems is used for aeration. In MBR, the proportion increases up to 80% due to the surplus of energy consumption by membrane aeration. It is therefore important to design the aeration system properly to avoid over or under estimating the aeration required that could lead to excessive energy costs or incomplete treatment, respectively.

6.4.1 Actual Oxygen Transfer Rate

Under field conditions, the oxygen transfer rate (i.e., actual oxygen transfer rate, AOTR) is much less than the transfer rate measured at standard conditions in clean water (SOTR). To calculate AOTR, it is first necessary to understand the theory explaining oxygen transfer in water. A two-film theory is commonly used in wastewater engineering in which gas film and liquid film exist between the bulk-gaseous and bulk-liquid phases as shown in Figure 6.14.

The theory assumes that the two films provide resistance for the transport of gas, and the difference in the concentration of gas at the two phases drives the transport of gas. If most of the mass transfer resistance occurs in the liquid film, which is assumed in wastewater treatment, the oxygen transfer rate (OTR) can be explained as the following equation.
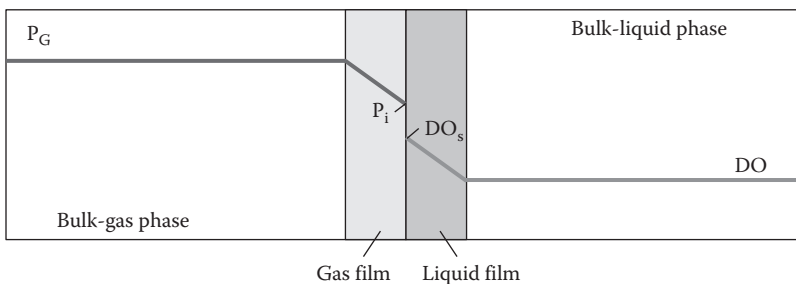
P_G = partial pressure of oxygen in the bulk-gas phase
P_i = partial pressure of oxygen at the interface in equilibrium with DO_s
DO = dissolved oxygen concentration in the bulk-liquid phase
DO_s = dissolved oxygen concentration at the interface in equilibrium with P_i

Figure 6.14   A schematic diagram explaining the two-film theory.

$$OTR = \frac{dDO}{dt} \cdot V = K_La \cdot (DO_S - DO) \cdot V \qquad (6.24)$$

where
   DO is the dissolved oxygen concentration in bulk-liquid phase, mg/L
   DO_S is the dissolved oxygen concentration in equilibrium with bulk-gas phase, mg/L
   K_La is the mass transfer coefficient, h^{-1}
   V is the reactor volume, m^3

SOTR represents the oxygen transfer rate at standard conditions (20°C, 1 atm, zero salinity, and zero DO in water), while AOTR is the oxygen transfer rate considering various field conditions including temperature, wastewater characteristics, aeration device, mixing intensity, and tank geometry. Temperature affects the rate of oxygen transfer by modifying the mass transfer coefficient. Higher temperatures lead to lower oxygen transfer coefficients.

$$K_La(T) = K_La(20°C)\theta^{T-20} \qquad (6.25)$$

where
   $K_La(T)$ is the mass transfer coefficient at temperature T, h^{-1}
   $K_La(20°C)$ is the mass transfer coefficient at 20°C, h^{-1}
   θ is the temperature corrector factor, unitless

Wastewater characteristics, aeration device, tank configuration, and mixing intensity also affect the mass transport coefficient. These effects are explained by an alpha correction factor that is defined in the following equation:

$$\alpha = \frac{K_La(\text{wastewater})}{K_La(\text{clean water})} \qquad (6.26)$$

It is reported that alpha factor values are highly variable ranging from 0.3 to 1.2 (Tchobanoglous et al., 2003) as determined by experiments. Alpha factors will be significantly lower in bioreactors of MBRs containing a high solids concentration than those in the bioreactor of CAS systems. A study conducted by Krampe and Krauth (2003) demonstrated that alpha factor decreased exponentially with increasing MLSS concentration. They formulated the correlation as $\alpha = e^{-0.08788 \cdot MLSS}$. The aeration system is also known to affect alpha factors. In practice, mechanical aeration systems tend to have higher values (0.6–1.2) than diffused aeration systems (0.4–0.8) (Tchobanoglous et al., 2003).

Wastewater characteristics also affect the solubility of oxygen. This effect is accounted for by β correction factors and is defined as the following equation:

$$\beta = \frac{DO_S(\text{wastewater})}{DO_S(\text{clean water})} \tag{6.27}$$

It is reported that a β value of 0.95 is generally acceptable for wastewater, although the values range from 0.7 to 0.98 (Tchobanoglous et al., 2003).

Considering all of the factors mentioned above, the oxygen transfer rate at field conditions (i.e., AOTR) can be explained as follows:

$$AOTR = SOTR \cdot \frac{\alpha(\beta DO_S - DO)}{DO_{S,20}} \theta^{T-20} \tag{6.28}$$

where
   AOTR is the actual oxygen transfer rate, kg/h
   SOTR is the standard oxygen transfer rate, kg/h

Example 6.6

Calculate the oxygen transfer rate in the field conditions (AOTR) provided in the following, and compare the rate with that estimated under standard conditions (SOTR).

   Volumetric oxygen transfer rate ($K_L a$) at 20°C = 4.9 h^{-1}
   The ratio of oxygen transfer rate of wastewater to that of clean water (α) = 0.6
   The temperature correction factor (θ) = 1.024
   The ratio of saturated DO concentration of wastewater to that of clean water
      (β) = 0.95
   Wastewater temperature = 25°C
   Henry's law constant at 20°C (293 K) = 790 L atm/mol
   Design DO concentration in a reactor = 2.0 mg/L
   Volume of a bioreactor = 223 m^3

Solution

It is necessary to estimate the saturation DO concentrations at temperatures of 20°C and 25°C for the calculations of SOTR and AOTR, respectively. The saturation DO concentration at temperature T ($DO_S(T)$) can be estimated using Henry's law constant at temperature T ($H_{O_2}(T)$) as the following equation:

$$DO_S(T) = \frac{P_{O_2(g)}}{H_{O_2}(T)} \tag{6.29}$$

where $P_{O_2(g)}$ is the partial pressure of oxygen, atm.

Henry's law constant at 25°C (298 K) can be estimated by the Van't Hoff equation as follows:

$$H_{O_2}(T_2) = H_{O_2}(T_1) \cdot \exp\left[\frac{\Delta H°}{R}\left(\frac{1}{T_1} - \frac{1}{T_2}\right)\right] \qquad (6.30)$$

where
$H_{O_2}(T_2)$ is the Henry's law constant of oxygen at the temperature T_2, K
$H_{O_2}(T_1)$ is the Henry's law constant of oxygen at the temperature T_1, K
$\Delta H°$ is the standard enthalpy change, kcal/mol
R is the gas constant, cal/K mol

$$H_{O_2}(298\ K) = 790\ (L\ atm)/mol \cdot \exp\left[\frac{3.56 \times 10^3\ cal/mol}{1.987\ cal/K\ mol}\left(\frac{1}{293\ K} - \frac{1}{298\ K}\right)\right]$$

$$= 875\ (L\ atm)/mol$$

The saturation DO concentration at the temperature 20°C and 25°C are

$$DO_S(293\ K) = \frac{P_{O_2(g)}}{H_{O_2}(293\ K)} = \frac{0.21\ atm}{790\ L\ atm/mol} = 2.66 \times 10^{-4}\ mol/L = 8.51\ mg/L$$

$$DO_S(298\ K) = \frac{P_{O_2(g)}}{H_{O_2}(298\ K)} = \frac{0.21\ atm}{875\ L\ atm/mol} = 2.40 \times 10^{-4}\ mol/L = 7.68\ mg/L$$

SOTR is the oxygen transfer rate at 20°C in clean water (zero DO demand) and can be expressed as follows:

$$SOTR = K_La(DO_{S,20} - 0)V = K_La \cdot DO_{S,20} \cdot V$$

$$= (4.9\ h^{-1})(8.51\ mg/L)(10^{-6}\ kg/mg)(10^3\ L/m^3)(223\ m^3) = 9.30\ kg/h$$

Now, AOTR can be estimated using Equation 6.28:

$$AOTR = SOTR \cdot \frac{\alpha(\beta DO_S - DO)}{DO_{S,20}}\theta^{T-20}$$

$$= (9.30\ kg/h) \times \frac{0.6(0.95 \times 7.68 - 2.0\ mg/L)}{8.51\ mg/L} \times 1.024^{(25-20)} = 3.91\ kg/h$$

It is necessary to note that the AOTR is only 42% of the SOTR, demonstrating the lower oxygen transfer efficiency in field conditions.

6.4.2 Calculating the Aeration Requirement
for Biological Treatment

The procedure for estimating the theoretical oxygen demand is based on COD consumption, nitrification, denitrification, and solids production. Let's revisit the equations for calculating theoretical oxygen demand (OD_{theory}):

$$OD_{theory} = Q(S_0 - S) + 4.32QN_{ox} - 2.86Q(N_{ox} - NO_{3,e}) - 1.42P_{X,bio} \quad (6.31)$$

This equation is based on an oxygen mass balance in which the OD_{theory} is the sum of COD removal ($Q(S_0 - S)$), oxygen consumption by nitrification ($4.32QN_{ox}$), oxygen credit via denitrification ($-2.86Q(N_{ox} - NO_{3,e})$), and oxygen credit via solids production ($-1.42P_{X,bio}$). $P_{X,bio}$ corresponds to the solids production rate due to biomass (heterotrophic + nitrifying biomass) and inert biomass production because both processes consume oxygen. $P_{X,bio}$ is expressed as the following equation:

$$P_{X,bio} = \frac{QY(S_0 - S)}{1 + k_d SRT} + \frac{QY_n N_{ox}}{1 + k_{dn} SRT} + f_d k_d \frac{QY(S_0 - S)}{1 + k_d SRT} SRT \quad (6.32)$$

Because the estimated OD_{theory} is the theoretical value, we need to convert it to the OD based on the aeration system's field conditions. The oxygen demand at field conditions (OD_{field}) can be obtained with the following expression:

$$OD_{field} = \left(\frac{OD_{theory}}{E}\right)\left(\frac{SOTR}{AOTR}\right) = \left(\frac{OD_{theory}}{E}\right)\left(\frac{DO_{S,20}}{\alpha \cdot (\beta DO_S - DO) \cdot \theta^{T-20}}\right)$$

$$(6.33)$$

where
OD_{field} is the oxygen demand at field condition, kg/day
OD_{theory} is the oxygen demand at theoretical condition, kg/day
$DO_{S,20}$ is the saturation DO concentration at 20°C, mg/L
E is the oxygen transfer efficiency of diffuser, unitless

Example 6.7

Estimate the OD at field conditions for the MBR system introduced in Example 6.4 (20 days of SRT). Assume that the field conditions are the same as Example 6.6 except for the diffuser efficiency (E) of 0.30.

Solution

Because nitrification is negligible in Example 6.4, $P_{X,bio}$ can be estimated as follows:

$$P_{X,bio} = \frac{QY(S_0 - S)}{1 + k_d SRT} + f_d k_d \frac{QY(S_0 - S)}{1 + k_d SRT} SRT$$

$$= \frac{(1,000\ m^3/day)(0.4g\ VSS/g\ COD)\left(400 - 0.31g\ COD/m^3\right)}{1 + (0.1g\ VSS/g\ VSS)(20\ days)}$$

$$+ (0.15\ g\ VSS/g\ VSS)(0.1\ g\ VSS/g\ VSS)$$

$$\times \left[\frac{(1,000\ m^3/day)(0.4g\ VSS/g\ COD)\left(400 - 0.31g\ COD/m^3\right)}{1 + (0.1g\ VSS/g\ VSS)(20\ days)}\right](20\ days)$$

$$= (53,292 + 15,988)g\ VSS/day = 69,280g\ VSS/day$$

OD_{theory} can be estimated as follows:

$$OD_{theory} = Q(S_0 - S) - 1.42P_{X,bio} = 1,000\ m^3/day \cdot (400 - 0.31)\ g/m^3 - 1.42 \times 69,280\ g/day$$

$$= 301,312\ g/day = 301\ kg/day = 12.5\ kg/h$$

Now, OD_{field} can be calculated as follows:

$$OD_{field} = \left(\frac{OD_{theory}}{E}\right)\left(\frac{DO_{S,20}}{\alpha \cdot (\beta DO_S - DO) \cdot \theta^{T-20}}\right)$$

$$= \left(\frac{301\ kg/day}{0.3}\right)\left(\frac{8.51\ mg/L}{0.6(0.95 \times 7.68 - 2.0\ mg/L) \cdot 1.024^{(25-20)}}\right)$$

$$= 2387\ kg/day = 99\ kg/h$$

The estimated OD_{field} is around 7.9 fold higher than the OD_{theory}. Assuming the density of air 1.2 kg/m³ (density is variable depending on temperature), the airflow rate based on OD_{field} can be calculated as 359 m³ air/h (=(99 kg O_2/h)/(0.23 kg O_2/kg air × 1.2 kg air/m³)).

6.4.3 Aeration Amount for Membrane Cleaning

Course bubble aerators are installed beneath the membrane modules to scour the solids accumulated on the surface of the membranes in submersed MBR systems. Membrane aeration is also important to improve filtration performance because flux tends to increase by increasing the bubbling rate to a certain extent (Chang, 2011). Providing the proper amount of aeration is essential to minimize the energy cost as well as to reduce fouling of the membranes. The energy cost for coarse bubble aeration is reported to increase the total energy cost for operating an MBR plant from 30% to 50% (Judd, 2008).

Table 6.3   Specific Aeration Demand (SAD$_m$) for Various Membrane Modules

Supplier	Membrane Type[a]	Model	SAD$_m$ (m³/m²/h)	Reference
Kubota	FS	EW	0.34	Judd (2006)
	FS	EM	0.48	Judd (2006)
	FS	EK	0.53	Judd (2006)
	FS	ES	0.75	Judd (2006)
Mitsubishi	HF	SUR334LA	0.34	Judd (2006)
GE Zenon	HF	500d	0.54	Judd (2006)
	HF	500d	0.34	Brepols (2004)
	HF	500d	0.18	Cote (2004)
Siemens	HF	B10R	0.36	Adham (2004)
Econity	HF	4005CF	0.15	Online MBR Info[b]
A3	HF	SADF	0.20	Grelot (2010)
Asahi	HF	MUNC-620A	0.24	Online MBR Info

[a] FS, flat-sheet membrane; HF, hollow-fiber membrane.
[b] Online MBR Info: http://www.onlinembr.info.

The amount of aeration required for membrane cleaning is directly dependent on the number of membrane modules installed in the bioreactor (i.e., membrane area). The estimation of aeration required is therefore calculated based on the membrane area and the specific aeration demand (SAD$_m$). SAD$_m$ is defined as the airflow rate per unit membrane area (e.g., m³ air/m² membrane/h). The values of SAD$_m$ vary for different membrane suppliers and specific membrane models. Typical values range from 0.3 to 0.8 m³ air/m² membrane/h and are presented in Table 6.3.

Sometimes the aeration demand for membrane aeration is reported based on permeate (SAD$_p$) instead of membrane area. SAD$_p$ is defined as the airflow rate per unit permeate production rate (e.g., m³ air/m³ permeate). SAD$_p$ ranges between 10 and 100 (Judd, 2006).

6.5 Membrane System Design

It is desirable to set water flux as high as possible to reduce the cost associated with membrane modules, but high flux rates may result in a low stability MBR system.
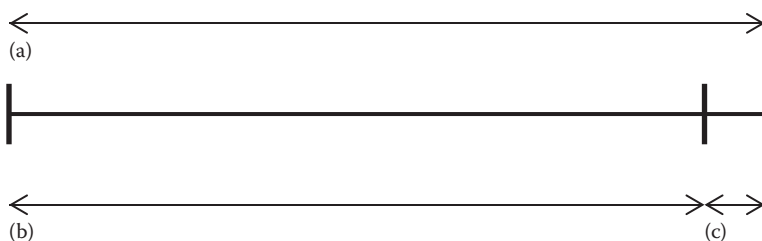
Figure 6.15 **A schematic diagram showing a typical filtration cycle: a—total cycle time = 10 min; b—time of filtration operation = 9.5 min; and c—regular downtime to allow particles to release from membranes to reduce fouling = 30 s.**

It is known that the membrane fouling rate in terms of transmembrane pressure (TMP) increases with time and exponentially increases with flux (Judd, 2006). Determining the design flux should consider the flow rate peaking factor (i.e., the ratio of hourly peak flow to daily average flow) and the pausing time due to filtration cycle and backwashing. A typical filtration cycle is shown in Figure 6.15. Membranes should be stably operated at peak flow conditions (i.e., no significant fouling). Therefore, the design flux should be determined based on the peak flow condition not daily average flow rate. If the peaking factor is >1.5, it is strongly recommended to install a flow equalization tank instead of increasing the number of membrane modules for a cost-effective solution.

Membrane filtration is operated discontinuously to minimize membrane fouling. Intermittent filtration is a conventional strategy for MBR operation. In addition, backwashing is routinely performed to also reduce membrane fouling. The pausing time due to the filtration cycle and backwashing reduces the design flux. Chemical cleaning periods during which filtration is not underway also contribute to a decrease in design flux. Therefore, design flux should consider the peaking factor, filtration cycle, and chemical cleaning and can be determined as the following equation:

$$\text{Design flux} = \frac{(\text{Maximum operating flux})(\text{Filtration ratio})(\text{Operating ratio})}{\text{Peaking factor}}$$

(6.34)

where
  Maximum operating flux = critical flux, $\text{L/m}^2/\text{h}$
  Filtration ratio = (filtration time)/(filtration + backwash + pausing times), unitless
  Operating ratio = (operating time)/(operating + cleaning times), unitless
  Peaking factor = (hourly peak flow)/(daily average flow), unitless

The number of membrane modules installed in an MBR can be determined based on the design flux. The number can be estimated using daily average flow rate, design flux, and membrane area per module using the following equation:

$$\text{Number of modules} = \frac{\text{Daily average flowrate}}{(\text{Design flux})(\text{Membrane area per module})} \quad (6.35)$$

Example 6.8

Permeate water is withdrawn with 30 LMH in an MBR plant. In order to minimize membrane fouling, 30 s of backwashing is practiced every 5 min of filtration cycle (i.e., 4.5 min of permeation and 0.5 min of backwashing). In addition to backwashing, maintenance cleaning is performed for 30 min every day. What is the net water flux considering backwashing and maintenance cleaning?

Solution

Because permeate water is not produced during the periods of backwashing and maintenance cleaning, the net flux should be calculated based on net filtration and operation times as follows:

$$\text{Net flux} = \left(\text{instant flux}\right)\left(\text{filtration ratio}\right)\left(\text{operating ratio}\right)$$

$$= \left(30\ \text{LMH}\right)\left(\frac{4.5\ \text{min}}{5\ \text{min}}\right)\left(\frac{23.5\ \text{h}}{24\ \text{h}}\right) = 26.4\ \text{LMH}$$

6.6 Design Example

This design example summarizes all the design procedures introduced in this chapter and will be of use for the readers who want to understand the big picture of MBR design. The challenge is to design the bioreactor and membrane systems for a newly built MBR plant treating municipal wastewater. The bioreactor consists of an anoxic tank and an aerobic tank, and the mixed liquor in the aerobic tank is recycled into the anoxic tank (i.e., internal recycle) to facilitate biological nitrogen removal via nitrification and denitrification. The anoxic and aerobic tanks are assumed to be operated by completely stirred tank reactor.

Designing should include (1) the volume of two completely mix tank reactors (i.e., anoxic and aerobic tanks), (2) flow rates for internal recycle, (3) aeration rates for biological treatment and membrane cleaning, and (4) the number of membrane modules installed in the aerobic tank. The target MLSS concentration in the bioreactor and SRT is 8000 g MLVSS/m³ and 20 days, respectively. In this example, the membrane system will be designed based on the GE-Zenon's ZeeWeed 500d immersed membranes. The ZeeWeed 500d cassette has maximum 48 modules and each module has 31.6 m² of membrane surface area (i.e., 1516.8 m²/cassette).

General information, wastewater characteristics, kinetic parameters, aeration parameters, and operating conditions of the membrane system are presented in Tables 6.4 through 6.8.

For a precise design, it is generally required to use design software based on activated sludge model (e.g., GPS-X, BioWin, WEST, etc.). Nevertheless, designing an MBR plant using a desktop approach will be of use for understanding the factors affecting the size of the bioreactor, total solids production, aeration amounts, and number of required membrane modules. Following is a desktop approach adapted from the procedure introduced in *Wastewater Engineering* (Tchobanoglous et al., 2003).

Table 6.4   General Information for the Design

Constituent	Value
Average influent wastewater flow rate (m³/day)	1000
Peaking factor for wastewater flow[a]	1.5
Solids retention time of the aerobic tank (day)	20
Average wastewater temperature during summer (°C)	25
Average wastewater temperature during winter (°C)	12
Maximum permeate biodegradable COD (g/m³)	5.0
Maximum permeate ammonia (g N/m³)	0.5
Maximum permeate nitrate (g N/m³)	25.0
DO concentration of aerobic tank (g/m³)	2.0

[a] Peaking factor is defined as the average daily flow per hourly peak flow. And the duration of peaking factor is assumed to be 2 h.

Table 6.5   Influent Wastewater Characteristics

Constituent	Concentration (mg/L)
Biodegradable COD	230
Nonbiodegradable soluble COD	20
TKN	50
Nitrate	0
Nonbiodegradable VSS	20
Alkalinity (as CaCO₃)	150

Table 6.6 Activated Sludge Kinetic Parameters

Parameter	Unit	Value
μ_m	g VSS/(g VSS/day)	6.0
K_s	g bCOD/m^3	20.0
Y	g VSS/g bCOD	0.40
k_d	g VSS/(g VSS/day)	0.12
f_d	Unitless	0.15
$\mu_{m,N}$	g VSS/(g VSS/day)	0.75
K_N	g N/m^3	0.74
K_{DO}	g DO/m^3	0.5
Y_N	g VSS/g N	0.12
$k_{d,N}$	g VSS/(g VSS/day)	0.08
θ values		
μ_m or $\mu_{m,N}$	Unitless	1.07
k_d or $k_{d,N}$	Unitless	1.04
K_s	Unitless	1.00
K_N	Unitless	1.05
SDNR	Unitless	1.08

Table 6.7 Parameters of Aeration for Biological Reaction

Parameter	Unit	Value
Alpha (α)	Unitless	0.45
Beta (β)	Unitless	1.0
DO in aeration basin (DO)	mg/L	2.0
Diffuser oxygen transfer rate (E)	%	30

6.6.1 *Checking Design SRT Based on Nitrification Kinetics*

Initially, it is necessary to check whether the design SRT value is greater than the minimum SRT required to achieve full nitrification in the aerobic tank. If the minimum SRT is greater than the design SRT, the design SRT needs to be redesigned

Table 6.8   Parameters of Membrane System Operation

Parameter	Unit	Value
Maximum operating flux[a]	L/m² h	40
Permeation cycle		
Filtration	min	15
Backwash	min	0.5
Maintenance cleaning		
Frequency	times/week	3
Duration	min	60
Coarse bubble aeration		
SAD	m³/m²/h	0.54
Aeration/pause	s	10/10

[a] Maximum operating flux indicates critical flux. And the flux condition over the maximum operating flux should be limited to <1 h.

(i.e., increase in SRT). As shown in Example 6.3, the minimum SRT for nitrification can be determined from the specific growth rate of AOB using the following equations:

$$\mu_{AOB} = \left(\frac{\mu_{m,AOB} \cdot NH_3}{K_N + NH_3} \right) \left(\frac{DO}{K_{DO} + DO} \right) - k_{d,AOB}$$

$$\mu_{m,AOB}(T) = \mu_{m,AOB}(20°C) \cdot \theta^{(T-20)}$$

$$K_N(T) = K_N(20°C) \cdot \theta^{(T-20)}$$

$$k_{d,AOB}(T) = k_{d,AOB}(20°C) \cdot \theta^{(T-20)}$$

At winter temperature conditions (i.e., 12°C),

$$\mu_{m,AOB}(12°C) = 0.75 \times 1.07^{(12-20)} = 0.44 \text{ g VSS/g VSS day}$$

$$K_N(12°C) = 0.74 \times 1.05^{(12-20)} = 0.50 \text{ g N/m}^3$$

$$k_{d,AOB}(12°C) = 0.08 \times 1.04^{(12-20)} = 0.06 \text{ g VSS/g VSS day}$$

Using the calculated values given, other kinetic parameters, and the design conditions, the specific growth rate of AOB can be calculated as follows:

$$\mu_{AOB} = \left(\frac{\mu_{m,AOB} \cdot NH_3}{K_N + NH_3} \right)\left(\frac{DO}{K_{DO} + DO} \right) - k_{d,AOB}$$

$$= \left(\frac{(0.44 \text{ g/g day})(0.5 \text{ g/m}^3)}{(0.50 + 0.5) \text{ g/m}^3} \right)\left(\frac{2.0 \text{ g/m}^3}{(0.5 + 2.0) \text{ g/m}^3} \right) - 0.06 \text{ g/g day}$$

$$= 0.12 \text{ g/g day}$$

The minimum SRT required in the aerobic tank can be calculated using Equation 6.9 as follows:

$$SRT = \frac{1}{\mu_{AOB}} = \frac{1}{0.12 \text{ g/g day}} = 8.3 \text{ days}$$

Even though we applied a safety factor (i.e., the ratio of peak influent TKN to average influent TKN concentration) of two, the calculated minimum SRT is shorter than the predetermined SRT of 20 days. Therefore, it is not necessary to reset the design SRT.

6.6.2 Determining the Solids Production Associated with Biological Reactions

Total solids production associated with biological reactions ($P_{X,bio}$, unit: mass per time) can be determined based on Equation 6.12. $P_{X,bio}$ can be calculated by subtracting solids production originated from inert material in influent wastewater from total solids production (P_{X_T}). To obtain $P_{X,bio}$, first it is required to estimate the permeate COD concentration and oxidizable ammonia concentration. Permeate COD can be determined using Equation 2.20 as follows:

$$S = \frac{K_S(1 + k_d SRT)}{SRT(\mu_m - k_d) - 1} = \frac{(20 \text{ g COD/m}^3)\left[1 + \left(0.09 \text{ g VSS/g VSS day}\right)(20 \text{ days})\right]}{20 \text{ days}\left[(3.50 - 0.09) \text{ g VSS/g VSS day}\right] - 1}$$

$$= 0.83 \text{ g COD/m}^3$$

$$k_d(12°C) = k_d(20°C) \cdot \theta^{(T-20)} = 0.12 \times 1.04^{(12-20)} = 0.09 \text{ g VSS/g VSS day}$$

$$\mu_m(12°C) = \mu_m(20°C) \cdot \theta^{(T-20)} = 6.0 \times 1.07^{(12-20)} = 3.50 \text{ g VSS/g VSS day}$$

Note that the permeate COD concentration is less than the design permeate biodegradable COD (5.0 g/m³). The oxidizable ammonia concentration (N_{ox})

can be determined by iterative calculations of $P_{X,bio}$ and N_{ox}. Initially, we assume N_{ox} as 35 g N/m^3 (70% of influent TKN concentration) and calculate $P_{X,bio}$ as follows:

$$P_{X,bio} = \frac{QY(S_0 - S)}{1 + k_d SRT} + \frac{QY_n N_{ox}}{1 + k_{d,AOB} SRT} + f_d k_d \frac{QY(S_0 - S)}{1 + k_d SRT} SRT$$

$$= \frac{(1{,}000 \text{ m}^3/\text{day})(0.40 \text{ g/g})\left[(230 - 0.83) \text{ g/m}^3\right]}{\left[1 + (0.09 \text{ g/g day})(20 \text{ days})\right]}$$

$$+ \frac{(1{,}000 \text{ m}^3/\text{day})(0.12 \text{ g/g})(35 \text{ g/m}^3)}{\left[1 + (0.06 \text{ g/g day})(20 \text{ days})\right]}$$

$$(0.15 \text{ g/g})(0.09 \text{ g/g day})(1{,}000 \text{ m}^3/\text{day})(0.40 \text{ g/g})$$

$$+ \frac{\times \left[(230 - 0.83) \text{ g/m}^3\right](20 \text{ days})}{\left[1 + (0.09 \text{ g/g day})(20 \text{ days})\right]}$$

$$= 43{,}487 \text{ g VSS/day}$$

N_{ox} is now calculated using Equation 6.13.

$$N_{ox} = \frac{TKN_0 - N_e - 0.12 P_{X,bio}}{Q}$$

$$= \frac{50 \text{ g/m}^3 - 0.5 \text{ g/m}^3 - 0.12 \times (43{,}487 \text{ g/day})}{(1000 \text{ m}^3/\text{day})} = 44.3 \text{ g/m}^3$$

The calculated N_{ox} is much bigger than the initial our estimate (44.3 > 35 g/m^3). It is thus necessary to reassume the value and calculate $P_{X,bio}$ and N_{ox} again until the assumed N_{ox} is same as the calculated N_{ox}. A spreadsheet program such as Microsoft Excel can be used to iterate the calculation. Iterative calculation results show N_{ox} as 44.2 g/m^3 and $P_{X,bio}$ as 43,990 g VSS/day.

6.6.3 Determining the Volume of an Aerobic Tank

The volume of the aerobic tank can be calculated based on the estimation of the total solids mass and the design total solids concentration (Equation 6.15). It is thus necessary to calculate daily solids production (P_{X_T}) for the estimation of the total solids mass in the aerobic tank (Equation 6.12).

$$P_{X_T} = P_{X,bio} + QX_{0,i} = 43,990 \, g/day + (1,000 \, m^3/day)(20 \, g/m^3)$$

$$= 63,990 \, g \, VSS/day$$

$$V = \frac{Mass \ of \ solids \ in \ a \ bioreactor}{Total \ solids \ concentration \ in \ a \ bioreactor}$$

$$= \frac{(63,990 \ g \ VSS/day)(20 \ days)}{8,000 \ g \ VSS/m^3} = 160 \ m^3$$

The volume of the aerobic tank corresponds to 3.8 h of HRT (=160 m³/(1000 m³/day)(24 h/day)).

6.6.4 Estimating the Volume of an Anoxic Tank

Estimating the required volume of anoxic tank begins with estimating the solids concentration in the anoxic tank (X_{ax}), which is used to calculate the F/M ratio in the anoxic tank (F/M_{ax}). The SDNR is a function of F/M_{ax} (Equation 6.19) and is used for the amount of biomass required for denitrification. Assuming the ratio of recycle activated sludge from aerobic tank to anoxic tank is high enough, X_{ax} is assumed to be equivalent to the solids concentration in the aerobic tank (X) (e.g., 8000 g VSS/m³). F/M_{ax} is now calculated based on the assumption of 2 h of HRT for the anoxic tank volume (e.g., 83.3 m³) using Equation 6.18:

$$\frac{F}{M_{ax}} = \frac{QS_0}{V_{ax}X_{ax}} = \frac{(1000 \ m^3/day)(230 \ g/m^3)}{(83.3 \ m^3)(8000 \ g/m^3)} = 0.345 \ g/g \ day$$

SDNR can be calculated using Equation 6.19.

$$SDNR(20°C) = 0.019 \left(\frac{F}{M_{ax}} \right) + 0.029 = 0.019(0.345 \ g/g \ day) + 0.029$$

$$= 0.036 \ g \ NO_3^- - N/g \ VSS \ day$$

$$SDNR(12°C) = SDNR(20°C) \cdot \theta^{(12-20)} = (0.036 \ g/g \ day)(1.08)^{(12-20)}$$

$$= 0.019 \ g \ NO_3^- - N/g \ VSS \ day$$

As previously determined, the nitrogen concentration to be oxidized (N_{ox}) is 44.2 g NO_3^-–N/m³ and the nitrate discharge limit is 25 g NO_3^-–N/m³. Therefore, the

amount of nitrogen to be denitrified is 19,200 g NO_3^-– N/day ($=(44.2 - 25)$ g/m³ × 1,000 m³/day) and the amount of biomass required for denitrification is 1,010,526 g VSS ($=(19,200$ g/day)/(0.019 g/g day)). The volume of anoxic tank (V_{ax}) can, therefore, be calculated as follows:

$$V_{ax} = \frac{\text{Activated sludge required for denitrification}}{\text{Activated sludge concentration in the anoxic tank}}$$

$$= \frac{1,010,526 \text{ g}}{8,000 \text{ g/m}^3} = 126.3 \text{ m}^3$$

The calculated volume of the anoxic tank (126.3 m³) is larger than our initial assumption (83.3 m³). The calculated value needs to be equalized to that of the initial assumption. Similar to the determination of $P_{X,bio}$ and N_{ox}, V_{ax} can be estimated by iterative calculation. Iterative calculation has resulted in the following values:

$$\frac{F}{M_{ax}} = 0.21 \text{ g COD/g VSS day}$$

$$\text{SDNR(20°C)} = 0.0331 \text{ g } NO_3^-\text{–N/g VSS day}$$

$$\text{SDNR(12°C)} = 0.0179 \text{ g } NO_3^-\text{–N/g VSS day}$$

$$\text{Activated sludge required for denitrification} = 1,074,754 \text{ g VSS}$$

$$V_{ax} = 134.3 \text{ m}^3 \text{ (=3.2 h of HRT)}$$

6.6.5 Determining the Internal Recycling Rate

The aforementioned calculations enable us to estimate the TNR efficiency and the fraction of nitrogen to be assimilated into biomass (f), which can be used for determining the internal recycle rate as described in Section 6.3.5.

$$\text{TNR efficiency} = \frac{TKN_0 - NO_{3,P}}{TKN_0} = \frac{(50 - 25) \text{ g/m}^3}{50 \text{ g/m}^3} = 0.5$$

$$f = \frac{TKN_0 - N_{ox}}{TKN_0} = \frac{(50 - 44.2) \text{ g/m}^3}{50 \text{ g/m}^3} = 0.1$$

$$\text{TNR efficiency} = 1 - \frac{Q \cdot (1 - f)}{Q + Q_r}$$

$$0.5 = 1 - \frac{(1000 \text{ m}^3/\text{day})(1 - 0.1)}{1000 \text{ m}^3/\text{day} + Q_r}$$

$$Q_r = 800 \text{ m}^3/\text{day}$$

6.6.6 Checking the Alkalinity Requirement

As discussed previously, alkalinity is consumed during nitrification (7.14 mg $CaCO_3$ per mg NH_3–N oxidized) and recovered during denitrification (3.60 mg $CaCO_3$ per mg NO_3^-–N reduced). It is thus necessary to check whether supplemental alkalinity is needed or not.

Alkalinity consumed during nitrification

$$= \left(7.14 \frac{\text{mg CaCO}_3}{\text{mg NH}_3 - \text{N}}\right)(44.2 \text{ mg/L}) = 316 \text{ mg/L as CaCO}_3$$

Alkalinity saved during denitrification

$$= \left(3.60 \frac{\text{mg CaCO}_3}{\text{mg NH}_3 - \text{N}}\right)(19.2 \text{ mg/L}) = 69 \text{ mg/L as CaCO}_3$$

Considering influent alkalinity (150 mg $CaCO_3$/L) and minimum residual alkalinity (50 mg $CaCO_3$/L), it is necessary to supplement 147 mg $CaCO_3$/L of alkalinity to the bioreactor.

$$\text{Supplemental alkalinity} = \text{Influent alkalinity} - \text{Consumed alkalinity}$$

$$+ \text{Saved alkalinity} - \text{Minimum alkalinity}$$

$$= (150 - 316 + 69 - 50) \text{ mg/L} = -147 \text{ mg CaCO}_3/\text{L}$$

6.6.7 Determining the Waste Activated Sludge

As discussed previously, the waste activated sludge rate is equivalent to the daily solids production rate (P_{X_T}). Because P_{X_T} was estimated using mass units, it is necessary to convert it into a volume unit for determining the waste activated sludge rate using the solids concentration in the aerobic tank. Note that, in practice, there is no thickening facility such as secondary sedimentation tanks in MBR plants. Therefore, the concentration of waste activated sludge is the same

as the MLVSS concentration of the aerobic tank where activated sludge wasting is performed.

$$P_{X_T} = 63,990 \text{ g VSS/day}$$

$$\text{Waste activated sludge} = \frac{63,990 \text{ g/day}}{8,000 \text{ g/m}^3} = 8.0 \text{ m}^3/\text{day}$$

6.6.8 Determining the Aeration Requirements for Biological Reactions

OD_{theory} for COD removal and nitrification in the aerobic tank can be obtained using Equation 6.31.

$$OD_{theory} = Q(S_0 - S) + 4.32QN_{ox} - 2.86Q(N_{ox} - NO_{3,e}) - 1.42P_{X,bio}$$

$$= (1,000 \text{ m}^3/\text{day})\left[(230 - 0.83) \text{ g/m}^3\right] + 4.32(1,000 \text{ m}^3/\text{day})(44.2 \text{ g/m}^3)$$

$$- 2.86(1,000 \text{ m}^3/\text{day})\left[(44.2 - 25) \text{ g/m}^3\right] - 1.42(43,487 \text{ g/day})$$

$$= 303,450 \text{ g O}_2/\text{day}$$

Oxygen demand at field conditions (OD_{field}) can be estimated based on the net OD_{theory}, wastewater characteristics, and mixing conditions using Equation 6.33.

$$OD_{field} = \left(\frac{OD_{theory}}{E}\right)\left(\frac{DO_{S,20}}{\alpha \cdot (\beta DO_S - DO) \cdot \theta^{T-20}}\right)$$

$$= \left(\frac{303 \text{ kg/day}}{0.3}\right)\left(\frac{8.51 \text{ g/m}^3}{0.6(0.95 \times 10.10 \text{ g/m}^3 - 2.0 \text{ g/m}^3) \cdot 1.024^{(12-20)}}\right)$$

$$= 2280 \text{ kg/day}$$

The saturation DO concentration at 12°C (285 K) is determined using Equations 6.29 and 6.30 as follows:

$$H_{O_2}(285 \text{ K}) = H_{O_2}(293 \text{ K}) \cdot \exp\left[\frac{\Delta H°}{R}\left(\frac{1}{293} - \frac{1}{285}\right)\right]$$

$$= 790 \text{ (L atm)/mol} \cdot \exp\left[1792\left(\frac{1}{293} - \frac{1}{285}\right)\right] = 665.4 \text{ (L atm)/mol}$$

$$\text{DO}_S(285\text{ K}) = \frac{P_{O_2(g)}}{H_{O_2}(285\text{ K})} = \frac{0.21\text{ atm}}{665.4\text{ (L atm)/bar}}$$

$$= 3.16 \times 10^{-4}\text{ mol/L} = 10.10\text{ mg/L}$$

If we apply 0.27 kg O_2 per m^3 air for the conversion from a mass rate into a volumetric rate, the OD is 8444 m^3 air/day or 5.86 m^3 air/min.

6.6.9 Designing the Membrane System

The design of the membrane system includes determining the design flux, required number of membrane modules, and aeration requirement for coarse bubble aeration.

First, the design flux can be determined based on wastewater flow characteristics and the membrane filtration cycle as follows:

$$\text{Design flux} = \frac{(\text{Maximum operating flux})(\text{Filtration ratio})(\text{Operating ratio})}{\text{Peaking factor}}$$

$$= \frac{(40\text{ L/m}^2\text{ h})(0.968)(0.982)}{1.5} = 25.35\text{ L/m}^2\text{ h}$$

where
   Peaking factor = (hourly peak flow)/(daily average flow) = 1.5
   Filtration ratio = (filtration time)/(filtration time + backwash time) = (15 min)/(15 + 0.5 min) = 0.968
   Operating ratio = (operating time)/(operating time + cleaning time) = [1 week – (3 times)(60 min/time)(1 week/10,080 min)]/(1 week) = 0.982

Second, the number of membrane modules can be estimated based on the design flux and daily average flow:

$$\text{Number of modules} = \frac{\text{Daily average flow}}{(\text{Design flux})(\text{Membrane area per module})}$$

$$= \frac{(1000\text{ m}^3/\text{day})(1000\text{ L/m}^3)(1\text{ day/24 h})}{(25.35\text{ L/m}^2\text{ h})(31.6\text{ m}^2/\text{module})} = 52\text{ modules}$$

ZeeWeed 500d cassettes can hold maximally 48 modules. Therefore, two cassettes are required with each cassette holding 26 modules.

Third, the coarse bubble aeration requirement for membrane scouring can be estimated based on the SAD and cyclic aeration strategy as follows:

Aeration requirement for coarse bubble aeration

$$= (SAD_m)(Membrane\ area)\frac{Aeration\ time}{Aeration\ time + Pause\ time}$$

$$= (0.54\ m^3/m^2/h)(52\ modules \times 31.6\ m^2/module)\frac{10\ s}{(10 + 10\ s)}$$

$$= 443.7\ m^3/h = 7.39\ m^3/min$$

6.6.10 Summary of Design

Design Parameter	Unit	Value
Aerobic tank		
Volume	m³	160
HRT	h	3.8
Anoxic tank		
Volume	m³	134
HRT	h	3.2
Internal recycle		
Flow rate	m³/day	800
Ratio to influent flow rate	Q	0.8
Alkalinity addition	mg CaCO₃/L	147
Wastage activated sludge		
Mass rate	kg VSS/day	64.0
Volumetric rate	m³/day	8.0
Aeration		
Biological reactions	m³/min	5.86
Coarse bubble aeration	m³/min	7.39
Membrane system		
Number of modules	ea	52
Number of cassettes	ea	2

Problems

6.1 You want to design a bar screen to remove coarse materials such as rages, paper, plastics, and metals from the flow stream.

Rack

Influent → Effluent

Rack chamber
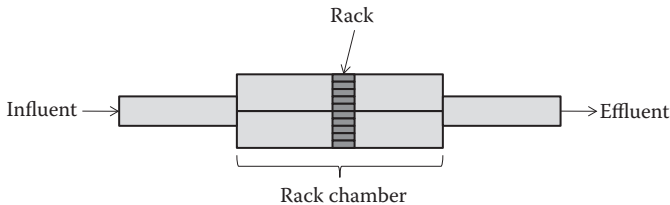
Assuming the design conditions are as follows:

- Peak design wet weather flow = 3.0 m³/s
- Depth of the conduit at peak design flow = 2.0 m
- Approach velocity = 0.6 m/s
- Velocity through clean bar screen = 0.9 m/s
- Headloss coefficient for a clean bar screen = 0.7
- Headloss coefficient for a clogged bar screen = 0.6
  a. Compute the headloss through the bar screen when the bar is clean.
  b. You want to design an automatic bar rake active when the headloss increases to 0.2 m. Compute the percentage of clogging of the bar screen when the headloss reaches 0.2 m.
  c. Determine the number of clear widths and the number of bars for a set of bar screens for the peak design flow condition, assuming the flow was equally distributed to each bar screen. Each bar is 10 mm thick, while each clear width has 25 mm of spacing.

6.2 A university has a plan to build a wastewater treatment plant on campus. The data in the following table consist of monthly average flow values generated from the campus. Assuming the data are distributed normally, determine wastewater flow rate corresponding to 60% and 90% probabilities graphically.

Month	*Flow rate (m³/day)*
January	3000
February	4500
March	5700
April	6200
May	6900

Month	Flow rate (m³/day)
June	7500
July	8700
August	8000
September	6600
October	5200
November	4800
December	3700

6.3 An in-line flow equalization basin is to be designed for an MBR plant. From plant records, a compilation has been made that gives the hourly flow rate vs. hour of the day as follows:

Hour (h)	m³/day	Hour (h)	m³/day
12 AM	11.4	1 PM	25.0
1	8.3	2	25.0
2	7.9	3	26.9
3	7.6	4	28.8
4	9.1	5	32.9
5	10.6	6	37.5
6	13.6	7	37.5
7	20.8	8	31.8
8	25.0	9	23.1
9	28.0	10	15.9
10	28.8	11	13.2
11	26.9	12 AM	11.4
12 noon	25.7		

6.4 Determine the fluctuating volume required for the basin in cubic meters. In order to reduce the size of the anoxic tank while designing an MBR plant (see Section 6.6), designers want to use an external carbon source for

denitrification. This will increase the F/M ratio in the anoxic tank and resultantly increase the SDNR and reduce the required size of the anoxic tank. Designers are planning to use methanol wastewater as the external carbon source. The concentration of methanol is 1000 mg/L and the amount of methanol available is 50 m³ per day. Estimate the altered size of the anoxic tank and the required flow rate for internal recycle. Assume that the maximum permeate nitrate level has not been changed (i.e., 25 mg N/L).

6.5 In order to produce better effluent quality, an existing wastewater treatment plant will be retrofitted to an MBR plant. Design a bioreactor and membrane system for the MBR plant and estimate the treated water quality. The bioreactor consists of an anoxic tank (volume = 125 m³) and an aerobic tank (volume = 250 m³), and the mixed liquor in the aerobic tank is recycled into the anoxic tank (e.g., internal recycle) with a flow rate of 2000 m³/day to facilitate biological nitrogen removal via nitrification and denitrification. The anoxic and aerobic tanks are operated by completely stirred tank reactor. Assuming all the design conditions except the target MLVSS concentration are the same as those introduced in Section 6.6, estimate (1) the MLVSS concentration in the bioreactor, (2) the amount of daily waste activated sludge, (3) the aeration rates for biological treatment and membrane cleaning, and (4) the nitrogen removal performance.

6.6 Influent wastewater entering a bioreactor was characterized to design a wastewater treatment bioreactor as follows:

Parameter	Unit	Value
Flow	m³/day	5000
Influent total COD	mg/L	320
Influent biodegradable COD	mg/L	200
Influent TSS	mg/L	100
Influent VSS	mg/L	70
Influent nonbiodegradable VSS	mg/L	30
HRT	h	8
SRT	day	6
Biomass yield, Y	g VSS/g bCOD	0.40
Fraction of biomass that remains as cell debris, f_d	g VSS/g VSS	0.10
Endogenous decay coefficient, k_d	g VSS/g VSS/day	0.10

Parameter	Unit	Value
Half-saturation constant, K_s	mg COD/L	10
Max. specific growth rate, μ_m	day^{-1}	3.00

    a. Estimate the effluent biodegradable COD concentration.
    b. Estimate the total sludge production rate ($P_{X_T,VSS}$) in kg VSS/day.
    c. Determine the solids concentration of the bioreactor in mg VSS/L.
    d. Determine the return flow rate in m³/day assuming the concentration of return activated sludge is 9000 mg VSS/L.
    e. Determine the bioreactor oxygen requirement in kg/day.

6.7   An engineer wants to design a wastewater treatment plant to treat wastewater containing phenol at a semiconductor company. Phenol is the sole organic matter of the wastewater and should be treated below 1 g/m³. The engineer has decided to design a treatment plant using an MBR process because the semiconductor company has limited space for constructing a conventional activated sludge plant. The space available for building a bioreactor is <500 m³ and 4 m³ is available for a holding tank for waste activated sludge. The engineer wants to design an MBR bioreactor <500 m³ and plans to empty the holding tank every week to dispose of the waste activated sludge. Wastewater is produced at a rate of 1000 m³ daily and contains 1000 g/m³ phenol. Nonbiodegradable solids ($X_{0,i}$) are not detectable in the influent wastewater. Kumar et al. (2005) had reported the kinetic data of a bacterium that can degrade phenol as follows: Y = 0.654 g phenol/g VSS, μ_{max} = 0.216 h^{-1}, K_s = 20.59 g/m³, k_d = 0.1 g VSS/g VSS day, and f_d = 0.15 g VSS/g VSS. Calculate the design SRT, daily solids production (P_{X_T}) in kg VSS/day, solids concentration in the bioreactor (X_T) in g VSS/m³, and required bioreactor volume using the provided conditions and the kinetic data of Kumar et al. In addition, assume that the density of the waste activated sludge is 1000 kg/m³.

6.8   The design flux and the number of modules need to be determined for an MBR plant. It is planned to install flat sheet membranes having 40 LMH of maximum operating flux. Each membrane module has 1.0 m² of surface area. Membranes will be operated cyclically with 9 min of operation and 1 min of pause. Backwashing will not be performed, but maintenance cleaning will be conducted for 30 min every day. The average wastewater inflow to the bioreactor is 500 m³/day and the flow rate peaking factor is 1.8.
    a. Calculate the design flux for the estimated number of membrane modules in the MBR plant.
    b. Estimate the number of modules required for the MBR plant.

6.9   An engineer monitored AOTR as a function of temperature from a bioreactor in an MBR plant (see the following graph). Based on the following information, deduce the volume of the bioreactor.
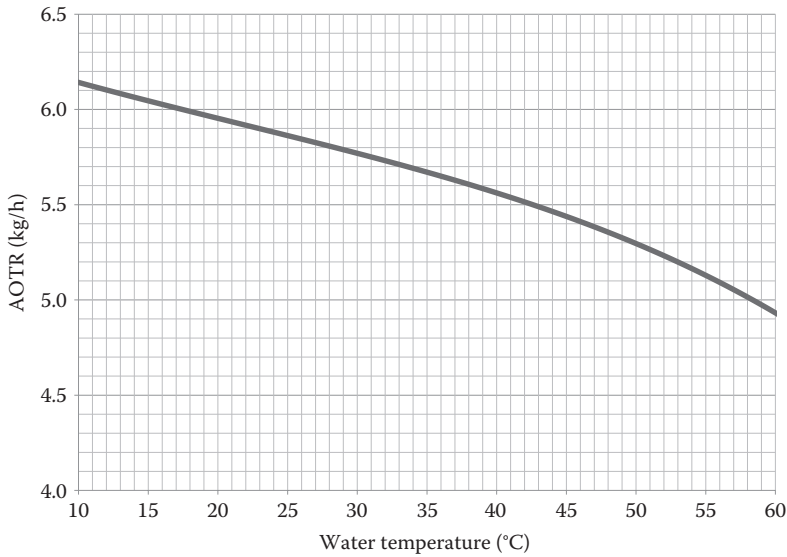
- Volumetric oxygen transfer rate (K_{La}) at 20°C = 4.9 h^{-1}
- The ratio of oxygen transfer rate of wastewater to that of clean water (α) = 0.6
- The temperature correction factor (θ) = 1.024
- The ratio of saturated DO concentration of wastewater to that of clean water (β) = 0.95
- Henry's law constant at 20°C (293 K) = 790 L atm/mol
- Design DO concentration in a reactor = 2.0 mg/L

6.10 Wu et al. (2008) conducted a set of experiments to evaluate relaxation (filtration and pause) and backwashing for membrane fouling control in a laboratory-scale MBR. They set up three relaxation conditions (R1–R3), five backwashing conditions (B1–B5), one continuous filtration without relaxation or backwashing (C1) as shown in the following table. To compensate for the loss of productivity (i.e., to generate net flux as 20 LMH) during backwashing or relaxation, instantaneous flux was applied.
Conditions applied in the experiment

Run	Operating Parameter for Relaxation or Backwashing			Instantaneous Flux (L/(m² h))
	Duration (s)	Interval (s)	Strength (L/(m² h))	
C1	—	—	—	20.0
R1	20	440	—	21.0
R2	20	220	—	22.0

| | Operating Parameter for Relaxation or Backwashing | | | Instantaneous |
Run	Duration (s)	Interval (s)	Strength (L/(m² h))	Flux (L/(m² h))
R3	40	440	—	22.0
B1	40	240	50	34.0
B2	20	240	50	26.4
B3	40	480	50	26.4
B4	20	240	30	24.5
B5	40	480	30	24.5

Source: Wu, J.L. et al., *J. Membr. Sci.*, 324(1–2), 26, 2008.

Duration indicates the applied time for pause (R1–R3) or backwashing (B1–B3). Strength indicate the flow rate of backwashing.

a. Explain the advantages of backwashing and relaxation in MBR operation, respectively.
b. Temporal changes in membrane fouling rates (dTMP/dt) for different relaxation conditions are shown in the following figure. What conclusions can be drawn from the results?
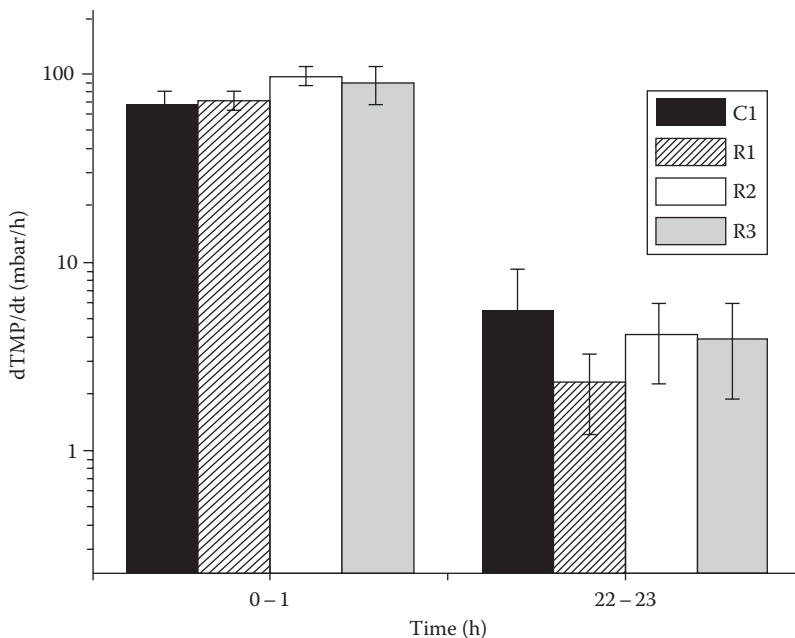
(a)   *Source*: Wu, J.L. et al., *J. Membr. Sci.*, 324(1–2), 26, 2008.

c. The fouled membrane was cleaned using appropriate methods after a filtration period. And the fouling layers were separated into three fractions: rinsed, backwashed, and desorbed. The hydraulic resistances of different fractions (i.e., total, rinsed, and desorbed) for the different backwashing conditions are shown in the following figure. What conclusions can be drawn from the results?
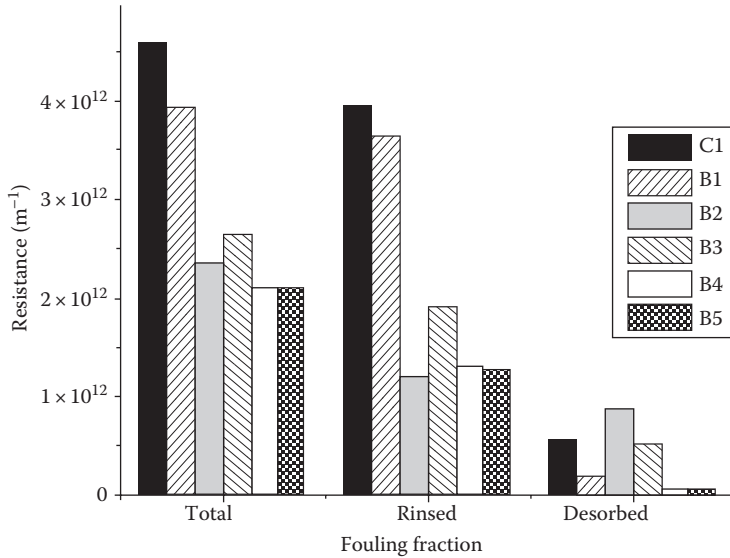
(b)   *Source*: Wu, J.L. et al., *J. Membr. Sci.*, 324(1–2), 26, 2008.

d. Pearson correlation analysis between instantaneous flux and final TMP is shown in the following figure. What conclusions can be drawn from the results?
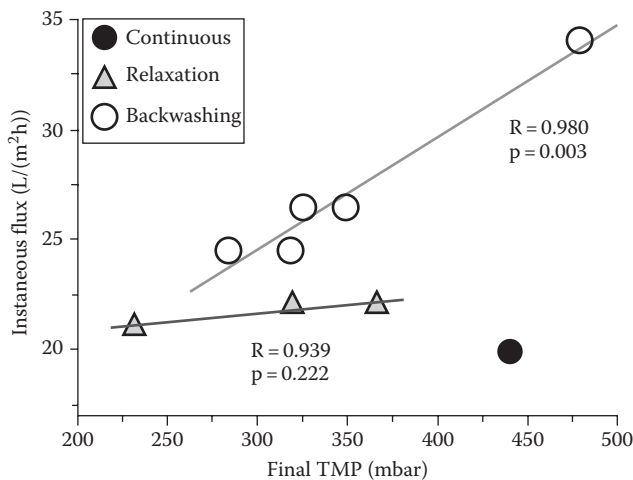
(c)   *Source*: Wu, J.L. et al., *J. Membr. Sci.*, 324(1–2), 26, 2008.

References

Chang, S. (2011) Application of submerged hollow fiber membrane in membrane bioreactors: Filtration principles, operation, and membrane fouling, *Desalination*, 283: 31–39.

Frechen, F. B., Schier, W., and Linden, C. (2008) Pre-treatment of municipal MBR applications, *Desalination*, 231: 108–114.

Henze, M., Gujer, W., Mino, T., and van Loosdrecht, M. (2000) *Activated Sludge Models ASM1, ASM2, ASM2d and ASM3*. IWA Publishing, London, U.K.

Judd, S. (2006) *The MBR Book*. Elsevier, London, U.K.

Judd, S. (2008) The status of membrane bioreactor technology, *Trends in Biotechnology*, 26(2): 109–116.

Krampe, J. and Kauth, K. (2003) Oxygen transfer into activated sludge with high MLSS concentrations, *Water Science and Technology*, 47(11): 297–303.

Kumar, A., Kumar S., and Kumar, S. (2005) Biodegradation kinetics of phenol and catechol using *Pseudomonas putida* MTCC 1194, *Biochemical Engineering Journal*, 22: 151–159.

Qasim, S. (1998) *Wastewater Treatment Plants: Planning, Design, and Operation*, 2nd edn. CRC Press, Boca Raton, FL.

Randal, C.W., Barnard, J.L., and Stensel, H.D. (1992) Design of activated sludge biological nutrient removal plants, in *Design and Retrofit of Wastewater Treatment Plants for Biological Nutrient Removal*, Randal, C.W., Barnard, J.L., and Stensel, H.D. (Eds.). Technomic Publishing, Lancaster, PA.

Reynolds, T.D. and Reynolds, P.A. (1996) *Unit Operations and Processes in Environmental Engineering*, 2nd edn. PWS Publishing Company, Boston, MA.

Rittmann, B.E. and McCarty, P.L. (2000) *Environmental Biotechnology: Principles and Applications*, McGraw-Hill Higher Education, Boston, MA.

Schier, W., Frechen, F.B., and Fisher, St. (2009) Efficiency of mechanical pre-treatment on European MBR plants, *Desalination*, 236: 85–93.

Tchobanoglous, G., Burton, F.L., and Stensel, H.D. (2003) *Wastewater Engineering: Treatment and Reuse*, 4th edn. McGraw-Hill, New York.

U.S. EPA (1993) Manual: Nitrogen control. U.S. Environmental Protection Agency, Washington, D.C.

Wu, J., Le-Clech, P., Stutz, R.M., Fane, A.G., and Chen, V. (2008) Effects of relaxation and backwashing conditions on fouling in membrane bioreactor, *Journal of Membrane Science*, 324(1–2): 26–32.

Chapter 7

Case Studies

7.1 Introduction

Membrane bioreactor (MBR) technology has been studied for over 40 years, beginning in 1969. In North America, full scale commercial MBR technology for the treatment of industrial wastewaters has been in use since 1991. In the early 1990s, most MBR configuration included pressurized modules. By the mid-1990s, submerged membranes had been developed and were adapted by MBR processes. Submerged membranes reduced the high electric power consumption and high fouling rate issues of the pressurized modules. Submerged membrane modules also expanded MBR applications from exclusive industrial treatment systems to include municipal wastewater treatment. Plant capacity has been increasing in proportion with the in number of operating MBR plants from less than 1,500 m^3/day to more than 200,000 m^3/day.

Table 7.1 shows the largest MBR plants worldwide. The list is ordered by peak daily flows (PDF, million liters per day). The world's largest MBR plant, currently, is the Seine Aval municipal WWTP in Acheres, France. It is currently under construction by GE and will treat 224,000 m^3/day of wastewater starting from 2016. Twelve out of the 33 plants listed in the table are located in the United States, 10 in China and Korea, 3 in Australia, and 3 in Europe. Although Japan invented the original MBR technology, they have no MBR plants on the list. European countries also have only a few large MBR plants, even though there are many applications there. Twenty-two out of the 33 MBR plants were provided by GE, which means GE and their engineering technologies are the dominant providers of larger MBR plants. The MBR plants listed in Table 7.1 will be studied in Sections 7.4 and 7.5 based on municipal or industrial wastewater treatment categorization.

Table 7.1   Largest MBR Plants Worldwide

Installation	Location	Technology Provider	Commissioned Date	PDF (MLD)	ADF (MLD)
Seine Aval	Acheres, France	GEWPT	2016	357	224
Canton WWTP	Ohio, USA	Ovivo, USA	Expected 2015–2017	333	159
Macau	China	GEWPT	2014	189	137
Riverside	California, USA	GEWPT	2014	186	124
Brightwater	Washington, USA	GEWPT	2011	175	122
Visalia	California, USA	GEWPT	2014	171	85
Qinghe	China	OW/MRC	2011	150	150
North Las Vegas	Nevada, USA	GEWPT	2011	136	97
Ballenger McKinney ENR WWTP	Maryland, USA	GEWPT	2013	135	58
Cox Creek WRF	Maryland, USA	GEWPT	2015	116	58
Yellow River	Georgia, USA	GEWPT	2011	114	71
Shiyan Shendinghe	China	OW/MRC	2009	110	110
Aquaviva	Cannes, France	GEWPT	2013	108	60
Busan City	Korea	GEWPT	2012	102	102
Guangzhou	China	Memstar	2010	100	
Wenyuhe	Beijing, China	OW/Asahi Kasei	2007	100	100
John's Creek	Georgia, USA	GEWPT	2009	96	42

(*Continued*)

Table 7.1 (*Continued*)   Largest MBR Plants Worldwide

Installation	Location	Technology Provider	Commissioned Date	PDF (MLD)	ADF (MLD)
Changi	Singapore	GEWPT	2014	92	61
Awaza/ Polimeks	Turkmenistan	GEWPT	2011	89	71
Songsan Green City	Korea	Econity	Planned 2015	84	
Beixiaohe	China	Siemens	2008	78	—
Al Ansab	Muscat, Oman	Kubota	2010	77	55
Cleveland Bay	Australia	GEWPT	2007	77	29
Broad Run WRF	Virginia, USA	GEWPT	2008	73	38
Gongchon	Korea	Econity	2012	65	65
Lusail STP	Doha, Qatar	GEWPT/ Degrémont	2013	62	58
La Moree	France	GEWPT	2013		61
Gaoyang	China	United Envirotech	Expected 2014	60	
Cairns North	Australia	GEWPT	2009	59	19
Cairns South	Australia	GEWPT	2009	59	19
Peoria	Arizona, USA	GEWPT	2008	58	38
Aquapolo	São Paulo, Brazil	Koch Membrane Systems	2013	56	56
Sabadell	Spain	Kubota	2009	55	
Jordan Basin WRF	Utah, USA	GEWPT	2010		54

7.2 Commercial Membranes, Modules, and Cassettes for MBR

There are hundreds of membrane providers in the world. However, in the MBR market there are two major companies. The largest company is GE Zenon and the second largest is Kubota. GE Zenon supplied membranes for 14 of the largest MBR plants out of the top 20 in the world according to data released in 2010. Koch Membrane Systems (KMS), which supplies MBR technology with Kubota membranes, has the most installations in the world. GE Zenon produces hollow fiber membranes and Kubota produces flat-sheet membranes. Both companies supply submerged membrane modules. Mitsubishi Rayon was the first company in the world to develop membranes and apply them in MBR processes. Therefore, they have the original patent for MBR membranes and systems.

7.2.1 GE Zenon

Zenon debuted the reinforced hollow fiber membranes and the corresponding immersed modules under the product name "ZeeWeed 145" in 1993. The membranes were made of polyvinylidene fluoride (PVDF) based on non-solvent-induced phase separation (NIPS) technology and were reinforced with braid made of PET. The membrane was an ultrafiltration (UF) membrane with pore size of 0.02 μm. The outer diameter of the membrane was 1.8 mm and the inner diameter was 0.8 mm. The effective membrane surface area in a module was 13.5 m^2.

Permeate water flowed from the outer membrane surface to both the ends of the membranes. A cassette consisted of 12 modules, which gave 167 m^2 of total effective membrane area in each module. The membrane packing density of a cassette was 168 m^2/m^3. This original model was developed in many aspects, and GE Zenon's most recent product is ZeeWeed 500d.

Its unit module and cassette are shown in Figure 7.1b. The major membrane specifications have not changed much, but the modules and their cassettes have been developed to be more efficient. The effective membrane surface area in each module has been increased to 34.4 m^2. A cassette can now accommodate 48 modules, resulting in a total effective membrane surface area of 1650 m^2, which is 10 times higher than the first product. The membrane packing density of the current cassette is 448 m^2, which is almost three times higher than the original. Figure 7.1 shows pictures of (a) ZeeWeed 145 and (b) ZeeWeed 500d.

The performance of the cassettes has also advanced. Membrane aeration is the main reason MBR systems are more expensive compared to conventional processes, which impedes more widespread use of MBR systems. Membrane aeration requires about 30% of the total operating energy. GE Zenon has adapted a stepwise cleaning process that includes backwashing, maintenance cleaning (MC), and recovery cleaning. They also developed cyclic aeration and ecoaeration and succeeded in
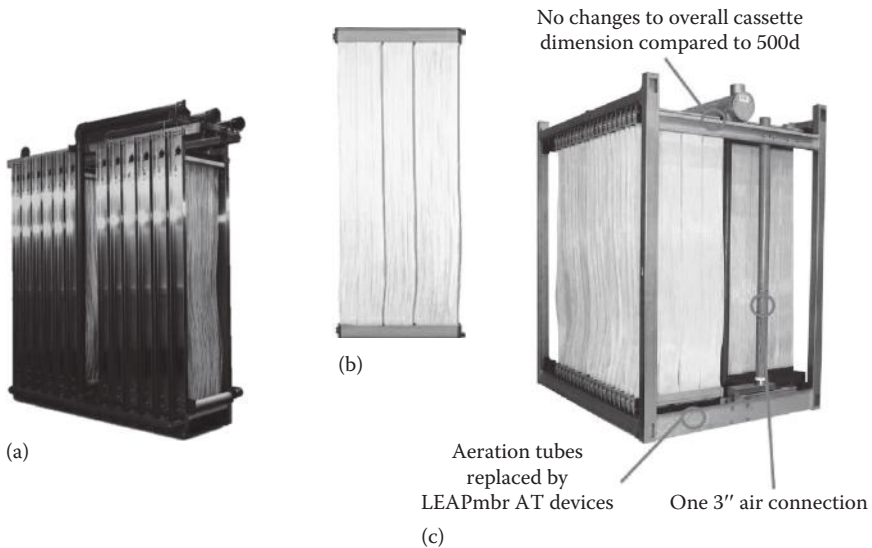
Figure 7.1 **(a) ZeeWeed 145 cassette, (b) its unit module, and (c) the cassette of ZeeWeed 500d.**

reducing the aeration energy from 0.9 kWh/m³ (ZeeWeed 150) to 0.1 kWh/m³ (ZeeWeed 500d). Their general aeration rate (SAD_m) is 0.54 Nm³/h·m².

Aim to reduce aeration cost was the reason why they adapted the interval aeration times. Cyclic aeration included 50% of downtime (no aeration) and now the new ecoaeration includes 75%. Recently they developed the "LEAPmbr" system, which additionally reduces the aeration by an additional 30% by changing the aeration intensity, that is, to say, varying the air flow. The new system could also eliminate many air-cycling valves and reduce capital costs.

7.2.2 Kubota

Kubota launched membranes for MBR several years before Zenon. The former product was named the "510" series and it has now advanced to the "515" series. Both membranes are made of chlorinated polyethylene, based on melting chemistry. The former membrane (510 series) was an MF membrane, and its pore size was 0.4 μm. The flat surface was further mounted on a flat plastic plate with a spacer material. The plate of 510 was 1000 mm high, 490 mm wide, and 6 mm thick and had a total surface of 0.8 m² per plate. The latest 515 model plate is 1560 mm high, 575 mm wide, and 6 mm thick and has a total surface of 1.45 m² per plate. The 515 module has two suction ports for efficient permeation. The effective membrane surface area in a "510" series module was 0.8 m². Permeate was extracted from the top ends of

the membranes. A cassette consisted of a maximum of 200 modules, which gave an effective surface area of 160 m². The membrane packing density of a cassette was 44 m²/m³, which was a quarter of the ZeeWeed 150.

Compared with the 510 series, the current 515 series has been developed considering many more aspects. Like the ZeeWeed series, the major membrane specifications have not changed a lot, but the modules and their cassettes have been developed to be more efficient. The effective membrane surface area in a module has increased to 1.45 m². A cassette can accommodate 200 modules resulting in a total effective membrane surface area of 290 m², which is 1.8 times higher than the first product.

The membrane packing density of a current cassette is 48 m², which is not a large improvement from the original series and is significantly lower compared to the current ZeeWeed. Increasing the packing density of membrane cassettes is resulted from stacking unit modules by two or three layers, which is called a double-deck (DD) system. Figure 7.2 shows a schematic of (a) 510 and 515 series modules, (b) their cassettes, and (c) the pictures of main cassettes such as ES, EK, and RW that have single, double, and triple stacks, respectively.

KMS is the major engineering partner of Kubota. KMS developed the MBR system for Kubota's membranes. They adapted a continuous aeration process, and they focused on and succeeded in reducing the aeration rate from 0.75 to 0.42 Nm³/h·m².

7.2.3 Mitsubishi Rayon Engineering

Mitsubishi Rayon Engineering (MRE) is the third largest MBR membrane supplier worldwide and the largest in Asia, and it holds the original technology patents for MBR membranes and processes. MRE provides two types of membranes. One is a single layer hollow fiber membrane made of polyethylene with the series brand name "SUR." The other is a braid-reinforced hollow fiber membrane made of PVDF on PET braid reinforcement with the series brand name "SADF." Both products are based on NIPS technology.

"SUR" has a nominal membrane pore size of 0.4 μm and is an MF membrane. The effective membrane surface area of the largest module is 3 m². Permeate is extracted from both side ends of the membranes. The modules have a horizontal configuration. The largest cassette, "SUR 50M0210LS," consists of 70 modules, which provides 210 m² of effective membrane area. The membrane packing density of a cassette is 131 m²/m³.

"SADF" has a nominal membrane pore size of 0.1 μm and is also an MF membrane. The effective membrane surface area of the largest module is 25 m². Permeate is extracted from both ends of the membranes and the modules have a vertical configuration. The largest cassette "SADF 50E0025SA" consists of 20 modules, which provides 500 m² of effective membrane area. The membrane
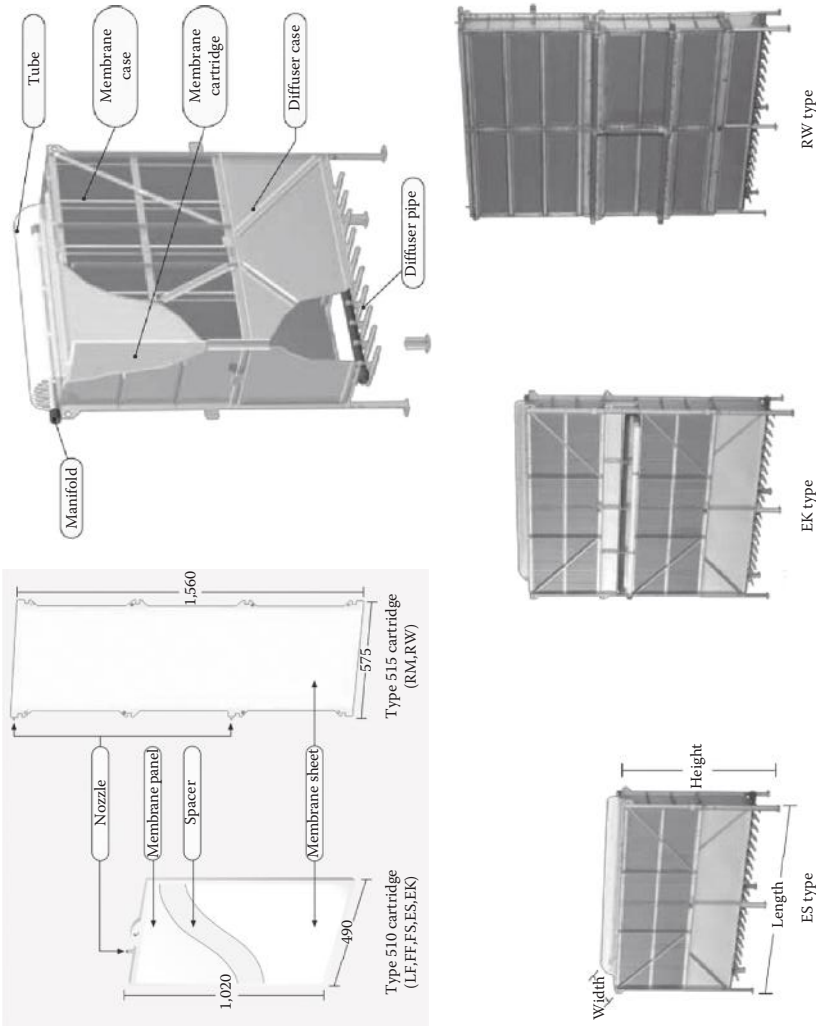
Figure 7.2   Schematic of Kubota membrane module and cassettes.

Membrane element—horizontal   Membrane module—horizontal

Membrane surface

Membrane element—vertical   Membrane module—vertical

H 2000 mm, W 1250 mm
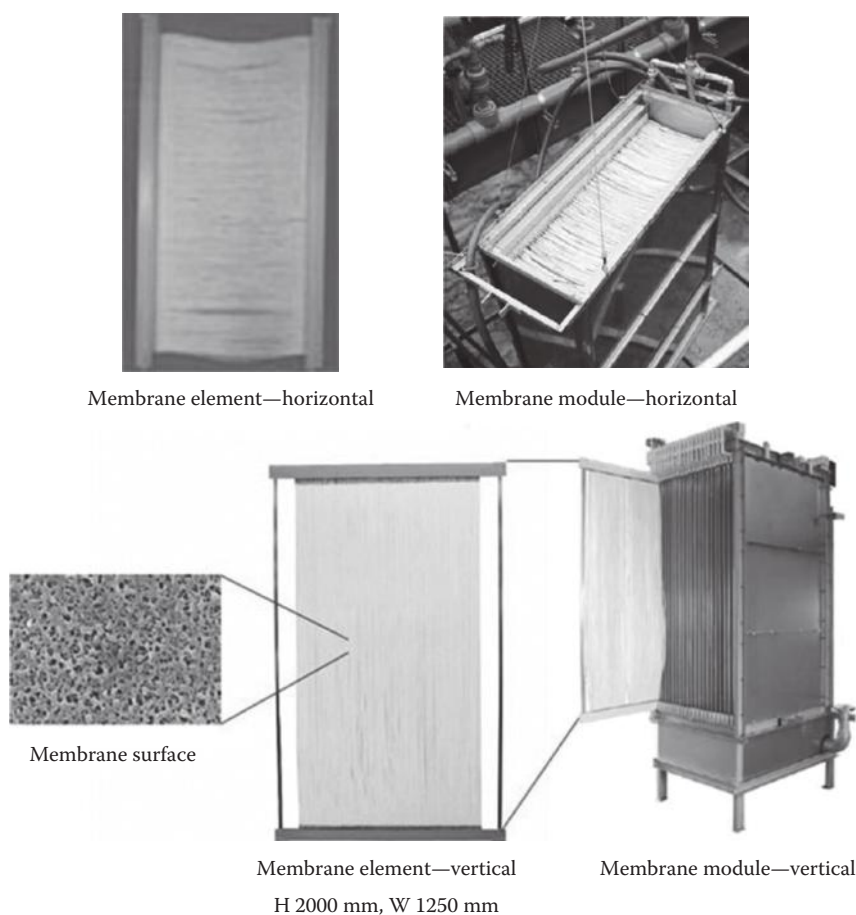
Figure 7.3   Schematic of MRE membrane module and cassettes. (From van der Roest, H.F. et al., *Membrane Bioreactors for Municipal Wastewater Treatment,* **IWA Publishing, London, U.K., 2002; Judd, C., The largest MBR plants worldwide?, http://www.thembrsite.com/about-mbrs/largest-mbr-plants/, 2014.)**

packing density of a cassette is 64 m²/m³. Figure 7.3 shows the pictures of SUR 50M0210LS and SADF 50E0025SA.

7.2.4 Pentair

Pentair provides membranes named "X-Flow." The X-Flow filtration surface has a 0.03 μm pore size (UF) made of PVDF coated on a tubular support. The water being treated passes from the inside of the membrane to the outside by

Compact 27

Compact 33V

Compact 32V MBR system
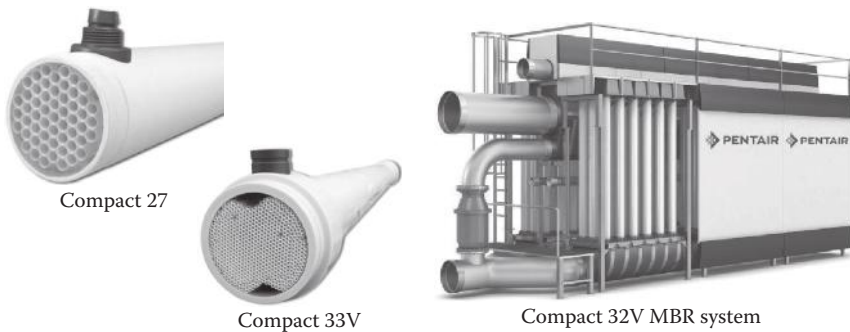
Figure 7.4   Schematic of Pentair membrane module and cassettes. (From van der Roest, H.F. et al., *Membrane Bioreactors for Municipal Wastewater Treatment*, IWA Publishing, London, U.K., 2002; Judd, C., The largest MBR plants worldwide?, http://www.thembrsite.com/about-mbrs/largest-mbr-plants/, 2014.)

a pressure-driven force. The external module system uses low-pressure sludge circulation with air in order to maintain turbulent flow along the hollow fiber or membrane tube. Figure 7.4 displays the current X-Flow technology.

7.2.5 Membranes, Modules, and Cassettes List for MBR Application

Table 7.2 presents a list consisting of the technical information of various membranes, modules, and cassettes for MBR processes. The table also shows the pictures of membrane modules and a unit system of the modules. It also gives some information about the providers, brand names of membrane modules, membrane materials, membrane pore size, classification by pore size, permeation direction, and module morphologies.

7.3 Case Studies of the MBR Processes Using Popular Membranes

In this section the performances of MBR pilot plants using popular membranes that were introduced in Section 7.2 are described in detail. This section is the summary of MBR pilot test result in Beverwijk wastewater treatment plant (WWTP) researched by STOWA, the Dutch Foundation for Applied Water Research. They invited four major membrane and MBR system providers and tested their technologies, and optimized the technologies for Beverwijk wastewater. During the test they had four different phases with different operation conditions for optimization. This section includes the general information of the membranes, modules, systems, and their results.
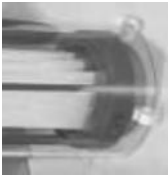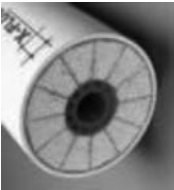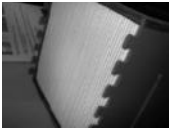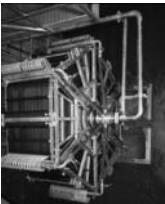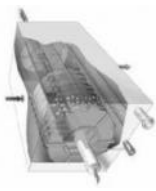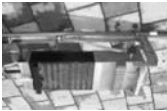
Table 7.2 Modules List for MBR Application

Module	System	Company Model	Chemistry	Pore Size	MF UF	Membrane Morphology	Permeation Direction	Module Morphology
		GE—Zenon ZeeWeed	PVDF	0.02	UF	H, R	Out → In	S, V
		Kubota 510	PVC	0.4	MF	P	Out → In	S, V
		MRE SUR	PE	0.4	MF	H	Out → In	S, H

(Continued)

Table 7.2 (Continued) Modules List for MBR Application

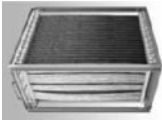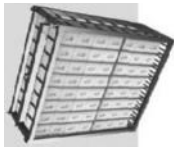| Module	System	Company Model	Chemistry	Pore Size	MF UF	Membrane Morphology	Permeation Direction	Module Morphology
		MRE SADF	PVDF	0.1	MF	H, R	Out → In	S, V
		US Memjet	PVDF	0.08	MF	H	Out → In	S, V
		Norit Xiga	PES	0.03	UF	H	In → Out	P, H
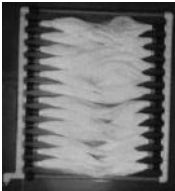
(Continued)

Table 7.2 (Continued) Modules List for MBR Application

Module	System	Company Model	Chemistry	Pore Size	MF UF	Membrane Morphology	Permeation Direction	Module Morphology
		KMS Puron	PES	0.05	MF	H,R	Out → In	S, V
		Toray Seghers Keppel	PVDF	0.08	MF	P	Out → In	S, V
		Max flow A3	Polyphenol	0.08	MF	P	Out → In	S, V
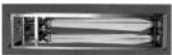
(Continued)

Table 7.2 (Continued) Modules List for MBR Application

Module	System	Company Model	Chemistry	Pore Size	MF UF	Membrane Morphology	Permeation Direction	Module Morphology
		Eidos	PP	0.1	MF	H	Out → In	S, V
		Huber VRM	PES	0.1	MF	P	Out → In	S, V
		Huber VUM	PES	0.1	MF	H	Out → In	S, V
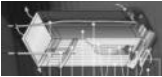
(Continued)

Table 7.2 (Continued)   Modules List for MBR Application

Module	System	Company Model	Chemistry	Pore Size	MF UF	Membrane Morphology	Permeation Direction	Module Morphology
		Asahi Kasei MUNC 620	PVDF	0.3	MF	H	Out → In	S, V
		Cleanfil®-S30V	PVDF	0.1	MF	H, R	Out → In	S, V
		KMS-600	PP	0.4	MF	H	Out → In	S, V

(Continued)

Table 7.2 (Continued) Modules List for MBR Application

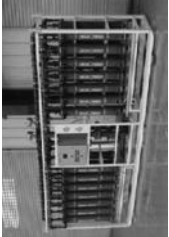| Module	System	Company Model	Chemistry	Pore Size	MF UF	Membrane Morphology	Permeation Direction	Module Morphology
		Martin Systems siClaro FM		0.1	UF	P	Out → In	S, V
		VSEP			UF	P	Out → In	P, V
		Norit Aquaflex	PVDF	0.03	UF	H	In → Out	P, V

(*Continued*)

Table 7.2 (Continued) Modules List for MBR Application

Module	System	Company Model	Chemistry	Pore Size	MF UF	Membrane Morphology	Permeation Direction	Module Morphology
		Norit Cross-flow MBR	PVDF	0.03	UF	H	In → Out	P, H
		DOW Omexell	PVDF	0.01	UF	H	Out → In	P, V
		Orelis SA Persep Novasep	PES		UF	H	In → Out	P, V
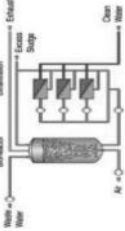
(Continued)

Table 7.2 (Continued) Modules List for MBR Application

Module	System	Company Model	Chemistry	Pore Size	MF UF	Membrane Morphology	Permeation Direction	Module Morphology
		Orelis SA Pleiade Novasep	PES		UF	P	Out → In	S, V
		Rochem BioFILT FM			UF	P	Out → In	S, H
		SFC Umwelttechnik—CMEM					Out → In	
		Motial Tianjin	PVDF		MF	H	Out → In	P/S, V

(Continued)

Table 7.2 (*Continued*)   Modules List for MBR Application

Module	System	Company Model	Chemistry	Pore Size	MF UF	Membrane Morphology	Permeation Direction	Module Morphology
		Spirasep Trisep	PES	0.05	UF	SW	Out → In	P, V
		Microclear Weise Water Systems		0.01	UF	P	Out → In	S, V
		Biomembrat Wehrie Werk				P	In → Out	P, V

(Continued)
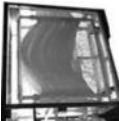
Table 7.2 (*Continued*) Modules List for MBR Application

Module	System	Company Model	Chemistry	Pore Size	MF UF	Membrane Morphology	Permeation Direction	Module Morphology
		Zao Membranes	PSF		MF	T	Out → In	S, V
		Motimo	PVDF		MF	H	Both	S/P, V
		Porous fibers	PVDF	0.1	MF	H	Out → In	S, V

(*Continued*)

Table 7.2 (*Continued*) Modules List for MBR Application

Module	System	Company Model	Chemistry	Pore Size	MF UF	Membrane Morphology	Permeation Direction	Module Morphology
		Litree			UF	H	Both	S/P, H
		Hyflux						
		BioCel Microdyne-Nadir	PES		MF	P	Out → In	S, V

Sources: van der Roest, H.F. et al., *Membrane Bioreactors for Municipal Wastewater Treatment*, IWA publishing, London, U.K., 2002; Judd, C., The largest MBR plants worldwide?, http://www.thembrsite.com/about-mbrs/largest-mbr-plants/, 2014.

Abbreviations: H, hollow fiber; P, plate (flat sheet); R, reinforced; M, mutibore; S, submerged; P, pressurized; V, vertical; H, horizontal.

The system configurations, design data, and the biological and membrane performances are presented. Finally the conclusions are summarized. In these Sections, we can apply our knowledge of MBR gathered through former Sections to case studies of pilot plants and compare MBR systems including membranes and their modules of each provider.

7.3.1 GE Zenon

7.3.1.1 System Configuration
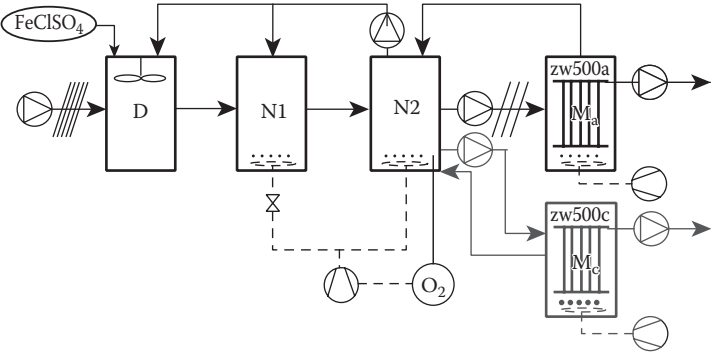
The picture of MBR pilot plant and the configuration and design of a GE Zenon pilot are presented in Figure 7.5 and Table 7.3. The recirculation began from N2 to reduce the oxygen recirculation to N1 to favor denitrification in this compartment. For the aeration of the activated sludge in N1 and N2 only one compressor was installed. The aeration in N1 could be shut down by the aeration control, which was based on the measured oxygen concentration in N2. The coarse bubble aeration in the membrane section was at a fixed constant level, but cycled over two of the four installed modules at all times.

Figure 7.5   Zenon's MBR pilot plant. (From van der Roest, H.F. et al., *Membrane Bioreactors for Municipal Wastewater Treatment*, IWA Publishing, London, U.K., 2002; Judd, C., The largest MBR plants worldwide?, http://www.thembrsite.com/about-mbrs/largest-mbr-plants/, 2014.)

Table 7.3   System Design Configuration and Figures of Zenon's MBR Plant

Process Part	Parameter	Unit	Values
Influent pump	Capacity	m³/h	15
	RWF[a] design flow	m³/h	7.6
	Design flow	m³/day	38.0
Influent screen	Type	—	Static half drum with brush
	Slot size	Mm	0.75
Biological tank	Total volume (and depth)	m³	26.6
	Anoxic volume (D)	m³ (m)	4.38 (1.75)
	Anoxic/oxic comp. (N1)	m³ (m)	7.66 (1.75)
	Oxic compartment (N2)	m³ (m)	7.66 (1.75)
	Membrane tank (M)	m³ (m)	3.0 (2.0)
Aeration source	Compressor capacity	Nm³/h	100
Ferric dosing	Type	—	FeClSO₄
	Ferric content	%	12.3
	Dose (at Me/P = 0.8)	mL/h	80–100
Membrane filtration	Number of modules	—	3
	Surface each module	m²	20
	Total surface	m²	60
	Maximum net flux (at RWF)	LMH	35

Table 7.3 (*Continued*)   System Design Configuration and Figures of Zenon's MBR Plant

Process Part	Parameter	Unit	Values
Aeration membranes	Compressor capacity	Nm³/h	60 (cycled)
	Specific capacity	Nm³/m² h	0.5
Recirculation flows	Sludge N2 → M	m³/h	18–30 (5:1)
	Internal N2 → N1	m³/h	8
	Nitrate N2 → D	m³/h	14.5
	Sludge N2 → M	m³/h	5–15 (x:1)

Sources: van der Roest, H.F. et al., *Membrane Bioreactors for Municipal Wastewater Treatment*, IWA Publishing, London, U.K., 2002; Judd, C., The largest MBR plants worldwide?, http://www.thembrsite.com/about-mbrs/largest-mbr-plants/, 2014.

[a] RWF, rain weather flow; DWF, dry weather flow.

7.3.1.2 Biological Performance

7.3.1.2.1 Process Conditions

The overall process conditions during the operation of the pilot are presented in Table 7.4. The average influent flow during the research period varied strongly due to excessive rainfall conditions. The average flow amounted to 140% of the design flow. The design sludge concentration was 10 kg MLSS/m³.

7.3.1.2.2 Results

In Table 7.5 the average feed and permeate concentrations are summarized.

The COD-effluent concentration was relatively low due to the fact that the non-soluble fraction was completely removed by the membrane filtration. The average COD removal of the MBR system was 95%. The permeate nitrogen concentration was relatively stable. Even though no chemical dosing occurred, the phosphorus permeate concentration was maintained to 1.9 mg P_{total}/L.

7.3.1.2.3 Sludge Characteristics

The main sludge characteristics are presented in Table 7.6. The diluted sludge volume index (DSVI, volume in mL occupied by 1 g of activated after settlement under specified conditions for 30 min) was relatively stable at a level of 100–120 mL/g. Both the capillary suction time (CST, a method to measure the filterability of activated sludge) and the Y-flow (a method to measure the dynamic viscosity of

Table 7.4 Zenon's MBR Process Conditions

Parameter	Unit	Values
Influent flow	m³/day	44
Process temperature	°C average	20
	°C range	10–28
pH	—	7.5
Biological loading	kg COD/kg MLSS day	0.086
Sludge concentration	kg MLSS/m³	11.2
Organic fraction	%	64
Sludge production	kg MLSS/day	10.1
Sludge age (SRT)	day	29
Ferric dosing AT	L/day	0
Ferric dosing ratio	mol Fe/mol P	0

Sources: van der Roest, H.F. et al., *Membrane Bioreactors for Municipal Wastewater Treatment*, IWA Publishing, London, U.K., 2002; Judd, C., The largest MBR plants worldwide?, http://www.thembrsite.com/about-mbrs/largest-mbr-plants/, 2014.

activated sludge) can be related to the sludge concentration. The viscosity of the MBR sludge varied from 5 to 12 MPa s, which was relatively low for the applied sludge concentrations. The sludge viscosity seemed to be related to the sludge concentration. At lower sludge concentrations viscosity decreased even further to 2 MPa s.

The α-factor with bubble aeration was seen to vary between 0.24 and 0.77 at a sludge concentration of 5–15 kg MLSS/m³. The average α-factor range at 10.5 kg MLSS/m³ was between 0.4 and 0.6. The average settling velocity at the beginning of the gravity-thickening test amounted to 3–6 cm/h, depending on the sludge concentration. The maximum concentration of MLSS after 24 h of gravity thickening was lower than 3%, indicating that gravity thickening was not efficient. The maximum sludge concentration with mechanical thickening amounted to 6%–8%. Figure 7.6 shows a microscopic view of the Zenon's MBR sludge.

During the start-up of the plant a few filamentous organisms were present. In the early stage of operation, monocultures were found, often larger than the sludge flocs. Mostly crawling ciliates (*Aspidisca*) and free swimming ciliates (*Euplotus*) were observed. Their occurrence indicated a well-aerated system with minor disturbances. During the operation no amoebas were observed.

Table 7.5 Average Concentrations of Feed and Permeate in Zenon's MBR plant

Parameter		Unit	Values
COD	Feed	mg/L	605
	Permeate	mg/L	33
	Efficiency	%	95
N_{kj}	Feed	mg/L	59
	Permeate	mg/L	2.7
NO_3–N	Permeate	mg/L	5.8
N_{total}	Permeate	mg/L	8.5
	Efficiency	%	86
P_{total}	Feed	mg/L	12.0
	Permeate	mg/L	1.9
	Efficiency	%	84

Sources: van der Roest, H.F. et al., *Membrane Bioreactors for Municipal Wastewater Treatment*, IWA Publishing, London, U.K., 2002; Judd, C., The largest MBR plants worldwide?, http://www.thembrsite.com/about-mbrs/largest-mbr-plants/, 2014.

7.3.1.3 Membrane Performance

Figure 7.7 depicts the difference between actual measured permeability and temperature-corrected permeability for a reference temperature of 15°C. The corrected permeability to 15°C (the average wastewater temperature at Beverwijk) shows no major deviation from the actual measured-value-based permeability at the process temperature. Even at the that temperature, the corrected membrane permeability was still stable.

In order to maintain membrane performance, a regular major chemical cleaning was executed with NaOCl and citric acid. As a result of cleaning, the permeability increased from around 150 to 320–350 LMH/bar, a level that was expected for Zenon membranes. The MC was required at an interval of once per week with a combination of NaOCl and citric acid.

Peak flux testing was done to establish the maximum operating against daily, weekly, monthly, yearly peak flow of influent. During the peak test, the biological loading was constant. The all permeate water was recirculated back to the bioreactor to artificially increase the hydraulic loading of the membranes but so as not to

Table 7.6 Sludge Characteristics of Zenon's MBR Plant

	Unit	Values
Sludge characteristics		
DSVI	mL/g	100
CST	s	50
Y-flow	s	120
Viscosity		
Viscosity value	MPa s	7.6
Shear rate	L/s	110
α-factor		
Surface aeration	—	0.52
Bubble aeration	—	0.64
Gravity thickening		
Settling velocity	cm/h	4.3
Maximum concentration	%	2.4
Mechanical thickening		
MLSS at 3900 rpm/10 min	%	7.9
MLSS at 1000 rpm/3 min	%	3.4

Sources: van der Roest, H.F. et al., *Membrane Bioreactors for Municipal Wastewater Treatment*, IWA Publishing, London, U.K., 2002; Judd, C., The largest MBR plants worldwide?, http://www.thembrsite.com/about-mbrs/largest-mbr-plants/, 2014.

overload the biological system. The total hydraulic loading was 7667 L/h, which corresponded with a net flux of 41.7 LMH and a gross flux of 50 LMH.

In Figure 7.8 the peak flux test results are graphically presented. The duration of the peak test per flux condition was 24 h. For a further period of 104 h the peak test was allowed to continue, which resulted in the permeability drop from 350 to 240 LMH/bar. The peak test was carried out at an average process temperature of 22.5°C.

7.3.1.4 Conclusions

The COD removal was constant at high levels; nitrogen removal was as expected, which was explicable to oxygen input issues. Simultaneous biological phosphorus

**Figure 7.6 Microscopic view of the activated sludge of Zenon's MBR plant.
(From van der Roest, H.F. et al.,** *Membrane Bioreactors for Municipal Wastewater
Treatment***, IWA Publishing, London, U.K., 2002; Judd, C., The largest MBR plants
worldwide?, http://www.thembrsite.com/about-mbrs/largest-mbr-plants/, 2014.)**

removal gave better effluent quality than preprecipitation. The sludge concentration
in the aeration tank was kept at a concentration of 10–11 kg MLSS/m^3 to avoid
too much sludge accumulation in the membrane zone and to optimize the energy
consumption as a result of an optimal α-factor.

A peak flux of 41.3 LMH net was achieved for the required operating period of
more than 3 days continuously (104 h proven). At lower temperatures of 5°C–10°C
the maximum design flux should be lowered to a more operable 30–32 LMH net.

Using the routine MC procedure lessened sludging problem of the membrane
module.

7.3.2 Kubota

7.3.2.1 System Configuration

The picture and the design configuration of a Kubota's MBR pilot plant using
DD cassette are presented in Figure 7.9 and Table 7.7. The coarse bubble aeration
required for the membrane operation was also responsible for the oxygen input for
the biological process. In the DD configuration, there was a separate compressor
for the aeration of the sludge in compartments N1 and N2. The aeration in com-
partment N1 could be shut down by the aeration control. The aeration control was
based on the oxygen measurement in the second aeration compartment (N2). The
coarse bubble aeration in the membrane tank depended on the membrane settings
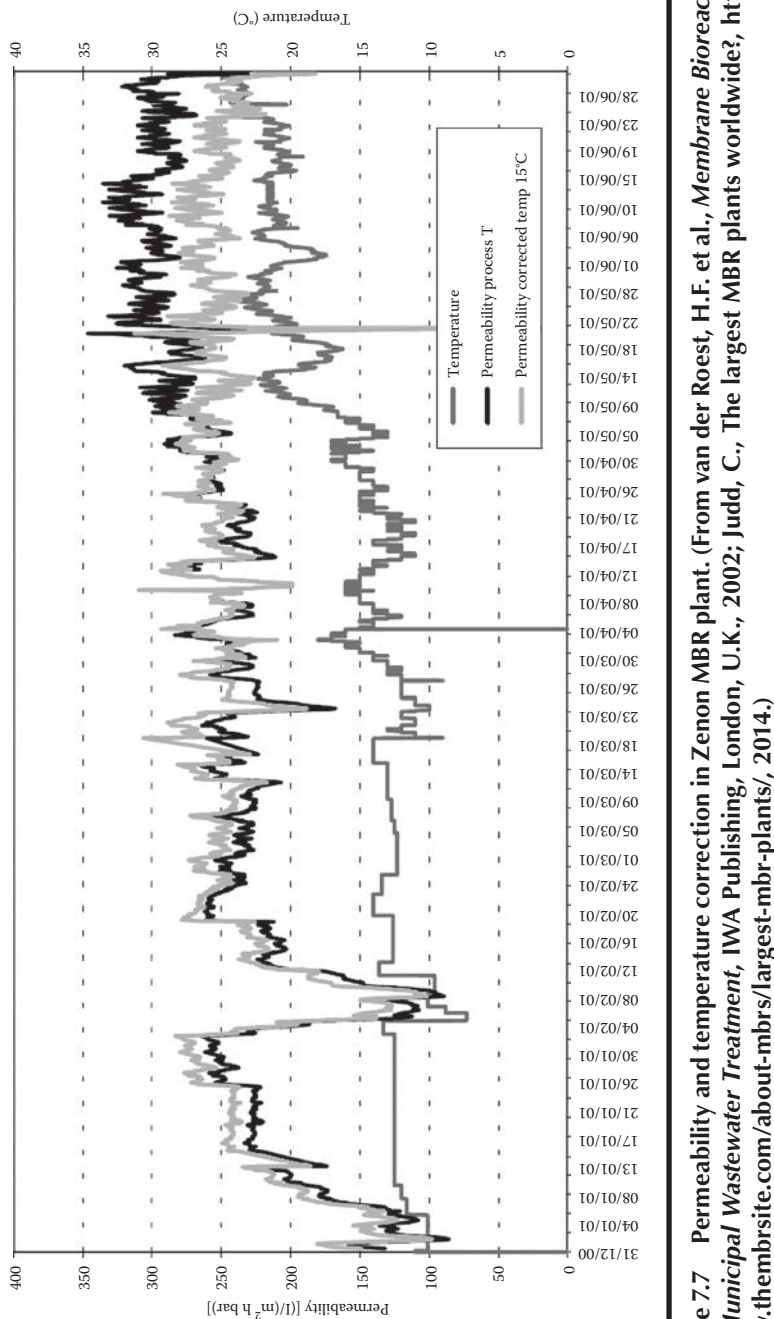
Figure 7.7 **Permeability and temperature correction in Zenon MBR plant. (From van der Roest, H.F. et al.,** *Membrane Bioreactors for Municipal Wastewater Treatment,* **IWA Publishing, London, U.K., 2002; Judd, C., The largest MBR plants worldwide?, http://www.thembrsite.com/about-mbrs/largest-mbr-plants/, 2014.)**
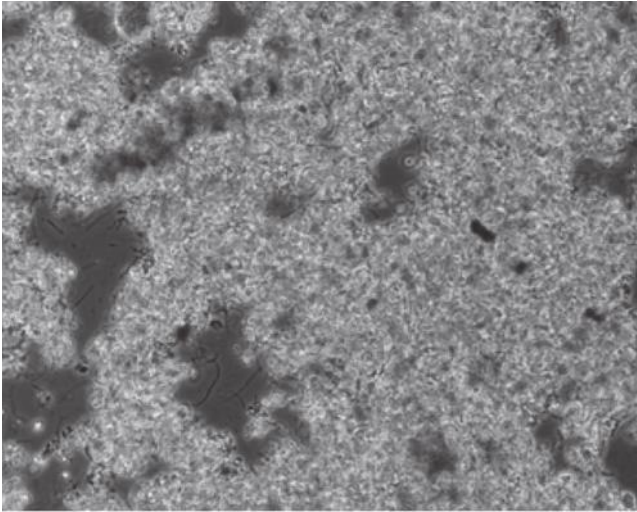
Figure 7.8   Permeability flux during peak test in Zenon's MBR plant. (From van der Roest, H.F. et al., *Membrane Bioreactors for Municipal Wastewater Treatment*, IWA Publishing, London, U.K., 2002; Judd, C., The largest MBR plants worldwide?, http://www. thembrsite.com/about-mbrs/largest-mbr-plants/, 2014.)

Figure 7.9   Kubota's MBR pilot plant. (From van der Roest, H.F. et al., *Membrane Bioreactors for Municipal Wastewater Treatment***, IWA Publishing, London, U.K., 2002; Judd, C., The largest MBR plants worldwide?, http://www.thembrsite.com/about-mbrs/largest-mbr-plants/, 2014.)**

and was set at a fixed flow. In common with the Zenon's plant, the feasibility of biological phosphorus removal was investigated. The mixing in the anoxic tank (D) is executed by intermittent aeration (10 s ON, 10 min OFF).

7.3.2.2 Biological Performance

7.3.2.2.1 Process Conditions

The overall process conditions during the operation of the pilot research are presented in Table 7.8. A typical sludge concentration for Kubota systems treating Japanese municipal wastewater is 15–20 kg MLSS/m³.

7.3.2.2.2 Results

In Table 7.9 the average feed and permeate concentrations are presented.

The COD-effluent concentration was relatively low due to the fact that the nonsoluble fraction had been completely removed by the membranes. The effect of bringing the recirculation flow from the membrane tank directly into the anoxic compartment was investigated. The effluent concentration did not improve in this period. The chemical dosing was stopped and biological phosphorus removal introduced.

Table 7.7   System Design Configuration and Figures of Kubota's MBR Plant

Process Part	Parameter	Unit	Values
Influent pump	Capacity	m³/h	15
	RWF design flow	m³/h	7.8
	Design flow	m³/day	39
Influent screen	Type	—	Rotating drum
	Slot size	mm	1.0
Aeration tank	Total volume (and depth)	m³	42.8
	Anaerobic volume (A)	m³ (m)	13.5 (2.7)
	Anoxic volume (D)	m³ (m)	8.4 (2.7)
	Fac compartment (D/N)	m³ (m)	—
	Oxic compartment (N)	m³ (m)	8.4 (2.7)
	Membrane tank (M)	m³ (m)	12.5 (4.1)
Aeration biology	Compressor capacity	Nm³/h	80
Ferric dosing	Type	—	$FeClSO_4$
	Ferric content	%	12.3
	Capacity (at Me/P=0.8)	mL/h	160
Membrane filtration	Number of modules	—	2 (× 150 plates)
	Total surface	m²	240
	Maximum net flux (at RWF)	LMH	41.7
Aeration membranes	Compressor capacity	Nm³/h	115
	Specific capacity	Nm³/m² h	0.5

(*Continued*)

Table 7.7 (*Continued*)   System Design Configuration and Figures of Kubota's MBR Plant

Process Part	Parameter	Unit	Values
Recirculation flows	Sludge D → N/M	m³/h	—
	Internal N → M	m³/h	10–30 (5:1)
	Nitrate N → D	m³/h	15
	Sludge D → A	m³/h	9

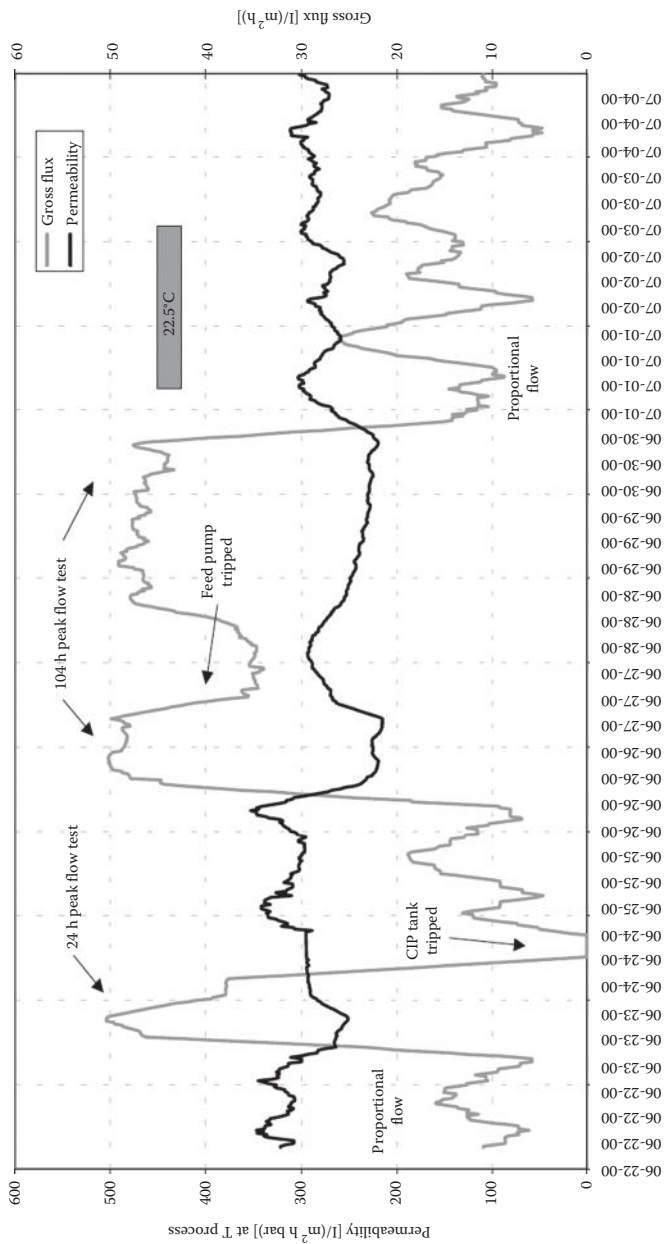*Sources:* van der Roest, H.F. et al., *Membrane Bioreactors for Municipal Wastewater Treatment*, IWA Publishing, London, U.K., 2002; Judd, C., The largest MBR plants worldwide?, http://www.thembrsite.com/about-mbrs/largest-mbr-plants/, 2014.

Table 7.8   Kubota MBR Process Conditions

Parameter	Unit	Values
Influent flow	m³/day	51
Process temperature	°C average	19
	°C range	10–28
pH	—	7.4
Biological loading	kg COD/kg MLSS day	0.100
Sludge concentration	kg MLSS/m³	10.8
Organic part	%	63
Sludge production	kg MLSS/day	10.3
Sludge age	day	30
Ferric dosing AT	L/day	0
Ferric dosing ratio	molFe/molP	0

Sources: van der Roest, H.F. et al., *Membrane Bioreactors for Municipal Wastewater Treatment*, IWA Publishing, London, U.K., 2002; Judd, C., The largest MBR plants worldwide?, http://www.thembrsite.com/about-mbrs/largest-mbr-plants/, 2014.

The hydraulic retention time in the anaerobic tank was about 1 h. The permeate phosphorus concentration decreased to an extreme low level (<0.1 mg/L) and remained very stable even at high influent peak concentrations. From September 2001, the phosphorus permeate concentration increased to an average concentration of 1.5 mg P_{total}/L.

Table 7.9   Average Concentrations of Feed and Permeate in Kubota's MBR Plant

Parameter		Unit	Values
COD	Feed	mg/L	621
	Permeate	mg/L	32
	Efficiency	%	95
N_{kj}	Feed	mg/L	58
	Permeate	mg/L	3.0
NO_3–N	Permeate	mg/L	7.9
N_{total}	Permeate	mg/L	10.8
	Efficiency	%	81
P_{total}	Feed	mg/L	10.9
	Permeate	mg/L	0.8
	Efficiency	%	93

Sources: van der Roest, H.F. et al., *Membrane Bioreactors for Municipal Wastewater Treatment*, IWA Publishing, London, U.K., 2002; Judd, C., The largest MBR plants worldwide?, http://www.thembrsite.com/about-mbrs/largest-mbr-plants/, 2014.

7.3.2.2.3 Sludge Characteristics

The main sludge characteristics are presented in Table 7.10. The DSVI was relatively stable at a level of 80–90 mL/g, which was rather lower than that of Zenon's plant. This stability was related to a good floc structure as described in the next section. Also the CST and the Y-flow were low. The viscosity of the MBR sludge was 8 MPa s on average, which was relatively similar to Zenon's result.

The average α-factor value for surface aeration remained constant at 0.50–0.55 during the operations. The α-factor with bubble aeration was eventually higher than with surface aeration. The average settling velocity at the beginning of the gravity-thickening test amounted to 4–6 cm/h on average, depending on the sludge concentration. The thickened sludge concentration (after 24 h) varied from 2.8% to 3.4% (Figure 7.10).

During the start-up, the flocs had a medium size with a compact structure; some filamentous organisms were also present. Since the start-up, more than 10 scale amoebas per sample were observed. In the early stage of operation most of the flocs showed an open structure and ciliates and monocultures were present. Normally, some crawling ciliates (*Aspidisca*) and free-swimming ciliates (*Euplotus*) were

Table 7.10 Sludge Characteristics of Kubota's MBR Plant

	Unit	Values
Sludge characteristics		
DSVI	mL/g	90
CST	S	50
Y-flow	S	100
Viscosity		
Viscosity value	MPa s	5.8
Shear rate	L/s	60
α-factor		
Surface aeration	—	0.50
Bubble aeration	—	0.54
Gravity thickening		
Settling velocity	cm/h	5.0
Maximum concentration	%	2.8
Mechanical thickening		
MLSS at 3900 rpm/10 min	%	10.4
MLSS at 1000 rpm/3 min	%	5.1

Sources: van der Roest, H.F. et al., *Membrane Bioreactors for Municipal Wastewater Treatment*, IWA Publishing, London, U.K., 2002; Judd, C., The largest MBR plants worldwide?, http://www.thembrsite.com/about-mbrs/largest-mbr-plants/, 2014.

observed. The number of filaments had dropped below 1 according to Eikelboom, but seemed to be a part of the microbial population.

7.3.2.3 Membrane Performance

At the site, Kubota membranes showed 42 LMH peak flow. During the cooling period, biomass was circulated through a heat exchanger to achieve an overall biomass temperature of 10°C. The membranes ran continuously between 12 and 25 LMH gross flux. After the low temperature test, Kubota's MBR system required the sludge concentration to be increased to 15 g/L.

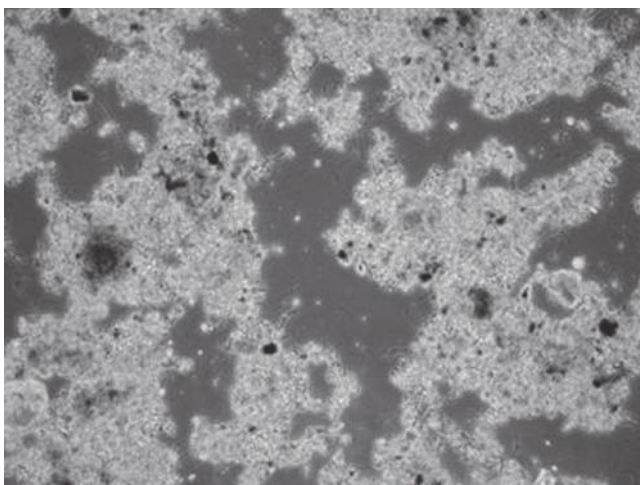**Figure 7.10 Microscopic view of the activated sludge of Kubota's MBR plant. (From van der Roest, H.F. et al., *Membrane Bioreactors for Municipal Wastewater Treatment*, IWA Publishing, London, U.K., 2002; Judd, C., The largest MBR plants worldwide?, http://www.thembrsite.com/about-mbrs/largest-mbr-plants/, 2014.)**

In order to increase membrane packing density per footprint, Kubota provides DD system, which has two layers of membrane modules. Modules at the top and bottom are subjected to different water heads and they have different transmembrane pressures even at the same suction pressure. Optimized balance of flux between top and bottom modules is required. The ratio of flux introduced by Kubota between the top and bottom modules is 60:40. To prevent plugging of aeration pipe, flushing was done once per day (Figure 7.11).

Figure 7.12 shows peak test result. Before the peak test started, the permeability, depending on the DWF variations, varied from 650 to 950 LMH/bar, indicating a clean membrane. The peak test was started at 42 LMH net or 52.5 LMH gross, and the permeability rapidly decreased to 550 LMH/bar and, subsequently, slowly to 450 LMH/bar in 48 h. The permeability further decreased to a minimum level of 360 LMH/bar. On stopping the peak test, the permeability recovered steadily to around 500 LMH/bar within 12–24 h. The relaxation showed positive impact on the membrane performance at peak flow.

After the membrane operation, a thickened sludge layer was formed between the membrane plates with a concentration up to 15%, and the membrane plates required mechanical cleaning; and a chemical disinfection with a 150 mg/L NaOCl solution was also carried out.

The cleaning procedure consisted of two separate chemical treatments: first a cleaning with a 5000 mg/L NaOCl solution, followed, a day later, by a cleaning with a 1% oxalic acid solution. Both steps were carried out in situ in biomass.

Figure 7.11 **Permeability and temperature correction in Zenon's MBR plant. (From van der Roest, H.F. et al.,** *Membrane Bioreactors for Municipal Wastewater Treatment***, IWA Publishing, London, U.K., 2002; Judd, C., The largest MBR plants worldwide?, http://www.thembrsite.com/about-mbrs/largest-mbr-plants/, 2014.)**
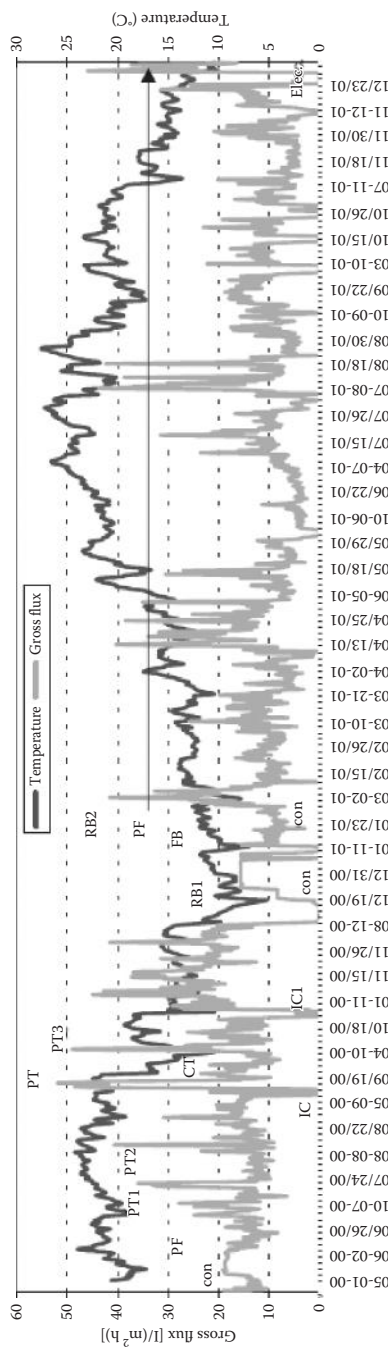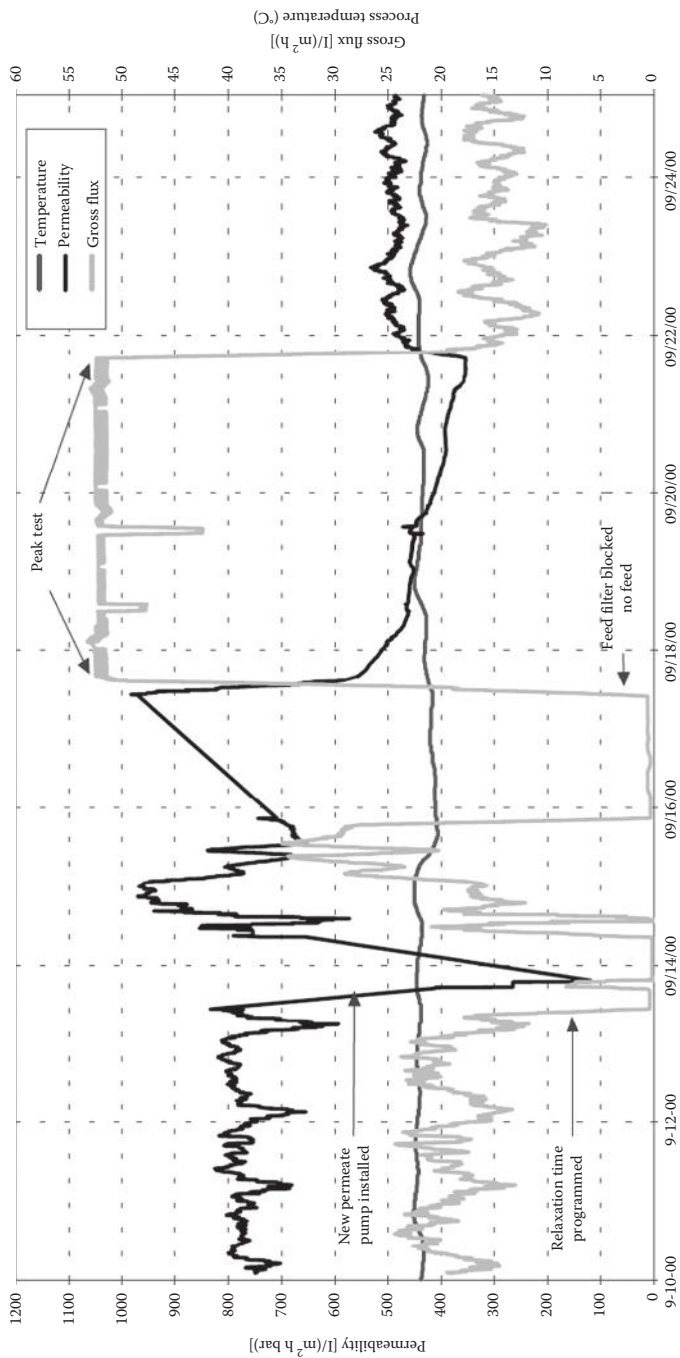
Figure 7.12 Permeability flux during peak test in Zenon's MBR plant. (From van der Roest, H.F. et al., *Membrane Bioreactors for Municipal Wastewater Treatment,* **IWA Publishing, London, U.K., 2002; Judd, C., The largest MBR plants worldwide?, http://www. thembrsite.com/about-mbrs/largest-mbr-plants/, 2014.)**

As a result of the NaOCl cleaning the permeability increased from 200 to 700 LMH/bar. This was equal to the clean process permeability as measured at the start of the project. The oxalic acid cleaning had little additional effect on the permeability. The fouling was predominately biomass surface fouling or organic in nature.

After the mechanical cleaning, the permeability recovered immediately to 600–800 LMH/bar and membrane integrity was maintained.

7.3.2.4 Conclusions

The COD removal was constant at high levels, nitrogen removal was as expected. Simultaneous phosphorus removal gave a better effluent quality than preprecipitation, even at very low ferric dosing ratios. Biological phosphorus removal resulted in a low and relatively stable permeate concentration.

The sludge concentration in the aeration tank was kept at a level of 12 kg MLSS/m³, to optimize the oxygen transfer in relation with the α-factor.

A peak flux of 42 LMH net was achieved for the required operating period of more than 3 continuous days (100 h proven) with relaxation at site. At reduced temperature, 10°C, the peak flux of 42 LMH net was achieved for the required operating period of 24 h continuous.

The suggested cleaning of the modules twice per year was proven to be unnecessary. The DD configuration suggested that one intensive cleaning per year would be sufficient. This cleaning should be planned prior to the onset of winter.

The DD configuration has proven to be a reliable permeate extraction ratio.

7.3.3 Mitsubishi Rayon Engineering

7.3.3.1 System Configuration

The picture of an MBR pilot plant and the configuration and design of an MRE pilot are presented in Figure 7.13 and Table 7.11. Aeration of sludge in compartments N1 and N2 was achieved with one compressor. The aeration in compartment N2 could be shut down manually if required. The aeration control was based on the oxygen measurement in the first aeration compartment (N1). In practice the aeration was in operation in both compartments almost continuously. The original design flow of the Mitsubishi aeration tank was set at 34 m³/day. Phosphorus removal was based only on biological uptake.

7.3.3.2 Biological Performance

7.3.3.2.1 Process Conditions

The overall process conditions during the operation of the pilot are presented in Table 7.12.

Figure 7.13   MRE's MBR pilot plant. (From van der Roest, H.F. et al., *Membrane Bioreactors for Municipal Wastewater Treatment*, IWA Publishing, London, U.K., 2002; Judd, C., The largest MBR plants worldwide?, http://www.thembrsite.com/ about-mbrs/largest-mbr-plants/, 2014.)

The average influent flow during the research period varied strongly due to rainfall conditions. The average flow amounted to 40 m^3/day. The design sludge concentration was 10 kg MLSS/m^3.

7.3.3.2.2 Results

In Table 7.13 the average feed and permeate concentrations are presented.

The COD-permeate concentration was relatively low due to the fact that the non-soluble fraction was completely removed by the membrane filtration. The nitrogen removal performed well at a permeate concentration <10 mg N_{total}/L. Phosphorus removal efficiency was 90% using the enhanced biological phosphorus removal.

7.3.3.2.3 Sludge Characteristics

The main sludge characteristics are presented in Table 7.14. DSVI was relatively stable at a level of 100–140 mL/g. The viscosity of MBR sludge varied from 6 to 13 MPa s, which was relatively low for the applied sludge concentrations.

The α-factor with bubble aeration varied between 0.3 and 0.5 at a sludge concentration of 5–12 kg MLSS/m^3. The average α-factor at 10 kg MLSS/m^3 was approximately 0.4. With a surface aerator 15% higher values were achieved. The average settling velocity at the beginning of the gravity-thickening test amounted to 2–6 cm/h, depending on the sludge concentration. The maximum concentration after 24 h was lower than 3%, indicating that gravity thickening was not efficient.

Table 7.11   System Configuration and Design Figures

Process Part	Parameter	Unit	Values
Influent pump	Capacity	m³/h	10
	RWF design flow	m³/h	6.4
	Design flow	m³/day	32
Influent screen	Type	—	Parabolic sieve
	Slot size	Mm	0.75
Aeration tank	Total volume (and depth)	m³	34.2
	Anoxic volume (D1/2/3/4)	m³ (m)	4×3.9 (1.70)
	Oxic compartment (N2)	m³ (m)	2×3.9 (1.70)
	Membrane tank (M)	m³ (m)	10.8 (5.0)
Aeration biology	Compressor capacity total	Nm³/h	160
	Capacity N1/N2	Nm³/h	80/80
Ferric dosing	Type	—	FeClSO$_4$
	Ferric content	%	12.3
	Capacity (at Me/P = 0.8)	mL/h	160
Membrane filtration	Number of modules	—	3
	Total surface	m²	315
	Maximum net flux (at RWF)	LMH	20.3
Aeration membranes	Compressor capacity	Nm³/h	75–120
	Specific capacity	Nm³/m² h	0.24–0.38

(*Continued*)

Table 7.11 (*Continued*) System Configuration and Design Figures

Process Part	Parameter	Unit	Values
Recirculation flows	Sludge N1 → M	m³/h	20–40
	Internal D4 → N1	m³/h	17–25
	Nitrate D4 → D1	m³/h	17–25

Sources: van der Roest, H.F. et al., *Membrane Bioreactors for Municipal Wastewater Treatment*, IWA Publishing, London, U.K., 2002; Judd, C., The largest MBR plants worldwide?, http://www.thembrsite.com/about-mbrs/largest-mbr-plants/, 2014.

Table 7.12 MRE's MBR Process Conditions

Parameter	Unit	Values
Influent flow	m³/day	55
Process temperature	°C average	18
	°C range	7–31
pH	—	7.4
Biological loading	kg COD/kg MLSS day	0.084
Sludge concentration	kg MLSS/m³	11.6
Organic part	%	65
Sludge production	kg MLSS/day	15.5
Sludge age	day	26
Ferric dosing AT	L/day	0
Ferric dosing ratio	mol Fe/mol P	0

Sources: van der Roest, H.F. et al., *Membrane Bioreactors for Municipal Wastewater Treatment*, IWA Publishing, London, U.K., 2002; Judd, C., The largest MBR plants worldwide?, http://www.thembrsite.com/about-mbrs/largest-mbr-plants/, 2014.

The maximum sludge concentration with mechanical thickening amounted to 6%–9%.

Since the start-up of the MBR system, the flocs had decreased to a small floc size with an open structure. Further, monocultures were present. The size of these monocultures increased a little, and sometimes they were larger than the flocs present. Toward the middle of operation their number decreased dramatically. Normally, some crawling ciliates (*Aspidisca*) and free-swimming ciliates (*Euplotus*)

Table 7.13 Average Concentrations of Feed and Permeate in MRE's MBR Plant

Parameter		Unit	Values
COD	Feed	mg/L	605
	Permeate	mg/L	34
	Efficiency	%	94
N_{kj}	Feed	mg/L	59
	Permeate	mg/L	4.2
$NO_3–N$	Permeate	mg/L	4.4
N_{total}	Permeate	mg/L	8.6
	Efficiency	%	85
P_{total}	Feed	mg/L	12.1
	Permeate	mg/L	1.1
	Efficiency	%	90

Sources: van der Roest, H.F. et al., *Membrane Bioreactors for Municipal Wastewater Treatment*, IWA Publishing, London, U.K., 2002; Judd, C., The largest MBR plants worldwide?, http://www.thembrsite.com/about-mbrs/largest-mbr-plants/, 2014.

were observed. Their occurrence indicated a well-aerated system with minor disturbances. Specifically during the start-up, some filamentous organisms occurred, but in the process, their number steadily dropped below 1. Figure 7.14 shows a microscopic view of the MRE's MBR sludge.

7.3.3.3 Membrane Performance

The maximum achievable flux was 32.5 LMH continuously (20.3LMH net). Cleaning was done twice per year and the cleaning mode used 5000 mg/L NaOCl followed by an acidic solution. Relaxation was used between process modes. Periodically the Mitsubishi membranes have relaxation. The MC procedures have helped maintain a high and stable permeability of around 400 LMH/bar (Figure 7.15).

7.3.3.4 Conclusions

The sludge concentration in the aeration tank was kept at a level of around 10 kg MLSS/m³ to avoid problems in the membrane zone and to optimize the oxygen

**Table 7.14   Sludge Characteristics in MRE's MBR Plant**

	Unit	*Values*
Sludge Characteristics		
DSVI	mL/g	100
CST	s	50
Y-flow	s	120
Viscosity		
Viscosity value	MPa s	7.6
Shear rate	L/s	110
α-factor		
Surface aeration	—	0.52
Bubble aeration	—	0.64
Gravity thickening		
Settling velocity	cm/h	4.3
Maximum concentration	%	2.4
Mechanical thickening		
MLSS at 3900 rpm/10 min	%	7.9
MLSS at 1000 rpm/3 min	%	3.4

Sources: van der Roest, H.F. et al., *Membrane Bioreactors for Municipal Wastewater Treatment*, IWA Publishing, London, U.K., 2002; Judd, C., The largest MBR plants worldwide?, http://www.thembrsite.com/about-mbrs/largest-mbr-plants/, 2014.

transfer in relation to the α-factor. The α-factor had increased during the operation, mainly due to system improvements resulting in a lower shear stress for the sludge.

A peak flux of 28.1 LMH net was achieved for the required operating period of more than three continuous days (95 h proven) at a temperature above 20°C. Continuous flow mode seemed to be the best mode of operation for the module at the site.

The maximum continuous design flux above temperatures of 10°C was established at 15–18 LMH net. At these fluxes, an in situ or intensive cleaning could be planned every 2 to 4 months of operation.
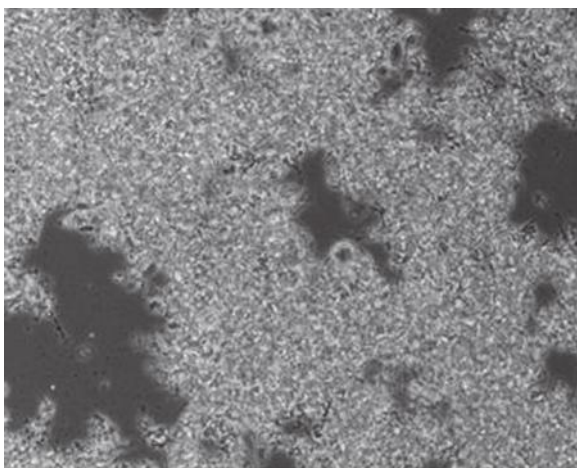
Figure 7.14   Microscopic view of the activated sludge. (From van der Roest, H.F. et al., *Membrane Bioreactors for Municipal Wastewater Treatment***, IWA Publishing, London, U.K., 2002; Judd, C., The largest MBR plants worldwide?, http://www.thembrsite.com/about-mbrs/largest-mbr-plants/, 2014.)**

7.3.4 Pentair

7.3.4.1 System Configuration

The picture of an MBR pilot plant and the configuration and design of an X-Flow's pilot are presented in Figure 7.16 and Table 7.15. For the aeration of sludge in the compartments N1 and N2 there is one compressor. The aeration in compartment N1 can be shut down using the aeration control. The aeration control was based on the oxygen measurement in the second aeration compartment (N2).

7.3.4.2 Biological Performance

7.3.4.2.1 Process Conditions

The overall process conditions during the operation of the pilot are presented in Table 7.16.

The design flow at dry weather flow conditions was 50 m³/day. The set point for the sludge concentration was 10 kg MLSS/m³.

7.3.4.2.2 Results

In Table 7.17, the average feed and permeate concentrations are summarized.

The COD-effluent concentration was relatively low because the nonsoluble fraction was completely removed by the membrane filtration; COD removal efficiency
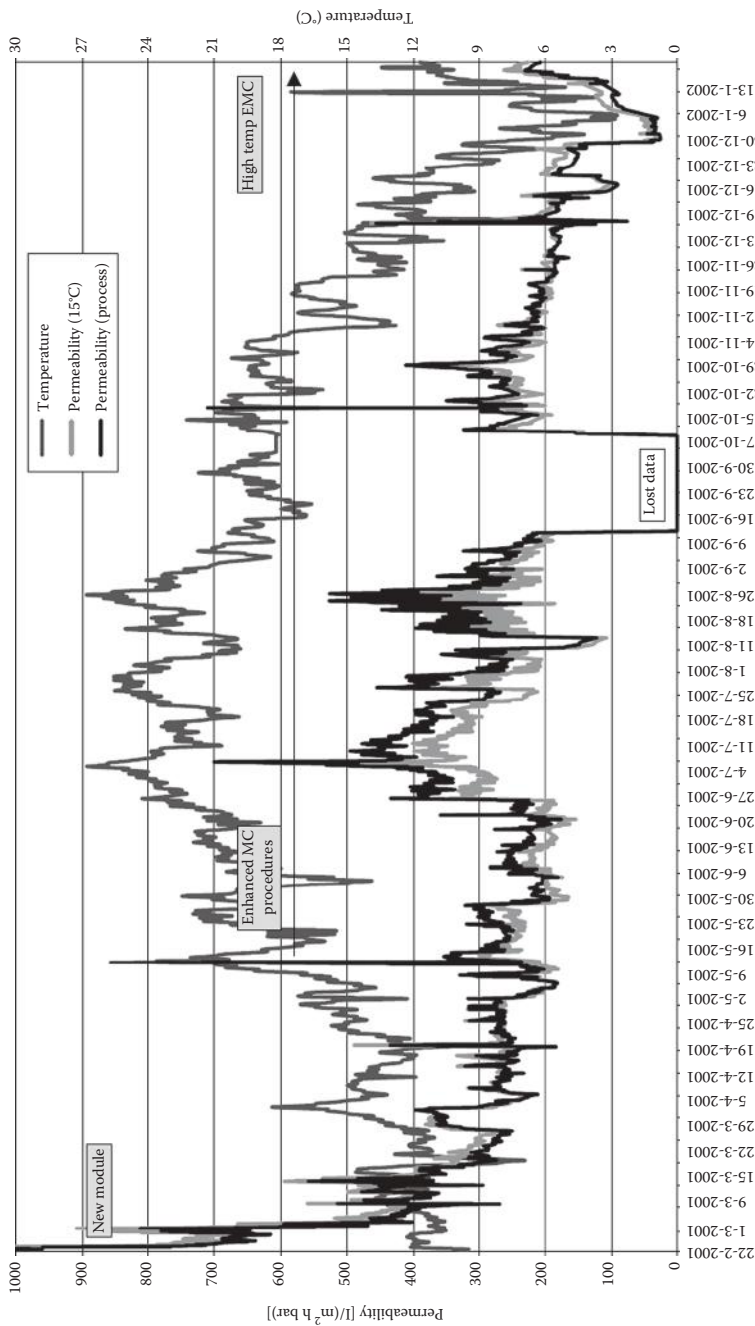
Figure 7.15 **Permeability and temperature correction in MRE's MBR plant. (From van der Roest, H.F. et al.,** *Membrane Bioreactors for Municipal Wastewater Treatment,* **IWA Publishing, London, U.K., 2002; Judd, C., The largest MBR plants worldwide?, http:// www.thembrsite.com/about-mbrs/largest-mbr-plants/, 2014.)**

Figure 7.16   Photographs of a new X-Flow plant. (From van der Roest, H.F. et al., *Membrane Bioreactors for Municipal Wastewater Treatment***, IWA Publishing, London, U.K., 2002; Judd, C., The largest MBR plants worldwide?, http://www. thembrsite.com/about-mbrs/largest-mbr-plants/, 2014.)**

remained at 90%–94%. In operation the nitrogen effluent concentration was lower than 8 mg N_{total}/L. This was partly due to the low loading of the pilot plant in this period. The phosphorus influent concentration was relatively high and the sludge loading was relatively low. As a consequence, the phosphorus effluent concentration was >1 mg P_{total}/L.
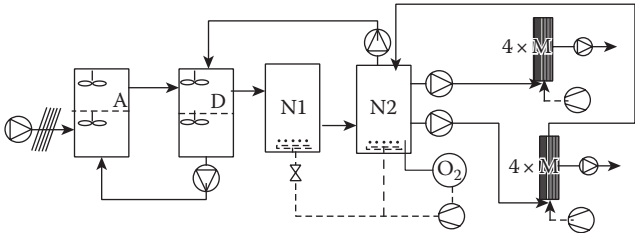
7.3.4.2.3 Sludge Characteristics

The main sludge characteristics are presented in Table 7.18. The DSVI was relatively stable at a level of 80–90 mL/g. The viscosity of the MBR sludge varied from 5 to 10 MPa s, which was relatively low for the applied sludge concentrations.

The α-factor with bubble aeration varied between 0.4 and 0.8 at a sludge concentration of 7–11 kg MLSS/m^3. The average α-factor at 10 kg MLSS/m^3 was approximately 0.6. The average settling velocity at the beginning of the gravity-thickening test amounted to 3–10 cm/h, strongly dependent on the sludge concentration. The maximum concentration after 24 h was lower than 3% in general, indicating that gravity thickening was not really efficient. The maximum sludge concentration with mechanical thickening was 6%–8%. Figure 7.17 shows a microscopic view of the X-Flow's MBR sludge.

The floc structure of the MBR sludge has changed dramatically from flocs with a medium size and a compact structure to a very small one, like pin flocs, with a somewhat open structure. Of course, the number of flocs also increased due to the increased dry solid content of the system.

Table 7.15   Design Figures X-Flow Plant

Process Part	Parameter	Unit	Values
Influent pump	Capacity	m³/h	10
	RWF design flow	m³/h	10
	Design flow	m³/day	50
Influent screen	Type	—	Rotating drum
	Slot size	mm	0.50
Aeration tank	Total volume	m³	40.8
	Anaerobic volume(A)	m³	12.0
	Anoxic comp. (D)	m³	7.0
	Anoxic/oxic comp. (N1)	m³	10.5
	Oxic compartment (N2)	m³	10.5
	Membrane tank (M)	m³	0.8
	Depth aeration tank	m	3.0
Aeration biology	Compressor capacity	Nm³/h	140
Membrane filtration	Number of modules	—	8
	Surface each	m²	30
	Total surface	m²	240
	Maximum net flux (at RWF)	LMH	41.7
Aeration membranes	Air flush	Nm³/h	15–20
	Air flush On/Off	s	7/200
	Continuous air lift	Nm³/h	10–15

(*Continued*)

Table 7.15 (*Continued*)   Design Figures X-Flow Plant

Process Part	Parameter	Unit	Values
Recirculation flows	Pumps N2 → M	m³/h	2×80
	Internal D → A	m³/h	15
	Internal N2 → D	m³/h	15

Sources: van der Roest, H.F. et al., *Membrane Bioreactors for Municipal Wastewater Treatment*, IWA Publishing, London, U.K., 2002; Judd, C., The largest MBR plants worldwide?, http://www.thembrsite.com/about-mbrs/largest-mbr-plants/, 2014.

Table 7.16   Process Conditions

Parameter	Unit	Values
Influent flow	m³/day	33
Process temperature	°C average	23
	°C range	15–35
pH	—	7.4
Biological loading	kg COD/kg MLSS day	0.054
Sludge concentration	kg MLSS/m³	10.6
Organic part	%	63
Sludge production	kg MLSS/day	8.8
Sludge age	Day	34
Ferric dosing AT	L/day	0
Ferric dosing ratio	mol Fe/mol P	0

Sources: van der Roest, H.F. et al., *Membrane Bioreactors for Municipal Wastewater Treatment*, IWA Publishing, London, U.K., 2002; Judd, C., The largest MBR plants worldwide?, http://www.thembrsite.com/about-mbrs/largest-mbr-plants/, 2014.

In the early stage of operation the floc became denser and solid and the size was very small. The number of monocultures more or less stabilized to a small number per sample.

During the test the number of filamentous organisms increased to 1, but during the last stage of operation the number varied between 1 and 2 according to Eikelboom. The type was not identified, but appeared floc bound.

Table 7.17 Average Concentration of Feed and Permeate in X-Flow's MBR Plant

Parameter		Unit	Values
COD	Feed	mg/L	569
	Permeate	mg/L	36
	Efficiency	%	94
N_{kj}	Feed	mg/L	56
	Permeate	mg/L	3.6
$NO_3–N$	Permeate	mg/L	4.2
N_{total}	Permeate	mg/L	7.8
	Efficiency	%	86
P_{total}	Feed	mg/L	11.3
	Permeate	mg/L	1.4
	Efficiency	%	88

Sources: van der Roest, H.F. et al., *Membrane Bioreactors for Municipal Wastewater Treatment*, IWA Publishing, London, U.K., 2002; Judd, C., The largest MBR plants worldwide?, http://www.thembrsite.com/about-mbrs/largest-mbr-plants/, 2014.

7.3.4.3 Membrane Performance

The maximum achievable flux was 60 LMH net. The cleaning was carried out at routine intervals dependent on the permeability, 2–4 times per year. Back flush was used between process modes and no other recovery steps/modes were anticipated. Figure 7.18 shows the permeability and temperature in X-Flow's MBR plant.

The system was run at a constant 3 m³/h for three vertical modules. Continuous fluxes of 50 LMH were achieved. A peak test of 70 LMH was performed. The system ran with weekly MC less than 1 m/s and good results were achieved at 0.5 m/s; the air flow supplied an additional 0.25–0.5 m/s to the biomass' turbulence but remained constant under normal processing conditions.

7.3.4.4 Conclusions

The sludge concentration in the aeration tank was kept at a level of around 10 kg MLSS/m³ to avoid problems with the membrane tubes and to optimize the energy consumption in relation to the α-factor. Continuous flow mode was

Table 7.18   Sludge Characteristics of the X-Flow's Plant

	Unit	*Values*
Sludge characteristics		
DSVI	mL/g	100
CST	s	70
Y-flow	s	120
Viscosity		
Viscosity value	MPa s	7.0
Shear rate	L/s	100
α-factor		
Surface aeration	—	0.58
Bubble aeration	—	0.52
Gravity thickening		
Settling velocity	cm/h	4.3
Maximum concentration	%	2.3
Mechanical thickening		
MLSS at 3900 rpm/10 min	%	6.4
MLSS at 1000 rpm/3 min	%	2.3

Sources: van der Roest, H.F. et al., *Membrane Bioreactors for Municipal Wastewater Treatment*, IWA Publishing, London, U.K., 2002; Judd, C., The largest MBR plants worldwide?, http://www.thembrsite.com/about-mbrs/largest-mbr-plants/, 2014.

applied and the maximum continuous design flux above temperatures of 5°C was established at 22.5 LMH net and further optimized to 37 LMH net. At these fluxes a weekly MC was required with an intensive clean estimated at 4–8 times per year.

7.4 Case Studies for Municipal Wastewater Treatment

Most large MBR plants worldwide are municipal WWTPs and most of them have adapted ZeeWeed hollow fiber membrane provided by GE Zenon.

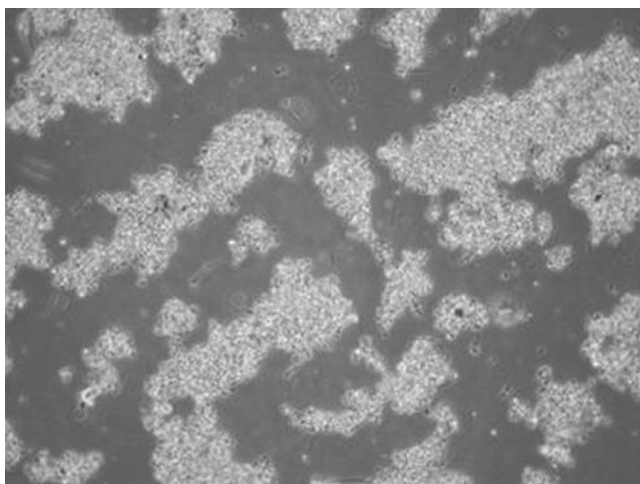**Figure 7.17   Microscopic view of the activated sludge of X-Flow's MBR plant. (From van der Roest, H.F. et al.,** *Membrane Bioreactors for Municipal Wastewater Treatment***, IWA Publishing, London, U.K., 2002; Judd, C., The largest MBR plants worldwide?, http://www.thembrsite.com/about-mbrs/largest-mbr-plants/, 2014.)**

7.4.1 Seine Aval Wastewater Treatment Facility

Originally, the Paris agglomeration's wastewater was supposed to be treated at a single site (Seine Aval) located downstream of the agglomeration on the Seine River at Achères. The WWTP was designed in 1933 to reach the capacity of 2.7 million m³/day. Service Public de L'Assainissement Francilien (SIAAP) owns and operates five WWTPs in Paris including the Seine Aval WWTP (Figure 7.19).

For many reasons this centralized sanitation design was first challenged in the late 1960s and then again in the late 1990s. This led to the reduction of its size in two steps. The first stage of downsizing started with the construction of the Marne Aval WWTP and then the Seine Amont WWTP. In the second stage, these WWTPs were built: Seine Centre, Seine Grésillons, and Seine Morée. At the same time, Seine Aval went through different stages of modernization including the first stage of adding physicochemical water treatment for combined sewer overflow that was also used for the removal of phosphorus. Then a nitrogen pollution processing unit was added in 2007. This MBR system will be completed and operational in 2016 (Table 7.1).

Figure 7.5a shows a schematic of the MBR process of Seine Aval MBR plant. The Seine Aval WWTP treats the wastewater generated from over 75% of the population in Paris, and the average influent is 1,210,000 m³/day. The plant divides the influent water into two process trains. 1,010,000 m³/day is treated by a conventional process and 200,000 m³/day is treated by an MBR process. In the case of the MBR
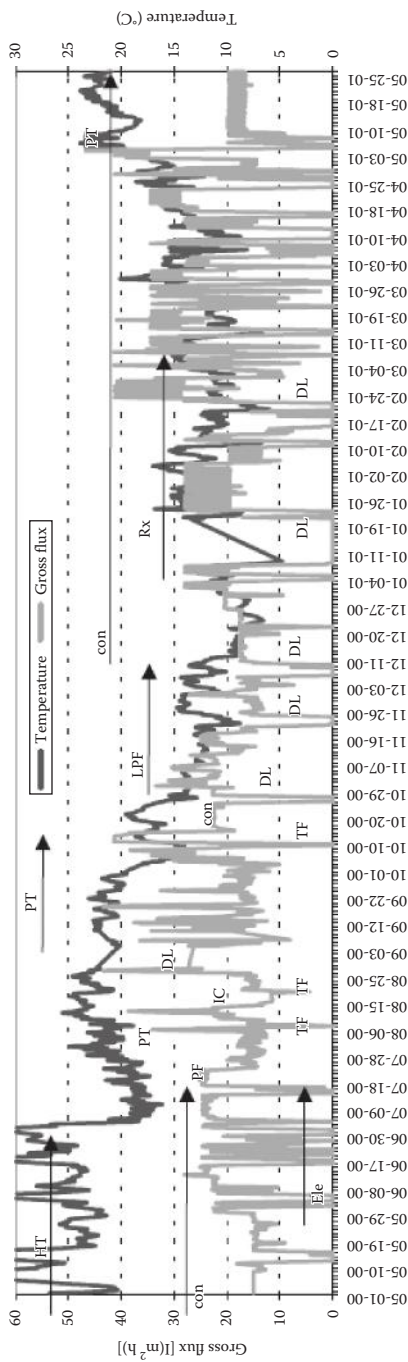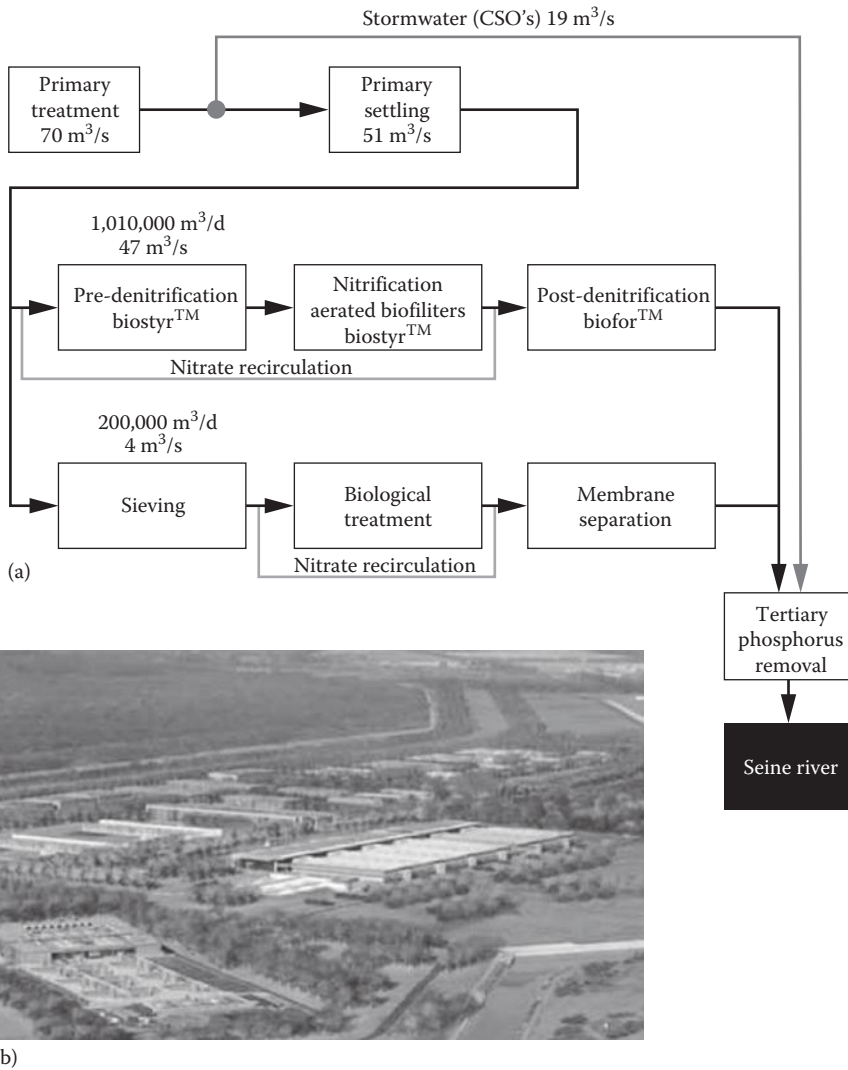
Figure 7.18   Permeability and temperature in X-Flow's MBR plant. (From van der Roest, H.F. et al., *Membrane Bioreactors for Municipal Wastewater Treatment*, IWA Publishing, London, U.K., 2002; Judd, C., The largest MBR plants worldwide?, http://www. thembrsite.com/about-mbrs/largest-mbr-plants/, 2014.

(a)

(b)

Figure 7.19 (a) Schematic of MBR process and (b) long-distance view of Seine Aval MBR plant.

process, after primary settling, influent water is sieved by 1 mm size screens. The activated sludge tanks are divided into 2 lanes with 6 tanks resulting in a total tank volume of 118,000 m³. The plant adapted ZeeWeed™ 500d with braid-reinforced hollow fiber membranes and vertically aligned submerged membrane modules provided by GE Zenon. Each lane has 14 cells or divisions and each cell has 11 membrane cassettes. The total effective membrane area installed is 462,000 m².

7.4.2 Brightwater Wastewater Treatment Facility

King County's Brightwater WWTP is the fourth largest MBR plant but the largest operating MBR plant in the world (the other three larger plants are still under construction). The plant is located in King County, Washington, United States. The plant was installed and commissioned in 2011 for municipal wastewater treatment. The average daily permeate water flow is 117,000 m³/day and PDF is 170,000 m³/day. The membranes and their modules are ZeeWeed™ 500d with braid-reinforced hollow fiber membranes and vertically aligned submerged membrane modules, provided by GE Zenon (Figure 7.20).

The plant was constructed by GE Water & Process Technologies and after construction was completed the ownership was transferred to the King County Wastewater Treatment Division. King County's Wastewater Treatment Division serves about 1.4 million people in the Seattle, Washington, area. Brightwater WWTF had become a necessity due to the expansion of population in the region.

As the Brightwater WWTF discharges treated effluent into Puget Sound, marine environment protection was a key factor in the selection of treatment process for the plant. In addition, King County wanted to be able to produce reclaimed water, allowing reuse of the treated wastewater for nonpotable applications such as landscape or agricultural irrigation, heating and cooling, and industrial processing. The produced effluent water from the facility is 7–10 times cleaner than effluent from a conventional activated sludge system.

Figure 7.20   Picture of Brightwater Wastewater Treatment Facility.

The procurement process, which included an evaluation of bids from two MBR suppliers, resulted in the selection of GE Water & Process Technologies to provide ZeeWeed MBR technology for the project. When awarded in 2005, the Brightwater WWTF was the largest awarded MBR in the world and has been the largest operating MBR in North America since its commissioning.

The Brightwater WWTF treatment process begins with preliminary treatment, including coarse screening and grit removal. Following primary clarification, the wastewater passes through fine screens prior to entering the MBR. The biological treatment process includes both anoxic and aerobic zones, which promote the removal of nitrogen from the wastewater, reduce aeration requirements, and improve the alkalinity of the system. The ZeeWeed membranes that form the basis of the MBR plant provide efficient solid/liquid separation, filtering out virtually all solid particles and even bacteria. The facility includes 10 parallel membrane trains, though initially only 8 trains were installed, with each train containing 20 membrane cassettes to meet the current flow requirements.

The modular nature of ZeeWeed membranes allows for simple expansion for future flows; two trains are anticipated to be added within the next 5 years, with the option for additional trains in the future. Downstream of membrane filtration, the treated water is disinfected with sodium hypochlorite.

The Brightwater WWTF incorporates a novel treatment strategy for large influent flows. Flow rates up to the MBR capacity are processed through conventional primary clarification and the MBR system. Peak flow rates above the capacity of the MBR, however, are diverted and treated simply with chemically-enhanced primary clarification, and then are blended with the MBR permeate. This approach was selected in order to most cost-effectively meet the secondary treatment requirements for the full peak flows through the plant.

An interesting aspect of the procurement process for this project was that King County combined the delivery of the Brightwater WWTF with the delivery of a smaller MBR plant, the Carnation WWTP. MBR technology was also selected for the Carnation WWTP, as this plant produces Class A reclaimed water that is utilized to enhance nearby wetlands. This smaller plant also served as a training and test site for the larger Brightwater plant. The Carnation WWTP has an average design flow of 0.39 MGD, and uses the same ZeeWeed membranes as the Brightwater plant. The Carnation WWTP started operation in May 2008, and a few months later was the recipient of the "Small Project of the Year" award from the WateReuse Association.

7.4.3 Yellow River Water Reclamation Facility

The Yellow River Water Reclamation Facility is the 11th largest MBR plant and the 5th largest operating MBR plant in the world. The plant is located in Lilburn, Georgia, United States. The plant was installed and commissioned in 2011 for

municipal wastewater treatment. The average daily flow is 69,000 m^3/day and the PDF is 111,000 m^3/day. The membranes and their modules are ZeeWeed™ 500d provided by GE Zenon. The plant was constructed by CH2M Hill and after construction was completed the ownership was transferred to Gwinnett County. Figure 7.21 displays site pictures from the facility.
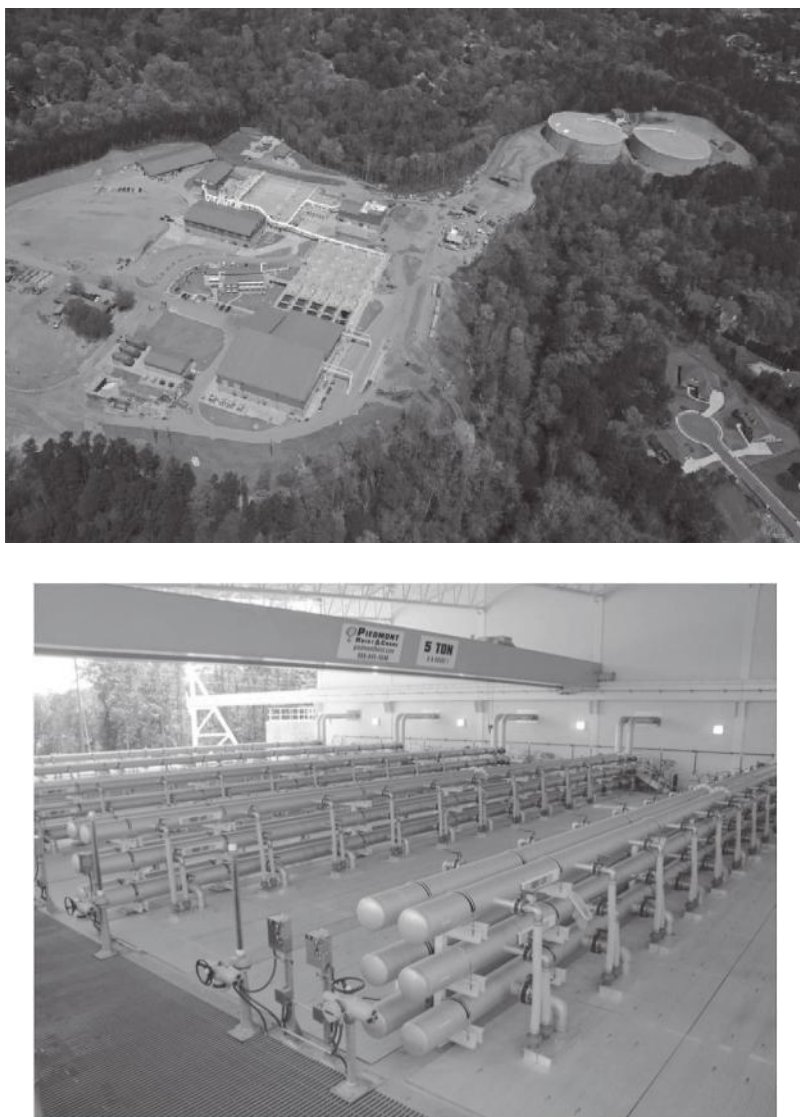
Figure 7.21   Pictures of the Yellow River Water Reclamation Facility.

7.4.4 Cannes Aquaviva Wastewater Treatment Facility

The Cannes Aquaviva WWTP is the 13th largest MBR plant and the 7th largest operating MBR plant in the world. The plant is located in Cannes, France. The plant was installed and commissioned in 2012 for municipal wastewater treatment. The average daily permeate water flow is 59,000 m^3/day and the PDF is 106,000 m^3/day. The membranes and their modules are ZeeWeed™ 500d. The plant was constructed by Degremont and after construction the ownership was transferred to Ville de Cannes. Figure 7.22 shows an aerial photo of the WWTP and a picture of the control building.

7.4.5 Busan Suyeong Sewage Treatment Plant

The Busan Suyeong sewage treatment plant is Korea's largest MBR system. It is a completely underground 102,000 m^3/day ZeeWeed MBR design, which made room for a residential park at ground level. The plant is located in Busan, South Korea and is the 14th largest MBR plant and the 8th largest operating MBR plant in the world. The plant was installed and commissioned in 2012 for municipal wastewater treatment. The average daily permeate water flow is 59,000 m^3/day and the PDF is 106,000 m^3/day. The membranes and their modules are ZeeWeed™ 500d. The plant was constructed by GS Engineering and after construction the ownership was transferred to Busan City Council. Pictures of the site and above-ground building are shown in Figure 7.13.

As the second largest city in Korea, Busan is home to more than 3.5 million people. When the city decided to replace the aging Suyeong conventional MWWTP, it faced a number of challenges including strict discharge effluent quality requirements and limited land area for construction. Figure 7.23 shows a picture of Busan Suyeong sewage treatment plant.

Residents also called for a more environmental-friendly and sanitary facility, especially since the old Suyeong MWWTP was then surrounded by a sprawling urban landscape. Following an increasingly common trend in Korea, the city decided to build the new MWWTP completely underground with a residential park at ground level. The new MWWTP became part of the city's 20-year three-phase infrastructure development plan to build/expand the Suyeong MWWTP.

The system utilizes GE's ZeeWeed MBR technology, which includes totally 5760 membrane modules having 31.6 m^2 of effective membrane area and 120 membrane cassettes that have 48 modules each. Ten membrane cassettes are immersed in a membrane train and total 12 membrane trains are installed. The system eliminates the need for secondary clarifier and tertiary filtration, has a smaller footprint than conventional alternatives, and boasts of reduced construction costs.

The MBR process meets the effluent quality limit of 7 mg/L biological oxygen demand (BOD), 40 mg/L chemical oxygen demand (COD), 20 mg/L total suspended solid (SS), 20 mg/L total nitrogen (TN), and 2 mg/L total phosphorus (TP).
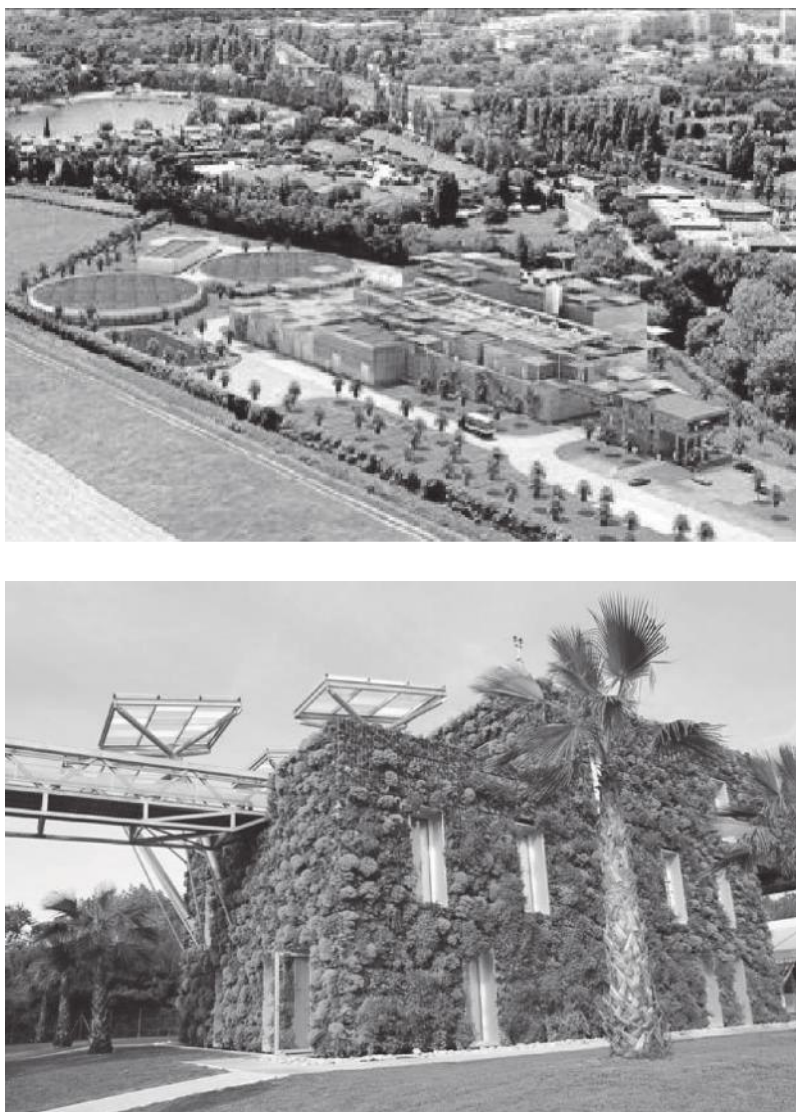
Figure 7.22   Pictures of Cannes Aquaviva Wastewater Treatment Plant.

Meeting these strict limits was extremely important for the city; the effluent from the STP is discharged into the Suyeong River, which flows directly to the ocean near some of Korea's most popular beach resorts.

The system has two stages of screening processes. Influent water overflows on the first settling tank is filtered by 6 mm of fine screen at first and then by 1 mm of mash screen. The linear velocities of each screen are 0.5 and 0.25 m/s each.

Figure 7.23   Pictures of Busan Suyeong sewage treatment plant.

A bioreactor is one of the typical A_2O processes. The reactor has an anaerobic tank, an anoxic tank, an aeration tank, and a membrane tank separated from the aeration tank. Additionally, backwashing tank and chemical tanks are installed near the membrane tank.

Membranes are operated by repeated sequence of permeation (12 min) and backwashing (0.5 min). Backwashing flux is 1.5 times higher than permeation flux. During the membrane operation, additional cleaning processes are applied. Cyclic aeration intermittently supplies air from the bottom of membrane cassettes to the top by cycles of 10 s on and 30 s off. When the source water flow is higher than the PDF, aeration cycle is changed to 10 s on and 10 s off in order to reduce the membrane operation load. SAD_m is 0.54 Nm^3/m^3 h. Membranes are washed by MC that

adds 200 mg/L of hypochlorite (at every 0.5 week) and 1000 mg/L of citric acid (at every 1 week) to backwashing water. When the TMP reaches the limit of membrane operation or the membrane operation interval reaches 6 months, recovery cleaning is done with higher concentration of hypochlorite (1000 mg/L) and citric acid (2000 mg/L). In recovery cleaning, membranes are immersed into the cleaning solution for 6 h by aeration.

7.4.6 Cleveland Bay Wastewater Treatment Plant

The Cleveland Bay WWTP is the 23rd largest MBR plant and the 15th largest operating MBR plant in the world. The plant is located in Cleveland Bay, Townsville, Queensland, Australia. The plant was installed and commissioned in 2008 for MWWT. The average daily permeate water flow is 29,000 m^3/day and the PDF is 75,000 m^3/day. The membranes and their modules are ZeeWeed™ 500d. The plant was designed as a clarifier retrofit using ZeeWeed membranes to increase plant throughput and to meet stringent effluent requirements in the Great Barrier Reef area. Aerial pictures from the site are shown in Figure 7.24.

Like everywhere in Australia, the Townsville area had been facing severe drought conditions. On top of the water restrictions, the Environmental Protection Agency had implemented more stringent license agreements for cities in the Great Barrier Reef area. Of particular concern was both nitrogen and phosphate in the effluent quality.

The Townsville Council had to rebuild their Cleveland Bay Wastewater Treatment Plant using state of the art technology. Due to the small footprint of its technology, GE Water & Process Technologies were chosen as the UF supplier utilizing their hollow fiber membranes for the MBR. The process consists of two MBR streams that have been constructed through the modification of existing secondary clarifiers. This was achieved through a novel circular design in which the membrane tanks are located centrally with an oxidation ditch forming the outer annulus. The plant is currently processing 23 ML of effluent a day with a design dry weather flow of 29 ML/day. It also has a design peak wet weather flow of 145 ML/day, of which 75 ML flows through the secondary treatment and the membrane system.

The plant was completely rebuilt over an 18-month period and is one of the largest MBR WWTPs of its type in the Southern Hemisphere. The plant has reduced the amount of nutrient discharge into the environment by around 140 m^3 per annum. The amount of nitrogen discharge has been reduced from 138 m^3 a year to 30 m^3, and the amount of phosphorus has been reduced from 43 m^3 to just 8 m^3 per year. The impact on local marine life has reduced with better quality water being discharged into the environment. With the Townsville population rapidly increasing, the council has to look at future plans to also reuse this treated water. The treated water can be recycled for civic and commercial purposes and this is the key area to focus on.
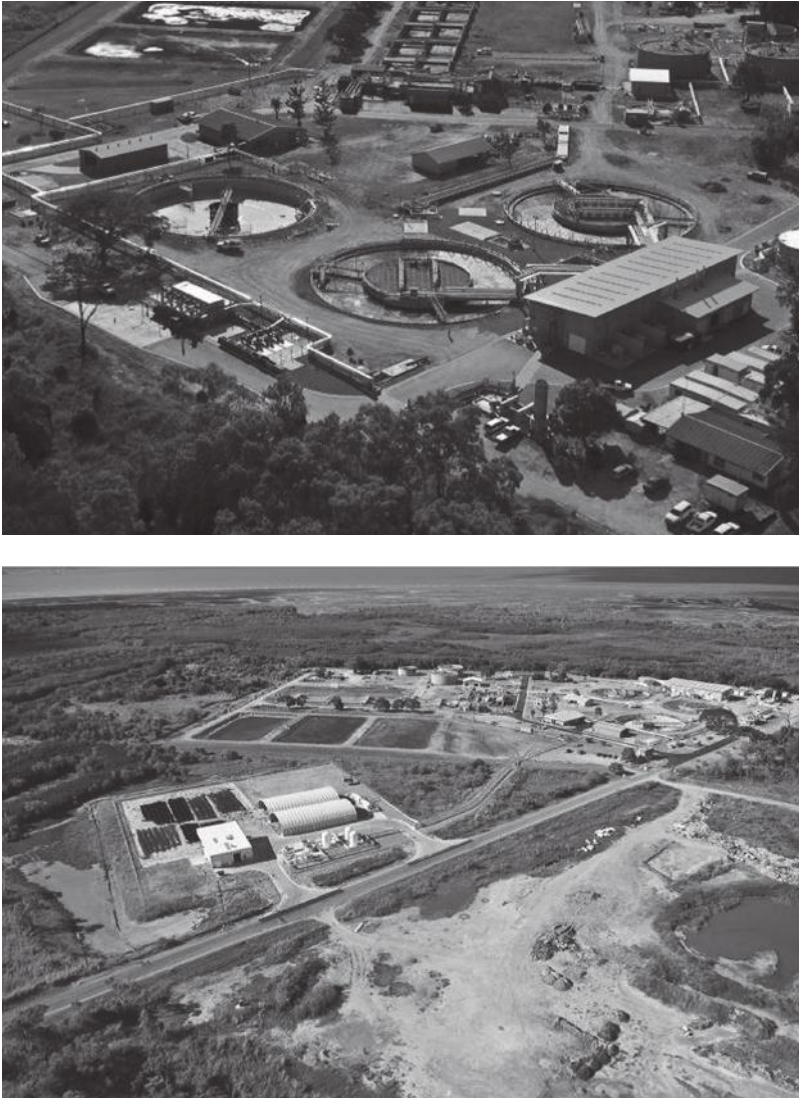
Figure 7.24   Cleveland Bay WWTP.

7.5 Case Studies for Industrial Wastewater Treatment

7.5.1 Basic American Foods Potato Processing Plant

At the Basic American Foods (BAF) Potato Processing Plant, a potato processing facility, GE's ZeeWeed MBR technology has been in use for more than 12 years to treat wastewater. The plant is located in Blackfoot, Idaho, United States, and

Figure 7.25   Picture of BAF potato processing plant.

was installed and commissioned in 2002. The average daily permeate water flow is 4900 m³/day. The membranes and their modules are ZeeWeed™ 500d. The plant is owned by BAF. Figure 7.25 displays a picture of the processing plant.

Based in Idaho, BAF is a leading manufacturer of potato products in the United States. The main potato processing plant was established in the 1950s and remains the company's largest manufacturing plant. Wastewater from the plant contains high levels of nitrogen; hence, BAF turned to an advanced wastewater treatment system to handle the difficult-to-treat water. Previously, the treatment process consisted of clarification and land irrigation. Although anaerobic treatment has traditionally been the preferred technology for potato processing facilities, anaerobic treatment does not remove nutrients (e.g., nitrogen) from the waste stream.

BAF needed a trouble-free system to treat wastewater to a high level that could be safely discharged back to the environment.

After considering a variety of options, BAF selected a ZeeWeed MBR system from GE's Water & Process Technologies. Leveraging GE's design/build capabilities, the entire 1.3 MGD (4920 m³/day) plant was constructed and commissioned in just 7 months.

The facility's influent wastewater is first fed to an existing primary clarifier. Effluent from the clarifier is fed to a 4542 m³ anoxic tank, which is then followed by three 3028 m³ aerobic bioreactors. In order for the denitrification to occur, the mixed liquor is recycled at a high rate from the aerobic tanks to the anoxic tank. To achieve the highest effluent quality, the mixed liquor is fed from three aerobic

tanks to three separate membrane tanks. To prevent solids concentration buildup in these membrane tanks, a portion of the flow is pumped back into the aerobic tanks. The ZeeWeed cassettes are immersed directly into the membrane tanks and a gentle suction of –6.9 to –55 kPa is applied. Once drawn inside the membrane fibers, the treated water is conveyed to the main effluent discharge pipe and released safely back into the environment.

7.5.2 *Frito-Lay Process Water Recovery Treatment Plant*

The Frito-Lay Process Water Recovery Treatment Plant (PWRTP) is an award-winning plant that uses ZeeWeed MBR technology to reclaim water for food processing. The plant is located in Casa Grande, Arizona, United States, and was installed and commissioned in 2010. The average daily permeate water flow is 2400 m^3/day. The membranes and their modules are ZeeWeed™ 500d. The plant is owned by Frito-Lay (Figure 7.26).

Frito-Lay's Casa Grande, Arizona, snack food manufacturing plant is a flagship project with ambitious goals: to nearly run the entire plant on renewable energy and recycled water while producing less than 1% landfill waste. A key component to this action was the installation of a new PWRTP that eliminates the need for land application of the plant's wastewater and provides space for a 5 MW PV solar system and a biomass boiler system to produce the steam and electricity needed to operate the plant.

CDM designed and built the 2650 m^3/day water recovery and recycling facility to reclaim and reuse more than 75% of the plant's process water. Using GE's advanced membrane technology to help meet US EPA primary and secondary drinking water standards, the recovery system cleans and reuses most of the facility's process water for other cleaning and production needs. The compact facility dramatically reduces the plant's discharged water, freeing up ground currently used for the land application of wastewater.

The innovative design and reliable MBR technology enables Frito-Lay to reduce the impact their manufacturing operations have on the environment by conserving water, reducing energy use, and minimizing waste.

In 2010, GE and Frito Lay received the Environmental Contribution of the Year Award from Global Water Intelligence for the Casa Grande Facility.

7.5.3 *Kanes Foods*

The Kanes Foods WWTP is located in Worcestershire, UK. The plant was installed and commissioned in 2001. The average daily permeate water flow is 2400 m^3/day. The membranes and their modules are multitube cylindrical tubular with pressurized modules provided by Aquabio Ltd—AMBR LE. The plant is owned by Kanes Foods.
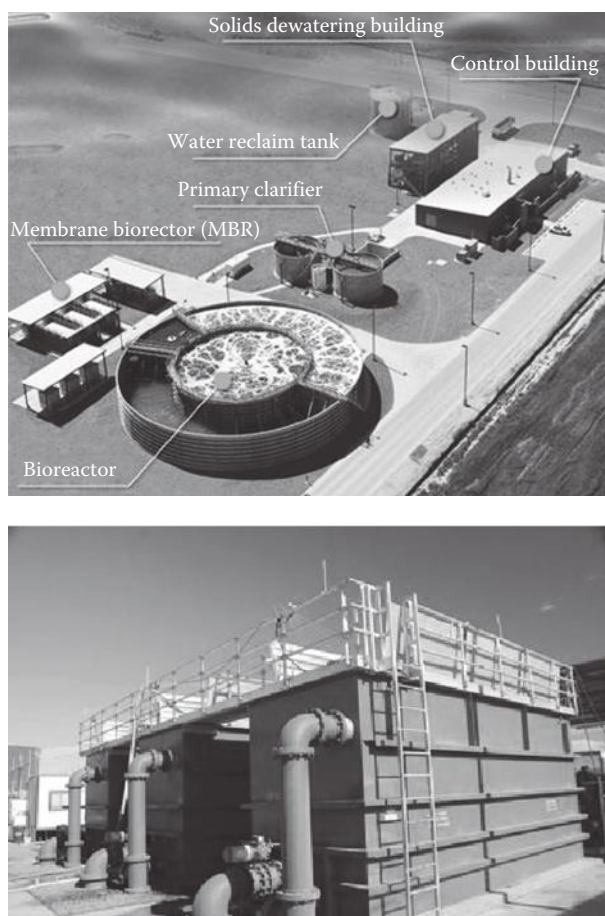
Figure 7.26   Picture of Frito-Lay Process Water Recovery Treatment Plant.

The plant is an example of food effluent recycling with a sidestream pumped MBR based on Aquabio's "AMBR" technology, and was commissioned in 2001. Eighty percent of the flow is recycled.

The process treatment scheme comprises upstream screening, flow balancing, DAF treatment (for fine vegetable solids removal), the MBR itself, and downstream treatment by reverse osmosis followed by UV disinfection. The permeate water is blended with main processing water for use within the factory. The MBR is composed of two 250 m^3 bioreactors with four banks of cross-flow membrane modules. The maximum MLSS concentration is 20 g/L, but the bioreactor is generally operated at around 10 g/L resulting in food-to-microorganism (F:M) ratios of around 0.13 kg COD/kg MLSS day.

Sludge production is calculated as being 0.14 kg DS (dry solid or dry sludge)/kg COD removed from when the sludge age is over 100 days. Each membrane bank is fitted with four 200 mm diameter MT UF Norit membranes. The membranes operate at an average flux of 153 LMH normalized to 25°C. The permeate water has average TSS, BOD, and COD concentrations of 4, 7, and 16 mg/L, respectively. The UF permeate is passed to a two-stage reverse osmosis plant that achieves an overall recovery of 75%–80%. The reject stream is discharged to the sewer, and the permeate, which typically has a conductivity of 40–100 μS/cm, is passed to the UV disinfection unit and then to the client's water supply tank.

The plant has performed consistently in terms of biological treatment, membrane performance, and final reuse water quality. For the majority of the time membrane performance has been better than design, allowing one bank to be maintained as a standby and, hence, offering greater process flexibility and lower energy use. Occasional reductions in membrane flux have been linked to poor biomass health, which has been rectified by closer management of the process.

7.5.4 Pfizer Wastewater Treatment Plant

The Pfizer WWTP is located in Ireland and was installed and commissioned in 2001. The average daily permeate water flow is 1500 m³/day. The membranes and their modules are ZeeWeed™ 500d. The plant is owned by Pfizer.

Pharmaceutical wastewater streams can be difficult to treat with conventional physical/chemical and biological treatment systems. High COD, variable strength waste streams, and shock loads are just a few conditions that limit the effectiveness of conventional systems. Physical/chemical systems are a common method of treating pharmaceutical wastewater; however, system results are limited due to high sludge production and relatively low efficiency of dissolved COD removal.

Biological aerobic treatment systems are also used extensively, often with limited success due to the final clarification step. The clarifiers are susceptible to sludge bulking and variations in total dissolved solids, often associated with batch process production, which can cause destabilization of bacterial floc formation, with a consequential loss of biomass in the final effluent. These systems require constant operator attention to adjust chemical dosing for the daily, even hourly changes in influent flow.

7.5.5 Taneco Refinery

The Taneco Refinery WWTP is located in Nizhnekamsk, Tatarstan, Russia. The plant was installed and commissioned in 2012. The average daily permeate water flow is 17,000 m³/day. The membranes and their modules are ZeeWeed™ 500d. The plant was constructed by GE Water & Process Technologies and after construction the ownership was transferred to OJSC Taneco. Figure 7.27 shows an aerial picture of the site.

Figure 7.27 Picture of Taneco refinery plant.

7.5.6 *Zhejiang Pharmaceutical WWTP*

The Zhejiang Pharmaceutical WWTP is located in Zhejiang, China, and was installed and commissioned in 2011. The average daily permeate water flow is 400 m³/day. The membranes and their modules are flat-sheet membranes and vertically aligned submerged membrane modules provided Shanghai MegaVision Membrane Engineering and Technology Co., Ltd. The plant was constructed by Shanghai MegaVision and after construction its ownership was transferred to Zhejiang Pharmaceutical. A picture of the facility is shown in Figure 7.28.

Figure 7.28 Picture of Zhejiang Pharmaceutical WWTP.

This new project was designed after several months of in situ tests to determine the best options to depurate the very complex mix of industrial wastewater. The designed solution is composed of previously built concrete tanks with a new anaerobic treatment as primary treatment based on ValorSabio's technology UASB (upflow anaerobic sludge blanket)-PRO and the secondary treatment is also based on ValorSabio's JET-LOOP SYSTEM + MBR technology.

In parallel to the secondary treatment based on biological processes (JET-LOOP SYSTEM + MBR), a chemical and physical unit was also installed in order to flocculate and remove nonbiodegradable substances in effluent water.

The UASB-PRO was installed and has been in operation since November 2011. It uses a new pulse process to solve the old problems found in large UASBs related to unbalanced and poor feed distribution, preferential flow paths inside the bioreactors, and difficulties in maintaining the up-flow wastewater within the design range.

The operation of the UASB-PRO is capable of reducing COD loads by more than 80% even with a poorly biologically degradable influent. It also produces a considerable volume of biogas, thus reducing the treatment operating expenses (OPEX) and creating a return of electrical energy and hot water from the biogas cogeneration burn.

The JET-LOOP SYSTEM + MBR process is operated with a low HRT (less than 25%) compared with the previous conventional activated sludge process and produces extremely high-quality treated water. The treated water quality is fully under the legal permits negotiated with the authorities and agencies.

References

Judd, C. (2014) The largest MBR plants worldwide?, http://www.thembrsite.com/about-mbrs/largest-mbr-plants.

van der Roest, H. F., Lawrence, D. P., and van Bentem, A. G. N. (2002) *Membrane Bioreactors for Municipal Wastewater Treatment*, IWA Publishing, London, U.K.

WASTEWATER ENGINEERING

Principles of Membrane Bioreactors for Wastewater Treatment covers the basic principles of membrane bioreactor (MBR) technology, including biological treatment, membrane filtration, and MBR applications. The book discusses concrete principles, appropriate design, and operational aspects.

It covers a wide variety of MBR topics, including filtration theory, membrane materials and geometry, fouling phenomena and properties, and strategies for minimizing fouling. Also covered are the practical aspects such as operation and maintenance.

Case studies and examples in the book help readers understand the basic concepts and principles clearly, while problems presented help advance relevant theories more deeply. Readers will find this book a helpful resource to understand the state of the art in MBR technology.